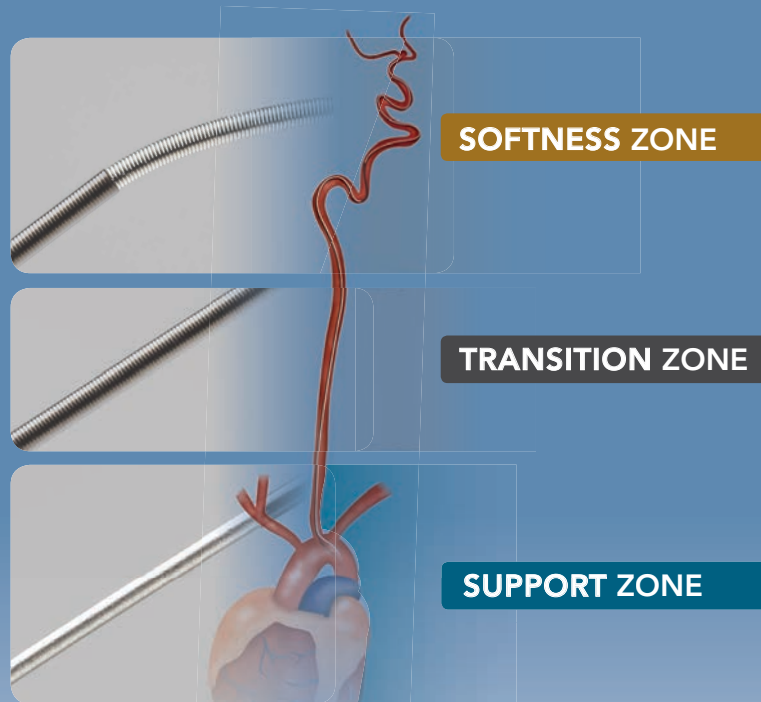


Advanced

by MicroVention



ENHANCED CONTROL TO MAXIMIZE COIL PERFORMANCE

The V-Trak® Advanced Coil System, the next generation to power the performance of our most technically advanced line of coils. Offering the optimal combination of support and flexibility.

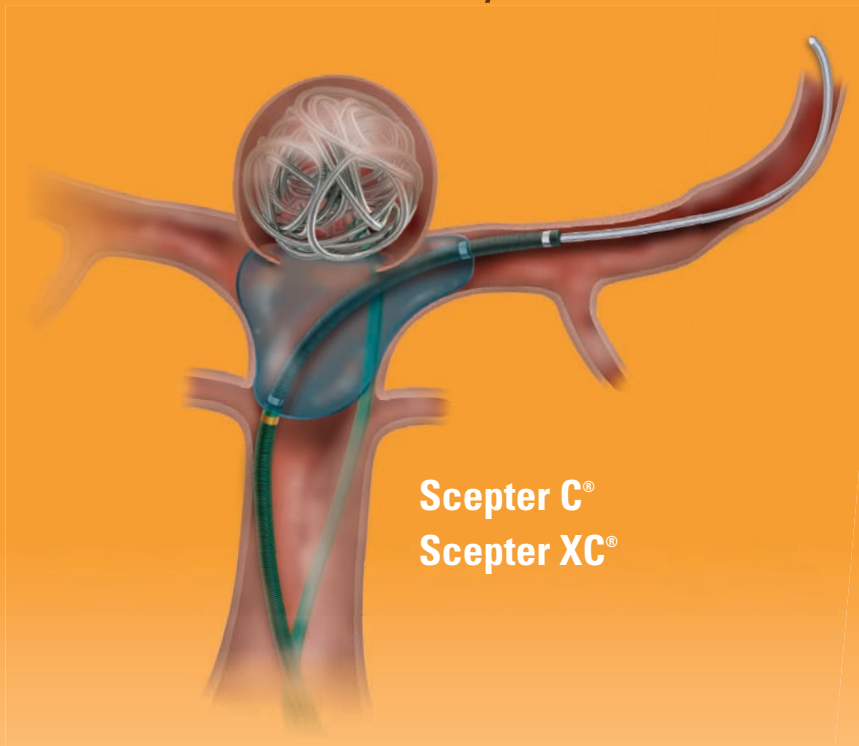
microvention.com

MICROVENTION, V-Trak, Scepter C, Scepter XC and Headway are registered trademarks of MicroVention, Inc. Scientific and clinical data related to this document are on file at MicroVention, Inc. Refer to Instructions for Use, contraindications and warnings for additional information. Federal (USA) law restricts this device for sale by or on the order of a physician. © 2015 MicroVention, Inc. 5/15

CE
0297

Versatility

by MicroVention



Scepter C®
Scepter XC®

Scepter
Occlusion Balloon
Catheter

REDEFINING DELIVERABILITY, VERSATILITY AND CONTROL

MicroVention has developed two occlusion balloon catheters. **Scepter C®** compliant balloon is designed for reliable vessel occlusion yet conforms to vessel anatomy. **Scepter XC®** x-tra compliant balloon conforms to extremely complex anatomies where neck coverage is more challenging.

• Used with



For more information or a product demonstration,
contact your local MicroVention representative:



MicroVention, Inc.

Worldwide Headquarters

1311 Valencia Avenue

Tustin, CA 92780 USA

MicroVention UK Limited

MicroVention Europe, S.A.R.L.

MicroVention Deutschland GmbH

PH +1.714.247.8000

PH +44 (0) 191 258 6777

PH +33 (1) 39 21 77 46

PH +49 211 210 798-0

COILING OPTIMIZED



NOW AVAILABLE

**BARRICADE COMPLEX
FINISHING COIL**

- ◆ Extremely soft profile of The Barricade Finishing coil now in a complex shape
- ◆ Excellent microcatheter stability for confident coil placement
- ◆ Available in a size range of 1mm-5mm

BARRICADE™ COIL SYSTEM



MADE IN AMERICA

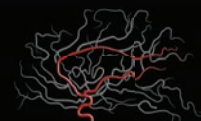
The Barricade Coil System is intended for the endovascular embolization of intracranial aneurysms and other neurovascular abnormalities such as arteriovenous malformations and arteriovenous fistulae. The System is also intended for vascular occlusion of blood vessels within the neurovascular system to permanently obstruct blood flow to an aneurysm or other vascular malformation and for arterial and venous embolizations in the peripheral vasculature. Refer to the instructions for use for complete product information.

18 TECHNOLOGY DRIVE #169, IRVINE CA 92618

p: 949.788.1443 | f: 949.788.1444

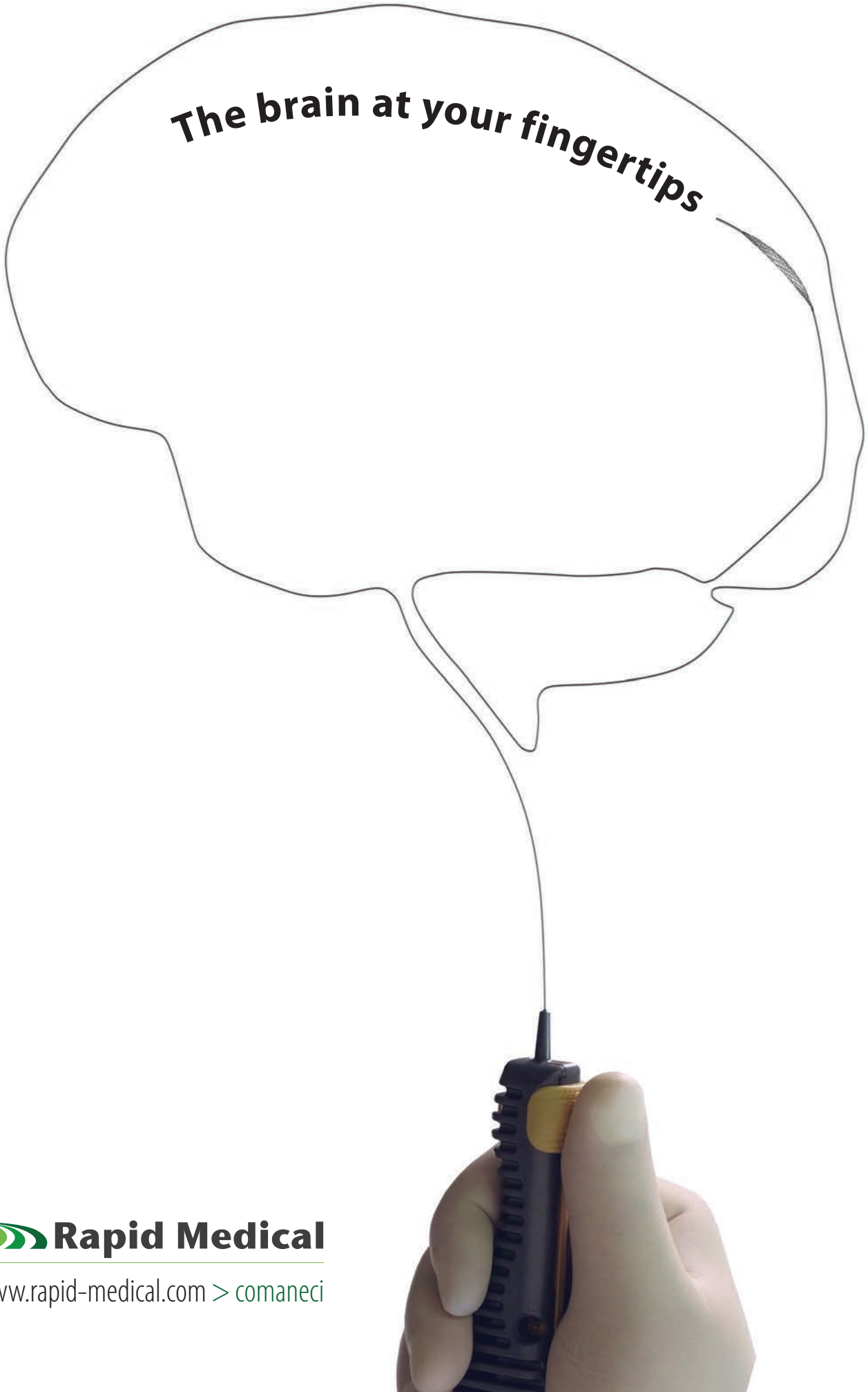
WWW.BLOCKADEMEDICAL.COM

MKTG-031 Rev. A



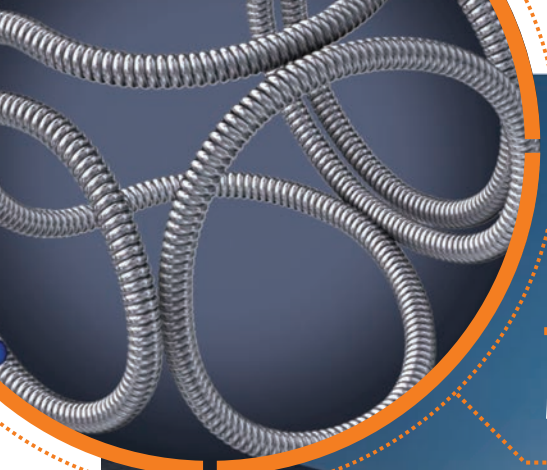
BLOCKADE
M E D I C A L

The brain at your fingertips



 **Rapid Medical**

www.rapid-medical.com > [comaneci](#)



Target[®] DETACHABLE COILS



Smooth and Stable

Whether you are framing, filling or finishing, Target Detachable Coils deliver consistently smooth deployment and exceptional microcatheter stability. Focused on design, Target Coils feature a host of advantages to ensure the high-powered performance you demand.

For more information, please visit www.strykerneurovascular.com/Target or contact your local Stryker Neurovascular sales representative.

stryker[®]
Neurovascular

CALL FOR AJNR EDITORIAL FELLOWSHIP CANDIDATES

ASNR and AJNR are pleased once again to join efforts with other imaging-related journals that have training programs on editorial aspects of publishing for trainees or junior staff (3–5 years after training), including Radiology (Olmsted fellowship), AJR (Figley and Rogers fellowships), JACR (Bruce J. Hillman fellowship), and Radiologia.

2016 Candidate Information and Requirements

GOALS

- Increase interest in “editorial” and publication-related activities in younger individuals.
- Increase understanding and participation in the AJNR review process.
- Incorporate into AJNR’s Editorial Board younger individuals who have previous experience in the review and publication process.
- Fill a specific need in neuroradiology not offered by other similar fellowships.
- Increase the relationship between “new” generation of neuroradiologists and more established individuals.
- Increase visibility of AJNR among younger neuroradiologists.

ACTIVITIES OF THE FELLOWSHIP

- Serve as Editorial Fellow for one year. This individual will be listed on the masthead as such.
- Review at least one manuscript per month for 12 months. Evaluate all review articles submitted to AJNR.
- Access to our electronic manuscript review system will be granted so that the candidate can learn how these systems work.
- Be involved in the final decision of selected manuscripts together with the Editor-in-Chief.
- Participate in all monthly Senior Editor telephone conference calls.
- Participate in all meetings of the Editors and Publications Committee during the annual meetings of ASNR and RSNA as per candidate’s availability. The Foundation of the ASNR will provide \$2000 funding for this activity.
- Evaluate progress and adjust program to specific needs in annual meeting or telephone conference with the Editor-in-Chief.
- Write at least one editorial for AJNR.
- Embark on an editorial scientific or bibliometric project that will lead to the submission of an article to AJNR or another appropriate journal as determined by the Editor-in-Chief. This project will be presented by the Editorial Fellow at the ASNR annual meeting.
- Serve as liaison between AJNR and ASNR’s Young Professionals Network and the 3 YPs appointed to AJNR as special consultants. Participate in meetings and telephone calls with this group. Design one electronic survey/year polling the group regarding readership attitudes and wishes.
- Recruit trainees as reviewers as determined by the Editor-in-Chief.
- Participate in Web improvement projects.
- Invite Guest Editors for AJNR’s News Digest to cover a variety of timely topics.

QUALIFICATIONS

- Be a fellow in neuroradiology from North America, including Canada (this may be extended to include other countries).
- Be a junior faculty neuroradiology member (< 3 years) in either an academic or private environment.
- Be an “in-training” or member of ASNR in any other category.

APPLICATION

- Include a short letter of intent with statement of goals and desired research project. CV must be included.
- Include a letter of recommendation from the Division Chief or fellowship program director. A statement of protected time to perform the functions outlined is desirable.
- Applications will be evaluated by AJNR’s Senior Editors and the Chair of the Publications Committee prior to the ASNR meeting. The name of the selected individual will be announced at the meeting.
- Applications should be received by March 4, 2016 and sent to Ms. Karen Halm, AJNR Managing Editor, electronically at khalm@asnr.org.



ASFNR • ASHNR • ASPNR • ASSR • SNIS

THE FOUNDATION OF THE ASNR



THE FOUNDATION OF THE ASNR SYMPOSIUM 2016: EMERGENCY NEURORADIOLOGY MAY 21-22

ASNR 54TH ANNUAL MEETING MAY 23-26



THE FOUNDATION OF THE ASNR SYMPOSIUM 2016: EMERGENCY NEURORADIOLOGY

The Symposium 2016 will be held from May 21-22 and will feature world-renowned speakers providing a comprehensive review of Emergency Neuroradiology and neuroimaging issues in critical care. Neuroimaging has become an indispensable tool for triage and management of both adults and children in emergency settings. Efficient and appropriate use of CT and MRI are critical to the urgent management of brain, spine, head & neck, and neurovascular emergencies, all of which will be highlighted by expert faculty. Best practices for traumatic and non-traumatic emergencies will be discussed, including methods to ensure optimal workflow, image post-processing, PACS integration, telemedicine, safety, and quality. Challenges and solutions for providing 24/7 coverage will be presented and debated.

ASNR 54TH ANNUAL MEETING: The meeting will be held from May 23-26 with an estimated 1,700 physicians and medical professionals worldwide who are interested in the latest products and services to deliver the highest quality care in the realm of Neuroradiology and allied professions. The Annual Meeting will provide informative updates on general Neuroradiology and showcase specialty programming from the ASFNR, ASHNR, ASPNR, ASSR, and SNIS. The heart of the meeting will be the invited lectures, original presentations, scientific posters and educational exhibits.

Howard A. Rowley, MD, ASNR 2016 Program Chair/President-Elect
Programming developed in cooperation with ...

American Society of Functional Neuroradiology (ASFNR)
Christopher G. Filippi, MD

American Society of Head and Neck Radiology (ASHNR)
Lindell R. Gentry, MD

American Society of Pediatric Neuroradiology (ASPNR)
Erin Simon Schwartz, MD

American Society of Spine Radiology (ASSR)
Gregory J. Lawler, MD

Society of NeuroInterventional Surgery (SNIS)
Charles J. Prestigiacomo, MD

American Society of Neuroradiology (ASNR) Committee Programming:
Health Policy Committee
Robert M. Barr, MD, FACR

Computer Science and Informatics (CSI) Committee
John L. Go, MD, FACR

Research Scientists Committee
Dikoma C. Shungu, PhD/Timothy P.L. Roberts, PhD

ASNR 54TH ANNUAL MEETING

c/o American Society of Neuroradiology
800 Enterprise Drive, Suite 205
Oak Brook, Illinois 60523-4216
Phone: 630-574-0220
Fax: 630 574-0661
www.asnr.org/2016

SCAN NOW
TO VISIT
OUR WEBSITE



SAVE THE DATE... MAY 21-26, 2016
WASHINGTON MARRIOTT WARDMAN PARK • WASHINGTON, DC



Simplify the MOC Process



Manage your CME Credits Online

CMEgateway.org

Available to Members of Participating Societies

American Board of Radiology (ABR)
American College of Radiology (ACR)
American Roentgen Ray Society (ARRS)
American Society of Neuroradiology (ASNR)
Commission on Accreditation of Medical
Physics Educational Programs, Inc. (CAMPEP)
Radiological Society of North America (RSNA)
Society of Interventional Radiology (SIR)
SNM
The Society for Pediatric Radiology (SPR)

It's Easy and Free!

Log on to CME Gateway to:

- View or print reports of your CME credits from multiple societies from a single access point.
- Print an aggregated report or certificate from each participating organization.
- Link to SAMs and other tools to help with maintenance of certification.

American Board of Radiology (ABR) participation!

By activating ABR in your organizational profile, your MOC-fulfilling CME and SAM credits can be transferred to your own personalized database on the ABR Web site.

Sign Up Today!

go to CMEgateway.org

Go Green!

AJNR urges American Society of Neuroradiology members to reduce their environmental footprint by voluntarily suspending their print subscription.

The savings in paper, printing, transportation, and postage not only help members cut down on clutter, but go to fund new electronic enhancements and expanded content.

The digital edition of *AJNR* presents the print version in its entirety, along with extra features including:

- Publication Preview
- Case of the Week
- Podcasts
- Special Collections
- The *AJNR* Blog
- Weekly Poll

It also **reaches subscribers much faster than print**. An **electronic table of contents** will be sent directly to your mailbox to notify you as soon as it publishes.

Readers can **search, reference, and bookmark** current and archived content 24 hours a day on www.ajnr.org, rather than thumb through stacks of accumulated paper issues for articles and images they need.



<http://www.ajnr.org/cgi/feedback>

ASNR members who wish to opt out of print can do so by using the Feedback form on the *AJNR* Website (<http://www.ajnr.org/cgi/feedback>). Just type "Go Green" in the subject line to stop print and spare our ecosystem.



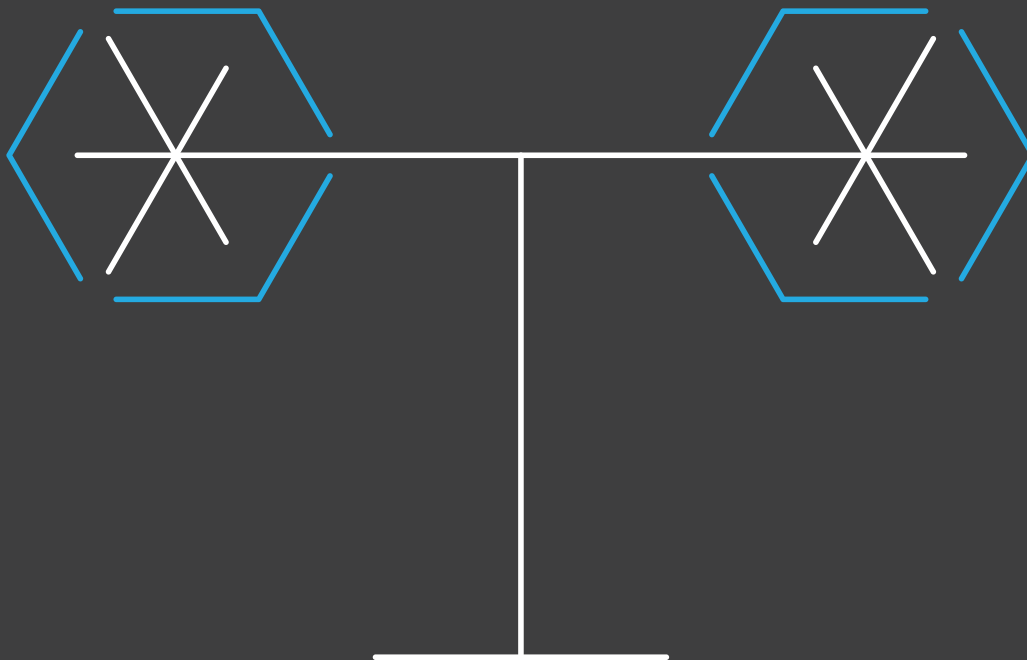
The Korean Society of Radiology

K-RAD  Open · Balanced
Sustainable

KCR 2016

The 72nd Korean Congress of Radiology
And Annual Delegate Meeting of
The Korean Society of Radiology

2016.9.21 Wed – 2016.9.24 Sat
Coex, Seoul, Korea



www.kcr4u.org

Target® Detachable Coil

See package insert for complete indications, contraindications, warnings and instructions for use.

INTENDED USE / INDICATIONS FOR USE

Target Detachable Coils are intended to endovascularly obstruct or occlude blood flow in vascular abnormalities of the neurovascular and peripheral vessels.

Target Detachable Coils are indicated for endovascular embolization of:

- Intracranial aneurysms
- Other neurovascular abnormalities such as arteriovenous malformations and arteriovenous fistulae
- Arterial and venous embolizations in the peripheral vasculature

CONTRAINDICATIONS

None known.

POTENTIAL ADVERSE EVENTS

Potential complications include, but are not limited to: allergic reaction, aneurysm perforation and rupture, arrhythmia, death, edema, embolus, headache, hemorrhage, infection, ischemia, neurological/intracranial sequelae, post-embolization syndrome (fever, increased white blood cell count, discomfort), TIA/stroke, vasospasm, vessel occlusion or closure, vessel perforation, dissection, trauma or damage, vessel rupture, vessel thrombosis. Other procedural complications including but not limited to: anesthetic and contrast media risks, hypotension, hypertension, access site complications.

WARNINGS

- Contents supplied STERILE using an ethylene oxide (EO) process. Do not use if sterile barrier is damaged. If damage is found, call your Stryker Neurovascular representative.
- For single use only. Do not reuse, reprocess or resterilize. Reuse, reprocessing or resterilization may compromise the structural integrity of the device and/or lead to device failure which, in turn, may result in patient injury, illness or death. Reuse, reprocessing or resterilization may also create a risk of contamination of the device and/or cause patient infection or cross-infection, including, but not limited to, the transmission of infectious disease(s) from one patient to another. Contamination of the device may lead to injury, illness or death of the patient.
- After use, dispose of product and packaging in accordance with hospital, administrative and/or local government policy.
- **This device should only be used by physicians who have received appropriate training in interventional neuroradiology or interventional radiology and preclinical training on the use of this device as established by Stryker Neurovascular.**
- Patients with hypersensitivity to 316LVM stainless steel may suffer an allergic reaction to this implant.
- MR temperature testing was not conducted in peripheral vasculature, arteriovenous malformations or fistulae models.
- The safety and performance characteristics of the Target Detachable Coil System (Target Detachable Coils, InZone Detachment Systems,

delivery systems and accessories) have not been demonstrated with other manufacturer's devices (whether coils, coil delivery devices, coil detachment systems, catheters, guidewires, and/or other accessories). Due to the potential incompatibility of non Stryker Neurovascular devices with the Target Detachable Coil System, the use of other manufacturer's device(s) with the Target Detachable Coil System is not recommended.

- To reduce risk of coil migration, the diameter of the first and second coil should never be less than the width of the ostium.
- In order to achieve optimal performance of the Target Detachable Coil System and to reduce the risk of thromboembolic complications, it is critical that a continuous infusion of appropriate flush solution be maintained between a) the femoral sheath and guiding catheter, b) the 2-tip microcatheter and guiding catheters, and c) the 2-tip microcatheter and Stryker Neurovascular guidewire and delivery wire. Continuous flush also reduces the potential for thrombus formation on, and crystallization of infusate around, the detachment zone of the Target Detachable Coil.
- Do not use the product after the "Use By" date specified on the package.
- Reuse of the flush port/dispenser coil or use with any coil other than the original coil may result in contamination of, or damage to, the coil.
- Utilization of damaged coils may affect coil delivery to, and stability inside, the vessel or aneurysm, possibly resulting in coil migration and/or stretching.
- The fluoro-saver marker is designed for use with a Rotating Hemostatic Valve (RHV). If used without an RHV, the distal end of the coil may be beyond the alignment marker when the fluoro-saver marker reaches the microcatheter hub.
- If the fluoro-saver marker is not visible, do not advance the coil without fluoroscopy.
- Do not rotate delivery wire during or after delivery of the coil. Rotating the Target Detachable Coil delivery wire may result in a stretched coil or premature detachment of the coil from the delivery wire, which could result in coil migration.
- Verify there is no coil loop protrusion into the parent vessel after coil placement and prior to coil detachment. Coil loop protrusion after coil placement may result in thromboembolic events if the coil is detached.
- Verify there is no movement of the coil after coil placement and prior to coil detachment. Movement of the coil after coil placement may indicate that the coil could migrate once it is detached.
- Failure to properly close the RHV compression fitting over the delivery wire before attaching the InZone® Detachment System could result in coil movement, aneurysm rupture or vessel perforation.
- Verify repeatedly that the distal shaft of the catheter is not under stress before detaching the Target Detachable Coil. Axial compression or tension forces could be stored in the 2-tip microcatheter causing the tip to move during coil delivery. Microcatheter tip movement could cause the aneurysm or vessel to rupture.
- Advancing the delivery wire beyond the microcatheter tip once the coil has been detached involves risk of aneurysm or vessel perforation.
- The long term effect of this product on extravascular tissues has not been established so care should be taken to retain this device in the intravascular space.

Damaged delivery wires may cause detachment failures, vessel injury or unpredictable distal tip response during coil deployment. If a delivery wire is damaged at any point during the procedure, do not attempt to straighten or otherwise repair it. Do not proceed with deployment or detachment. Remove the entire coil and replace with undamaged product.

- After use, dispose of product and packaging in accordance with hospital, administrative and/or local government policy.

CAUTIONS / PRECAUTIONS

- Federal Law (USA) restricts this device to sale by or on the order of a physician.
- Besides the number of InZone Detachment System units needed to complete the case, there must be an extra InZone Detachment System unit as back up.
- Removing the delivery wire without grasping the introducer sheath and delivery wire together may result in the detachable coil sliding out of the introducer sheath.
- Failure to remove the introducer sheath after inserting the delivery wire into the RHV of the microcatheter will interrupt normal infusion of flush solution and allow back flow of blood into the microcatheter.
- Some low level overhead light near or adjacent to the patient is required to visualize the fluoro-saver marker; monitor light alone will not allow sufficient visualization of the fluoro-saver marker.
- Advance and retract the Target Detachable Coil carefully and smoothly without excessive force. If unusual friction is noticed, slowly withdraw the Target Detachable Coil and examine for damage. If damage is present, remove and use a new Target Detachable Coil. If friction or resistance is still noted, carefully remove the Target Detachable Coil and microcatheter and examine the microcatheter for damage.
- If it is necessary to reposition the Target Detachable Coil, verify under fluoroscopy that the coil moves with a one-to-one motion. If the coil does not move with a one-to-one motion or movement is difficult, the coil may have stretched and could possibly migrate or break. Gently remove both the coil and microcatheter and replace with new devices.
- Increased detachment times may occur when:
 - Other embolic agents are present.
 - Delivery wire and microcatheter markers are not properly aligned.
 - Thrombus is present on the coil detachment zone.
- Do not use detachment systems other than the InZone Detachment System.
- Increased detachment times may occur when delivery wire and microcatheter markers are not properly aligned.
- Do not use detachment systems other than the InZone Detachment System.

Copyright © 2014 Stryker
NV00006677.AA

Trevo® XP ProVue Retrievers

See package insert for complete indications, complications, warnings, and instructions for use.

INDICATIONS FOR USE

The Trevo Retriever is intended to restore blood flow in the neurovasculature by removing thrombus in patients experiencing ischemic stroke within 8 hours of symptom onset. Patients who are ineligible for intravenous tissue plasminogen activator (IV t-PA) or who fail IV t-PA therapy are candidates for treatment.

COMPLICATIONS

Procedures requiring percutaneous catheter introduction should not be attempted by physicians unfamiliar with possible complications which may occur during or after the procedure. Possible complications include, but are not limited to, the following: air embolism; hematoma or hemorrhage at puncture site; infection; distal embolization; pain/headache; vessel spasm, thrombosis, dissection, or perforation; emboli; acute occlusion; ischemia; intracranial hemorrhage; false aneurysm formation; neurological deficits including stroke; and death.

COMPATIBILITY

3x20 mm retrievers are compatible with Trevo® Pro 14 Microcatheters (REF 90231) and Trevo® Pro 18 Microcatheters (REF 90238). 4x20 mm retrievers are compatible with Trevo® Pro 18 Microcatheters (REF 90238). Compatibility of the Retriever with other microcatheters has not been established. Performance of the Retriever device may be impacted if a different microcatheter is used. The Merci® Balloon Guide Catheters are recommended for use during thrombus removal procedures. Retrievers are compatible with the Abbott Vascular DOC® Guide Wire Extension (REF 22260).

WARNINGS

- Contents supplied STERILE, using an ethylene oxide (EO) process. Nonpyrogenic.
- To reduce risk of vessel damage, adhere to the following recommendations:
 - Take care to appropriately size Retriever to vessel diameter at

intended site of deployment.

- Do not perform more than six (6) retrieval attempts in same vessel using Retriever devices.
- Maintain Retriever position in vessel when removing or exchanging Microcatheter.
- To reduce risk of kinking/fracture, adhere to the following recommendations:
 - Immediately after unsheathing Retriever, position Microcatheter tip marker just proximal to shaped section. Maintain Microcatheter tip marker just proximal to shaped section of Retriever during manipulation and withdrawal.
 - Do not rotate or torque Retriever.
 - Use caution when passing Retriever through stented arteries.
- Do not resterilize and reuse. Structural integrity and/or function may be impaired by reuse or cleaning.
- The Retriever is a delicate instrument and should be handled carefully. Before use and when possible during procedure, inspect device carefully for damage. Do not use a device that shows signs of damage. Damage may prevent device from functioning and may cause complications.
- Do not advance or withdraw Retriever against resistance or significant vasospasm. Moving or torquing device against resistance or significant vasospasm may result in damage to vessel or device. Assess cause of resistance using fluoroscopy and if needed resheath the device to withdraw.
- If Retriever is difficult to withdraw from the vessel, do not torque Retriever. Advance Microcatheter distally, gently pull Retriever back into Microcatheter, and remove Retriever and Microcatheter as a unit. If undue resistance is met when withdrawing the Retriever into the Microcatheter, consider extending the Retriever using the Abbott Vascular DOC guidewire extension (REF 22260) so that the Microcatheter can be exchanged for a larger diameter catheter such as a DAC® catheter. Gently withdraw the Retriever into the larger diameter catheter.
- Administer anti-coagulation and anti-platelet medications per standard institutional guidelines.

PRECAUTIONS

- Prescription only – device restricted to use by or on order of a physician.
- Store in cool, dry, dark place.
- Do not use open or damaged packages.
- Use by "Use By" date.
- Exposure to temperatures above 54°C (130°F) may damage device and accessories. Do not autoclave.
- Do not expose Retriever to solvents.
- Use Retriever in conjunction with fluoroscopic visualization and proper anti-coagulation agents.
- To prevent thrombus formation and contrast media crystal formation, maintain a constant infusion of appropriate flush solution between guide catheter and Microcatheter and between Microcatheter and Retriever or guidewire.
- Do not attach a torque device to the shaped proximal end of DOC® Compatible Retriever. Damage may occur, preventing ability to attach DOC® Guide Wire Extension.



Concentric Medical
301 East Evelyn
Mountain View, CA 94041



EMERGO Europe
Molenstraat 15
2513 BH, The Hague
The Netherlands



Stryker Neurovascular
47900 Bayside Parkway
Fremont, CA 94538-6515

stryker.com/neurovascular

Date of Release: FEB/2014

EX_EN_US



Stryker Neurovascular
47900 Bayside Parkway
Fremont, CA 94538-6515

stryker.com/neurovascular
stryker.com/emea/neurovascular

Date of Release: JUN/2014

EX_EN_GL

Copyright © 2014 Stryker
NV00009028.AA

66%

of Patients in MR CLEAN
Were Treated with a
Trevo® Stent Retriever

stryker[®]
Neurovascular

Trevo[®]
PROVUE RETRIEVER

MR CLEAN¹

**First clinical evidence for intra-arterial
treatment with stent retrievers**

- **Largest** of the randomized AIS trials², with over 500 patients enrolled
- The Trevo Retriever was the **#1** device used in the **MR CLEAN** Trial

¹O.A. Berkhemer et al. A Randomized Trial for Intra-arterial Treatment for Acute Ischemic Stroke. *N Eng J Med* December 2014.

²MR CLEAN is the largest AIS Trial in which stent retrievers were used.
<http://www.mrclean-trial.org/>

DERIVO[®] Embolisation Device



VISIBLE PERFORMANCE

- New visibility concept
- Unique BlueXide[®] surface

AJNR

AMERICAN JOURNAL OF NEURORADIOLOGY

FEBRUARY 2016
VOLUME 37
NUMBER 2
WWW.AJNR.ORG

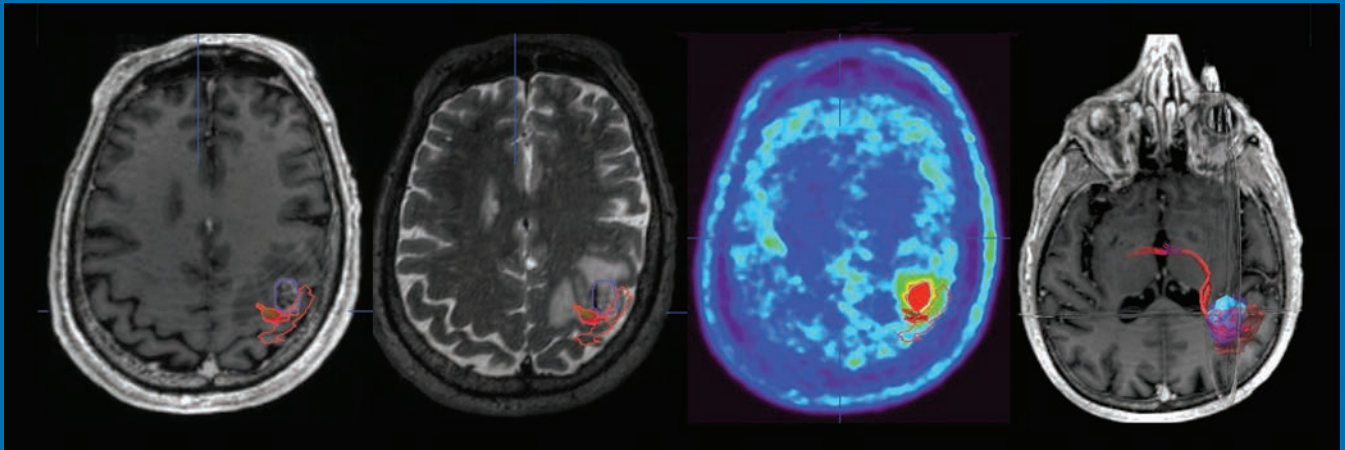
THE JOURNAL OF DIAGNOSTIC AND
INTERVENTIONAL NEURORADIOLOGY

Multimodal imaging of brain tumors

MRA-guided sclerotherapy

Flow-diverter stents for middle cerebral bifurcation aneurysms

Official Journal ASNR • ASFNR • ASHNR • ASPNR • ASSR



AJNR

AMERICAN JOURNAL OF NEURORADIOLOGY

FEBRUARY 2016
VOLUME 37
NUMBER 2
WWW.AJNR.ORG

Publication Preview at www.ajnr.org features articles released in advance of print. Visit www.ajnrblog.org to comment on AJNR content and chat with colleagues and AJNR's News Digest at <http://ajnrdigest.org> to read the stories behind the latest research in neuroimaging.

199 **PERSPECTIVES** *M.I. Vargas*

REVIEW ARTICLE



200 **Carotid Near-Occlusion: A Comprehensive Review, Part 2—Prognosis and Treatment, Pathophysiology, Confusions, and Areas for Improvement** *E. Johansson, et al.*

**EXTRACRANIAL
VASCULAR
INTERVENTIONAL**

PATIENT SAFETY



205 **MR Angiographic–Guided Percutaneous Sclerotherapy for Venous Vascular Malformations: A Radiation Dose-Reduction Strategy** *S.G. Imbesi, et al.*

**INTERVENTIONAL
HEAD & NECK**

HEALTH CARE REFORM VIGNETTE

210 **Sustainable Growth Rate Repealed, MACRA Revealed: Historical Context and Analysis of Recent Changes in Medicare Physician Payment Methodologies** *J.A. Hirsch, et al.*

GENERAL CONTENTS



215 **Prevalence of Brain Microbleeds in Alzheimer Disease: A Systematic Review and Meta-Analysis on the Influence of Neuroimaging Techniques** *A.A. Sepehry, et al.*

ADULT BRAIN



223 **Diagnostic Significance of Cortical Superficial Siderosis for Alzheimer Disease in Patients with Cognitive Impairment** *Y. Inoue, et al.*

ADULT BRAIN



228 **Acute Preoperative Infarcts and Poor Cerebrovascular Reserve Are Independent Risk Factors for Severe Ischemic Complications following Direct Extracranial-Intracranial Bypass for Moyamoya Disease** *M.U. Antonucci, et al.*

ADULT BRAIN



236 **Diagnostic Impact of Bone-Subtraction CT Angiography for Patients with Acute Subarachnoid Hemorrhage** *P. Aulbach, et al.*

ADULT BRAIN



244 **Cerebral Perfusion Pressure is Maintained in Acute Intracerebral Hemorrhage: A CT Perfusion Study** *A.S. Tamm, et al.*

ADULT BRAIN



252 **A Potential Biomarker in Amyotrophic Lateral Sclerosis: Can Assessment of Brain Iron Deposition with SWI and Corticospinal Tract Degeneration with DTI Help?** *R. Sheelakumari, et al.*

ADULT BRAIN



259 **FLAIR²: A Combination of FLAIR and T2 for Improved MS Lesion Detection** *V. Wiggermann, et al.*

ADULT BRAIN



266 **Multimodal Imaging in Malignant Brain Tumors: Enhancing the Preoperative Risk Evaluation for Motor Deficits with a Combined Hybrid MRI-PET and Navigated Transcranial Magnetic Stimulation Approach** *V. Neuschmelting, et al.*

ADULT BRAIN

	274	Principal Component Analysis of Diffusion Tensor Images to Determine White Matter Injury Patterns Underlying Postconcussive Headache <i>A. Ghodadra, et al.</i>	ADULT BRAIN
	279	Flow-Diverter Stents for the Treatment of Saccular Middle Cerebral Artery Bifurcation Aneurysms <i>J. Caroff, et al.</i>	INTERVENTIONAL
	285	The Revascularization Scales Dilemma: Is It Right to Apply the Treatment in Cerebral Ischemia Scale in Posterior Circulation Stroke? <i>C. Jung, et al.</i>	INTERVENTIONAL
	290	Autosomal Dominant Polycystic Kidney Disease and Intracranial Aneurysms: Is There an Increased Risk of Treatment? <i>M.N. Rozenfeld, et al.</i>	INTERVENTIONAL ADULT BRAIN
	294	<i>Commentary</i> Treatment of Unruptured Intracranial Aneurysms in Autosomal Dominant Polycystic Kidney Disease: Primum Non Nocere <i>M. Niemczyk</i>	
	296	<i>Reply</i> <i>M.N. Rozenfeld, et al.</i>	
	297	Cerebral Angiography for Evaluation of Patients with CT Angiogram-Negative Subarachnoid Hemorrhage: An 11-Year Experience <i>JJ. Heit, et al.</i>	INTERVENTIONAL ADULT BRAIN
	305	Stent Retriever Thrombectomy in Patients Who Are Ineligible for Intravenous Thrombolysis: A Multicenter Retrospective Observational Study <i>F. Dorn, et al.</i>	INTERVENTIONAL
	311	Combination of Multicatheter Plus Stent or Balloon for Treatment of Complex Aneurysms <i>HJ. Jeon, et al.</i>	INTERVENTIONAL
	317	High-Resolution C-Arm CT and Metal Artifact Reduction Software: A Novel Imaging Modality for Analyzing Aneurysms Treated with Stent-Assisted Coil Embolization <i>I. Yuki, et al.</i>	INTERVENTIONAL ADULT BRAIN
	324	Evaluation of the Angiographic Grading Scale in Aneurysms Treated with the WEB Device in 80 Rabbits: Correlation with Histologic Evaluation <i>A. Rouchaud, et al.</i>	INTERVENTIONAL
  	330	Evaluation for Blunt Cerebrovascular Injury: Review of the Literature and a Cost-Effectiveness Analysis <i>A. Malhotra, et al.</i>	EXTRACRANIAL VASCULAR ADULT BRAIN
	336	The Moving Carotid Artery: A Retrospective Review of the Retropharyngeal Carotid Artery and the Incidence of Positional Changes on Serial Studies <i>D.E. Lukins, et al.</i>	EXTRACRANIAL VASCULAR HEAD & NECK
 	342	Usefulness of Pseudocontinuous Arterial Spin-Labeling for the Assessment of Patients with Head and Neck Squamous Cell Carcinoma by Measuring Tumor Blood Flow in the Pretreatment and Early Treatment Period <i>N. Fujima, et al.</i>	HEAD & NECK
	349	Protrusion of the Infraorbital Nerve into the Maxillary Sinus on CT: Prevalence, Proposed Grading Method, and Suggested Clinical Implications <i>J.E. Lantos, et al.</i>	HEAD & NECK
	354	Ultrasound of the Hypoglossal Nerve in the Neck: Visualization and Initial Clinical Experience with Patients <i>S. Meng, et al.</i>	HEAD & NECK
	360	Elucidating Metabolic Maturation in the Healthy Fetal Brain Using ¹ H-MR Spectroscopy <i>I.E. Evangelou, et al.</i>	PEDIATRICS
	367	Intensity of MRI Gadolinium Enhancement in Cerebral Adrenoleukodystrophy: A Biomarker for Inflammation and Predictor of Outcome following Transplantation in Higher Risk Patients <i>W.P. Miller, et al.</i>	PEDIATRICS
 	373	Treatment of 213 Patients with Symptomatic Tarlov Cysts by CT-Guided Percutaneous Injection of Fibrin Sealant <i>K. Murphy, et al.</i>	SPINE INTERVENTIONAL
	380	Clinical Outcomes of Patients with Delayed Diagnosis of Spinal Dural Arteriovenous Fistulas <i>W. Brinjikji, et al.</i>	SPINE INTERVENTIONAL

B. Amini, et al.

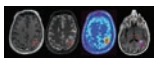
ONLINE FEATURES

LETTERS

- E11 **Low Signals on T2* and SWI Sequences in Patients with MS with Progressive Multifocal Leukoencephalopathy** *P. Labauge, et al.*
- E12 **Reply** *J. Hodel, et al.*
- E13 **Flow-Diverter Stents for the Treatment of Sacular Middle Cerebral Artery Bifurcation Aneurysms: Is “Unsuitable” the Right Conclusion?**
C. Iosif, et al.
- E14 **Reply** *J. Caroff, et al.*
- E15 **Stents for Idiopathic Intracranial Hypertension: Meta-Analyzed, Hypo-Analyzed, and In Need of a Trial** *P. Noonan*
- E17 **Reply** *S.R. Satti, et al.*
- E19 **ERRATUM**

BOOK REVIEWS *R.M. Quencer, Section Editor*

Please visit www.ajnrblog.org to read and comment on Book Reviews.



Contralateral upper limb weakness in this patient shown by the overlap of the metastasis on MR (left 2 images), FET-PET (*light blue* in the right 2 images), and hand-motor representation (*red*). Integration of functional, metabolic, and anatomic data shown in the right image.



Indicates Editor's Choices selection



Indicates Fellows' Journal Club selection



Indicates open access to non-subscribers at www.ajnr.org



Indicates article with supplemental on-line table



Indicates article with supplemental on-line photo



Indicates article with supplemental on-line video



Evidence-Based Medicine Level 1



Evidence-Based Medicine Level 2

Official Journal:

American Society of Neuroradiology
 American Society of Functional Neuroradiology
 American Society of Head and Neck Radiology
 American Society of Pediatric Neuroradiology
 American Society of Spine Radiology

EDITOR-IN-CHIEF

Jeffrey S. Ross, MD

Professor of Radiology, Department of Radiology,
 Mayo Clinic College of Medicine, Phoenix, Arizona

SENIOR EDITORS

Harry J. Cloft, MD, PhD

Professor of Radiology and Neurosurgery,
 Department of Radiology, Mayo Clinic College of
 Medicine, Rochester, Minnesota

Thierry A.G.M. Huisman, MD

Professor of Radiology, Pediatrics, Neurology, and
 Neurosurgery, Chairman, Department of Imaging
 and Imaging Science, Johns Hopkins Bayview,
 Director, Pediatric Radiology and Pediatric
 Neuroradiology, Johns Hopkins Hospital,
 Baltimore, Maryland

C.D. Phillips, MD, FACR

Professor of Radiology, Weill Cornell Medical
 College, Director of Head and Neck Imaging,
 New York-Presbyterian Hospital, New York,
 New York

Pamela W. Schaefer, MD

Clinical Director of MRI and Associate Director of
 Neuroradiology, Massachusetts General Hospital,
 Boston, Massachusetts, Associate Professor,
 Radiology, Harvard Medical School, Cambridge,
 Massachusetts

Charles M. Strother, MD

Professor of Radiology, Emeritus, University of
 Wisconsin, Madison, Wisconsin

Jody Tanabe, MD

Professor of Radiology and Psychiatry,
 Chief of Neuroradiology,
 University of Colorado, Denver, Colorado

STATISTICAL SENIOR EDITOR

Bryan A. Comstock, MS

Senior Biostatistician,
 Department of Biostatistics,
 University of Washington, Seattle, Washington

EDITORIAL BOARD

Ashley H. Aiken, *Atlanta, Georgia*
 A. James Barkovich, *San Francisco, California*
 Walter S. Bartynski, *Charleston, South Carolina*
 Barton F. Branstetter IV, *Pittsburgh, Pennsylvania*
 Jonathan L. Brisman, *Lake Success, New York*
 Julie Bykowski, *San Diego, California*
 Donald W. Chakeres, *Columbus, Ohio*
 Asim F. Choudhri, *Memphis, Tennessee*
 Alessandro Cianfoni, *Lugano, Switzerland*
 Colin Derdeyn, *St. Louis, Missouri*
 Rahul S. Desikan, *San Francisco, California*
 Richard du Mesnil de Rochemont, *Frankfurt, Germany*
 Clifford J. Eskey, *Hanover, New Hampshire*
 Massimo Filippi, *Milan, Italy*
 David Fiorella, *Cleveland, Ohio*
 Allan J. Fox, *Toronto, Ontario, Canada*
 Christine M. Glastonbury, *San Francisco, California*
 John L. Go, *Los Angeles, California*
 Wan-Yuo Guo, *Taipei, Taiwan*
 Rakesh K. Gupta, *Lucknow, India*
 Lotfi Hacin-Bey, *Sacramento, California*
 David B. Hackney, *Boston, Massachusetts*
 Christopher P. Hess, *San Francisco, California*
 Andrei Holodny, *New York, New York*
 Benjamin Huang, *Chapel Hill, North Carolina*
 George J. Hunter, *Boston, Massachusetts*
 Mahesh V. Jayaraman, *Providence, Rhode Island*
 Valerie Jewells, *Chapel Hill, North Carolina*
 Timothy J. Kaufmann, *Rochester, Minnesota*
 Kenneth F. Layton, *Dallas, Texas*
 Ting-Yim Lee, *London, Ontario, Canada*
 Michael M. Lell, *Erlangen, Germany*
 Michael Lev, *Boston, Massachusetts*
 Karl-Olof Lovblad, *Geneva, Switzerland*
 Franklin A. Marden, *Chicago, Illinois*
 M. Gisele Matheus, *Charleston, South Carolina*
 Joseph C. McGowan, *Merion Station, Pennsylvania*
 Kevin R. Moore, *Salt Lake City, Utah*
 Christopher J. Moran, *St. Louis, Missouri*
 Takahisa Mori, *Kamakura City, Japan*
 Suresh Mukherji, *Ann Arbor, Michigan*
 Amanda Murphy, *Toronto, Ontario, Canada*
 Alexander J. Nemeth, *Chicago, Illinois*
 Laurent Pierot, *Reims, France*
 Jay J. Pillai, *Baltimore, Maryland*
 Whitney B. Pope, *Los Angeles, California*
 M. Judith Donovan Post, *Miami, Florida*
 Tina Young Poussaint, *Boston, Massachusetts*
 Joana Ramalho, *Lisbon, Portugal*

Otto Rapalino, *Boston, Massachusetts*
 Àlex Rovira-Cañellas, *Barcelona, Spain*
 Paul M. Ruggieri, *Cleveland, Ohio*
 Zoran Rumboldt, *Rijeka, Croatia*
 Amit M. Saindane, *Atlanta, Georgia*
 Erin Simon Schwartz, *Philadelphia, Pennsylvania*
 Aseem Sharma, *St. Louis, Missouri*
 J. Keith Smith, *Chapel Hill, North Carolina*
 Maria Vittoria Spampinato, *Charleston, South Carolina*
 Gordon K. Sze, *New Haven, Connecticut*
 Krishnamoorthy Thamburaj, *Hershey, Pennsylvania*
 Kent R. Thielen, *Rochester, Minnesota*
 Cheng Hong Toh, *Taipei, Taiwan*
 Thomas A. Tomsick, *Cincinnati, Ohio*
 Aquilla S. Turk, *Charleston, South Carolina*
 Willem Jan van Rooij, *Tilburg, Netherlands*
 Arastoo Vossough, *Philadelphia, Pennsylvania*
 Elysa Widjaja, *Toronto, Ontario, Canada*
 Max Wintermark, *Charlottesville, Virginia*
 Ronald L. Wolf, *Philadelphia, Pennsylvania*
 Kei Yamada, *Kyoto, Japan*

EDITORIAL FELLOW

Hillary R. Kelly, *Boston, Massachusetts*

SPECIAL CONSULTANTS TO THE EDITOR

AJNR Blog Editor

Neil Lall, *Denver, Colorado*

Case of the Month Editor

Nicholas Stence, *Aurora, Colorado*

Case of the Week Editors

Juan Pablo Cruz, *Santiago, Chile*

Sapna Rawal, *Toronto, Ontario, Canada*

Classic Case Editor

Sandy Cheng-Yu Chen, *Taipei, Taiwan*

Clinical Correlation Editor

Christine M. Glastonbury, *San Francisco, California*

Facebook Editor

Peter Yi Shen, *Sacramento, California*

Health Care and Socioeconomics Editor

Pina C. Sanelli, *New York, New York*

Physics Editor

Greg Zaharchuk, *Stanford, California*

Podcast Editor

Yvonne Lui, *New York, New York*

Twitter Editor

Ryan Fitzgerald, *Little Rock, Arkansas*

YOUNG PROFESSIONALS ADVISORY COMMITTEE

Asim K. Bag, *Birmingham, Alabama*

Anna E. Nidecker, *Sacramento, California*

Peter Yi Shen, *Sacramento, California*

Founding Editor

Juan M. Taveras

Editors Emeriti

Mauricio Castillo, Robert I. Grossman,

Michael S. Huckman, Robert M. Quencer

Managing Editor

Karen Halm

Electronic Publications Manager

Jason Gantenberg

Executive Director, ASNR

James B. Gantenberg

Director of Communications, ASNR

Angelo Artemakis

AJNR (Am J Neuroradiol ISSN 0195–6108) is a journal published monthly, owned and published by the American Society of Neuroradiology (ASNR), 800 Enterprise Drive, Suite 205, Oak Brook, IL 60523. Annual dues for the ASNR include \$170.00 for journal subscription. The journal is printed by Cadmus Journal Services, 5457 Twin Knolls Road, Suite 200, Columbia, MD 21045; Periodicals postage paid at Oak Brook, IL and additional mailing offices. Printed in the U.S.A. POSTMASTER: Please send address changes to American Journal of Neuroradiology, P.O. Box 3000, Denville, NJ 07834, U.S.A. Subscription rates: nonmember \$380 (\$450 foreign) print and online, \$305 online only; institutions \$440 (\$510 foreign) print and basic online, \$875 (\$940 foreign) print and extended online, \$365 online only (basic), extended online \$790; single copies are \$35 each (\$40 foreign). Indexed by PubMed/Medline, BIOSIS Previews, Current Contents (Clinical Medicine and Life Sciences), EMBASE, Google Scholar, HighWire Press, Q-Sensei, RefSeek, Science Citation Index, and SCI Expanded. Copyright © American Society of Neuroradiology.



Title: Sunrise in the Promenade des Anglais. The “English Promenade” runs 8 km along the coast of Nice, France. The many blue chairs, as seen in the photo, are used mainly for contemplation of the azure water of the Bay of Angels (la Baie des Anges). In the next few years, the Promenade likely will become a UNESCO World Heritage Site, with the city having submitted its application in 2015.

Maria Isabel Vargas, MD, Geneva University Hospitals, Division of Neuroradiology, Geneva, Switzerland

Carotid Near-Occlusion: A Comprehensive Review, Part 2—Prognosis and Treatment, Pathophysiology, Confusions, and Areas for Improvement

E. Johansson and A.J. Fox



ABSTRACT

SUMMARY: In Part 1 of this review, the definition, terminology, and diagnosis of carotid near-occlusion were presented. Carotid near-occlusions (all types) showed a lower risk of stroke than other severe stenoses. However, emerging evidence suggests that the near-occlusion prognosis with full collapse (higher risk) differs from that without full collapse (lower risk). This systematic review presents what is known about carotid near-occlusion. In this second part, the foci are prognosis and treatment, pathophysiology, the current confusion about near-occlusion, and areas in need of future improvement.

ABBREVIATIONS: ARR = absolute risk reduction; CCA = common carotid artery; ECA = external carotid artery; PCA = posterior cerebral artery; ECST = European Carotid Surgery Trial

Carotid near-occlusion is distal luminal collapse of the internal carotid artery beyond a tight stenosis.¹ Please refer to the first part of this review for the literature review, definition, terminology, and diagnosis of carotid near-occlusion.² Near-occlusion without full collapse seems to be commonly overlooked by some researchers and clinicians. Emerging evidence suggests a difference in prognosis, depending on the degree of collapse.³

The aim of Parts 1 and 2 of this review was to present the definition, terminology, diagnosis, prognosis, treatment, and pathophysiology of carotid near-occlusion; and highlight areas of confusion and those in need of future improvement. In this second part, the foci are prognosis and treatment, pathophysiology, the current confusion about near-occlusion, and areas in need of improvement.

Prognosis and Treatment

The NASCET and European Carotid Surgery Trial (ECST) included 246 cases of near-occlusion without full collapse and 16 cases of near-occlusion with full collapse.¹ The cases with full collapse were few, and none had recurrent stroke, so all cases of

near-occlusion were analyzed together. For near-occlusions randomized to medical treatment or surgery, the 3-year risk of ipsilateral stroke was 15.1% and 10.9%, respectively (absolute risk reduction [ARR], 4.2%; $P = .33$). In cases with 70%–99% stenosis without near-occlusion randomized to medical treatment or surgery, the 3-year risk of ipsilateral stroke was 26.0% and 8.2%, respectively (ARR, 17.8%; $P < .001$).¹ The risk of perioperative stroke and death was similar for near-occlusion (5.4%; 8/148) and 70%–99% stenosis (6.2%; 36/581),⁴ and slightly lower periprocedural risks have been reported since then.⁵ Because 94% of near-occlusions were without full collapse, the findings from NASCET and ECST are mostly applicable to this group of near-occlusions.¹ However, there was no indication that near-occlusion with full collapse differed.¹

In 1983, Ringelstein et al⁶ concluded that “immediate diagnostic clarification and emergency endarterectomy are mandatory” for near-occlusion with full collapse, diagnosed with low-flow findings on continuous-wave Doppler. However, this opinion was not an observed high risk of recurrent stroke but was based on that of 9 patients: Two had crescendo TIA at baseline, 2 had crescendo amaurosis fugax at baseline, and 2 rapidly progressed to occlusion. In fact, no risk of recurrent stroke was reported.⁶ In 1989, O’Leary et al⁷ reported that of 9 patients with near-occlusion (most likely with full collapse) who did not undergo carotid endarterectomy, 2 had an angiographic stroke and 3 had a recurrent ipsilateral stroke within 1 year. Presumably, the angiographic strokes affected further management. Recently, in a small study of 10 cases with near-occlusion with full collapse, 4 (40%) had an ipsilateral ischemic stroke within 1 month of presentation,

From the Department of Pharmacology and Clinical Neuroscience (E.J.), Umeå University, Umeå, Sweden; and Department of Neuroradiology (A.J.F.), Sunnybrook Health Sciences Centre, University of Toronto, Toronto, Ontario, Canada.

This work was funded by the Swedish Stroke Foundation, the Northern Swedish Stroke Fund, the foundation for neuroscientific research at Umeå University Hospital, the County of Västerbotten, and the Medical Faculty of Umeå University.

Please address correspondence to Elias Johansson, MD, Department of Neurology, Institution of Pharmacology and Clinical Neuroscience, Umeå University, 901 82 Umeå, Sweden; e-mail: elias.johansson@umu.se

Indicates open access to non-subscribers at www.ajnr.org

<http://dx.doi.org/10.3174/ajnr.A4429>

whereas none of 15 patients with near-occlusion without full collapse had recurrent stroke ($P = .023$).³

Even if near-occlusion with full collapse might show a high risk of recurrent stroke, the evidence level is poor. Indeed, because only approximately half ($n \approx 8$) of the near-occlusions with full collapse were observed without an operation in NASCET and ECST, and Ringelstein et al⁶ did not report the risk of recurrent stroke, the risk of recurrent stroke without or before carotid endarterectomy has only been reported for approximately 27 patients.^{1,3,7} Of these, 26% (7/27; 95% CI, 8%–44%) had a recurrent stroke within 1 year—ie, roughly equal to the 3-year risk of 70%–99% stenoses (but with a wide margin of error). If anything, 26% might be an underestimation because some were not followed for a full year and some were not followed from the presenting event. This high risk was not observed in NASCET and ECST, possibly because of the long delay between the last event and the study entry (an overall delay of >4 weeks in >50% of cases),¹ whereas a recent study found that all recurrent strokes occurred within 4 weeks.³

Asymptomatic near-occlusion prognosis has not been studied. Some near-occlusion cases without full collapse were likely, but unintentionally, included in the Asymptomatic Carotid Surgery Trial.⁸ In this trial, the diagnosis of carotid stenosis was mostly made with sonography, which cannot distinguish carotid stenosis and near-occlusion without full collapse. Because near-occlusions were not identified, they were not separately analyzed.

Pathophysiology

Nature of Near-Occlusion. A few studies shed light on the nature of near-occlusion:

- Conventional stenoses can progress to near-occlusion.¹
- Intraoperative back pressure is higher in cases of near-occlusion with full collapse (mean, 56 ± 15 mm Hg) than for those with conventional stenosis (mean, 33 ± 13 mm Hg).⁹
- Flow velocities are high in near-occlusion without full collapse and can be high or low in near-occlusion with full collapse.^{3,10–12}
- Collaterals reaching the ipsilateral MCA via the anterior communicating artery, posterior communicating artery, and/or the ophthalmic artery on conventional angiography are present in 64%, 43%, 25%, and <5% in cases with near-occlusion (with and without full collapse), with 85%–99% stenosis, 70%–84% stenosis, and <70% stenosis respectively.¹³ Any flow in intracranial collaterals has been reported in 96% of cases with near-occlusion (with and without full collapse).¹⁴
- Both CBF and SPECT blood flow reactions to acetazolamide are lower among patients with near-occlusion (likely with full collapse alone) than in both patients with 70%–99% stenoses and disease-free controls.¹⁵ Before carotid stenting, 20% (3/15) of those with near-occlusions had >10% blood flow increase with acetazolamide; after carotid stenting, 100% (15/15) had >10% increase.¹⁵ Some studies included measurements of intracerebral hemodynamics, without analyzing them in detail.^{16–19}
- Near-occlusion with full collapse (diagnosed with low-flow velocities on sonography) and high-grade stenosis cause similar infarction patterns with approximately half of patients having

infarctions in watershed areas, though occlusions often have large territorial infarctions.²⁰

- Some near-occlusions looked similar to conventional stenoses histologically, whereas some were actually recanalized thrombotic occlusions.²¹ However, the underlying study included both symptomatic and asymptomatic near-occlusions with a mean interval between the last symptom and surgery of 2.2 months.²¹

A theoretic model presented by Spencer and Reid²² noted that if a stenosis is sufficiently severe, incurring a large pressure drop, the flow from intracranial collaterals will create back pressure. With a sufficiently large pressure difference, the flow through the stenosis will decrease and the artery will collapse. Because stenoses can progress to near-occlusion,¹ cases with near-occlusion have high back pressures⁹ and visible collaterals.^{13,14} When flow is poised to reduce, the flow velocities are still high, as seen in cases without full collapse having high flow velocities.^{3,10} This model seems robust in vivo and may explain varying sonographic findings in near-occlusion.

Usable circle of Willis and/or external carotid collaterals should exist for developing near-occlusion, though some individuals may not have usable collaterals.²³ It may be that without intracranial collaterals, near-occlusion may not develop when stenosis progresses; rather, hemodynamic strokes may occur instead. No report examined this possibility, to our knowledge.

The diagnosis of near-occlusion is more difficult in cases with contralateral disease.^{2,24} However, the impact of contralateral disease on collateral use and prognosis has not been studied.

True hypoplasia is rare, between 0.01% and 0.24%.^{25–27} Most cases of near-occlusion show true artery collapse with a reduced outer diameter, and it inflates after the stenosis is removed.⁹ However, on CTA, the cross-section of the carotid canal can look like “an island in a lake” or a “small brook in a large river bed” in cases of near-occlusion with full collapse (Fig 1). In contrast, true ICA hypoplasia is seen as a thin artery with a thin bony canal on CTA (Fig 1), without prominent ICA bulb stenosis.

Mechanism behind Recurrent Strokes. Near-occlusion with full collapse might cause a high risk of recurrent stroke.^{1,3,7} If confirmed, by what mechanism can near-occlusion with full collapse cause the observed higher stroke risk? It has been reported that untreated near-occlusions often progress to occlusion.⁷ However, a recent article found that none of 4 fully collapsed near-occlusions progressed to occlusion when examined after presumed embolic recurrent stroke.³ Other pathophysiologic mechanisms of near-occlusion with and without full collapse have not been studied. Both hemodynamic and embolic mechanisms are reasonable for the possible high risk of stroke among patients with symptomatic near-occlusion with full collapse.

As near-occlusion progresses from without-to-full collapse, the ipsilateral hemisphere receives less from its carotid artery and more from collaterals. Patients with near-occlusion with full collapse show compromised cerebral hemodynamics¹⁵; it is reasonable to suspect a hemodynamic mechanism for recurrent strokes. The presence or absence of systemic hypotension at the time of recurrence was not analyzed in previous studies.^{1,3,7}

Severe flow reduction of near-occlusion with full collapse stimulates blood stagnation with presumed increased risk of

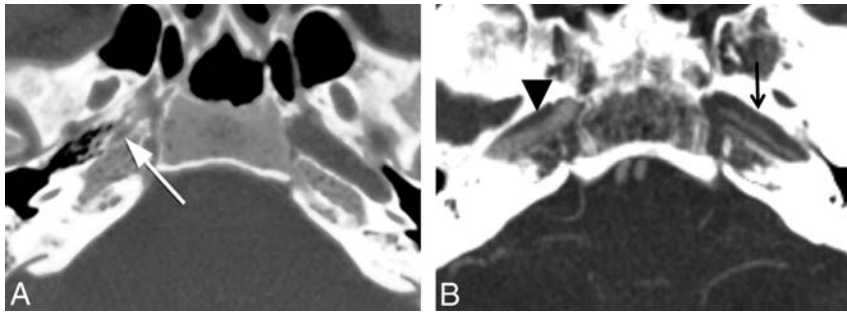


FIG 1. Comparison of bony carotid canals with ICA hypoplasia and near-occlusion. A, A case of right ICA hypoplasia. A narrow bony carotid canal (*white arrow*)—smaller than that on the contralateral side. Reprinted with permission from Ibrahim et al.⁵⁸ B, A case of left near-occlusion with full collapse. The narrow left ICA (*black arrow*) is in a normal-sized bone channel—“a small brook in a large river bed.” Bone channels are similar on the left (*black arrow*) and right (*black arrowhead*).

thrombus formation, leading to embolic risk from the ICA bifurcation up to the first good intracranial collateral. Comparably, ischemic events from embolic mechanisms were seen for 3% of cases undergoing balloon occlusion for unclippable aneurysms.²⁸ Such embolic risk seems greatest before thrombus organization, likely a short-lived phenomenon. Most stroke recurrences occurred early (within 1 month),^{1,3,7} indicating a short-lived stroke-risk increase followed by stability, supporting the embolic mechanism. Even though reduced flow may lower embolic transportation in near-occlusion, full-collapse cases might still be at increased risk of embolic strokes overall from increased thrombus formation. Indeed, some near-occlusions are likely recanalized thrombotic occlusions.²¹

Confusion about Near-Occlusion

In Part 1 of this review, we presented the terminology, definition, and diagnosis of near-occlusion.² Because some of the confusion in terminology definition and diagnosis is interwoven with prognosis, treatment, and pathophysiology, all issues are presented here.

Terminology and Definition. The multitude of terms for near-occlusion and their interchangeable use may contribute to confusion. The expanded near-occlusion definition, including subtle collapse in NASCET,¹⁴ was not recognized by all. “Near-occlusion” was used interchangeably with the “string sign” (or similar variations), even though the “string sign” (full collapse) is a subset of near-occlusion.

Near-occlusion without full collapse continues to be ignored, unknown by many. Existing guidelines do not clearly acknowledge this diagnosis.^{29,30} Educational articles,^{31,32} reviews,³³ editorials,^{34,35} and book chapters³⁶ do not acknowledge this diagnosis (with few exceptions).^{37,38} Without recognition, incorrect calculations for NASCET percentage stenosis are performed for near-occlusion without full collapse. In addition, near-occlusion without full collapse is the natural intermediate step between severe stenosis with normal-caliber ICA beyond it and near-occlusion with full collapse. Yet near-occlusion without full collapse is well documented—but ignored. Many authors^{10,16,34,39-43} have cited outcomes of near-occlusions with full collapse from the 1997 NASCET article¹⁴ as the outcome of all near-occlusions, without mention or explanation of those

without full collapse. In contrast, fewer correctly made this distinction when citing that article.^{17,18}

In some articles, terms for near-occlusion (“pseudo-occlusion” and “string sign”) were used differently from those for severe atherosclerotic stenosis, and clearly for another entity.⁴⁴⁻⁵³ However, in other articles, terms for near-occlusion have been used inappropriately by also including carotid stenoses without distal collapse in the term but without clarification that something else was intended; rather the findings were directly compared with those in near-occlusion studies,^{42,54} or the article was

educational without references.³¹ Specifically, with high-flow velocities on sonography, many high-grade conventional stenoses can be called “near-total occlusion.”⁴² In 2 articles, threadlike stenosis without distal collapse was called the “string sign.”^{54,31}

Diagnosis. Near-occlusion should be listed as “near-occlusion,” not as a “percentage stenosis.” Suggestions that the contralateral ICA be used as a denominator when the ipsilateral ICA is collapsed, creating tight percentage stenosis,⁵⁵ seem an extraordinary devotion to percentage stenosis without recognizing the reality of near-occlusion. The prognosis of part-near-occlusion seems to differ from that in severe stenosis¹; using the contralateral ICA as a denominator for percentage seems inappropriate. Some argued that the NASCET method is fallacious because the distal artery can collapse,⁵⁶ though this argument ignores the fact that NASCET called for recognition of near-occlusions and requested that such stenoses not be graded with percentages.³⁷ Those who do otherwise are not performing the NASCET grading as recommended. It is important to exclude distal artery collapse before grading a carotid stenosis; subtle collapses can be overlooked and not identified as near-occlusion if not actively sought consistently. If you do not seek it, you will not find it.

Prognosis and Treatment. Smaller studies,^{6,7} before NASCET and ECST, suggested that near-occlusions with full collapse have a high risk of stroke; this suggestion was negated by NASCET and ECST.¹ However, NASCET and ECST mostly included near-occlusion without full collapse. Recently suggested are relevant differences of short-term prognosis between symptomatic near-occlusion with and without full collapse,³ differing from previous knowledge,¹ with symptomatic near-occlusion without full collapse associated with a lower risk of recurrent stroke. However, symptomatic near-occlusion with full collapse is rarely studied, with conflicting results; it could have a high risk of recurrent stroke,^{1,3,6,7} which was not picked up by NASCET and ECST. After all, those studies were both randomized trials requiring patients to be acceptable candidates for both medical and surgical treatment arms, the equipoise requirement for a randomized treatment trial. In the late 1980s and early 1990s, few cases with fully collapsed ICA beyond a bulb stenosis would have been randomized.

Need for Future Improvement

Near-occlusion without full collapse needs recognition for future studies, guidelines, and clinical practice. Many seem unaware of this diagnostic category. As a result, patients can presumably be misdiagnosed as having conventional carotid stenosis, even non-significant stenosis, severely affecting management. Current guidelines simply state that near-occlusion has a low risk of stroke.^{29,30} Awareness of near-occlusion with only full collapse will not pick up partial near-occlusion. Guidelines should be revised to highlight the 2 types of near-occlusion, that near-occlusion without full collapse has been well-studied but misunderstood by many, and that only this type may have a lower risk of stroke. On the other hand, near-occlusion with full collapse is widely known, but its real stroke risk is less known.

Further studies of symptomatic near-occlusion prognosis with full collapse are warranted. Some small studies suggest a high risk of recurrent stroke,^{3,7} despite being thought of as low.¹ If this high risk is further documented, a randomized trial is warranted.

Several Other Areas for Improvement.

- More high-quality studies comparing sonography, CTA, and MR imaging with conventional angiography are warranted.
- Sonography, common as the first and often only carotid imaging, cannot distinguish near-occlusion without full collapse from conventional stenosis with peak systolic velocity analyzed. Other velocity or diameter measurements or both need analysis.
- A small sonographic study reported how often different pathologic flow profiles indicate distal occlusion or near-occlusion in situ.⁵⁷ This should be reproduced.
- The value of contrast-enhanced sonography to better distinguish near-occlusion from occlusion should be evaluated.
- The prognosis of asymptomatic near-occlusion is unknown.
- It is not well worked out if the mechanism for recurrent strokes in patients with near-occlusion with and without full collapse is predominantly hemodynamic or predominantly embolic.

Disclosures: Elias Johansson—RELATED: Grant: Several smaller stroke funds contributed, with funding listed in the footnotes*; none had any influence on the content. Conforms to “no disclosures.” Allan J. Fox—UNRELATED: Expert Testimony: medical malpractice suits, none relevant to the topic of this work. *Money paid to the institution.

REFERENCES

1. Fox AJ, Eliasziw M, Rothwell PM, et al. **Identification, prognosis, and management of patients with carotid artery near occlusion.** *AJNR Am J Neuroradiol* 2005;26:2086–94 Medline
2. Johansson E, Fox AJ. **Carotid near-occlusion: a comprehensive review, part 1—definition, terminology and diagnosis carotid near-occlusion.** *AJNR Am J Neuroradiol* 2016;37:2–10 CrossRef Medline
3. Johansson E, Öhman K, Wester P. **Symptomatic carotid near-occlusion with full collapse might cause a very high risk of stroke.** *J Intern Med* 2015;277:615–23 CrossRef Medline
4. Rothwell PM, Eliasziw M, Gutnikov SA, et al; Carotid Endarterectomy Trialists' Collaboration. **Analysis of pooled data from the randomised controlled trials of endarterectomy for symptomatic carotid stenosis.** *Lancet* 2003;361:107–16 CrossRef Medline
5. Koutsoumpelis A, Kouvelos G, Peroulis M, et al. **Surgical and endovascular intervention on internal carotid artery near occlusion.** *Int Angiol* 2015;34:172–81 Medline
6. Ringelstein EB, Berg-Dammer E, Zeumer H. **The so-called atheromatous pseudoocclusion of internal carotid artery: a diagnostic and therapeutical challenge.** *Neuroradiology* 1983;25:147–55 CrossRef Medline
7. O'Leary DH, Mattle H, Potter JE. **Atheromatous pseudo-occlusion of the internal carotid artery.** *Stroke* 1989;20:1168–73 CrossRef Medline
8. Halliday A, Mansfield A, Marro J, et al; MRC Asymptomatic Carotid Surgery Trial (ACST) Collaborative Group. **Prevention of disabling and fatal strokes by successful carotid endarterectomy in patients without recent neurological symptoms: randomised controlled trial.** *Lancet* 2004;363:1491–502 CrossRef Medline
9. Archie JP. **Carotid endarterectomy when the distal internal carotid artery is small or poorly visualized.** *J Vasc Surg* 1994;19:23–30; discussion 30–31 CrossRef Medline
10. El-Saden SM, Grant EG, Hathout GM, et al. **Imaging of the internal carotid artery: the dilemma of total versus near total occlusion.** *Radiology* 2001;221:301–08 CrossRef Medline
11. Mansour MA, Mattos MA, Hood DB, et al. **Detection of total occlusion, string sign, and preocclusive stenosis of the internal carotid artery by color-flow duplex scanning.** *Am J Surg* 1995;170:154–58 CrossRef Medline
12. Hetzel A, Eckenweber B, Trummer B, et al. **Colour-coded duplex sonography of preocclusive carotid stenoses.** *Eur J Ultrasound* 1998; 8:183–91 CrossRef Medline
13. Henderson R, Eliasziw M, Fox AJ, et al; North American Symptomatic Carotid Endarterectomy Trial (NASCET) Group. **Angiographically defined collateral circulation and risk of stroke in patients with severe carotid artery stenosis.** *Stroke* 2000;31:128–32 CrossRef Medline
14. Morgenstern LB, Fox AJ, Sharpe BL, et al; North American Symptomatic Carotid Endarterectomy Trial (NASCET) Group. **The risks and benefits of carotid endarterectomy in patients with near occlusion of the carotid artery.** *Neurology* 1997;48:911–15 CrossRef Medline
15. Oka F, Ishihara H, Kato S, et al. **Cerebral hemodynamic benefits after carotid artery stenting in patients with near occlusion.** *J Vasc Surg* 2013;58:1512–17 CrossRef Medline
16. Terada T, Tsuru M, Matsumoto H, et al. **Endovascular treatment for pseudo-occlusion of the internal carotid artery.** *Neurosurgery* 2006;59:301–09; discussion 301–09 CrossRef Medline
17. González A, Gil-Peralta A, Mayol A, et al. **Internal carotid artery stenting in patients with near occlusion: 30-day and long-term outcome.** *AJNR Am J Neuroradiol* 2011;32:252–58 CrossRef Medline
18. Choi BS, Park JW, Shin JE, et al. **Outcome evaluation of carotid stenting in high-risk patients with symptomatic carotid near occlusion.** *Interv Neuroradiol* 2010;16:309–16 Medline
19. Greiner C, Wassmann H, Palkovic S, et al. **Revascularization procedures in internal carotid artery pseudo-occlusion.** *Acta Neurochir (Wien)* 2004;146:237–43; discussion 243 CrossRef Medline
20. Szabo K, Kern R, Gass A, et al. **Acute stroke patterns in patients with internal carotid artery disease: a diffusion-weighted magnetic resonance imaging study.** *Stroke* 2001;32:1323–29 CrossRef Medline
21. Hirata Y, Sakata N, Inoue T, et al. **Histopathological features with angiographic correlates of internal carotid artery pseudo-occlusion: impact of plaque compositions—clinical article.** *J Neurosurg* 2011;115:350–58 CrossRef Medline
22. Spencer MP, Reid JM. **Quantitation of carotid stenosis with continuous-wave (C-W) Doppler ultrasound.** *Stroke* 1979;10:326–30 CrossRef Medline
23. Hoksbergen AW, Legemate DA, Ubbink DT, et al. **Collateral variations in circle of Willis in atherosclerotic population assessed by means of transcranial color-coded duplex ultrasonography.** *Stroke* 2000;31:1656–60 CrossRef Medline
24. Bartlett ES, Walters TD, Symons SP, et al. **Diagnosing carotid stenosis near-occlusion by using CT angiography.** *AJNR Am J Neuroradiol* 2006;27:632–37 Medline
25. Chen CJ, Lee TH, Hsu HL, et al. **Multi-slice CT angiography in diagnosing total versus near occlusions of the internal carotid artery:**

- comparison with catheter angiography. *Stroke* 2004;35:83–85 Medline
26. Okahara M, Kiyosue H, Mori H, et al. **Anatomic variations of the cerebral arteries and their embryology: a pictorial review.** *Eur Radiol* 2002;12:2548–61 CrossRef Medline
 27. Ito S, Miyazaki H, Iino N, et al. **Unilateral agenesis and hypoplasia of the internal carotid artery: a report of three cases.** *Neuroradiology* 2005;47:311–15 CrossRef Medline
 28. Fox AJ, Viñuela F, Pelz DM, et al. **Use of detachable balloons for proximal artery occlusion in the treatment of unclippable cerebral aneurysms.** *J Neurosurg* 1987;66:40–46 CrossRef Medline
 29. European Stroke Organisation (ESO) Executive Committee, ESO Writing Committee. **Guidelines for management of ischaemic stroke and transient ischaemic attack 2008.** *Cerebrovasc Dis* 2008;25:457–507 CrossRef Medline
 30. Furie KL, Kasner SE, Adams RJ, et al; American Heart Association Stroke Council, Council on Cardiovascular Nursing, Council on Clinical Cardiology, and Interdisciplinary Council on Quality of Care and Outcomes Research. **Guidelines for the prevention of stroke in patients with stroke or transient ischemic attack: a guideline for healthcare professionals from the American Heart Association/American Stroke Association.** *Stroke* 2011;42:227–76 CrossRef Medline
 31. Gross K, Wang H. **The string sign.** *J Vasc Nurs* 2000;18:72 CrossRef Medline
 32. Pappas JN. **The angiographic string sign.** *Radiology* 2002;222:237–38 CrossRef Medline
 33. Giannoukas AD, Labropoulos N, Smith FC, et al. **Management of the near total internal carotid artery occlusion.** *Eur J Vasc Endovasc Surg* 2005;29:250–55 CrossRef Medline
 34. Yadav JS. **Functional occlusions of the carotid artery (string signs): to treat or not to treat?** *JACC Cardiovasc Interv* 2010;3:305–06 CrossRef Medline
 35. Bazan HA. **Carotid string sign is not necessarily a functional occlusion: admit, anticoagulate, and revascularize urgently.** *Cather Cardiovasc Interv* 2010;75:1110 CrossRef Medline
 36. Biller J, Love BB, Schneck MJ. **Vascular diseases of the nervous system: ischemic cerebrovascular disease.** In: Daroff RB, Fenichel GM, Jankovic J, et al, eds. *Bradley's Neurology in Clinical Practice*. 6th ed. Philadelphia: Elsevier; 2012:1046
 37. Fox AJ. **How to measure carotid stenosis.** *Radiology* 1993;186:316–18 CrossRef Medline
 38. Fox AJ, Symons SP, Aviv RI, et al. **Falsely claiming use of NASCET percentage stenosis method.** *Radiology* 2009;253:574–75; author reply 575 CrossRef Medline
 39. Son S, Choi DS, Kim SK, et al. **Carotid artery stenting in patients with near occlusion: a single-center experience and comparison with recent studies.** *Clin Neurol Neurosurg* 2013;115:1976–81 CrossRef Medline
 40. Sakamoto S, Kiura Y, Kajihara Y, et al. **Carotid artery stenting using the proximal or dual protection method for near occlusion of the cervical internal carotid artery.** *Neurosurg Rev* 2013;36:551–57; discussion 557–58 CrossRef Medline
 41. Nikas DN, Ghany MA, Stabile E, et al. **Carotid artery stenting with proximal cerebral protection for patients with angiographic appearance of string sign.** *JACC Cardiovasc Interv* 2010;3:298–304 CrossRef Medline
 42. Radak DJ, Tanaskovic S, Ilijevski NS, et al. **Eversion carotid endarterectomy versus best medical treatment in symptomatic patients with near total internal carotid occlusion: a prospective nonrandomized trial.** *Ann Vasc Surg* 2010;24:185–89 CrossRef Medline
 43. Ferguson GG. **Comment on "Revascularization procedures in ICA pseudo-occlusion."** *Acta Neurochir (Wien)* 2004;146:243
 44. Kniemeyer HW, Aulich A, Schlachetzki F, et al. **Pseudo- and segmental occlusion of the internal carotid artery: a new classification, surgical treatment and results.** *Eur J Vasc Endovasc Surg* 1996;12:310–20 CrossRef Medline
 45. Ascher E, Markevich N, Hingorani A, et al. **Pseudo-occlusions of the internal carotid artery: a rationale for treatment on the basis of a modified duplex scan protocol.** *J Vasc Surg* 2002;35:340–45 CrossRef Medline
 46. Macpherson P. **Pseudo-occlusion of the internal carotid artery.** *Br J Radiol* 1978;51:5–10 CrossRef Medline
 47. Regina G, Testini M, Fullone M, et al. **Pseudo-occlusion of the internal carotid artery: report of 15 cases and review of the literature.** *Int Angiol* 1997;16:147–50 Medline
 48. Sitzer M, Fürst G, Fischer H, et al. **Between-method correlation in quantifying internal carotid stenosis.** *Stroke* 1993;24:1513–18 CrossRef Medline
 49. Ammar AD, Turrentine MW, Farha SJ. **The importance of arteriographic interpretation in occlusion or pseudo-occlusion of the carotid artery.** *Surg Gyn Obst* 1988;167:119–23 Medline
 50. Mehigan JT, Olcott C 4th. **The carotid "string" sign: differential diagnosis and management.** *Am J Surg* 1980;140:137–43 CrossRef Medline
 51. Marquering HA, Nederkoorn PJ, Beenen LF, et al. **Carotid pseudo-occlusion on CTA in patients with acute ischemic stroke: a concerning observation.** *Clin Neurol Neurosurg* 2013;115:1591–94 CrossRef Medline
 52. Ojemann RG, Fisher CM, Rich JC. **Spontaneous dissecting aneurysm of the internal carotid artery.** *Stroke* 1972;3:434–40 CrossRef Medline
 53. Ehrenfeld WK, Wylie EJ. **Spontaneous dissection of the internal carotid artery.** *Arch Surg* 1976;111:1294–1301 CrossRef Medline
 54. Berman SS, Devine JJ, Erdoes LS, et al. **Distinguishing carotid artery pseudo-occlusion with color-flow Doppler.** *Stroke* 1995;26:434–38 CrossRef Medline
 55. Dix JE, McNulty BJ, Kallmes DF. **Frequency and significance of a small distal ICA in carotid artery stenosis.** *AJNR Am J Neuroradiol* 1998;19:1215–18 Medline
 56. Ruiz-Salmerón RJ, Gamero MA, Carrascosa C, et al. **Carotid artery stenting: clinical and procedural implications for near-occlusion stenosis.** *Neurologia* 2013;28:535–42 CrossRef Medline
 57. Fujimoto S, Toyoda K, Kishikawa K, et al. **Accuracy of conventional plus transoral carotid ultrasonography in distinguishing pseudo-occlusion from total occlusion of the internal carotid artery.** *Cerebrovasc Dis* 2006;22:170–76 CrossRef Medline
 58. Ibrahim M, Branson HM, Buncic JR, et al. **A case of Horner syndrome with intermittent mydriasis in a patient with hypoplasia of the internal carotid artery.** *AJNR Am J Neuroradiol* 2006;27:1318–20 Medline

MR Angiographic–Guided Percutaneous Sclerotherapy for Venous Vascular Malformations: A Radiation Dose-Reduction Strategy

S.G. Imbesi, D.A. Green, A. Cho, and R.S. Pakbaz



ABSTRACT

SUMMARY: We present a new technique using MRA instead of the usual DSA to provide guidance in the treatment of venous vascular malformations. When one performs this embolization procedure, appropriate needle positioning within the malformation must be confirmed before injection of the sclerosing agent to prevent untoward complications. Time-resolved imaging of contrast kinetics–MRA can accurately depict the angioarchitecture of the lesion, which substantially reduces the total radiation dose in these patients who are commonly in the pediatric age group and usually require numerous treatment episodes.

Venous malformations are the most common vascular malformation and can be found throughout the body but tend to be located in the head and neck region or the extremities.^{1–3} They are low-flow lesions of an abnormal venous network of dilated vascular spaces consisting of thin-walled sponge-like channels of varying size with adventitial fibrosis, sparse clumped smooth-muscle cells, internal regions of thrombosis, and occasional phleboliths. On examination, venous malformations are compressible, nonpulsatile masses, usually exhibiting a bluish tint of the overlying skin. Provocative maneuvers such as Valsalva can show enlargement of the lesion. They present in childhood; mostly enlarge with time, especially during puberty and pregnancy due to hormonal effects; and do not regress. Thus, these lesions may require treatment. Accurate diagnosis is required to confirm the nature of the vascular malformation so that appropriate treatment can be planned.

Mulliken and Glowacki⁴ differentiated vascular anomalies as either vascular neoplasms or vascular malformations. The vascular neoplasms (or true hemangiomas) show endothelial hyperplasia, while the vascular malformations, being an error of embryologic development, show normal endothelial turnover. This scheme was further subclassified by the International Society for the Study of Vascular Anomalies, which divided the vascular malformations between simple (capillary, venous, or lymphatic malformations) or combined (arteriovenous malformation, arterio-

venous fistula, and capillary and/or venous and/or lymphatic malformation) forms.⁵ Finally, vascular malformations can also be categorized as either low-flow (capillary, venous, lymphatic, or any combination of these) or high-flow (arteriovenous malformation, arteriovenous fistula). On imaging, Doppler sonography can be used to show the low-flow profile of the venous malformation. On CT, a heterogeneous lesion is usually seen with fat and calcified phleboliths easily identifiable. The lesion enhances slowly and peripherally after contrast administration. MR imaging is best to delineate the lesion margins and detect invasion into surrounding structures, with T2-weighted STIR imaging showing the mostly bright-blood-filled channels.

Patient symptoms are related to lesion size and location. While venous malformations are noted in the skin and adjacent subcutaneous tissues, they usually also involve the underlying muscle, bone, and other tissues. Thrombosis, bleeding, and swelling can lead to pain. Lesions of the head and neck can present aesthetic issues for the patient but can also distort speech and even obstruct the upper airway. In particular in these instances, treatment of the venous malformation is necessary. This is performed via direct needle puncture of the lesion. Rapid blood return from the needle hub assumes correct needle positioning within the lesion; however, a phlebogram must be obtained (presently via digital subtraction angiography) to confirm the exact needle localization (Fig 1). A sclerosing agent such as absolute ethanol or sodium tetradecyl sulfate is then injected. The confirmation of correct needle positioning is mandatory because extravasation of the sclerosant can lead to direct tissue necrosis or nerve injury. Observation of large draining veins may also preclude treatment because the peripheral extent of the sclerosant into the systemic circulation may lead to hemolysis or cardiac/pulmonary/renal complications. We propose MR angiography–time-resolved imaging of

Received March 17, 2015; accepted after revision June 24.

From the Department of Radiology (S.G.I., D.A.G., A.C.), University of California, San Diego Health System, San Diego, California; and Department of Radiology (R.S.P.), VA San Diego Healthcare System, San Diego, California.

Please address correspondence to Steven G. Imbesi, MD, Department of Radiology, University of California, San Diego Health System, 200 West Arbor Dr, Mail Code #8756, San Diego, CA 92103; e-mail: simbesi@ucsd.edu

<http://dx.doi.org/10.3174/ajnr.A4518>

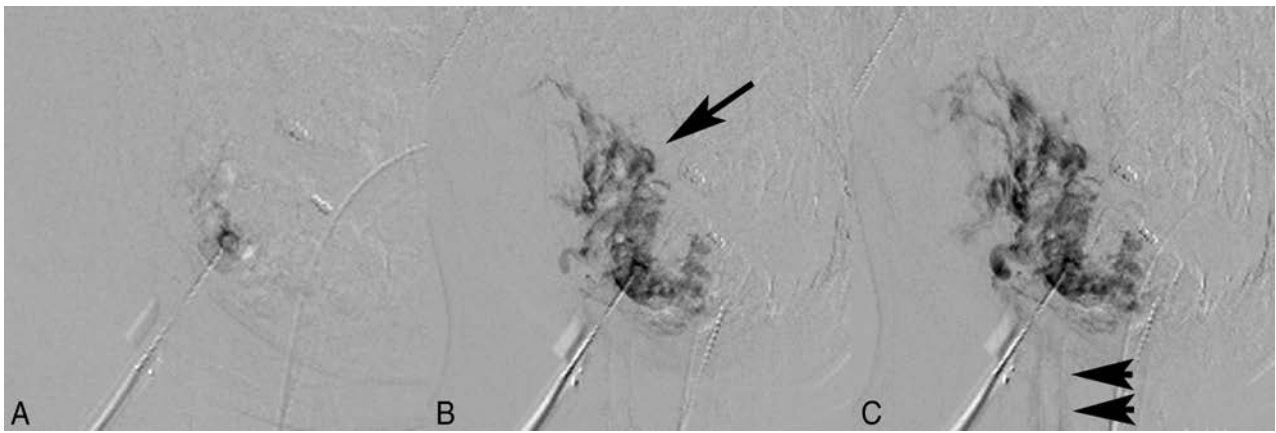


FIG 1. Early (A), mid (B), and late (C) phase direct needle puncture phlebography of a left facial venous malformation by using a traditional digital subtraction angiography technique shows appropriate needle localization for subsequent embolization. There is satisfactory sequential opacification of the venous channels of the lesion (*arrow*) and only faint flow into small draining veins (*arrowheads*), with no evidence of contrast extravasation or demonstration of large draining veins.

contrast kinetics to obtain appropriate needle positioning and depict the angioarchitecture of the venous malformation to decrease the radiation dose when treating these lesions.

Case Series

In 5 patients, including 4 with venous malformations of the head/neck and 1 with a peripheral limb venous malformation of the knee, 14 sclerotherapy sessions have been performed. A standard 1.5T superconducting magnet was used for all the procedures. The study was approved by the local institutional review board. The patients were placed under general anesthesia and prepped and draped in the usual sterile manner in the MR imaging suite, and sterile covers were placed over the MR imaging coils that were eventually positioned over the ROI. Initial multiplanar, multisequence MR images were obtained to assess the lesion. Twenty-two-gauge titanium needles were then inserted through the skin for direct puncture access to the venous malformation. Along the tubing adjacent to the needle, a 3-way stopcock was also placed to allow attachment of a second shorter tubing that is connected to a syringe prefilled with contrast material. Gadobenate dimeglumine (MultiHance; Bracco Diagnostics, Princeton, New Jersey) in a 1:100 dilution with normal saline solution was used for the contrast administration. Approximately 1.0–1.5 mL of contrast material was preloaded into the needle and the most distal portion of the tubing beyond the stopcock. The stopcock was then opened to the long connecting tubing so that injection could be performed by the operator outside the bore of the magnet.

Once the patients were positioned within the magnet bore, continuous MRA–time-resolved imaging of contrast kinetics was obtained before and during the injection of the 1.0–1.5 mL of contrast medium followed by 10 mL of normal saline solution flush. The parameters of the image acquisition were as follows: sagittal plane slab orientation with 10 sections by using TR, 4.028 milliseconds; TE, 1.672 milliseconds; NEX, 0.5; section thickness, 2.6 mm; FOV, 220 × 220 mm; matrix, 256 × 192, echo-train, 1; flip angle, 30°; bandwidth, 488.3 hertz. The precontrast images (13-second acquisition) were used as a mask and were digitally subtracted from the postcontrast images (51-second acquisition). The sequential images were then viewed as a cine loop to demonstrate intralésional vascular flow with time. The chosen param-

eters result in a relatively fast 1.8 seconds per frame for the cine loop, which also achieves reasonable spatial resolution that enables appropriate evaluation of the venous vascular flow. Finally, summation maximum-intensity-projection images can also be viewed and 3D rotated to observe the entirety of the opacification of the vascular lesion and venous runoff altogether in a single slab. If a satisfactory needle position was achieved, the sclerosant (absolute ethanol, 0.1 mL/Kg body weight) was then injected. Following a dwell time of 10 minutes, the contrast injection was repeated and the result of embolization was observed (Figs 2–4).

Following completion of the sclerotherapy session, the patient was closely observed with airway management (in particular for the head/neck embolizations) and placed on methylprednisolone corticosteroids for reduction of potential subsequent soft-tissue swelling and given hydrocodone and acetaminophen for pain control. Excellent response to therapy was achieved in every case, evidenced by diminished flow within the lesions and pruning of the lesion vasculature. No procedural complications were encountered, and all patients had an uneventful postprocedural recovery.

DISCUSSION

When treatment of venous vascular malformations is required due to lesion bleeding, pain, mass effect, or esthetic problems, an angiogram must be obtained to confirm appropriate needle positioning within the lesion before injection of the sclerosing agent to prevent complications and untoward effects of the procedure.^{6,7} This information is traditionally obtained by using digital subtraction angiography. While the radiation dose is relatively low for each individual treatment episode, in many instances, numerous treatment sessions are usually required due to the intrinsic multiloculated, trans-spatial nature of the lesion. In addition, only a small amount of sclerosant (in particular absolute ethanol) can be delivered to the tissues in a given treatment session to limit systemic toxicity. Thus, the total accumulated radiation dose to achieve complete lesion obliteration can become rather substantial. Additionally, because these lesions commonly occur in the head and neck region, adjacent very radiosensitive structures such as the thyroid gland and ocular lenses are frequently in the field of

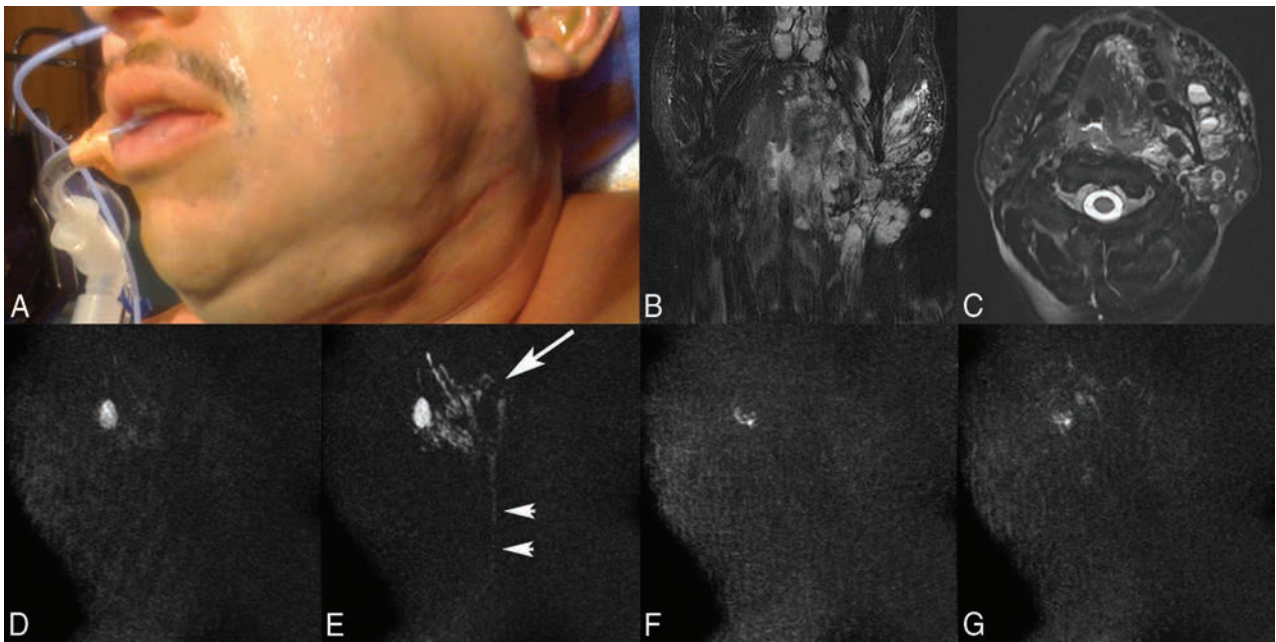


FIG 2. A 36-year-old man with a left facial venous malformation who undergone 14 treatments during the past 3 years, the last 2 with MR imaging guidance. Overview of the direct-injection MR angiography technique for embolization of the lesion. A, Patient photograph before MR sclerotherapy shows left facial swelling from a persistent left facial venous malformation. Coronal (B) and axial (C) T2-weighted fat-saturated MR images demonstrate the typical imaging characteristics of a venous vascular malformation, including a mixed signal intensity but mostly bright trans-spatial lesion extending both superficial and deep to the left mandible composed of multiloculated blood-filled channels with fluid-fluid levels producing local mass effect. Pretreatment MR angiograms, early (D) and late (E) phase, show appropriate needle positioning within the loculated blood-filled channels of the venous malformation (arrow) with slow venous runoff into a small draining vein (arrowheads). Posttreatment MR angiograms, early (F) and late (G) phase, demonstrate pruning of the vascular channels of the venous malformation with markedly diminished flow into the draining vein, compatible with satisfactory embolization of the lesion.

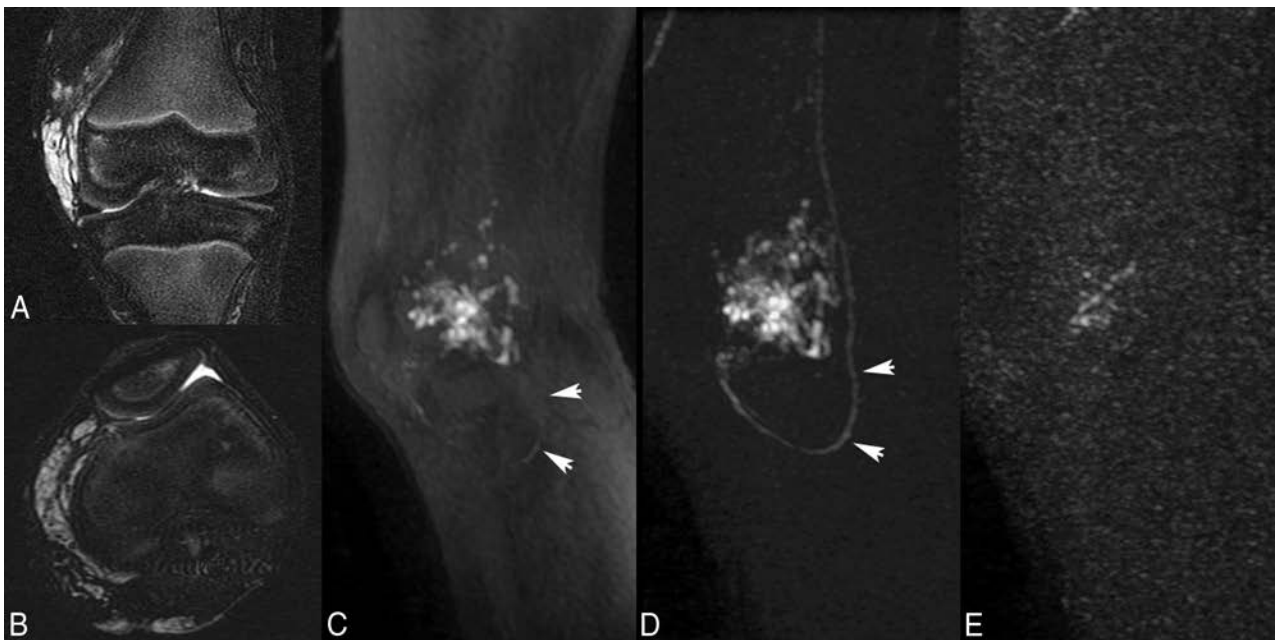


FIG 3. A 6-year-old boy with a peripheral venous malformation of the left knee. Note depiction of the mask subtraction technique that results in more complete visualization of the vascular structures on MR angiography. Coronal (A) and axial (B) T2-weighted fat-saturated MR images demonstrate a multiloculated increased T2-signal venous vascular malformation in the left knee, particularly surrounding the medial and posterior portions of the distal femur. Pretreatment MR angiogram, without (C) and with (D) digital mask subtraction, shows opacification of the venous malformation but limited visualization of the draining vein (arrowheads) without mask subtraction; however, there is not only improved visualization of the venous malformation but also excellent visualization of the draining vein (arrowheads) achieved following mask subtraction of the images. E, Posttreatment MR angiogram again shows pruning of the vascular channels of the venous malformation with no significant flow into the draining vein, compatible with satisfactory embolization of the lesion.

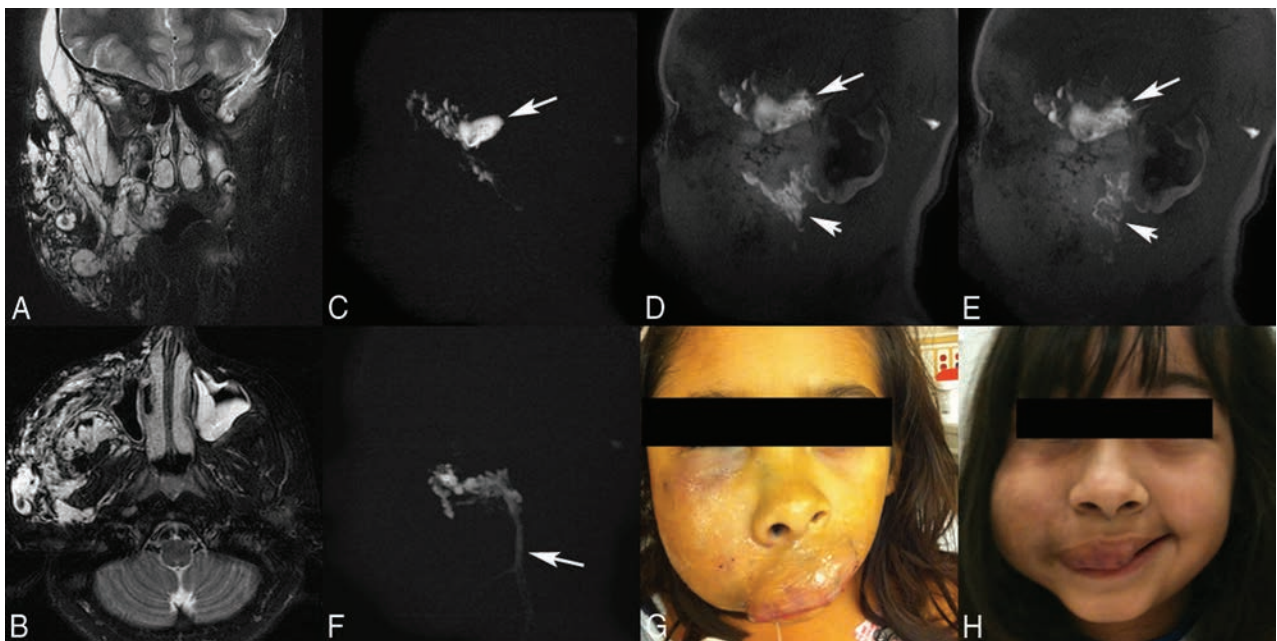


FIG 4. A 10-year-old girl with a very large venous malformation of the right face, who has had >20 previous treatment episodes with traditional digital subtraction angiography guidance, now being treated with MR imaging guidance. These images demonstrate the necessity of angiography to assure proper needle positioning. Coronal (A) and axial (B) T2-weighted fat-saturated MR images show the very large venous vascular malformation extending essentially throughout all superficial and deep spaces of the right face, producing significant local mass effect. C, Pretreatment MR angiogram, initial needle placement, demonstrates opacification of the venous malformation but also a focus of stagnation of contrast material that remained on the late-phase images, indicating extravasation (arrow). Thus, this is not a safe location to treat, and sclerotherapy was not performed. Note that normal venous backflow from the needle hub was initially detected, but adequate needle placement can only be assured following angiography. Early (D) and late (E) phase pretreatment MR angiograms, second needle placement, again demonstrate opacification of the venous malformation but now also show runoff of the contrast material on the late-phase image, indicating safe needle placement for embolization (arrowheads). Note the continued presence of the previously extravasated contrast material from the first injection on this nonmask subtracted image (arrows). F, Early-phase pretreatment MR angiogram, third needle placement, depicts needle localization within the venous malformation; however, there is very rapid filling of an enlarged draining vein (arrow). Thus, this is not a safe location to treat, and sclerotherapy was not performed. Again, adequate needle placement can only be assured following angiographic visualization of the lesion. Patient photographs before (G) and following (H) MR sclerotherapy show significant improvement in right facial swelling; however, a persistent right facial venous malformation is still present, requiring additional multiple future treatment sessions.

treatment and thus receive overall large doses of radiation. Finally, these lesions usually occur in the pediatric population, warranting further concern regarding the total radiation dose given to the patient, because the longer subsequent life span of these young patients markedly increases the potential for future development of neoplastic disease.

For example, regarding radiation-induced thyroid cancer, the following can be surmised: The excess relative risk of thyroid cancer per sievert of x-ray radiation is 10× that of baseline for patients 0–9 years of age, 3× baseline for patients 10–19 years, and 0.3× baseline for patients 20–39 years.^{8–11} Thus, while the excess relative risk is not that significant for adults, it becomes very significant for the pediatric population because the pediatric risk is 10–30× that of the adult. One minute of fluoroscopy yields approximately 3-mSv x-ray radiation effective dose to the thyroid gland, which is mostly due to internal scatter and therefore cannot be further reduced, even with dose-reduction techniques, including tight collimation or thyroid shielding (without thyroid shielding, the dose can be as high as 10 mSv/min). Of note, 3 mSv is equivalent to 1 year of background radiation or approximately 30 chest radiographs.

The average procedural fluoroscopy time for each venous malformation sclerotherapy treatment session at our institution is usually 1.5 minutes (including dose-reduction techniques such as

pulsed fluoroscopy and reduced frame rate). Therefore, each procedure results in approximately 0.005-Sv radiation exposure to the thyroid gland, leading to a pediatric excess relative risk of 0.05 above baseline. Our patient (Fig 4), who has undergone >20 prior treatment sessions, now has an excess relative risk of 1.0, which is 2× the natural risk of the disease. Because the lifetime natural risk of thyroid cancer in a young female is 1.5%, her risk is now 3%, assuming that all her procedures were performed with thyroid shielding. Without thyroid shielding, her risk could be as high as 10%, and because her lesion is still not fully resolved, she will require numerous additional treatment sessions. This risk underscores the need to reduce the radiation dose as much as possible, especially in the pediatric population, and exemplifies the ongoing effort of the Alliance for Radiation Safety in Pediatric Imaging with their “Image Gently” campaign and the joint effort of the American College of Radiology, Radiological Society of North America, American Society of Radiologic Technologists, and the American Association of Physicians in Medicine with their “Image Wisely” campaign.^{12–14}

We have developed a method to completely eliminate digital subtraction angiography x-ray radiation exposure during treatment of venous vascular malformations. Using MR imaging, angiographic images of the venous malformation can be obtained to eventually directly guide sclerotherapy of the lesion. Angiography

is achieved by direct needle puncture into the malformation with subsequent injection of very dilute gadolinium contrast agent during MR imaging. The time-resolved imaging technique produces an angiographic “runoff” observation of the venous malformation and the draining venous system. Lack of contrast extravasation into the adjacent soft tissues and lack of rapid flow into large draining veins confirms appropriate needle localization and allows safe embolization of the lesion. Following embolization, repeat contrast injection can show efficacy of the treatment by demonstrating pruning of the venous malformation vasculature and slowing of flow into the draining veins. The needle is then repositioned into another region of the lesion, and the process can be repeated. To our knowledge, this is the first time MR angiographic guidance has been used to completely supplant digital subtraction angiography in the real-time evaluation of angiographic vascular flow during active neurovascular embolization. Obviously, this new technique fully exemplifies the principle and radiologists’ duty to obtain a radiation dose as low as reasonably achievable by completely eliminating radiation exposure for this procedure. The lack of ionizing radiation by using this technique is extremely promising for the future development of additional applications in the neurointerventional armamentarium, especially when treating pediatric patients who are most susceptible to the harmful effects of x-ray radiation.

Limitations of the technique include extended use of the MR imaging system and an angiographic frame rate of approximately 1.8 seconds. With regard to the extended time in the MR imaging suite, experience performing the procedure has reduced the initial time of a treatment session from 2 hours to 1 hour. This reduction has been achieved by further streamlining the process, including patient and technologist education, staff familiarity with the examination protocol, and placement of multiple needles simultaneously into different portions of the lesion for rapid transition from one treatment site to the next. While the current technology only provides an MR angiographic temporal resolution of 1.8 seconds/frame to maintain the necessary detailed spatial resolution to clearly evaluate the lesion, this is sufficient to visualize venous flow and allows safe embolization of venous vascular malformations. Although this is slow compared with the current DSA temporal resolution, as improvements in magnet performance and image acquisition software continue, more rapid frame rates may one day result in the ability to adequately visualize detailed arterial flow, with the promise of performing many other types of embolization with this technique. Finally, metallic objects such as braces on the patient’s teeth (common in the pediatric age group) can result in marked susceptibility artifacts preventing visualization of the lesion on MR imaging and precluding MR imaging-guided embolization.

However, an additional benefit of the technique is the ability to acquire pre-embolization MR images of the lesion, either for de novo lesion evaluation or follow-up assessment of the prior sclerotherapy session, saving the patient time and expense because this 1 technique can now be used for both lesion visualization and lesion treatment in a single patient visit/setting. To date, 5 patients at our institution (4 with venous malformations of the head/neck and 1 with peripheral limb venous malformation of the knee) with a total of 14 sclerotherapy sessions have been treated with this technique. Excellent response to therapy was achieved in every case, evidenced by dimin-

ished flow within the lesions and pruning of the lesion vasculature. No procedural complications were encountered, and all patients had an uneventful postprocedural recovery.

CONCLUSIONS

MRA–direct-puncture time-resolved imaging of contrast kinetics for guidance during venous malformation sclerotherapy allows adequate lesion visualization and sufficient temporal resolution to assess vascular flow and evaluate treatment results. The obvious benefit of this technique is that no additional radiation is necessary to treat these lesions, which typically occur in the pediatric population and usually require numerous treatment sessions, resulting in significant reduction in total radiation dose. Limitations of this technique include a low temporal resolution compared with conventional digital subtraction angiography and high use of the MR imaging during relatively long procedural times. In the future, continued optimization of the technique will improve temporal resolution and increase patient throughput.

REFERENCES

1. Dubois J, Garel L. **Imaging and therapeutic approach of hemangiomas and vascular malformations in the pediatric age group.** *Pediatr Radiol* 1999;29:879–93 CrossRef Medline
2. Dubois J, Soulez G, Oliva VL, et al. **Soft-tissue venous malformations in adult patients: imaging and therapeutic issues.** *Radiographics* 2001;21:1519–31 CrossRef Medline
3. Navarro OM, Laffan EE, Ngan BY. **Pediatric soft-tissue tumors and pseudo-tumors: MR imaging features with pathologic correlation, part 1—imaging approach, pseudotumors, vascular lesions, and adipocytic tumors.** *Radiographics* 2009;29:887–906 CrossRef Medline
4. Mulliken JB, Glowacki J. **Hemangiomas and vascular malformations in infants and children: a classification based on endothelial characteristics.** *Plast Reconstr Surg* 1982;69:412–22 CrossRef Medline
5. Dasgupta R, Fishman SJ. **ISSVA classification.** *Semin Pediatr Surg* 2014;23:158–61 CrossRef Medline
6. Hyodoh H, Hori M, Akiba H, et al. **Peripheral vascular malformations: imaging, treatment approaches, and therapeutic issues.** *Radiographics* 2005;25:S159–71 CrossRef Medline
7. Goyal M, Causer PA, Armstrong D. **Venous vascular malformations in pediatric patients: comparison of results of alcohol sclerotherapy with proposed MR imaging classification.** *Radiology* 2002;223:639–44 CrossRef Medline
8. Ron E, Lubin JH, Shore RE, et al. **Thyroid cancer after exposure to external radiation: a pooled analysis of seven studies.** *Radiat Res* 1995;141:259–77 CrossRef Medline
9. Ron E. **Cancer risks from medical radiation.** *Health Phys* 2003;85:47–59 CrossRef Medline
10. Kleinerman RA. **Cancer risks following diagnostic and therapeutic radiation exposure in children.** *Pediatr Radiol* 2006;36(suppl 2):121–25 CrossRef Medline
11. Sinnott B, Ron E, Schneider AB. **Exposing the thyroid to radiation: a review of its current extent, risks, and implications.** *Endocr Rev* 2010;31:756–73 CrossRef Medline
12. Farman AG. **Image gently: enhancing radiation protection during pediatric imaging.** *Oral Surg Oral Med Oral Pathol Oral Radiol* 2014;117:657–58 CrossRef Medline
13. Brink JA, Amis ES Jr. **Image Wisely: a campaign to increase awareness about adult radiation protection.** *Radiology* 2010;257:601–02 CrossRef Medline
14. Goske MJ, Frush DP, Brink JA, et al. **Curbing potential radiation-induced cancer risks in oncologic imaging: perspectives from the “image gently” and “image wisely” campaigns.** *Oncology (Williston Park)* 2014;28:232–38, 243 Medline

Sustainable Growth Rate Repealed, MACRA Revealed: Historical Context and Analysis of Recent Changes in Medicare Physician Payment Methodologies

J.A. Hirsch, H.B. Harvey, R.M. Barr, W.D. Donovan, R. Duszak Jr, G.N. Nicola, P.W. Schaefer, and L. Manchikanti

ABBREVIATIONS: APM = Alternative Payment Models; CHIP = Children's Health Insurance Program; CMS = Centers for Medicare and Medicaid Services; MACRA = Medicare Access and CHIP Reauthorization Act of 2015; MIPS = Merit-Based Incentive Payment System; SGR = Sustainable Growth Rate

Intended to provide long-term control of Medicare physician spending, the Sustainable Growth Rate (SGR) tied certain Medicare Part B payments to the economic performance of the United States. Although sensible in concept, the political implementation of the SGR resulted in a failed and perilous policy that challenged sensibilities and practice since its implementation in 1997. Few professions or businesses could function with the potential for an overnight diminution in compensation of double-digit percentages, yet physicians have survived under this methodology for almost 2 decades. Given the payment structure of imaging centers, many radiology practices have been particularly vulnerable. The Medicare Access and CHIP Reauthorization Act of 2015 (MACRA) eliminated this sword of Damocles of the SGR once and for all.¹ However, by mandating the Merit-Based Incentive Payment System (MIPS) and Alternative Payment Models (APM), MACRA creates both challenges and opportunities for radiologists—and all other Medicare-participating health care professionals. For instance, by 2022, certain providers could experience adjustments in certain Medicare Part B payments by as much as $\pm 9\%$ based on performance metrics collected in 2021: fluctuations comparable in magnitude to the envisioned SGR cuts. This Vignette describes the political and health care environment leading to the SGR repeal and describes, in detail, the new physician payment methodologies advanced under MACRA.

From the Department of Radiology (J.A.H., H.B.H., P.W.S.), Massachusetts General Hospital, Boston, Massachusetts; Harvard Medical School (J.A.H., H.B.H., P.W.S.), Boston, Massachusetts; Mecklenburg Radiology Associates P.A. (R.M.B.), Charlotte, North Carolina; Norwich Diagnostic Imaging Associates (W.D.D.), Norwich, Connecticut; Department of Radiology and Imaging Sciences (R.D.), Emory University, Atlanta, Georgia; Harvey L. Neiman Health Policy Institute (R.D.), Reston, Virginia; Hackensack University Medical Center (G.N.N.), Hackensack, New Jersey; Pain Management Center of Paducah (L.M.), Paducah, Kentucky; and Department of Anesthesiology and Perioperative Medicine (L.M.), University of Louisville, Louisville, Kentucky.

Please address correspondence to H. Benjamin Harvey, MD, JD, Department of Radiology, Massachusetts General Hospital, 175 Cambridge St, Suite 200, Boston, MA 02114; e-mail: hbharvey@partners.org

<http://dx.doi.org/10.3174/ajnr.A4522>

INTRODUCTION AND FOCUSED HISTORY

In 1997, the federal government enacted what, in retrospect, seems to have been a confusing policy: to assist balancing the federal budget by curtailing growth in professional-side medical spending. The Balanced Budget Act of 1997 introduced the SGR into Medicare payment policy.² The SGR concept is not novel to the medical profession: It was derived from the business world, where it describes best-case-scenario growth. For example, an SGR may be used to define an expansion strategy for a given line of business based on preconceived plans, definitions, and limitations.

Parts B and D of the Medicare program are financed from the Supplementary Medical Insurance Trust Fund. The Supplementary Medical Insurance is financed through fees paid by beneficiaries and federal dollars derived from taxation. Part B provides professional-component reimbursement to physicians and allied health professionals and the global fees to free-standing imaging centers. (Payment of the technical component of hospital-based imaging services is made through Medicare Part A and was not addressed by the SGR.)

Targets set by the SGR were not direct limits on expenditures. Instead, the Medicare Fee Schedule Update is adjusted to reflect the comparison of actual expenditures with target expenditures. Thus, if service expenditures exceed the SGR target, the Medicare fee schedule update is reduced to meet the deficit, and vice versa. The SGR target is calculated on the basis of projected changes in 4 factors: 1) fees for physicians' services, 2) the number of Medicare beneficiaries, 3) US gross domestic product, and 4) service expenditures based on changing law or regulations.³ Simply stated, the SGR formula tied growth in physician spending to the economic performance of the United States, theoretically preventing growth in Medicare physician spending from exceeding the annual growth in gross domestic product.⁴ The Centers for Medicare and Medicaid Services (CMS) used money spent between April 1, 1996, and March 31, 1997 (\$48.9 billion dollars) as the basis for its calculation of future program goals.

Since the 1970s, growth of health care expenditures has typi-

cally outstripped rates of gross domestic product growth in the United States.⁵ This difference naturally raises questions about the wisdom of linking professional-side physician reimbursement to gross domestic product. The early years of the SGR included a period in which the federal budget was, in fact, balanced, and the formula-based correction did not result in lower physician reimbursement rates. However, this changed in 2001 and subsequent years when the SGR methodology indicated that health care spending was above its target, which meant that Part B payments needed to be cut to stay within the legislated goal.^{6,7}

ORGANIZED MEDICINE SPRINGS INTO ACTION

At its height, the SGR methodology called for an overnight reduction in Part B payments of over 25%. The medical community vociferously argued that such reimbursement cuts constituted a direct threat to patient care by making resource planning impossible, among other challenges. Innumerable medical professional societies—including but not limited to the American Medical Association, the American College of Radiology, the American Society of Neuroradiology, the American Society of Interventional Pain Physicians, and the Society of NeuroInterventional Surgery—issued formal opinions or published articles calling for the elimination of the SGR.⁸ The Medicare Payment Advisory Commission also threw its support behind SGR reform.⁹

Understanding the disruption that SGR-mandated cuts would mean for federally supported patient care, Congress perennially blocked the implementation of the cuts through last-minute legislative actions, while repeatedly declining to enact permanent reform. By 2010, the cumulative cost of these Congressional fixes was estimated to be nearly \$300 billion dollars.¹⁰

THE TIDE TURNS

Health care reform was the pre-eminent domestic policy issue in the first term of the Obama presidency, resulting in the Affordable Care Act of 2010.¹¹ Interestingly, the Affordable Care Act did not explicitly address the SGR, despite the potential of the SGR to dramatically affect health care services in the United States.¹² Around the time of the Affordable Care Act, many policy experts were discussing a potential 10-year freeze in physician payments, as a longer term workaround to the SGR; outright repeal of the SGR was still deemed too difficult. However, in 2013, an opportunity for action was facilitated by publication of a Congressional Budget Office report, which cut the cost estimates for an SGR solution by nearly half compared with prior years, namely due to the recession and slow subsequent economic growth.¹³ This report resulted in a fresh set of ideas and rejuvenated interest in permanently repealing the SGR. Several proposals were generated, but Congress was unable to unite behind a single bill.¹⁴

In a move that took many in the health policy and physician communities by surprise, an SGR repeal bill was introduced in Congress and was speedily passed by both houses earlier this year. On March 26, 2015, the House overwhelmingly, by a vote of 392 to 37, passed House Resolution 2: the Medicare Access and CHIP Reauthorization Act of 2015. On April 14, 2015, the Senate ratified MACRA by a similar overwhelming vote of 92 to 8. Two days later on April 16, President Obama signed MACRA into law.¹ MACRA represents a crescendo of bipartisan health care reform

efforts during the past decade, including the Physician Quality Reporting System, Physician Quality Reporting Initiative, and Medicare Advantage.

Among its many aims, MACRA was intended to improve the milieu of physician reimbursement by encouraging payments based on quality rather than volume.¹⁵ Supported by pundits and the broader medical community, the President hailed the new Medicare package as a “significant bipartisan achievement.” However, beyond just further codifying “value-based payment models,” MACRA repealed the SGR, thereby eliminating the association between Part B payments and the gross domestic product.¹ As such, MACRA did away with the 21.2% correction to physician payments that was scheduled to go into effect in 2015. Instead, MACRA provides annual 0.5% reimbursement increases from July 2015 through 2019; then from 2020 through 2025, physician reimbursement will be held steady; and finally in 2026 and beyond, the law provides for 2 separate update paths based on the physician payment methodology selected by the provider (described in detail below). However, the current schedule of increases and freezes could be altered in any subsequent Congress.

NO MORE SGR, BUT IS MACRA JUMPING FROM THE FRYING PAN INTO THE FIRE?

In January 2015, the Secretary of the Department of Health and Human Services, Sylvia Burwell, presented her vision for the future of health care delivery and Medicare payment policy in a comment in the *New England Journal of Medicine*.¹⁶ Burwell described several goals for transforming the volume-based, fee-for-service system predominating US health care into one that is value-based.¹⁷ However, a clear strategy for reaching those goals was not explicitly described. Enter MACRA.

MACRA provides the bridge from ethereal ideas of value-based payment to on-the-ground implementation. By providing a detailed strategy for enacting value-based payments, MACRA has taken the Burwell doctrine from proselytization into practice. The 2 major value-based physician payment methodologies laid out in MACRA are the Merit-Based Incentive Payment System and Alternative Payment Models. The former, MIPS, represents “value-based light” and essentially continues traditional fee-for-service but imbues it with new value-based performance requirements. APMs are risk-sharing, value-based payment schema and represent a more complete departure from traditional fee-for-service. These 2 physician payment methodologies are described in detail in dedicated sections below.

RELATIVITY IN A VALUE-BASED PARADIGM

Before MACRA, it was uncertain how historical concepts of relativity and actual reimbursement would play into value-based paradigms of the future. In the pre-MACRA fee-for-service system, determining values for physician reimbursement relied on a complex interplay between several committees of the American Medical Association and CMS. The Current Procedural Terminology Committee establishes the codes that are then used to characterize procedures.¹⁸ On a code-by-code basis, the Relative Value Scale Update Committee values physicians’ work to establish relative values across specialty lines.¹⁹ The American Society of Neuroradiology is very active in this process, with formal representation

on both the Current Procedural Terminology Committee and the Relative Value Scale Update Committee to foster fair valuation of neuroradiology services relative to services of other physician providers.^{20,21} MACRA preserves elements of the relativity-based system by providing a methodology for relating fee-for-service to value-based payments. As such, the relative value unit system and the Relative Value Scale Update Committee are likely to continue to play central roles in determining physician payment reimbursement under MACRA payment schemes. This necessitates an enduring commitment to data-driven evidence to support Relative Value Scale Update Committee decisions and strong and effective neuroradiology representation on the Relative Value Scale Update Committee.

MERIT-BASED INCENTIVE PAYMENT SYSTEM

The Merit-Based Incentive Payment System will allow physicians to continue practicing in a fee-for-service environment, but new quality metrics must be reported to qualify for ongoing reimbursement. Recognizing that there is a complex first generation of quality metrics in existence (eg, Value-Based Payment Modifier program, Physician Quality Reporting System incentive), MACRA envisions a consolidation of the current quality metrics into a unified quality framework. As such, Congress charged CMS with the task of establishing a system that brings the current quality programs together into a comprehensive scheme that will assess the performance of health care professionals participating in Medicare.¹

To this end, MACRA introduces 4 performance categories. These performance categories repackage some of the existing quality metrics and introduce a new one. For instance, the MIPS simplifies the names of the Value-Based Modifier program and Physician Quality Reporting System Incentive/Disincentive Program to “Resource Use” and “Quality,” respectively, representing 2 of the performance categories. The third performance category, “Clinical Practice Improvement Activities,” is new and will focus on improvement in the domains of patient access (particularly for urgent care), population health management and care coordination, beneficiary engagement, patient safety, and practice assessment. The Meaningful Use Incentive Program for Electronic Health Records, the fourth performance category, remains largely unchanged under MIPS.

MACRA attempts to reduce the hassle and administrative challenge of demonstrating compliance by uniting these 4 performance categories via the use of Qualified Clinical Data Registries. Qualified Clinical Data Registries are CMS-approved entities that can satisfy each of the 4 performance categories created by MIPS. The good news for the radiology community is that the National Radiology Data Registry, created and maintained by the American College of Radiology, is now CMS-approved as a Qualified Clinical Data Registry.²² The National Radiology Data Registry currently supports 14 Physician Quality Reporting System measures, allowing eligible providers to reach the requirement of at least 9 Physician Quality Reporting System measures across 3 National Quality Strategy domains.²²

Starting in 2019, eligible health care providers participating in MIPS will receive a composite numeric score for their performance relating to the 4 value-based categories described above. The score will range from 0 to 100. Using a set threshold, the

Secretary of Health and Human Services will compare the provider’s performance score with the performance of the broader community. Although not yet set in stone, it is envisioned that the performance threshold for each year will likely be the median or mean of the performance scores of all MIPS-eligible professionals from a prior time period as determined by the Secretary. Only those providers continuing to participate in fee-for-service Medicare will be eligible for MIPS, whereas providers participating in an Alternative Payment Model are governed by a different reimbursement framework described in detail below.

Under MIPS, payment adjustments (up or down) will be tied to how the eligible provider performs on his or her performance measures. If one exceeds the threshold, starting in 2019, a bonus (“positive adjustment”) will be applied. The better one does, the larger the adjustment, within the limits of budget neutrality. The policy even allows super bonuses for those with exceptional performance, with aggregate additional payments of up to \$500 million dollars annually from 2019 to 2024.¹ For those providers who have performance measures at the threshold, no adjustment will be made. Last, for those that do not achieve the performance threshold, a penalty (“negative adjustment”) will be enacted. The MIPS positive or negative adjustment factor will be 4% in 2019, 5% in 2020, 7% in 2021, and 9% in 2022 and thereafter.¹ This methodology essentially results in a shifting of payments from underperformers to performers. At its peak, MIPS could result in payment fluctuations comparable in magnitude with those envisioned at the height of the SGR. The effectiveness of this incentive structure on improving health care quality and the potential negative impact of said adjustments on practice finances remain unclear and are largely untested on this scale.

ALTERNATIVE PAYMENT MODELS

Under MACRA, the second new pathway for physician payment from Medicare is through participation in an Alternative Payment Model. APMs target volume-based incentives and have grown from nonexistent entities to prevalent health care payment models within the past 5 years. Multiple approaches are currently being assessed in trials.^{23,24}

By November 2016, the Health and Human Services Secretary is required to establish specific criteria for physician-focused APMs, including models for specialist physicians. Stakeholders are being given the opportunity to submit proposals for such payment models, and these will be reviewed by a new Physician-Focused Payment Model Technical Advisory Committee. This advisory committee will report directly to the Secretary of Health and Human Services for policy-making decisions that relate to reimbursement.

Of particular note to radiologists, MACRA provides different ways to achieve APM status. The first approach requires that a substantial portion of a physician’s or group’s Medicare revenue come through an APM. A second approach would recognize APM revenue from both Medicare and other payers. This recognition would allow eligible professionals to qualify for bonuses even if APM options in their area are limited. One could envision this applying to radiologists because traditional participation in accountable care organizations can be challenging for certain types of specialists.²⁵

In 2019–2020, at least 25% of Part B services must be provided by an eligible APM entity, such as a Medicare Shared Savings Program for Accountable Care Organizations or similar programs created by the Centers for Medicare and Medicaid Innovation. In 2021–2022, this escalates to 50% of Part B services being provided by an eligible APM entity or via another approved risk-based, quality-measured arrangement. Finally, in 2023 and thereafter, 75% percent of Part B services must meet this criterion. If this rapid, and arguably hasty, pace can be achieved, the inertia-ridden US health care system will have been transitioned from volume-based to value-based care in less than a decade's time.²⁵

MACRA encourages providers to choose the APM physician payment model over the MIPS model by giving APM participants more favorable reimbursement. If providers participate in a qualifying APM, they will receive a bonus each year from 2019 through 2024 equal to 5% of the estimated aggregate payment amounts for covered Part B professional services for the preceding year. Starting in 2026, APM participants will benefit from a more favorable annual conversion factor update of 0.75% compared with 0.25% for participants in the MIPS program.

SELECTED ADDITIONAL ELEMENTS OF MACRA

Several other areas are of interest to radiologists and neuroradiologists in MACRA. One example is the mandate to have interoperable, certified electronic health records by the start of 2019. Radiologists are keenly aware of the difficulties of getting electronic health record systems to interact with each other in a functional manner. However, it seems likely that the exchange of electronic health records might include digital images. For this reason, radiologists should anticipate the implications for their practices going forward.

CMS has recently begun releasing provider payment information to the public. The information released to date has been spotty and poorly contextualized, and the lay media has been left to explore the findings.²⁶ As part of MACRA, CMS will expand the information released to the public domain.

The reauthorization of the Children's Health Insurance Program (CHIP) is another important achievement of MACRA. CHIP assists millions of children and pregnant women who do not qualify for Medicaid because their income is too high. MACRA extends funding for this program through fiscal year 2017.

HOW WILL MACRA BE FINANCED?

Above, we described how previous effort in Congress to permanently repeal the SGR fell short because there was no accepted mechanism to pay for the cost of doing so. How was that solved with this legislation? In reality, it was not. First, Medicare is going to expand what is generally known as means testing. As such, MACRA decreases the thresholds at which high-income beneficiaries pay higher Medicare premiums. Second, Medicare reimbursements for post-acute care facilities such as inpatient rehabilitation and skilled nursing facilities will be limited to a 1% increase in 2018. Furthermore, MACRA replaces an expected one-time payment increase of 3.2% to inpatient hospital payment rates in 2018, with 0.5% increases from 2018 through 2023. As a result, MACRA fundamentally shifts money previously earmarked

for hospitals and other facilities to physicians. Taken together, these offsets will only cover a portion of the cost of the legislation.

TAKE-HOME POINTS

- The Sustainable Growth Rate was a sensible attempt to limit historically rapid growth in physician spending to the economic performance of the United States; but the political implementation resulted in a failed and perilous policy.
- The Medicare Access and CHIP Reauthorization Act of 2015 eliminated the SGR and, in doing so, removed the perennial threat of 20% cuts in physician payments, which would have threatened patient access to health care services.
- By defining 2 new Medicare physician payment methodologies, the Merit-Based Incentive Payment System and the Alternative Payment Models, MACRA charts a path away from fee-for-service payments and toward value-based payments. Congress has mandated a rapid, and arguably hasty, transition to value-based payments models, with widespread adoption of these new payment models required as early as 2019. By understanding the risks and opportunities under these varying payment models, radiologists can proactively seek the value-based physician payment methodology that best meets their needs or can even craft specialty-specific APMs themselves.

Disclosures: Joshua A. Hirsch—UNRELATED: Consultancy: Medtronic, CareFusion, Comments: Medtronic, Interventional Spine, ongoing; CareFusion, single non-Continuing Medical Education event in past 12 or 36 months; Stock/Stock Options: Intratech (development-stage stroke company). Robert M. Barr—UNRELATED: Board Membership: I serve on the board of Novant Health and the Harvey L. Neiman Health Policy Institute. These are both unpaid positions; Payment for Lectures (including service on Speakers Bureaus): academic institutions only. Laxmaiah Manchikanti—UNRELATED: Semnur Pharmaceuticals, Comments: provided limited consulting services to Semnur Pharmaceuticals, which is developing nonparticulate steroids.

REFERENCES

1. Medicare Access and CHIP Reauthorization Act of 2015. (2015). 42 USC 1305.
2. Balanced Budget Act of 1997. (1997). 42 USC 4511, 4512.
3. Hirsch JA, Rosman DA, Liu RW, et al. **Sustainable growth rate 2013: time for definitive intervention.** *J Neurointerv Surg* 2013;5:382–86 CrossRef Medline
4. Thrall JH. **Unintended consequences of health care legislation.** *J Am Coll Radiol* 2011;8:687–91 CrossRef Medline
5. United States Department of Labor, Bureau of Labor Statistics. Spotlight on Statistics: Health Care. November 2009. http://www.bls.gov/spotlight/2009/health_care/. Accessed June 7, 2015
6. Congressional Budget Office. Medicare's payments to physicians: the budgetary impact of alternative policies relative to CBO's March 2012 baseline. July 30, 2012. <http://www.cbo.gov/sites/default/files/cbofiles/attachments/43502-SGR%20Options2012.pdf>. Accessed June 7, 2015
7. Medicare Payment Advisory Commission. Report to the Congress: Medicare and the Health Care Delivery System. Review of CMS's preliminary estimate of the 2013 update for physician and other professional services. June 2012. http://www.medpac.gov/documents/reports/jun12_appa.pdf?sfvrsn=0. Accessed June 7, 2015
8. House Energy and Commerce Committee. Re: The need to move beyond the SGR. Statement of the American Medical Association before the House Energy and Commerce Committee Subcommittee on Health Presented by Cecil B. Wilson, MD, May 5, 2011. <http://www.medsocdel.org/Portals/1/Health%20Care%20Reform%20Info/Proposal%20from%20the%20AMA.pdf>. Accessed June 7, 2015
9. Medicare Payment Advisory Commission. Report to the Congress. Medicare and the Health Care Delivery System. June 2012.

- http://www.medpac.gov/documents/reports/jun12_entirereport.pdf?sfvrsn=0. Accessed June 7, 2015
10. Fiegl C. **Medicare SGR repeal price tag plummets.** *American Medical News*. February 25, 2013. <http://www.amednews.com/article/20130218/government/130219946/1/>. Accessed June 7, 2015
 11. Patient Protection and Affordable Care Act. (2010). 42 USC 18001.
 12. Manchikanti L, Hirsch JA. **Patient Protection and Affordable Care Act of 2010: a primer for neurointerventionalists.** *J Neurointerv Surg* 2012;4:141–46 CrossRef Medline
 13. Congressional Budget Office. The budget and economic outlook; fiscal years 2013 to 2023. February 2013. www.cbo.gov/sites/default/files/cbofiles/attachments/43907-BudgetOutlook.pdf. Accessed June 7, 2015
 14. Hirsch JA, Manchikanti L. **The sustainable growth rate: a 2014 update.** *J Neurointerv Surg* 2014;6:411–12 CrossRef Medline
 15. Manchikanti L, Staats PS, Boswell MV, et al. **Analysis of the carrot and stick policy of repeal of the sustainable growth rate formula: the good, the bad, and the ugly.** *Pain Physician* 2015;18:E273–92 Medline
 16. Burwell SM. **Setting value-based payment goals: HHS efforts to improve U.S. health care.** *N Engl J Med* 2015;372:897–99 CrossRef Medline
 17. Hirsch JA, Leslie-Mazwi TM, Barr RM, et al. **The Burwell roadmap.** *J Neurointerv Surg* 2015 Mar 5. [Epub ahead of print] CrossRef Medline
 18. Hirsch JA, Leslie-Mazwi TM, Nicola GN, et al. **Current procedural terminology; a primer.** *J Neurointerv Surg* 2015;7:309–12 CrossRef Medline
 19. Hirsch JA, Silva E 3rd, Nicola GN, et al. **The RUC: a primer for neurointerventionalists.** *J Neurointerv Surg* 2014;6:61–64 CrossRef Medline
 20. Hirsch JA, Donovan WD, Leslie-Mazwi TM, et al. **Component coding and the neurointerventionalist: a tale with an end.** *J Neurointerv Surg* 2013;5:615–19 CrossRef Medline
 21. Donovan WD, Leslie-Mazwi TM, Silva E 3rd, et al. **Diagnostic carotid and cerebral angiography: a historical summary of the evolving changes in coding and reimbursement in a complex procedure family.** *J Neurointerv Surg* 2014;6:712–17 CrossRef Medline
 22. American College of Radiology. NRDR PQRS Qualified Clinical Data Registry. <http://www.acr.org/Quality-Safety/National-Radiology-Data-Registry/Qualified-Clinical-Data-Registry>. Accessed June 7, 2015
 23. Meehan TM, Harvey HB, Duszak R Jr, et al. **Accountable Care Organizations: what they mean for the country and for neurointerventionalists.** *J Neurointerv Surg* 2015 May 18. [Epub ahead of print] CrossRef Medline
 24. Harvey HB, Gowda V, Gazelle GS, et al. **The ephemeral accountable care organization: an unintended consequence of the Medicare shared savings program.** *J Am Coll Radiol* 2014;11:121–24 CrossRef Medline
 25. McCurdy DA, Carder-Thompson EB, Cody DA, et al. President Signs MACRA: Permanently Reforms Medicare Physician Reimbursement Framework, Includes Other Medicare Payment, Program Integrity, and Policy Provisions. Reed Smith Client Alerts. April 16, 2015. www.reedsmith.com/Congress-Approves-MACRA-Permanently-Reforms-Medicare-Physician-Reimbursement-Framework-Includes-Other-Medicare-Payment-Program-Integrity-and-Policy-Provisions-04-16-2015/. Accessed June 7, 2015
 26. USA Today. First look at Medicare data in 35 years. <http://www.usatoday.com/story/news/nation/2014/04/09/government-releases-medicare-physician-payment/7462923/>. Accessed June 7, 2015

Prevalence of Brain Microbleeds in Alzheimer Disease: A Systematic Review and Meta-Analysis on the Influence of Neuroimaging Techniques

A.A. Sepehry, D. Lang, G.-Y. Hsiung, and A. Rauscher



ABSTRACT

BACKGROUND AND PURPOSE: The literature on the prevalence of Alzheimer disease–associated cerebral microbleeds assessed with MR imaging shows considerable heterogeneity in terms of imaging techniques and parameters. Our aim was to perform a meta-analysis of the role of imaging techniques, including image acquisition, field strength and scanner type, and clinical and demographic factors on the reported prevalence of microbleeds in Alzheimer disease.

MATERIALS AND METHODS: The prevalence of microbleeds was examined with respect to a priori–selected moderating variables via meta-analytic tools of literature reports.

RESULTS: Fourteen unique studies providing 15 microbleed prevalence rates met the selection criteria for inclusion. The aggregate prevalence of microbleeds was 24% (95% CI, 19%–28%). Scan (SWI = 40%, gradient echo = 18%, EPI = 19%) and field strength (slope = 0.39; standard error = 15, $P < .01$) influenced the prevalence of microbleeds. The associations between microbleeds and age, sex, and global cognitive status were not significant. After updating the literature, the aggregate prevalence remained in the 95% CI range.

CONCLUSIONS: Imaging technique and field strength are strongly associated with the prevalence of microbleeds over the global aggregate. Standardized imaging protocols for identification of microbleeds are recommended to minimize confounds.

ABBREVIATIONS: AD = Alzheimer disease; ER = event rate; GRE = gradient recalled-echo imaging; MB = microbleed; MCI = mild cognitive impairment; STROBE = Strengthening the Reporting of Observational studies in Epidemiology

A growing number of studies have suggested that the presence of microbleeds (MBs) and the overall microbleed burden have prognostic significance for Alzheimer disease (AD).^{1,2} In AD, MBs are thought to contribute to the pathophysiology of the illness, demonstrating a link between amyloid pathology and neurovascular change.³ Although still controversial, the impact of MBs on the progression of mild cognitive impairment (MCI) due to incipient AD and subsequent emergence of AD has been suggested.⁴ It is not clear whether MBs are consequences of AD or cerebral amyloid angiopathy, or just a bystander. Current data on the impact of MBs on global cognition have been equivocal, and

most studies showed a minimal effect of MBs.⁵ The lack of effect has been associated with small sample size, insufficient MB counts to cause any cognitive change, or AD severity masking the subtle effect of MBs on neurocognitive functioning.⁶ Heterogeneous classifications and poor validation of both the presence and prevalence of MBs have further obscured potential relationships between neurocognitive functioning and MBs.^{7,8} With respect to subregional neuropathology, few studies have directly examined the effect of MBs on other markers of AD such as CSF-associated amyloid antibodies or hippocampal atrophy.^{8,9}

A number of clinical human studies examining the prevalence of MBs in AD have been published since 2000. The most recent review on the prevalence of MBs in AD included 4 unique studies.³ Those studies reported heterogeneous samples of patients with AD with varying severity of cognitive impairment, age ranges, sex, study design, and other confounds. Reported prevalence rates ranging between 17% and 32% were described, likely due to considerable heterogeneity of imaging acquisition techniques and MB identification approaches.

In MR imaging, paramagnetic hemosiderin in MBs gives rise to local field inhomogeneities, which affect both the magnitude

Received March 31, 2015; accepted after revision July 11.

From the Division of Neurology (A.A.S., G.-Y.H.), Department of Medicine; Departments of Paediatrics (A.A.S., A.R.) and Radiology (D.L.); University of British Columbia, Vancouver, British Columbia, Canada.

Please address correspondence to Amir A. Sepehry, MSc, PhD, University of British Columbia, University of British Columbia Hospital, Division of Neurology, 2211 Westbrook Mall, Vancouver, BC, Canada; e-mail: sepehryaa@alumni.ubc.ca; @rauscherMRI, @asmetaanalysis

Indicates article with supplemental on-line tables.

Indicates article with supplemental on-line photos.

<http://dx.doi.org/10.3174/ajnr.A4525>

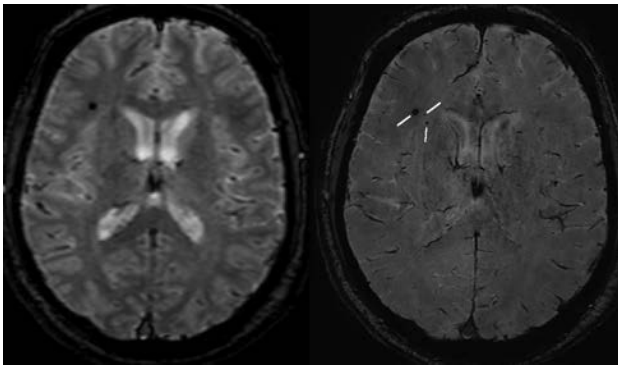


FIG 1. Gradient-echo MR imaging (*left*) and SWI (*right*) acquired in the same subject on a 3T Achieva (Philips Healthcare, Best, the Netherlands) with an 8-channel sensitivity encoding head coil and sensitivity encoding reconstruction of multichannel data. The gradient-echo scan shows 1 microhemorrhage when the more sensitive SWI scan detects 3.

and the frequency of the MR imaging signal. Conventional gradient recalled-echo imaging (GRE) makes use of changes in the magnitude via loss in the $T2^*$ -weighted signal. Susceptibility-weighted imaging is a gradient-echo technique with high spatial resolution that generates images with improved sensitivity to MBs by also incorporating the MB effects on the MR signal frequency.^{10,11} Because SWI is a 3D sequence, it allows thin sections without intersection gaps. Typical spatial resolution of SWI is $0.5 \times 0.5 \times 2$ mm, whereas GRE sections are up to 5 mm thick with intersection gaps of up to 2 mm. The improved spatial resolution allows SWI to capture small MBs, which may be missed with GRE. Imaging of MBs also benefits from increased magnetic field strength, which leads to a higher signal-to-noise ratio and makes the field inhomogeneities around MBs more pronounced, resulting in increased image contrast. The choices of both field strength and imaging technique have, therefore, a substantial influence on the visibility of small bleeds (Fig 1). With technical developments, the sensitivity of MR imaging to MBs has increased and the prevalence reported on previous reviews may have to be revised.

The purpose of this study was to conduct a meta-analysis of MB prevalence in AD that takes into account imaging, clinical, and demographic parameters.

MATERIALS AND METHODS

Search Strategy

MEDLINE and EMBASE were queried for a priori–defined key words with key terms and subject headings on September 9, 2014. The following were combined to yield our search outcome: SWI OR “susceptibility weighted imaging” OR “gradient echo imaging” OR “gradient echo MR imaging” OR “susceptibility-weighted MR imaging” OR MR imaging OR nuclear MR imaging AND Microbleed* OR microhemorrhage OR “petechial hemorrhage” OR hemosiderin OR “cerebral amyloid angiopathy” OR cerebral hemorrhage OR intracranial hemorrhages AND Alzheimer disease OR dementia OR Alzheimer*. Examining the reference list of review articles relevant to the study substantiated the search. The search of the literature was updated on May 11, 2015.

Selection Criteria

Two reviewing authors (A.A.S. and A.R.) examined all retrieved abstracts independently. Studies were retained when they reported both the diagnosis of AD and the prevalence of MBs. Articles were excluded if they were the following: 1) a case report, review, meta-analysis, letter, editorial, case-control or cross-sectional studies; 2) a treatment study; or 3) reported duplicate data on the following: 4) on postmortem brain; 5) atypical AD (eg, logopenic); 6) explicitly on familial AD type; or 7) included mixed groups (eg, AD with MCI). The same method was applied to studies found by a hand search of reference lists of review articles. When disagreement occurred in study classification, further discussion was undertaken to reach concordance. Additionally, quantitative analysis of between-rater agreement was performed. The selection criteria were formulated to minimize statistical and sample heterogeneity.

A Priori–Selected Moderating Variables

The selected moderating variables were the following: imaging parameters including scanner type, field strength, and scan techniques; MB definition; age of patients with AD (total AD sample); global cognitive scores of the sample; sex; diagnosis of AD (possible or probable); study design; hemorrhage; infarct/lacuna; stroke; and the anatomic distribution of MBs. Due to the limited number of included studies and the large number of variables, exploratory single-variable meta-regressions were performed.

Effect Size and Calculations

Event rates (effect sizes) were generated by using the reported prevalence rate for MBs (>1) in patients with AD for each study. Subsequently, an aggregate measure was computed by using the random-effects model that takes into account the sample size from each study. For categoric and continuous-type moderating variables, meta-regression or categoric analyses were performed. All the analyses and graphs were implemented by using Comprehensive Meta-Analysis (Version 2.0, <https://www.meta-analysis.com>).¹²

Each study contributed 1 time to the aggregate event rate estimate, unless the authors provided different event rates for different techniques. For the study reporting field strengths of 1T and 1.5T, the lower field strength was used. For studies reporting cognitive scores or mean age for patients with and without MBs, an aggregate mean and SD were calculated by using D-STAT¹³ and were subsequently used in the overall analyses. Comparison between the prevalence of MBs in patients with AD versus healthy controls and those with subjective cognitive impairment and other dementias was performed by using odd ratios. Examination of the effect of antiplatelet medication, the *apolipoprotein E4* allele (presence and percentage reported), hypertension, and immunotherapy when possible was performed by using categoric and meta-regression analyses. For all analyses, the critical level of significance was set to 5%. For all meta-regressions, secondary (aggregate) statistics were used. The reported prevalence (event rate) from each study was transformed to a log scale to allow both continuous and dichotomized moderating variables. For single-variable meta-regressions, we regressed the moderating variable

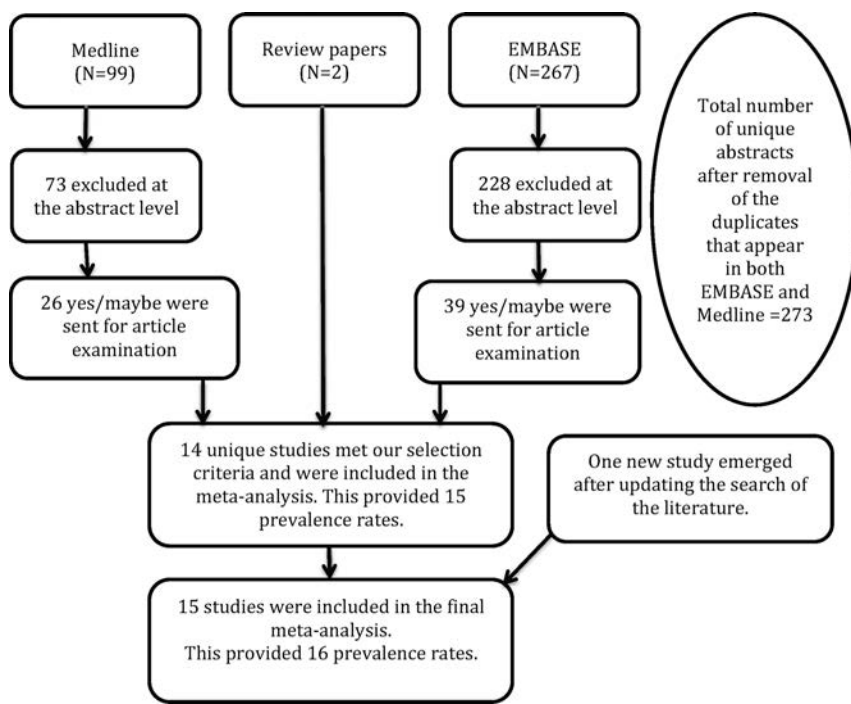


FIG 2. Flow diagram showing the progress of data collection.

on the prevalence rate. The R^2 analog was used to report the explained magnitude of between-study variance.

Quality Assessment

The quality of the included studies was assessed according to STrengthening the Reporting of OBservational studies in Epidemiology (STROBE) guidelines.¹⁴ For reporting of the meta-analysis data, when applicable, reference has been made to Meta-analysis of Observational Studies in Epidemiology or the Preferred Reporting Items for Systematic Reviews and Meta-Analyses (PRISMA) statement.^{15,16}

Assessment of Bias

For examination of publication bias, the funnel plot and the Begg and Mazumdar rank correlation test¹⁷ and the test of the intercept of Egger et al¹⁸ were used. A significant P value for both Begg and Mazumdar and Egger test is indicative of possible bias.

Heterogeneity

Statistical heterogeneity was examined for global and subsequent moderating variables by using the Q -statistic and I^2 .¹⁹ To minimize the magnitude of bias resulting from selectively dropping studies to explain heterogeneity and to keep the maximum number of studies in the analyses, we assessed the heterogeneity by using multivariable meta-regressions (incremental or diagonal approach) when applicable. The incremental approach was used when variables could have been added, and the diagonal was used when there was collinearity among variables. The first category consisted of imaging parameters including field strength, scan technique, and scanner type. The second category included demographics and Mini-Mental State Examination score. The third category pertained to clinical variables, including the effect of MB

location and definition, lacunae, stroke, hemorrhage, AD diagnosis, and risk factors. Subsequently, analyses were performed of the following: 1) prevalence for other dementias and control groups, 2) risk factors including *apolipoprotein E4* carriers (heterozygote, homozygotes, or both) and percentage with hypertension, 3) publication date on the prevalence of MBs, and 4) analyses based on updated literature.

RESULTS

Study Selection

The search of electronic literature yielded 273 unique abstracts (99 from MEDLINE and 267 from EMBASE). Also, 2 studies^{20,21} emerged from the search of review articles. From these, 73 studies from MEDLINE and 228 from EMBASE were excluded at abstract screening. The remaining 26 from MEDLINE and 39 from EMBASE were examined for data and selection criteria in more detail. At this stage, the interrater

κ agreement was at 0.87. From MEDLINE/EMBASE and emerging studies, 14 published studies met selection criteria and had no overlap with any other included study. One study²² reported results from 2 techniques in the same cohort, resulting in 15 reported prevalence rates for the subsequent analyses (see Online Table 1 for excluded studies, and flow-diagram, Fig 2). Therefore, the final included number of studies was 15 (Table 1 and Online Table 2).

Demographic Data and Acquisition Platforms of the Included Studies

The sample sizes ranged from 10 to 550. For the studies reporting global cognition scores as assessed by the Mini-Mental State Examination, the values ranged from 17.9 to 26. The mean age range was 67–79.5 years; the percentage of male subjects was between 29% and 51%. AD diagnoses were reported as probable AD, a mix of probable and possible AD as per the 1984 criteria of McKhann et al,²³ and unspecified.

Scanners used were Signa 1.5T and Signa 3T (GE Healthcare, Milwaukee, Wisconsin); Intera 1.5T, Intera 3T, and Achieva 3T (Philips Healthcare, Best, the Netherlands); and 1T Impact, 1.5T Avanto, 1.5T Vision, 1.5T Sonata, and 3T Trio (Siemens, Erlangen, Germany). The field strengths were 1T, 1.5T, and 3T; the techniques used were T2*-weighted gradient echo, echo-planar imaging, and SWI. Most studies reported on diffuse/global distribution of the MBs and explicitly considered MBs as round and ≤ 10 mm.

Prevalence Aggregate

The global event rate (ER) estimate for at least 1 MB included 583 cases from a sample of 2333 (ER = 0.24, $n = 15$) and was heterogeneous ($I^2 = 85.99$). Both graphic (funnel plot) and quantita-

Table 1: Neuroimaging parameters of the included studies

Studies	Scanner/Technique/Field Strength	Gap/Raters
Benedictus et al, 2013 ²⁸	GE Healthcare/EPI/3T	Unknown/1 neuroradiologist
Cordonnier et al, 2006 ⁷	Siemens/GRE/1T	1.5/1 observer, type unknown
Fukui et al, 2013 ^{21,a}	Unknown/GRE/1.5T	Unknown
Goos et al, 2011 ^{22,b}	Siemens/GRE/1.5T	1.5/1 rater, type unknown
Kester et al, 2014 ^{29,a}	Siemens/SWI/1.5T	NA/1 rater, type unknown
Kirsch et al, 2009 ⁴	GE Healthcare, Siemens/GRE/IT, 1.5T, and 3T	Unknown
Nagasawa et al, 2014 ²⁰	Siemens/SWI/1.5T	NA/4 readers +1 neuroradiologist
Nagata et al, 2012 ⁴⁰	Unknown/GRE/1.5T	0.5/2 neurologists, 1 neuroradiologist
Nakata-Kudo et al, 2006 ⁴¹	Unknown/EPI/1.5T	Unknown/unknown
Park et al, 2013 ⁴²	Philips/GRE/1.5T	1/1 neurologist, 1 radiologist
Qiu et al, 2010 ⁴³	Philips/GRE/3T	2/2 neurologists in consensus
Staekenborg et al, 2009 ⁴⁴	GE Healthcare/EPI/1.5T	NA/1 neuroradiologist and subsequent raters
Uetani et al, 2013 ²⁴	Siemens/GRE/IT	1.5/unknown
van der Vlies et al, 2012 ⁴⁵	Siemens/SWI/3T	NA/2 neuroradiologists in consensus
Yates et al, 2014 ⁴⁶	Siemens/GRE/IT or 1.5T	1/unknown
Zonnefeld et al, 2014 ⁴⁷	Siemens/SWI/3T	NA/2 neuroradiologists in consensus
Postupdate	GE Healthcare/SWI/3T	NA/1 of 2 neuroradiologists
Olazarán et al, 2014 ²⁷	GE Healthcare/EPI/3T	NR/neuroradiologist

Note:—NA indicates not applicable; NR, examined but not reported.

^a Studies are excluded at the moderating factor analyses. Only the van der Vlies et al⁴⁵ 2012 study reported the percentage of medicated patients with AD.

^b Two different techniques were used with the same cohort.

Table 2: Mixed-effects single meta-regressions (method of moment) on the event rate estimate as a function of moderating variables

Variables	Slope	SE	P Value	No.
Quality (STROBE)	0.0545	0.1184	.6455	15
Field strength	0.3924	0.1482	.0081	15
Male (%)	-0.0085	0.0260	.7449	12
Age AD (mean, yr)	0.0484	0.0456	.2881	12
MMSE (mean score)	-0.1919	0.1119	.0864	9
ApoE-ε4 (%)	0.0117	0.0091	.1992	5
No. of image raters	0.1330	0.1598	.4055	12
Postupdate ^a				
Year of publication	0.1099	0.0518	.0340	16

Note:—SE indicates standard error; MMSE, Mini-Mental State Examination; No., number of outcomes included in the analysis; imaging technique: TE and TR.

^a No statistical change was observed for all other variables in the Table after analyzing with the new study.

tive analyses for publication bias were nonsignificant ($P > .05$), suggesting a lack of significant bias.

Global/diffuse distribution of the MB event rate was similar to the global effect (ER = 0.24, $n = 11$); and for cortical, subcortical, or nonspecified MB locations, various prevalence rates were reported. For those that reported explicitly and used a size of ≤ 10 mm to define MBs, the prevalence of MBs was 25 (ER = 0.25, $n = 13$).

Moderating Factors

Imaging Techniques. With SWI (ER = 0.40, $n = 5$), the prevalence was more than twice as high as that in those studies conducted with GRE imaging (ER = 0.18, $n = 7$) or EPI (ER = 0.19, $n = 3$). For Siemens scanners, the prevalence of MB was 27% (ER = 0.27, $n = 8$).

Demographics. Age ($P = .29$), sex ($P = .75$), and global cognition ($P = .09$) assessed by single mixed-effects meta-regression did not modify the prevalence of MBs (Table 2). For cigarette smoking, the prevalence of MBs was nearly 25% (ER = 0.246; 95% CI, 0.200–0.298). Details for medication and substance use were insufficient for further analyses.

Diagnostic Characteristics. For studies reporting explicitly on probable AD as per the diagnostic framework of McKhann et al,²³ the prevalence of MBs (ER = 0.27, $n = 7$) was slightly higher compared with those studies that did not specify an AD diagnostic criterion (ER = 0.24, $n = 6$) but was significantly higher than those reporting a combination of probable and possible AD groups (ER = 0.14, $n = 2$). The associations between MBs and age, sex, and global cognitive status were not significant factors that affected the prevalence of MBs for probable AD ($P > .1$).

Quality Assessment. The quality of studies as assessed by STROBE guidelines did not appear to affect the overall event rate estimate (slope = 0.055, standard error = 0.118, $P = .646$, $n = 15$).

Details on event rates and meta-regression results are listed in Table 2 and On-line Table 3.

Heterogeneity

The heterogeneity was assessed by using multivariable meta-regressions. For the imaging model, independently, the field strength was significant ($P < .002$) and explained approximately 34% of the between-study variability but was no longer significant when the scanner type and, subsequently, the technique were included in the model. When including the field strength and scanner type, GRE explained 73% and SWI explained 93% of the variability. When all 3 variables were included in the model, only the Philips scanner was significant. This effect was not present when initially the technique and then the scanner type were entered into the model.

None of the other models (demographic, clinical factors, lacunae/stroke/hemorrhage) and clinical AD diagnoses (probable/probable-possible/not specified) and none of the risk factors (*apolipoprotein E4* carriers, hypertension), alone or in combination, were statistically significant or resulted in a between-study variability of $>3\%$. Immunotherapy and antiplatelet therapy were not examined due to limited data.

Prevalence of Other Dementias

Within the subset of studies that provided a comparison group, the presence of MBs in vascular dementia was 58% (71 of 122 cases of vascular dementia, 4 studies), 16% for healthy controls or the subjective cognitive impairment group (92 of 553 cases of controls, 7 studies), 28% for mild cognitive impairment (105 of 376 cases of MCI, 7 studies), and 14% for a group containing mixed diagnoses (eg, including AD, vascular dementia, mixed dementia) (50 of 358 cases of mixed diagnosis, 6 studies). Analyses comparing the prevalence of MBs in AD with frontotemporal lobar dementia and Lewy body dementia were not possible, given that only 1 study²⁴ made these comparisons. The ORs for these comparisons are given in On-line Fig 1.

Risk Factors

The MB prevalence rate for the studies reporting the percentage of *apolipoprotein E4* carriers (heterozygote, homozygote, or both) was similar to the global aggregate (On-line Table 3). The effect of the percentage of *apolipoprotein E4* carriers on the prevalence rate via single meta-regression was nonsignificant (Table 2). There was no effect of hypertension on the prevalence of MBs (slope = 0.015, standard error = 0.042, $P = .71$).

Literature Update

Update of the literature review, based on screening, yielded 3 studies. Two of the 3 studies were excluded,^{25,26} and the only study meeting our selection criteria²⁷ was added to the remaining of studies. To avoid investigator bias, we also performed analyses of the added new article separately. Small changes were observed in the global prevalence of MBs (24.9% versus 24.1%) and other variables, which are listed in Table 2 and On-line Table 3. On-line Fig 2 shows the forest plot for the updated aggregate event rate.

Effect of Publication Year

Single-variable meta-regression analysis to examine the effect of publication year on the MB prevalence rates was significant ($P = .034$).

DISCUSSION

The aggregate MB prevalence emerging from this meta-analysis for patients with AD was 24%, and 25% after including an additional study that emerged from a search update in May 2015, and was similar to the earlier findings from studies reported by Cordonnier and van der Flier (23%).³ Apparent prevalence is particularly affected by the image-acquisition technique (GRE, EPI, SWI). Those studies applying SWI had twice the prevalence rates for MBs as studies using GRE or EPI. SWI is highly sensitive to susceptibility-related contrast because of combining phase and magnitude images. In studies of neurotrauma, SWI was found to detect up to 5 times as many hemorrhages compared with GRE.²⁸ However, SWI requires appropriate reconstruction of data acquired with multichannel coils. If the data from the individual channels are combined incorrectly, the phase images may exhibit singularities that lead to artifactual MBs in the final SWI.²² These singularities are avoided if complex valued coil sensitivity maps are used for the channel combination (sensitivity encoding reconstruction).^{10,22,29} On some scanner platforms, the correct coil

combination is implemented by default,¹⁰ whereas on other platforms, it must be implemented by the end user.^{4,29}

Patients with AD have increased prevalence rates of MBs compared with healthy controls and those with subjective cognitive impairment. Our aggregate prevalence of MBs for AD was considerably higher than that reported in the literature for asymptomatic or healthy elderly individuals (11.1 versus 25%),³⁰ and it is consistent with the literature reporting higher prevalence in atypical AD compared with AD.³¹

The prevalence of MBs from studies reporting explicitly on probable AD was higher than that in those reporting a combination of probable and possible AD (14% versus 27%). This is potentially because in the latter group, the balance in the number of patients included between possible and probable AD was not clear and the pathology could have been frontotemporal lobar dementia or Lewy body dementia-like, which are expected to have lower prevalences of MBs.

The current results have implications for disease monitoring and imaging outcomes in drug development. SWI would show more bleeds at baseline and would be more sensitive to detecting new MBs, which may have implications for safety monitoring in phase II trials. Also, a change in the MB number and size could be associated with the severity of primary pathology and secondary symptoms.

Whether an increase in MB detection translates into a clinically meaningful difference remains debatable.²² MBs contribute to the pathophysiology of the illness, and they potentially indicate a link between amyloid pathology and neurovascular change.^{3,32} Moreover, the presence of MBs and the overall MB burden have prognostic significance for AD³³⁻³⁵ and may affect cognition.^{8,36} Better imaging of the MBs in AD may allow better understanding of the pathophysiology of MBs in AD and the role that small-vessel disease plays in AD pathology.

The strength of our study is that we examined multiple moderating variables that to date, no other study has performed, to our knowledge. Scanner type (Siemens and GE Healthcare), use of SWI technique, field strength, and diagnosis of probable AD and MB definition (≤ 10 mm) were factors that increased the prevalence over the global aggregate. We also found that great variability existed as a function of AD diagnosis, but not because of age, sex, or cognitive status.

Our meta-analysis has certain limitations. Given the requirement for multiple single-variable meta-regression analysis, an increased probability of type I error exists. However, the results remain unchanged when examined at a significance level of $P = .01$. Additionally, multivariable meta-regressions were used to investigate heterogeneity without dropping studies that would have been limitations in other approaches. Nonetheless, the limited number of studies and some missing data, which preclude sufficient analyses of publication bias and multivariable modeling, suggest that some results should be considered with caution.

Most of the studies included in our analyses did not explicitly state that patients with a history of brain injury, stroke, or other sources of hemorrhage were excluded. Because these events can result in localized regions of tissue damage that could be misconstrued as AD-associated MBs instead of injury-associated MBs by raters, there is a risk that inclusion of patients with head injury,

neurovascular pathology, or hemorrhage would have skewed their reported results. Additionally, we were unable to contact the authors for missing data, which would have added power to each component of the analyses, specifically at the meta-regression level.

Because of a paucity of detailed data on patients' medication regimens, we could not determine the effect of immunotherapy on the rate of MBs. Certain types of A β -42-based immunotherapy are hypothesized to aggravate cerebral amyloid angiopathy-related vascular damage or dysfunction.^{37,38} We found no significant effect of the presence of the *apolipoprotein E4* allele on the prevalence of MBs. This lack of effect could be due to heterogeneity in reporting the status of the *apolipoprotein E4* allele carriers (heterozygote, homozygote, or both). In fact, some studies reported the percentage of the carrier without specifying allele variants, whereas others reported exact rates for homozygotes and heterozygotes.

Future Directions

Future studies examining the prevalence of MBs in AD should report the number, size, and location of MBs more precisely, which may allow analysis of the relationship between these factors and neurocognitive outcomes. Given the large differences in prevalence among different imaging technologies, future studies should attempt to use technologies that can be standardized and are sensitive, yet widely available. SWI with 3T scanners is now emerging as the standard for identifying MBs. This is consistent with our finding that the year of publication is positively correlated with the prevalence of MBs. In addition, MR imaging scanner manufacturers need to ensure that artifact-free SWI is provided. Field strengths of 7T and above are gaining importance in research and may eventually be used in clinical settings, which may result in a further increase in the prevalence of MBs in patients imaged on such systems.³⁹

CONCLUSIONS

Imaging technique and field strength are strongly associated with the prevalence of microbleeds over the global aggregate. Standardized imaging protocols for identification of microbleeds are recommended to minimize confounds.

ACKNOWLEDGMENTS

We thank Charlotte Beck (University of British Columbia medical librarian) for assisting with the search methodology.

Disclosures: Ging-Yuek Hsiung—UNRELATED: Grants/Grants Pending: Canadian Institutes of Health Research,* Brain Canada,* National Institutes of Health/National Institute on Aging,* Heart and Stroke Foundation,* Hoffmann-La Roche,* TauRx,* AstraZeneca,* Eli Lilly,* and Genentech.* Comments: I have received grants from the Canadian Institutes of Health Research, Brain Canada, the National Institutes of Health/National Institute on Aging, and the Heart and Stroke Foundation of Canada for academic research projects. I have also received funds from sponsors for conduction of clinical trials, including Hoffmann-La Roche, TauRx, AstraZeneca, Eli Lilly, and Genentech. Alexander Rauscher—UNRELATED: Board Membership: Hoffmann-La Roche. Drs Sepehry and Lang have no financial interest or conflict of interest to report. *Money paid to the institution.

REFERENCES

1. Gorelick PB, Scuteri A, Black SE, et al; American Heart Association Stroke Council, Council on Epidemiology and Prevention, Council

- on Cardiovascular Nursing, Council on Cardiovascular Radiology and Intervention, and Council on Cardiovascular Surgery and Anesthesia. **Vascular contributions to cognitive impairment and dementia: a statement for healthcare professionals from the American Heart Association/American Stroke Association.** *Stroke* 2011; 42:2672–713 CrossRef Medline
2. Heringa SM, Reijmer YD, Leemans A, et al; Utrecht Vascular Cognitive Impairment (VCI) Study Group. **Multiple microbleeds are related to cerebral network disruptions in patients with early Alzheimer's disease.** *J Alzheimers Dis* 2014;38:211–21 CrossRef Medline
3. Cordonnier C, van der Flier WM. **Brain microbleeds and Alzheimer's disease: innocent observation or key player?** *Brain* 2011;134: 335–44 CrossRef Medline
4. Kirsch W, McAuley G, Holshouser B, et al. **Serial susceptibility weighted MRI measures brain iron and microbleeds in dementia.** *J Alzheimers Dis* 2009;17:599–609 CrossRef Medline
5. Hommet C, Mondon K, Constans T, et al. **Review of cerebral microangiopathy and Alzheimer's disease: relation between white matter hyperintensities and microbleeds.** *Dement Geriatr Cogn Disord* 2011;32:367–78 CrossRef Medline
6. van der Flier WM. **Clinical aspects of microbleeds in Alzheimer's disease.** *J Neurol Sci* 2012;322:56–58 CrossRef Medline
7. Cordonnier C, van der Flier WM, Sluimer JD, et al. **Prevalence and severity of microbleeds in a memory clinic setting.** *Neurology* 2006; 66:1356–60 CrossRef Medline
8. Goos JD, Kester MI, Barkhof F, et al. **Patients with Alzheimer disease with multiple microbleeds: relation with cerebrospinal fluid biomarkers and cognition.** *Stroke* 2009;40:3455–60 CrossRef Medline
9. Frisoni GB, Fox NC, Jack CR Jr, et al. **The clinical use of structural MRI in Alzheimer disease.** *Nat Rev Neurol* 2010;6:67–77 CrossRef Medline
10. Denk C, Rauscher A. **Susceptibility weighted imaging with multiple echoes.** *J Magn Reson Imaging* 2010;31:185–91 CrossRef Medline
11. Haacke EM, Xu Y, Cheng YC, et al. **Susceptibility weighted imaging (SWI).** *Magn Reson Med* 2004;52:612–18 CrossRef Medline
12. Borenstein M, Hedges L, Higgins J, et al. *Comprehensive Meta-Analysis*. 2nd ed. Englewood, New Jersey: Biostat; 2005
13. Johnson BT. *DSTAT: Software for the Meta-Analytic Review of Research Literatures*. Version 1. Hillsdale, New Jersey: Lawrence Erlbaum Associates; 1993
14. von Elm E, Altman DG, Egger M, et al; STROBE Initiative. **The Strengthening of Reporting of Observational Studies in Epidemiology (STROBE) statement: guidelines for reporting observational studies.** *Epidemiology* 2007;18:800–04 CrossRef Medline
15. Stroup DF, Berlin JA, Morton SC, et al. **Meta-analysis of observational studies in epidemiology: a proposal for reporting—Meta-analysis Of Observational Studies in Epidemiology (MOOSE) group.** *JAMA* 2000;283:2008–12 CrossRef Medline
16. Moher D, Liberati A, Tetzlaff J, et al; PRISMA Group. **Preferred reporting items for systematic reviews and meta-analyses: the PRISMA statement.** *Int J Surg* 2010;8:336–41 CrossRef Medline
17. Begg CB, Mazumdar M. **Operating characteristics of a rank correlation test for publication bias.** *Biometrics* 1994;50:1088–101 CrossRef Medline
18. Egger M, Davey Smith G, Schneider M, et al. **Bias in meta-analysis detected by a simple, graphical test.** *BMJ* 1997;315:629–34 CrossRef Medline
19. Higgins JP, Thompson SG, Deeks JJ, et al. **Measuring inconsistency in meta-analyses.** *BMJ* 2003;327:557–60 CrossRef Medline
20. Nagasawa J, Kiyozaka T, Ikeda K. **Prevalence and clinicoradiological analyses of patients with Alzheimer disease coexisting multiple microbleeds.** *J Stroke Cerebrovasc Dis* 2014;23:2444–49 CrossRef Medline
21. Fukui T, Oowan Y, Yamazaki T, et al. **Prevalence and clinical implication of microbleeds in dementia with Lewy bodies in comparison with microbleeds in Alzheimer's disease.** *Dement Geriatr Cogn Dis Extra* 2013;3:148–60 CrossRef Medline

22. Goos JD, van der Flier WM, Knol DL, et al. **Clinical relevance of improved microbleed detection by susceptibility-weighted magnetic resonance imaging.** *Stroke* 2011;42:1894–900 CrossRef Medline
23. McKhann G, Drachman D, Folstein M, et al. **Clinical diagnosis of Alzheimer's disease: report of the NINCDS-ADRDA Work Group under the auspices of Department of Health and Human Services Task Force on Alzheimer's Disease.** *Neurology* 1984;34:939–44 CrossRef Medline
24. Uetani H, Hirai T, Hashimoto M, et al. **Prevalence and topography of small hypointense foci suggesting microbleeds on 3T susceptibility-weighted imaging in various types of dementia.** *AJNR Am J Neuroradiol* 2013;34:984–89 CrossRef Medline
25. Shams S, Martola J, Granberg T, et al. **Cerebral microbleeds: different prevalence, topography, and risk factors depending on dementia diagnosis—the Karolinska Imaging Dementia Study.** *AJNR Am J Neuroradiol* 2015;36:661–66 CrossRef Medline
26. Shams S, Martola J, Cavallin L, et al. **SWI or T2*: Which MRI sequence to use in the detection of cerebral microbleeds? The Karolinska Imaging Dementia Study.** *AJNR Am J Neuroradiol* 2015;36:1089–95 CrossRef Medline
27. Olazarán J, Ramos A, Boyano I, et al. **Pattern of and risk factors for brain microbleeds in neurodegenerative dementia.** *Am J Alzheimers Dis Other Demen* 2014;29:263–69 CrossRef Medline
28. Benedictus MR, Goos JDC, Binnewijzend MA, et al. **Specific risk factors for microbleeds and white matter hyperintensities in Alzheimer's disease.** *Neurobiol Aging* 2013;34:2488–94 CrossRef Medline
29. Kester MI, Goos JD, Teunissen CE, et al. **Associations between cerebral small-vessel disease and Alzheimer disease pathology as measured by cerebrospinal fluid biomarkers.** *JAMA Neurol* 2014;71:855–62 CrossRef Medline
30. Cordonnier C. **Brain microbleeds: more evidence, but still a clinical dilemma.** *Curr Opin Neurol* 2011;24:69–74 CrossRef Medline
31. Whitwell JL, Kantarci K, Weigand SD, et al. **Microbleeds in atypical presentations of Alzheimer's disease: a comparison to dementia of the Alzheimer's type.** *J Alzheimers Dis* 2015;45:1109–17 CrossRef Medline
32. Staekenborg SS, Koedam ELGE, Henneman WJP, et al. *Progression of Mild Cognitive Impairment to Dementia Contribution of Cerebrovascular Disease Compared with Medial Temporal Lobe Atrophy.* 4th ed. Philadelphia: Lippincott Williams and Wilkins; 2009:1269–74
33. Martinez-Ramirez S, Greenberg SM, Viswanathan A. **Cerebral microbleeds: overview and implications in cognitive impairment.** *Alzheimers Res Ther* 2014;6:33 CrossRef Medline
34. Poels MM, Ikram MA, van der Lugt A, et al. **Cerebral microbleeds are associated with worse cognitive function: the Rotterdam Scan Study.** *Neurology* 2012;78:326–33 CrossRef Medline
35. van Norden AG, van Uden IW, de Laat KF, et al. **Cognitive function in small vessel disease: the additional value of diffusion tensor imaging to conventional magnetic resonance imaging: the RUN DMC study.** *J Alzheimers Dis* 2012;32:667–76 CrossRef Medline
36. Pettersen JA, Sathiyamoorthy G, Gao FQ, et al. **Microbleed topography, leukoariosis, and cognition in probable Alzheimer disease from the Sunnybrook dementia study.** *Arch Neurol* 2008;65:790–95 CrossRef Medline
37. Sperling R, Salloway S, Brooks DJ, et al. **Amyloid-related imaging abnormalities in patients with Alzheimer's disease treated with bapineuzumab: a retrospective analysis.** *Lancet Neurol* 2012;11:241–49 CrossRef Medline
38. Werring DJ, Sperling R. **Inflammatory cerebral amyloid angiopathy and amyloid-modifying therapies: variations on the same ARIA?** *Ann Neurol* 2013;73:439–41 CrossRef Medline
39. Brundel M, Heringa SM, de Bresser J, et al. **High prevalence of cerebral microbleeds at 7Tesla MRI in patients with early Alzheimer's disease.** *J Alzheimers Dis* 2012;31:259–63 CrossRef Medline
40. Nagata K, Takano D, Yamazaki T, et al. **Cerebrovascular lesions in elderly Japanese patients with Alzheimer's disease.** *J Neurol Sci* 2012;322:87–91 CrossRef Medline
41. Nakata-Kudo Y, Mizuno T, Yamada K, et al. **Microbleeds in Alzheimer disease are more related to cerebral amyloid angiopathy than cerebrovascular disease.** *Dement Geriatr Cogn Disord* 2006;22:8–14 CrossRef Medline
42. Park JH, Seo SW, Kim C, et al. **Pathogenesis of cerebral microbleeds: in vivo imaging of amyloid and subcortical ischemic small vessel disease in 226 individuals with cognitive impairment.** *Ann Neurol* 2013;73:584–93 CrossRef Medline
43. Qiu C, Cotch MF, Sigurdsson S, et al. **Cerebral microbleeds, retinopathy, and dementia: the AGES-Reykjavik Study.** *Neurology* 2010;75:2221–28 CrossRef Medline
44. Staekenborg SS, Koedam EL, Henneman WJ, et al. **Progression of mild cognitive impairment to dementia: contribution of cerebrovascular disease compared with medial temporal lobe atrophy.** *Stroke* 2009;40:1269–74 CrossRef Medline
45. van der Vlies AE, Goos JD, Barkhof F, et al. **Microbleeds do not affect rate of cognitive decline in Alzheimer disease.** *Neurology* 2012;79:763–69 CrossRef Medline
46. Yates PA, Desmond PM, Phal PM, et al. **Incidence of cerebral microbleeds in preclinical Alzheimer disease.** *Neurology* 2014;82:1266–73 CrossRef Medline
47. Zonneveld HI, Goos JD, Wattjes MP, et al. **Prevalence of cortical superficial siderosis in a memory clinic population.** *Neurology* 2014;82:698–704 CrossRef Medline
48. Atri A, Locascio JJ, Lin JM, et al. **Prevalence and effects of lobar microhemorrhages in early-stage dementia.** *Neurodegener Dis* 2005;2:305–12 CrossRef Medline
49. Guro ME, Viswanathan A, Gidicsin C, et al. **Cerebral amyloid angiopathy burden associated with leukoariosis: a positron emission tomography/magnetic resonance imaging study.** *Ann Neurol* 2013;73:529–36 CrossRef Medline
50. Danve A, Grafe M, Deodhar A. **Amyloid beta-related angiitis: a case report and comprehensive review of literature of 94 cases.** *Semin Arthritis Rheum* 2014;44:86–92 CrossRef Medline
51. Ghostine S, Raghavan R, Khanlou N, et al. **Cerebral amyloid angiopathy: micro-haemorrhages demonstrated by magnetic resonance susceptibility-weighted imaging.** *Neuropathol Appl Neurobiol* 2009;35:116–19 CrossRef Medline
52. Henneman WJ, Sluimer JD, Cordonnier C, et al. **MRI biomarkers of vascular damage and atrophy predicting mortality in a memory clinic population.** *Stroke* 2009;40:492–98 CrossRef Medline
53. Hilal S, Saini M, Tan CS, et al. **Ankle-brachial index, cognitive impairment and cerebrovascular disease in a Chinese population.** *Neuroepidemiology* 2014;42:131–38 CrossRef Medline
54. Kimberly WT, Gilson A, Rost NS, et al. **Silent ischemic infarcts are associated with hemorrhage burden in cerebral amyloid angiopathy.** *Neurology* 2009;72:1230–35 CrossRef Medline
55. Ku HL, Chi NF. **Cerebral lobar microhemorrhages detection by high magnetic field susceptibility weighted image: a potential diagnostic neuroimage technique of Alzheimer's disease.** *Med Hypotheses* 2011;76:840–42 CrossRef Medline
56. Kuijf HJ, Brundel M, de Bresser J, et al. **Semi-automated detection of cerebral microbleeds on 3.0 T MR images.** *PLoS One* 2013;8:e66610 CrossRef Medline
57. Ii Y, Maeda M, Kida H, et al. **In vivo detection of cortical microinfarcts on ultrahigh-field MRI.** *J Neuroimaging* 2013;23:28–32 CrossRef Medline
58. van Assema DM, Goos JD, van der Flier WM, et al. **No evidence for additional blood-brain barrier P-glycoprotein dysfunction in Alzheimer's disease patients with microbleeds.** *J Cereb Blood Flow Metab* 2012;32:1468–71 CrossRef Medline
59. Van Rooden S, Goos JD, van Opstal AM, et al. **Increased number of microinfarcts in Alzheimer disease at 7-T MR imaging.** *Radiology* 2014;270:205–11 CrossRef Medline
60. van Veluw SJ, Heringa SM, Kuijf HJ, et al. **Cerebral cortical micro-**

- infarcts at 7Tesla MRI in patients with early Alzheimer's disease.** *J Alzheimers Dis* 2014;39:163–67 CrossRef Medline
61. Vidal JS, Sigurdsson S, Jonsdottir MK, et al. **Coronary artery calcium, brain function and structure: the AGES-Reykjavik Study.** *Stroke* 2010;41:891–97 CrossRef Medline
62. Wollenweber FA, Buerger K, Mueller C, et al. **Prevalence of cortical superficial siderosis in patients with cognitive impairment.** *J Neurol* 2014;261:277–82 CrossRef Medline
63. Yates PA, Sirisriro R, Villemagne VL, et al; AIBL Research Group. **Cerebral microhemorrhage and brain β -amyloid in aging and Alzheimer disease.** *Neurology* 2011;77:48–54 CrossRef Medline
64. Yokoyama S, Kajiya Y, Yoshinaga T, et al. **Imaging discrepancies between magnetic resonance imaging and brain perfusion single-photon emission computed tomography in the diagnosis of Alzheimer's disease, and verification with amyloid positron emission tomography.** *Psychogeriatrics* 2014;14:110–17 CrossRef Medline

Diagnostic Significance of Cortical Superficial Siderosis for Alzheimer Disease in Patients with Cognitive Impairment

Y. Inoue, M. Nakajima, H. Uetani,  T. Hirai, M. Ueda, M. Kitajima, D. Utsunomiya, M. Watanabe, M. Hashimoto, M. Ikeda, Y. Yamashita, and Y. Ando



ABSTRACT

BACKGROUND AND PURPOSE: Because the diagnostic significance of cortical superficial siderosis for Alzheimer disease and the association between cortical superficial siderosis and the topographic distribution of cerebral microbleeds have been unclear, we investigated the association between cortical superficial siderosis and clinicoradiologic characteristics of patients with cognitive impairment.

MATERIALS AND METHODS: We studied 347 patients (217 women, 130 men; mean age, 74 ± 9 years) who visited our memory clinic and underwent MR imaging (3T SWI). We analyzed the association between cortical superficial siderosis and the topographic distribution of cerebral microbleeds plus clinical characteristics including types of dementia. We used multivariate logistic regression analysis to determine the diagnostic significance of cortical superficial siderosis for Alzheimer disease.

RESULTS: Twelve patients (3.5%) manifested cortical superficial siderosis. They were older ($P = .026$) and had strictly lobar cerebral microbleeds significantly more often than did patients without cortical superficial siderosis (50.0% versus 19.4%, $P = .02$); the occurrence of strictly deep and mixed cerebral microbleeds, however, did not differ in the 2 groups. Alzheimer disease was diagnosed in 162 (46.7%) patients. Of these, 8 patients (4.9%) had cortical superficial siderosis. In the multivariate logistic regression analysis for the diagnosis of Alzheimer disease, lacunar infarcts were negatively and independently associated with Alzheimer disease ($P = .007$).

CONCLUSIONS: Although cortical superficial siderosis was associated with a strictly lobar cerebral microbleed location, it was not independently associated with Alzheimer disease in a memory clinic setting. Additional studies are required to investigate the temporal changes of these cerebral amyloid angiopathy–related MR imaging findings.

ABBREVIATIONS: AD = Alzheimer disease; CAA = cerebral amyloid angiopathy; cSS = cortical superficial siderosis; DLB = dementia with Lewy bodies; MBs = cerebral microbleeds; MCI = mild cognitive impairment

Cortical superficial siderosis (cSS) is characterized by linear hypointensities on the surface of cerebral cortex gyri on T2*-weighted gradient-echo MR imaging or SWI.^{1,2} cSS reflects subtle hemorrhages from amyloid-affected fragile cortical or leptomeningeal vessels and occurs often in patients with cerebral amyloid angiopathy (CAA); associations of cSS with repeat lobar hemorrhages have been reported.^{3–5} Several studies showed that patients with cognitive impairment manifested a higher prevalence of cSS compared with the general population.^{6,7} cSS, along with lobar cerebral microbleeds

(MBs), was described as a characteristic neuroimaging marker of CAA.^{8,9}

Alzheimer disease (AD) is the most common cause of dementia in the elderly, and CAA is assumed to have a pivotal function in the underlying pathogenesis of AD.¹⁰ In the aforementioned studies, cSS was associated with the presence of MBs, and the authors speculated that a relatively high prevalence of cSS in patients with AD indicates this pathogenesis.^{6,7} We therefore hypothesized that cSS itself may be a significant diagnostic marker of AD and that lobar MBs would be observed more frequently in patients with cSS than in patients without cSS.

The primary aim of the present study was thus to clarify the diagnostic significance of cSS for AD, with the secondary aim being to explore the radiologic markers of small-vessel disease in relation to cSS in patients with cognitive impairment.

MATERIALS AND METHODS

Study Population

This study consisted of a subanalysis of a prospective clinicoradiologic study described previously.¹¹ Consecutive patients who

Received January 12, 2015; accepted after revision June 18.

From the Departments of Neurology (Y.I., M.N., M.U., M.W., Y.A.), Diagnostic Radiology (H.U., T.H., M.K., D.U., Y.Y.), and Psychiatry and Neuropathobiology (M.H., M.I.), Graduate School of Medical Sciences, Kumamoto University, Kumamoto, Japan.

Please address correspondence to Yasuteru Inoue, MD, Department of Neurology, Graduate School of Medical Sciences, Kumamoto University, 1-1-1 Honjo, Kumamoto 860-8556, Japan; e-mail: yinoue@fc.kuh.kumamoto-u.ac.jp

 Indicates article with supplemental on-line table.

<http://dx.doi.org/10.3174/ajnr.A4496>

attended the Dementia Clinic of the Department of Neuropsychiatry, Kumamoto University Hospital, were recruited prospectively from January 2008 to February 2010. The Ethics Committee of Kumamoto University Hospital approved this study. The patients received information about the purpose and method of the study, and written informed consent for participation in the study was obtained from them or their caregivers.

Patients with cognitive impairment associated with posttraumatic brain injury, brain tumor, idiopathic normal pressure hydrocephalus, history of psychiatric diseases or substance abuse, and neurodegenerative diseases, including Pick disease, corticobasal degeneration, and spinocerebellar degeneration, were excluded from this study. Patients whose MR images had severe motion artifacts and patients who did not provide informed consent were also excluded.

All patients received independent neuropsychological evaluations conducted by 2 neuropsychiatrists (M.I., M.H.). Neuropsychological tests including the Mini-Mental State Examination, brain MR imaging, and SPECT were used for diagnosing dementia. Diagnostic criteria included the following: for AD, criteria from the National Institute of Neurological and Communicative Disorders and Stroke–Alzheimer Disease and Related Disorders Association¹²; for vascular dementia, criteria from the National Institute of Neurological Disorders and Stroke–Association Internationale pour la Recherche et l’Enseignement en Neurosciences¹³; for mild cognitive impairment (MCI), general criteria from the International Working Group on Mild Cognitive Impairment¹⁴; for dementia with Lewy bodies (DLB), clinical criteria from the Consortium on Dementia with Lewy Bodies¹⁵; and for frontotemporal lobar dementia, the Lund-Manchester criteria for behavioral variant frontotemporal lobar dementia, semantic dementia, or progressive nonfluent aphasia.¹⁶ If results of all clinical investigations were normal, patients were classified in a subgroup labeled “subjective memory symptoms.”

MR Imaging Protocol

MR imaging was performed with a 3T whole-body system (Magnetom Trio; Siemens, Erlangen, Germany). Axial SWI, axial FLAIR, axial T2-weighted turbo spin-echo sequences, 3D T1-weighted magnetization-prepared rapid acquisition of gradient echo sequences, diffusion-weighted imaging, MR spectroscopy, and MRA were performed by using the same section thickness, matrix, and parameters as described previously.¹¹

Evaluation of cSS and Other Radiologic Data

We defined cSS as linear hypointensities on the surface of cerebral cortex gyri on SWI; cSS related to previous symptomatic subarachnoid hemorrhage, traumatic subdural hematoma, or intracranial surgery was not included. cSS was classified as focal (restricted to 3 sulci) or disseminated (≥ 4 sulci).

We defined MBs as small (< 10 mm in diameter), homogeneous, round foci of low signal intensity. We excluded symmetric hypointensities in the globi pallidi and dentate nuclei, which we identified as physiologic calcifications or iron deposits; we also excluded hypointense signals inside a lesion that were consistent with infarcts. Lacunar infarcts and white matter hyperintensities were defined according to criteria reported previously.^{11,17,18} The distribution of MBs

was categorized as lobar (frontal, temporal, parietal, and occipital) or deep (thalamoganglionic, brain stem, and cerebellum).

Patients with MBs were divided into 3 groups according to the microbleed distribution. The strictly lobar group had MBs localized exclusively in the lobar region. The strictly deep group had MBs located only in the thalamoganglionic and infratentorial regions. The mixed group had MBs throughout both lobar and deep regions. All radiologic findings were assessed by 2 experienced neuroradiologists (H.U., T.H.) who were blinded to the clinical information.

Clinical Data Collection

Baseline clinical information, including age, sex, history of hypertension, length of education, and Mini-Mental State Examination results, was recorded at registration. Hypertension was defined as a history of hypertension or prescription of antihypertensive medications.

Statistical Analyses

We compared baseline demographics and clinical characteristics for patients with any cSS and patients with no cSS. Categorical data were evaluated by using the χ^2 test and the Fisher 2-tailed exact test. Continuous variables were compared by using the Mann-Whitney *U* test. We next conducted multivariate logistic regression analysis to investigate the predictors for diagnosing AD. The independent variables included age, sex, hypertension, length of education, distribution of MBs (strictly lobar, strictly deep, or mixed), lacunar infarcts, white matter hyperintensities, and cSS. Backward stepwise logistic regression analysis was performed by adjusting for age,^{19–21} sex,²² length of education,²³ and variables that were automatically selected in a backward stepwise selection method. We performed a backward selection procedure for each outcome by using $P > .10$ of the likelihood ratio test for exclusion of variables. The OR and 95% CI were obtained. The statistical significance level was set at $P < .05$. In addition, we calculated the sensitivity, specificity, positive predictive value, and negative predictive value of cSS for the clinical diagnosis of AD. Statistical analyses were performed by using JMP 9.0 statistical software (SAS Institute, Cary, North Carolina).

RESULTS

Prevalence of cSS

A total of 347 patients (217 women, 130 men; mean age, 74 ± 9 years) with cognitive impairment visited our hospital from January 2008 to February 2010. Of these patients, 12 (3.5%) had cSS.

Clinical Characteristics Related to cSS

Table 1 provides demographic and clinical characteristics of the patients. Patients with cSS were older ($P = .026$) compared with patients without cSS. No significant differences were observed in the occurrence of cSS across different types of dementia ($P = .337$), and a bivariate analysis also demonstrated no differences between patients with and without AD ($P = .239$). Sensitivity, specificity, positive predictive value, and negative predictive value of cSS for the clinical diagnosis of AD were 4.9%, 97.8%, 66.7%, and 54.0%, respectively (4 patients had cSS but no AD, 8 patients had both cSS and AD, 181 patients had no cSS or AD, and 154 patients had AD but no cSS).

Table 1: Demographic and clinical characteristics of patients with or without cSS

Parameter	No. of Patients (%)			P Value
	Total	Any cSS	No cSS	
No. of patients	347	12	335	
Age (yr) (mean)	74 ± 9	79 ± 5	74 ± 9	.026
No. of women	217 (62.5%)	6 (50.0%)	211 (63.0%)	.361
No. of patients with hypertension	160 (46.1%)	9 (75.0%)	151 (45.1%)	.073
Length of education (yr) (mean) (range)	11 (9–12)	11 (9–13)	11 (9–12)	.506
MMSE (mean)	21 ± 5	19 ± 7	21 ± 5	.457
Types of dementia				.337
AD	162 (46.7%)	8 (66.7%)	154 (46.0%)	
DLB	41 (11.8%)	1 (8.3%)	40 (11.9%)	
FTLD	33 (9.5%)	0 (0%)	33 (9.9%)	
VaD	28 (8.1%)	1 (8.3%)	27 (8.1%)	
MCI	51 (14.7%)	2 (16.7%)	49 (14.6%)	
SC	32 (9.2%)	0 (0%)	32 (9.6%)	

Note:—MMSE indicates Mini-Mental State Examination; FTLD, frontotemporal lobar dementia; VaD, vascular dementia; SC, subjective symptoms.

Table 2: Radiologic characteristics of patients with or without cSS

Type of MBs	No. of Patients (%)			P Value
	Total	Any cSS	No cSS	
No. of patients	347	12	335	
Lobar MBs				
Frontal	69 (19.9%)	7 (58.3%)	62 (18.5%)	.003
Temporal	65 (18.7%)	8 (66.7%)	57 (17.0%)	<.001
Parietal	78 (22.5%)	7 (58.3%)	71 (21.2%)	.007
Occipital	63 (18.2%)	7 (58.3%)	56 (16.7%)	.002
Deep MBs				
Thalamoganglionic	62 (17.9%)	3 (25.0%)	59 (17.6%)	.456
Brain stem	32 (9.2%)	3 (25.0%)	29 (8.7%)	.088
Cerebellum	48 (13.8%)	3 (25.0%)	45 (13.4%)	.222
Topographic distribution of MBs				
Strictly lobar	71 (20.5%)	6 (50.0%)	65 (19.4%)	.020
Strictly deep	10 (2.9%)	0 (0%)	10 (3.0%)	1.00
Mixed	79 (22.8%)	5 (41.7%)	74 (22.1%)	.154
No MBs	187 (53.9%)	1 (8.3%)	186 (55.5%)	.002
Lacunar infarcts	71 (20.5%)	6 (50.0%)	65 (19.4%)	.020
WMH (mean) ^a	1.5 ± 0.8	1.9 ± 0.8	1.4 ± 0.8	.053
0	32 (9.2%)	0 (0%)	32 (9.6%)	
1	166 (47.8%)	4 (33.3%)	162 (48.4%)	
2	107 (30.8%)	5 (41.7%)	102 (30.4%)	
3	42 (12.1%)	3 (25.0%)	39 (11.6%)	

Note:—WMH indicates white matter hyperintensities.

^a WMH were graded according to the scale of Fazekas et al¹⁷: 0, absent; 1, punctate; 2, early confluent; and 3, confluent.

Location and Topographic Distribution of MBs

Strictly lobar MBs were observed more frequently in patients with cSS than in patients without cSS ($P = .020$), whereas the 2 groups did not differ with regard to the occurrence of strictly deep MBs ($P = 1.00$) and mixed MBs ($P = .154$). MBs in each cerebral lobe (frontal [$P = .003$], temporal [$P < .001$], parietal [$P = .007$], and occipital [$P = .002$]) had a significant association with the presence of cSS. However, patients with cSS and those without cSS showed no significant differences in the presence of thalamoganglionic MBs ($P = .456$), brain stem MBs ($P = .088$), and cerebellar MBs ($P = .222$) (Table 2). We also performed a separate analysis of demographic and clinicoradiologic characteristics in patients with AD and found similar tendencies in location and topographic distribution of MBs for that whole population (On-line Table). Among patients with AD, strictly lobar MBs were ob-

served more frequently in patients with cSS than in patients without cSS ($P = .004$). MBs in each cerebral lobe (frontal [$P = .040$], temporal [$P < .001$], parietal [$P = .040$], and occipital [$P = .006$]) also had a significant association with the presence of cSS.

Clinicoradiologic Characteristics of Patients with cSS

We further investigated the clinicoradiologic characteristics of 12 patients with cSS (6 women, 6 men; mean age, 79 ± 5 years) (Table 3). Of these, AD was diagnosed in 8 patients (66.7%); DLB, in 1 patient (8.3%); and MCI, in 2 patients (16.7%). cSS was observed in 22 cerebral lobes, and its location corresponded to locations of MBs in 13 lobes (72.2%). We noted a tendency of cSS to occur in temporal and occipital lobes, and the distribution was focal in 7 patients (58.3%) and disseminated in 5 patients (41.7%). Six patients (50%) had strictly lobar MBs, 5 patients (41.7%) had mixed MBs, no patient with cSS had strictly deep MBs, and 1 patient (8.3%) had no MBs (case 2, Table 3). Four patients (33.3%) were classified as having grade 1 white matter hyperintensities; 5 patients (41.7%), grade 2 white matter hyperintensities; and 3 patients (25.0%), grade 3 white matter hyperintensities. No correlations between age-related white matter change rating scores and the location of cSS were found.

Relationship among cSS, MBs, and AD

Table 4 shows the results of multivariate logistic regression analysis for the diagnosis of AD. In the multivariate model, lacunar infarcts (OR, 0.46; 95% CI, 0.25–0.81; $P = .007$) were negatively and independently associated with AD, and the presence of cSS was not associated with AD (OR, 2.99; 95% CI, 0.88–12.0; $P = .08$).

DISCUSSION

This study is the first to investigate the diagnostic significance of cSS for AD and the relationships between cSS and the location of MBs in patients with cognitive impairment. The major new finding was that patients with cSS had strictly lobar MBs significantly more often than patients without cSS.

With respect to spatial distributions of MBs, past histopathologic studies of patients with intracerebral hemorrhage revealed that strictly lobar MBs strongly suggested CAA.²⁴ The population-based Rotterdam Scan Study showed a tendency for MBs to be located in the lobar region, especially in the temporal lobes.²⁵ A

Table 3: Clinoradiologic characteristics of patients with cSS

Subject No.	Type of Dementia	Age (yr)	Sex	Location of cSS	Topographic Distribution				Topographic Distribution of MBs	WMH ^a	ARWMC Rating Scale ^b (R/L)		
					Frontal	Temporal	Parietal	Occipital			Frontal	Temporal	Parieto-Occipital
1	AD	79	M	Right frontal	—	—	+	+	Mixed	1	1/1	1/0	1/1
2	AD	81	F	Left occipital	—	—	—	—	No MBs	2	1/0	2/2	2/2
3	AD	84	M	Right occipital	—	+	—	—	Strictly lobar	3	2/2	3/3	2/1
4	AD	83	F	Left temporal	+	+	—	—	Strictly lobar	2	2/2	2/2	2/2
5	AD	78	F	Right temporal	—	+	+	+	Strictly lobar	1	0/0	1/1	0/0
6	AD	80	M	Right frontal	+	+	+	+	Strictly lobar	2	2/2	2/2	2/2
7	AD	78	F	Right temporal	+	+	+	+	Strictly lobar	1	0/1	1/0	1/1
8	AD	70	F	Right frontal	+	+	—	+	Strictly lobar	1	1/1	1/1	1/1
9	DLB	69	F	Right parietal	+	—	+	—	Mixed	2	2/2	2/2	2/2
10	VaD	87	M	Right occipital	+	+	—	+	Mixed	2	1/1	2/2	2/2
11	MCI	82	M	Right temporal	—	—	+	—	Mixed	3	3/3	3/2	3/3
12	MCI	80	M	Left occipital	+	+	+	+	Mixed	3	3/3	3/3	3/3

Note:—ARWMC indicates age-related white matter changes; R/L, right/left; WMH, white matter hyperintensities; VaD, vascular dementia.

^a WMH were graded according to the scale of Fazekas et al¹⁷: 0, absent; 1, punctate; 2, early confluent; and 3, confluent.

^b ARWMC rating scale¹⁸: 0, no lesions (including symmetric, well-defined caps, or bands); 1, focal lesions; 2, beginning confluence of lesions; 3, diffuse involvement of the entire region, with or without involvement of U fibers.

Table 4: Multivariate logistic regression analysis for AD^a

Parameter	OR (95% CI)	P Value
Age (per 1-yr increase)	0.99 (0.96–1.02)	.400
Female sex	0.88 (0.55–1.41)	.593
Education (per 1-yr increase)	1.72 (0.43–7.02)	.448
Lacunar infarcts	0.46 (0.25–0.81)	.007
cSS	2.99 (0.88–12.0)	.080

^a The model was adjusted for age, sex, length of education, and variables that showed a relationship to AD in a backward stepwise selection method.

case-control and memory clinic–based cross-sectional study including patients with AD showed that the microbleed topography was significantly predominant in the occipital region.²⁶ Our study indicated that strictly lobar MBs are closely related to cSS, which was shown to be a marker of CAA. This tendency also persisted among patients with AD with or without cSS, 2 groups who were barely distinguishable from each other except for a higher prevalence of a lobar microbleed location in patients with AD and cSS.

With respect to the diagnostic significance of cSS for AD, though AD was diagnosed in most patients with cSS, multivariate logistic regression analysis showed that neither cSS nor MBs in any location were independent significant predictors for the diagnosis of AD. An explanation of this result is that CAA pathogenesis also occurs in patients with dementias other than AD. Other histopathologic studies reported CAA in patients with DLB and vascular dementia and a low prevalence of CAA in patients with frontotemporal lobar dementia.^{27–29} MCI was reportedly a transitional state of AD,³⁰ so our patients with cognitive impairment may have had CAA pathologic features. Thus, the similar occurrence of cSS and pathologic findings of CAA in patients with cognitive impairment again indicated the same underlying pathophysiologic mechanisms.

As an interesting finding, 1 female patient had AD and cSS without MBs in the present study, whereas all other patients manifested both cSS and MBs. As with convexity subarachnoid hemorrhage, cSS has causes other than CAA: posterior reversible leukoencephalopathy syndrome, reversible cerebral vasoconstriction syndrome, and lupus vasculitis.³¹ One study indicated that cSS or convexity subarachnoid hemorrhage does not always reflect CAA pathogenesis.³¹ Given the older age and impaired cognition of our patients, however, most cSS in our study presumably resulted from CAA, as in another study that found CAA in >80% of patients with AD.³² A cross-sectional study including patients with probable or definite CAA, diagnosed on the basis of the Boston criteria,³³ found inverse associations among the severity of cSS, number of MBs, and *apolipoprotein E ε4*.³⁴ These authors also speculated that cSS may arise from vasculopathic mechanisms different from those associated with CAA-related microbleeds.³⁴ Because this patient in our study had no history of possible underlying causes of cSS other than CAA, cSS may have manifested as an initial radiologic finding of CAA.

Limitations of the present study included using a relatively small population and a heterogeneous patient population without AD (DLB, frontotemporal lobar dementia, vascular dementia, MCI, and subjective symptoms) as a reference group in the multivariate logistic regression analysis.

Our study results indicated that cSS was associated with a lobar location of MBs and may be an initial radiologic finding of CAA in patients with cognitive impairment. Additional prospective studies to investigate temporal changes of these CAA-related MR imaging findings may help in understanding the mechanisms of cognitive decline.

CONCLUSIONS

The prevalence of cSS was 3.9% in our memory clinic. Most patients with cSS were diagnosed as having AD, and the specificity of cSS for the clinical diagnosis of AD was high. Strictly lobar MBs were observed more frequently in patients with cSS than in patients without cSS.

Disclosures: Mitsuharu Ueda—UNRELATED: Grants/Grants Pending: Grants-in-Aid for Science Research from the Ministry of Education, Culture, Sports, Science and Technology of Japan (No. 25870541). *Manabu Ikeda—UNRELATED: Grants/Grants Pending: Daiichi Sankyo, Eisai, FUJIFILM RI, Janssen Pharmaceuticals, Nihon Medi-Physics, Novartis, Pfizer, Takeda, Tsumura. *Comments: as the chairman of the department; Payment for Lectures (including service on Speakers Bureaus): Daiichi Sankyo, Eisai, FUJIFILM RI, Janssen Pharmaceuticals, Nihon Medi-Physics, Novartis, Pfizer, Takeda, Tsumura, MSD, Ono Pharmaceutical. *Money paid to the institution.

REFERENCES

1. Kumar N. Neuroimaging in superficial siderosis: an in-depth look. *AJNR Am J Neuroradiol* 2010;31:5–14 CrossRef Medline
2. Linn J, Herms J, Dichgans M, et al. Subarachnoid hemosiderosis and superficial cortical hemosiderosis in cerebral amyloid angiopathy. *AJNR Am J Neuroradiol* 2008;29:184–86 CrossRef Medline
3. Feldman HH, Maia LF, Mackenzie IR, et al. Superficial siderosis: a potential diagnostic marker of cerebral amyloid angiopathy in Alzheimer disease. *Stroke* 2008;39:2894–97 CrossRef Medline
4. Linn J, Wollenweber FA, Lummler N, et al. Superficial siderosis is a warning sign for future intracranial hemorrhage. *J Neurol* 2013;260:176–81 CrossRef Medline
5. Charidimou A, Peeters AP, Jäger R, et al. Cortical superficial siderosis and intracerebral hemorrhage risk in cerebral amyloid angiopathy. *Neurology* 2013;81:1666–73 CrossRef Medline
6. Zonneveld HI, Goos JD, Wattjes MP, et al. Prevalence of cortical superficial siderosis in a memory clinic population. *Neurology* 2014;82:698–704 CrossRef Medline
7. Wollenweber FA, Buerger K, Mueller C, et al. Prevalence of cortical superficial siderosis in patients with cognitive impairment. *J Neurol* 2014;261:277–82 CrossRef Medline
8. Charidimou A, Gang Q, Werring DJ. Sporadic cerebral amyloid angiopathy revisited: recent insights into pathophysiology and clinical spectrum. *J Neurol Neurosurg Psychiatry* 2012;83:124–37 CrossRef Medline
9. Ellis RJ, Olichney JM, Thal LJ, et al. Cerebral amyloid angiopathy in brains of patients with Alzheimer's disease: the CERAD experience, part XV. *Neurology* 1996;46:1592–96 CrossRef Medline
10. Yamada M. Risk factors for cerebral amyloid angiopathy in the elderly. *Ann N Y Acad Sci* 2002;977:37–44 CrossRef Medline
11. Uetani H, Hirai T, Hashimoto M, et al. Prevalence and topography of small hypointense foci suggesting microbleeds on 3T susceptibility-weighted imaging in various types of dementia. *AJNR Am J Neuroradiol* 2013;34:984–89 CrossRef Medline
12. McKhann G, Drachman D, Folstein M, et al. Clinical diagnosis of Alzheimer's disease: report of the NINCDS-ADRDA Work Group under the auspices of Department of Health and Human Services Task Force on Alzheimer's Disease. *Neurology* 1984;34:939–44 CrossRef Medline
13. Román GC, Tatemichi TK, Erkinjuntti T, et al. Vascular dementia: diagnostic criteria for research studies—report of the NINDS-AIREN International Workshop. *Neurology* 1993;43:250–60 CrossRef Medline
14. Winblad B, Palmer K, Kivipelto M, et al. Mild cognitive impairment beyond controversies—towards a consensus: report of the International Working Group on Mild Cognitive Impairment. *J Intern Med* 2004;256:240–46 CrossRef Medline
15. McKeith IG, Galasko D, Kosaka K, et al. Consensus guidelines for the clinical and pathologic diagnosis of dementia with Lewy bodies (DLB): report of the consortium on DLB international workshop. *Neurology* 1996;47:1113–24 CrossRef Medline
16. Neary D, Snowden JS, Gustafson L, et al. Frontotemporal lobar degeneration: a consensus on clinical diagnostic criteria. *Neurology* 1998;51:1546–54 CrossRef Medline
17. Fazekas F, Chawluk JB, Alavi A, et al. MR signal abnormalities at 1.5 T in Alzheimer's dementia and normal aging. *AJR Am J Roentgenol* 1987;149:351–56 CrossRef Medline
18. Wahlund LO, Barkhof F, Fazekas F, et al; European Task Force on Age-Related White Matter Changes. A new rating scale for age-related white matter changes applicable to MRI and CT. *Stroke* 2001;32:1318–22 CrossRef Medline
19. Evans DA, Funkenstein HH, Albert MS, et al. Prevalence of Alzheimer's disease in a community population of older persons: higher than previously reported. *JAMA* 1989;262:2551–56 CrossRef Medline
20. Jorm AF, Korten AE, Henderson AS. The prevalence of dementia: a quantitative integration of the literature. *Acta Psychiatr Scand* 1987;76:465–79 CrossRef Medline
21. Rocca WA, Amaducci LA, Schoenberg BS. Epidemiology of clinically diagnosed Alzheimer's disease. *Ann Neurol* 1986;19:415–24 CrossRef Medline
22. Gao S, Hendrie HC, Hall KS, et al. The relationships between age, sex, and the incidence of dementia and Alzheimer disease: a meta-analysis. *Arch Gen Psychiatry* 1998;55:809–15 CrossRef Medline
23. Lindsay J, Laurin D, Verreault R, et al. Risk factors for Alzheimer's disease: a prospective analysis from the Canadian Study of Health and Aging. *Am J Epidemiol* 2002;156:445–53 CrossRef Medline
24. Fazekas F, Kleinert R, Roob G, et al. Histopathologic analysis of foci of signal loss on gradient-echo T2*-weighted MR images in patients with spontaneous intracerebral hemorrhage: evidence of microangiopathy-related microbleeds. *AJNR Am J Neuroradiol* 1999;20:637–42 Medline
25. Mesker DJ, Poels MM, Ikram MA, et al. Lobar distribution of cerebral microbleeds: the Rotterdam Scan Study. *Arch Neurol* 2011;68:656–59 CrossRef Medline
26. Shams S, Martola J, Granberg T, et al. Cerebral microbleeds: different prevalence, topography, and risk factors depending on dementia diagnosis—the Karolinska Imaging Dementia Study. *AJNR Am J Neuroradiol* 2015;36:661–66 CrossRef Medline
27. Esiri MM, Wilcock GK. Cerebral amyloid angiopathy in dementia and old age. *J Neurol Neurosurg Psychiatry* 1986;49:1221–26 CrossRef Medline
28. De Reuck J, Deramecourt V, Cordonnier C, et al. Prevalence of small cerebral bleeds in patients with a neurodegenerative dementia: a neuropathological study. *J Neurol Sci* 2011;300:63–66 CrossRef Medline
29. De Reuck J, Deramecourt V, Cordonnier C, et al. Detection of microbleeds in post-mortem brains of patients with frontotemporal lobar degeneration: a 7.0-Tesla magnetic resonance imaging study with neuropathological correlates. *Eur J Neurol* 2012;19:1355–60 CrossRef Medline
30. Markesbery WR. Neuropathologic alterations in mild cognitive impairment: a review. *J Alzheimers Dis* 2010;19:221–28 CrossRef Medline
31. Kumar S, Goddeau RP Jr, Selim MH, et al. Atraumatic convexal subarachnoid hemorrhage: clinical presentation, imaging patterns, and etiologies. *Neurology* 2010;74:893–99 CrossRef Medline
32. Pettersen JA, Sathiyamoorthy G, Gao FQ, et al. Microbleed topography, leukoariosis, and cognition in probable Alzheimer disease from the Sunnybrook dementia study. *Arch Neurol* 2008;65:790–95 CrossRef Medline
33. Knudsen KA, Rosand J, Karluk D, et al. Clinical diagnosis of cerebral amyloid angiopathy: validation of the Boston criteria. *Neurology* 2001;56:537–39 CrossRef Medline
34. Shoamanesh A, Martinez-Ramirez S, Oliveira-Filho J, et al. Interrelationship of superficial siderosis and microbleeds in cerebral amyloid angiopathy. *Neurology* 2014;83:1838–43 CrossRef Medline

Acute Preoperative Infarcts and Poor Cerebrovascular Reserve Are Independent Risk Factors for Severe Ischemic Complications following Direct Extracranial-Intracranial Bypass for Moyamoya Disease

M.U. Antonucci, T.C. Burns, T.M. Pulling, J. Rosenberg, M.P. Marks, G.K. Steinberg, and G. Zaharchuk



ABSTRACT

BACKGROUND AND PURPOSE: Severe ischemic changes are a rare but devastating complication following direct superficial temporal artery to MCA bypass in patients with Moyamoya disease. This study was undertaken to determine whether preoperative MR imaging and/or cerebrovascular reserve assessment by using reference standard stable xenon-enhanced CT could predict such complications.

MATERIALS AND METHODS: Among all adult patients undergoing direct bypass at our institution between 2005 and 2010 who received a clinically interpretable xenon-enhanced CT examination, we identified index cases (patients with >15-mL postoperative infarcts) and control cases (patients without postoperative infarcts and without transient or permanent ischemic symptoms). Differences between groups were evaluated by using the Mann-Whitney *U* test. Univariate and multivariate generalized linear model regression was used to test predictors of postoperative infarct.

RESULTS: Six index cases were identified and compared with 25 controls. Infarct size in the index cases was 95 ± 55 mL. Four of 6 index cases (67%), but no control patients, had preoperative acute infarcts. Baseline CBF was similar, but cerebrovascular reserve was significantly lower in the index cases compared with control cases. For example, in the anterior circulation, median cerebrovascular reserve was -0.4% (range, -38.0% – -16.6%) in index versus 26.3% (range, -8.2% – -60.5%) in control patients ($P = .003$). Multivariate analysis demonstrated that the presence of a small preoperative infarct (regardless of location) and impaired cerebrovascular reserve were independent, significant predictors of severe postoperative ischemic injury.

CONCLUSIONS: Acute infarcts and impaired cerebrovascular reserve on preoperative imaging are independent risk factors for severe ischemic complications following superficial temporal artery to MCA bypass in Moyamoya disease.

ABBREVIATIONS: CVR = cerebrovascular reserve; STA-MCA = superficial temporal artery to middle cerebral artery; XeCT = xenon-enhanced CT

Moyamoya disease is a cerebrovascular disorder characterized by steno-occlusion of the supraclinoid internal carotid, proximal anterior, and middle cerebral arteries. The entity is discernible on cerebral angiography, on which these findings are frequently associated with a characteristic collateral network at the base of the brain.^{1,2} In addition, leptomeningeal anastomoses

from the posterior circulation and transdural anastomoses from the external carotid artery can develop to preserve cerebral perfusion.³⁻⁵ Patients present with transient ischemic attacks, ischemic strokes, intracranial hemorrhage, seizures, and/or headaches.^{6,7} Its natural history, while variable, is typically relentlessly progressive.

Surgical revascularization has emerged as an effective treatment to prevent future ischemic episodes.^{1,3,8} Revascularization procedures can be characterized as either direct (eg, superficial temporal artery to MCA [STA-MCA] bypass), indirect (eg, encephaloduroarteriosynangiosis), or combined.^{3,9} While direct bypass shows no benefit over medical therapy for treating atherosclerotic disease,^{10,11} it continues to be successfully used for Moyamoya disease. The overwhelming majority of these procedures are uncomplicated, with low perioperative morbidity.⁹ Rarely, ischemic complications can lead to disability or death. In the present study, we tested whether preoper-

Received April 27, 2015; accepted after revision July 3.

From the Department of Radiology (M.U.A.), Medical University of South Carolina, Charleston, South Carolina; and Departments of Neurosurgery (T.C.B., G.K.S.) and Radiology (T.M.P., J.R., M.P.M., G.Z.), Stanford University and Stanford University Medical Center, Stanford, California.

M.U. Antonucci and T.C. Burns contributed equally.

This work was supported by National Institutes of Health 1R01-NS066506.

Please address correspondence to Greg Zaharchuk, MD, PhD, Department of Radiology, Stanford University, 1201 Welch Rd, mail code 5488, Stanford, CA 94305-5488; e-mail: gregz@stanford.edu

Indicates open access to non-subscribers at www.ajnr.org

<http://dx.doi.org/10.3174/ajnr.A4535>

ative imaging and cerebrovascular reserve (CVR) assessment can identify patients at higher risk of severe early ischemic postoperative complications.

MATERIALS AND METHODS

Patient Population

We performed a retrospective case-control study, comprising populations drawn from the 279 adult patients with Moyamoya disease who underwent 438 STA-MCA bypasses at Stanford University between 2005 and 2010. These patients underwent a standardized, extensive preoperative work-up, including cerebral angiography, MR imaging, and CVR assessment. All patients were participants in an ongoing Moyamoya disease study, for which institutional review board approval and informed consent were obtained. All procedures were in accordance with institutional guidelines.

Our analysis focused on 2 subgroups of the full cohort. Given our interest in CVR, patients were eligible for inclusion if they had a diagnostic pre- and postacetazolamide xenon-enhanced CT (XeCT) study as part of their preoperative assessment. The index cases are patients with severe ischemic complications. We defined “severe ischemia” as a postoperative infarct of >15 mL on diffusion-weighted imaging coupled with new symptoms within 1 week of surgery. The control cases are patients with no new postoperative symptoms, even if transient, and no new DWI lesion of any size on postoperative MR imaging.

Imaging

All patients had preoperative MR imaging and XeCT imaging within 1 month of surgery. “Acute infarct” was defined as high DWI signal, confirmed on apparent diffusion coefficient maps to exclude T2 shingthrough. Postoperative MR imaging with DWI was performed in all patients within 1 week of the operation. Infarct volume was calculated by using automated software (RAPid processing of Perfusion and Diffusion; iSchemaView, Stanford, California).¹²

Cerebral hemodynamic assessment was performed by using pre- and postacetazolamide XeCT CBF imaging. The study was performed by using a LightSpeed 8-detector scanner (GE Healthcare, Milwaukee, Wisconsin) integrated with a stable xenon-enhancer system (Enhancer 3000; Diversified Diagnostic Products, Houston, Texas). Following an initial noncontrast CT, 4 contiguous 10-mm sections, aligned with the orbitomeatal axis and beginning at the level of the basal ganglia, were obtained. Images were acquired at 45-second intervals during which the patient breathed a mixture containing 27% stable xenon gas. CBF in units of milliliter/100 g/min was calculated by using the Kety-Schmidt method as implemented by the manufacturer’s (Diversified Diagnostic Products) software. This software also permits the brain to be segmented into peripheral mixed cortical ROIs in each section (Fig 1). The regions were combined on the basis of anatomic territories to generate values for 4 vascular territories: right and left, anterior (anterior and middle cerebral artery territories) and posterior regions.^{13,14}

Cerebrovascular reserve assessment was performed by using CBF values obtained before (pre) and 20 minutes following

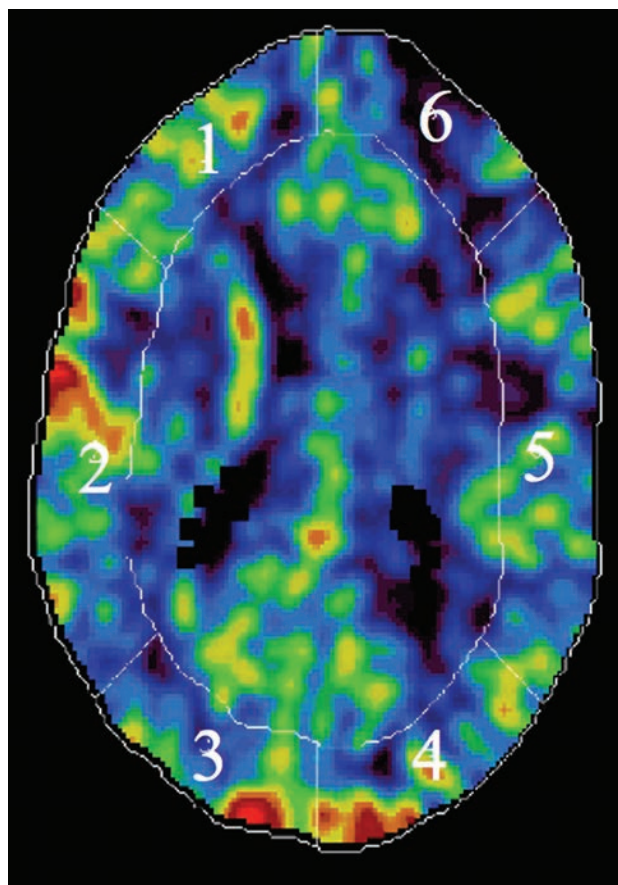


FIG 1. A representative xenon-enhanced CT study with ROIs for analysis. At each of 4 contiguous 10-mm sections starting at the level of the basal ganglia, the brain is segmented into 6 peripheral mixed cortical ROIs (a single section is shown here for clarity). For the anterior circulation CBF levels reported, the weighted average of regions 1 and 2 (right hemisphere) and 5 and 6 (left hemisphere) for all 4 levels was determined; likewise, the same method by using regions 3 and 4 was used to determine the right and left posterior circulation CBF values.

(post) 1 g of acetazolamide administered intravenously. CVR is defined as

$$CVR = \frac{CBF_{\text{post}} - CBF_{\text{pre}}}{CBF_{\text{pre}}}$$

and expressed as percentage change. In the normal brain, acetazolamide will produce a 30%–60% CBF increase.¹⁵ However, in Moyamoya disease, areas of the brain under ischemic stress may demonstrate an insufficient response to vasodilatory stimuli or even a paradoxically decreased postacetazolamide CBF, known as the “steal phenomenon.”

STA-MCA Bypass

The surgical technique of the STA-MCA bypass has been described in detail previously.^{16–18} In brief, the frontal or parietal branch of the STA is anastomosed end-to-side with an M4 MCA branch. Graft patency is confirmed intraoperatively, and strict blood pressure control is maintained throughout the operation. Care is taken to avoid significant hypotensive periods intraoperatively. Patients are maintained on aspirin and kept well-hydrated postoperatively with close hemodynamic monitoring.^{16–18} In pa-

Table 1: Demographic, clinical, and imaging characteristics of index and control cases^a

Factor	Index (n = 6)	Control (n = 25)	Group Effect (P Value)
Age (yr)	39 (27–67)	35 (18–59)	.39
Sex (% female)	67	68	.67
Anterior territory CBF baseline (mL/100 g/min)	36.6 (33.3–57.9)	50.2 (31.2–62.9)	.14
Anterior territory CBF post-ACZ (mL/100 g/min)	34.3 (23.4–64.5)	63.7 (39.0–74.3)	.007
Anterior change CBF (CVR) (%)	–0.4 (–38.7–16.6)	26.3 (–8.2–60.5)	.003
Posterior territory CBF baseline (mL/100 g/min)	41.7 (33.4–48.8)	38.8 (27.1–54.5)	.36
Posterior territory CBF post-ACZ (mL/100 g/min)	54.2 (31.7–64.7)	55.6 (38.2–72.2)	.39
Posterior change CBF (CVR) (%)	31.9 (–19.1–55.4)	39.1 (0.9–117.7)	.16
Volume of acute infarcts following surgery (mL)	95.0 (17.0–181.0)	0	NA
Patients with acute (DWI+) infarcts on preop MRI (%)	4 (66.7%)	0 (0%)	NA

Note:—ACZ indicates acetazolamide; preop, preoperative; NA, not applicable; DWI+, DWI with positive findings.

^a Values are median (range) where applicable.

tients with bilateral disease, staged unilateral operations are typically performed 1 week apart.

Statistical Analysis

Differences between index and control groups were assessed by using the Mann-Whitney *U* test. Sex correlation was evaluated by using the χ^2 test. Because the presence of preoperative infarcts, CVR, and postoperative infarcts may vary between hemispheres, analyses were further performed in each right and left anterior and right and left posterior territory. Because several patients underwent bilateral bypasses, assessment of these variables using an ipsilateral/contralateral convention was not possible and a right/left distinction was used. When practical, measured parameters such as CBF and CVR were combined to produce anterior and posterior values. Predictors of preoperative augmentation were tested with univariate Wilcoxon rank sum tests and multivariate mixed-effects linear regression with patient as the random effect. Predictors of postoperative infarct were tested with univariate and multivariate generalized linear model regression adjusted for clustering within patient. Because of the low frequency of strokes, a loglog link was used instead of the usual logit link. For univariate and multivariate regression, we dichotomized CVR to a greater than or less than 10% CBF increase¹⁹ and <0% increase (cerebrovascular steal). All statistical analyses were performed by using STATA 13.1 (StataCorp, College Station, Texas).

RESULTS

Six index cases (with 3 patients undergoing bilateral surgeries for 9 bypassed hemispheres) and 25 control cases (with 36 bypassed hemispheres) were identified. Demographic data and preoperative imaging characteristics for each group are presented in Table 1.

DWI Analysis

The mean size of the postoperative DWI lesions in the index group was large (95 ± 55 mL). Figure 2 shows representative MR images from each index patient demonstrating the infarct patterns, which were not restricted to the bypassed territory and often involved both cortical and subcortical structures. On preoperative MR imaging, 4 of the 6 index cases (67%) had small acute infarcts. In 3 patients, there were bilateral anterior territory infarcts preoperatively, and the fourth patient had a small left anterior infarct (Fig 2). One patient (patient 5) had an acute infarct 3 months before surgery, which was not considered because no

acute infarct was present on the immediate preoperative MR imaging. No posterior territory infarcts were observed before surgery. No control patient had a preoperative infarct.

To test whether the presence of an acute preoperative DWI lesion and/or impaired CVR correlated with the presence and location of postoperative infarcts, we evaluated 124 vascular regions in 31 patients (4 in each patient: left and right, anterior and posterior circulation). Of 8 anterior circulation territories with preoperative infarcts, 5 developed postoperative infarcts. Of 3 additional postoperative anterior circulation infarcts, 2 were contralateral to the preoperative DWI lesion. Overall, the presence of a preoperative DWI lesion was a strong predictor of postoperative infarct (OR = 9.8; 95% confidence range, 2.2–44.2; $P = .003$; Table 2).

CBF and CVR Analysis

Baseline anterior CBF showed a nonsignificant trend toward being lower in index patients (median, 36.6 versus 50.2 mL/100 g/min; $P = .14$) but a significant difference in CBF following acetazolamide administration (median, 34.3 versus 63.7 mL/100 g/min; $P = .007$). This finding corresponded to lower anterior circulation CVR in the index patients compared with controls (median, –0.4% versus 26.3%, respectively; $P = .003$). There was no difference between groups for posterior circulation baseline CBF or CVR, in keeping with the known tendency of Moyamoya disease to preferentially involve the anterior circulation. In addition, within each hemisphere, there was significantly lower preoperative CVR in the regions with postoperative infarctions (Fig 3). Figure 4 shows an example of normal augmentation in a patient in the control group. Figure 5 highlights index patient 3, with poor anterior augmentation, with additional evidence of reduced flow-related enhancement on an MR angiogram within the contralateral ICA following bypass, suggesting widespread hemodynamic changes following bypass.

Univariate and Multivariate Analyses by Hemisphere

Although preoperative DWI lesions showed the largest effect size as a predictor of postoperative infarct, impaired preoperative CVR (Fig 3) was also a highly consistent and significant risk factor for postoperative infarcts in univariate analysis by region (Table 2). This held true regardless of whether CVR was considered a continuous variable (OR = 0.97; 95% CI, 0.96–0.98; $P < .001$) or

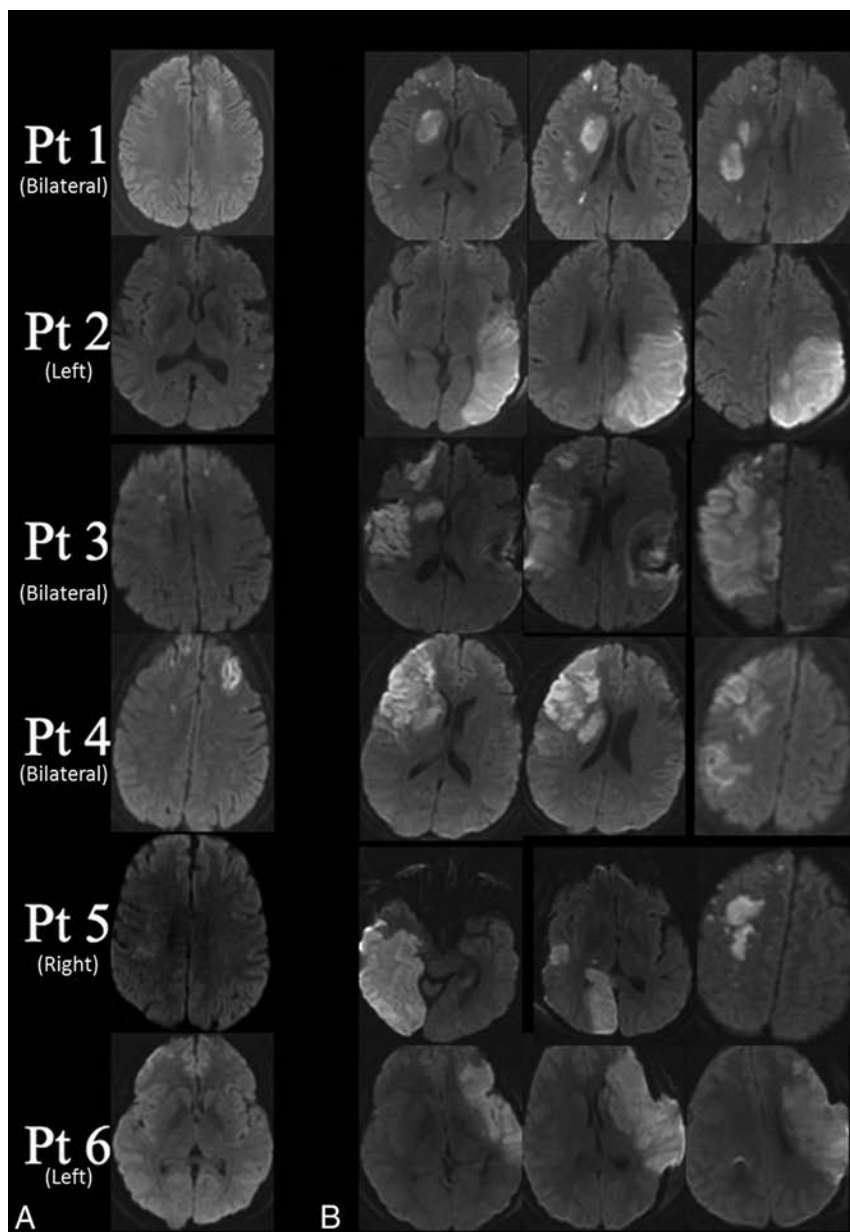


FIG 2. DWI in each index patient with the laterality of bypasses indicated in parentheses. *A*, Preoperative images demonstrate small acute infarcts in 4 of the 6 index patients. Patient 5 demonstrates a DWI region with positive findings in the right hemisphere that had negative findings on ADC (representing T2-shinethrough related to a subacute, rather than acute, infarct). *B*, Postoperative images demonstrate the extent of the infarct in the 6 index patients on MR imaging performed within 1 week of direct STA-MCA bypass.

Table 2: Univariate predictors of large postoperative infarcts

Variable	Odds Ratio	95% CI	P Value
Presence of an infarct on preoperative MRI	9.8	2.2–44.2	.003
Anterior location of preoperative infarct	2.0	1.2–3.4	.01
Post-ACZ CBF augmentation (continuous, per mL/100 g/min)	0.97	0.96–0.98	<.001
Absolute CBF augmentation anterior circulation (10% change) ^a	0.88	0.82–0.96	.002
Impaired CVR (augmentation of <10%)	2.8	1.8–4.3	<.001
Steal phenomenon (augmentation <0%)	2.4	1.3–4.5	.005

^a The reported odds ratio is the effect of a 10 mL/100 g/min increase in absolute CBF change, a 10% increase in percentage difference for CBF change. For example, for absolute CBF change in the anterior circulation, for every increase of 10 mL/100 g/min (ie, better augmentation), there is a 12% decrease in the odds (ie, 0.88) that the patient will be in the index (ischemic complications) group.

a binary variable, whether defined as <10% increase (OR = 2.8; 95% CI, 1.8–4.3; $P < .001$) or <0% (steal) (OR = 2.4; 95% CI, 1.3–4.5; $P = .005$).

There were strong interactions between these predictors. For example, with the Wilcoxon rank sum analysis, the presence of a preoperative infarct strongly predicted impaired augmentation (–12.7% versus 31.2%, $P < .001$). As such, we asked whether preoperative infarcts and impaired CVR may be independent risk factors. The results of multivariate generalized linear model regression adjusted for clustering are shown in Fig 6. Different probability fit curves depict the presence and absence of preoperative infarcts; the presence of preoperative infarct (red) shifts the curve up the probability axis relative to no preoperative infarct (blue). The best model incorporated the presence of a pre-bypass infarct and impaired CVR (<10% increase) (Table 3).

DISCUSSION

While the risk of developing a large infarct is very low following STA-MCA bypass, a small subset of patients do experience this complication shortly after the operation. Our results suggest that certain features evident on preoperative imaging may be related to this clinical outcome. While baseline CBF does not differ between the index and control groups, both univariate and multivariate regression analyses demonstrated that CVR is significantly lower in patients who develop large postoperative infarcts. Multiple prior studies suggest that reduced CVR is an independent risk factor for stroke.^{20,21} A recent meta-analysis demonstrated a significant positive relationship between reduced CVR and stroke risk in patients with carotid stenosis or occlusion, with an odds ratio of 3.86.²² Despite this relationship, it is not immediately clear why patients would experience strokes so soon after revascularization.

One potential explanation for the observed infarcts is that any surgical procedure represents a physiologic stress that portends an elevated risk of ischemic complications. Indeed, for this reason, a cardiac stress test is routinely performed in patients considered at high risk before surgical intervention.

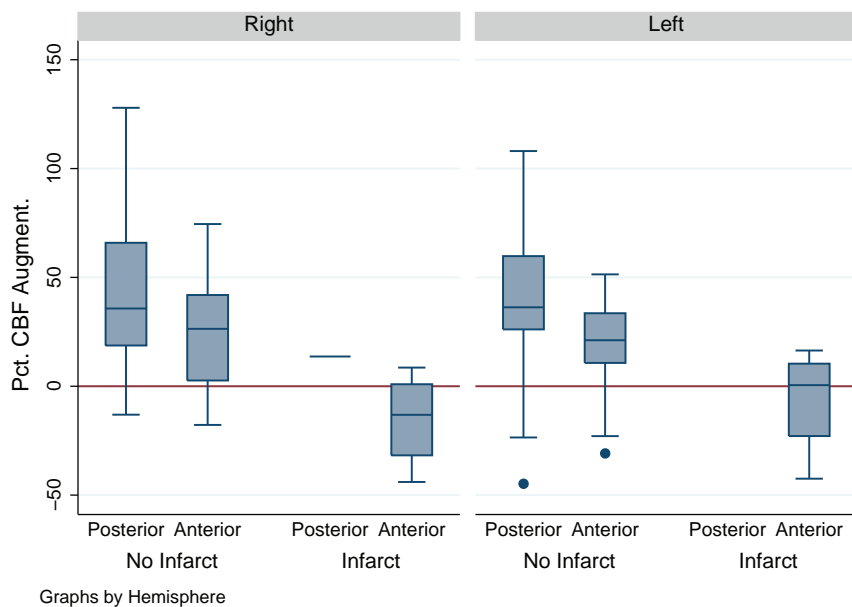


FIG 3. Cerebrovascular reserve expressed as percentage change from baseline within the right and left anterior and posterior circulation ROIs, segregated by the presence or absence of postoperative infarcts. All postoperative infarcts were in the anterior circulation, with the exception of 1 patient who developed a posterior circulation infarct on the side of a fetal posterior cerebral artery. CVR was lower in the hemispheres that subsequently developed infarcts, compared with those that did not. There was no difference between hemispheres. Circles indicate individual outlier measurements.

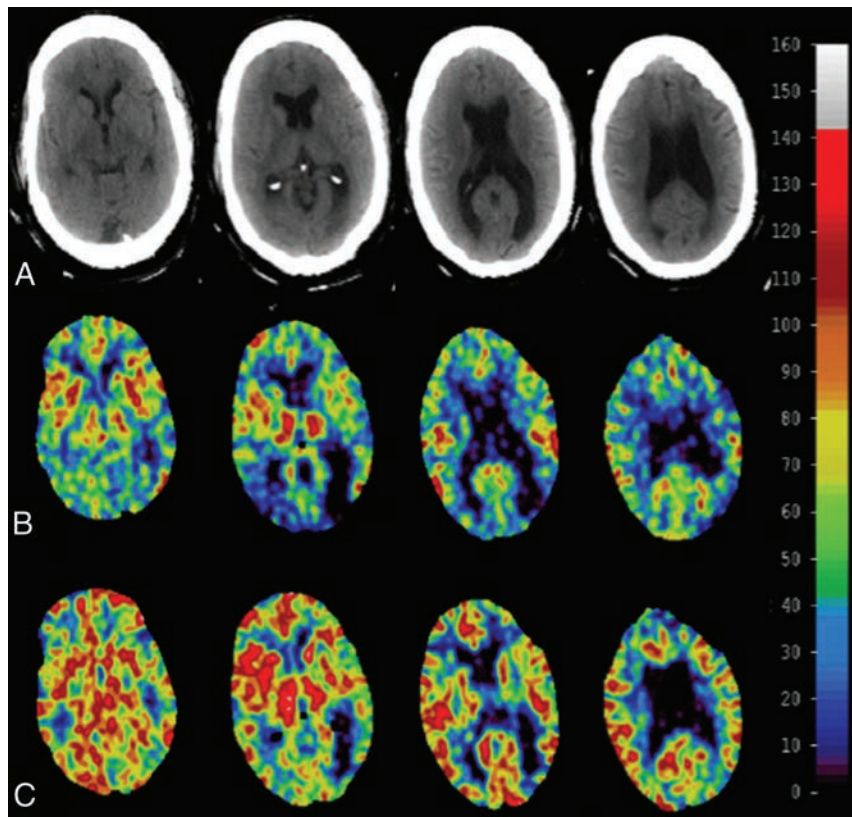


FIG 4. In this representative control patient, quantitative XeCT CBF maps (scale at right in milliliters/100 g/min) at 4 representative axial levels (A) obtained before (B) and after (C) the administration of acetazolamide are shown. CVR, calculated from these images, through the Equation referenced in the “Materials and Methods” section, is within the normal expected range (>30%) in all vascular territories, and this patient had no postoperative infarcts or clinical symptoms.

Similarly, patients with reduced CVR may be at an elevated risk of ischemic complications following any operation. Schoof et al²³ explored this concept in patients who underwent a coronary artery bypass graft and were screened with carotid sonography. If stenosis was identified, CVR was calculated by using transcranial Doppler before and after carbon dioxide administration. Patients with reduced CVR had a 27.3% stroke rate following cardiothoracic surgery, compared with a 1.5% risk in patients with normal CVR. Patients with reduced CVR may similarly have an elevated stroke risk following cerebral revascularization.

The rationale behind operative intervention in patients with Moyamoya disease is that for the long term, the risk of ischemic events will be lowered. As such, patients with reduced CVR may benefit the most. Indeed, the presence of reduced CVR appears to promote the success of revascularization. In a study assessing the postoperative course of patients with Moyamoya disease who underwent bilateral encephaloduroarteriosynangiosis, revascularization occurred selectively in areas of reduced CVR,²⁴ suggesting that abnormal CVR may itself promote angiogenesis. With time, this possibility is obviously advantageous. However, during an operation or in the immediate postoperative period, during which mean flow through the microanastomosis increases 5-fold (from 4.4 to 22.2 mL/min),⁹ the balance of cerebral hemodynamics may be very fragile. Increased flow related to the bypass may paradoxically represent a new hemodynamic stress and induce altered perfusion parameters by competing with the underlying stenotic vasculature and the native collateral network. This concept has been explored in prior studies, in part to account for the presence of postoperative perfusion abnormalities contralateral to the bypass.^{1,6} Indeed, it has previously been shown that increased STA flow following bypass is correlated with a higher incidence of postoperative infarct,⁹ though it is not clear whether this association is causative or correlative.

As in our study, infarcts have been reported both ipsilateral and contralateral to the most recently revascularized

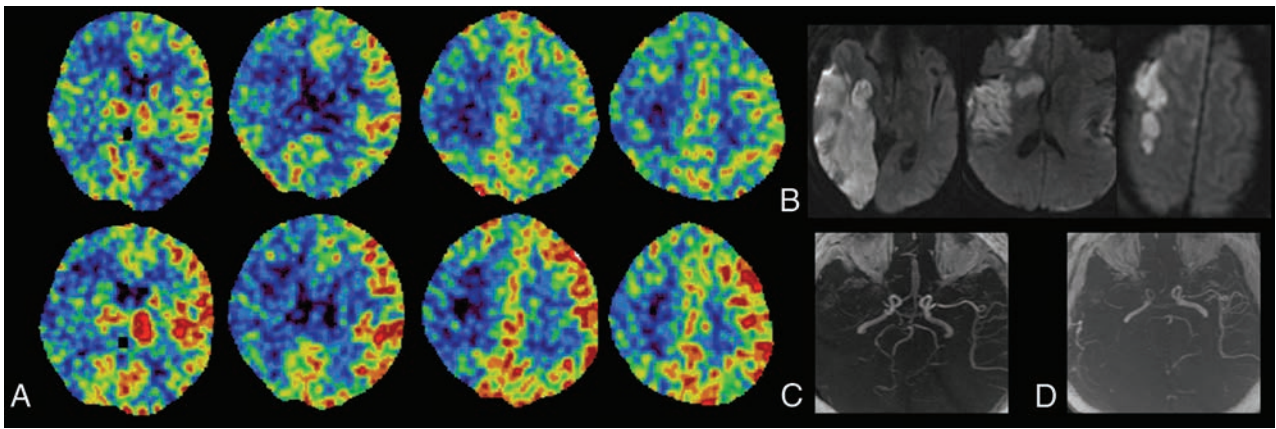


FIG 5. A 51-year-old man with Moyamoya disease and a history of transient left arm numbness and left lower extremity weakness (patient 3). *A*, XeCT imaging demonstrates mildly reduced baseline CBF in the right anterior circulation (*top row*). Postacetazolamide CBF paradoxically decreases in the right anterior circulation (*bottom row*), representing steal physiology, while augmenting normally on the left. Following right STA-MCA bypass, he experienced progressive left hemiplegia. *B*, Postoperative MR imaging within the first week after bypass revealed an extensive new infarct involving the right MCA territory and a portion of the right PCA territory. We believe that the posterior circulation involvement was due to the presence of a large posterior communicating artery on this side. *C*, Preoperative MR angiography reveals severe steno-occlusive disease involving the right-greater-than-left supraclinoid ICAs with complete occlusion of the right M1 MCA segment. *D*, MRA obtained after revascularization demonstrates a patent right STA-MCA bypass but decreased conspicuity of the patient's native vasculature, despite the study being performed on the same scanner. In particular, there is no appreciable flow-related enhancement in the bilateral anterior cerebral arteries or in the right posterior communicating or posterior cerebral artery, and there is continued occlusion of the right MCA. While the changes seen could be multifactorial and could be related to changes in other factors, such as sedation or intracranial pressure, we suggest that the hemodynamic changes related to the operation may have caused worsening of the patient's tenuous native right-sided arterial circulation, particularly given the lack of significant changes on the left side.

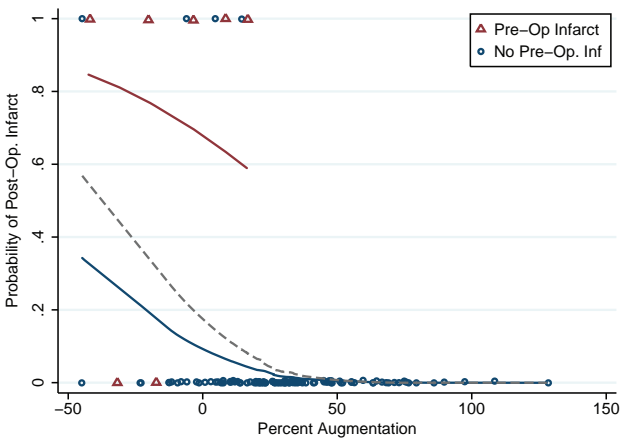


FIG 6. Probability fit curves based on multivariate analysis. Findings illustrate that impaired augmentation strongly increases the probability of infarct both in the presence (*red line*) and absence (*blue line*) of a preoperative infarct. The *dashed line* shows the overall probability of infarct based on percentage augmentation, regardless of preoperative infarct.

Table 3: Multivariate analysis summary

Variable	Odds Ratio	95% CI	P Value
Presence of an acute infarct on preop MRI	6.9	1.3–36.1	.02
Anterior location of preop infarct	1.1	0.7–1.8	.632
Impaired CVR (CBF augmentation <10%)	2.0	1.4–3.0	<.001

Note:—preop indicates preoperative.

hemisphere. The concept of competitive flow might further explain the prominent changes in vascular flow dynamics following bypass in several of the index cases. For instance, a postoperative MR angiogram obtained in 1 patient (Fig 5) demonstrated new decreased flow-related enhancement in the bilateral anterior

and right posterior communicating/posterior cerebral artery territories, which was confirmed as a change on cerebral angiography. It is possible that such rapid progression could arise in response to hemodynamic changes related to the flow through the new bypass in conjunction with altered perfusion parameters in the setting of a large acute infarct.

Most of the index cases demonstrated small acute infarcts on MR imaging examinations performed shortly before the operation. On univariate and multivariate analyses, the presence of a preoperative acute infarct was found to be a significant and independent predictor of infarct in the postoperative period. Most interesting, although the DWI lesions predicted the vascular territory in 5 of 8 anterior circulation territories, 2 anterior circulation infarcts occurred contralateral to the preoperative DWI lesion. These occurred in patients with large infarcts after the first bypass but who had significant contralateral stenosis and poor CVR. While such spatially removed infarcts may be explained by the hemodynamic changes described above, systemic factors (such as alterations in platelet function) may render a patient with recent infarcts more generally susceptible to a postoperative infarct than would be expected on the basis of vascular pathology alone. In addition, while hypotension was strictly avoided during the operation, other operative stresses, such as cortisol release and platelet activation, may collectively contribute to perioperative ischemia. Whether delaying operative revascularization to allow infarct evolution/stabilization in such high-risk patients would have altered the postoperative course is presently unknown because our data were collected as part of the preoperative work-up of operative patients and similar data were not available to assess the effect of acute infarct and impaired CVR on a matched nonoperative patient cohort. Nonetheless, the risks

and benefits of delaying the operation in patients with ongoing ischemic change must be carefully weighed, given the inherently progressive nature of Moyamoya disease.

Prior researchers have noted the association between preoperative infarct and perioperative complications in Moyamoya disease. In a review of 165 adult patients (undergoing 265 revascularization procedures), Hyun et al²⁵ found that the presence of a preoperative diffusion abnormality was significantly correlated with 19 perioperative infarcts. However, most of these complications were transient in nature and occurred primarily in indirect revascularization procedures. By comparison, our series assesses variables associated with large, clinically significant infarctions in patients undergoing direct bypass, a distinctly less well-studied patient population.

There are several potential limitations to our study. The first is its retrospective design and the relatively small number of index cases. Our institutional morbidity associated with cerebral revascularization is low, and despite a large number of bypasses, only a small number of patients with large postoperative infarcts were available for analysis. To maximize the power of this small patient cohort, we analyzed multiple vascular territories in each patient independently, while correcting for clustering. We also performed multivariate analysis, maximizing our ability to detect meaningful predictors of postoperative infarct. Second, this analysis focused on 2 smaller subsets of a larger group of patients with Moyamoya disease. The study was specifically designed in this manner to identify factors associated with profound operative morbidity relative to the optimal clinical outcome.

While prior studies have assessed factors associated with transient postoperative neurologic deficits,²⁶ our index patients represent a small, relatively unstudied subgroup. Given the low risk of postoperative stroke in this patient population and the fact that most of these strokes tend to be small, investigation of the factors that lead to severe infarcts was deemed most clinically relevant. Nonetheless, additional patients who underwent bypass at our institution included those with either small postoperative diffusion abnormalities (often clinically asymptomatic) or those with mild or transient neurologic symptoms. Further studies are ongoing to address contributors to adverse outcomes in these larger patient cohorts. Only acute (DWI with positive findings) preoperative infarcts were considered in the evaluation of preoperative risk factors because only acute infarcts could be consistently evaluated in all patients. Although 4 of the 6 index cases had acute preoperative infarcts, another index patient had a small infarct on a 3-month preoperative scan, which was subacute on immediate preoperative MR imaging. Although the presence of subacute infarcts could not be consistently evaluated for all patients in this study, we cannot exclude the possibility that the presence of subacute infarcts could also portend a worse prognosis.

Finally, we used XeCT CBF measurements for the CVR measurements. While XeCT is considered a reference standard method, others have proposed the use of MR imaging–based perfusion measurements.²⁷ Regardless of the methodology, our results underscore the importance of quantitative assessment of CVR to identify patients at high risk for stroke. Thus,

we are now investigating the use of MR perfusion with and without acetazolamide, which, if comparable, may represent a technique more amenable to widespread use outside specialized centers.

CONCLUSIONS

Our results indicate that an acute infarct on preoperative MR imaging and the presence of impaired CVR can help identify the small subset of patients with Moyamoya who experience a severe ischemic complication following extracranial-intracranial bypass.

Disclosures: Gary K. Steinberg—UNRELATED: Consultancy: Medtronic Neuroscience Strategic Advisory Board; Grants/Grants Pending: National Institutes of Health,* California Institute for Regenerative Medicine*; Patents (planned, pending or issued): Stanford University*; Stock/Stock Options: Qool Therapeutics. Greg Zarchuk—RELATED: Grant: National Institutes of Health,* Comments: part of a larger study of patients with Moyamoya disease, 5R01-NS066506; UNRELATED: Consultancy: GE Healthcare; Grants/Grants Pending: National Institutes of Health,* Comments: multiple grants unrelated to the current work; Royalties: Cambridge University Press. *Money paid to the institution.

REFERENCES

1. Ma Y, Meng L, Jiao LQ, et al. **Contralateral cerebral hemodynamic changes after unilateral direct revascularization in patients with Moyamoya disease.** *Neurosurg Rev* 2011;34:347–54 CrossRef Medline
2. Ikezaki K. **Rational approach to treatment of Moyamoya disease in childhood.** *J Child Neurol* 2000;15:350–56 CrossRef Medline
3. Togao O, Mihara F, Yoshiura T, et al. **Cerebral hemodynamics in Moyamoya disease: correlation between perfusion-weighted MR imaging and cerebral angiography.** *AJNR Am J Neuroradiol* 2006;27:391–97 Medline
4. Suzuki J, Takaku A. **Cerebrovascular “Moyamoya” disease: disease showing abnormal net-like vessels in base of brain.** *Arch Neurol* 1969;20:288–99 CrossRef Medline
5. Yun TJ, Cheon JE, Na DG, et al. **Childhood Moyamoya disease: quantitative evaluation of perfusion MR imaging—correlation with clinical outcome after revascularization surgery.** *Radiology* 2009;251:216–23 CrossRef Medline
6. Pandey P, Steinberg GK. **Neurosurgical advances in the treatment of Moyamoya disease.** *Stroke* 2011;42:3304–10 CrossRef Medline
7. Karasawa J, Kikuchi H, Furuse S, et al. **Treatment of Moyamoya disease with STA-MCA anastomosis.** *J Neurosurg* 1978;49:679–88 CrossRef Medline
8. Guzman R, Lee M, Achrol A, et al. **Clinical outcome after 450 revascularization procedures for Moyamoya disease: clinical article.** *J Neurosurg* 2009;111:927–35 CrossRef Medline
9. Lee M, Guzman R, Bell-Stephens T, et al. **Intraoperative blood flow analysis of direct revascularization procedures in patients with Moyamoya disease.** *J Cereb Blood Flow Metab* 2011;31:262–74 CrossRef Medline
10. Powers WJ, Clarke WR, Grubb RL Jr, et al; COSS Investigators. **Extracranial-intracranial bypass surgery for stroke prevention in hemodynamic cerebral ischemia: the Carotid Occlusion Surgery Study randomized trial.** *JAMA* 2011;306:1983–92 CrossRef Medline
11. EC/IC Bypass Study Group. **Failure of extracranial-intracranial arterial bypass to reduce the risk of ischemic stroke: results of an international randomized trial.** *N Engl J Med* 1985;313:1191–200 CrossRef Medline
12. Straka M, Albers GW, Bammer R. **Real-time diffusion-perfusion mismatch analysis in acute stroke.** *J Magn Reson Imaging* 2010;32:1024–37 CrossRef Medline
13. Qiu D, Straka M, Zun Z, et al. **CBF measurements using multilayer pseudocontinuous and velocity-selective arterial spin label-**

- ing in patients with long arterial transit delays: comparison with xenon CT CBF. *J Magn Reson Imaging* 2012;36:110–19 CrossRef Medline
14. Zaharchuk G, Bammer R, Straka M, et al. **Improving dynamic susceptibility contrast MRI measurement of quantitative cerebral blood flow using corrections for partial volume and nonlinear contrast relaxivity: a xenon computed tomographic comparative study.** *J Magn Reson Imaging* 2009;30:743–52 CrossRef Medline
 15. Settakis G, Molnar C, Kerenyi L, et al. **Acetazolamide as a vasodilatory stimulus in cerebrovascular disease and in conditions affecting the cerebral vasculature.** *Eur J Neurol* 2003;10:609–20 CrossRef Medline
 16. Chang SD, Steinberg GK. **Surgical management of Moyamoya disease.** Moyamoya.com. <http://www.moyamoya.com/journals/moyamoya.html>. Last update January 1, 2013. Accessed April 1, 2015
 17. Li G, Lim M, Khan N, et al. **Cerebral revascularization for Moyamoya disease.** In: Abdulrauf SI, ed. *Cerebral Revascularization: Techniques in Extracranial-to-Intracranial Bypass Surgery*. Philadelphia: Elsevier; 2011:185–92
 18. Guzman R, Steinberg GK. **Direct bypass technique for the treatment of pediatric Moyamoya disease.** *Neurosurg Clin N Am* 2010;21:565–73 CrossRef Medline
 19. JET Study Group. **Japanese EC-IC bypass trial (JET study): study design and interim analysis** [in Japanese]. *Surg Cereb Stroke (Jpn)* 2002;30:97–100 CrossRef
 20. Kuroda S, Houkin K, Kamiyama H, et al. **Long-term prognosis of medically treated patients with internal carotid or middle cerebral artery occlusion: can acetazolamide test predict it?** *Stroke* 2001;32:2110–16 CrossRef Medline
 21. Grubb RL Jr, Derdeyn CP, Fritsch SM, et al. **Importance of hemodynamic factors in the prognosis of symptomatic carotid occlusion.** *JAMA* 1998;280:1055–60 CrossRef Medline
 22. Gupta A, Chazen JL, Hartman M, et al. **Cerebrovascular reserve and stroke risk in patients with carotid stenosis or occlusion: a systematic review and meta-analysis.** *Stroke* 2012;43:2884–91 CrossRef Medline
 23. Schoof J, Lubahn W, Baeumer M, et al. **Impaired cerebral autoregulation distal to carotid stenosis/occlusion is associated with increased risk of stroke at cardiac surgery with cardiopulmonary bypass.** *J Thorac Cardiovasc Surg* 2007;134:690–96 CrossRef Medline
 24. Nariai T, Suzuki R, Matsushima Y, et al. **Surgically induced angiogenesis to compensate for hemodynamic cerebral ischemia.** *Stroke* 1994;25:1014–21 CrossRef Medline
 25. Hyun SJ, Kim JS, Hong SC. **Prognostic factors associated with perioperative ischemic complications in adult-onset Moyamoya disease.** *Acta Neurochir (Wien)* 2010;152:1181–88 CrossRef Medline
 26. Ohue S, Kumon Y, Kohno K, et al. **Postoperative temporary neurological deficits in adults with Moyamoya disease.** *Surg Neurol* 2008;69:281–86; discussion 286–87 CrossRef Medline
 27. Tanaka Y, Nariai T, Nagaoka T, et al. **Quantitative evaluation of cerebral hemodynamics in patients with Moyamoya disease by dynamic susceptibility contrast magnetic resonance imaging: comparison with positron emission tomography.** *J Cereb Blood Flow Metab* 2006;26:291–300 CrossRef Medline

Diagnostic Impact of Bone-Subtraction CT Angiography for Patients with Acute Subarachnoid Hemorrhage

P. Aulbach, D. Mucha, K. Engelland, K. Hädrich,  M. Kuhn, and R. von Kummer

ABSTRACT

BACKGROUND AND PURPOSE: Detection and evaluation of ruptured aneurysms is critical for choosing an appropriate endovascular or neurosurgical intervention. Our aim was to assess whether bone-subtraction CTA is capable of guiding treatment for cerebral aneurysms in patients with acute SAH and could replace DSA.

MATERIALS AND METHODS: We prospectively studied 116 consecutive patients with SAH with 16–detector row bone-subtraction CTA and DSA before intracranial aneurysm treatment. Two independent neuroradiologists reviewed the bone-subtraction CTA blinded to DSA (reference standard). We determined the accuracy of bone-subtraction CTA for aneurysm detection and the measurement of aneurysm dimensions and compared the radiation doses of the 2 imaging modalities.

RESULTS: Seventy-one patients (61%) had 74 aneurysms on DSA. Bone-subtraction CTA detected 73 of these aneurysms, but it detected 1 additional aneurysm. On a per-aneurysm basis, sensitivity, specificity, and positive and negative predictive values for bone-subtraction CTA were 99%, 98%, and 99% and 98%, respectively. For aneurysms of ≤ 3 mm, sensitivity was 94% (95% CI, 73%–99%). Bone-subtraction CTA slightly overestimated neck and dome diameters by <0.2 mm and overestimated the dome-to-neck ratios by 2% on average. Dose-length product was 565 ± 201 mGy \times cm for bone-subtraction CTA and 1609 ± 1300 mGy \times cm for DSA.

CONCLUSIONS: Bone-subtraction CTA is as accurate as DSA in detecting cerebral aneurysms after SAH, provides similar information about aneurysm configuration and measures, and reduces the average effective radiation dose for vascular diagnostics by 65%. Diagnostic equivalence in association with dose reduction suggests replacing DSA with bone-subtraction CTA in the diagnostic work-up of spontaneous SAH.

ABBREVIATIONS: BSCTA = bone-subtraction CTA; D/N = dome-to-neck; NECT = nonenhanced CT

Prompt detection and evaluation of ruptured intracranial aneurysms is critical for choosing an appropriate endovascular or neurosurgical intervention.¹ Invasive digital subtraction angiography carries an overall risk of neurologic complications, resulting in permanent deficits in 0.5%.^{2,3} Providing false-negative results in 5%–10% of patients,⁴ it also may increase the risk of rebleeding.^{5,6}

Multidetector CT angiography with high spatial resolution and bone-subtraction CTA (BSCTA) approaches the diagnostic accuracy of DSA in the detection of intracranial aneurysms.^{7–12}

Thus, BSCTA can be considered an alternative to DSA in treatment planning.^{13,14} Some authors already recommend BSCTA as the primary imaging in acute SAH.^{7,15,16} However, it still seems unclear whether BSCTA can provide sufficient information for therapy decisions, making diagnostic DSA redundant.^{17,18}

We therefore tested the hypothesis that BSCTA is as accurate as DSA for the identification and characterization of cerebral aneurysms in patients with SAH, even for small aneurysms and for those at the level of the skull base. We additionally studied the reliability of BSCTA and radiation-exposure reduction by avoiding diagnostic DSA.

MATERIALS AND METHODS

Participants

After University Hospital Dresden review board approval (EK No. 73042008) and informed consent, from November 2007 to June 2011, neuroradiologists or neurosurgeons familiar with the protocol prospectively enrolled patients with acute SAH able to undergo CTA and DSA. We classified SAH severity with the Fisher score. Patients underwent nonenhanced CT (NECT) and BSCTA

Received January 29, 2015; accepted after revision June 22.

From the Department of Neuroradiology (P.A., K.E., K.H., R.v.K.), University Hospital Carl Gustav Carus, Technische Universität, Dresden, Germany; Institute for Medical Informatics and Biometry at the Medical Faculty (M.K.), Technische Universität, Dresden, Germany; and Department of Neuroradiology (D.M.), Heinrich Braun Hospital, Zwickau, Germany.

Please address correspondence to Rüdiger von Kummer, MD, Department of Neuroradiology, University Hospital Carl Gustav Carus, Technische Universität, Fetscherstr 74, 01307 Dresden, Germany; e-mail: ruediger.vonkummer@uniklinikum-dresden.de

 Indicates open access to non-subscribers at www.ajnr.org

<http://dx.doi.org/10.3174/ajnr.A4497>

Table 1: Scan parameters for CT examinations

Scan Parameters	BSCTA		
	NECT	Low-Dose	
		CT	CTA
Tube voltage (kV)	120	100	100
Tube current (effective mAs)	320	70	140
Rotation time (sec)	1.0	0.5	0.5
Section acquisition (mm)	16 × 1.5	16 × 0.75	16 × 0.75
Table speed/rotation (mm)	13.2	13.8	13.8
Recon. section thickness (mm)	8	1.0	1.0
Reconstruction increment (mm)	8	0.5	0.5
Automated exposure control	Off	Off	Off
Contrast material (mL) ^a	NA	NA	80
Injection rate (mL/s)	NA	NA	4–5

Note:—Recon. indicates reconstruction; NA, not applicable.

^aIopromide, Ultravist, 370 mg I/mL; Bayer HealthCare, Berlin, Germany.

followed by DSA with 3D reconstructions. We documented the time interval between CT and DSA. Patients with typical exclusion criteria for CTA or previous coiling or clipping were excluded. Because we aimed to assess the accuracy of BSCTA for the detection and description of cerebral aneurysms, we did not follow patients with perimesencephalic SAH further.

CTA Imaging Technique

Examinations were performed with the patient in the supine position from the C1 vertebral body to the vertex on a 16–detector row spiral CT (Somatom Sensation 16; Siemens, Malvern, Pennsylvania). We performed BSCTA after low-dose NECT (bone mask) and CTA, avoiding motion by head fixation and minimizing the delay between the 2 scans.

We did not use standard NECT for bone masking because standard NECT is acquired with a gantry tilt preventing direct x-ray to the eye lenses, whereas CTA data are acquired with no gantry tilt. The BSCTA algorithm used requires similar, narrow, section acquisition (0.75 mm for high spatial resolution) and datasets with minimum motion artifacts (0.5 seconds for minimized motion artifacts during acquisition). Standard-dose NECT, however, requires a slower rotation time of 1.0 second (to collect a sufficient amount of x-ray quanta) and a wider collimation of 1.5 mm. The CT scan parameters are listed in Table 1. The acquisition time was approximately 10 seconds. Bone-subtraction was performed automatically by using special prototype software on a workstation (syngo 2006G and syngo MultiTechnique Workplace, VE31D; Siemens).

DSA and 3D-DSA

We used a rotational biplane DSA unit (Allura Xper FD 20 biplane; Philips Healthcare, Best, the Netherlands) for panangiography (all cerebral arteries). Per acquisition, we administered 3–6 mL of non-ionic contrast agent (iohexol, Accupaque, 300 mg I/mL; GE Healthcare, Milwaukee, Wisconsin). 3D reformatted images of rotational angiographic data were generated at the DSA workstation.

Image Analysis

Two neuroradiologists (D.M., K.E.), with 14 and 10 years of experience, reviewed the DSA images independently and blinded to BSCTA. Readers were informed of the patient's clinical symptoms and initial CT findings. Reading of BSCTA and DSA datasets was separated by 8–10 weeks to prevent bias. To assess intraobserver

reliability, reader 1 analyzed 15 randomly selected BSCTA imaging studies (12.9%) twice, separated by an interval of 1 month.

An aneurysm was considered entirely characterized if all 3 orthogonal dimensions were obtained and the aneurysm neck and dome and arterial incorporations into the sac or neck were visualized and precisely measured. We categorized aneurysms as “berry-formed,” “fusiform,” and “branching” if they were located at an arterial bifurcation.

The readers generated maximum intensity projections, volume rendering technique reformations, and multiplanar reconstructions searching for aneurysms. If multiple aneurysms were detected, the most likely source of bleeding was estimated. Dome-to-neck (D/N) ratios were calculated for both modalities. The 2 readers evaluated images in consensus in case of discrepancies. We evaluated the effect of patient motion on image quality for DSA and BSCTA and rated the quality of BSCTA images on a 4-point scale as “excellent,” “good,” “moderate,” or “poor.”

Radiation Dose

We measured the dose-length product of both modalities and calculated the effective doses. Among the recorded values for DSA examinations, we only considered the diagnostic portion of the dose-length product for comparison. Exposure information was reported automatically, as required by the standard of the International Electrotechnical Commission (IEC 60601-2-43) for total fluoroscopy time in minutes, total number of exposures in numbers, accumulated fluoroscopy dose in milligrays, accumulated exposure dose in milligrays, total dose in milligrays, total number of frames in numbers, image-area dose product in milligrays, entrance dose and air kerma in milligrays, exposure start time, kilovolt (peak), distance source-to-image receptor distance, exposure time, x-ray tube current, positioner primary angle, positioner secondary angle, and frame rate.

Examination and dose reporting for both BSCTA and DSA examinations are provided through Radiology Information DICOM 2-way interface, by using the DICOM Worklist Management and Technique Performed Procedure Step Standards.

Statistical Methods

We used MedCalc for Windows 12 (Version 12.3.0; MedCalc Software, Mariakerke, Belgium) for statistical analysis. We considered DSA, including 3D reconstructions, as the reference standard for aneurysm evaluation. We calculated the sensitivity, specificity, and accuracy of BSCTA on per-aneurysm and per-patient bases and used the Wilson procedure, without a correction for continuity, for the limits of the CI. We used the Cohen κ to quantify inter- and intrareader agreement beyond chance in detecting aneurysms with BSCTA. A *P* value $\leq .05$ was statistically significant. We compared the DSA and BSCTA differences for aneurysm dome and neck diameter and the D/N ratio, applying the Bland-Altman method and a paired Student *t* test, to analyze differences in radiation doses.

RESULTS

Participants

During 44 months, 269 consecutive patients presented to our department with SAH. We excluded 6 patients with prior clipping or

coiling and 147 patients due to imaging protocol violations. Finally, 116 patients (50% women) (mean age, 53.9 ± 13.6 years) were prospectively examined with BSCTA and DSA according to the study protocol.

CT Findings

All patients had SAH, with a Fisher grade 1 in 8 patients (6.9%), 2 in 7 patients (6.0%), 3 in 42 patients (36.2%), and 4 in 59 patients (50.9%).

DSA Reference

The time between BSCTA and DSA varied from 20 minutes to 43 hours (median time, 7.0 hours). Of 116 patients, 71 patients (61.2%) had 74 intracranial aneurysms on initial DSA. Table 2

Table 2: Location and sizes of cerebral aneurysms as detected by DSA

Location	Size Categories		
	Small (≤ 3.0 mm)	Medium (3.1–5.0 mm)	Large (> 5 mm)
ICA			
Intraclinoid	0	0	1
Ophthalmic	0	0	1
PcomA	1	6	2
Carotid-T	1	0	0
ACA			
A1	0	1	0
A1/A2	5	16	7
A2 and A3	3 ^a	0	3
MCA			
Trifurcation	4 ^b	8	2
PCA	0	1	1
BA			
Oral	1	0	3
VA			
PICA	0	3	2
V4	0	0	1
All	15	35	23

Note:—PcomA indicates posterior communicating artery; Carotid-T, intracranial ICA bifurcation; ACA, anterior cerebral artery; A1, A2, A3, segments of the ACA; PCA, posterior cerebral artery; BA, basilar artery; VA, vertebral artery; PICA, posterior inferior cerebellar artery; V4, distal segment of VA.

^a One aneurysm missed by bone-subtraction CTA.

^b One aneurysm missed by DSA but detected by bone-subtraction CTA.

shows the locations and sizes of intracranial aneurysms as detected and characterized by DSA. We found 53 branching aneurysms (71.6%), 20 berry-form aneurysms (27.0%), and 1 fusiform aneurysm (1.4%). Among the 45 patients without aneurysms, 6 had arteriovenous malformations. We could not identify the cause of SAH in 39 patients, among them 27 patients with additional intracerebral hematomas. We did not have any observations because our patients with acute SAH had not shown signs of vasospasm. The average amount of contrast media used for diagnostic DSA was 106.4 ± 39.8 mL, with a median of 100 mL. The maximum amount was 230 mL, and the lowest, 50 mL.

BSCTA Findings

BSCTA detected 73 aneurysms in 70 patients, confirmed by DSA (Fig 1), and missed 1 anterior cerebral artery A2/A3 segment aneurysm with a diameter of 1.7 mm that was detected by DSA (Fig 2). Bone-subtraction CTA detected a 2.5-mm left

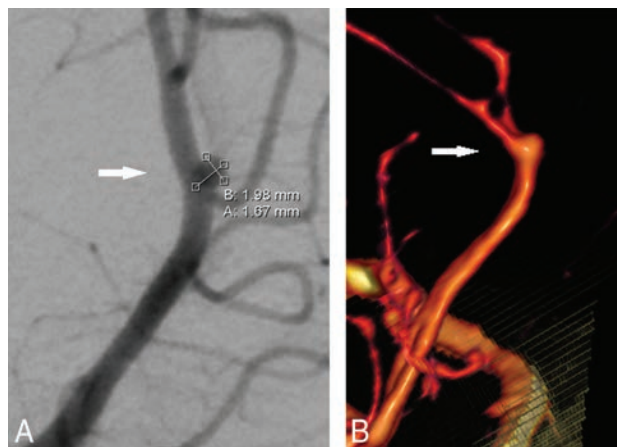


FIG 2. False-negative bone-subtraction CTA findings of an aneurysm of the right anterior cerebral artery in a 50-year-old woman. **A**, The right anterior oblique projection DSA shows a small broad-based aneurysm (arrow). **B**, On volume-rendering reconstruction, the aneurysm (arrow) appears fusiform. The white surface in the lower part of the image represents the bone-to-vessel boundary of the bone-removal processing.

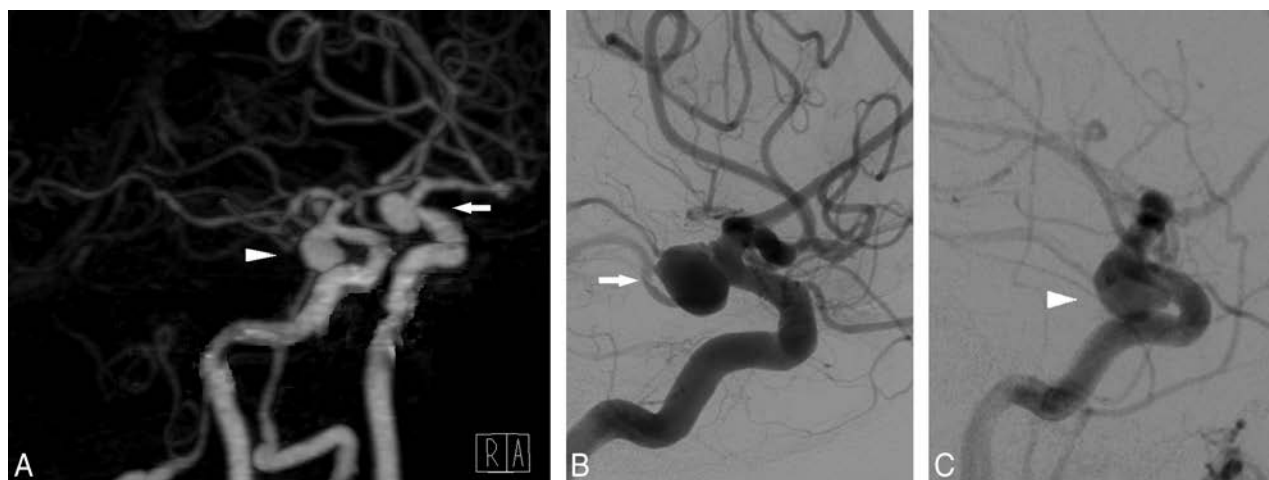


FIG 1. A 78-year-old-female patient with symmetric infraclinoid aneurysms of the ICA. **A**, Volume-rendering of BSCTA displays both aneurysms (arrowhead: right aneurysm; arrow: left aneurysm). **B** and **C**, DSA confirms both aneurysms in size and configuration.

MCA M2 segment aneurysm that was missed by DSA and finally confirmed by both readers in consensus (Fig 3). Both findings did not change clinical decisions.

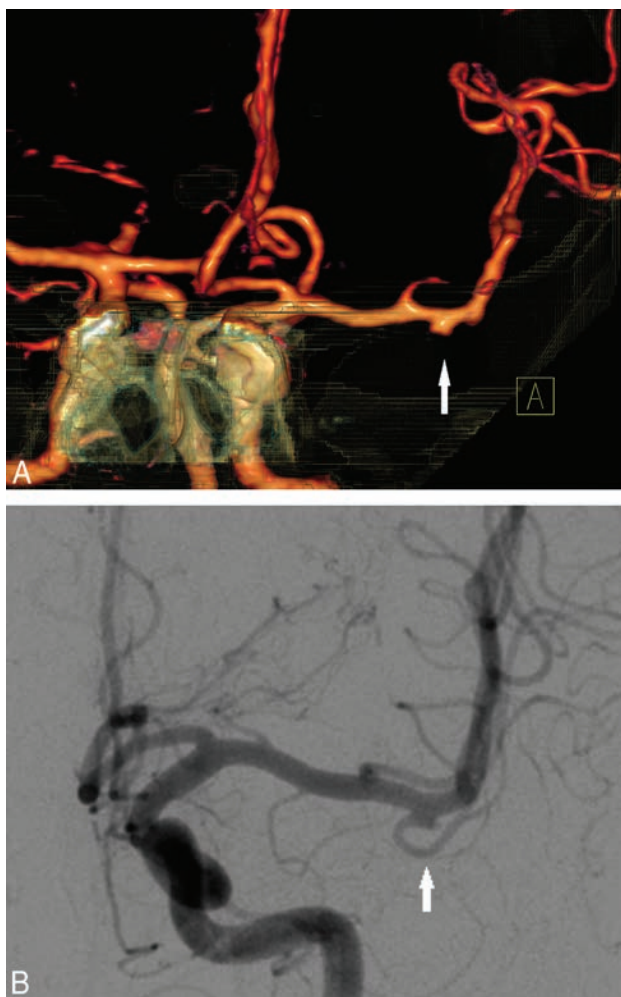


FIG 3. False-positive bone-subtraction CTA findings in an aneurysm (2.5 mm) of the left middle cerebral artery distal to the trifurcation in a 50-year-old man with 2 aneurysms. *A*, Volume-rendering of bone-subtraction CTA depicts the aneurysm (anteroposterior view) that was missed by DSA. *B*, 3D-DSA image of the initially missed M2 MCA trifurcation aneurysm (left anterior oblique view) that was confirmed in retrospect.

Table 3: Accuracy of BSCTA in detecting cerebral aneurysms

	TP (No.)	TN (No.)	FP (No.)	FN (No.)	Sensitivity (%) (No.)	Specificity (%) (No.)	PPV (%) (No.)	NPV (%) (No.)	Accuracy (%) (No.)
Per patient	70	45	0	1	99 (70/71)	100 (45/45)	100 (70/70)	98 (45/46)	99 (115/116)
95% CI					92–100	92–100	95–100	89–100	95–100
Per aneurysm	73	45	1	1	99 (73/74)	98 (45/46)	99 (73/74)	98 (45/46)	98 (118/120)
95% CI					93–100	89–100	93–100	89–100	94–100

Note:—TP indicates true-positive; TN, true-negative; FP, false-positive; FN, false-negative; PPV, positive predictive value; NPV, negative predictive value.

Table 4: Accuracy of BSCTA in detecting cerebral aneurysms of different sizes

Diameter	TP (No.)	TN (No.)	FP (No.)	FN (No.)	Sensitivity (%) (No.)	Specificity (%) (No.)	PPV (%) (No.)	NPV (%) (No.)	Accuracy (%) (No.)
>5.0 mm	23	45	0	0	100 (23/23)	100 (45/45)	100 (23/23)	100 (45/45)	100 (68/68)
95% CI					86–100	92–100	86–100	92–100	95–100
3.1–5.0 mm	35	45	0	0	100 (35/35)	100 (45/44)	100 (35/35)	100 (45/45)	100 (80/80)
95% CI					90–100	92–100	90–100	92–100	94–100
≤3.0 mm	16	45	1	1	94 (16/17)	98 (45/46)	94 (16/17)	98 (45/46)	97 (61/63)
95% CI					73–99	89–100	73–99	89–100	89–100

Note:—TP indicates true-positive; TN, true-negative; FP, false-positive; FN, false-negative; PPV, positive predictive value; NPV, negative predictive value.

Sensitivity and specificity of BSCTA for intracranial aneurysms are presented in Tables 3 and 4.

Aneurysm dome diameters were slightly longer with a 0.17-mm bias (95% CI, -0.04 to 0.39 mm) measured on BSCTA compared with DSA (Fig 4A). The measurement differences are relatively constant over all aneurysm diameters. Aneurysm neck diameters of BSCTA did not differ from those on DSA (Fig 4B). Figure 4C shows that BSCTA aneurysm D/N ratios differ by -0.04 only (95% CI, -0.16 to 0.08) from the DSA D/N ratios. The average DSA D/N ratio was 1.90 ± 0.86 , and the average BSCTA D/N ratio was 1.86 ± 0.84 . On average, BSCTA D/N ratios were 2% smaller than DSA D/N ratios ($P = .4678$). The highest agreement of methods was for the D/N ratio of 1.5–2.0. Comparison of the distribution of D/N ratios in DSA versus BSCTA is shown in Fig 4C.

Image Quality and Reliability

Overall bone-subtraction quality was high (91.4% good or excellent). Ten of 116 datasets were rated moderate or poor. Fifteen of 74 aneurysms were near or surrounded by bone and were correctly detected and characterized with BSCTA. Motion artifacts impaired DSA in 28 patients (23.9%) and BSCTA in 2 patients (1.7%). The effect of the motion-impaired data on the diagnosis is shown in Table 5. The interobserver agreement for the identification of aneurysms was substantial ($\kappa = 0.950$; 95% CI, 0.894 – 1.000). Agreement per patient was also high with ($\kappa = 0.965$; 95% CI, 0.916 – 1.000). Both readers agreed substantially on aneurysm configuration ($\kappa = 0.969$; 95% CI, 0.941 – 0.996 ; $P < .001$). Reader 1 agreed in all repeated cases with his initial reading.

Radiation Dose

The mean dose-length product was 564.7 ± 201.4 mGy \times cm for BSCTA and 1608.9 ± 1299.6 mGy \times cm for DSA, meaning a reduction of 65% ($P < .001$, 2-sample Student *t* test). The effective dose for BSCTA was between 0.8 and 3.6 mSv, with an average effective dose of 1.3 ± 0.3 mSv. The average effective radiation dose for diagnostic DSA was 3.7 ± 2.98 mSv, ranging from 0.37 to 17.3 mSv.

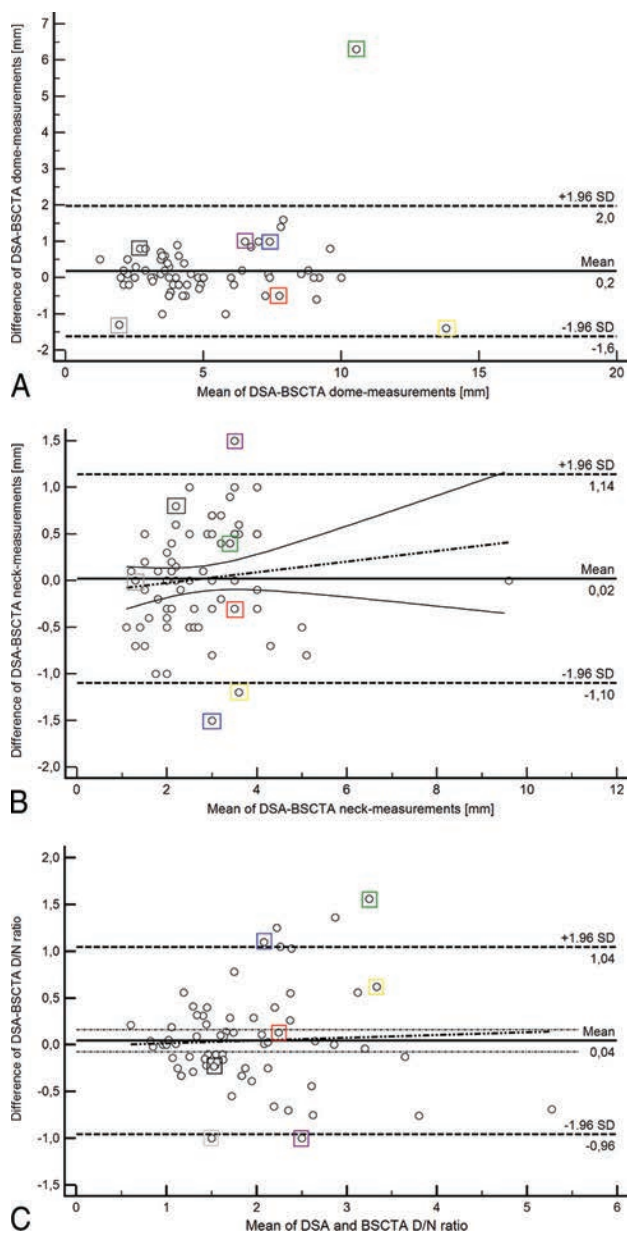


FIG 4. Bland-Altman plots show the relationship between differences and means of DSA and BSCTA in aneurysm dome (A) and neck (B) measurements and dome/neck ratios (C). The *black dotted line* indicates the regression line of the differences. The *2 thin black lines* represent the 95% confidence interval for the regression line of the differences. A, Bone subtraction CTA tends to overestimate aneurysm domes by 0.17 mm (95% CI, 0.04–0.39 mm) and has a mild trend toward higher values for dome diameters with larger values. The colored *rectangular boxes* highlight manual measurements with interpolation of DSA results because DSA millimeter calibrations were not transferred with the other DSA data. The outlier case is 1 large 14.0-mm aneurysm that was overestimated by 6.0 mm and belongs to the manually calculated measurements. B, Bone-subtraction CTA measurements of the aneurysm neck are in good agreement with DSA (0 ± 1.96 mm). Outlier cases are small 2.5- and 2.7-mm aneurysms that were underestimated by -1.5 and -1.2 mm. The third outlier was a 2.7-mm aneurysm that was overestimated by 1.5 mm. C, Bone-subtraction CTA slightly overestimates dome/neck ratios compared with DSA (mean, 0.04; 95% CI, 0.08–0.16). Four of the 6 outliers belong to the manually calculated DSA measurements (colored *rectangular boxes*).

Table 5: Patient motion artifacts and performance on aneurysm detection

Method	Intubated Patients	Motion Artifacts			Aneurysm Detection	
		Mild	Moderate	Severe	FN	FP
DSA	1	15	6	7	0	0
CT	0	1	1	0	0	0

Note:—FP indicates false-positive; FN, false-negative.

DISCUSSION

Our study confirmed a high accuracy of 16–detector row BSCTA in depicting and characterizing intracranial aneurysms. Immediate selection and planning of treatment was possible, even for complex and small aneurysms. This effect was true even for the relatively small amount of aneurysms that were close to bony structures. Furthermore, we demonstrated that the BSCTA method is already delivering high accuracy and robustness, even with widely available, outdated, 16–detector row multidetector CT hardware.

Therefore given the radiation-exposure reduction, BSCTA could replace diagnostic DSA. More advanced CT technology will probably perform as well or even better.

CTA has a high sensitivity and specificity in detecting intracranial aneurysms,^{8,9,11,12,17,19,20} but skull base structures can hide adjacent aneurysms.^{17,21} Bone-subtraction CTA^{22,23} has been developed to overcome this problem. A feasibility study²² and a study with 100 patients²⁴ showed that BSCTA can improve the detection of vascular pathology closely adjacent to bony structures. These studies, however, did not use DSA as the reference standard to determine the diagnostic accuracy of BSCTA under clinical conditions. A recent 320–detector row BSCTA study evaluated the diagnostic accuracy of nonsubtracted and subtracted volumetric CTA data.¹² The sensitivity for nonsubtracted CTA was 96.7% compared with 99.2% for subtracted CTA with 100% specificity for both.

Our findings are concordant with those in previous reports^{8–11} and compare well with a meta-analysis of twelve 16–detector row BSCTA studies.¹⁰ The sensitivity and specificity of BSCTA for small aneurysms (<3.0 mm) were lower than those in our population.

Our study results also compare well with 8 pooled 64–detector row BSCTA studies.¹⁰ Similar results were seen in a 64–detector row multidetector CT study with 89 patients.⁷ Our study results are also in line with those in 2 other studies by using modern dual-source and 320–detector row BSCTA.¹²

In our study, 1 aneurysm of <3 mm (2.5 mm) in diameter was missed by DSA (Fig 3). Another <3 -mm (1.7 mm) aneurysm was initially missed by BSCTA (Fig 2). In both cases, these findings did not change the treatment strategy. Both methods have a small risk of missing small aneurysms. The diagnostic accuracy of DSA was limited by complex vascular anatomy (vessel trifurcation, small diameter of <3 mm) and inadequate projections due to patient motion. In a study with 50 patients presenting with diffuse aneurysmal pattern, 2 aneurysms were missed initially by DSA and BSCTA.²⁵

False-positive cases on both 16– and 64–detector row BSCTA can be explained by focal venous plexus overlying the MCA.¹⁷ Venous contrast has been described as a potential source of error.^{26,27} Venous enhancement is, however, not a crucial factor in the detection of cerebral aneurysms, except for extensive en-

hancement of the cavernous sinus.²⁸ In contrast, with 16–detector row CTA and bolus triggering, arterial and venous structures can be distinguished by their different attenuations. Whether modern, wide-detector (>64–detector row), multidetector CT is capable of further improving the diagnostic accuracy of BSCTA, beyond the known 16– and 64–detector row multidetector CT results, needs to be investigated. With wider z-coverage, the negative effect of scatter radiation and conebeam artifacts increases and may not lead to a further gain in accuracy.^{29,30}

The most common and well-studied geometric determinant of treatment decisions and outcome is the dome-to-neck ratio.²¹ Aspects of aneurysm geometry such as shape, size, dome-to-neck ratio, and location and the relationship to the parent vessels all may impact treatment decisions.^{31,32}

Interobserver agreement in our study was somewhat higher than that reported previously.^{11,17,19,26} Intraobserver agreement was excellent as in another study by Lu et al.¹¹

We had excellent interreader agreement for aneurysm identification and configuration. Our results are in line with those in other studies,^{17,26} even with a recent study with 320–detector row BSCTA³³ comparing CTA with intraoperative observations.

Only 1 study evaluated the D/N ratios in a comparable fashion, but not in the same level of detail.²⁶ In contrast to our results, this study reported a general overestimation of D/N ratio with 16–detector row BSCTA due to partial volume sampling effects.²⁴ Considerable overestimation of the D/N ratio of aneurysms may have led to therapeutic option changes.²⁶ Endovascular treatment of wide-neck or “difficult” aneurysms requires special techniques such as balloon- or stent-assisted coiling.²¹ Because we did not document the decisions of our interventionists and neurosurgeons, we do not know to what extent the information provided by BSCTA has influenced patient management. We can state, however, that BSCTA assessed the site and shape of cerebral aneurysms as accurately as DSA.

Radiation is an important factor for patients with SAH,³⁴ because many are younger and need repeat brain imaging. Our BSCTA dose values were below the European reference value (2.4 mSv) for CT angiography of the brain.³⁵ Our average DSA radiation dose remained at the lower limit of doses reported for DSA (3.5–6.5 mSv).³⁶ A disadvantage of BSCTA is the radiation dose, due to 2 consecutive scans, which means an increase of exposure by 20%–25% above the level of standard CTA according to our and others’ experience.^{37,38} Low-dose settings for nonenhanced CT are acceptable in achieving an effective dose below 3 mSv. Recently new approaches are being evaluated to replace the low-dose NECT with either a standard-dose NECT or a late venous CT dataset, to receive the subtraction bone mask.^{39–41} Optimally, the work-up of SAH before the selection of a method of aneurysm treatment should be exclusively noninvasive diagnostics. In contrast to diagnostic DSA, BSCTA can reduce the door-to-treatment time by providing the relevant information instantly.^{17,26} It may even prevent DSA in cases with a clear indication for clipping.^{26,27,42} The accuracy of BSCTA being comparable with DSA now allows clipping of these aneurysms without additional DSA when transarterial intervention is not possible. In cases where the

first CTA does not show the cause of SAH, it is not necessary to perform DSA. A second CTA is sufficient.

Moreover, BSCTA can exclude an aneurysm as the cause of spontaneous SAH.¹⁷

Our study has limitations. Although BSCTA was feasible in almost all patients, we could recruit patients only when the involved neuroradiologist was on duty and had ordered the new BSCTA protocol. We cannot safely exclude the possibility that the patients identified by study neuroradiologists were different from those with SAH seen by a radiologist not familiar with the study. We aimed to consecutively identify all patients with acute SAH and without previous aneurysm treatment, which means we had no knowledge of the source of bleeding. We thought this population was the best to study the accuracy of BSCTA. We lost patients for the study when radiologists on call were not yet familiar with the study protocol. We think, however, that the patients we recruited represented the population typical for acute SAH. Consequently, we extended the observation period to reach the planned sample size.

In our institution, we now recommend BSCTA in addition to NECT as the first imaging technique in patients with acute SAH. Our neurosurgeons clip aneurysms solely on the basis of this information in urgent cases that cannot be coiled. We have reduced the DSA protocol before intervention to the artery affected and do not further perform panangiographies. We further recommend repeat BSCTA in cases of CTA with negative findings in patients with SAH, but we admit that not all of our neurosurgeons consistently follow this advice.

CONCLUSIONS

The widely available 16–detector row BSCTA allows reliable and accurate detection and characterization of cerebral aneurysms in patients with acute SAH and thus can guide treatment decisions faster and more efficiently. If the location and shape of aneurysms favor surgical clipping, an additional DSA is no longer necessary because all information needed by neurosurgeons is provided. If coiling is preferred, complete diagnostic 4-vessel panangiography is no longer routinely required. Interventionists can focus DSA on the site of the symptomatic aneurysm. This new strategy will not only reduce the risks and radiation dose for patients and physicians, but also reduce cost and time. More modern CT technology may make BSCTA more efficient, more standardized, and finally easier to apply.

Disclosures: Peter Aulbach—*RELATED: Support for Travel to Meetings for the Study or Other Purposes:* Siemens, *Comments:* Siemens, as my employer, supports my studies through payments for traveling to the university and back. It is just the cost for hotel, car, and fuel; *UNRELATED: Employment:* Siemens, *Comments:* I am an employee of Siemens. My PhD is tolerated there as part of my personal development. My employer just compensates the cost for me to travel to the University (car, fuel, and hotel). Additionally, Siemens allows me to spend time at the university if it is not too many days. As long as my work output does not suffer, they tolerate it. Rüdiger von Kummer—*UNRELATED: Board Membership:* Lundbeck; *Consultancy:* Lundbeck, Penumbra, Covidien, Boehringer Ingelheim; *Payment for Lectures (including service on Speakers Bureaus):* Penumbra; *Royalties:* Elsevier, Springer, *Comments:* book chapter authorship.

REFERENCES

1. Connolly ES Jr, Rabinstein AA, Carhuapoma JR, et al; American Heart Association Stroke Council, Council on Cardiovascular Radi-

- ology and Intervention, Council on Cardiovascular Nursing, Council on Cardiovascular Surgery and Anesthesia, Council on Clinical Cardiology. **Guidelines for the management of aneurysmal subarachnoid hemorrhage: a guideline for healthcare professionals from the American Heart Association/American Stroke Association.** *Stroke* 2012;43:1711–37 CrossRef Medline
2. Dawkins AA, Evans AL, Wattam J, et al. **Complications of cerebral angiography: a prospective analysis of 2,924 consecutive procedures.** *Neuroradiology* 2007;49:753–59 CrossRef Medline
 3. Fifi JT, Meyers PM, Lavine SD, et al. **Complications of modern diagnostic cerebral angiography in an academic medical center.** *J Vasc Interv Radiol* 2009;20:442–47 CrossRef Medline
 4. Velthuis BK, Van Leeuwen MS, Witkamp TD, et al. **Computerized tomography angiography in patients with subarachnoid hemorrhage: from aneurysm detection to treatment without conventional angiography.** *J Neurosurg* 1999;91:761–67 CrossRef Medline
 5. Rinkel GJ, van Gijn J, Wijdicks EF. **Subarachnoid hemorrhage without detectable aneurysm: a review of the causes.** *Stroke* 1993;24:1403–09 CrossRef Medline
 6. Saitoh H, Hayakawa K, Nishimura K, et al. **Rerupture of cerebral aneurysms during angiography.** *AJNR Am J Neuroradiol* 1995;16:539–42 Medline
 7. Li Q, Lv F, Li Y, et al. **Evaluation of 64-section CT angiography for detection and treatment planning of intracranial aneurysms by using DSA and surgical findings.** *Radiology* 2009;252:808–15 CrossRef Medline
 8. Zhang LJ, Wu SY, Niu JB, et al. **Dual-energy CT angiography in the evaluation of intracranial aneurysms: image quality, radiation dose, and comparison with 3D rotational digital subtraction angiography.** *AJR Am J Roentgenol* 2010;194:23–30 CrossRef Medline
 9. Zhang LJ, Wu SY, Poon CS, et al. **Automatic bone removal dual-energy CT angiography for the evaluation of intracranial aneurysms.** *J Comput Assist Tomogr* 2010;34:816–24 CrossRef Medline
 10. Menke J, Larsen J, Kallenberg K. **Diagnosing cerebral aneurysms by computed tomographic angiography: meta-analysis.** *Ann Neurol* 2011;69:646–54 CrossRef Medline
 11. Lu L, Zhang LJ, Poon CS, et al. **Digital subtraction CT angiography for detection of intracranial aneurysms: comparison with three-dimensional digital subtraction angiography.** *Radiology* 2012;262:605–12 CrossRef Medline
 12. Chen W, Xing W, Peng Y, et al. **Cerebral aneurysms: accuracy of 320-detector row nonsubtracted and subtracted volumetric CT angiography for diagnosis.** *Radiology* 2013;269:841–49 CrossRef Medline
 13. Papke K, Kuhl CK, Fruth M, et al. **Intracranial aneurysms: role of multidetector CT angiography in diagnosis and endovascular therapy planning.** *Radiology* 2007;244:532–40 CrossRef Medline
 14. Westerlaan HE, van Dijk JMC, van Dijk MJ, et al. **Intracranial aneurysms in patients with subarachnoid hemorrhage: CT angiography as a primary examination tool for diagnosis—systematic review and meta-analysis.** *Radiology* 2011;258:134–45 CrossRef Medline
 15. Agid R, Willinsky RA, Farb RI, et al. **Life at the end of the tunnel: why emergent CT angiography should be done for patients with acute subarachnoid hemorrhage.** *AJNR Am J Neuroradiol* 2008;29:e45; author reply e46–47 CrossRef Medline
 16. Fox AJ, Symons SP, Aviv RI. **CT angiography is state-of-the-art first vascular imaging for subarachnoid hemorrhage.** *AJNR Am J Neuroradiol* 2008;29:e41–42; author reply e46–47 CrossRef Medline
 17. McKinney AM, Palmer CS, Truwit CL, et al. **Detection of aneurysms by 64-section multidetector CT angiography in patients acutely suspected of having an intracranial aneurysm and comparison with digital subtraction and 3D rotational angiography.** *AJNR Am J Neuroradiol* 2008;29:594–602 CrossRef Medline
 18. Donmez H, Serifov E, Kahrman G, et al. **Comparison of 16-row multislice CT angiography with conventional angiography for detection and evaluation of intracranial aneurysms.** *Eur J Radiol* 2011;80:455–61 CrossRef Medline
 19. Romijn M, Gratama van Andel HA, van Walderveen MA, et al. **Diagnostic accuracy of CT angiography with matched mask bone elimination for detection of intracranial aneurysms: comparison with digital subtraction angiography and 3D rotational angiography.** *AJNR Am J Neuroradiol* 2008;29:134–39 CrossRef Medline
 20. Li Q, Lv F, Li Y, et al. **Subtraction CT angiography for evaluation of intracranial aneurysms: comparison with conventional CT angiography.** *Eur Radiol* 2009;19:2261–67 CrossRef Medline
 21. Brinjikji W, Cloft HJ, Kallmes DF. **Difficult aneurysms for endovascular treatment: overdue or undertall?** *AJNR Am J Neuroradiol* 2009;30:1513–17 CrossRef Medline
 22. Lell MM, Ruehm SG, Kramer M, et al. **Cranial computed tomography angiography with automated bone subtraction: a feasibility study.** *Invest Radiol* 2009;44:38–43 CrossRef Medline
 23. Lell M, Anders K, Klotz E, et al. **Clinical evaluation of bone-subtraction CT angiography (BSCTA) in head and neck imaging.** *Eur Radiol* 2006;16:889–97 CrossRef Medline
 24. Morhard D, Fink C, Becker C, et al. **Value of automatic bone subtraction in cranial CT angiography: comparison of bone-subtracted vs. standard CT angiography in 100 patients.** *Eur Radiol* 2008;18:974–82 CrossRef Medline
 25. Agid R, Andersson T, Almqvist H, et al. **Negative CT angiography findings in patients with spontaneous subarachnoid hemorrhage: when is digital subtraction angiography still needed?** *AJNR Am J Neuroradiol* 2010;31:696–705 CrossRef Medline
 26. Yoon DY, Lim KJ, Choi CS, et al. **Detection and characterization of intracranial aneurysms with 16-channel multidetector row CT angiography: a prospective comparison of volume-rendered images and digital subtraction angiography.** *AJNR Am J Neuroradiol* 2007;28:60–67 Medline
 27. Agid R, Lee SK, Willinsky RA, et al. **Acute subarachnoid hemorrhage: using 64-slice multidetector CT angiography to “triage” patients’ treatment.** *Neuroradiology* 2006;48:787–94 CrossRef Medline
 28. Lell MM, Anders K, Uder M, et al. **New techniques in CT angiography.** *Radiographics* 2006;26(suppl 1):S45–62 CrossRef Medline
 29. Li B, Toth TL, Hsieh J, et al. **Simulation and analysis of image quality impacts from single source, ultra-wide coverage CT scanner.** *J Xray Sci Technol* 2012;20:395–404 CrossRef Medline
 30. Boas FE, Fleischmann D. **CT artifacts: causes and reduction techniques.** *Imaging Med* 2012;4:229–40 CrossRef
 31. Gonzalez N, Sedrak M, Martin N, et al. **Impact of anatomic features in the endovascular embolization of 181 anterior communicating artery aneurysms.** *Stroke* 2008;39:2776–82 CrossRef Medline
 32. Brinjikji W, Cloft H, Lanzino G, et al. **Comparison of 2D digital subtraction angiography and 3D rotational angiography in the evaluation of dome-to-neck ratio.** *AJNR Am J Neuroradiol* 2009;30:831–34 CrossRef Medline
 33. Hayashida E, Sasao A, Hirai T, et al. **Can sufficient preoperative information of intracranial aneurysms be obtained by using 320-row detector CT angiography alone?** *Jpn J Radiol* 2013;31:600–07 CrossRef Medline
 34. Gelfand AA, Josephson SA. **Substantial radiation exposure for patients with subarachnoid hemorrhage.** *J Stroke Cerebrovasc Dis* 2011;20:131–33 CrossRef Medline
 35. European Commission. **European guidelines on quality criteria for computed tomography.** Report EUR 16262. Brussels, Belgium: European Commission, 1999
 36. Westerlaan HE, Gravendeel J, Fiore D, et al. **Multislice CT angiography in the selection of patients with ruptured intracranial aneurysms suitable for clipping or coiling.** *Neuroradiology* 2007;49:997–1007 CrossRef Medline
 37. Venema HW, Hulsmans FJ, den Heeten GJ. **CT angiography of the circle of Willis and intracranial internal carotid arteries: maximum intensity projection with matched mask bone elimination—feasibility study.** *Radiology* 2001;218:893–98 CrossRef Medline
 38. Tomandl BF, Hammen T, Klotz E, et al. **Bone-subtraction CT angiography for the evaluation of intracranial aneurysms.** *AJNR Am J Neuroradiol* 2006;27:55–59 Medline
 39. Huang A, Lee CW, Yang CY, et al. **Using standard nonenhanced**

- axial scans for cerebral CT angiography bone elimination: feasibility study. *Invest Radiol* 2010;45:225–32 CrossRef Medline
40. Lell MM, Ditt H, Panknin C, et al. **Cervical CT angiography comparing routine noncontrast and a late venous scan as masks for automated bone subtraction: feasibility study and examination of the influence of patient motion on image quality.** *Invest Radiol* 2008;43:27–32 CrossRef Medline
41. Gratama van Andel HA, Venema HW, Streekstra GJ, et al. **Removal of bone in CT angiography by multiscale matched mask bone elimination.** *Med Phys* 2007;34:3711–23 CrossRef Medline
42. Pozzi-Mucelli F, Bruni S, Doddi M, et al. **Detection of intracranial aneurysms with 64 channel multidetector row computed tomography: comparison with digital subtraction angiography.** *Eur J Radiol* 2007;64:15–26 CrossRef Medline

Cerebral Perfusion Pressure is Maintained in Acute Intracerebral Hemorrhage: A CT Perfusion Study

A.S. Tamm, R. McCourt, B. Gould, M. Kate, J.C. Kosior, T. Jeerakathil, L.C. Gioia, D. Dowlatshahi,  M.D. Hill, S.B. Coutts,  A.M. Demchuk, B.H. Buck, D.J. Emery, A. Shuaib, and K.S. Butcher; on behalf of the ICH ADAPT Investigators



ABSTRACT

BACKGROUND AND PURPOSE: Although blood pressure reduction has been postulated to result in a fall in cerebral perfusion pressure in patients with intracerebral hemorrhage, the latter is rarely measured. We assessed regional cerebral perfusion pressure in patients with intracerebral hemorrhage by using CT perfusion source data.

MATERIALS AND METHODS: Patients with acute primary intracerebral hemorrhage were randomized to target systolic blood pressures of <150 mm Hg ($n = 37$) or <180 mm Hg ($n = 36$). Regional maps of cerebral blood flow, cerebral perfusion pressure, and cerebrovascular resistance were generated by using CT perfusion source data, obtained 2 hours after randomization.

RESULTS: Perihematoma cerebral blood flow (38.7 ± 11.9 mL/100 g/min) was reduced relative to contralateral regions (44.1 ± 11.1 mL/100 g/min, $P = .001$), but cerebral perfusion pressure was not (14.4 ± 4.6 minutes⁻¹ versus 14.3 ± 4.8 minutes⁻¹, $P = .93$). Perihematoma cerebrovascular resistance (0.34 ± 0.11 g/mL) was higher than that in the contralateral region (0.30 ± 0.10 g/mL, $P < .001$). Ipsilateral and contralateral cerebral perfusion pressure in the external (15.0 ± 4.6 versus 15.6 ± 5.3 minutes⁻¹, $P = .15$) and internal (15.0 ± 4.8 versus 15.0 ± 4.8 minutes⁻¹, $P = .90$) borderzone regions were all similar. Borderzone cerebral perfusion pressure was similar to mean global cerebral perfusion pressure (14.7 ± 4.7 minutes⁻¹, $P \geq .29$). Perihematoma cerebral perfusion pressure did not differ between blood pressure treatment groups (13.9 ± 5.5 minutes⁻¹ versus 14.8 ± 3.4 minutes⁻¹, $P = .38$) or vary with mean arterial pressure ($r = -0.08$, $[-0.10, 0.05]$).

CONCLUSIONS: Perihematoma cerebral perfusion pressure is maintained despite increased cerebrovascular resistance and reduced cerebral blood flow. Aggressive antihypertensive therapy does not affect perihematoma or borderzone cerebral perfusion pressure. Maintenance of cerebral perfusion pressure provides physiologic support for the safety of blood pressure reduction in intracerebral hemorrhage.

ABBREVIATIONS: BP = blood pressure; BZ = borderzone; CPP = cerebral perfusion pressure; CVR = cerebrovascular resistance; ICH = intracerebral hemorrhage; ICH ADAPT = Intracerebral Hemorrhage Acutely Decreasing Arterial Pressure Trial

Patients with intracerebral hemorrhage (ICH) most often present with elevated blood pressure (BP), but acute treatment remains controversial.^{1,2} Despite the results of recent randomized controlled trials of BP management demonstrating no excess of adverse clinical events,^{3,4} many physicians are reluctant to aggres-

sively use antihypertensive agents in the acute phase of ICH. This reluctance is primarily based on persisting theoretic concerns that there is a zone of tissue at risk for ischemic injury surrounding the acute hematoma.⁵ In addition, more recent MR imaging studies have suggested that subacute ischemic injury occurs in areas remote from the hematoma, including borderzone (BZ, also known as watershed) regions.⁶⁻¹¹ The etiology of these ischemic injuries has been postulated to be hemodynamic compromise secondary to BP reduction.¹⁰ Studies of CBF in the perihematoma region indicate that this region is relatively hypoperfused, but not se-

Received February 23, 2015; accepted after revision July 14.

From the Division of Neurology (R.M., B.G., M.K., J.C.K., T.J., L.C.G., B.H.B., A.S., K.S.B.) and Department of Diagnostic Imaging (A.S.T., D.J.E.), University of Alberta, Edmonton, Alberta, Canada; Division of Neurology (D.D.), University of Ottawa, Ottawa, Ontario, Canada; and Department of Clinical Neurosciences (M.D.H., S.B.C., A.M.D.), University of Calgary, Calgary, Alberta, Canada.

This work was supported by a grant-in-aid from Alberta Innovates Health Solutions (G513000128) and the Heart and Stroke Foundation of Canada (G220170180). K.S.B. holds a Canada Research Chair in Cerebrovascular Disease, a Heart and Stroke Foundation of Alberta Professorship in Stroke Medicine, and a New Investigator Award from Alberta Innovates Health Solutions. M.D.H. has a Heart and Stroke Foundation of Alberta Professorship in Stroke Medicine. A.M.D. has a Chair in Stroke Medicine (Heart and Stroke Foundation of Alberta). S.B.C. has an Alberta Innovates Health Solutions New Investigator award. B.G. and R.M. were supported by Alberta Innovates Health Solutions studentships.

Preliminary data previously presented at: International Stroke Congress, February 9–11, 2011; Los Angeles, California.

Please address correspondence to Ken Butcher, MD, 2E3 WMC Health Sciences Centre, University of Alberta, 8440 112th St, Edmonton, AB, Canada T6G 2B7; e-mail: ken.butcher@ualberta.ca

 Indicates open access to non-subscribers at www.ajnr.org

<http://dx.doi.org/10.3174/ajnr.A4532>

verely enough to result in ischemia.¹²⁻¹⁴ Previous PET studies have demonstrated that the perihematoma region is, in fact, hypometabolic, likely secondary to the primary brain injury, and that the oxygen extraction fraction is not elevated, indicating the absence of misery perfusion.^{12,15} Nonetheless, it is possible that reduction of BP will result in a fall in cerebral perfusion pressure (CPP), subsequently precipitating ischemia.¹⁶ In the Intracerebral Hemorrhage Acutely Decreasing Arterial Pressure Trial (ICH ADAPT), we demonstrated that acute BP reduction is not associated with a significant fall in CBF.¹⁷ It has been demonstrated, however, that CPP is more sensitive than CBF or CBV to changes in blood pressure.¹⁸ The relationship between CPP and BP reduction in patients with intracerebral hemorrhage is unknown.

Global CPP is normally calculated as the difference between the mean arterial pressure and intracranial pressure, which requires insertion of an intraventricular manometer. Monitoring of intracranial pressure and CPP is generally reserved for patients with a decreased level of consciousness and/or obstructive hydrocephalus requiring ventricular drainage. In these cases, current consensus guidelines recommend that BP be titrated to ensure that CPP is between 50 and 70 mm Hg.^{19,20} In addition, global CPP may not reflect local variations in intracranial pressure due to the mass effect of a hematoma, particularly in small hematomas.²¹ Measurements of regional CPP might inform clinical BP management decisions. With PET, it has been demonstrated that CPP can be calculated as a ratio of CBF to CBV.¹⁸ We adapted this technique by using CTP source data from ICH ADAPT to assess local CPP in acute ICH. We tested the hypothesis that aggressive antihypertensive therapy reduces CPP in the perihematoma and borderzone regions.

MATERIALS AND METHODS

Patients

The ICH ADAPT protocol (clinicaltrials.gov, NCT00963976) has been published previously.⁴ Briefly, patients 18 years of age or older presenting with acute primary (spontaneous) ICH diagnosed on noncontrast CT within 24 hours of symptom onset were prospectively enrolled. Exclusion criteria included evidence of secondary ICH (ie, related to underlying tumors, arteriovenous malformations, or drug use), planned surgical resection, contraindications to BP reduction or an indication for urgent reduction, or inability to undergo CTP imaging. A standardized antihypertensive treatment protocol was applied with the sequential use of labetalol, hydralazine, and IV enalapril. Informed consent was obtained from each patient or an authorized representative, and the human ethics committees at each site approved the study protocol.

Imaging Protocol

Two hours after randomization, all patients underwent a standard repeat noncontrast CT scan of the brain. The scan consisted of 5-mm sections (120 KV[peak], 300 mA per section) through the entire brain (18–20 sections with a 512 × 512 matrix). Due to differences in CT scanner capabilities between sites, a variable 38- to 80-mm-thick section was selected to assess perfusion (CTP) centered over the section where the hematoma had the greatest diameter on noncontrast CT. Intravenous iodinated contrast (40

mL) was administered at 4–7 mL/s via an 18-ga angiocatheter in an antecubital vein. CTP images were acquired every 1 second for 50 seconds (80 KV[p], 200 mA per image), and all sections were 5-mm-thick. All patients had a repeat NCCT scan at 24 ± 3 hours.

Image Processing and Analysis

Raw contrast-enhanced CT images were imported into the PerfScape analysis package (2.0 CT Edition; Olea Medical, La Ciotat, France) software. An arterial input function was manually selected over the contralateral anterior cerebral artery, while the venous output function was obtained over the confluence of the sinuses. Perfusion maps were derived from the tissue time-attenuation curve on the basis of the change in x-ray attenuation, which is linearly related to iodinated contrast concentration on a per-voxel basis with time. Errors introduced by delay and dispersion of the contrast bolus before arrival in the cerebral circulation were corrected for by using a block-circulant deconvolution algorithm.²² Quantitative perfusion indices, including CBF and CBV, were calculated on a voxelwise basis and used to generate color-coded maps.

All perfusion maps were transferred to the Analyze 11.0 software package (AnalyzeDirect, Overland Park, Kansas).²³ Maps of CPP and cerebrovascular resistance (CVR) were generated by using a voxelwise calculation of CBF/CBV and 1/CBV, respectively (Fig 1), as previously described.¹⁸ The perimeter of the hematoma was outlined on the precontrast arrival CT source image by using a semiautomated intensity Hounsfield unit threshold technique, as previously described.²⁴ Internal and external BZ and 7-mm perihematoma ROIs were manually outlined (Fig 1). In cases in which the hematoma itself involved a BZ, the latter was not outlined. All voxels containing blood vessels were removed from the ROI by using an intensity-threshold function. On the basis of previous studies, voxels with CBF of >100 mL/100 g/min or CBV of >8 mL/100 g were assumed to contain vessels and removed from the ROI.²⁵⁻²⁷ Mean perfusion indices were measured in all ROIs, contralateral homologous regions, and the entire hemispheres (excluding the hematoma) ipsilateral and contralateral to the hematoma.

Statistical Analysis

Statistical analysis was performed by using SPSS Statistics 21.0 2008 (IBM, Armonk, New York). Differences in perfusion parameters were assessed with paired *t* tests. Linear regression was used to assess the relationship between the perfusion parameters and blood pressure. Differences in perfusion parameters between treatment groups were assessed with independent-samples *t* tests.

RESULTS

Patient Characteristics and Outcomes

Seventy-five patients were randomized in ICH ADAPT.¹⁷ Two patients were excluded from this analysis due to inadequate quality of raw CTP data required to complete CPP and CVR calculations. This study, therefore, included 73 patients (54 men), with a median age of 70 years (interquartile range, 60–80 years). Hematoma locations were as follows: 55 basal ganglia, 17 lobar, and 1 posterior fossa. Median time from symptom onset to CTP imag-

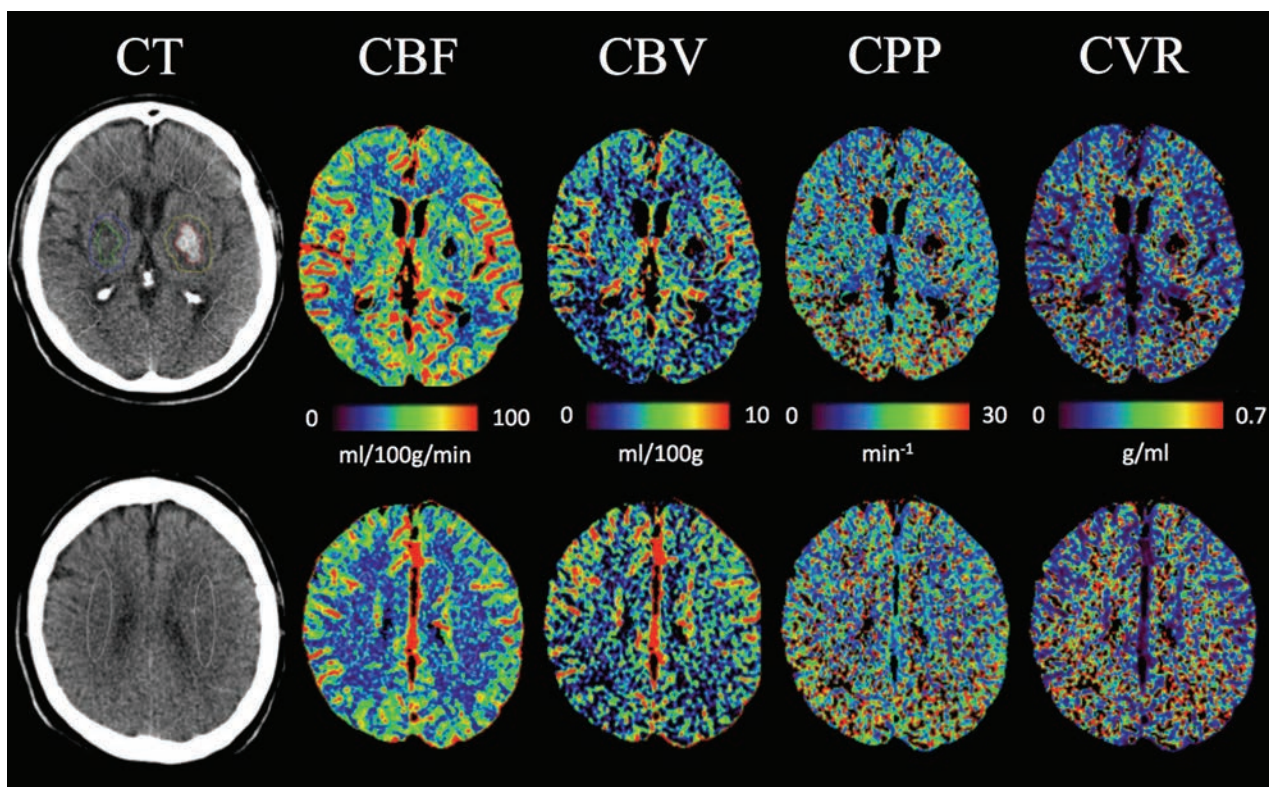


FIG 1. Examples of CT perfusion source data with perihematoma and external and internal borderzone ROIs. Maps of cerebral blood flow, cerebral blood volume, cerebral perfusion pressure, and cerebrovascular reserve at 2 different sections from a patient in the <180-mm Hg treatment group.

ing was 9.8 hours (interquartile range, 6.0–19.2 hours), and from the acute diagnostic CT to the CTP study, it was 4.8 hours (interquartile range, 3.4–14.5 hours). The delay between the diagnostic CT and randomization was variable with a median of 2.3 hours (interquartile range, 1.0–11.6 hours). Four patients in each treatment arm had antithrombotic-associated ICH (either antiplatelet or anticoagulant; Table 1).

The mean systolic and diastolic BP at the time of the CTP scan was 150 ± 20 and 77 ± 15 mm Hg, respectively. The number of patients receiving each of the 3 antihypertensive therapies along with the mean dose is recorded in Table 1. The median acute Glasgow Coma Scale and NIHSS scores were 15 (range, 4–15; interquartile range, 13–15) and 10 (range, 1–35; interquartile range, 6–17), respectively.

The mean intraparenchymal hematoma volume at the time of CTP imaging was 23.9 ± 28.3 mL. Follow-up imaging was performed at a median of 21.8 hours (interquartile range, 21–23.7 hours) later. Mean hematoma volume at that time was 25.5 ± 27.3 mL. Eleven patients (15%) had large-volume ICHs, with hematoma volumes of >40 mL. Hematoma expansion of >6 mL was seen in 16 patients (8 in each treatment group, $P = .86$). Thirty-seven patients were randomized to a target BP of <150 mm Hg, and 36, to a target BP of <180 mm Hg. No significant differences in patient characteristics were seen between the treatment groups (Table 1).

There were no differences in any clinical outcome events between the 2 groups (Table 1). Mortality was 19% in the 150-mm Hg treatment group and 11% in the 180-mm Hg treatment group

($P = .52$). Functional disability as measured by the modified Rankin Scale score was comparable between the 150-mm Hg (median, 3 mm Hg; interquartile range, 1.5–5.5 mm Hg) and 180-mm Hg (median, 4 mm Hg; interquartile range, 2–5 mm Hg) treatment groups ($P = .43$). No patient in the trial had an ischemic lesion on 24-hour follow-up CT.

Cerebral Blood Flow and Volume

Mean perihematoma CBF in all 73 patients (38.7 ± 11.9 mL/100 g/min; Fig 2) was significantly lower than that in contralateral homologous regions (44.1 ± 11.1 mL/100 g/min, $P < .001$). Mean ipsilateral hemispheric CBF (42.1 ± 10.5 mL/100 g/min) was lower than that in the contralateral hemisphere (43.4 ± 10.5 mL/100 g/min, $P < .001$).

There was a reduction in perihematoma CBV (3.65 ± 0.70 mL/100 g; Fig 2) compared with the contralateral regions (4.21 ± 1.53 mL/100 g, $P = .001$). Mean ipsilateral hemispheric CBV (3.83 ± 0.63 mL/100 g) was lower than that in the contralateral hemisphere (3.88 ± 0.64 mL/100 g, $P = .033$).

Cerebral Perfusion Pressure and Cerebrovascular Resistance

Perihematoma CPP (14.4 ± 4.6 minutes⁻¹) was similar to that in contralateral homologous regions (14.3 ± 4.8 minutes⁻¹, $P = .93$; Fig 2). Ipsilateral hemispheric CPP (14.6 ± 4.6 minutes⁻¹) was also comparable with that in the contralateral hemispheric CPP (14.8 ± 4.9 minutes⁻¹, $P = .28$). There were no differences in CPP within the ipsilateral and contralateral external (15.0 ± 4.6

Table 1: Baseline characteristics and outcomes of randomized patients^a

Characteristic	<150-mm Hg Target (n = 37)	<180-mm Hg Target (n = 36)	P Value
Age (yr)	71.0 ± 12.5	68.7 ± 11.1	.40
Male	26 (70%)	28 (78%)	.47
Symptom onset to randomization (hr)	10.5 ± 7.4	9.7 ± 7.0	.65
Medical history			
Hypertension	26 (70%)	27 (75%)	.71
Previous ICH	4 (11%)	1 (3%)	.19
Antiplatelet/anticoagulation	4 (11%)	4 (11%)	.74
Ischemic stroke	6 (16%)	2 (6%)	.17
Clinical characteristics			
Systolic BP (mm Hg)	182 ± 20	184 ± 25	.66
Diastolic BP (mm Hg)	94 ± 19	97 ± 23	.53
Mean arterial pressure (mm Hg)	123 ± 17	126 ± 22	.54
Glasgow Coma Scale	13.3 ± 2.7	13.9 ± 1.9	.27
NIHSS score	12.3 ± 7.7	11.5 ± 6.3	.64
Hematoma characteristics			
Basal ganglia	28 (76%)	27 (75%)	.99
Lobar	9 (24%)	8 (22%)	
Cerebellum	0 (0%)	1 (3%)	
Intraparenchymal volume (mL)	24.5 ± 28.9	22.61 ± 21.35	.75
Intraventricular volume (mL)	2.20 ± 6.26	4.25 ± 8.78	.26
Total ICH volume (mL)	26.68 ± 31.50	26.86 ± 25.24	.98
Antihypertensive therapy ^b			
Labetalol (No.) (mean dose ± SD in mg)	34 (38 ± 25)	16 (29 ± 25)	
Hydralazine (No.) (mean dose ± SD in mg)	18 (22 ± 14)	5 (14 ± 8)	
IV enalapril (No.) (mean dose ± SD in mg)	9 (1.25 ± 0)	3 (1.25 ± 0)	
Outcomes			
Mortality (No.) (%)	7 (19)	4 (11)	.52
Modified Rankin Scale score (median) (IQR)	3 (1.5–5.5)	4 (2–5)	.43
Hematoma growth >6 mL (No.) (%)	8 (21)	8 (22)	.86

Note.—IQR indicates interquartile range.

^a Data are means unless otherwise specified.

^b Nineteen patients in the <150-mm Hg group and 2 patients in the <180-mm Hg group received multiple antihypertensives.

and 15.6 ± 5.3 minutes⁻¹, respectively; $P = .15$) or ipsilateral and contralateral internal (15.0 ± 4.8 and 15.0 ± 4.8 minutes⁻¹, respectively; $P = .90$) BZ regions. Similarly, there were no significant differences when the CPP in the above ipsilateral and contralateral external and internal BZ regions was compared with the mean bilateral hemispheric CPP (14.7 ± 4.7 minutes⁻¹, $P \geq .29$; Table 2). On linear regression analysis, CPP was not related to intraparenchymal hematoma volume ($\beta = -0.001 [-0.002, 0.001]$).

Mean perihematoma CVR (0.34 ± 0.11 g/mL) was slightly higher than that in contralateral homologous regions (0.30 ± 0.10 g/mL, $P < .001$; Fig 2). Ipsilateral hemispheric CVR was also elevated (0.31 ± 0.08) relative to the contralateral hemisphere (0.30 ± 0.09 g/mL, $P = .04$). There were no hemispheric differences in CVR within the external (0.34 ± 0.12 versus 0.35 ± 0.12 g/mL, $P = .53$) or internal (0.41 ± 0.15 versus 0.39 ± 0.14 g/mL, $P = .17$) BZ regions.

Effect of Blood Pressure Treatment on Cerebral Perfusion Pressure and Cerebrovascular Resistance

At the time of CTP imaging, systolic BP was significantly lower in the <150-mm Hg target group (140 ± 19 mm Hg) than that in the <180-mm Hg target group (162 ± 12 mm Hg, $P < .001$). Mean CPP and CVR in the perihematoma and most BZ regions was similar between BP treatment groups (Table 2). Mean CPP in the ipsilateral internal BZ (13.5 ± 4.6 minutes⁻¹) in the

<150-mm Hg group was lower than that in the <180-mm Hg group (16.5 ± 4.7 minutes⁻¹, $P = .02$; Table 2). Mean CVR in the contralateral internal BZ (0.32 ± 0.11 g/mL) in the <150-mm Hg group was lower than that in the <180-mm Hg group (0.38 ± 0.12 g/mL, $P = .04$; Table 2).

There was no relationship between perihematoma CPP and BP in all patients at the time of the CTP scan (systolic BP, $\beta = -0.04 [-0.07, 0.05]$; diastolic BP, $\beta = -0.10 [-0.11, 0.04]$); or mean arterial pressure, $\beta = -0.08 [-0.10, 0.05]$; Fig 3). Similarly, perihematoma CVR was unrelated to BP at the time of the CTP scan (systolic BP, $\beta = -0.10 [-0.002, 0.001]$; diastolic BP, $\beta = -0.10 [-0.002, 0.001]$); or mean arterial pressure ($\beta = -0.11 [-0.003, 0.001]$, Fig 3).

DISCUSSION

This assessment of local cerebral perfusion pressure and cerebrovascular resistance in patients with acute primary intracerebral hemorrhage indicates that CPP is maintained in all potentially hemodynamically vulnerable regions. There is also a slight increase in CVR within the perihematoma region. Neither CPP nor CVR appear to be affected

by acute BP reduction.

Cerebral Perfusion Pressure Assessment

Changes in CPP are relevant to the management of BP in patients with acute ICH, though measurement of CPP in patients with ICH is challenging. In this study, we adapted the method originally described by Schumann et al (1998)¹⁸ to estimate regional CPP on the basis of positron-emission tomography–derived measurements of CBF. In a primate model of cerebral ischemia, these authors demonstrated that CPP is strongly correlated with mean arterial pressure, the major physiologic determinant of CPP in patients with vascular insults. In fact, CPP (or the CBF/CBV ratio) was shown to be more sensitive to slight variations in mean arterial pressure compared with individual measurements of CBF or CBV.¹⁸ These data indicated that blood pressure reduction did not have a subtle effect on CPP, which may not have been evident on the more conventional measures of CBF and CBV alone at this single point in time. Although PET and CTP differ with respect to tracer kinetics (diffusible versus nondiffusible), the physiologic data are comparable both qualitatively and quantitatively,²⁸ permitting application of the method described by Schumann et al to both perfusion imaging modalities. Additionally, intermittent CTP studies in severe traumatic head injuries have been shown to provide additional information with respect to preservation of autoregulation compared with continuous CPP measurements.²⁹

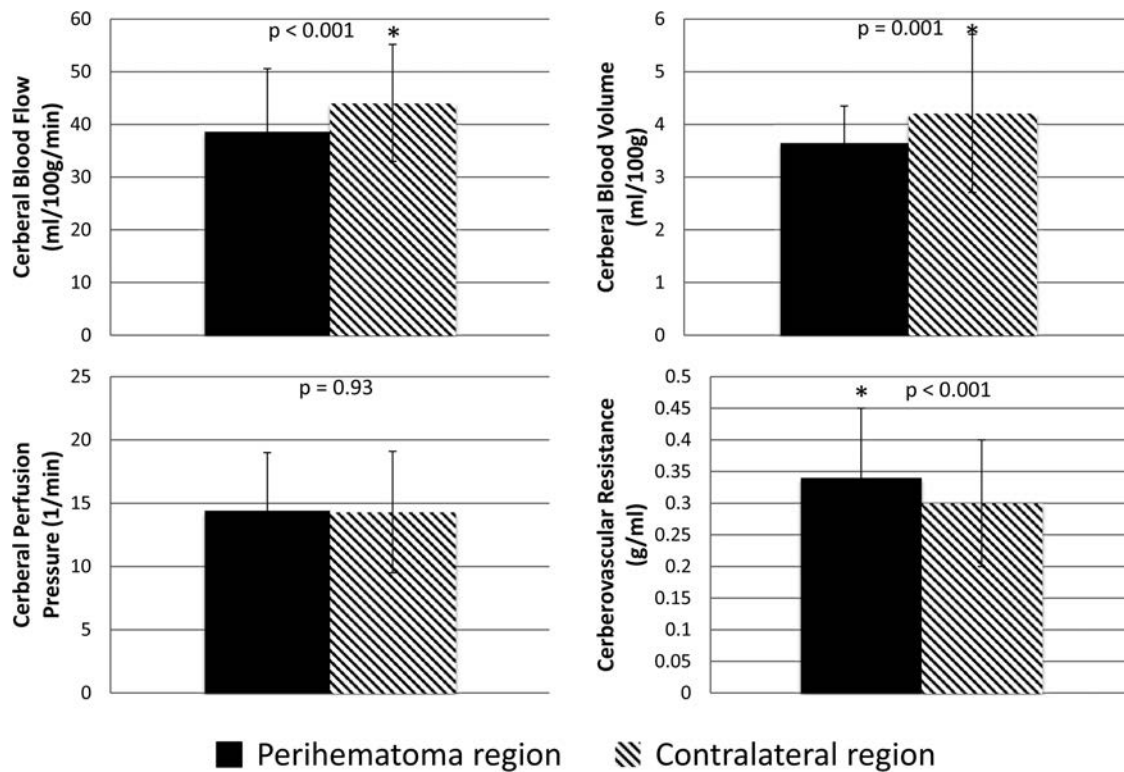


FIG 2. Mean (\pm SD) perihematoma and contralateral homologous region cerebral blood flow, cerebral blood volume, cerebral perfusion pressure, and cerebrovascular reserve.

Thus, CPP measured by noninvasive imaging techniques may be of particular interest in patients with traumatic brain injuries.

Perihematoma Perfusion Pressure

Our results and those of a PET study completed in patients with acute ICH¹² confirm that CBF and CBV are modestly reduced in the perihematoma region. Although estimates of CPP and CVR were not included in the PET studies, these parameters could, in fact, be derived from source data in the same manner as that described by Schumman et al (1998).¹⁸ The elevated CVR within the perihematoma region is presumably secondary to compression of the microvasculature by the space-occupying effect of the hematoma and edema. Maintenance of CPP suggests that this increase in CVR is not responsible for the reduction in CBF, however. Both direct (PET) and indirect (CTP) measurements of oxygen metabolism suggest that CBF reduction is related to decreased metabolic demand within the perihematoma region.^{12,15,30}

Blood Pressure and Perihematoma Perfusion Pressure

We have previously demonstrated that acute BP reduction does not result in reduced perihematoma CBF in patients with acute ICH.^{15,17,31} In the present study, we found no relationship between BP treatment target or actual BP and perihematoma CPP. The maintenance of CPP despite marked reductions in BP in many of our patients suggests some preservation of autoregulation in patients with acute ICH. This is consistent with serial measurements of CBF pre- and post-BP reduction by using both PET and CTP.^{15,31}

Borderzone Cerebral Perfusion Pressure

Our CPP measurements may be relevant to the results of diffusion-weighted MR imaging studies indicating that subacute ischemic injury occurs in areas remote from the hematoma, including BZ regions, in up to one-third of patients with acute ICH.⁶⁻¹¹ The retrospective association shown between BP reduction in the setting of chronic hypertensive vasculopathy and these ischemic lesions raises the possibility that they are a consequence of hemodynamic compromise. Given that CPP has been shown to be more sensitive to slight variations in mean arterial pressure than individual measurements of CBF or CBV,¹⁸ we postulated that subtle perfusion changes in the BZ regions may only become apparent by using this analysis. External and internal BZ CPP was not different from that in surrounding hemispheric tissue and did not vary between the ipsilateral and contralateral hemispheres. The modest reduction in the absolute CPP in the ipsilateral internal BZ in the <150-mm Hg treatment group is of dubious clinical significance, particularly given the lack of difference in relative CPP. Furthermore, the slight decrease in ipsilateral CPP in our more aggressive BP target group is an unlikely mechanism for DWI lesion formation, which has been reported with equal frequency in both the ipsilateral and contralateral hemispheres.¹⁰ Very recent research suggests that the small DWI lesions outside the perihematoma region are associated with larger hematoma volumes. The precise etiology of these lesions is unknown, though they may represent an epiphenomenon with an underlying microvascular pathogenesis rather than a hemodynamic mechanism of ischemic injury after primary ICH.³²

Nonetheless, the possibility that very localized hemodynamic changes, including variations in CPP, are related to the development of these small DWI lesions cannot be excluded on the basis of our results.

Clinical Implications

Our findings are consistent with those in previous studies of perfusion in patients with acute ICH, suggesting that acute BP reduction is safe. These data are also consistent with the lack of indicators of clinical harm in randomized trials of BP reduction after ICH.^{17,33,34}

Although concerns persist that BZ regions may be hemodynamically vulnerable to rapid BP reduction, we can find no objective evidence to support this hypothesis. We are currently testing the hypothesis that BP reduction is associated with the development of MR imaging ischemic lesions as part of an ongoing randomized trial (NCT02281838).

Limitations

This study has a number of limitations. Regional CPP was measured indirectly, but noninvasively, by using the ratio of CBF to CBV maps. Global CPP has been correlated with the CBF/CBV ratio,¹⁸ but regional evaluation of CPP by using CTP has not been confirmed with direct measurements of intracranial pressure. Invasive intracranial pressure measurements were not included in this study; consequently, our noninvasive, indirect measurements of CPP cannot be validated. Furthermore, CTP studies are single-time-point assessments in a potentially dynamic process. This study cannot exclude the possibility that CPP does, in fact, drop transiently after BP

Table 2: Effect of BP reduction on perfusion parameters

Perfusion Parameters and Region	Treatment Group		P Value
	<150 mm Hg (n = 37)	<180 mm Hg (n = 36)	
Absolute ipsilateral CPP			
Perihematoma	13.9 ± 5.5	14.8 ± 3.4	.38
Hemisphere	14.0 ± 5.3	15.2 ± 3.9	.27
External BZ	14.1 ± 4.6	15.8 ± 4.6 (n = 35)	.11
Internal BZ	13.5 ± 4.6 (n = 27)	16.5 ± 4.7 (n = 29)	.02 ^a
Absolute contralateral CPP			
Perihematoma	13.9 ± 5.5	14.8 ± 4.0	.43
Hemisphere	14.3 ± 5.8	15.2 ± 3.8	.45
External BZ	15.1 ± 6.5	16.0 ± 3.7 (n = 35)	.46
Internal BZ	15.0 ± 7.1 (n = 27)	16.0 ± 4.6 (n = 29)	.48
Absolute ipsilateral CVR			
Perihematoma	0.32 ± 0.10	0.36 ± 0.11	.11
Hemisphere	0.29 ± 0.08	0.32 ± 0.08	.14
External BZ	0.31 ± 0.11	0.37 ± 0.12 (n = 35)	.05 ^a
Internal BZ	0.37 ± 0.13 (n = 27)	0.44 ± 0.16 (n = 29)	.08
Absolute contralateral CVR			
Perihematoma	0.28 ± 0.09	0.33 ± 0.11	.56
Hemisphere	0.28 ± 0.08	0.32 ± 0.09	.09
External BZ	0.32 ± 0.11	0.38 ± 0.12 (n = 35)	.04 ^a
Internal BZ	0.36 ± 0.12 (n = 27)	0.40 ± 0.14 (n = 29)	.16
Relative CPP			
Perihematoma	1.02 ± 0.16	1.02 ± 0.15	.96
Hemisphere	0.99 ± 0.09	1.00 ± 0.10	.75
External BZ	0.99 ± 0.19	1.00 ± 0.26 (n = 35)	.76
Internal BZ	1.01 ± 0.17 (n = 27)	1.01 ± 0.16 (n = 29)	.99
Relative CVR			
Perihematoma	1.16 ± 0.23	1.11 ± 0.17	.36
Hemisphere	1.04 ± 0.10	1.02 ± 0.08	.32
External BZ	1.01 ± 0.18	1.01 ± 0.22 (n = 35)	.91
Internal BZ	1.02 ± 0.17 (n = 27)	1.04 ± 0.15 (n = 29)	.52

^a Significant.

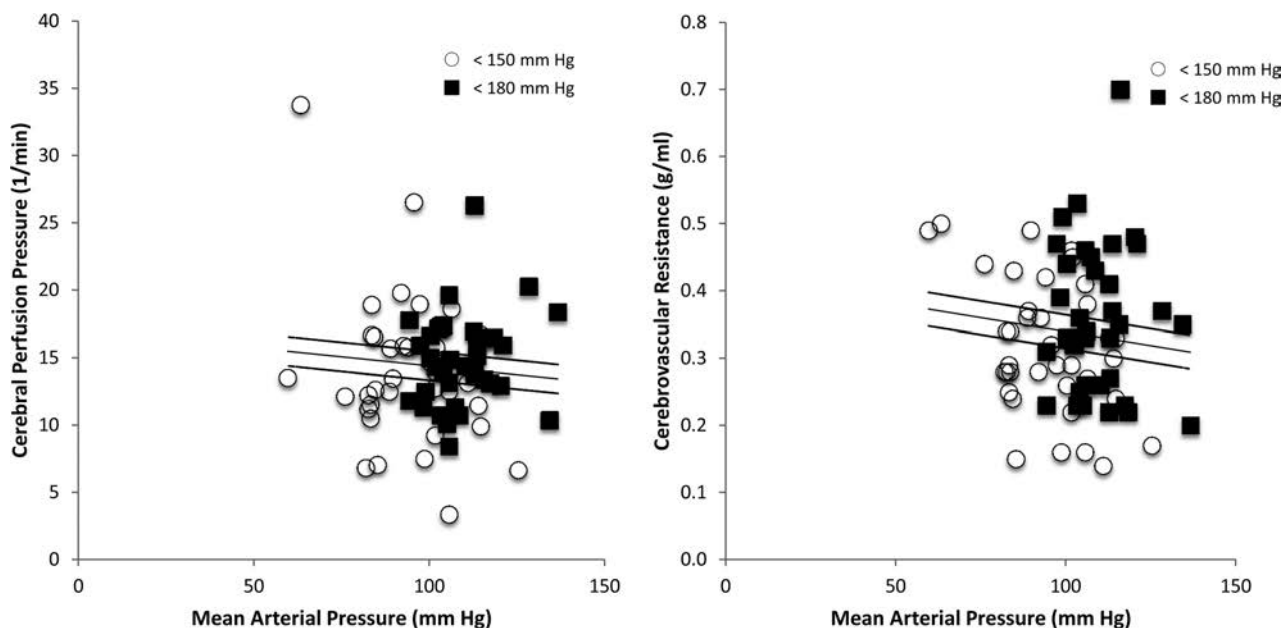


FIG 3. Plots of cerebral perfusion pressure and cerebrovascular resistance against mean arterial pressure. The open circles refer to the <150-mm Hg treatment group, while the filled squares represent the <180-mm Hg treatment group. There was no relationship between mean arterial pressure and CPP ($\beta = -0.08 [-0.10, 0.05]$) or CVR ($\beta = -0.11 [-0.003, 0.001]$).

reduction either before or after the CTP study. Finally, these data are from a relatively small sample of patients with ICH with predominately small-to-moderate hematoma volumes. In our study, only 15% of patients had ICH volumes of >40 mL. This is consistent with other ICH trials.^{33,35} Patients with large-volume ICH are less likely to be enrolled in trials because they are treated either conservatively or alternatively with surgical resection from the onset; consequently, these patients make up the minority in this clinical trial. All patients in our study were stable enough and lacked contraindications to CTP scanning 2 hours after randomization, which certainly introduced a selection bias. Nonetheless, these results provide further insight into cerebral perfusion patterns in acute ICH.

CONCLUSIONS

Perihematoma CPP is maintained, despite a modest increase in CVR, in acute primary ICH. Vascular borderzone CPP and CVR are normal in patients with ICH. Reduction of BP does not affect CPP in perihematoma or borderzone regions. These results provide further physiologic support for the safety of BP reduction in ICH.

Disclosures: Bronwen Gould—RELATED: Grant: Alberta Innovates Health Solutions (summer studentship). Thomas Jeerakathil—RELATED: Grant: Canadian Institutes for Health Research.* Comments: I am a collaborator on the grant that funded this research project. This was a peer-reviewed grant from a government funding agency. There is no conflict of interest. Dariush Dowlatshahi—UNRELATED: Expert Testimony: Canadian Medical Protective Association (medicolegal consultation for ischemic stroke); Grants/Grants Pending: Heart and Stroke Foundation, Comments: grant funding to study CTA, spot sign, and ICH; Patents (planned, pending or issued): patent on CT imaging software for the ICH spot sign; Travel/Accommodations/Meeting Expenses Unrelated to Activities Listed: BI Worldwide (travel grant to the meeting). Michael D. Hill—UNRELATED: Board Membership: Heart and Stroke Foundation of Alberta Board (volunteer charity board); Consultancy: Merck, Comments: Adjudication Committee for clinical trials in diabetes; Grants/Grants Pending: Covidien.* Comments: grant for clinical trial. Shelagh B. Coutts—UNRELATED: Canadian Institutes of Health Research,* Genome Canada,* Heart and Stroke Foundation of Canada.* Comments: grant funding for research not related to this article. Kenneth S. Butcher—RELATED: Grant: Alberta Institutes of Health Research and Heart and Stroke Foundation of Canada.* Comments: A grant-in-aid supported the ICH ADAPT trial; UNRELATED: Grants/Grants Pending: Canadian Institutes of Health Research.* Comments: Two grants-in-aid for unrelated work (blood pressure reduction in ischemic stroke and novel anticoagulant therapy in acute noncardioembolic stroke); Payment for Lectures (including service on Speakers Bureaus): speaker fees for new oral anticoagulants use by Boehringer Ingelheim, Bayer, and Pfizer/Bristol-Myers Squibb Canada.* Money paid to the institution.

REFERENCES

1. Fogelholm R, Avikainen S, Murros K. **Prognostic value and determinants of first-day mean arterial pressure in spontaneous supratentorial intracerebral hemorrhage.** *Stroke* 1997;28:1396–400 CrossRef Medline
2. Okumura K, Ohya Y, Maehara A, et al. **Effects of blood pressure levels on case fatality after acute stroke.** *J Hypertens* 2005;23:1217–23 CrossRef Medline
3. Anderson CS, Huang Y, Wang JG, et al; INTERACT Investigators. **Intensive blood pressure reduction in acute cerebral haemorrhage trial (INTERACT): a randomised pilot trial.** *Lancet Neurol* 2008;7:391–99 CrossRef Medline
4. Butcher K, Jeerakathil T, Emery D, et al. **The Intracerebral Haemorrhage Acutely Decreasing Arterial Pressure Trial: ICH ADAPT.** *Int J Stroke* 2010;5:227–33 CrossRef Medline
5. Mendelow AD. **Mechanisms of ischemic brain damage with intracerebral hemorrhage.** *Stroke* 1993;24(12 suppl):1115–17; discussion 1118–19 Medline
6. Brazzelli M, Sandercock PA, Chappell FM, et al. **Magnetic resonance imaging versus computed tomography for detection of acute vascular lesions in patients presenting with stroke symptoms.** *Cochrane Database Syst Rev* 2009;CD007424 CrossRef Medline
7. Kimberly WT, Gilson A, Rost NS, et al. **Silent ischemic infarcts are associated with hemorrhage burden in cerebral amyloid angiopathy.** *Neurology* 2009;72:1230–35 CrossRef Medline
8. Singer OC, Kurre W, Humpich MC, et al; MR Stroke Study Group Investigators. **Risk assessment of symptomatic intracerebral hemorrhage after thrombolysis using DWI-ASPECTS.** *Stroke* 2009;40:2743–48 CrossRef Medline
9. Singer OC, Berkefeld J, Lorenz MW, et al; MR Stroke Study Group Investigators. **Risk of symptomatic intracerebral hemorrhage in patients treated with intra-arterial thrombolysis.** *Cerebrovasc Dis* 2009;27:368–74 CrossRef Medline
10. Menon RS, Burgess RE, Wing JJ, et al. **Predictors of highly prevalent brain ischemia in intracerebral hemorrhage.** *Ann Neurol* 2012;71:199–205 CrossRef Medline
11. Arsava EM, Kayim-Yildiz O, Oguz KK, et al. **Elevated admission blood pressure and acute ischemic lesions in spontaneous intracerebral hemorrhage.** *J Stroke Cerebrovasc Dis* 2013;22:250–54 CrossRef Medline
12. Zazulia AR, Diringer MN, Videen TO, et al. **Hypoperfusion without ischemia surrounding acute intracerebral hemorrhage.** *J Cereb Blood Flow Metab* 2001;21:804–10 CrossRef Medline
13. Schellinger PD, Fiebach JB, Hoffmann K, et al. **Stroke MRI in intracerebral hemorrhage: is there a perihemorrhagic penumbra?** *Stroke* 2003;34:1674–79 CrossRef Medline
14. Butcher K, Baird T, MacGregor L, et al. **Perihematomal edema in primary intracerebral hemorrhage is plasma derived.** *Stroke* 2004;35:1879–85 CrossRef Medline
15. Powers WJ, Zazulia AR, Videen TO, et al. **Autoregulation of cerebral blood flow surrounding acute (6 to 22 hours) intracerebral hemorrhage.** *Neurology* 2001;57:18–24 CrossRef Medline
16. Adams RE, Powers WJ. **Management of hypertension in acute intracerebral hemorrhage.** *Crit Care Clin* 1997;13:131–61 CrossRef Medline
17. Butcher KS, Jeerakathil T, Hill M, et al; ICH ADAPT Investigators. **The Intracerebral Hemorrhage Acutely Decreasing Arterial Pressure Trial.** *Stroke* 2013;44:620–26 CrossRef Medline
18. Schumann P, Touzani O, Young A, et al. **Evaluation of the ratio of cerebral blood flow to cerebral blood volume as an index of local cerebral perfusion pressure.** *Brain* 1998;121:1369–79 CrossRef Medline
19. Brain Trauma Foundation; American Association of Neurological Surgeons; Congress of Neurological Surgeons; Joint Section on Neurotrauma and Critical Care, AANS/CNS, Carney NA, Ghajar J. **Guidelines for the management of severe traumatic brain injury.** *J Neurotrauma* 2007;24(suppl 1):S1–106. CrossRef Medline
20. Kirkman MA, Smith M. **Intracranial pressure monitoring, cerebral perfusion pressure estimation, and ICP/ CPP-guided therapy: a standard of care or optional extra after brain injury?** *Br J Anaesth* 2014;112:35–46 CrossRef Medline
21. Mayer SA, Lignelli A, Fink ME, et al. **Perilesional blood flow and edema formation in acute intracerebral hemorrhage: a SPECT study.** *Stroke* 1998;29:1791–98 CrossRef Medline
22. Wu O, Ostergaard L, Weisskoff RM, et al. **Tracer arrival timing-insensitive technique for estimating flow in MR perfusion-weighted imaging using singular value decomposition with a block-circulant deconvolution matrix.** *Magn Reson Med* 2003;50:164–74 CrossRef Medline
23. Robb RA. **The biomedical imaging resource at Mayo Clinic.** *IEEE Trans Med Imaging* 2001;20:854–67 CrossRef Medline
24. McCourt R, Gould B, Gioia L, et al; ICH ADAPT Investigators. **Cerebral perfusion and blood pressure do not affect perihematomal edema growth in acute intracerebral hemorrhage.** *Stroke* 2014;45:1292–98 CrossRef Medline
25. Wintermark M, Thiran JP, Maeder P, et al. **Simultaneous measurement of regional cerebral blood flow by perfusion CT and stable**

- xenon CT: a validation study. *AJNR Am J Neuroradiol* 2001;22:905–14 Medline
26. Kudo K, Terae S, Katoh C, et al. **Quantitative cerebral blood flow measurement with dynamic perfusion CT using the vascular-pixel elimination method: comparison with H2(15)O positron emission tomography.** *AJNR Am J Neuroradiol* 2003;24:419–26 Medline
 27. Murphy BD, Fox AJ, Lee DH, et al. **Identification of penumbra and infarct in acute ischemic stroke using computed tomography perfusion-derived blood flow and blood volume measurements.** *Stroke* 2006;37:1771–77 CrossRef Medline
 28. Gillard JH, Minhas PS, Harball MP, et al. **Assessment of quantitative computed tomographic cerebral perfusion imaging with H2(15)O positron emission tomography.** *Neurol Res* 2000;22:457–64 Medline
 29. Wintermark M, Chioléro R, van Melle G, et al. **Relationship between brain perfusion computed tomography variables and cerebral perfusion pressure in severe head trauma patients.** *Crit Care Med* 2004;32:1579–87 CrossRef Medline
 30. Kate MP, Hansen MB, Mouridsen K, et al. **Blood pressure reduction does not reduce perihematoma oxygenation: a CT perfusion study.** *J Cereb Blood Flow Metab* 2014;34:81–86 CrossRef Medline
 31. Gould B, McCourt R, Asdagh N, et al; ICH ADAPT investigators. **Autoregulation of cerebral blood flow is preserved in primary intracerebral hemorrhage.** *Stroke* 2013;44:1726–28 CrossRef Medline
 32. Gioia LC, Kate M, Choi V, et al. **Ischemia in intracerebral hemorrhage is associated with leukoaraiosis and hematoma volume, not blood pressure reduction.** *Stroke* 2015;46:1541–47 CrossRef Medline
 33. Qureshi AI, Palesch YY, Martin R, et al; Antihypertensive Treatment of Acute Cerebral Hemorrhage Study Investigators. **Effect of systolic blood pressure reduction on hematoma expansion, perihematomal edema, and 3-month outcome among patients with intracerebral hemorrhage: results from the antihypertensive treatment of acute cerebral hemorrhage study.** *Arch Neurol* 2010;67:570–76 CrossRef Medline
 34. Anderson CS, Heeley E, Huang Y, et al; INTERACT2 Investigators. **Rapid blood-pressure lowering in patients with acute intracerebral hemorrhage.** *N Engl J Med* 2013;368:2355–65 CrossRef Medline
 35. Arima H, Anderson CS, Wang JG, et al; Intensive Blood Pressure Reduction in Acute Cerebral Haemorrhage Trial Investigators. **Lower treatment blood pressure is associated with greatest reduction in hematoma growth after acute intracerebral hemorrhage.** *Hypertension* 2010;56:852–58 CrossRef Medline

A Potential Biomarker in Amyotrophic Lateral Sclerosis: Can Assessment of Brain Iron Deposition with SWI and Corticospinal Tract Degeneration with DTI Help?

R. Sheelakumari, M. Madhusoodanan, A. Radhakrishnan, G. Ranjith, and B. Thomas



ABSTRACT

BACKGROUND AND PURPOSE: Iron-mediated oxidative stress plays a pivotal role in the pathogenesis of amyotrophic lateral sclerosis. This study aimed to assess iron deposition qualitatively and quantitatively by using SWI and microstructural changes in the corticospinal tract by using DTI in patients with amyotrophic lateral sclerosis.

MATERIALS AND METHODS: Seventeen patients with amyotrophic lateral sclerosis and 15 age- and sex-matched controls underwent brain MR imaging with SWI and DTI. SWI was analyzed for both signal-intensity scoring and quantitative estimation of iron deposition in the anterior and posterior banks of the motor and sensory cortices and deep gray nuclei. The diffusion measurements along the corticospinal tract at the level of pons and medulla were obtained by ROI analysis.

RESULTS: Patients with amyotrophic lateral sclerosis showed reduced signal-intensity grades in the posterior bank of the motor cortex bilaterally. Quantitative analysis confirmed significantly higher iron content in the posterior bank of the motor cortex in patients with amyotrophic lateral sclerosis. In contrast, no significant differences were noted for the anterior bank of the motor cortex, anterior and posterior banks of the sensory cortex, and deep nuclei. Receiver operating characteristic comparison showed a cutoff of $35\mu\text{g Fe/g}$ of tissue with an area under the curve of 0.78 ($P = .008$) for the posterior bank of the motor cortex in discriminating patients with amyotrophic lateral sclerosis from controls. Fractional anisotropy was lower in the pyramidal tracts of patients with amyotrophic lateral sclerosis at the pons and medulla on either side, along with higher directionally averaged mean diffusivity values. The combination of SWI and DTI revealed an area under the curve of 0.784 for differentiating patients with amyotrophic lateral sclerosis from controls.

CONCLUSIONS: Measurements of motor cortex iron deposition and diffusion tensor parameters of the corticospinal tract may be useful biomarkers for the diagnosis of clinically suspected amyotrophic lateral sclerosis.

ABBREVIATIONS: ALS = amyotrophic lateral sclerosis, CST = corticospinal tract; D_{av} = directionally averaged mean diffusivity; FA = fractional anisotropy; PBMC = posterior bank of the motor cortex

Amyotrophic lateral sclerosis (ALS) is a fatal neurodegenerative disorder of the motor system characterized by progressive degeneration of corticospinal tracts, brain stem, and lower motor neurons in the spinal cord.^{1,2} The clinical presentation of ALS includes progressive involvement of the upper motor neu-

ron, lower motor neuron, and craniobulbar musculature due to degeneration of the anterior horn cells and motor neurons. The disease shows great variation in its onset, clinical presentation, and survival, with diagnosis usually depending on changes in needle electromyography from various muscles sampled, which include even the tongue and paraspinal muscles. Needle electromyography is invasive and rather cumbersome to perform. Hence, a reliable and objective noninvasive surrogate biomarker of motor neuron dysfunction, if available, may play a pivotal role in the diagnosis and monitoring of disease progression in ALS.

Recent investigations proved that ALS pathology is associated with abnormal iron homeostasis inducing excessive oxidative stress in the motor neurons.^{3,4} There is also evidence to suggest that reduced fractional anisotropy (FA) and increased directionally averaged mean diffusivity (D_{av}) along the pyra-

Received March 14, 2015; accepted after revision July 9.

From the Department of Neurology (R.S., M.M., A.R.), Devices Testing Laboratory, Biomedical Technology Wing (G.R.), and Department of Imaging Sciences and Interventional Radiology (B.T.), Sree Chitra Thirunal Institute of Medical Sciences and Technology, Trivandrum, Kerala, India.

Please address correspondence to Bejoy Thomas, MD, DNB, Department of Imaging Sciences and Interventional Radiology, Sree Chitra Thirunal Institute for Medical Sciences and Technology, Trivandrum, India; e-mail: bejoy@sctimst.ac.in



Indicates article with supplemental on-line table.



Indicates article with supplemental on-line photos.

<http://dx.doi.org/10.3174/ajnr.A4524>

midal tracts indicate microstructural tissue changes in ALS.⁵⁻⁷ Hence, detection of elevated iron levels in the motor cortex and associated corticospinal tract (CST) degeneration in these patients could be useful for demonstrating the underlying pathology.

MR imaging techniques that can quantify this tissue iron include T2, T2*, magnetic field correlation, field-dependent relaxation rate increase, and SWI.⁸⁻¹⁴ Recent studies advocated SWI as a potential in vivo marker to detect susceptibility changes among tissues, which aids in the identification of paramagnetic nonheme iron (ferritin and transferrin), which would appear hyperintense on filtered phase images.¹⁵⁻¹⁸ These finding opened a new window to estimate the regional changes in iron content associated with ALS. The aim of this study was to measure iron in various GM regions in ALS by using qualitative and quantitative SWI and to investigate the microstructural tissue changes in CST by DTI.

MATERIALS AND METHODS

Study Participants

The study was approved by the Institutional Ethics Committee. Seventeen patients (7 men and 10 women) with definite or probable ALS according to revised EI Escorial criteria¹⁹ were included in this retrospective analysis. All had undergone a detailed clinical and psychometric evaluation to exclude any associated neurologic conditions. We have subclassified the cohort (On-line Table) according to the latest phenotypic classification of ALS by Chiò et al,²⁰ though the staging proposed by Roche et al²¹ was not possible in this retrospective cohort. Clinical and imaging data were retrieved from the electronic medical records and PACS, respectively. Imaging and demographic data of 15 age- and sex-matched healthy volunteers (8 men, 7 women) were also included from another prospective Institutional Ethics Committee-approved study (R. Sheelakumari, MPhil, unpublished data, 2014).

Image Acquisition

MR imaging was performed on a 1.5T (Avanto; Siemens, Erlangen, Germany) whole-body scanner by using a transmit-receive head coil array with 12 elements. All participants had undergone multisection diffusion tensor imaging by using a single-shot spin-echo echo-planar sequence. For the acquisition, diffusion sensitizing gradients were applied in 30 noncollinear directions with the following imaging parameters: TR, 6000 ms; TE, 88 ms; matrix, 128 × 128; FOV, 230 mm; 3-mm section thickness with a 1.5-mm gap averaged twice with b-values of 0 and 1000 s/mm².

SWI was obtained with a 3D spoiled gradient recalled-echo sequence (TR/TE, 49 ms/40 ms; flip angle, 20°; section thickness, 2.1 mm; number of sections, 56; matrix, 260 × 320). We selected both SWI and corrected phase images for the analysis. In the corrected phase images, there is a direct correlation between the phase and iron content of the tissue.

For left-hand MR systems, the phase is given by the following relation:

$$\phi = \gamma \cdot \Delta B \cdot TE$$

where γ , ΔB , TE represents the gyromagnetic ratio, the magnetic field change between tissues, and echo time, respectively. Iron being a paramagnetic element, it aligns with the main magnetic field and thus creates a positive ΔB . Thus, the larger the iron

content in the tissue, the larger will be the value of ΔB and thus the larger the phase change ϕ will be relative to its surroundings.

$$\Delta B = \Delta \chi B_0,$$

$$\Delta \chi \propto c,$$

where $\Delta \chi$ is the change in susceptibility and c is the concentration of iron.

Our MR imaging processing uses the phase convention

$$\Phi = 2048 \left[\left(\frac{\phi}{\pi} \right) + 1 \right],$$

where Φ varies from $-\pi$ to $+\pi$ and ϕ varies from 0 to 4096. We take 180 U (0.276 radians) of phase to be equivalent to 60 $\mu\text{g Fe/g}$ of tissue.^{13,15} The iron content is then given by the relation

$$\text{Iron Concentration } (\mu\text{g Fe/g tissue}) = \frac{(\phi - 2048)\pi}{2048 \times 0.276} \times \frac{60 \mu\text{g Fe}}{\text{Gram Tissue}}.$$

A simplification of the above equation shows that 3 Siemens phase units are equal to 1 $\mu\text{g Fe/g}$ tissue.^{14,15} The phase images obtained were high-pass-filtered by a 64×64 k-space filter and resulted in an SWI filtered phase image.

Image Analysis

Qualitative Assessment of SWI. All the SWI was visually examined in the regular clinical settings by an experienced neuroradiologist (B.T.) and a neurologist (A.R.) with >15 years of experience in their respective fields. Qualitative visual rating scores were assigned at the posterior bank of the motor cortex (PBMC), globus pallidus, putamen, and caudate nucleus. The central sulcus was used as an anatomic landmark to identify the motor cortex. Each observation was independent and blinded to the diagnosis (patients or controls). The magnitude of hypointensity was graded as 0 = absent, 1 = present (mild to moderate), 2 = present (marked) (Fig 1).

Quantitative Regional Assessment of Iron Content (Microgram Iron/Gram of Tissue). ROI-based quantitative analysis of regional iron (Fe) content was performed by using Signal Processing In NMR software (SPIN; MR Imaging Institute for Biomedical Research, Detroit, Michigan). The ROIs were drawn manually by 2 doctoral scholars (R.S. and M.M.), who were trained in the procedure. The images were magnified 2 times, and the phase values obtained from 9 structures in both hemispheres included the following: GM at the PBMC, adjacent subcortical WM and CSF in the central sulcus, GM of anterior bank of the motor cortex, anterior bank of the sensory cortex, posterior bank of the sensory cortex, and basal ganglia regions (On-line Fig 1), with extreme care to minimize partial volume effects. For all the subjects, phase values were measured by the 2 observers to determine the interobserver agreement.

The ROIs were copied to phase images to obtain the mean phase shift values within. To compare data across patients, we assumed that the CSF in each patient contained zero iron.¹⁴ Thus the iron content in an ROI was directly proportional to the shift in

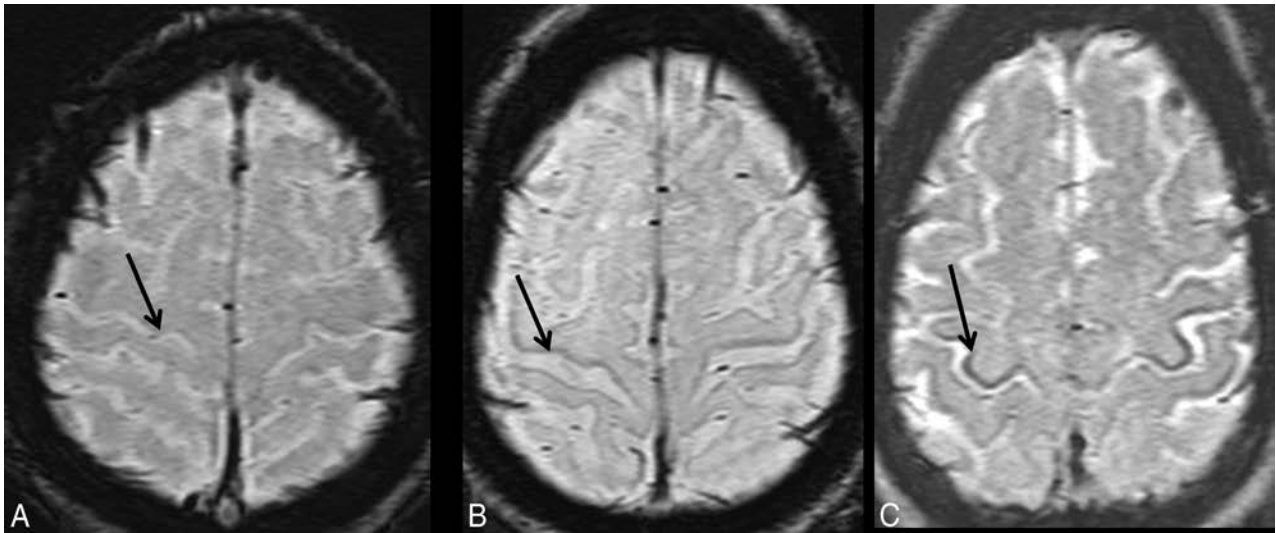


FIG 1. Motor cortex hypointensity visual scoring on SWI: absent (grade 0) (A), mild to moderately present (grade 1) (B), and severely present (grade 2) (C).

phase between the CSF and the particular ROI. Mean phase shift values were calculated for each ROI by averaging the values obtained from both hemispheres.

DTI ROI Analysis of CST. DTI data were transferred to a Leonardo workstation (Siemens) and postprocessed with Neuro3D software (Siemens). The off-line tensor images and color maps were generated by using the built-in “DTI Task Card” (Version 1). T1-weighted images were coregistered on the color maps for selecting the ROI in the specific anatomic region. The datasets were then analyzed by 2 observers blinded to patients or controls. On the basis of the prior anatomic knowledge and relevant literature,^{5,22} 2 circular ROIs of same size, 3 mm², were placed along the CST on FA and D_{av} maps in the brain stem at the level of cerebellar peduncles and medullary pyramids (On-line Fig 2); care was taken to exclude non-structure-of-interest pixels. The FA and D_{av} values were calculated on a pixel-by-pixel basis, and average values for each position on both sides were tabulated for statistical analysis.

Statistical Analysis

Statistical analyses of all datasets were performed by using SPSS, Version 20.0 (IBM, Armonk, New York). We used the Student *t* test and χ^2 test, respectively, to compare age and sex distributions between patients and controls. Interrater agreement of visual scoring of the hypointensity of gray matter on SWI was determined by κ statistics. To investigate whether the visual rating is effective to discriminate between groups of hypointensity scores on SWI (absent versus present, ie, group 0 versus groups 1 + 2), we performed sensitivity and specificity analysis by using cross-tabs. Analyses were also repeated for the absent or mild to moderately present group versus the markedly present group (ie, 0 + 1 versus group 2). The combined hemispheric mean values of iron in micrograms/gram and FA and D_{av} values of each ROI were compared between subjects with ALS and controls by using the Mann-Whitney *U* test for independent samples with Bonferroni correction for multiple comparisons. In addition, we compared the estimated means of iron values in the posterior motor cortex

with the visual rating score by using 1-way ANOVA. Furthermore, the correlation between quantitative iron and diffusion values in the CST was performed by the Pearson correlation coefficient. In addition, receiver operating characteristic analysis curves were computed to calculate the cutoff values of iron in the motor cortex in distinguishing patients and controls. To establish a best cutoff value, we considered a value that presented with the highest sum of sensitivity and specificity. Finally, a combined receiver operating characteristic was obtained with SWI and DTI measures [iron + {(1-FA) + ADC}].

RESULTS

Subject Characteristics

Patients were in the age range of 32–76 years (mean, 54.41 ± 13.99 years), and controls were 45–75 years of age (mean, 56.8 ± 8.28 years). Patients and controls were comparable in age ($P = .551$) and sex ($P = .492$). The average age at onset of ALS was 51.94 years. The demographic and clinical information of the patients is shown in On-line Table 1.

Visual Rating Measurements of the Motor Cortex

Between the 2 observers in SWI, visual scoring for hypointensity showed excellent agreement for PBMC ($\kappa = 0.97, P < .001$), while other regions such as the caudate nucleus ($\kappa = 0.75, P < .001$), putamen ($\kappa = 0.75, P < .001$), and globus pallidus ($\kappa = 0.7, P < .001$) also revealed good interrater agreement.

Sensitivity and Specificity Analysis

The visual assessment of hypointensity scores in the PBMC was highly sensitive (91.15%) in differentiating patients with ALS from healthy controls while considering absent-versus-present groups. However, the specificity was less (13.35%) when the magnitude of hypointensity was considered this way. Similar analysis between the absent/mild to moderately present versus the markedly present group showed 100% specificity but very low sensitivity (20.55%). There was no statistically significant correlation among Fe scores in other GM regions.

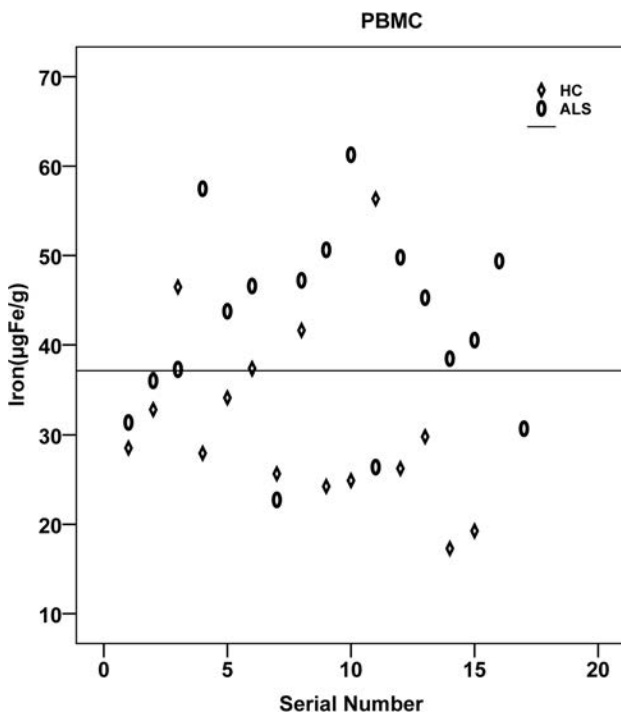


FIG 2. Distribution of iron content in the posterior bank of the motor cortex plotted for patients and controls. HC indicates healthy controls.

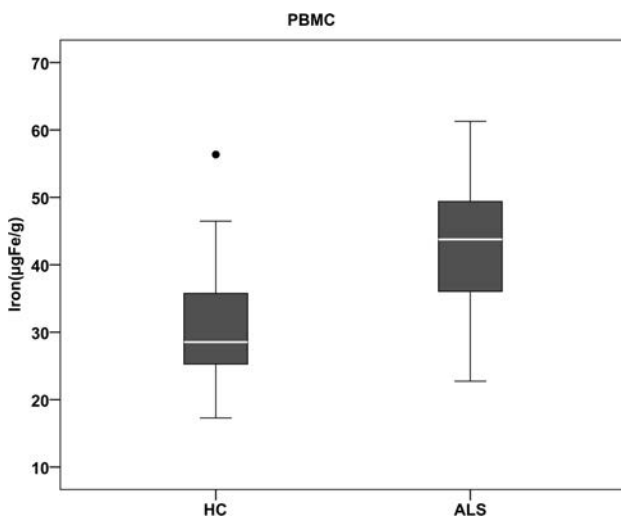


FIG 3. Boxplot showing group comparison of iron content in the posterior banks of motor cortex in patients and controls. HC indicates healthy controls.

Quantitation of Regional Iron Deposition in Gray Matter Structures

The regional assessment of iron content (micrograms iron/gram of tissue) in various gray matter regions revealed significantly increased iron deposition in the PBMC ($P = .007$) in patients with ALS compared with controls (Figs 2 and 3). However, the iron deposition in the anterior bank of the motor cortex, anterior bank of the sensory cortex, anterior bank of the sensory cortex, posterior bank of the sensory cortex, globus pallidus, putamen, and caudate nucleus, though higher than that in the control group, was not statistically significant (Table 1). One-way ANOVA of estimated means of iron values, and the

Table 1: Iron content ($\mu\text{g Fe/g}$ of tissue) of each ROI in the ALS and control groups^a

ROI	ALS	Healthy Controls	P Value ^b
PBMC			
GM	42.05 (10.42)	31.51 (10.42)	.007 ^c
WM	11.84 (5.24)	11.33 (4.75)	.911
ABMC	29 (6.42)	28.39 (10.04)	.502
PBSC	31.66 (7.62)	30.18 (11.65)	.766
ABSC	28.69 (13.29)	25.15 (10.32)	.278
GP	30.28 (7.48)	29.00 (7.62)	.602
PUT	24.14 (5.62)	22.44 (10.03)	.911
CAU	29.41 (6.81)	25.38 (13.14)	.455

Note:—ABSC indicates anterior bank of the sensory cortex; ABMC, anterior bank of the motor cortex; PBSC, posterior bank of the sensory cortex; GP, globus pallidus; PUT, putamen; CAU, caudate nucleus.

^a Data are in mean (SD) or in a number range.

^b P value is calculated with the Mann-Whitney U test.

^c Post hoc Bonferroni correction.

Table 2: Diffusion property measurement of corticospinal tract by ROI analysis^a

Region	FA			D_{av} ($10^{-3} \text{ mm}^2/\text{S}$)		
	ALS	Healthy Controls	P Value ^b	ALS	Healthy Controls	P Value ^b
Pons	0.53 (0.08)	0.61 (0.04)	.001 ^c	0.83 (0.06)	0.74 (0.05)	.003 ^c
Medulla	0.50 (0.01)	0.58 (0.05)	.06 ^c	1.01 (0.23)	0.85 (0.12)	.011 ^c

^a Data are in mean (SD) or in number range.

^b P value is calculated with the Mann-Whitney U test.

^c Post hoc Bonferroni correction.

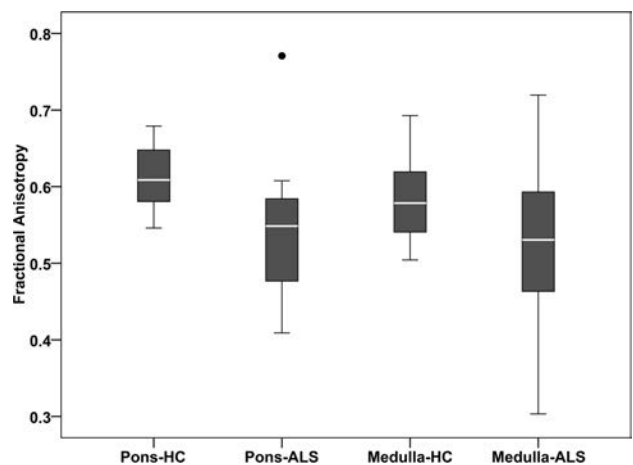


FIG 4. Boxplot showing group comparison of fractional anisotropy along the corticospinal tracts at the levels of pons and medulla. HC indicates healthy controls.

visual rating score in the PBMC also revealed a significant difference between groups ($P = .004$).

Diffusion Measurements of the Corticospinal Tract

The mean values of FA and D_{av} for patients with ALS and controls at various levels of the CST are shown in Table 2. Patients with ALS showed lower FA values than controls along the CST in the pons ($P = .001$). A similar trend was observed for the medullary pyramid (Fig 4), though this did not survive after multiple comparisons. In addition, the D_{av} values were significantly elevated in the pons ($P = .003$) and pyramid ($P = .011$) (Fig 5). No significant correlation was found in any of the ROIs between the amount of iron deposition and FA values in the CST. A similar pattern was observed between D_{av} and iron values.

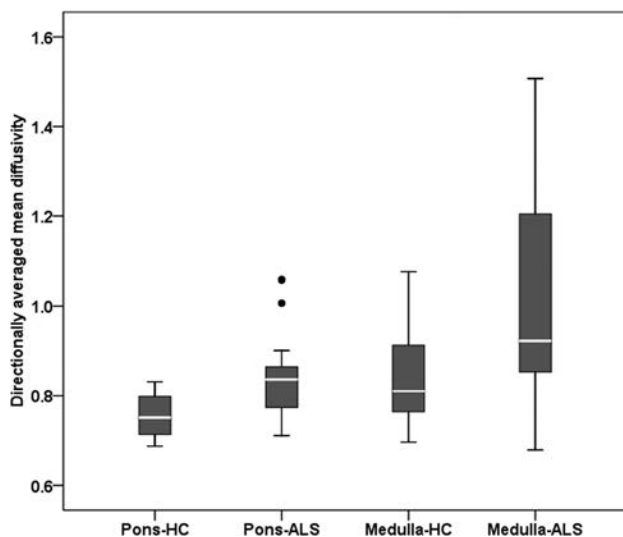


FIG 5. Boxplot showing group comparison of directionally averaged mean diffusivity ($\times 10^{-3} \text{ mm}^2/\text{s}$) along the corticospinal tracts at the levels of the pons and medulla. HC indicates healthy controls.

Receiver Operating Characteristic Curve Analysis

The receiver operating characteristic curve analysis predicted the cutoff of iron in the PBMC and FA values. Identification of the greatest sum of sensitivity and specificity determined an iron value of $\geq 35 \mu\text{g Fe/g}$ of tissue as the best cutoff value for the PBMC, with a sum of sensitivity and specificity of 149% and area under the curve = 0.78 (95% CI, 0.61–0.94; $P = .008$). Of the 17 patients, 13 presented with an iron content of $\geq 35 \mu\text{g Fe/g}$ of tissue for the PBMC. Of the values of the 15 controls, only 4 were at or above the cutoff for the PBMC. When DTI measurements were added to SWI, only marginal improvement was observed in the area under the curve = 0.784 (95% CI, 0.62–0.95; $P = .006$) with a sum of sensitivity and specificity of 150.6% (Fig 6).

DISCUSSION

In this study, we qualitatively and quantitatively assessed the putative iron content in various gray matter structures, especially the motor cortex of the brain in patients with ALS in conjunction with microstructural changes along the CST by using SWI and DTI, respectively. A few earlier cross-sectional studies have investigated the phase differences between tissues in a number of regions of the human brain as a means of detecting iron abnormalities and CST degeneration by using MR imaging separately. To the best of our knowledge, no previous studies have performed the simultaneous assessment of brain iron content in the motor cortex and the changes in the CST by using SWI and DTI together.

It is well-known that degenerative brain disorders like Alzheimer disease,²³ Parkinson disease,¹⁶ multiple sclerosis,²⁴ and ALS have been associated with region-specific iron accumulation.²⁵ Increased iron deposition in the motor cortex of patients with ALS has been proved in histologic analysis,²⁶ MR imaging studies,¹⁷ and postmortem examinations.²⁷ Conventional MR imaging sequences such as FLAIR,²⁸ T2-weighted,²⁹ proton-density weighted,³⁰ and magnetization transfer imaging have revealed signal-intensity changes and a reduced magnetization transfer ratio³¹ in the internal capsule in patients with ALS. However, the

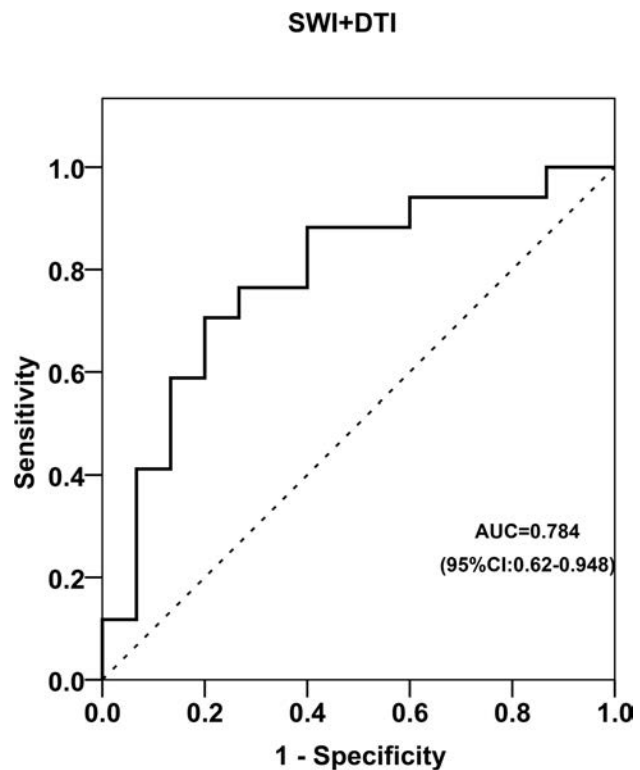


FIG 6. Receiver operating characteristics curve for the combined SWI in the PBMC and DTI values in the CST.

clinical utility of these techniques in individual patient management is questionable.³² Advanced imaging techniques like MR spectroscopy³³ and DTI have shown a significantly reduced NAA-to-creatine ratio and FA at various locations of CST, respectively,³⁴ in patients with ALS. In ALS, the signal alteration in the deeper layers of the motor cortex is correlated with accumulation of iron-laden microglia. The microglial cells in the motor cortex play a vital role in maintaining iron homeostasis, and enhanced microglial iron accumulation leads to the pathologic changes in ALS. In addition, excessive iron deposition in the motor cortex is considered a marker of disruption in the regulatory pathways of iron in the brain. Approximately 20% of familial ALS is caused by mutations in the superoxide dismutase gene. Earlier observations confirmed such findings in which elevated levels of ferritin transcripts were found in the *SOD1G93A* mouse model.³⁵ Moreover, lines of evidence indicate the presence of polymorphism in *HFE* genes and increased expression of the *H63D* variant of *HFE* genes with abnormal iron metabolism contributing to ALS pathology.³⁶

Compared with other imaging sequences, SWI is more robust and has been shown to provide sensitive measures of iron on the order of micrograms iron/gram of tissue. Adachi et al¹⁷ proved the supremacy of SWI to detect the iron deposition in the precentral cortex in ALS. They described much lower signal intensity on SWI than on T2- and T2*-weighted images and proved the presence of Fe-laden microglia and macrophages in the precentral cortex after staining with antiferritin antibody. A more recent analysis of DTI data by using tract-based spatial statistics determined reduced FA at the distal portion of CST in patients with ALS compared with those with primary lateral sclerosis. Regional

analysis of diffusion characteristics along the CST in ALS revealed a marked reduction of FA values at the levels of the internal capsule and pyramids.³⁷

We performed the visual assessment of hypointensities in patients with ALS as a measure of iron deposition in ALS, to analyze its clinical utility as a quick visual imaging tool to differentiate patients with ALS from age-matched healthy individuals. The hypointensity scoring in bilateral PBMC regions was found to be highly sensitive in differentiating patients with ALS from individuals with normal brains. The overall specificity was, however, low, but it improved once severe hypointensity was considered for the diagnosis of ALS. We also found no significant difference between the visual rating of Fe content in patients with ALS and controls in the caudate nucleus, putamen, and globus pallidus regions. To confirm these results and to make it more objective, we performed a quantitative analysis of iron content in terms of phase shift values in the motor cortex and basal ganglia regions. Our observations of significantly increased iron accumulation in the motor cortex of patients with ALS are in agreement with recent findings.¹² However, no significant differences were noted between patients with ALS and controls in other regions, including the anterior motor and sensory cortices, posterior sensory cortex, globus pallidus, putamen, and caudate nucleus. Yu et al,¹² who used the phase shift values of SWI by a 3T scanner, found that there was no difference in the iron levels in the globus pallidus, putamen, head of caudate nucleus, substantia nigra, and red nucleus in patients with ALS compared with controls. In contrast, a previous study by R2* mapping reported increased iron deposition in the caudate nucleus of patients with ALS compared with age- and sex-matched controls.¹

Besides iron deposition in the PBMC, there were significantly reduced FA and increased D_{av} in the CST of patients with ALS compared with controls,^{5,38,39} and the pattern was maintained from the pons to the medulla. When one considered multiple comparisons, the significance of FA in the medulla disappeared due to lack of statistical power. A previous report showed significant changes in FA and D_{av} in the bulbar-onset groups and correlated FA changes with measures of disease severity and the upper motor neuron index.⁴⁰ It is evident that FA is highly variable among the sections of the pons and medulla.³⁹ Increased D_{av} probably detects striking and chronic changes at these levels.

No correlation was found between regional iron values and any of the diffusion characteristics. The exact cause of this remains unexplained; however, they might represent relatively independent processes of degeneration within the natural course of the disease progression. Hence, we think that combined assessment of iron deposition and diffusion characteristics might be useful as a potential biomarker for the diagnosis and characterization of motor neuron diseases. However, this needs confirmation with future prospective studies.

The present study has a few limitations. These results were established in a relatively small cohort of clinically probable cases of ALS in this retrospective study, but a higher sample size would have contributed further to the validity. Second, this was a cross-sectional image-analysis study of patients with various clinical presentations in differing stages of the disease; hence, it is unable to provide details on the dynamic changes expected in correlation

with the clinical progression of the disease. The data were from a 1.5T scanner, and better results could be expected on a 3T scanner by improving the SNR and susceptibility effects. Our results need to be confirmed in future prospective studies by using larger samples.

CONCLUSIONS

This study demonstrates the usefulness of analysis of SWI and DTI in estimating motor cortex iron deposition and CST changes in patients with ALS. Quantitative estimation showed abnormal brain iron deposition in the posterior bank of the motor cortex in patients with ALS. The diffusion characteristics suggest altered microstructural organization of the CST at different brain stem levels. However, no statistically significant correlation was found among these processes, suggesting their possible independent evolution. Hence, a combined analysis of them might provide meaningful insights into the pathophysiologic changes in ALS and can serve as an in vivo objective biomarker for the diagnosis of ALS. Moreover, combining multimodal neuroimaging techniques along with clinical, genetic, and pathologic markers is a promising way to understand the underlying disease mechanisms, which might lead to the development of more robust biomarkers for the diagnosis and staging of this disease. However, future longitudinal prospective studies are warranted to prove this.

ACKNOWLEDGMENTS

We thank Dr Ravi Prasad Varma for his valuable suggestions on the statistical analysis.

REFERENCES

1. Langkammer C, Enzinger C, Quasthoff S, et al. **Mapping of iron deposition in conjunction with assessment of nerve fiber tract integrity in amyotrophic lateral sclerosis.** *J Magn Reson Imaging* 2010;31:1339–45 CrossRef Medline
2. Kiernan MC, Vucic S, Cheah BC, et al. **Amyotrophic lateral sclerosis.** *Lancet* 2011;377:942–55 CrossRef Medline
3. Petri S, Körner S, Kiaei M. **Nrf2/ARE signaling pathway: key mediator in oxidative stress and potential therapeutic target in ALS.** *Neurol Res Int* 2012;2012:878030 CrossRef Medline
4. Jomova K, Vondrakova D, Lawson M, et al. **Metals, oxidative stress and neurodegenerative disorders.** *Mol Cell Biochem* 2010;345:91–104 CrossRef Medline
5. Toosy AT, Werring DJ, Orrell RW, et al. **Diffusion tensor imaging detects corticospinal tract involvement at multiple levels in amyotrophic lateral sclerosis.** *J Neurol Neurosurg Psychiatry* 2003;74:1250–57 CrossRef Medline
6. Aoki S, Iwata NK, Masutani Y, et al. **Quantitative evaluation of the pyramidal tract segmented by diffusion tensor tractography: feasibility study in patients with amyotrophic lateral sclerosis.** *Radiat Med* 2005;23:195–99 Medline
7. Oshiro S, Morioka MS, Kikuchi M. **Dysregulation of iron metabolism in Alzheimer's disease, Parkinson's disease, and amyotrophic lateral sclerosis.** *Adv Pharmacol Sci* 2011;2011:378278 CrossRef Medline
8. Péran P, Hagberg G, Luccichenti G, et al. **Voxel-based analysis of R2* maps in the healthy human brain.** *J Magn Reson Imaging* 2007;26:1413–20 CrossRef Medline
9. Jensen JH, Szulc K, Hu C, et al. **Magnetic field correlation as a measure of iron-generated magnetic field inhomogeneities in the brain.** *Magn Reson Med* 2009;61:481–85 CrossRef Medline
10. Bartzokis G, Tishler TA, Lu PH, et al. **Brain ferritin iron may influ-**

- ence age- and gender-related risks of neurodegeneration. *Neurobiol Aging* 2007;28:414–23 CrossRef Medline
11. Harder SL, Hopp KM, Ward H, et al. **Mineralization of the deep gray matter with age: a retrospective review with susceptibility-weighted MR imaging.** *AJNR Am J Neuroradiol* 2008;29:176–83 CrossRef Medline
 12. Yu J, Qi F, Wang N, et al. **Increased iron level in motor cortex of amyotrophic lateral sclerosis patients: an in vivo MR study.** *Amyotroph Lateral Scler Frontotemporal Degener* 2014;15:357–61 CrossRef Medline
 13. Haacke EM, Xu Y, Cheng YC, et al. **Susceptibility weighted imaging (SWI).** *Magn Reson Med* 2004;52:612–28 CrossRef Medline
 14. Haacke EM, Ayaz M, Khan A, et al. **Establishing a baseline phase behavior in magnetic resonance imaging to determine normal vs. abnormal iron content in the brain.** *J Magn Reson Imaging* 2007;26:256–64 CrossRef Medline
 15. Haacke EM, Makki M, Ge Y, et al. **Characterizing iron deposition in multiple sclerosis lesions using susceptibility weighted imaging.** *J Magn Reson Imaging* 2009;29:537–44 CrossRef Medline
 16. Wu SF, Zhu ZF, Kong Y, et al. **Assessment of cerebral iron content in patients with Parkinson's disease by the susceptibility-weighted MRI.** *Eur Rev Med Pharmacol Sci* 2014;18:2605–08 Medline
 17. Adachi Y, Sato N, Saito Y, et al. **Usefulness of SWI for the detection of iron in the motor cortex in amyotrophic lateral sclerosis.** *J Neuroimaging* 2015;25:443–51 CrossRef Medline
 18. Thomas B, Somasundaram S, Thamburaj K, et al. **Clinical applications of susceptibility weighted MR imaging of the brain: a pictorial review.** *Neuroradiology* 2008;50:105–16 CrossRef Medline
 19. Brooks BR. **El Escorial World Federation of Neurology criteria for the diagnosis of amyotrophic lateral sclerosis: Subcommittee on Motor Neuron Diseases/Amyotrophic Lateral Sclerosis of the World Federation of Neurology Research Group on Neuromuscular Diseases and the El Escorial "Clinical limits of amyotrophic lateral sclerosis" workshop contributors.** *J Neurol Sci* 1994;124(suppl):96–107 CrossRef Medline
 20. Chiò A, Calvo A, Moglia C, et al. **Phenotypic heterogeneity of amyotrophic lateral sclerosis: a population based study.** *J Neurol Neurosurg Psychiatry* 2011;82:740–46 CrossRef Medline
 21. Roche JC, Rojas-García R, Scott KM, et al. **A proposed staging system for amyotrophic lateral sclerosis.** *Brain* 2012;135:847–852 CrossRef Medline
 22. Hirayama K, Tsubaki T, Toyokura Y, et al. **The representation of the pyramidal tract in the internal capsule and basis pedunculi: a study based on three cases of amyotrophic lateral sclerosis.** *Neurology* 1962;12:337–42 CrossRef Medline
 23. Zhou B, Li S, Huijin H, et al. **The evaluation of iron content in Alzheimer's disease by magnetic resonance imaging: phase and R2* methods.** *Adv Alzheimer Dis* 2013;2:51–59 CrossRef
 24. Ropele S, de Graaf W, Khalil M, et al. **MRI assessment of iron deposition in multiple sclerosis.** *J Magn Reson Imaging* 2011;34:13–21 CrossRef Medline
 25. Zecca L, Youdim MB, Riederer P, et al. **Iron, brain ageing and neurodegenerative disorders.** *Nat Rev Neurosci* 2004;5:863–73 CrossRef Medline
 26. Kwan JY, Jeong SY, Van Gelderen P, et al. **Iron accumulation in deep cortical layers accounts for MRI signal abnormalities in ALS: correlating 7 Tesla MRI and pathology.** *PLoS One* 2012;7:e35241 CrossRef Medline
 27. Oba H, Araki T, Ohtomo K, et al. **Amyotrophic lateral sclerosis: T2 shortening in motor cortex at MR imaging.** *Radiology* 1993;189:843–46 CrossRef Medline
 28. Cheung G, Gawel MJ, Cooper PW, et al. **Amyotrophic lateral sclerosis: correlation of clinical and MR imaging findings.** *Radiology* 1995;194:263–70 CrossRef Medline
 29. Hofmann E, Ochs G, Pelzl A, et al. **The corticospinal tract in amyotrophic lateral sclerosis: an MRI study.** *Neuroradiology* 1998;40:71–75 CrossRef Medline
 30. Hecht MJ, Fellner F, Fellner C, et al. **MRI-FLAIR images of the head show corticospinal tract alterations in ALS patients more frequently than T2-, T1- and proton-density-weighted images.** *J Neurol Sci* 2001;186:37–44 CrossRef Medline
 31. Kato Y, Matsumura K, Kinosada Y, et al. **Detection of pyramidal tract lesions in amyotrophic lateral sclerosis with magnetization-transfer measurements.** *AJNR Am J Neuroradiol* 1997;18:1541–47 Medline
 32. Cudkowicz M, Qureshi M, Shefner J. **Measures and markers in amyotrophic lateral sclerosis.** *NeuroRx* 2004;1:273–83 CrossRef Medline
 33. Mitsumoto H, Ulug AM, Pullman SL, et al. **Quantitative objective markers for upper and lower motor neuron dysfunction in ALS.** *Neurology* 2007;68:1402–10 CrossRef Medline
 34. Iwata NK, Kwan JY, Danielian LE, et al. **White matter alterations differ in primary lateral sclerosis and amyotrophic lateral sclerosis.** *Brain* 2011;134(pt 9):2642–55 CrossRef Medline
 35. Olsen MK, Roberds SL, Ellerbrock BR, et al. **Disease mechanisms revealed by transcription profiling in SOD1-G93A transgenic mouse spinal cord.** *Ann Neurol* 2001;50:730–40 CrossRef Medline
 36. Restagno G, Lombardo F, Ghiglione P, et al. **HFE H63D polymorphism is increased in patients with amyotrophic lateral sclerosis of Italian origin.** *J Neurol Neurosurg Psychiatry* 2007;78:327 CrossRef Medline
 37. Jacob S, Finsterbusch J, Weishaupt JH, et al. **Diffusion tensor imaging for long-term follow-up of corticospinal tract degeneration in amyotrophic lateral sclerosis.** *Neuroradiology* 2003;45:598–600 CrossRef Medline
 38. Wang S, Poptani H, Bilello M, et al. **Diffusion tensor imaging in amyotrophic lateral sclerosis: volumetric analysis of the corticospinal tract.** *AJNR Am J Neuroradiol* 2006;27:1234–38 Medline
 39. Hong YH, Lee KW, Sung JJ, et al. **Diffusion tensor MRI as a diagnostic tool of upper motor neuron involvement in amyotrophic lateral sclerosis.** *J Neurol Sci* 2004;227:73–78 CrossRef Medline
 40. Sage CA, Peeters RR, Görner A, et al. **Quantitative diffusion tensor imaging in amyotrophic lateral sclerosis.** *Neuroimage* 2007;34:486–99 CrossRef Medline

FLAIR²: A Combination of FLAIR and T2 for Improved MS Lesion Detection

V. Wiggermann, E. Hernández-Torres, A. Trabousee, D.K.B. Li, and A. Rauscher



ABSTRACT

BACKGROUND AND PURPOSE: FLAIR and double inversion recovery are important MR imaging scans for MS. The suppression of signal from CSF in FLAIR and the additional suppression of WM signal in double inversion recovery improve contrast between lesions, WM and GM, albeit at a reduced SNR. However, whether the acquisition of double inversion recovery is necessary is still debated. Here, we present an approach that allows obtaining CSF-suppressed images with improved contrast between lesions, WM and GM without strongly penalizing SNR.

MATERIALS AND METHODS: 3D T2-weighted and 3D-FLAIR data acquired from September 2014 to April 2015 in healthy volunteers (23.4 ± 2.4 years of age; female/male ratio, 3:2) and patients (44.1 ± 14.0 years of age; female/male ratio, 4:5) with MS were coregistered and multiplied (FLAIR²). SNR and contrast-to-noise measurements were performed for focal lesions and GM and WM. Furthermore, data from 24 subjects with relapsing-remitting and progressive MS were analyzed retrospectively (52.7 ± 8.1 years of age; female/male ratio, 14:10).

RESULTS: The GM-WM contrast-to-noise ratio was by 133% higher in FLAIR² than in FLAIR and improved between lesions and WM by 31%, 93%, and 158% compared with T2, DIR, and FLAIR, respectively. Cortical and juxtacortical lesions were more conspicuous in FLAIR². Furthermore, the 3D nature of FLAIR² allowed reliable visualization of callosal and infratentorial lesions.

CONCLUSIONS: We present a simple approach for obtaining CSF suppression with an improved contrast-to-noise ratio compared with conventional FLAIR and double inversion recovery without the acquisition of additional data. FLAIR² can be computed retrospectively if T2 and FLAIR scans are available.

ABBREVIATIONS: CNR = contrast-to-noise ratio; DIR = double inversion recovery

MR imaging is important for the diagnosis and monitoring of MS. Formation of MS lesions creates a hydrophilic environment, resulting in an increase in the T2 and proton density-weighted MR signal and a signal reduction on T1-weighted scans.¹ Ovoid hyperintense areas on T2-weighted MR imaging are

therefore a radiologic hallmark of MS. Lesion conspicuity is often affected by the bright CSF signal, for instance, close to the ventricles or cortical sulci. FLAIR is a T2-weighted scan that suppresses CSF selectively with an inversion pulse.² Yet, the CSF signal suppression comes at the cost of reduced SNR. Usually, FLAIR scans are acquired in 2D with sections parallel to the subcallosal line. Additional sagittal FLAIR scans are required to reliably detect corpus callosum lesions.^{2,3} Furthermore, 2D-FLAIR has artifacts due to CSF and blood inflow and often provides insufficient T2-weighting,⁴ requiring additional proton density/T2-weighted images for the detection of lesions in infratentorial areas. The brain MR imaging protocol for MS studies⁵ includes proton density and T2-weighted spin-echo, axial, and sagittal FLAIR and recommends pre- and postcontrast T1-weighted spin-echo MR imaging.

Apart from diagnosis, conventional MR images play an im-

Received May 4, 2015; accepted after revision June 21.

From the Departments of Physics and Astronomy (V.W.), Pediatrics (V.W., E.H.T., A.R.), Medicine (Neurology) (A.T., D.K.B.L.), and Radiology (D.K.B.L.); and University of British Columbia MRI Research Centre (V.W., E.H.T., A.R.); Centre for Brain Health (D.K.B.L., A.R.); and Child and Family Research Institute (A.R.), University of British Columbia, Vancouver, British Columbia, Canada.

This work was supported by a graduate studentship award from the MS Society of Canada (EGID 2002 [V.W.]), a Canadian Institutes of Health Research New Investigator Award (261306 [A.R.]), and a postdoctoral award by Consejo Nacional de Ciencia y Tecnología (237961 [E.H.T.]).

Paper previously presented at: 23rd Annual Meeting of the International Society for Magnetic Resonance in Imaging, May 30–June 5, 2015; Toronto, Ontario, Canada.

Please address correspondence to Alexander Rauscher, PhD, UBC MRI Research Centre and Department of Pediatrics, G33 Purdy Pavilion, 2221 Wesbrook Mall, University of British Columbia, Vancouver, BC, V6T 2B5, Canada; e-mail: rauscher@physics.ubc.ca; @rauscherMRI

Indicates open access to non-subscribers at www.ajnr.org

Indicates article with supplemental on-line photos.

<http://dx.doi.org/10.3174/ajnr.A4514>

Table 1: Imaging parameter overview for the SNR/CNR estimations and the retrospectively analyzed patient study

Study	Sequence	TR/TE _{eff} /TE _{equiv} /T ₁ /T ₂ (ms)	Acq. Voxel Size (mm ³)	Recon. Voxel Size (mm ³)	SENSE Acceleration	Acquisition Time (min)
SNR	FLAIR	8000/353/162/2400	0.8 × 0.8 × 1.6	0.8 × 0.8 × 0.8	2.5 (AP)2 (RL)	6:16
SNR	T2	2500/363/133	1 × 1 × 1.6	0.8 × 0.8 × 0.8	2 (AP) 2 (RL)	3:33
SNR	DIR	8000/337/156/3200/500	1 × 1 × 2	1 × 1 × 1	2.5 (AP) 2 (RL)	7:52
RS	FLAIR	8000/337/156/2400	1 × 1 × 1.6	0.8 × 0.8 × 0.8	2.5 (AP) 2 (RL)	5:04
RS	T2	2500/363/133	1 × 1 × 1.6	0.8 × 0.8 × 0.8	2 (AP) 1.5 (RL)	4:42
RS	DIR	8000/337/156/3200/500	1 × 1 × 1.6	0.8 × 0.8 × 0.8	2.5 (AP) 2 (RL)	9:44

Note:—RS indicates retrospectively analyzed patient study; Acq., acquired; Recon., reconstructed; SENSE, sensitivity encoding; AP, anterior-posterior; RL, right-left; TE_{equiv}, TE equivalent; TE_{eff}, effective TE.

portant role as outcome measures in clinical trials of new MS therapies.^{5,6} New lesion activity (eg, gadolinium-enhancing lesions and new or enlarging T2-lesions) and estimates of disease burden (eg, total T2-lesion volume or count; T1-hypointense lesion volume; brain atrophy) are typical imaging end points in clinical trials.⁵ These scans are directed toward lesion identification in WM. Demyelination and the appearance of lesions is, however, not limited to the WM; it also involves the deep and cortical GM.⁷ Focal GM lesions appear in the earliest stages of MS^{8,9} and are associated with physical and cognitive disability.^{10,11} Moreover, cortical lesion load was shown to be a predictor of progression of clinical disability during 5 years¹² and to improve predictions for the conversion from relapsing-remitting to secondary-progressive MS compared with assessing WM lesions alone.¹³ Given the importance of cortical lesions in MS, there is great interest in their visualization. However, the cortex is thin, its myelin content is low, and inflammation is low in cortical lesions. Contrast between lesions and healthy tissue is therefore low, making the detection of cortical damage challenging.

In double inversion recovery (DIR),¹⁴ both CSF and the WM signal are suppressed; this suppression results in enhanced contrast between lesions, GM and WM. T1-relaxation times of GM and WM are similar. Therefore, both tissues are affected by the inversion pulse, resulting in reduced SNR. Long data-acquisition times further limit the spatial resolution of DIR to 1 mm³ isotropic at 3T. In a postmortem study, the specificity of 3D-DIR was found to be 90%, whereas sensitivity was only 18%.¹⁵ DIR detected most leukocortical lesions; however, intracortical and subpial lesions were still missed.¹⁵ Intracortical and subpial lesions are the most common cortical lesions in patients with chronic MS, yet subpial lesions are rarely detected with DIR or other techniques.^{16,17} More recently, 3D versions of MR imaging sequences for MS have become available¹⁸ but are not yet used widely in clinical imaging of MS.¹⁹ 3D sequences with isotropic voxels of 1 mm³ volume or smaller are particularly suitable for the assessment of the cortex. Moreover, these scans allow simultaneous assessment of all 3 orthogonal image planes. A drawback is the increased acquisition time per scan, in particular for DIR. Lesion detection, especially within the cortex, would benefit from a rapid 3D imaging approach with high spatial resolution, suppressed CSF, higher SNR than DIR, and a good contrast-to-noise ratio (CNR) between lesions, GM and WM.

This study aims to develop and test a method that combines the good SNR of T2-weighted images with the CSF suppression of FLAIR to achieve GM-WM contrast similar to that in DIR and good contrast between lesions, healthy tissue. We compared SNR and CNR of this new approach with conventional FLAIR, T2, and

DIR; and we present images acquired in patients with relapsing-remitting and progressive MS.

MATERIALS AND METHODS

The Clinical Research Ethics Board of University of British Columbia approved the protocol. All subjects gave written informed consent in accord with the Declaration of Helsinki. The authors declare that there is no conflict of interest.

Subjects

Five healthy volunteers (23.4 ± 2.4 years of age; female/male ratio, 3:2) and 9 subjects with MS (44.1 ± 14.0 years of age; female/male ratio, 4:5, median Expanded Disability Status Scale score, 2.5; and mean disease duration, 10.4 ± 6.7 years; 6 with relapsing-remitting, 2 with primary-progressive MS, 1 with secondary-progressive MS) underwent MR imaging for this study. Furthermore, data from 24 subjects with MS (17 relapsing-remitting, 4 secondary-progressive MS, 3 primary-progressive MS; mean age, 52.7 ± 8.1 years; female/male ratio, 14:10; median Expanded Disability Status Scale score, 3.5; and mean age of disease onset, 38.2 ± 10.2 years) were analyzed retrospectively.

MR Imaging Protocol

MR imaging data were acquired on a 3T scanner (Achieva; Philips Healthcare, Best, the Netherlands) equipped with an 8-channel sensitivity encoding head coil. The imaging protocol included sagittal 3D-T2, 3D-FLAIR, and 3D-DIR scans. Detailed imaging parameters used for the CNR/SNR measurements and the retrospectively analyzed patient study are listed in Table 1.

The MR imaging protocol was refined after the study in the 24 patients and in parallel with the measurements of SNR and CNR. A range of spatial resolutions was tested in patients and controls. The specific imaging parameters are listed in the respective figure captions.

Data Processing and SNR/CNR Estimates

3D-FLAIR images were registered into the 3D T2 space by using FLIRT (FMRIB Linear Image Registration Tool; <http://www.fmrib.ox.ac.uk>)^{20,21} (12 *df*, search angle of 10°, mutual information as a cost function, sinc interpolation) and then multiplied with the T2 image, resulting in a heavily T2-weighted, CSF-suppressed image, which we refer to as FLAIR² (FLAIR squared).

For SNR and CNR measurements, every scan was acquired twice. The 2 consecutively acquired T2-weighted images were used to create a T2 half-way space by image registration with FLIRT.^{20,21} FLAIR and DIR images were then registered into the half-way space by using FLIRT with 6 *df*, a search angle of 10°, and

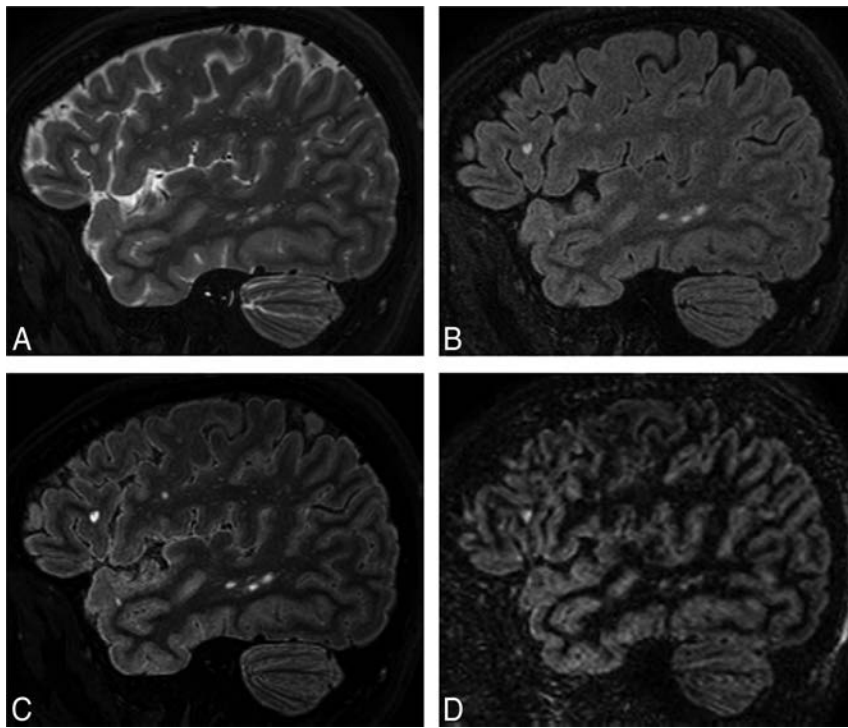


FIG 1. Comparison of standard MR images of MS with FLAIR² within the same patient (a 35-year-old woman): T2 (A), FLAIR (B), FLAIR² (C), and DIR (D). Here, T2 and FLAIR were acquired at $0.67 \times 0.76 \times 1.34 \text{ mm}^3$ within 6 minutes and 8 seconds and 7 minutes and 51 seconds, respectively, and were reconstructed to isotropic 0.3-mm^3 voxels, resulting in exquisite image contrast of the FLAIR² image compared with DIR (acquired within 13 minutes and 35 seconds and reconstructed to 1 mm^3), however, with much higher SNR. FLAIR² exhibits the highest contrast-to-noise levels between GM and WM and between lesions and surrounding normal-appearing brain tissue.

Table 2: Summary of SNR and CNR values in 5 healthy volunteers and 7 patients with MS

Imaging Technique	SNR	CNR (WM and GM)	CNR (WM and WM Lesions) (48 Lesions in 7 Patients)
FLAIR	19.3 ± 2.0	3.1 ± 0.7	7.1 ± 2.0
T2	23.9 ± 7.1	7.0 ± 3.0	13.9 ± 4.2
FLAIR ²	15.2 ± 2.3	7.1 ± 1.6	18.2 ± 6.1
DIR	4.5 ± 0.7	6.7 ± 1.1	9.4 ± 2.6

mutual information as a cost function. SNR and CNR were computed for FLAIR², FLAIR, and T2 in 5 healthy volunteers and 7 of our 9 patients with MS. Additionally, SNR and CNR for DIR were assessed for all patients with MS. The image noise was estimated within a large WM region as the SD of the subtraction of the consecutively acquired and coregistered images. The signal (S) was calculated as the mean signal within the same region in 1 of the 2 images, and SNR was calculated as $\text{SNR} = \sqrt{2} S / \text{SD}$.²² GM-WM CNR was computed as the signal difference between a representative part of the cortical GM and adjacent WM across multiple sections divided by the SD in the ROI of the subtraction image. In patients with MS, CNR was computed for up to 7 focal MS lesions and the surrounding WM within each patient.

RESULTS

Multiplication of the coregistered FLAIR with the T2-weighted scan results in an image (FLAIR²) in which the CSF is suppressed

due to the signal inversion on FLAIR and where WM signal is reduced due to the T2-weighted image contrast. Areas that are bright in both images, such as lesions and GM, are further enhanced in the resulting image. Figure 1 shows 3D-T2 (A), 3D-FLAIR (B), 3D-FLAIR² (C), and 3D-DIR (D) of a person with relapsing-remitting MS. Here, FLAIR² was acquired at $0.67 \times 0.76 \times 1.34 \text{ mm}^3$ and reconstructed to 0.3 mm^3 voxels, while DIR was acquired and reconstructed to 1 mm^3 . Data acquisition took 6 minutes and 8 seconds for T2 and 7 minutes and 51 seconds for FLAIR, whereas the acquisition of DIR alone took 13 minutes and 35 seconds. The DIR shows some cortical areas of hyperintense signal, which appear normal on FLAIR².

SNR and CNR values are shown in Table 2. In summary, T2-weighted images had the highest SNR levels, while CNR levels were similar among 3D-DIR, 3D-T2, and 3D-FLAIR². Being the result of multiplication, FLAIR² had lower SNR than both FLAIR and T2. However, the CNR between GM and WM of FLAIR² was 133% higher than in FLAIR, and across the 48 analyzed lesions and

their adjacent WM, FLAIR² achieved an improvement in CNR of 31%, 93%, and 158% compared with T2, DIR, and FLAIR, respectively.

An example of a high-spatial-resolution FLAIR² image of a patient with MS with cortical involvement is shown in Fig 2. A leukocortical U-fiber lesion is seen on sagittal FLAIR (A), FLAIR² (B), DIR (C), and T1-weighted (D) images, respectively. Here, FLAIR and T2 were acquired at $0.67 \times 0.76 \times 1.34 \text{ mm}^3$ and reconstructed to 0.3 mm^3 isotropic voxels. Additional coronal sections of the same lesion are shown (Fig 2). The T1-weighted image, which was acquired within 4 minutes and 12 seconds at the same spatial resolution, shows the lesion as a hypointense area.

The appearance of a large mixed GM-WM lesion on T2 (A), FLAIR (B), and FLAIR² (C) is compared in Fig 3. Here, FLAIR and T2 were acquired as described for the retrospective patient study. T2 exhibits the most signal within the lesion area and, in comparison with FLAIR, highlights how the WM lesion extends into the cortex. However, the heterogeneity of the lesion that is apparent on FLAIR is not seen on T2. FLAIR² can display a combination of these effects.

The large FOV of the sagittal 3D acquisition allows good visualization of lesions in the corpus callosum, infratentorial areas, and the cervical spine. In Fig 4, FLAIR² was calculated on the basis of the retrospectively analyzed patient study protocol. On axial (A), coronal (B), and sagittal (C) sections, an infratentorial, pontine lesion (A and C) and a corpus callosum (C) and a cervical spinal cord lesion (B and C) are visible.

Visually, the FLAIR² images reflected the quantitative assess-

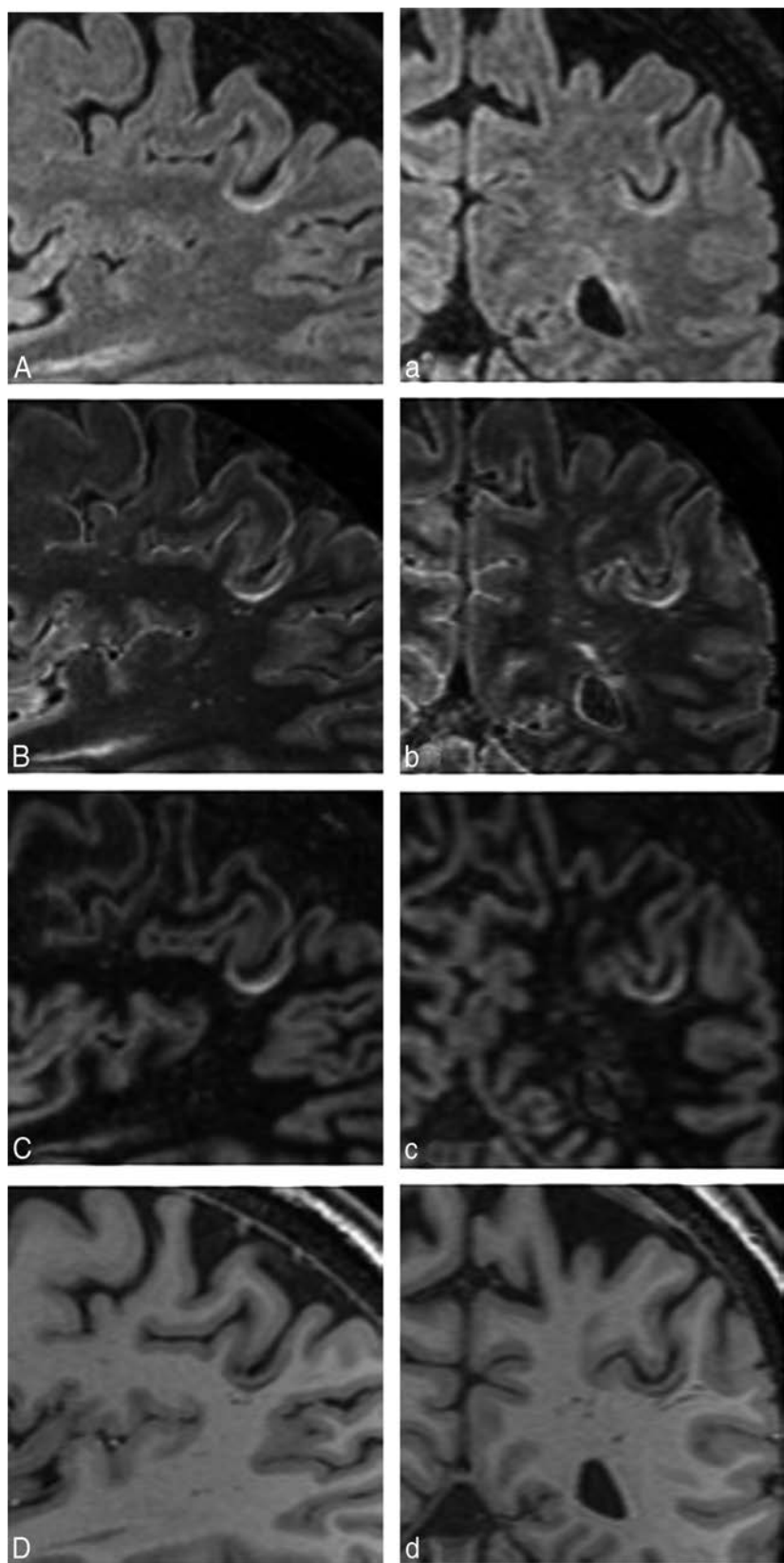


FIG 2. Depiction of a leukocortical U-fiber lesion on sagittal FLAIR (A), FLAIR² (B), DIR (C), and a T1-weighted image (D) of a patient with relapsing-remitting MS (a 54-year-old man). The same lesion is clearly visible on all coronal images (a–d). Here, FLAIR and T2 were reconstructed to 0.3-mm³ isotropic imaging voxels (acquired at $0.6 \times 0.68 \times 1.2$ mm³ in 7 minutes and 51 seconds and 7 minutes and 12 seconds, respectively), resulting in a visible SNR reduction, especially on FLAIR (A), and influencing the image quality of our FLAIR² (B).

ment of CNR and SNR, showing excellent CNR between lesions and GM and WM. The conspicuity of cortical involvement was good, without false-positive areas often seen on DIR (On-line Figs 1 and 2). Scans with approximately 0.3-mm³ voxel volume appear best for image quality and data-acquisition time.

DISCUSSION

Reliable detection of existing and new MS lesions is essential for the diagnosis and disease monitoring of MS. We presented a simple and robust approach for obtaining fluid-attenuated images with high contrast between lesions, GM and WM. Areas that are bright in both FLAIR and T2 are enhanced, whereas signal from areas that are dark in 1 of the 2 scans are suppressed. In particular, CSF remains hypointense on FLAIR². Moreover, because WM is more hypointense on T2-weighted images than on FLAIR and MS lesions are bright on both images, the FLAIR² images resemble DIR scans, but at much higher SNR and CNR compared with DIR (Fig 1 and Table 2). It may seem counterintuitive to multiply 2 images because the SNR of the resulting image will always be smaller than the SNR of any of the 2 input images. However, the CNR for both lesions-WM and GM-WM was larger in FLAIR² than in FLAIR, facilitating easier manual lesion detection and potentially better automated lesion segmentation.

Considerations for Data

Acquisition

We acquired all scans in a sagittal orientation by using 3D sequences, allowing coverage of the whole brain and parts of the spinal cord with 1 scan. We tested a range of spatial resolutions and found that the SNR penalty at an imaging voxel size of 0.2 mm³ appears to be too large (results are not shown here), while FLAIR² images with 0.3-mm³ voxels (Figs 1 and 2) present excellent contrast and good SNR. The retrospective FLAIR² study acquired 3D-FLAIR within 5:04 minutes, 3D-T2 in 4:42 minutes, and 3D-DIR in 9:44 minutes. When these images were acquired with a resolution of $1 \times 1.15 \times 1$ mm³, acquisition times for 3D-T2 and 3D-FLAIR extended to 5:27 min-

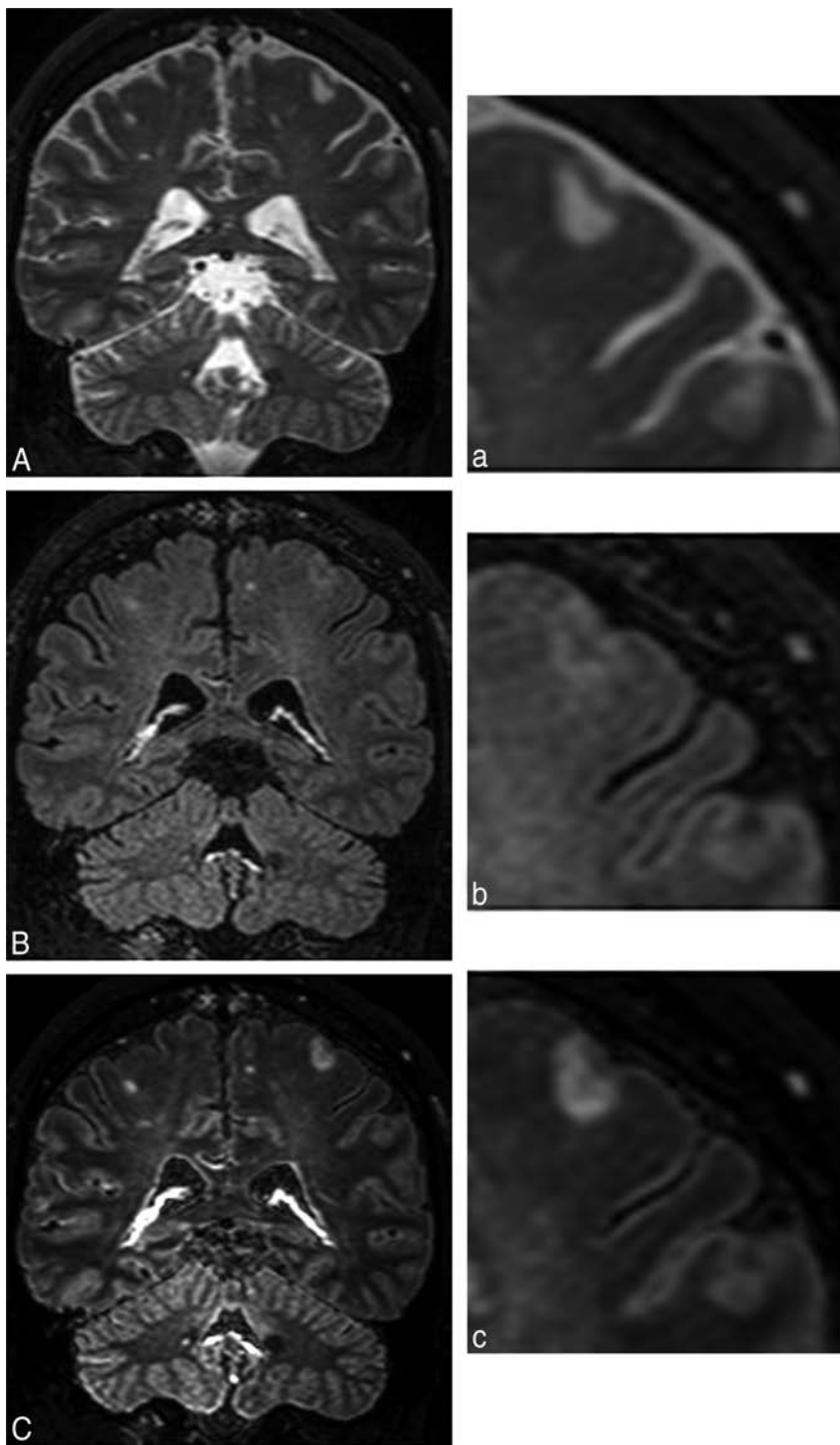


FIG 3. A large mixed GM-WM (leukocortical) lesion is present on T2 (A), FLAIR (B), and FLAIR² (C), acquired following the clinical imaging protocol in a patient with primary-progressive MS (a 44-year-old man). Their respective zoom-ins highlight the heterogeneity of the lesion, which is seen on FLAIR. Through the multiplication with T2, however, the lesion and its heterogeneity become more prominent (voxel size = $1.0 \times 1.0 \times 1.6 \text{ mm}^3$ acquired, $0.8 \times 0.8 \times 0.8 \text{ mm}^3$ reconstructed; T2 and FLAIR were acquired in 4 minutes and 43 seconds and 5 minutes, respectively).

utes and 6:56 minutes compared with 13:36 minutes for the 3D-DIR with the same spatial resolution. The gain in time and CNR by omitting DIR can be used to acquire the T2 and FLAIR scans at a higher spatial resolution.

The GM signal intensity on DIR scans varies considerably

across the cortex, which is due to partial volume effects, variations in cortical thickness, and differences in relaxation times. The higher spatial resolution achievable with FLAIR² mitigates partial volume effects.

While FLAIR² could, in principle, be computed from 2D scans, performing sagittal 3D data acquisition has several advantages. The sagittal readout offers the possibility of using partial parallel imaging²³ along both phase-encoding directions. Subtle ghosting due to partial parallel imaging can be exacerbated on multiplication if the 2 images have similar ghosting characteristics. The use of different acceleration factors for FLAIR (eg, 2.5, 2) and T2 (eg, 2, 1.5) may help mitigate this effect. However, we did not test whether identical sensitivity encoding factors lead to any amplification of ghosting artifacts. The sagittal acquisition furthermore allows large FOVs along the foot-head direction that extend into the cervical spine, even with a conventional head coil (Fig 4). With dedicated head-neck coils, the brain, the cervical spine, and superior aspects of the thoracic spine can be imaged with 1 sagittal acquisition, which would capture most of the clinically relevant spinal cord lesions.²⁴

Images acquired in 3D usually have isotropic voxels and, by definition, no intersection gap. Image registration works well with such data, which is essential for the FLAIR² approach. Moreover, 3D scans can be easily reformatted without loss of image quality. Due to the nonselective inversion pulse, there are no artifacts due to the inflow of noninverted blood and CSF in 3D-FLAIR images. Therefore, the additional proton density-weighted scan,⁵ which is necessary for detecting infratentorial lesions in 2D protocols, becomes obsolete with 3D protocols (Fig 4). However, it has been suggested that low T2-weighting of fast FLAIR acquisitions⁴ and the different T2-characteristics of infratentorial lesions²⁵ may limit their visibility on FLAIR. The combination of 3D-FLAIR and 3D-T2 should overcome insufficient T2-weighting in regions of the posterior fossa.

A study of 11 patients with relapsing-remitting MS and 5 with secondary-progressive MS at 1.5T showed that most infratentorial lesions were detected with 3D-FLAIR and 3D-DIR.¹⁹ Finally, due to the high isotropic spatial resolution of 3D-FLAIR², corpus

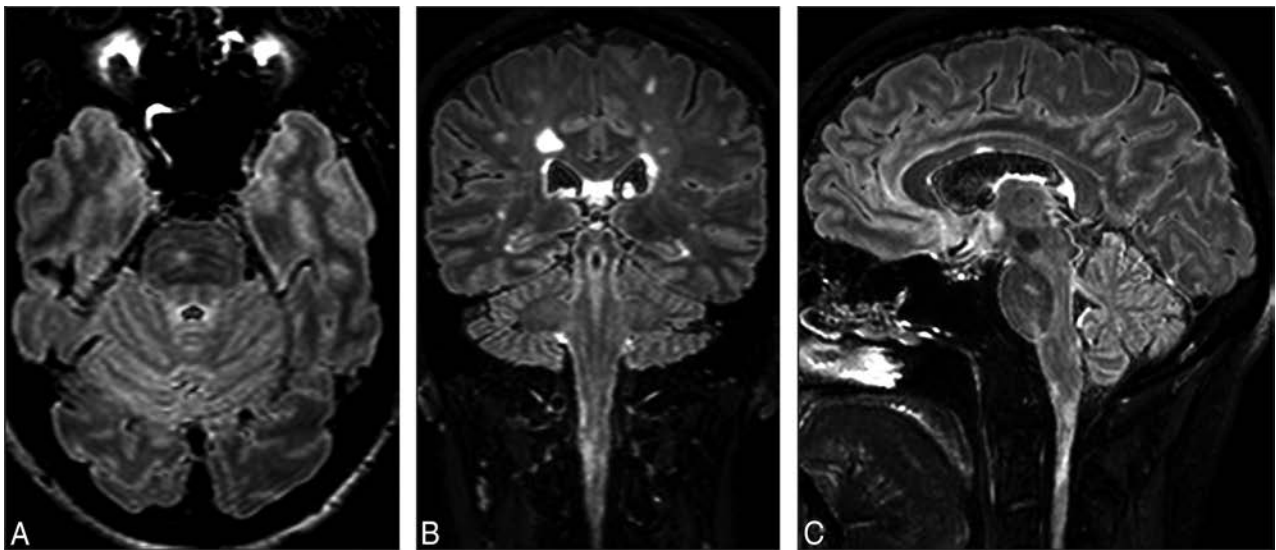


FIG 4. FLAIR² acquired at $1 \times 1 \times 1.6 \text{ mm}^3$ and reconstructed to 0.51 mm^3 shows an infratentorial lesion located in the pons (A and C), a lesion in the cervical spinal cord (B and C), and a lesion in the corpus callosum (C) in the same patient with MS. Due to the isotropic spatial resolution, the large FOV, and the insensitivity to flow in the infratentorial parts of the brain, no additional 2D or proton-density weighted scans are required to visualize these lesions.

callosum lesions are detectable without a separate acquisition of a sagittal 2D-FLAIR (Fig 4). By omitting the acquisition of the sagittal 2D-FLAIR, the 2D proton density-weighted image, and potentially the DIR, approximately 20 minutes of acquisition time is saved, which can be invested in acquiring 3D sequences at higher spatial resolution, for instance. In research studies, the remaining scanning time can also be used in the acquisition of advanced MR images, such as myelin water,²⁶ magnetization transfer imaging,²⁷ or susceptibility-weighted imaging²⁸⁻³⁰ for the calculation of frequency maps as measures of MS tissue damage³¹ and of R2* maps.³²

Improved Assessment of the Cortical GM

An improved visualization of the cortical GM and cortical damage is an important step in finding new markers for disease progression in patients with MS. Currently, GM thickness and GM lesion count are attractive markers. However, WM lesions close to GM or mixed GM-WM lesions are often misclassified. FLAIR² contrast could be helpful in automatically generating lesion masks. Automated segmentation should be improved, considering the high CNR between lesions and adjacent WM and surrounding GM.

Juxtacortical and leukocortical lesions are often seen within or close to the cortical U-fibers (Fig 2 and On-line Figs 1 and 2). It has been suggested that these areas promote lesion development due to reduced CSF circulation.¹⁰ DIR suppresses the WM component of the signal, which aids in lesion classification. However, the SNR reduction and the detection of a considerable number of false-positive lesions aggravate the use of DIR to mirror cortical damage.

Limitations

The hyperintense rim on the surface of the brain seen on FLAIR is also visible on FLAIR². However, the rim becomes less prominent with increasing spatial resolution. The quality of FLAIR² depends on good image registration between the 2 input scans. Due to the brightness of the CSF signal in the T2-weighted scan, any misregistration would be immediately apparent on FLAIR². Here, we

saw no signs of misregistration in >30 scans, suggesting that the approach can be implemented as a fully automated step on MR imaging systems. The robustness of image registration was previously demonstrated for the fusion of FLAIR and venograms computed from susceptibility-weighted images.^{33,34} The resulting FLAIR* images feature lesions and veins, which are often associated with MS lesions, but less often with WM hyperintensities of different etiology. Image-registration artifacts are a particular caveat for the detection of subpial lesions because CSF signal may leak into the FLAIR² images, which could be falsely interpreted as lesions. However, separate evaluation of T2 and FLAIR in all 3 orthogonal imaging planes can mitigate this problem. Furthermore, FLAIR is known to present sometimes diffusely abnormal signal in the periventricular WM, even in healthy subjects. This effect of unknown origin is not reduced in FLAIR². Therefore, the definition of diffusely abnormal WM requires a scan that is not susceptible to this effect (eg, a proton density-weighted scan). Finally, the sensitivity and specificity of FLAIR² compared with FLAIR or DIR were not assessed in this proof-of-principle study.

CONCLUSIONS

The proposed approach results in fluid-attenuated images with improved CNR between lesions, WM and GM compared with conventional FLAIR scans. FLAIR² can be computed retrospectively from T2 and FLAIR, which are available in most clinical and research studies on MS. The wide availability of the input data and the simplicity of the technique allow other research groups to quickly verify the usefulness of FLAIR² in a wide range of settings. We propose a protocol of 3D-T1, 3D-T2, 3D-FLAIR, and FLAIR², which can be acquired within 20 minutes at a spatial resolution of 0.3 mm^3 , compared with 33 minutes if DIR is included. This protocol captures WM lesions in the entire brain, including infratentorial regions, the corpus callosum, and most of the cervical cord (the entire cervical cord and parts of the thoracic cord if a head-

neck coil is used), and cortical lesions at high spatial resolution. With its DIR-like contrast, but higher SNR and CNR, FLAIR² may elegantly resolve the debate as to whether to include DIR in the standard imaging protocol of MS.

ACKNOWLEDGMENTS

The authors thank the participants of this study, Philips Healthcare for their continuing support, and the University of British Columbia MRI Research Centre and its staff and technologists for their support and service.

Disclosures: Vanessa Wiggermann—UNRELATED: *Travel/Accommodations/Meeting Expenses Unrelated to Activities Listed*: F. Hoffmann-La Roche, *Comments*: travel reimbursements; *OTHER RELATIONSHIPS*: recipient of a Doctoral Studentship Award from the MS Society of Canada (EGID 2002). Anthony Traboulsee—UNRELATED: *Board Membership*: F. Hoffmann-La Roche, *Comments*: Steering Committee member; *Consultancy*: Biogen, Teva, EMD Serono, Chugai, Roche, Genzyme, MedImmune; *Grants/Grants Pending*: Genzyme, F. Hoffman La Roche; *Payment for Lectures (including service on Speakers Bureaus)*: Genzyme, EMD Serono. David K.B. Li—UNRELATED: *Board Membership*: Opexa Therapeutics, Novartis, Nuron, and Roche, *Comments*: member of the Data and Safety Advisory Board for Opexa Therapeutics and the Scientific Advisory Board for Novartis, Nuron, and Roche; *Consultancy*: Vertex Pharmaceutical (advisor for product development); *Expert Testimony*: Genzyme,* F. Hoffmann-La Roche,* Merck-Serono,* Nuron,* Perceptives,* Sanofi-Aventis.* Alexander Rauscher—RELATED: *Grant*: Canadian Institutes of Health Research, *Comments*: Canadian Institutes of Health Research New Investigator Award (salary award); UNRELATED: *Board Membership*: F. Hoffmann-La Roche, *Comments*: Imaging Advisory Board. *Money paid to the institution.

REFERENCES

- Stewart WA, Hall LD, Berry K, et al. **Correlation between NMR scan and brain slice data in multiple sclerosis.** *Lancet* 1984;2:412 Medline
- Traboulsee A, Li DK. **Conventional MR imaging.** *Neuroimaging Clin N Am* 2008;18:651–73, x CrossRef Medline
- Simon JH, Li D, Traboulsee A, et al. **Standardized MR imaging protocol for multiple sclerosis: Consortium of MS Centers consensus guidelines.** *AJNR Am J Neuroradiol* 2006;27:455–61 Medline
- Okuda T, Korogi Y, Shigematsu Y, et al. **Brain lesions: when should fluid-attenuated inversion-recovery sequences be used in MR evaluation?** *Radiology* 1999;212:793–98 CrossRef Medline
- Paty DW, Li DK, Oger JJ, et al. **Magnetic resonance imaging in the evaluation of clinical trials in multiple sclerosis.** *Ann Neurol* 1994;36(suppl):S95–96 CrossRef Medline
- Bermel RA, Fisher E, Cohen JA. **The use of MR imaging as an outcome measure in multiple sclerosis clinical trials.** *Neuroimaging Clin N Am* 2008;18:687–701, xi CrossRef Medline
- Kutzelnigg A, Lucchinetti CF, Stadelmann C, et al. **Cortical demyelination and diffuse white matter injury in multiple sclerosis.** *Brain* 2005;128(pt 11):2705–12 CrossRef Medline
- Lucchinetti CF, Popescu BF, Bunyan RF, et al. **Inflammatory cortical demyelination in early multiple sclerosis.** *N Engl J Med* 2011;365:2188–97 CrossRef Medline
- Calabrese M, Gallo P. **Magnetic resonance evidence of cortical onset of multiple sclerosis.** *Mult Scler* 2009;15:933–41 CrossRef Medline
- Kutzelnigg A, Lassmann H. **Cortical demyelination in multiple sclerosis: a substrate for cognitive deficits?** *J Neurol Sci* 2006;245:123–26 CrossRef Medline
- Nielsen AS, Kinkel RP, Madigan N, et al. **Contribution of cortical lesion subtypes at 7T MRI to physical and cognitive performance in MS.** *Neurology* 2013;81:641–49 CrossRef Medline
- Calabrese M, Poretto V, Favaretto A, et al. **Cortical lesion load associates with progression of disability in multiple sclerosis.** *Brain* 2012;135:2952–61 CrossRef Medline
- Calabrese M, Romualdi C, Poretto V, et al. **The changing clinical course of multiple sclerosis: a matter of gray matter.** *Ann Neurol* 2013;74:76–83 CrossRef Medline
- Redpath TW, Smith FW. **Technical note: use of a double inversion recovery pulse sequence to image selectively grey or white brain matter.** *Br J Radiol* 1994;67:1258–63 CrossRef Medline
- Seewann A, Kooi EJ, Roosendaal SD, et al. **Postmortem verification of MS cortical lesion detection with 3D DIR.** *Neurology* 2012;78:302–08 CrossRef Medline
- Seewann A, Vrenken H, Kooi EJ, et al. **Imaging the tip of the iceberg: visualization of cortical lesions in multiple sclerosis.** *Mult Scler* 2011;17:1202–10 CrossRef Medline
- Kilsdonk ID, de Graaf WL, Soriano AL, et al. **Multicontrast MR imaging at 7T in multiple sclerosis: highest lesion detection in cortical gray matter with 3D-FLAIR.** *AJNR Am J Neuroradiol* 2013;34:791–96 CrossRef Medline
- Mugler JP 3rd, Bao S, Mulkern RV, et al. **Optimized single-slab three-dimensional spin-echo MR imaging of the brain.** *Radiology* 2000;216:891–99 CrossRef Medline
- Moraal B, Roosendaal SD, Pouwels PJ, et al. **Multi-contrast, isotropic, single-slab 3D MR imaging in multiple sclerosis.** *Eur Radiol* 2008;18:2311–20 CrossRef Medline
- Jenkinson M, Bannister P, Brady M, et al. **Improved optimization for the robust and accurate linear registration and motion correction of brain images.** *Neuroimage* 2002;17:825–41 CrossRef Medline
- Jenkinson M, Smith S. **A global optimisation method for robust affine registration of brain images.** *Med Image Anal* 2001;5:143–56 CrossRef Medline
- Price RR, Axel L, Morgan T, et al. **Quality assurance methods and phantoms for magnetic resonance imaging: report of AAPM nuclear magnetic resonance Task Group No. 1.** *Med Phys* 1990;17:287–95 CrossRef Medline
- Pruessmann KP, Weiger M, Scheidegger MB, et al. **SENSE: sensitivity encoding for fast MRI.** *Magn Reson Med* 1999;42:952–62 Medline
- Okuda DT, Mowry EM, Cree BA, et al. **Asymptomatic spinal cord lesions predict disease progression in radiologically isolated syndrome.** *Neurology* 2011;76:686–92 CrossRef Medline
- Bastianello S, Bozzao A, Paolillo A, et al. **Fast spin-echo and fast fluid-attenuated inversion-recovery versus conventional spin-echo sequences for MR quantification of multiple sclerosis lesions.** *AJNR Am J Neuroradiol* 1997;18:699–704 Medline
- Prasloski T, Rauscher A, MacKay AL, et al. **Rapid whole cerebrum myelin water imaging using a 3D GRASE sequence.** *Neuroimage* 2012;63:533–39 CrossRef Medline
- Loevner LA, Grossman RI, McGowan JC, et al. **Characterization of multiple sclerosis plaques with T1-weighted MR and quantitative magnetization transfer.** *AJNR Am J Neuroradiol* 1995;16:1473–79 Medline
- Reichenbach JR, Venkatesan R, Schillinger DJ, et al. **Small vessels in the human brain: MR venography with deoxyhemoglobin as an intrinsic contrast agent.** *Radiology* 1997;204:272–77 CrossRef Medline
- Haacke EM, Xu Y, Cheng YC, et al. **Susceptibility weighted imaging (SWI).** *Magn Reson Med* 2004;52:612–18 CrossRef Medline
- Denk C, Rauscher A. **Susceptibility weighted imaging with multiple echoes.** *J Magn Reson Imaging* 2010;31:185–91 CrossRef Medline
- Wiggermann V, Hernández Torres E, Vavasour IM, et al. **Magnetic resonance frequency shifts during acute MS lesion formation.** *Neurology* 2013;81:211–18 CrossRef Medline
- Walsh AJ, Blevins G, Lebel RM, et al. **Longitudinal MR imaging of iron in multiple sclerosis: an imaging marker of disease.** *Radiology* 2014;270:186–96 CrossRef Medline
- Grabner G, Dal-Bianco A, Scherthaner M, et al. **Analysis of multiple sclerosis lesions using a fusion of 3.0 T FLAIR and 7.0 T SWI phase: FLAIR SWI.** *J Magn Reson Imaging* 2011;33:543–49 CrossRef Medline
- Sati P, George IC, Shea CD, et al. **FLAIR*: a combined MR contrast technique for visualizing white matter lesions and parenchymal veins.** *Radiology* 2012;265:926–32 CrossRef Medline

Multimodal Imaging in Malignant Brain Tumors: Enhancing the Preoperative Risk Evaluation for Motor Deficits with a Combined Hybrid MRI-PET and Navigated Transcranial Magnetic Stimulation Approach

 V. Neuschmelting,  C. Weiss Lucas,  G. Stoffels,  A.-M. Oros-Peusquens,  H. Lockau,  N.J. Shah,  K.-J. Langen,  R. Goldbrunner, and  C. Grefkes



ABSTRACT

BACKGROUND AND PURPOSE: Motor deficits in patients with brain tumors are caused mainly by irreversible infiltration of the motor network or by indirect mass effects; these deficits are potentially reversible on tumor removal. Here we used a novel multimodal imaging approach consisting of structural, functional, and metabolic neuroimaging to better distinguish these underlying causes in a preoperative setting and determine the predictive value of this approach.

MATERIALS AND METHODS: Thirty patients with malignant brain tumors involving the central region underwent a hybrid O-(2-[¹⁸F]fluoroethyl)-L-tyrosine–PET-MR imaging and motor mapping by neuronavigated transcranial magnetic stimulation. The functional maps served as localizers for DTI tractography of the corticospinal tract. The spatial relationship between functional tissue (motor cortex and corticospinal tract) and lesion volumes as depicted by structural and metabolic imaging was analyzed.

RESULTS: Motor impairment was found in nearly all patients in whom the contrast-enhanced T1WI or PET lesion overlapped functional tissue. All patients who functionally deteriorated after the operation showed such overlap on presurgical maps, while the absence of overlap predicted a favorable motor outcome. PET was superior to contrast-enhanced T1WI for revealing a motor deficit before the operation. However, the best correlation with clinical impairment was found for T2WI lesion overlap with functional tissue maps, but the prognostic value for motor recovery was not significant.

CONCLUSIONS: Overlapping contrast-enhanced T1WI or PET-positive signals with motor functional tissue were highly indicative of motor impairment and predictive for surgery-associated functional outcome. Such a multimodal diagnostic approach may contribute to the risk evaluation of operation-associated motor deficits in patients with brain tumors.

ABBREVIATIONS: CE = contrast-enhanced; CST = corticospinal tract; FA = fractional anisotropy; FET = O-(2-[¹⁸F]fluoroethyl)-L-tyrosine; KPS = Karnofsky Performance Scale; M1 = primary motor area; nTMS = navigated transcranial magnetic stimulation; SPACE = T2-weighted sampling perfection with application-optimized contrasts using different flip angle evolution

Multimodal imaging is a criterion standard in the diagnosis of brain tumors.¹ The combination of anatomic, functional, and metabolic imaging by MR imaging and PET helps differentiate tumor tissue from functionally relevant brain regions (eg, the primary motor cortex [M1]).² A frequently encountered phenomenon in patients presenting with tumors in the vicinity of motor regions is that some of them have motor impairment while

others do not, and some deteriorate after the operation while others may even improve.³⁻⁵ In some patients, motor deficits can be explained by direct infiltration of the tumor into the motor cortex or corticospinal tract (CST), while in other patients, compression effects resulting from the tumor mass and/or perifocal edema may cause motor symptoms.⁵ Differentiating causes is, however, highly relevant with respect to the reversibility of symptoms and planning of operations.⁶⁻⁹

In clinical practice, such preoperative diagnostics usually rely on analyses of structural MR imaging sequences such as T1- or

Received May 5, 2015; accepted after revision July 14.

From the Departments of Neurosurgery (V.N., C.W.L., R.G.), Radiology (H.L.) and Neurology (C.G.), University of Cologne, Cologne, Germany; Department of Radiology (V.N., H.L.), Memorial Sloan Kettering Cancer Center, New York, New York; Institute for Neuroscience and Medicine (G.S., A.-M.O.-P., N.J.S., K.-J.L., C.G.), Forschungszentrum Jülich, (Institute for Neuroscience and Medicine [INM]-2, INM-3, INM-4), Juelich, Germany; and Departments of Neurology (N.J.S.) and Nuclear Medicine (K.-J.L.), Rheinisch-Westfälische Technische Hochschule Aachen University, Aachen, Germany.

This work was supported by a Deutsche Forschungsgemeinschaft grant No. INST 1856/50-1 LAGG (R.G.) and a Deutsche Forschungsgemeinschaft research fellowship grant No. NE 1922/2-1 (V.N.).

Please address correspondence to Volker Neuschmelting, MD, Department of Neurosurgery, University Hospital Cologne, Kerpener Str 62, 50931 Cologne, Germany; e-mail: volker.neuschmelting@uk-koeln.de

 Indicates open access to non-subscribers at www.ajnr.org

 Indicates article with supplemental on-line tables.

 Indicates article with supplemental on-line photos.

<http://dx.doi.org/10.3174/ajnr.A4536>

T2-weighted scans without integrating individual information on functional anatomy. Direct cortical stimulation remains the criterion standard for motor function mapping but is limited to the intraoperative setting and, thus, not suitable for preoperative planning and risk evaluation. However, the repertoire of methods available in brain mapping has considerably advanced in the past decade and now allows elaborate analyses of structure-function relationships. For example, a useful tool for assessing the functional anatomy of the primary motor cortex in a noninvasive fashion is navigated transcranial magnetic stimulation (nTMS).¹⁰⁻¹² This technique has a reliability similar to that of fMRI mapping, however, with less demand for the cooperation of patients who may have reduced alertness, compliance, and functional impairment such as those with brain tumors.^{13,14} Another technique that adds information to structure-function relationships is diffusion imaging, especially DTI.^{9,15,16} For example, DTI-based tractography has been developed to visualize the subcortical fiber tracts in individual subjects; this is especially useful in conditions in which the functional anatomy can be heavily distorted such as in patients with brain tumors.^{17,18} In addition, DTI can also be used to characterize the altered diffusion metrics within the tumor mass and the surrounding tissue, thereby allowing quantification of the integrity of fiber tracts.^{19,20}

In summary, there are currently rather limited data on how to preoperatively evaluate patients with brain tumors for operation-associated risks related to motor impairment and recovery thereof.^{7,12,21-23} Thus, the objective of our study was to use a multimodal imaging setup to delineate malignant brain tumor lesions from functionally relevant motor cortex and fibers in patients undergoing an operation. As such, the study was based on a multimodal imaging approach by the coregistered integration of the following: 1) MR imaging data for anatomically defining lesion extent (T2WI and T1WI) and allowing structural analysis by DTI tractography; 2) O-(2-[¹⁸F]fluoroethyl)-L-tyrosine (FET)-PET for outlining the metabolic extent of the tumor because FET is the most evaluated ¹⁸F-labeled amino acid for PET of brain tumors, in particular in treatment planning and monitoring²²⁻²⁵; and 3) nTMS data for a functional definition of the M1 region and allowing nTMS-based DTI tractography. We hypothesized the following: 1) The integration of FET-PET and nTMS data advances the preoperative evaluation of motor impairment more than with MR imaging alone by contrast-enhanced T1WI (T1-CE), T2WI, and DTI; and 2) lesional signal within primary motor functional tissue as depicted by the multimodal approach may then serve as a potential predictive imaging marker for motor function outcome.

MATERIALS AND METHODS

Patient Enrollment and Study Design

We prospectively examined 30 consecutive patients (16 men; mean age, 60 years) enrolled by referral for tumor removal in the vicinity of the M1 and/or the CST between November 2011 and September 2013 (see On-line Tables 1 and 2 for clinical characteristics and study criteria). While 25 patients were diagnosed for the first time, 5 were referred due to suspicious recurrent tumor growth. At admission and at discharge, upper limbs, lower limbs, and facial muscles were tested for strength and scored according to the widely used Medical Research Council scale from 0 to 5 by

the same experienced individual neurosurgeon. Any score <5 in any body part defined the presence of a motor deficit. In addition, the Karnofsky Performance Scale (KPS) was assessed at both time points (On-line Table 1).

The study was approved by the University of Cologne ethics committee. Written informed consent was obtained from all patients. Three patients were not scanned by PET due to a recently performed PET before the study. All other patients underwent a standardized hybrid MRI-PET protocol followed by an nTMS motor cortex mapping shortly thereafter, on average within 1 week before the operation. One patient declined surgical tumor removal; hence, this patient was excluded when testing for relationships to postoperative outcome. All other patients underwent a standard tumor-removal operative protocol with the use of state-of-the-art neurosurgical and technical equipment for a brain tumor operation in eloquent brain regions, including intraoperative navigation and neurophysiologic monitoring.

Hybrid MRI-PET Imaging and nTMS Data Acquisition

The hybrid 3T MRI-PET scanner used in the present study consisted of a commercially available 3T MR imaging system (Magnetom Tim Trio; Siemens, Erlangen, Germany) and a PET insert for brain imaging as described elsewhere.²⁵ In summary, the BrainPET (Siemens, Erlangen, Germany) ring consisted of 32 copper-shielded detector cassettes coupled with an array of Avalanche Photodiodes (Excelitas Technologies, Asslar, Germany) at the front end so that it was not sensitive to the magnetic field of the MR imaging system (FOV diameter, 31.4 cm; length, 19.2 cm), which allows a central image resolution of approximately 3 mm.^{2,25}

FET-PET

PET was performed by using FET (see Neuner et al²⁵ for details). In brief, after the intravenous injection of 200 MBq of FET, a hybrid MRI-PET protocol was performed with a duration of 40–50 minutes (see On-line Table 3 for the protocol summary). The corrections for a component-based normalization, attenuation, and scatter, dead-time, and decay were performed within the reconstruction process thereafter.²⁵ The reconstructed images had 256 × 256 × 153 isotropic voxels of 1.25 mm³ and were subsequently filtered with a 3D Gaussian kernel (filter width, 3 mm) to increase the SNR.

MR Imaging

Anatomic MR images were acquired by using a T2WI spin-echo sampling perfection with application-optimized contrasts using different flip angle evolution (SPACE; Siemens) sequence and a T1WI MPRAGE sequence before and after intravenous injection of a gadolinium-based contrast-enhancing agent (T1-CE) (gadoterate meglumine, Dotarem; Guerbet, Aulnay-sous-Bois, France).

For DTI tractography, whole-brain volumes were acquired with a double spin-echo diffusion-weighted EPI sequence (2 averages jointly used). Thirty diffusion gradient directions were used with a b-value of 800 s/mm² and a single acquisition with a b-value of zero (On-line Table 3).

nTMS Motor Mapping

nTMS was performed by using the eXimia NBS System (V4.2; Nexstim, Helsinki, Finland). As in earlier studies,^{13,17} motor-evoked potentials were recorded of the abductor pollicis brevis muscle as the M1 hand representation, the plantar toe flexors representing the foot M1 region, and the anterior lateral tongue muscles as the M1 face representation. The “hotspot” was defined as the cortical stimulation site at which coil positioning, orientation, and tilt yielded the highest amplitude of the motor-evoked potentials. In areas of critical interest such as the tumor border, the spatial attenuation of stimulation was increased and the coil orientation and tilt were varied to maximize topographic accuracy.¹⁰ The outer margin of a given functional area was determined by 2 adjacent negative stimulation spots (On-line Table 3).

Functional Tractography

Functional tractography was performed deterministically on the basis of the DTI and nTMS data by using the iPlan fibertracking software (V2.6; Brainlab, Feldkirchen, Germany).^{17,26,27} For each M1 muscle representation, a 5-mm sphere centered around the nTMS hotspot was concentrically enlarged by 5 mm to form a standardized seed volume for the tractography in an anterograde direction for each voxel in the respective ROI (vector step length, 1.6 mm; angular threshold, 30°).^{15,26} The course of the reconstructed fibers was verified as part of the CST by an experienced neuroradiologist. The minimum fractional anisotropy (FA) value in the CST voxels was determined by increasing the FA threshold stepwise up in 0.01 U until it resembled the thinnest tract possible in each individual.²⁷ This procedure allows exclusion of aberrant non-CST fibers.¹⁷

Image Volumetry

For each subject, the volumes of the tumor and the peritumoral T2WI lesion and the nTMS mapping volumes of both M1 and the CST were calculated by using the iPlan software volumetry tool, which is based on the Cavalieri principle to provide unbiased volume estimates.²⁸ Briefly, the lesion contours were manually segmented on sequential axial images and verified in the coronal and sagittal reconstruction planes by an experienced neuroradiologist, blinded to the patient’s clinical status and confirmed by a neurosurgeon. The sum of tumor contour surfaces of an MR imaging study was multiplied by the section thickness to obtain the estimated volume in cubic centimeters. T1-CE tumor volumes were determined on the MPRAGE sequence on the basis of the hyperintense T1WI signal of the gadolinium-enhanced acquisition compared with the baseline MPRAGE as a measure of tumor extent with a disrupted blood-brain barrier. The FET-PET hotspot volume was resolved on the fused PET image set on the basis of a significant FET uptake at a tumor-to-brain-ratio of at least 1:6 to represent the extent of the tumor with upregulated amino acid metabolism.²⁴ The T2WI lesion volume was calculated according to the alteration of the tumoral and peritumoral signal intensity compared with normal brain tissue in the SPACE sequence. Its volume served as a measure of the extent of peritumoral edema and diffuse infiltrative glial tumor growth. The overlap volumes of the lesions with the CST and the M1 ROI were calculated with the use of the overlap calculation tool of the iPlan software.

Statistical Analyses

Patients were dichotomized according to their initial clinical presentation in regard to the presence of motor impairment. The contingency tables were used to determine the sensitivity, specificity, and negative and positive predictive values. The 2-tailed Fisher exact probability test was used to determine whether there were nonrandom associations between the spatial overlap of lesional and functional tissue and the presence of motor impairment before and the change in motor performance after the operation. Differences in total lesional and functional tissue volumes, their overlapping volumes, the FA values, or the resting motor threshold between the groups of patients with motor impairment versus unaffected patients were calculated separately by the independent *t* tests. The potential influences of confounding factors on the presented results were tested by 1-way ANOVA ($F[DFn, DFd]$). Statistical significance was considered when passing a threshold of $P < .05$ (Bonferroni-corrected for multiple comparisons if appropriate) with the use of the SPSS software (V20.0; IBM, Armonk, New York).

RESULTS

Clinical Findings

Eight of the 30 patients enrolled in this study did not show any affection of motor function at clinical presentation, while most ($n = 22$) demonstrated an isolated motor weakness of the face or limbs, or a hemiparesis, respectively. At discharge after surgery (mean hospital length of stay, 8.5 ± 2.6 days), 4 patients (14%) had new or worsened motor deficits, while the others benefited from tumor removal with their motor performance either remaining unchanged or improved ($n = 25$, 86%). In subgroup analysis, the factor “tumor entity” (metastases versus high-grade gliomas) had no significant effect on the patients’ motor functions after surgery ($F[2,53] = 0.16$, $P = .85$).

In 55% of patients ($n = 16$), a gross total tumor resection could be achieved, indicated by complete removal of the contrast-enhancing tumor parts in postoperative MR imaging. In 45% of patients ($n = 13$), resection remained subtotal (see On-line Table 1 for further clinical characteristics). However, there was no significant effect of the factor “extent of tumor removal” (gross total versus subtotal resection) on postsurgical motor function ($F[2,55] = 0.15$, $P = .87$).

nTMS Motor Mapping

Motor mapping by nTMS was feasible in all subjects for the hand representation area but not for all in the foot and face regions. In 3 patients, the resting motor threshold of the foot representation area exceeded the maximum stimulator output intensity so that motor maps could not be obtained for this body part in these patients.¹³ Likewise, detailed cartography of the cortical tongue representation could only be obtained in 83% of the patients ($n = 25$). In the remaining patients ($n = 5$), stimulation thresholds of facial nerve fibers were lower than those of the M1 representation, leading to false-positive motor-evoked potentials in the lateral tongue as evident by very short latencies (range, 3–6 ms). Overall, nTMS motor mapping did not cause any seizures or neurologic side effects. The average resting motor threshold of the muscle representations of the hand, tongue, and foot did not differ

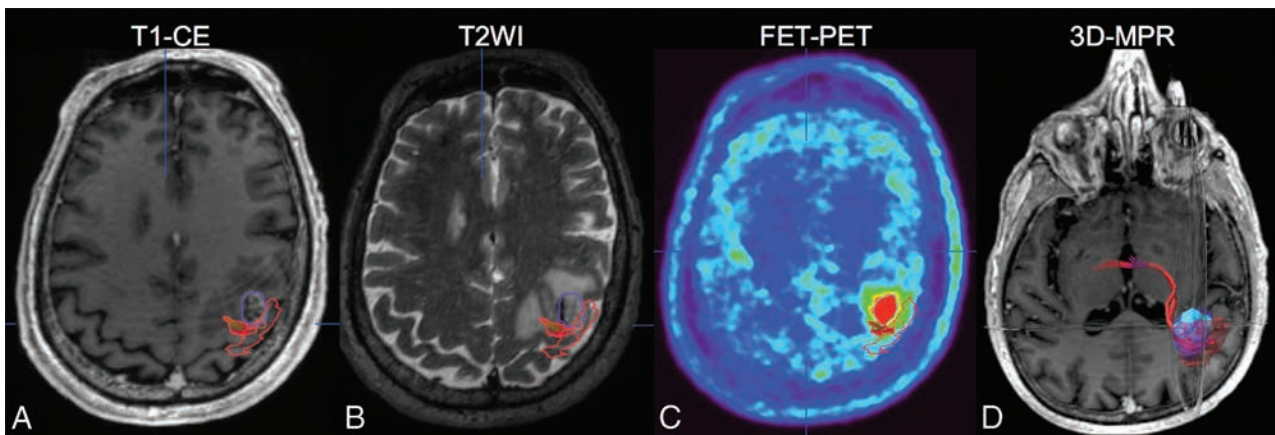


FIG 1. A 72-year-old male patient with contralateral upper limb weakness as depicted by an overlap between his carcinoma-metastasis on T1-CE (purple in A, B, and D) and FET-PET (light blue in C and D) and the hand-motor representation (red in A–D). 3D multiplanar reconstruction image with integration of functional, metabolic, and anatomic data is shown in (D).

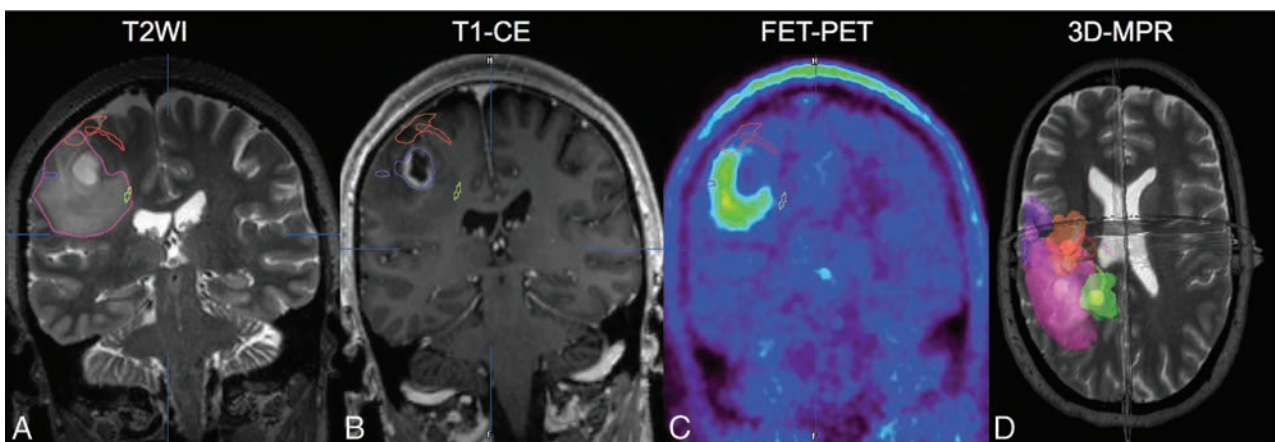


FIG 2. No overlap between the extent of the tumor on T1-CE and motor tissue is found in a 51-year-old female patient with glioblastoma and contralateral hemiparesis (B). The M1 representation of the hand (red in A–D) and CST of the face (purple in A–D) border the FET-PET lesion (C) but do not overlap the thresholded pathologic volume. However, the M1 representation of the hand (red in A–D) and the CST of the foot (yellow in A–D) are affected by the peritumoral T2WI lesion (pink in A and D) as the 3D multiplanar reconstruction image with integration of multimodal data reveals (D). The motor deficit proved reversible; this patient fully recovered her motor function on tumor removal.

between patients with motor impairment and those without deficits ($P > .1$) (On-line Fig 1).

Functional Tractography and MR Imaging Volumetry

Total Volumes. There was no statistical difference found in the comparison of the total tumor size based on the T1-CE or FET-PET lesion volumes between the patients with (T1-CE: $17.9 \pm 15.1 \text{ cm}^3$; FET-PET: $9.4 \pm 5.6 \text{ cm}^3$) and without a motor deficit (T1-CE: $9.7 \pm 14.9 \text{ cm}^3$; FET-PET: $5.2 \pm 5.7 \text{ cm}^3$; $P > .1$). Yet, there was a statistical trend for a greater extent of the perifocal T2WI lesion in patients with a motor deficit ($60.9 \pm 34.8 \text{ cm}^3$) compared with the others (38.1 ± 27.2 , $P = .08$) (On-line Fig 2A). Cortical M1 representations (3.4 ± 1.1 versus $3.6 \pm 0.8 \text{ cm}^3$) and the mean CST volumes (0.7 ± 0.3 versus $0.5 \pm 0.2 \text{ cm}^3$) were of equal size between the 2 groups ($P > .1$) (On-line Fig 2B).

Clinical Correlation of the Spatial Overlap between M1/CST Volumes and Lesional Tissue on FET-PET/T1-CE

Nearly all patients who showed an overlap between the T1-CE or the FET-PET-defined lesion and the functional tissue as depicted

by the nTMS M1 volumes and the DTI-defined CST had a motor deficit (T1-CE/FET-PET: positive predictive value = 91.7%/100%, sensitivity = 50%/63.2%) (Fig 1 and On-line Table 4). In contrast, in patients without motor deficits, functional tissue maps rarely overlapped the anatomically defined FET-PET or T1-CE extent of the tumor (T1-CE/FET-PET: 1/0, specificity = 87.5%/100%, negative predictive value = 38.9%/53.3%). Statistically, FET-PET lesion signal within functional tissue showed a significant effect on the likelihood of a motor deficit ($P < .01$) (On-line Table 4). In contrast, the effect of the T1-CE lesion signal within the functional tissue on the likelihood of a motor deficit was limited to a statistical trend ($P = .099$) (On-line Table 4).

Quantitatively, the relative overlap of the FET-PET-based tumor volume and the functional tissue was significantly higher in the patients with ($2.4 \pm 4.3\%$) compared with patients without ($P < .05$) motor deficits (Fig 3). With regard to T1-CE lesion signal within the M1 or the CST, we found only a statistical trend for greater overlaps in patients with motor impairments ($3.2 \pm 8.2\%$) compared with patients without deficits ($0.04 \pm 0.1\%$, $P = .09$).

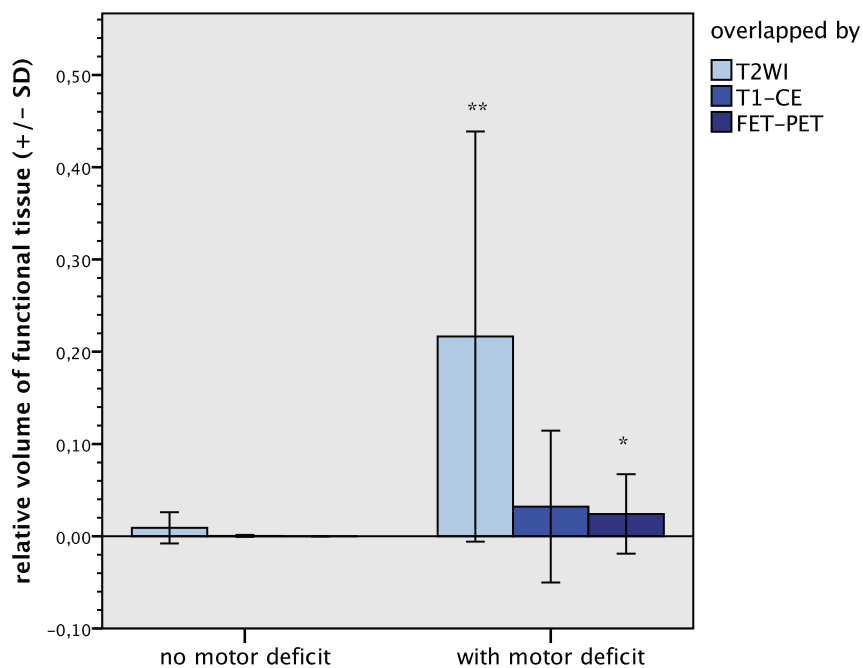


FIG 3. The overlapping volume of the motor functional tissue with the T2WI lesion and with the FET-PET lesion, respectively, is significantly greater in the motor-impaired group than the preserved group. Double asterisks indicate $P < .01$; asterisk, $P < .05$. The difference of the overlap volume between functional tissue and T1-CE tumor extent in the patients with motor weakness compared with the preserved patients is limited to a statistical trend ($P = .09$).

With respect to the postoperative outcome at discharge, all patients who had new or deteriorated motor deficits after the operation ($n = 4$) showed an overlap between tumor extent on FET-PET and T1-CE and the functional tissue (M1 and/or CST) before the operation (T1-CE/FET-PET: sensitivity = 100%/100%, positive predictive value = 33.3%/33.3%) (On-line Table 5). In other words, in the group of patients with functional tissue being affected by FET-PET and/or a T1-CE lesion before the operation ($n = 12$), the operation-associated risk of motor deterioration was 33.3% and, thus, more than double compared with the overall operation-associated risk of new or worsened motor deficits of all operated patients (13.8%, $n = 29$). On the other hand, all patients who did not show an overlap between the functional tissue and the lesion extent on T1-CE or FET-PET on preoperative maps ($n = 16$) benefited from tumor removal with their motor function remaining unchanged or even improved after surgery (T1-CE/FET-PET: negative predictive value = 100%/100%, specificity = 68.0%/65.2%) (On-line Table 5). In summary, the presence of T1-CE and FET-PET signal overlapping functional tissue on preoperative maps showed a significant impact on the likelihood of operation-associated motor deterioration, while the absence of such overlaps on preoperative maps indicated a higher chance of preserved motor function after the operation.

Clinical Correlation of the Spatial Overlap between M1/CST Volumes and Lesional Tissue on T2WI

Most ($n = 21$) patients with motor impairment ($n = 22$) showed an overlap between the T2WI lesion and the functional M1 and/or CST volumes (sensitivity = 95.5%, positive predictive value = 91.3%, specificity = 75.0%, negative predictive value = 85.7%) (Fig 2 and On-line Table 6). Overall, T2WI lesion signal within the

M1 representation and/or the CST showed a significant effect with respect to the likelihood of a motor deficit before the operation ($P < .001$) (On-line Table 6). Quantitatively, the mean relative overlap volume between the T2WI lesion and the functional tissue in the group of patients with motor impairment ($21.6 \pm 22.2\%$) was significantly higher compared with patients without motor deficits before the operation ($0.9 \pm 1.7\%$, $P < .01$) (Fig 3).

Within the group of patients with motor impairment who showed an overlap between functional tissue and the T2WI lesion on preoperative maps ($n = 20$), we found that nearly all of those who were affected by the T2WI lesion only and showed no additional overlap with the T1-CE or FET-PET lesion ($n = 7$) improved in motor function after the operation (positive predictive value = 87.5%, sensitivity = 53.8%, specificity = 85.7%, negative predictive value = 50.0%) (On-line Table 7). However, there were almost as many patients ($n = 6$) found to improve in motor impairment

after the operation despite an overlap between functional tissue and T1-CE and/or the FET-PET lesion. Thus, the value of the functional/T2WI overlap in predicting the reversibility in motor deficits due to tumor removal did not reach statistical significance ($P = .16$) (On-line Table 7).

Fractional Anisotropy

The mean minimum FA value of the CST was found to be significantly lower in the group of patients with a motor deficit (0.22 ± 0.06 U) than in patients without motor impairment (0.28 ± 0.06 U, $P = .04$) (On-line Fig 3). The FA values of the CST affected by altered T2WI signal overlap and by T1-CE or FET-PET tumor bulk are reported in On-line Fig 4. Moreover, no difference was found in the FA values of the CST in the patients with metastases versus those with high-grade gliomas (On-line Fig 5).

DISCUSSION

The understanding of the spatial relationship of lesional and motor function tissue in neuro-oncologic patients is critical for preoperative planning to choose the best therapeutic approach and to reduce postoperative morbidity. The deterioration of existing or newly developed motor deficits does not only reduce the quality of life but also reduces overall survival of the affected patients independent of the extent of resection and the adjuvant therapy.^{3,29} Tumor size, location, and infiltrative growth patterns have been discussed as underlying causes of neurologic impairment in those patients.⁵ Here, we found that patients with tumor masses directly within motor functional tissue as depicted by FET-PET or T1-CE merely accounted for approximately half of the patients with motor deficits. In this subgroup, FET-PET lesion signal within the M1 representation or the CST was associated

with the presence of a motor deficit with high specificity. With regard to T1-CE, this effect was less robust (statistical trend). Therefore, FET-PET was superior to T1-CE MR imaging in revealing a motor deficit before the operation. This observation is in line with previous studies and suggests that the combined use of PET and MR imaging is better for delineating tumor extent.³⁰ However, both T1-CE and FET-PET were of equal value for the prediction of postoperative functional outcome: While the absence of overlap with functional tissue maps predicted a favorable outcome, the presence of overlap before the operation was associated with a considerably higher risk of motor deterioration after the operation (33%) compared with the risk of the entire sample (14%) or with the risk reported in the literature, ranging from 6% to 19%.³⁻⁵ These findings need to be confirmed in a larger series but may be of great value in more wisely selecting and advising patients with brain tumors in the proximity of the CST or M1 for operative tumor removal.

Not surprising, the sensitivity of either FET-PET or T1-CE in revealing motor deficits before the operation was limited. In half of patients, motor impairment could not be explained by an overlap of FET-PET or T1-CE lesion extent with functional tissue maps. Hence, factors other than the lesion itself seem to contribute to motor impairment. In fact, we found almost all of the patients with motor impairment demonstrated T2WI signal hyperintensity within the motor functional tissue. This observation may serve as a highly sensitive measure to mirror motor impairment. In this regard, T2WI may have demonstrated superiority to FET-PET and T1-CE due to its ability to account for peritumoral edema formation and diffuse tumor cell infiltration, which may have caused motor function tissue disturbance in those cases.^{16,19,31} However, the potential of T2WI lesion overlap with functional tissue to serve as an imaging marker to predict the reversibility of motor impairment was limited: On one hand, most patients with motor impairment and a T2WI overlap but no involvement of FET-PET or T1-CE signal within the functional tissue maps improved in motor impairment after tumor resection. On the other hand, almost as many patients improved as well despite an overlap between functional tissue and the T1-CE and/or FET-PET lesion. Thus, despite such a relatively high positive predictive value, predictions were not statistically significant.

The findings were supported by the diffusion metrics of the CST. Malignant brain tumors are usually surrounded by a hyperintense signal of varying extent on T2WI, implying the presence of at least a minimum amount of extra- or intracellular water excess. Diffusion metrics such as FA have been shown to be significantly altered in these peritumoral regions. Such a lesion leads to an increasing magnitude of diffusion and, thus, to a decreasing directionality, expressed by a lower FA value in DTI.²⁰ Accordingly, the patients of the present sample with altered signals in T2WI voxels within the CST demonstrated a significantly lower FA value than those with CST voxels without T2WI overlap. With regard to motor impairment, we were able to verify that the FA was significantly lower in the group of patients with motor impairment than in the patients without motor deficits. This finding may, thus, support the hypothesis that the cause of motor impairment in the group of patients without overlaps of FET-PET/T1-CE with motor functional tissue is an indirect effect resulting

from, for example, edema interfering with the structural integrity of the motor system.^{6-8,32}

Moreover, there has been an ongoing debate about the utility of diffusion metrics in the differentiation of glial-versus-metastatic growth patterns in the white matter. While some authors found the FA to be reduced in the surroundings of glial tumors compared with metastatic lesions,^{19,31} others found the opposite.³³ In contrast, very low FA values were found not only in tumor-infiltrated T2WI lesions of gliomas but also in purely vasogenic edema, implying the limitation in differentiating the 2 on the basis of diffusion metrics alone.¹⁶ Accordingly, we did not find a difference in the FA values of the CST surrounded by high-grade glioma compared with metastases.

This observation also implied 2 of the limitations of our study: 1) the heterogeneity of the tumor entities within our study population; and 2) the small number of patients with respect to the tumor entities included in the study, the nonglial lesions in particular (ranging from 1 lymphoma to 7 metastases). While malignant cerebral lesions of different entities have various imaging features in common, some imaging features may also significantly differ depending on the tumor entity, for example, in T2WI and DWI as previously mentioned.^{16,32,33} Differences in the growth patterns of various tumor entities (eg, diffuse infiltration of glioblastoma versus less cell invasion in the brain-to-tumor interface of metastases) with infiltrated tissue below the detection threshold of current neuroimaging techniques certainly limit the diagnostic value of MR imaging and PET in tumor surgery. In addition, our study design was limited in providing control for the steroid therapy that was administered in 80% of the patients before inclusion in the study because steroids are known to potentially reduce the content of extracellular water in the brain tissue and, thus, for example, potentially affect imaging features on T2WI and DWI.

Overall, our findings are in line with those in other studies in which motor performance of patients with brain tumor correlated with structural or anatomic MR imaging parameters.⁶⁻⁸ However, most studies did not consider functional maps. The anatomic appearance of brain tissue can be heavily distorted by the tumor mass, especially for lesions close to the M1 and CST.¹² Likewise, previous studies did not consider nTMS mappings—that is, in putative lesions to motor cortical regions. Furthermore, previous studies primarily relied on T1-CE lesion volumes but did not consider metabolic information provided by PET.³⁰ We here intended to overcome these limitations by the integration of functional data of the M1 with a combined FET-PET and MR imaging dataset. The present study demonstrates the feasibility of a multimodal imaging approach, integrating functional information obtained by nTMS. The reliability of localizing the M1 region by nTMS has previously been shown to be of a value comparable with that of fMRI in healthy subjects.¹³ In patients with brain tumors, fMRI might be less useful due to the patients' motor impairments (leading to stronger task-related head movement artifacts), reduced alertness/compliance, and potential changes in neurovascular coupling.¹⁴ These effects are much less present in nTMS mapping performed in patients with brain tumors.¹¹ Hence, the combination of FET-PET, MR imaging, and nTMS

may help in the future to select patients more wisely for an operation and plan operations more precisely to possibly prevent operation-associated neurologic deterioration.

Only 1 patient's motor deficit could not be sufficiently explained on the basis of the multimodal imaging data obtained in this study. The patient showed neither FET-PET, T1-CE, nor T2WI signal alterations affecting the primary motor pathway. One alternative explanation could be a general disruption of the motor network connectivity itself rather than a single component—that is, diaschisis involving the premotor cortex, the supplemental motor cortex, the superior parietal lobule, and their interhemispheric connections.³⁴ Functional connectivity MR imaging seems to be a promising tool in this respect to further study the underlying network behind primary and secondary motor function, with the aim of predicting operative risks under these circumstances as well in the future.

CONCLUSIONS

The multimodal imaging approach demonstrated in this study allows insight into the spatial relationship between lesional and functional tissue and, thus, the putative cause of motor deficits in patients with brain tumors. The present study demonstrates that tumor infiltration of the M1 region or the CST as depicted by FET-PET is highly indicative of motor impairment, better than T1-CE alone, and is of predictive value for operative-risk evaluation. Furthermore, we also found the presence of motor deficits to be well-mirrored by the overlap of the peritumoral T2WI signal alteration with functional tissue. However, such overlap of functional tissue and T2WI signal alteration was of limited value in predicting tumor-removal-associated reversibility of motor impairment in our series. Further studies are required to evaluate the value of this approach for the preservation of function in patients with brain tumors.

ACKNOWLEDGMENTS

We thank the MR imaging staff of the Forschungszentrum Jülich for the acquisition of the MR imaging and PET data and their technical support.

Disclosures: Volker Neuschmelting—UNRELATED: Grants/Grants Pending: Deutsche Forschungsgemeinschaft, Comments: research fellowship grant. Carolin Weiss Lucas—RELATED: Grant: German Research Foundation (Deutsche Forschungsgemeinschaft). * Comments: funding for a TMS machine; no personal grant; UNRELATED: Payment for Lectures (including service on Speakers Bureaus): Roche Pharma, Comments: Young Advisory Board Meeting; compensation for presentation (single event)/payment; amount <€1000; Travel/Accommodations/Meeting Expenses Unrelated to Activities Listed: University of Cologne, German Society for Neurosurgery, Nexstim, Comments: travel costs regarding scientific meetings as an invited speaker. Roland Goldbrunner—UNRELATED: Board Membership: Roche, Comments: medical treatment of brain tumors; Travel/Accommodations/Meeting Expenses Unrelated to Activities Listed: Roche, Comments: travel expenses for the Society for NeuroOncology Annual Meetings 2013 and 2014. Christian Grefkes—UNRELATED: Grants/Grants Pending: German Research Foundation. * Money paid to the institution.

REFERENCES

1. Nabors LB, Ammirati M, Bierman PJ, et al; National Comprehensive Cancer Network. **Central nervous system cancers.** *J Natl Compr Canc Netw* 2013;11:1114–51 Medline
2. Shah NJ, Oros-Peusquens AM, Arrubla J, et al. **Advances in multimodal neuroimaging: hybrid MR-PET and MR-PET-EEG at 3 T and 9.4 T.** *J Magn Reson* 2013;229:101–15 CrossRef Medline
3. Obermueller T, Schaeffner M, Gerhardt J, et al. **Risks of postoperative paresis in motor eloquently and non-eloquently located brain metastases.** *BMC Cancer* 2014;14:21 CrossRef Medline
4. Krieg SM, Schnurbus L, Shiban E, et al. **Surgery of highly eloquent gliomas primarily assessed as non-resectable: risks and benefits in a cohort study.** *BMC Cancer* 2013;13:51 CrossRef Medline
5. Mukand JA, Blackinton DD, Crincoli MG, et al. **Incidence of neurologic deficits and rehabilitation of patients with brain tumors.** *Am J Phys Med Rehabil* 2001;80:346–50 CrossRef Medline
6. Morita N, Wang S, Kadakia P, et al. **Diffusion tensor imaging of the corticospinal tract in patients with brain neoplasms.** *Magn Reson Med Sci* 2011;10:239–43 CrossRef Medline
7. Kim CH, Chung CK, Kim JS, et al. **Use of diffusion tensor imaging to evaluate weakness.** *J Neurosurg* 2007;106:111–18 CrossRef Medline
8. Bobek-Billewicz B, Stasik-Pres G, Majchrzak K, et al. **Fibre integrity and diffusivity of the pyramidal tract and motor cortex within and adjacent to brain tumour in patients with or without neurological deficits.** *Folia Neuropathol* 2011;49:262–70 Medline
9. Laundre BJ, Jellison BJ, Badie B, et al. **Diffusion tensor imaging of the corticospinal tract before and after mass resection as correlated with clinical motor findings: preliminary data.** *AJNR Am J Neuroradiol* 2005;26:791–96 Medline
10. Picht T, Mularski S, Kuehn B, et al. **Navigated transcranial magnetic stimulation for preoperative functional diagnostics in brain tumor surgery.** *Neurosurgery* 2009;65:93–98; discussion 98–99 CrossRef Medline
11. Krieg SM, Sabih J, Bulbasova L, et al. **Preoperative motor mapping by navigated transcranial magnetic brain stimulation improves outcome for motor eloquent lesions.** *Neuro Oncol* 2014;16:1274–82 CrossRef Medline
12. Pouratian N, Bookheimer SY. **The reliability of neuroanatomy as a predictor of eloquence: a review.** *Neurosurg Focus* 2010;28:E3 CrossRef Medline
13. Weiss C, Nettekoven C, Rehme AK, et al. **Mapping the hand, foot and face representations in the primary motor cortex: retest reliability of neuronavigated TMS versus functional MRI.** *Neuroimage* 2013;66:531–42 CrossRef Medline
14. Forster MT, Hattingen E, Senft C, et al. **Navigated transcranial magnetic stimulation and functional magnetic resonance imaging: advanced adjuncts in preoperative planning for central region tumors.** *Neurosurgery* 2011;68:1317–24; discussion 1324–25 CrossRef Medline
15. Nimsy C, Ganslandt O, Merhof D, et al. **Intraoperative visualization of the pyramidal tract by diffusion-tensor-imaging-based fiber tracking.** *Neuroimage* 2006;30:1219–29 CrossRef Medline
16. Kinoshita M, Goto T, Okita Y, et al. **Diffusion tensor-based tumor infiltration index cannot discriminate vasogenic edema from tumor-infiltrated edema.** *J Neurooncol* 2010;96:409–15 CrossRef Medline
17. Weiss C, Tursunova I, Neuschmelting V, et al. **Improved nTMS- and DTI-derived CST tractography through anatomical ROI seeding on anterior pontine level compared to internal capsule.** *Neuroimage Clin* 2015;7:424–37 CrossRef Medline
18. Clark CA, Barrick TR, Murphy MM, et al. **White matter fiber tracking in patients with space-occupying lesions of the brain: a new technique for neurosurgical planning?** *Neuroimage* 2003;20:1601–08 CrossRef Medline
19. Wang W, Steward CE, Desmond PM. **Diffusion tensor imaging in glioblastoma multiforme and brain metastases: the role of p, q, L, and fractional anisotropy.** *AJNR Am J Neuroradiol* 2009;30:203–08 Medline
20. Sternberg EJ, Lipton ML, Burns J. **Utility of diffusion tensor imaging in evaluation of the peritumoral region in patients with primary and metastatic brain tumors.** *AJNR Am J Neuroradiol* 2014;35:439–44 CrossRef Medline
21. Baciu M, Le Bas JF, Segebarth C, et al. **Presurgical fMRI evaluation of cerebral reorganization and motor deficit in patients with tumors and vascular malformations.** *Eur J Radiol* 2003;46:139–46 CrossRef Medline
22. Stadlbauer A, Pölking E, Prante O, et al. **Detection of tumour inva-**

- sion into the pyramidal tract in glioma patients with sensorimotor deficits by correlation of (18)F-fluoroethyl-L-tyrosine PET and magnetic resonance diffusion tensor imaging. *Acta Neurochir (Wien)* 2009;151:1061–69 CrossRef Medline
23. Stadlbauer A, Hammen T, Grummich P, et al. Classification of peritumoral fiber tract alterations in gliomas using metabolic and structural neuroimaging. *J Nucl Med* 2011;52:1227–34 CrossRef Medline
 24. Rapp M, Heinzel A, Galldiks N, et al. Diagnostic performance of 18F-FET PET in newly diagnosed cerebral lesions suggestive of glioma. *J Nucl Med* 2013;54:229–35 CrossRef Medline
 25. Neuner I, Kaffanke JB, Langen KJ, et al. Multimodal imaging utilizing integrated MR-PET for human brain tumour assessment. *Eur Radiol* 2012;22:2568–80 CrossRef Medline
 26. Mori S, Frederiksen K, van Zijl PC, et al. Brain white matter anatomy of tumor patients evaluated with diffusion tensor imaging. *Ann Neurol* 2002;51:377–80 CrossRef Medline
 27. Frey D, Strack V, Wiener E, et al. A new approach for corticospinal tract reconstruction based on navigated transcranial stimulation and standardized fractional anisotropy values. *Neuroimage* 2012;62:1600–09 CrossRef Medline
 28. Mayhew TM, Olsen DR. Magnetic resonance imaging (MRI) and model-free estimates of brain volume determined using the Cavalieri principle. *J Anat* 1991;178:133–44 Medline
 29. McGirt MJ, Mukherjee D, Chaichana KL, et al. Association of surgically acquired motor and language deficits on overall survival after resection of glioblastoma multiforme. *Neurosurgery* 2009;65:463–69; discussion 469–470 CrossRef Medline
 30. Pauleit D, Floeth F, Hamacher K, et al. O-(2-[18F]fluoroethyl)-L-tyrosine PET combined with MRI improves the diagnostic assessment of cerebral gliomas. *Brain* 2005;128:678–87 CrossRef Medline
 31. Lu S, Ahn D, Johnson G, et al. Diffusion-tensor MR imaging of intracranial neoplasia and associated peritumoral edema: introduction of the tumor infiltration index. *Radiology* 2004;232:221–28 CrossRef Medline
 32. Lu S, Ahn D, Johnson G, et al. Peritumoral diffusion tensor imaging of high-grade gliomas and metastatic brain tumors. *AJNR Am J Neuroradiol* 2003;24:937–41 Medline
 33. Byrnes TJ, Barrick TR, Bell BA, et al. Diffusion tensor imaging discriminates between glioblastoma and cerebral metastases in vivo. *NMR Biomed* 2011;24:54–60 CrossRef Medline
 34. Otten ML, Mikell CB, Youngerman BE, et al. Motor deficits correlate with resting state motor network connectivity in patients with brain tumours. *Brain* 2012;135:1017–26 CrossRef Medline

Principal Component Analysis of Diffusion Tensor Images to Determine White Matter Injury Patterns Underlying Postconcussive Headache

A. Ghodadra, L. Alhilali, and S. Fakhran

ABSTRACT

BACKGROUND AND PURPOSE: Principal component analysis, a data-reduction algorithm, generates a set of principal components that are independent, linear combinations of the original dataset. Our study sought to use principal component analysis of fractional anisotropy maps to identify white matter injury patterns that correlate with posttraumatic headache after mild traumatic brain injury.

MATERIALS AND METHODS: Diffusion tensor imaging and neurocognitive testing with the Immediate Post-Concussion Assessment and Cognitive Test were performed in 40 patients with mild traumatic brain injury and 24 without posttraumatic headache. Principal component analysis of coregistered fractional anisotropy maps was performed. Regression analysis of the major principal components was used to identify those correlated with posttraumatic headache. Finally, each principal component that correlated with posttraumatic headache was screened against other postconcussive symptoms and demographic factors.

RESULTS: Principal component 4 (mean, 7.1 ± 10.3) correlated with the presence of posttraumatic headache in mild traumatic brain injury (odds ratio per SD, 2.32; 95% CI, 1.29–4.67; $P = .01$). Decreasing principal component 4 corresponded with decreased fractional anisotropy in the midsplenium and increased fractional anisotropy in the genu of the corpus callosum. Principal component 4 identified patients with posttraumatic headache with an area under the receiver operating characteristic curve of 0.73 and uniquely correlated with posttraumatic headache and no other postconcussive symptom or demographic factors.

CONCLUSIONS: Principal component analysis can be an effective data-mining method to identify white matter injury patterns on DTI that correlate with clinically relevant symptoms in mild traumatic brain injury. A pattern of reduced fractional anisotropy in the splenium and increased fractional anisotropy in the genu of the corpus callosum identified by principal component analysis can help identify patients at risk for posttraumatic headache after mild traumatic brain injury.

ABBREVIATIONS: FA = fractional anisotropy; ImPACT = Immediate Post-Concussion Assessment and Cognitive Test; mTBI = mild traumatic brain injury; PC = principal component; PCA = principal component analysis; PCS = postconcussive symptoms; PTH = posttraumatic headache

Mild traumatic brain injury (mTBI), commonly referred to as “concussion,” is a far-reaching disease, affecting up to 1.7 million individuals in the United States annually.¹ Many of these patients have chronic neurologic symptoms that profoundly impact daily life,² with approximately 15% of patients having persistent neurologic symptoms beyond 3 months.³ This “miserable minority” with persistent symptoms such as headache, fatigue,

photophobia, nausea, and visual deficits⁴ include many individuals in the prime of life with notable repercussions on the quality of life and productivity.⁵

Among postconcussion symptoms (PCS), posttraumatic headache (PTH) is one of the most frequent, enduring, and debilitating symptoms, with estimates of up to 90% prevalence following mTBI.⁶ The morbidity associated with PTH is high, with poorer neurocognitive test performance, exacerbation of other PCS, and longer recovery times.⁷ Unfortunately, imaging of mTBI and PTH has proved to be difficult because routine CT and MR imaging findings are often negative in these patients. However, recently, diffusion tensor imaging has emerged as a powerful MR imaging technique to identify disruption of major white matter fiber tracts in the brain after trauma^{8,9} and has detected white matter injuries underlying several postconcussion symptoms.^{1,10} While DTI continues to show promise as an imaging tool in detecting injuries underlying mTBI and PCS, analysis of the large

Received June 26, 2015; accepted July 2.

From the Department of Radiology, University of Pittsburgh Medical Center, Pittsburgh, Pennsylvania.

Abstract previously presented at: American Society of Neuroradiology Annual Meeting and the Foundation of the ASNR Symposium, April 25–30, 2015; Chicago, Illinois.

Please address correspondence to Anish Ghodadra, MD, University of Pittsburgh Medical Center, Department of Radiology, 200 Lothrop St, Suite 201 East Wing, Pittsburgh, PA 15213; e-mail: ghodadraag@upmc.edu; @AGhodadraMD

<http://dx.doi.org/10.3174/ajnr.A4505>

DTI datasets traditionally involves complex voxelwise techniques such as tract-based spatial statistics.¹¹ Analytic methods of this type have many advantages; however, at best, these methods simply identify regions of the brain in which DTI metrics, such as fractional anisotropy (FA), are different among groups of subjects. As a result, assessment of the correlation among brain regions is more difficult.

In an effort to overcome the limitations of traditional voxelwise methods, we sought to use principal component analysis (PCA) to analyze FA changes in patients with mTBI. PCA is a data-reduction algorithm that generates a set of new variables or principal components (PCs) that are orthogonal linear combinations of the original dataset to maximally explain the variance of the dataset.¹² This process allows a large number of redundant variables to be condensed into a relatively few new variables, or PCs, that give the most information about the data. These PCs can then be analyzed to determine which ones correlate with outcomes of interest. The purpose of our study was to use PCA of FA maps to identify white matter injury patterns that correlate with PTH after mTBI.

MATERIALS AND METHODS

Study Population

Our institutional review board approved this study, with a waiver of informed consent. All studies included were performed as standard of care, and results were retrospectively reviewed.

We searched our electronic medical record to retrospectively identify MR imaging studies with DTI performed for mTBI. Radiology reports from January 1, 2006, to March 1, 2013, were searched by using keywords “concussion,” “mild traumatic brain injury,” and “diffusion tensor imaging.” Inclusion criteria were 10–50 years of age, witnessed closed head trauma, no focal neurologic deficit, loss of consciousness of <1 minute, posttraumatic amnesia of <30 minutes, and English language proficiency. Exclusion criteria were a prior neuropsychiatric illness (2 patients), abnormal CT or conventional brain MR imaging findings (3 patients), history of substance abuse (3 patients), lack of DTI (4 patients), lack of neurocognitive assessment (6 patients), total symptom score of zero (3 patients), or inability to affine align FA images (2 patients). Demographic data collected from the electronic medical record included age and sex, type of trauma (sports injury versus non-sports injury), and any history of a prior concussion as diagnosed by an athletic trainer, neuropsychologist, or other medical personnel at any facility.

Neuropsychological and neurocognitive testing was performed by a neuropsychologist with >14 years of experience in treating patients with mTBI. Computerized neurocognitive testing was performed with the Immediate Post-Concussion Assessment and Cognitive Testing (ImPACT), in which a total symptom score was calculated for each patient using a 7-point Likert survey encompassing 22 PCS. Patients were classified as having headaches on the basis of the International Headache Society guidelines¹³ following the postconcussion clinical examination. Time to recovery was defined as when the ImPACT total symptom score was zero or the patient stated that he or she was asymptomatic.

Imaging

Conventional MR imaging and DTI were performed with a 1.5T unit (Signa; GE Healthcare, Milwaukee, Wisconsin) and a standard head coil. Despite the relatively long time span of this study, all patients and controls included in this study underwent the same imaging sequences on the same system, as follows: sagittal and axial T1-weighted (TR, 600 ms; TE, minimum; section thickness, 5 mm; NEX, 1), axial proton attenuation-weighted (TR, 2000–2500 ms; TE, minimum; section thickness, 5 mm; NEX 1), T2-weighted (TR/TE, 2000–2500/84–102 ms; section thickness, 5 mm; NEX, 1), fluid-attenuated inversion recovery (TR/TE, 9000–10,000/149 ms; TI, 2200 ms), and diffusion-weighted (single-shot echo-planar sequence; TR, 10,000 ms; TE, minimum; section thickness, 5 mm; matrix, 128 × 128). T2*-weighted gradient recalled-echo (TR/TE, 4400/21 ms; NEX, 1; 90° flip angle; section thickness, 3 mm) or susceptibility-weighted (TR/TE, 37/23 ms; NEX, 1; 15° flip angle; section thickness, 2.4 mm) sequences were performed. The FOV ranged from 200 to 240 mm.

DTI was performed with a single-shot echo-planar sequence (TR/TE, 4000/80 ms; NEX, 2; section thickness, 5 mm; 128 × 128 matrix; FOV, 260 mm). Diffusion gradients were set in 25 non-collinear directions by using 2 b-values ($b=0$ and 1000 s/mm²).

Image Analysis

Fractional anisotropy maps were generated as a measure of white matter integrity by using the fMRI of the Brain Diffusion Toolbox (<http://fsl.fmrib.ox.ac.uk/fsl/fslwiki/FDT>) as part of the fMRI of the Brain Software Library (FSL; <http://www.fmrib.ox.ac.uk/fsl>). The FA maps included both gray and white matter and were registered to the Montreal Neurological Institute atlas by using a 12-parameter affine transformation.

A mean FA map was created from the 64 coregistered FA images. For each subject, a new 3D matrix was calculated by subtracting the subject's FA map from the mean FA image. The resulting volumes were subjected to PCA, in which each voxel represented a variable. To facilitate interpretation of the PCs, a mean FA map was generated. Additional maps showing the effect of increasing and decreasing the value of each principal component by 2 SDs were then generated. Analysis was conducted by using a custom script in Matlab (MathWorks, Natick, Massachusetts).

Statistical Analysis

To prevent overfitting, we performed a multistep regression analysis. Initially, the first 20 PCs were screened with univariate analyses for correlation with the presence of PTH. Subsequently, forward stepwise nominal regression with the PCs whose univariate *P* values were <.25 was used to identify correlation with the presence of PTH. Finally, each PC that correlated with the presence of PTH was screened against demographic factors (age, sex) and other postconcussive symptoms, including sleep-wake disturbances, anxiety, tinnitus, and cervicgia by using univariate *t* testing or linear regression when appropriate. Receiver operating characteristic curves were created for PCs and the prediction of PTH. Areas under the receiver operating characteristic curve for PCs and PTH were obtained and interpreted according to the guidelines put forth by Hosmer and Lemeshow: no discrimina-

Table 1: Demographics by study group^a

	No PTH	PTH	P Value
Age (yr)	17.08 (2.99)	17.58 (5.87)	.7
ImPACT total symptom score	37.46 (24.87)	29.20 (24.65)	.2
% Male	254%	278%	.09
% Prior concussion	29%	250%	.12
Time to recovery (days)	56 (70)	55 (57)	.98

^a Data are mean (SD) unless otherwise noted.

Table 2: Descriptive statistics and results of univariate regression analysis of PCs and PTH

PC	Mean (SD)	Regression Coefficient	P Value
1	1.35 (13.62)	-0.002	.897
2	37.81 (11.67)	-0.006	.785
3	7.59 (11.58)	-0.036	.141
4 ^a	7.09 (10.32)	0.081	.010
5	-14.15 (9.68)	0.010	.712
6	30.59 (9.61)	-0.014	.621
7	-17.36 (9.11)	-0.011	.699
8	11.23 (9.02)	-0.051	.105
9	13.66 (8.83)	-0.033	.294
10	10.29 (8.84)	-0.003	.917
11	-4.83 (8.82)	0.012	.685
12	3.99 (8.55)	0.053	.112
13	11.26 (8.30)	-0.044	.196
14	-16.63 (8.15)	-0.026	.419
15	-1.70 (8.03)	0.015	.645
16	-5.50 (8.02)	-0.037	.274
17	-3.74 (7.92)	0.016	.627
18	-0.33 (7.65)	-0.051	.152
19	-5.82 (7.61)	0.048	.180
20	-9.34 (7.74)	-0.013	.691

^a Principal component 4 was the only statistically significant predictor for posttraumatic headache.

tion (area under the receiver operating characteristic curve = 0.5), acceptable discrimination ($0.7 \leq$ area under the receiver operating characteristic curve ≤ 0.8), excellent discrimination ($0.8 \leq$ area under the receiver operating characteristic curve ≤ 0.9), and outstanding discrimination (area under the receiver operating characteristic ≥ 0.9).¹⁴ Statistical analysis was conducted with the software package JMP 11 (SAS Institute, Cary, North Carolina).

RESULTS

Sixty-four patients with mTBI were included in our study, of which 40 (63%) had PTH. The mean age was 17.4 ± 5.0 years, with 69% male. There was no statistically significant difference in mean age (17.6 versus 17.1 years, $P = .70$) or percentage male (54% versus 78%, $P = .09$) between patients with and without PTH. These data are summarized in Table 1. The median time to presentation was not significantly different in patients with and without PTH (22 versus 24 days, $P = .79$). All patients had normal brain MR imaging findings.

Univariate analysis of the first 20 principal components demonstrated only PC 4 (mean, 7.1 ± 10.3) correlated with the presence of PTH in patients with mTBI. The odds ratio per SD of PC 4 was 2.32, (95% CI, 1.29–4.67; $P = .01$). Table 2 summarizes the results of univariate analysis of the correlation between PTH and each principal component.

Receiver operating characteristic analysis for PC 4 demonstrated acceptable performance with an area under the curve of

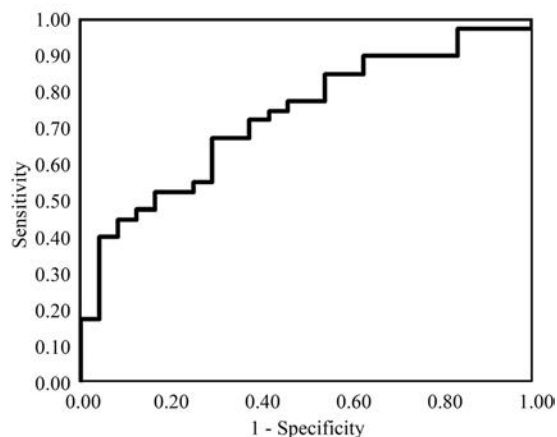
ROC Curve for Post-traumatic Headache using PC 4

FIG 1. Receiver operating characteristic curve for the presence of posttraumatic headache based on principal component 4. Receiver operating characteristic curve analysis demonstrates an acceptable diagnostic performance of FA values described by principal component 4 for the presence of posttraumatic headache, with an area under the curve of 0.73.

0.73 (Fig. 1). Figure 2 shows the effect of changing principal component 4 on the average FA map by 2 SDs. Lower values of PC 4 primarily indicated relatively decreased FA in the splenium and increased FA in the genu of the corpus callosum and corresponded to increased risk of postconcussive headache. Additionally, there were more subtle decreases within the corticospinal tract with decreasing PC 4. This principal component uniquely correlated with the presence of PTH and did not correlate with any other postconcussive symptom or demographic factor.

DISCUSSION

Our results show that PCA of DTI in patients with mTBI can successfully identify patterns of FA that correlate with PTH. PCA of FA maps revealed a unique principal component that correlated with increased risk of PTH in patients with mTBI. Decreased values of this principal component, PC 4, most prominently corresponded to decreased FA in the midsplenium of the corpus callosum and increased FA in the genu.

Previous studies of mTBI by using DTI have used 3 major analysis techniques: selection of a priori ROIs, voxelwise analysis (whole-brain or tract-based spatial statistics), and histogram analysis.¹⁵ While these techniques have shown promise in the analysis of DTI data, histogram analysis cannot identify focal regions of injury and voxelwise analysis and ROI analysis essentially treat each voxel/region as a unique variable that is tested against a clinical outcome of interest. These methods fail to capture the relationship among multiple regions of the brain. Furthermore, despite attempts at compensation for multiple comparisons, there is a higher risk of type 1 statistical errors.

Our technique builds on previous work investigating changes in white matter integrity in patients with mTBI with postconcussion syndrome that used voxel-based approaches.^{1,10,15,16} These reports have demonstrated white matter abnormalities in patients with mTBI relative to controls¹⁷⁻¹⁹; however, these differences have not correlated with symptoms.²⁰ Similarly, attempts to correlate structural injuries with postconcussive cognitive perfor-

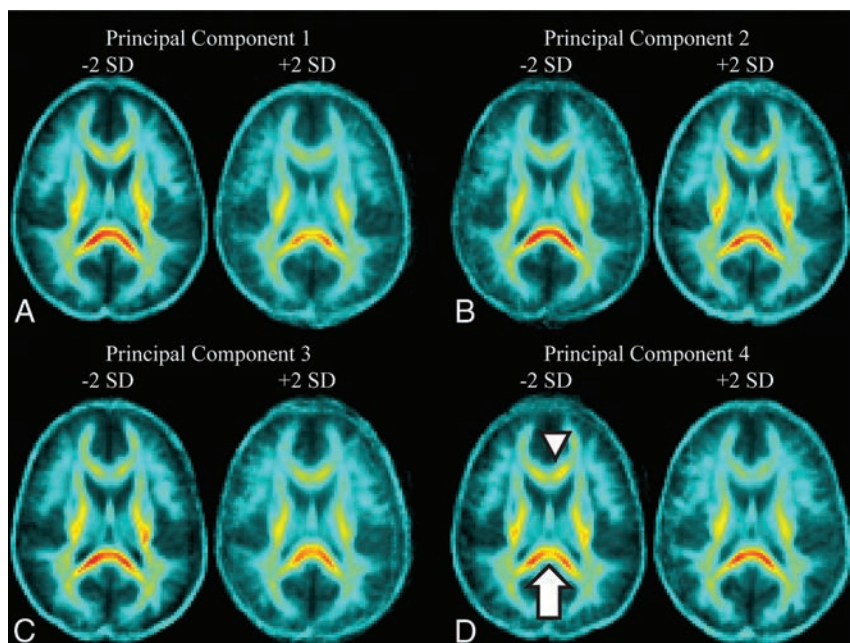


FIG 2. Effect of changing each principal component by ± 2 SDs on fractional anisotropy in a representative section through the corpus callosum. A, PC 1 corresponds to the overall average FA in the brain, with decreasing PC 1 resulting in an increase in the overall FA throughout the brain. B, PC 2 corresponds most closely with FA in the corticospinal tracts. A decrease in PC 2 results in a noticeable decrease in FA in the corticospinal tracts bilaterally. C, Changes to PC 3 correspond to changes in FA in both the corticospinal tracts and the splenium. Decreases in PC 3 increase the FA in both in the splenium and corticospinal tracts. D, PC 4, the only predictor of posttraumatic headache, corresponds closest to changes in FA in the splenium and genu of the corpus callosum. Decreasing PC 4 results in decreased FA in the splenium of the corpus callosum (white arrow) and increased FA in the genu (white arrowhead).

mance have shown mixed results without a strong anatomic/pathologic correlation, with deficits detected in regions as diverse as the occipital cortex and corticospinal tracts.²¹⁻²⁵ This finding suggests that not all regions with differences in FA between patients and controls are necessarily symptomatic.¹ Reduced FA in 1 region alone may not, in and of itself, be clinically relevant. Given the complex interconnectivity within the brain, it may not be sufficient to simply identify individual, isolated regions of FA variance. Rather, it would be more meaningful to view changes in FA in 1 region in the context of potentially related changes elsewhere in the brain. In short, identifying unique patterns of FA changes in multiple brain regions is needed, rather than merely identifying isolated regions of FA variance.

Our application of PCA to FA maps provides a novel analysis method of complex DTI data as a means of identifying patterns of change in FA. These data-reduction techniques allow distilling complex relationships between variables, in this case FA throughout the brain, to a relatively small set of principal components. Each principal component describes a unique way in which the variables “move” together. Furthermore, to aid in recognition of disease in a clinical setting, these PCs can be visualized in an image (eg, Fig 2).

The finding of a unique principal component that corresponds to FA abnormalities in the genu and splenium of the corpus callosum offers a means of stratifying patients with postconcussive syndrome into groups with high and low risk of the development of posttraumatic headache. Identification of patients at risk for the development of PTH would potentially allow

early intervention in an attempt to improve symptoms and outcome, because early comprehensive treatment of PTH has been shown to significantly reduce both the frequency of PTH and headache-related disability.⁷

Additionally, the areas of injury underlying PTH identified by PCA may help elucidate the pathophysiology underlying headache after mTBI. Identifying injury in the splenium is not surprising after mTBI because it is at high risk of direct impact by the falx cerebri and tentorium during trauma.²⁶ However, most interesting, abnormalities of this region are also seen in other forms of chronic headache, such as migraine.^{27,28} In fact, in nontraumatic migraine, abnormalities of the splenium are associated with a more chronic disease course, greater headache frequency, and comorbid neuropsychiatric conditions.¹⁵

Lower values of PC 4 also corresponded to increased FA in the genu of the corpus callosum. This could represent compensatory increases in FA in the genu related to the decreased FA/injury identified in the splenium. Compensatory increases in FA in areas of the corpus callosum in response to other cal-

losal injuries have been seen in many pathologies, including schizophrenia, white matter injury from prematurity, and age-related white matter loss.²⁹⁻³¹ The fact that PC 4 represents not only decreased FA in the splenium but also increased FA in the genu may indicate that injury to the splenium only results in PTH when it is substantial enough to trigger compensatory increases in FA in the genu. This pattern of FA identified by PC4 highlights the importance of detecting not simply differences in FA but relationships of changes in FA in different brain regions. PC 4 is not only a marker of FA in the splenium and genu, but rather it represents a unique pattern of FA in the entire brain and describes a complex relationship among these values. Further analysis of FA in the genu and splenium may yield more refined markers for identification of patients at risk for developing PTH.

While our study shows the potential of PCA in FA analysis, there are a few limitations of our findings. First, our study population consisted of a single-center retrospective cohort; thus, larger, multicenter prospective studies are needed to confirm these findings. Second, while our cohort is relatively large, given the relatively large number of voxels and the complexity of the FA structure, larger sample sizes would allow generation of more refined principal components. Furthermore, the registration process, while robust, introduces its own noise into the FA maps that can bias the principal components, particularly along edges. Finally, our analysis focused on a single time point after initial injury. The relationship we found between FA in the corpus callosum and PTH could be confounded by a more longitudinal process of injury. Applying this PCA tech-

nique to a longitudinal dataset would provide a more robust analysis and could shed light on the pathophysiology of post-concussive headache.

CONCLUSIONS

PCA can be used as a data-mining method to identify white matter injury patterns on DTI that correlate with clinically relevant symptoms in mTBI. PCA of FA maps in patients with mTBI identified a pattern of reduced FA in the splenium and increased FA in the genu of the corpus callosum that correlates with postconcussive headache in patients with mTBI. Our results suggest that analysis of the FA patterns in the corpus callosum may offer a means of identifying patients at risk for the development of PTH and thus allow early treatment.

REFERENCES

1. Fakhran S, Yaeger K, Alhilali L. **Symptomatic white matter changes in mild traumatic brain injury resemble pathologic features of early Alzheimer dementia.** *Radiology* 2013;269:249–57 CrossRef Medline
2. Bohnen N, Jolles J, Twijnstra A. **Neuropsychological deficits in patients with persistent symptoms six months after mild head injury.** *Neurosurgery* 1992;30:692–95; discussion 695–96 CrossRef Medline
3. Shenton ME, Hamoda HM, Schneiderman JS, et al. **A review of magnetic resonance imaging and diffusion tensor imaging findings in mild traumatic brain injury.** *Brain Imaging Behav* 2012;6:137–92 CrossRef Medline
4. Ganti L, Khalid H, Patel PS, et al. **Who gets post-concussion syndrome? An emergency department-based prospective analysis.** *Int J Emerg Med* 2014;7:31 CrossRef Medline
5. Emanuelson I, Andersson Holmkvist E, Björklund R, et al. **Quality of life and post-concussion symptoms in adults after mild traumatic brain injury: a population-based study in western Sweden.** *Acta Neurol Scand* 2003;108:332–38 CrossRef Medline
6. Kontos AP, Elbin RJ, Lau B, et al. **Posttraumatic migraine as a predictor of recovery and cognitive impairment after sport-related concussion.** *Am J Sports Med* 2013;41:1497–504 CrossRef Medline
7. Erickson JC. **Treatment outcomes of chronic post-traumatic headaches after mild head trauma in US soldiers: an observational study.** *Headache* 2011;51:932–44 CrossRef Medline
8. Bazarian JJ, Zhong J, Blyth B, et al. **Diffusion tensor imaging detects clinically important axonal damage after mild traumatic brain injury: a pilot study.** *J Neurotrauma* 2007;24:1447–59 CrossRef Medline
9. Wilde EA, McCauley SR, Hunter JV, et al. **Diffusion tensor imaging of acute mild traumatic brain injury in adolescents.** *Neurology* 2008;70:948–55 CrossRef Medline
10. Alhilali LM, Yaeger K, Collins M, et al. **Detection of central white matter injury underlying vestibulopathy after mild traumatic brain injury.** *Radiology* 2014;272:224–32 CrossRef Medline
11. Smith SM, Jenkinson M, Johansen-Berg H, et al. **Tract-based spatial statistics: voxelwise analysis of multi-subject diffusion data.** *Neuroimage* 2006;31:1487–505 CrossRef Medline
12. Jolliffe I. **Principal component analysis.** In: *Wiley StatsRef: Statistics Reference Online*. New York: John Wiley & Sons; 2014 CrossRef
13. Headache Classification Subcommittee of the International Headache Society. **The International Classification of Headache Disorders: 2nd edition.** *Cephalalgia* 2004;24(suppl 1):9–160 CrossRef Medline
14. Hosmer DW Jr, Lemeshow S, Sturdivant RX. *Applied Logistic Regression, 3rd Edition*. New York: John Wiley & Sons; 2013
15. Hulkower MB, Poliak DB, Rosenbaum SB, et al. **A decade of DTI in traumatic brain injury: 10 years and 100 articles later.** *AJNR Am J Neuroradiol* 2013;34:2064–74 CrossRef Medline
16. Zhang K, Johnson B, Pennell D, et al. **Are functional deficits in concussed individuals consistent with white matter structural alterations: combined FMRI & DTI study.** *Exp Brain Res* 2010;204:57–70 CrossRef Medline
17. Kasahara K, Hashimoto K, Abo M, et al. **Voxel- and atlas-based analysis of diffusion tensor imaging may reveal focal axonal injuries in mild traumatic brain injury: comparison with diffuse axonal injury.** *Magn Reson Imaging* 2012;30:496–505 CrossRef Medline
18. Messé A, Caplain S, Paradot G, et al. **Diffusion tensor imaging and white matter lesions at the subacute stage in mild traumatic brain injury with persistent neurobehavioral impairment.** *Hum Brain Mapp* 2011;32:999–1011 CrossRef Medline
19. Yallampalli R, Wilde EA, Bigler ED, et al. **Acute white matter differences in the fornix following mild traumatic brain injury using diffusion tensor imaging.** *J Neuroimaging* 2013;23:224–27 CrossRef Medline
20. Lange RT, Iverson GL, Brubacher JR, et al. **Diffusion tensor imaging findings are not strongly associated with postconcussional disorder 2 months following mild traumatic brain injury.** *J Head Trauma Rehabil* 2012;27:188–98 CrossRef Medline
21. Niogi SN, Mukherjee P, Ghajar J, et al. **Structural dissociation of attentional control and memory in adults with and without mild traumatic brain injury.** *Brain* 2008;131:3209–21 CrossRef Medline
22. Lipton ML, Gulko E, Zimmerman ME, et al. **Diffusion-tensor imaging implicates prefrontal axonal injury in executive function impairment following very mild traumatic brain injury.** *Radiology* 2009;252:816–24 CrossRef Medline
23. Levin HS, Wilde E, Troyanskaya M, et al. **Diffusion tensor imaging of mild to moderate blast-related traumatic brain injury and its sequelae.** *J Neurotrauma* 2010;27:683–94 CrossRef Medline
24. Little DM, Kraus MF, Joseph J, et al. **Thalamic integrity underlies executive dysfunction in traumatic brain injury.** *Neurology* 2010;74:558–64 CrossRef Medline
25. Wada T, Asano Y, Shinoda J. **Decreased fractional anisotropy evaluated using tract-based spatial statistics and correlated with cognitive dysfunction in patients with mild traumatic brain injury in the chronic stage.** *AJNR Am J Neuroradiol* 2012;33:2117–22 CrossRef Medline
26. Yaeger K, Alhilali L, Fakhran S. **Evaluation of tentorial length and angle in sleep-wake disturbances after mild traumatic brain injury.** *AJR Am J Roentgenol* 2014;202:614–18 CrossRef Medline
27. Li XL, Fang YN, Gao QC, et al. **A diffusion tensor magnetic resonance imaging study of corpus callosum from adult patients with migraine complicated with depressive/anxious disorder.** *Headache* 2011;51:237–45 CrossRef Medline
28. Yu D, Yuan K, Qin W, et al. **Axonal loss of white matter in migraine without aura: a tract-based spatial statistics study.** *Cephalalgia* 2013;33:34–42 CrossRef Medline
29. Xydis V, Astrakas L, Drougia A, et al. **Myelination process in preterm subjects with periventricular leucomalacia assessed by magnetization transfer ratio.** *Pediatr Radiol* 2006;36:934–39 CrossRef Medline
30. Kim SN, Park JS, Jang JH, et al. **Increased white matter integrity in the corpus callosum in subjects with high genetic loading for schizophrenia.** *Prog Neuropsychopharmacol Biol Psychiatry* 2012;37:50–55 CrossRef Medline
31. Schulte T, Maddah M, Müller-Oehring EM, et al. **Fiber tract-driven topographical mapping (FTTM) reveals microstructural relevance for interhemispheric visuomotor function in the aging brain.** *Neuroimage* 2013;77:195–206 CrossRef Medline

Flow-Diverter Stents for the Treatment of Saccular Middle Cerebral Artery Bifurcation Aneurysms

J. Caroff, H. Neki, C. Mihalea, F. D'Argento, H. Abdel Khalek, L. Ikka, J. Moret, and L. Spelle



ABSTRACT

BACKGROUND AND PURPOSE: The flow-diverter stent has been proved a feasible, safe, and efficient technique, particularly for the treatment of large and broad-neck carotid siphon aneurysms. Wide-neck bifurcation aneurysms remain, in some cases, a challenge for neurointerventionalists. We report the outcomes of the treatment of saccular middle cerebral artery bifurcation aneurysms with flow diversion in our institution.

MATERIALS AND METHODS: From the institution data base, all saccular, nondissecting MCA bifurcation aneurysms, treated with flow-diverter stents, were retrospectively reviewed. Technical issues, immediate posttreatment and follow-up angiographic findings, and clinical outcomes were assessed.

RESULTS: Fourteen patients with 15 aneurysms were included in the study. Ischemic complications, as confirmed by MR imaging, occurred in 6 patients (43%). Procedure-related morbidity and mortality at last follow-up were 21% and 0%, respectively. Angiographic follow-up was available for 13 aneurysms, with a mean follow-up of 16 months. Complete occlusion was obtained for 8 aneurysms (62%).

CONCLUSIONS: Compared with other available therapeutic options, the flow-diverter stent does not appear to be a suitable solution for the treatment of saccular MCA bifurcation aneurysms.

ABBREVIATIONS: EVT = endovascular treatment; FDS = flow-diverter stent

Endovascular treatment (EVT) of middle cerebral artery aneurysms is considered safe and effective.¹⁻³ However the choice between surgical and endovascular approaches for the treatment of aneurysms in this location is still a matter of debate.⁴ Furthermore, wide-neck MCA bifurcation lesions can sometimes prove challenging for traditional EVT approaches, and numerous techniques have been developed to address these cases. Simple coil embolization and remodeling techniques, including single-balloon- or multiple-balloon-assisted coiling^{5,6}; the dual-catheter technique⁷; stent-assisted coiling⁸⁻¹⁰; the “Y-stent placement” technique with and without coiling^{11,12}; the “waffle cone”

technique^{13,14}; neck-bridge devices^{15,16}; and intra-aneurysmal flow disruptors^{17,18} have all been trialed.

Flow-diverter stents (FDSs) have proved feasible, safe, and efficient for the treatment of large and broad-neck carotid siphon aneurysms.¹⁹ They have been designed to induce aneurysm sac thrombosis through flow disruption at the level of the neck, while preserving normal flow into parent vessels and adjacent branches.²⁰ Few studies have been published concerning FDS use for bifurcation lesion treatment, to our knowledge. In this report, our aim was to evaluate the feasibility, safety, and efficacy of the use of the FDSs for MCA saccular bifurcation aneurysms, with special consideration regarding the effects on the covered branches.

MATERIALS AND METHODS

Population

Between May 2013 and June 2014, 77 FDS procedures for intracranial aneurysm treatment were performed in the Beaujon Hospital (APHP, Paris). From our prospectively maintained data base, we extracted all MCA bifurcation saccular aneurysms treated with an FDS and collected the following data for each patient: age, sex, aneurysm location and biometry (max-

Received April 3, 2015; accepted after revision June 12.

From the Department of Interventional Neuroradiology (J.C., H.N., C.M., H.A.K., L.I., J.M., L.S.), Neuro Brain Vascular Center, Hôpital Bicêtre, APHP, Paris Sud Université, France; Department of Neurosurgery (H.N.), Saitama University, Saitama, Japan; Department of Neurosurgery (C.M.), University of Medicine and Pharmacy “Victor Babes,” Timisoara, Romania; Department of Bioimaging and Radiological Sciences (F.D.), Policlinico “A. Gemelli,” Rome, Italy; and Department of Neuropsychiatry (H.A.K.), Tanta University Hospital, Tanta, Egypt.

Please address correspondence to Jildaz Caroff, MD, Service de Neuroradiologie Interventionnelle, Hôpital Bicêtre, 78 rue du Général Leclerc, 94270 Le Kremlin Bicêtre, France; e-mail: Jildaz.caroff@bjn.aphp.fr

<http://dx.doi.org/10.3174/ajnr.A4540>

imum diameter, neck size, aspect ratio), rupture status, previous treatment, the modified Rankin Scale scores at the time of admission and discharge, modalities of treatment, intraoperative complications (aneurysm rupture, thromboembolic events, deployment failure), and postoperative complications (delayed bleeding, thromboembolic events). Immediate postoperative DSA, 3D rotational angiography, and VasoCT images (Philips Healthcare, Best, the Netherlands)^{21,22} were collected along with any available follow-up imaging data. The last mRS evaluation during follow-up was also recorded.

In this study, only saccular aneurysms were included, and nonsaccular aneurysms (fusiform, blood blister-like, or dissecting) were excluded. Those lesions were considered very difficult to treat for both interventionists and neurosurgeons. Conventional EVT approaches were judged not suitable. Some relatively small lesions were treated because of a patient history of multiple aneurysms and previous rupture. In each case, the decision to treat was made by a multidisciplinary team, which included interventionists and surgeons. Informed consent was obtained in each case.

Endovascular Treatment

All patients were treated preoperatively with a dual antiplatelet therapy of 160 mg of aspirin and 75 mg of clopidogrel per day for 7 days before treatment. The effectiveness of the platelet inhibition therapy was tested by hematologic analysis, and in cases of insufficiency, loading doses were administered.

Endovascular treatment was performed with the patient under general anesthesia and systemic heparinization. The protocol for heparinization was administration of a 50-U/kg bolus at the beginning of the procedure, followed by a continuous intravenous injection of 35–50 U/kg to maintain an activated clotting time of 2–2.5 times the baseline.

We used 3 types of commercial FDSs: the Silk flow diverter (Balt, Montmorency, France), the Pipeline Embolization Device (Covidien, Irvine, California), and the FRED stent (Microvention, Tustin, California). The selection of the specific FDS in each case depended on operator preference, and sizing was performed on the basis of artery measurement, acquired from 3D rotational angiography data.

For the postprocedural medication regimen, aspirin and clopidogrel were both maintained for 3 months and aspirin was continued for a further 9 months.

Procedural Assessment and Follow-Up

Follow-up angiographies were performed at 3–6 months then at 1.5 and 3.5 years after treatment, depending on the previous results. Standard projections, 3D rotational angiography, and VasoCT analyses were used to evaluate residual flow within the aneurysm and to assess the patency of both the FDS and MCA bifurcation branches. Aneurysm occlusion was graded as either complete, residual neck, residual aneurysm, or unchanged. Permanent morbidity and mortality rates subsequent to treatment were evaluated at discharge and at follow-up when possible. MR imaging studies were performed only in cases of acute neurologic deficit. Morbidity was defined as an

mRS of >1. When the preoperative mRS was >1, morbidity was defined by any increase in the mRS score.

RESULTS

Population

Fourteen patients (9 women and 5 men; age range, 40–67 years; median age, 57 years), with 15 MCA bifurcation aneurysms were included in this study. Five aneurysms had a history of rupture and recanalization after coil treatment, but none were treated with an FDS at the acute phase of bleeding. In 2 cases, the reason to treat was incomplete occlusion or recanalization after WEB aneurysm embolization system (Sequent Medical, Aliso Viejo, California) treatment. Twelve aneurysms (80%) were located on the right side. Initial aneurysm size varied from 2.6 to 14 mm (mean, 6.1 ± 3.6 mm), neck size varied from 2.3 to 7 mm (mean, 4.1 ± 1.5 mm), and the aspect ratio varied from 0.6 to 1.2 mm (mean, 0.8 ± 0.2 mm).

Feasibility

FDS delivery was possible in all cases. All patients except 1 were treated with only 1 FDS. The remaining patient had 2 aneurysms on the same bifurcation; stent shortening was perceived during follow-up and a new FDS was secondarily implanted, in a telescopic fashion, because one of the aneurysm necks was no longer sufficiently covered.

Additional sac coiling was performed during 1 procedure in 1 patient.

Complication Rate

One patient had intraoperative occlusion of the covered branch; however, collateral flow was excellent and the patient was asymptomatic on waking after the operation. The day 2 angiogram demonstrated reopening of the artery. This patient was also the only one who presented with a weak sensitivity to antiplatelet medications, thus requiring a loading dose of 300 mg of clopidogrel (Plavix) before treatment.

In another case, slight flow modification was depicted at the end of the treatment in the covered branch, and hemiparesis was evident when the patient awoke. A new angiogram was immediately obtained, and covered branch occlusion leading to neurologic deficit was confirmed, despite efficient abciximab infusion and artery reopening.

For 1 patient, a second FDS, positioned in a telescopic fashion, was deemed necessary due to original FDS shortening. Within 20 hours of the second intervention, the patient presented with left hemiplegia and DSA analysis showed dual-FDS occlusions, extending into both bifurcation branches. Intra-arterial thrombolysis allowed efficient reopening of both FDS devices and bifurcation branches. The patient recovered from all motor deficits within days and was able to return to work, having only minor cognitive impairment. In this case, treatment with aspirin and a double dose of Plavix was continued for 6 months, though biologic tests did not demonstrate any antiplatelet resistance. After 6 months, Plavix therapy was stopped. Two years after EVT, on termination of aspirin treatment, the patient reported a transient ischemic attack in the MCA territory, so aspirin was re-instated for life.

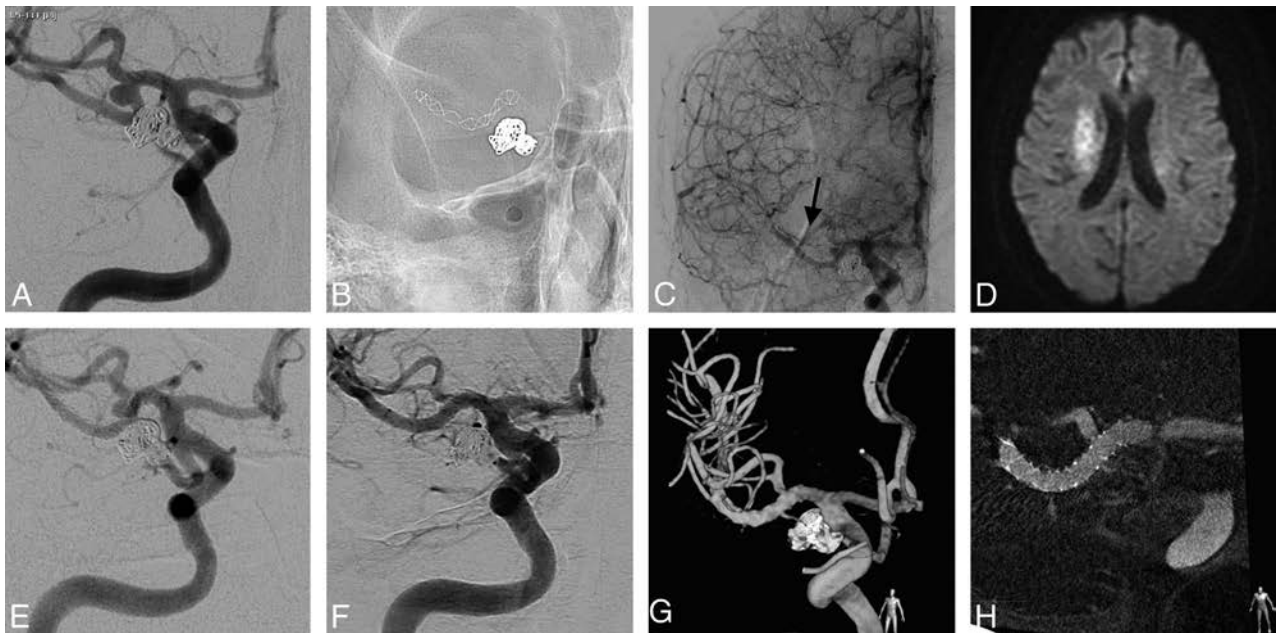


FIG 1. A 58-year-old woman was previously treated in our institution for a right posterior communicating artery ruptured aneurysm. Three months later, she was scheduled for the treatment of a second aneurysm. *A*, The right internal carotid angiogram shows a saccular MCA bifurcation aneurysm. *B*, The unsubtracted picture after FDS placement in the inferior bifurcation branch. *C*, The final angiogram shows slow flow in the covered branch (*arrow*). Five hours after the treatment, the patient presented with transient right hemiparesis when the mean blood pressure dropped to <80 mm Hg. *D*, MR imaging shows limited DWI-positive findings in the corresponding territory. The patient then remained asymptomatic. *E*, Six-month follow-up shows a reduction in the size of the aneurysm. *F–H*, DSA, 3D rotational angiography, and VasoCT at 2.5-year follow-up demonstrate complete occlusion of the aneurysm and the unchanged aspect of the covered branch.

Slow flow was observed in the covered branch on the final angiograms in 4 patients. This led to postoperative presentation of no deficits in 1 case, transient deficits in 1 case, and permanent deficits in 2 cases.

One of those 4 patients exhibited covered branch occlusion during follow-up. This patient presented with slight left hemiparesis due to slow flow in the covered branch after treatment and was admitted to our institution 1 month later with complete left-sided motor deficits. The patient had discontinued clopidogrel medication a few days before admission, and DSA showed complete occlusion of the stent, though the collateral flow was relatively good. The patient partially overcame the deficit within days.

Overall in this study, no hemorrhagic complications occurred. Immediate flow modifications in the covered branch were not identified in only 7 patients (50%).

Clinical ischemic complications, defined as new neurologic deficits and confirmed by MR imaging, occurred in 43% of patients, though most were small DWI lesions caused by flow restriction in the covered branch. Procedure-related morbidity and mortality at last follow-up were 21% and 0%, respectively.

Angiographic Follow-Up

Angiographic follow-up data were available for 12 patients and 13 aneurysms (87%). The remaining 2 patients have yet to undergo their first follow-up DSA. The average length of angiographic follow-up for this cohort was 16 months (range, 3–41; median, 8 months).

On the basis of the most recent angiogram in each case, we observed, in total, 2 covered branch occlusions and 6 other cases (50%) presented with a significantly reduced caliber. Overall, covered branch modifications were present in 66% of cases.

We noted complete aneurysm occlusion in 62% of patients, aneurysm remnants with partial occlusion in 31% of patients, and a neck remnant in 8% of patients.

DISCUSSION

Wide-neck bifurcation aneurysms can, in some cases, be difficult and challenging for traditional EVT approaches. Most can be successfully treated with the balloon-remodeling technique,⁵ especially in ruptured cases. However, attenuated and complete coil occlusion is not always possible, and recurrence rates are not negligible.^{23,24}

In these cases, stent-assisted coiling has been increasingly favored,^{10,11} but although efficiency rates are good, complication rates appear high for “X” and “Y” configurations, with a 10.0% occurrence of procedure-related permanent neurologic deficits and a 1.0% death rate reported in the study of Bartolini et al.²⁵

The use of FDSs in the treatment of intracranial aneurysms is gradually increasing. The FDS concept is to induce intra-aneurysmal thrombosis by disrupting the flow near the aneurysmal neck while preserving the patency of the parent vessels and the covered branches.¹⁹ It has been shown that it is safe to cover the supraclinoid internal carotid branch while treating internal carotid aneurysms with FDSs and that in these cases, the occlusion rate of the covered branches is low.^{26,27}

A small number of articles describe the safety and efficiency of FDSs in the treatment of bifurcation aneurysms. Very recently, some articles investigating their use in the treatment of MCA aneurysms were published, though study populations were sometimes heterogeneous and included saccular and fusiform aneurysms and both bifurcation and nonbifurcation types.^{28–30}

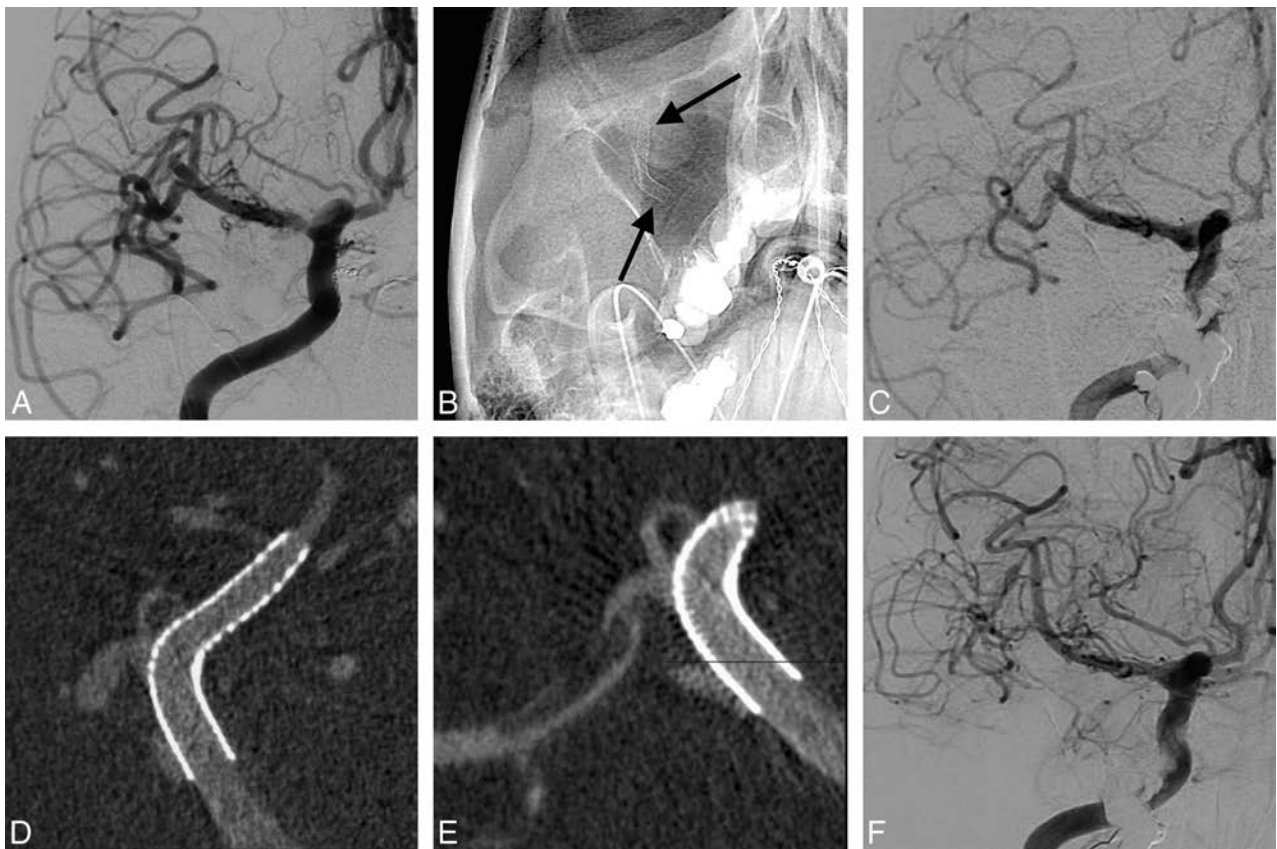


FIG 2. A 44-year-old woman who presented with an incidentally found aneurysm was treated in our institution. Although the aneurysm was small, the patient requested treatment. *A*, The right internal carotid angiogram shows a saccular MCA bifurcation aneurysm. *B*, The unsubtracted view after FDS placement in the superior bifurcation branch. *C*, The final internal carotid angiogram confirms the partial thrombosis but shows very good collateral flow. After stent delivery, VasoCT curved reconstructions of the superior (*D*) and inferior branches (*E*) show good patency of the FDS but immediate partial thrombosis in the covered branch and aneurysm. The patient was kept under a double dose of antiplatelet therapy, heparin, and noradrenaline for 48 hours. She did not develop any symptoms, and early follow-up DSA showed the normal aspect of the covered branch. However, the angiogram obtained at 2-year follow-up (*F*), demonstrates asymptomatic complete occlusion of both the covered branch and aneurysm.

From 25 MCA aneurysms (including 21 bifurcation lesions) treated with FDSs, Yavuz et al²⁸ reported good results, with 84% complete occlusion at follow-up. Although the last follow-up showed that 43% of covered branches had reduced caliber or were occluded, no permanent neurologic deficits occurred. Subsequent articles did not show similar results.

In the Saleme et al²⁹ study of FDS-treated bifurcation aneurysms, 19 were located at the MCA bifurcation (89% saccular type). The complete occlusion rate was good (92%), but the overall procedure-related complication rate was 8%, with new permanent neurologic deficits occurring in 9.4% of patients during hospitalization and new DWI-positive findings reported in 64.8% of cases. Middle cerebral artery bifurcation covered branch modifications remained unchanged in only 37% of cases, and symptomatic narrowing or occlusion occurred in 16% of cases.

In a small MCA aneurysm study, with 15 subjects, Briganti et al³⁰ claimed that EVT with FDS was a relatively safe treatment for those lesions, though they described high rates of permanent postprocedural neurologic deficits (27% of cases).

In our study, the ischemic complication rate was also very high. In 43% of cases, neurologic deficits with DWI-positive findings were reported. We did not encounter perforator branch occlusion. The infarct zones were usually relatively small and were

due to flow impairment inside the covered branch. Infarctions were limited because potential collateral flow was always tested with balloon MCA occlusion before FDS treatment, though existing, collateral flow was sometimes insufficient. Balloon test occlusion in these situations obviously cannot be used to guarantee sufficient collateral flow because of the absence of a clinical evaluation during the test. However, balloon test occlusion was used to determine cases in which balloon test occlusion would clearly be insufficient. Thus, if no collateral flow was perceived, the FDS technique was rejected in favor of other approaches.

Also, because 80% of the lesions were located in the nondominant hemisphere, clinical consequences were not as devastating as one might anticipate. Nonetheless, 21% of patients had an mRS score of >1 at last follow-up.

Antiplatelet therapy certainly plays a crucial role in ensuring the safety of FDS treatment, particularly in cases of bifurcation aneurysms. Individual antiplatelet sensitivity was not related to thromboembolic complications in our study because only 1 patient was shown to be weakly sensitive, in which case a loading dose had been administered. It is conceivable that more intensive antiplatelet therapy with prasugrel or ticagrelor could lower the complication rates. Apart from 1 incident of TIA after complete interruption of antiplatelet therapy, no posthospitalization com-

plications were reported for our cohort. Therefore, it seems that hemodynamic changes in the covered branch are most likely during the very acute phase, and medical management of coagulation and blood pressure should be optimized at that time to avoid ischemic strokes. Because most complications occurred at the acute phase, there is no evidence that an extension of the double-antiplatelet regimen would modify the result. On the other hand, a life-long aspirin therapy could be discussed in this population at risk of ischemia. Furthermore, our patients did not experience any hemorrhagic complications.

Angiographic follow-up demonstrated complete occlusion in only 62% of the patients in our study. The aneurysms treated with this technique were very challenging, and though anatomic results were superior in other FDS studies (80%–92%),^{28–30} better results could be achieved with other techniques.

Recently, numerous devices for the EVT of wide-neck bifurcation aneurysms have been developed. Most have not yet been clinically evaluated. The WEB device is intended for the treatment of the same population as seen in our study. Some midterm follow-up studies have been published^{17,31,32} and show good safety with morbidity rates of between 1.3% and 3.1%, with no mortality reported. Midterm anatomic results^{17,31,33} have shown complete occlusion in 26.7%–56.9% of aneurysms.

However, it is imperative that new EVT techniques compare favorably with neurosurgical results. In a recent, large study of unruptured MCA aneurysms, the mortality and morbidity rates of surgical repair were 0.4% and 4.9%, respectively.³⁴ In another large series,⁴ 5.4% of patients were worse after surgery for non-ruptured MCA aneurysms, with a 1.9% mortality rate. However, anatomic results were excellent, with complete occlusion in 97.4% of patients.

Our study has several limitations. First, it was limited by a relatively small number of patients, though numbers were sufficient to show high complication rates. Our angiographic follow-up was short (median, 8 months), so longer term follow-up is needed to evaluate the effect of FDSs for the treatment of MCA bifurcation aneurysms, not in the least because the effect of this treatment is based on progressive flow reduction inside the sac and side branch and occlusion rates could improve with time. We did not include dissecting MCA aneurysms in this study. For this very specific population, results would possibly favor FDS treatment because other therapeutic options, including surgery, present high complication risks.

CONCLUSIONS

From our experience and compared with other therapeutic options, flow-diverter stents do not appear to be suitable for the treatment of saccular MCA bifurcation aneurysms.

Disclosures: Jacques Moret—UNRELATED: Consultancy: Covidien, MicroVention; OTHER RELATIONSHIPS: My son is an employee of MicroVention. Laurent Spelle—UNRELATED: Consultancy: Sequent Medical, Stryker, Medtronic.

REFERENCES

1. Molyneux AJ, Kerr RSC, Yu LM, et al; International Subarachnoid Aneurysm Trial (ISAT) Collaborative Group. **International subarachnoid aneurysm trial (ISAT) of neurosurgical clipping versus endovascular coiling in 2143 patients with ruptured intracranial**

- aneurysms: a randomised comparison of effects on survival, dependency, seizures, rebleeding, subgroups, and aneurysm occlusion. *Lancet* 2005;366:809–17 CrossRef Medline
2. Pierot L, Spelle L, Vitry F. **Immediate clinical outcome of patients harboring unruptured intracranial aneurysms treated by endovascular approach: results of the ATENA study.** *Stroke* 2008;39:2497–504 CrossRef Medline
3. Brinjikji W, Lanzino G, Cloft HJ, et al. **Endovascular treatment of middle cerebral artery aneurysms: a systematic review and single-center series.** *Neurosurgery* 2011;68:397–402; discussion 402 CrossRef Medline
4. Rodríguez-Hernández A, Sughrue ME, Akhavan S, et al. **Current management of middle cerebral artery aneurysms: surgical results with a “clip first” policy.** *Neurosurgery* 2013;72:415–27 CrossRef Medline
5. Moret J, Cognard C, Weill A, et al. **The “remodelling technique” in the treatment of wide neck intracranial aneurysms: angiographic results and clinical follow-up in 56 cases.** *Interv Neuroradiol* 1997;3:21–35 Medline
6. Arat A, Cil B. **Double-balloon remodeling of wide-necked aneurysms distal to the circle of Willis.** *AJNR Am J Neuroradiol* 2005;26:1768–71 Medline
7. Baxter BW, Rosso D, Lownie SP. **Double microcatheter technique for detachable coil treatment of large, wide-necked intracranial aneurysms.** *AJNR Am J Neuroradiol* 1998;19:1176–78 Medline
8. Piotin M, Blanc R, Spelle L, et al. **Stent-assisted coiling of intracranial aneurysms: clinical and angiographic results in 216 consecutive aneurysms.** *Stroke* 2010;41:110–15 CrossRef Medline
9. Lubicz B, Bandeira A, Bruneau M, et al. **Stenting is improving and stabilizing anatomical results of coiled intracranial aneurysms.** *Neuroradiology* 2009;51:419–25 CrossRef Medline
10. Shapiro M, Becske T, Sahlein D, et al. **Stent-supported aneurysm coiling: a literature survey of treatment and follow-up.** *AJNR Am J Neuroradiol* 2012;33:159–63 CrossRef Medline
11. Fargen KM, Mocco J, Neal D, et al. **A multicenter study of stent-assisted coiling of cerebral aneurysms with a Y configuration.** *Neurosurgery* 2013;73:466–72 CrossRef Medline
12. Zhao KJ, Yang PF, Huang QH, et al. **Y-configuration stent placement (crossing and kissing) for endovascular treatment of wide-neck cerebral aneurysms located at 4 different bifurcation sites.** *AJNR Am J Neuroradiol* 2012;33:1310–16 CrossRef Medline
13. Liu W, Kung DK, Policeni B, et al. **Stent-assisted coil embolization of complex wide-necked bifurcation cerebral aneurysms using the “waffle cone” technique: a review of ten consecutive cases.** *Interv Neuroradiol* 2012;18:20–28 Medline
14. Horowitz M, Levy E, Sauvageau E, et al. **Intra/extra-aneurysmal stent placement for management of complex and wide-necked bifurcation aneurysms: eight cases using the waffle cone technique.** *Neurosurgery* 2006;58(4 suppl 2):ONS-258–62; discussion ONS-262 Medline
15. Raymond J, Guilbert F, Roy D. **Neck-bridge device for endovascular treatment of wide-neck bifurcation aneurysms: initial experience.** *Radiology* 2001;221:318–26 CrossRef Medline
16. Aguilar-Pérez M, Kurre W, Fischer S, et al. **Coil occlusion of wide-neck bifurcation aneurysms assisted by a novel intra- to extra-aneurysmal neck-bridging device (pCONus): initial experience.** *AJNR Am J Neuroradiol* 2014;35:965–71 CrossRef Medline
17. Pierot L, Klisch J, Cognard C, et al. **Endovascular WEB flow disruption in middle cerebral artery aneurysms: preliminary feasibility, clinical, and anatomical results in a multicenter study.** *Neurosurgery* 2013;73:27–34; discussion 34–25 CrossRef Medline
18. Caroff J, Mihalea C, Dargento F, et al. **Woven Endobridge (WEB) device for endovascular treatment of ruptured intracranial wide-neck aneurysms: a single-center experience.** *Neuroradiology* 2014;56:755–61 CrossRef Medline
19. Alderazi YJ, Shastri D, Kass-Hout T, et al. **Flow diverters for intracranial aneurysms.** *Stroke Res Treat* 2014;2014:415653 CrossRef Medline

20. D'Urso PI, Lanzino G, Cloft HJ, et al. **Flow diversion for intracranial aneurysms: a review.** *Stroke* 2011;42:2363–68 CrossRef Medline
21. Caroff J, Mihalea C, Neki H, et al. **Role of C-arm VasoCT in the use of endovascular WEB flow disruption in intracranial aneurysm treatment.** *AJNR Am J Neuroradiol* 2014;35:1353–57 CrossRef Medline
22. Kizilkilic O, Kocer N, Metaxas GE, et al. **Utility of VasoCT in the treatment of intracranial aneurysm with flow-diverter stents.** *J Neurosurg* 2012;117:45–49 CrossRef Medline
23. Pierot L, Cognard C, Spelle L, et al. **Safety and efficacy of balloon remodeling technique during endovascular treatment of intracranial aneurysms: critical review of the literature.** *AJNR Am J Neuroradiol* 2012;33:12–15 CrossRef Medline
24. Shapiro M, Babb J, Becske T, et al. **Safety and efficacy of adjunctive balloon remodeling during endovascular treatment of intracranial aneurysms: a literature review.** *AJNR Am J Neuroradiol* 2008;29:1777–81 CrossRef Medline
25. Bartolini B, Blanc R, Pistocchi S, et al. **“Y” and “X” stent-assisted coiling of complex and wide-neck intracranial bifurcation aneurysms.** *AJNR Am J Neuroradiol* 2014;35:2153–58 CrossRef Medline
26. Vedantam A, Rao VY, Shaltoni HM, et al. **Incidence and clinical implications of carotid branch occlusion following treatment of internal carotid artery aneurysms with the Pipeline embolization device.** *Neurosurgery* 2015;76:173–78; discussion 178 CrossRef Medline
27. Neki H, Caroff J, Jittapiromsak P, et al. **Patency of the anterior choroïdal artery covered with a flow-diverter stent.** *J Neurosurg* 2015 Jun 5. [Epub ahead of print] Medline
28. Yavuz K, Geyik S, Saatci I, et al. **Endovascular treatment of middle cerebral artery aneurysms with flow modification with the use of the Pipeline embolization device.** *AJNR Am J Neuroradiol* 2014;35:529–35 CrossRef Medline
29. Saleme S, Iosif C, Ponomarjova S, et al. **Flow-diverting stents for intracranial bifurcation aneurysm treatment.** *Neurosurgery* 2014; 75:623–31; quiz 631 CrossRef Medline
30. Briganti F, Delehay L, Leone G, et al. **Flow diverter device for the treatment of small middle cerebral artery aneurysms.** *J Neurointerv Surg* 2015 Jan 20. [Epub ahead of print] CrossRef Medline
31. Papagiannaki C, Spelle L, Januel AC, et al. **WEB intrasaccular flow disruptor—prospective, multicenter experience in 83 patients with 85 aneurysms.** *AJNR Am J Neuroradiol* 2014;35:2106–11 CrossRef Medline
32. Caroff J, Mihalea C, Klisch J, et al. **Single layer WEBS: intrasaccular flow disrupters for aneurysm treatment—feasibility results from a European study.** *AJNR Am J Neuroradiol* 2015 Jul 9. [Epub ahead of print] Medline
33. Lubicz B, Klisch J, Gauvrit JY, et al. **WEB-DL endovascular treatment of wide-neck bifurcation aneurysms: short- and midterm results in a European study.** *AJNR Am J Neuroradiol* 2014;35:432–38 CrossRef Medline
34. Morgan MK, Mahattanakul W, Davidson A, et al. **Outcome for middle cerebral artery aneurysm surgery.** *Neurosurgery* 2010;67:755–61; discussion 761 CrossRef Medline

The Revascularization Scales Dilemma: Is It Right to Apply the Treatment in Cerebral Ischemia Scale in Posterior Circulation Stroke?

C. Jung, W. Yoon, S.J. Ahn, B.S. Choi, J.H. Kim, and S.H. Suh

ABSTRACT

BACKGROUND AND PURPOSE: Although various revascularization scales are used in the angiographic evaluation of acute ischemic stroke, observer reliability tests of these scales have been rarely performed for posterior circulation stroke. We aimed to evaluate inter- and intraobserver variability of 2 scales, the modified Treatment in Cerebral Ischemia and the Arterial Occlusive Lesion, in posterior circulation stroke.

MATERIALS AND METHODS: Three independent readers interpreted pre- and postthrombolytic angiographies of 62 patients with posterior circulation stroke by using the modified Treatment in Cerebral Ischemia and Arterial Occlusive Lesion scales. The κ statistic was used to measure observer agreement for both scales, and $\kappa > 0.6$ was considered substantial agreement.

RESULTS: For the Arterial Occlusive Lesion scale, inter- and intraobserver agreement was >0.6 . While intraobserver agreement of the modified Treatment in Cerebral Ischemia scale was >0.6 except for 1 reader, interobserver agreement was lower in dichotomized and original scales. In 49 cases with solely basilar artery occlusion, inter- and intraobserver agreement of both scales was similar to that in all 62 patients with posterior circulation stroke. In 2 consecutive readings, there was a significant decrease in the proportion of mTICI 2a reads (22.58% in the first versus 13.44% in the second session, $P < .03$) and a reciprocal increase in the sum of proportions for modified Treatment in Cerebral Ischemia 2b and modified Treatment in Cerebral Ischemia 3 reads (62.37% in the first versus 72.58% in the second session, $P < .046$).

CONCLUSIONS: In angiographic assessment of posterior circulation stroke, inter- and intraobserver agreement for the Arterial Occlusive Lesion scale was reliable, while the modified Treatment in Cerebral Ischemia failed to achieve substantial interobserver agreement. The clinical impact of this result needs to be validated in future studies.

ABBREVIATIONS: AOL = Arterial Occlusive Lesion; BAO = basilar artery occlusion; mTICI = modified Treatment in Cerebral Ischemia; TICI = Thrombolysis in Cerebral Infarction; TIMI = Thrombolysis in Myocardial Infarction

In the treatment of acute ischemic stroke with large intracranial arterial occlusion, endovascular techniques are becoming the mainstream with higher revascularization rates.¹⁻³ While various grading schemes, such as the Thrombolysis in Myocardial Infarction (TIMI) or Thrombolysis in Cerebral In-

farction (TICI), are widespread, their reliability in angiographic assessment of anterior circulation stroke remains controversial.⁴⁻⁸ Recently, the modified Treatment in Cerebral Ischemia (mTICI) and the Arterial Occlusive Lesion (AOL) scales were strongly recommended as standards of reperfusion and recanalization in the angiographic evaluation of anterior circulation stroke.⁹

Despite applying similar scales to the posterior circulation, it is also unclear which scales might be reliably implemented for the vertebrobasilar territory. Recently, Gerber et al¹⁰ questioned whether it is right to use the TIMI or TICI scale in posterior circulation stroke and demonstrated that interobserver variability tests of these scales had never been performed in case of posterior circulation stroke.

Therefore, we aimed to evaluate intra- and interobserver agreement of the mTICI and AOL scales in the angiographic evaluation of posterior circulation stroke.

Received June 3, 2015; accepted after revision July 22.

From the Department of Radiology (C.J., B.S.C., J.H.K.), Seoul National University College of Medicine, Seoul National University Bundang Hospital, Seongnam, Korea; Department of Radiology (W.Y.), Chonnam National University Medical School, Gwangju, Korea; Department of Radiology (S.J.A., S.H.S.), Gangnam Severance Hospital, Yonsei University, Seoul, Korea; and Severance Institute of Vascular and Metabolic Research (S.H.S.), Yonsei University College of Medicine, Seoul, Korea.

This study was supported by a faculty research grant from Yonsei University College of Medicine (6-2015-0051).

Please address correspondence to Sang Hyun Suh, MD, Department of Radiology, Gangnam Severance Hospital, Yonsei University College of Medicine, 712 Eonjoro, Gangnam-gu, Seoul, 135-720 Korea; e-mail: suhsh11@yuhs.ac

<http://dx.doi.org/10.3174/ajnr.A4529>

Table 1: The modified Treatment in Cerebral Ischemia and the Arterial Occlusive Lesion scale scores

	mTICI	AOL
0	No perfusion	Complete occlusion of the target artery
1	Antegrade reperfusion past the initial occlusion but limited distal branch filling with little or slow distal reperfusion	Incomplete or partial local recanalization at the target artery with no distal flow
2		Incomplete or partial local recanalization at the target artery with any distal flow
2a	Antegrade reperfusion of less than half of the previously occluded target artery ischemic territory	
2b	Antegrade reperfusion of more than half of the previously occluded target artery ischemic territory	
3	Complete antegrade reperfusion of the previously occluded target artery territory, with absence of visualized occlusion in all distal branches	Complete recanalization and restoration of the target artery with any distal flow

Table 2: Interobserver agreement of 62 cases and subset of 49 cases with basilar artery occlusion by using original versus dichotomized outcomes

Reader	κ Values (SE)			
	Original Scale		Dichotomized Scale	
	All (N = 62)	BAO (n = 49)	All (N = 62)	BAO (n = 49)
mTICI				
A versus B	0.418 (0.088)	0.43 (0.093)	0.315 (0.116)	0.334 (0.131)
A versus C	0.484 (0.074)	0.471 (0.082)	0.506 (0.111)	0.469 (0.126)
B versus C	0.503 (0.077)	0.523 (0.08)	0.478 (0.11)	0.466 (0.121)
AOL				
A versus B	0.696 (0.089)	0.7 (0.091)	0.815 (0.127)	0.810 (0.130)
A versus C	0.631 (0.086)	0.659 (0.088)	0.742 (0.142)	0.734 (0.145)
B versus C	0.709 (0.081)	0.775 (0.075)	0.914 (0.085)	0.911 (0.087)

Note.—SE indicates standard error.

MATERIALS AND METHODS

Patients

After approval of the institutional review board for this retrospective study, 62 patients (men/women = 37:25, mean age = 68 ± 11.4 years) with acute posterior circulation stroke, who underwent intra-arterial thrombolysis from April 2004 to December 2013, were consecutively enrolled from a single institutional data base. All patients underwent digital subtraction angiography before and after the procedure.

In these patients, the mean NIHSS score at admission was 17 ± 8, and the levels of arterial occlusion in the basilar (n = 49) and vertebral arteries (n = 13) were 79% and 21%, respectively. At 3 months, 21 patients (33.9%) had a good outcome (modified Rankin Scale score 0–2) and 12 (19%) had died.

Image Acquisition

DSA images from angiograms of the bilateral vertebral arteries were acquired by using a biplane angiography system. Consecutive anteroposterior and lateral angiographic images before and after intra-arterial thrombolysis, from the arterial to the delayed venous phase, were obtained in JPEG format, and were converted to a movie file format (Adobe Flash authoring file). Each reader interpreted them via on-line storage by making a comparison between preoperative and postoperative DSA images.

Image Interpretation

Three experienced readers (S.H.S., C.J., and W.Y.), who worked in 3 different tertiary medical centers as interventional neuroradiologists (with >10 years of experience), independently reviewed all images of 62 cases twice, 3–4 months apart. There was no training or required consensus of readers to perform this task.

Regardless of the others' reads, each reader assessed his own read by using the mTICI and AOL scales. In Table 1, the mTICI scale is defined in 5 grades according to the Stroke Treatment Academic Industry Roundtable consensus⁹ and the AOL scale is classified into 4 grades.¹¹ For this study, we did not provide any special information to the readers.

Statistical Analysis

As parameters of intraobserver and interobserver agreement, the κ statistic was used for the mTICI and AOL scales. The κ value was interpreted according to Landis and Koch¹² with a κ value of 0 = poor, 0.01–0.20 = slight, 0.21–0.40 = fair, 0.41–0.60 = moderate, 0.61–0.80 substantial, and 0.81–1.0 = almost-perfect agreement. The κ statistic was also calculated for 49 cases with basilar artery occlusion (BAO) and the dichotomized groups, including those with poor revascularization (AOL = 0–2, mTICI = 0–2a) versus good revascularization (AOL = 3, mTICI = 2b–3). Comparison of the κ values was performed by using 95% CIs for the difference between the κ statistics, with 1000 bootstrapped samples. The difference was statistically significant if 95% CIs did not include zero. Statistical analyses were performed by using SAS (Version 9.2; SAS Institute, Cary, North Carolina).

RESULTS

Contrary to the AOL scale, all pair-wise κ values for the mTICI were lower than 0.6 in interobserver agreement (Table 2). Intraobserver agreement for the AOL and mTICI scales was substantial to almost perfect in most cases, except for 1 reader for the mTICI scale (reader A, κ = 0.444 in all and 0.462 in BAO, respectively; Table 3). Regardless of the scale used, intraobserver and interob-

Table 3: Intraobserver agreement between 62 cases and subset of 49 cases with basilar artery occlusion

Scale	κ Values (SE)					
	All (N = 62)			BAO (n = 49)		
	Reader A	Reader B	Reader C	Reader A	Reader B	Reader C
mTICI	0.444 (0.085)	0.79 (0.061)	0.855 (0.045)	0.462 (0.092)	0.757 (0.073)	0.855 (0.050)
AOL	0.646 (0.079)	0.816 (0.085)	0.833 (0.055)	0.633 (0.083)	0.807 (0.089)	0.859 (0.052)

Table 4: Proportions in all ratings of 3 readers by categories of the scales

	Reads (%; n = 186)	
	First Reading	Second Reading
mTICI		
0	12 (6.45)	13 (6.99)
1	16 (8.60)	13 (6.99)
2a ^a	42 (22.58)	25 (13.44)
2b	82 (44.09)	98 (52.69)
3	34 (18.28)	37 (19.89)
AOL		
0	12 (6.45)	12 (6.45)
1	7 (3.76)	10 (5.38)
2	31 (16.67)	28 (15.05)
3	136 (73.12)	136 (73.12)

^a Statistically significant ($P < .05$).

server agreement for 49 cases with BAO was not significantly different from that for all 62 patients. For the dichotomized scales, there was an increasing trend of κ values in the AOL, but not in the mTICI scale.

Table 4 shows the distribution of all reads by using either the mTICI or the AOL scale. In 2 consecutive readings, there was a significant decrease in the proportion of mTICI 2a (42/186, 22.58%, in the first session versus 25/186, 13.44%, in the second session; $P < .03$) and a reciprocal increment in the sum of proportions for mTICI 2b and mTICI 3 (116/186, 62.37%, in the first session versus 135/186, 72.58%, in the second session; $P < .046$). In the proportion of unanimity, the mTICI was also significantly lower than the AOL (14/62, 23%, in mTICI, versus 44/62, 71%, in the AOL; $P < .001$).

DISCUSSION

In the 17 recent studies regarding intra-arterial thrombolysis in acute posterior circulation stroke,¹³⁻²⁹ 5 (29.4%) did not provide any scheme and 12 (70.6%) used the TIMI or TICI scale, of which 58% (7/12) used TIMI ≥ 2 and 42% (5/12), TICI $\geq 2b$ as a cutoff level of “successful reperfusion.” In 10 studies with only BAO cases,^{14,17,20-23,25,27-29} the TIMI scale was used in 5 and the TICI scale in 4. However, observer reliability tests in those previous studies had never been performed for angiographic assessment of posterior circulation stroke. If such heterogeneous and inconsistent scoring systems are used in defining end points of revascularization success, it is difficult to compare or combine results of clinical studies.³⁰ Therefore, selection of a reliable biomarker for revascularization is relevant to the prediction of procedural efficacy and the outcome in posterior circulation stroke. To our knowledge, this is the first study to evaluate inter- and intraobserver agreement for 2 common scales in the angiographic evaluation following intra-arterial thrombolysis of posterior circulation stroke.

In this study, we found the observer variability of the mTICI inherent in the angiographic assessment of posterior circulation stroke. While inter- and intraobserver variability for the AOL was reliable, the mTICI failed to achieve substantial interobserver agreement with a low concordance rate of 23% (14/62 cases). We also demonstrated a significant difference in the proportion of mTICI 2a reads that had a direct influence on the sum of proportions of mTICI 2b and 3, which may affect the judgment of angiographic end points in intra-arterial thrombolysis. The mTICI was inferred inferior to the AOL for the following reason¹: the relative complexity of the mTICI with more responses and semi-quantitative descriptors. Gaha et al⁴ explained that inter- and intraobserver disagreement in adjudicating treatment results may be caused by multiple problems: intrinsic ambiguities in the definitions of the classifications; discrepancies in the various ways the definitions are interpreted by various readers; and even if the definitions were understood in the same way, discrepancies in applying the definitions to individual cases. Kundel and Polansky³¹ also showed that the κ value in observer agreement was likely to increase as the number of categories decreased.² It is possible to have inconsistency in interpreting the mTICI 2 grade, such as mTICI 2a versus mTICI 2b, especially for posterior circulation. In fact, angiographic evaluation of the vertebrobasilar territory has some limitations, such as interference with abundant collateral flows, incomplete visualization of the perforating arteries to the brain stem, and the necessity to consider the antegrade flow from the anterior circulation.

Because endovascular revascularization therapy is becoming the main strategy for acute ischemic stroke, it is important to use the optimal scale with high reliability in decisions of revascularization end points. In fact, revascularization can be understood as angiographic recanalization of the primary arterial occlusive lesion or reperfusion in the arterial bed distal to the occlusion (TIMI, TICI, mTICI). The AOL scale has been the sole scoring system for measuring the degree of recanalization at the target arterial lesion since its introduction in the Interventional Management of Stroke trials,³²⁻³⁴ and the posterior circulation occlusions were categorized according to AOL recanalization in Interventional Management of Stroke III.³² Although Gaha et al⁴ reported that observer variability for the AOL was “moderate” in anterior circulation stroke, we found that this scheme had high reliability in posterior circulation stroke. Considering its ease of use and consistency, it is possible to evaluate the AOL as a recanalization scale in a further posterior circulation stroke study.

This study had some limitations. First, the study design was retrospective with a limited number of cases. Second, the predictive power of both scales in this study was not analyzed due to the sampling heterogeneity. In fact, whether to choose the recanalization or reperfusion scale as a determinant of clinical outcome in posterior circulation stroke is still controversial. Cho et al³⁵ re-

ported that reperfusion was a reliable surrogate and the strongest predictor of clinical outcome in anterior circulation stroke, and Singer et al³⁶ reported that independent predictors of clinical outcome were not the TICl scale, but the collateral status in BAO. In contrast, Mourand et al³⁷ proposed a DWI brain lesion score for prediction of clinical outcome in patients with BAO by using brain MR imaging. Finally, unfortunately in this study, only bilateral vertebral angiographies were used for interpretation, which may cause underdiagnosis of the mTICl because of the imperfect evaluation of collateral flows from the circle of Willis circulation.

CONCLUSIONS

In angiographic assessment of posterior circulation stroke, this is the first study to evaluate inter- and intraobserver variability for 2 commonly used scales; while the AOL as a recanalization scale showed a higher reliability, the mTICl, as a reperfusion criterion, failed to achieve substantial interobserver agreement among readers. In future studies, it will be necessary to validate the clinical impact of this result in posterior circulation stroke.

ACKNOWLEDGMENTS

We thank Kyung Hwa Han, MS, for her assistance with statistics for this study.

REFERENCES

- Berkhemer OA, Fransen PS, Beumer D, et al. **A randomized trial of intraarterial treatment for acute ischemic stroke.** *N Engl J Med* 2015; 372:11–20 CrossRef Medline
- Campbell BC, Mitchell PJ, Kleinig TJ, et al; EXTEND-IA Investigators. **Endovascular therapy for ischemic stroke with perfusion-imaging selection.** *N Engl J Med* 2015;372:1009–18 CrossRef Medline
- Goyal M, Demchuk AM, Menon BK, et al; ESCAPE Trial Investigators. **Randomized assessment of rapid endovascular treatment of ischemic stroke.** *N Engl J Med* 2015;372:1019–30 CrossRef Medline
- Gaha M, Roy C, Estrade L, et al. **Inter- and intraobserver agreement in scoring angiographic results of intra-arterial stroke therapy.** *AJNR Am J Neuroradiol* 2014;35:1163–69 CrossRef Medline
- Suh SH, Cloft HJ, Fugate JE, et al. **Clarifying differences among Thrombolysis in Cerebral Infarction scale variants: is the artery half open or half closed?** *Stroke* 2013;44:1166–68 CrossRef Medline
- Bar M, Mikulik R, Jonszta T, et al. **Diagnosis of recanalization of the intracranial artery has poor inter-rater reliability.** *AJNR Am J Neuroradiol* 2012;33:972–74 CrossRef Medline
- Tomsick T. **TIMI, TIBI, TICl: I came, I saw, I got confused.** *AJNR Am J Neuroradiol* 2007;28:382–84 Medline
- Kallmes DF. **TICl: if you are not confused, then you are not paying attention.** *AJNR Am J Neuroradiol* 2012;33:975–76 CrossRef Medline
- Zaidat OO, Yoo AJ, Khatri P, et al; Cerebral Angiographic Revascularization Grading (CARG) Collaborators, STIR Revascularization working group, STIR Thrombolysis in Cerebral Infarction (TICl) Task Force. **Recommendations on angiographic revascularization grading standards for acute ischemic stroke: a consensus statement.** *Stroke* 2013;44:2650–63 CrossRef Medline
- Gerber JC, Miaux YJ, von Kummer R. **Scoring flow restoration in cerebral angiograms after endovascular revascularization in acute ischemic stroke patients.** *Neuroradiology* 2015;57:227–40 CrossRef Medline
- Khatri P, Neff J, Broderick JP, et al; IMS-I Investigators. **Revascularization end points in stroke interventional trials: recanalization versus reperfusion in IMS-I.** *Stroke* 2005;36:2400–03 CrossRef Medline
- Landis JR, Koch GG. **The measurement of observer agreement for categorical data.** *Biometrics* 1977;33:159–74 CrossRef Medline
- Becker KJ, Monsein LH, Ulatowski J, et al. **Intraarterial thrombolysis in vertebrobasilar occlusion.** *AJNR Am J Neuroradiol* 1996;17:255–62 Medline
- Egan R, Clark W, Lutsep H, et al. **Efficacy of intraarterial thrombolysis of basilar artery stroke.** *J Stroke Cerebrovasc Dis* 1999;8:22–27 CrossRef Medline
- Lin DD, Gailloud P, Beauchamp NJ, et al. **Combined stent placement and thrombolysis in acute vertebrobasilar ischemic stroke.** *AJNR Am J Neuroradiol* 2003;24:1827–33 Medline
- Macleod MR, Davis SM, Mitchell PJ, et al. **Results of a multicentre, randomised controlled trial of intra-arterial urokinase in the treatment of acute posterior circulation ischaemic stroke.** *Cerebrovasc Dis* 2005;20:12–17 CrossRef Medline
- Bergui M, Stura G, Daniele D, et al. **Mechanical thrombolysis in ischemic stroke attributable to basilar artery occlusion as first-line treatment.** *Stroke* 2006;37:145–50 CrossRef Medline
- Schulte-Altendorneburg G, Hamann GF, Mull M, et al. **Outcome of acute vertebrobasilar occlusions treated with intra-arterial fibrinolysis in 180 patients.** *AJNR Am J Neuroradiol* 2006;27:2042–47 Medline
- Lutsep HL, Rymer MM, Nesbit GM. **Vertebrobasilar revascularization rates and outcomes in the MERCI and multi-MERCI trials.** *J Stroke Cerebrovasc Dis* 2008;17:55–57 CrossRef Medline
- Pfefferkorn T, Mayer TE, Opherck C, et al. **Staged escalation therapy in acute basilar artery occlusion: intravenous thrombolysis and on-demand consecutive endovascular mechanical thrombectomy: preliminary experience in 16 patients.** *Stroke* 2008;39:1496–500 CrossRef Medline
- Nagel S, Schellinger PD, Hartmann M, et al. **Therapy of acute basilar artery occlusion: intraarterial thrombolysis alone vs bridging therapy.** *Stroke* 2009;40:140–46 CrossRef Medline
- Schonewille WJ, Wijman CA, Michel P, et al; BASICS study group. **Treatment and outcomes of acute basilar artery occlusion in the Basilar Artery International Cooperation Study (BASICS): a prospective registry study.** *Lancet Neurol* 2009;8:724–30 CrossRef Medline
- Yu YY, Niu L, Gao L, et al. **Intraarterial thrombolysis and stent placement for acute basilar artery occlusion.** *J Vasc Interv Radiol* 2010;21:1359–63 CrossRef Medline
- Roth C, Mielke A, Siekmann R, et al. **First experiences with a new device for mechanical thrombectomy in acute basilar artery occlusion.** *Cerebrovasc Dis* 2011;32:28–34 CrossRef Medline
- Andersson T, Kuntze Söderqvist Å, Söderman M, et al. **Mechanical thrombectomy as the primary treatment for acute basilar artery occlusion: experience from 5 years of practice.** *J Neurointerv Surg* 2013;5:221–25 CrossRef Medline
- Espinosa de Rueda M, Parrilla G, Zamarro J, et al. **Treatment of acute vertebrobasilar occlusion using thrombectomy with stent retrievers: initial experience with 18 patients.** *AJNR Am J Neuroradiol* 2013;34:1044–48 CrossRef Medline
- Mordasini P, Brekenfeld C, Byrne JV, et al. **Technical feasibility and application of mechanical thrombectomy with the Solitaire FR Revascularization device in acute basilar artery occlusion.** *AJNR Am J Neuroradiol* 2013;34:159–63 CrossRef Medline
- Möhlenbruch M, Stampfl S, Behrens L, et al. **Mechanical thrombectomy with stent retrievers in acute basilar artery occlusion.** *AJNR Am J Neuroradiol* 2014;35:959–64 CrossRef Medline
- Mourand I, Machi P, Milhaud D, et al. **Mechanical thrombectomy with the Solitaire device in acute basilar artery occlusion.** *J Neurointerv Surg* 2014;6:200–4 CrossRef Medline
- Fugate JE, Klunder AM, Kallmes DF. **What is meant by “TICl”?** *AJNR Am J Neuroradiol* 2013;34:1792–97 CrossRef Medline
- Kundel HL, Polansky M. **Measurement of observer agreement.** *Radiology* 2003;228:303–08 CrossRef Medline
- Broderick JP, Palesch YY, Demchuk AM, et al; Interventional Management of Stroke (IMS) III Investigators. **Endovascular therapy af-**

- ter intravenous t-PA versus t-PA alone for stroke. *N Engl J Med* 2013;368:893–903 CrossRef Medline
33. Tomsick T, Broderick J, Carrozella J, et al; Interventional Management of Stroke II Investigators. **Revascularization results in the Interventional Management of Stroke II trial.** *AJNR Am J Neuroradiol* 2008;29:582–87 CrossRef Medline
34. Tomsick TA, Yeatts SD, Liebeskind DS, et al; IMS III Investigators. **Endovascular revascularization results in IMS III: intracranial ICA and M1 occlusions.** *J Neurointerv Surg* 2014 Oct 23. [Epub ahead of print] CrossRef Medline
35. Cho TH, Nighoghossian N, Mikkelsen IK, et al. **Reperfusion within 6 hours outperforms recanalization in predicting penumbra salvage, lesion growth, final infarct, and clinical outcome.** *Stroke* 2015;46:1582–89 CrossRef Medline
36. Singer OC, Berkefeld J, Nolte CH, et al; ENDOSTROKE Study Group. **Mechanical recanalization in basilar artery occlusion: the ENDOSTROKE study.** *Ann Neurol* 2015;77:415–24 CrossRef Medline
37. Mourand I, Machi P, Nogue E, et al. **Diffusion-weighted imaging score of the brain stem: a predictor of outcome in acute basilar artery occlusion treated with the Solitaire FR device.** *AJNR Am J Neuroradiol* 2014;35:1117–23 CrossRef Medline

Autosomal Dominant Polycystic Kidney Disease and Intracranial Aneurysms: Is There an Increased Risk of Treatment?

M.N. Rozenfeld, S.A. Ansari, P. Mohan, A. Shaibani, E.J. Russell, and M.C. Hurley

ABSTRACT

BACKGROUND AND PURPOSE: Autosomal dominant polycystic kidney disease is associated with an increased risk of intracranial aneurysms. Our purpose was to assess whether there is an increased risk during aneurysm coiling and clipping.

MATERIALS AND METHODS: Data were obtained from the National Inpatient Sample (2000–2011). All subjects had an unruptured aneurysm clipped or coiled and were divided into polycystic kidney ($n = 189$) and control ($n = 3555$) groups. Primary end points included in-hospital mortality, length of stay, and total hospital charges. Secondary end points included the International Classification of Diseases, Ninth Revision codes for iatrogenic hemorrhage or infarction; intracranial hemorrhage; embolic infarction; and carotid and vertebral artery dissections.

RESULTS: There was a significantly greater incidence of iatrogenic hemorrhage or infarction, embolic infarction, and carotid artery dissection in the patients with polycystic kidney disease compared with the control group after endovascular coiling. There was also a significantly greater incidence of iatrogenic hemorrhage or infarction in the polycystic kidney group after surgical clipping. However, the hospital stay was not longer in the polycystic kidney group, and the total hospital charges were not higher. Additional analysis within the polycystic kidney group revealed a significantly shorter length of stay but similar in-hospital costs when subjects underwent coiling versus clipping.

CONCLUSIONS: Patients with polycystic kidney disease face an increased risk during intracranial aneurysm treatment, whether by coiling or clipping. This risk, however, does not translate into longer hospital stays or increased hospital costs. Despite the additional catheterization-related risks of dissection and embolization, coiling results in shorter hospital stays and similar mortality compared with clipping.

ABBREVIATIONS: ADPCKD = autosomal dominant polycystic kidney disease; ICD9-CM = International Classification of Diseases, Ninth Revision, Clinical Modification; NIS = National Inpatient Sample

Autosomal dominant polycystic kidney disease (ADPCKD) is a genetic disorder affecting 1 in 1000 individuals worldwide and is associated with an increased risk of intracranial aneurysms, ranging from 4% to 23%^{1–6} compared with the general population risk of 2%–3%.^{7–10} Patients with ADPCKD are also at increased risk for aneurysm rupture earlier in life (mean age, 35–45 years),^{1,11–13} compared with the general population (mean age, 50–54 years).^{14,15}

There is evidence that the associated vascular defects in

ADPCKD may be due to mutations in the *PKD1* and *PKD2* genes, located on the short arm of chromosomes 16 and 4.^{16,17} Abnormalities of these genes in mouse models correspond with increased rates of arterial dissection, arterial rupture, and intracranial vascular abnormalities.¹⁸ To our knowledge, only 1 study to date has investigated whether these issues engender an increased risk when treating intracranial aneurysms (whether by endovascular coiling or surgical clipping).² The purpose of this investigation was to assess whether ADPCKD confers an increased peri- and immediate postprocedural risk of aneurysm coiling and clipping.

MATERIALS AND METHODS

Data for this study were obtained from the National Inpatient Sample (NIS; <http://www.entnet.org/content/nationwide-inpatient-sample-nis>) provided by the Healthcare Cost and Utilization Project, sponsored by the Agency for Healthcare Research and Quality under the US Department of Health and Human

Received May 18, 2015; accepted after revision June 17.

From the Department of Radiology (M.N.R.), University of Chicago Medical Center, Chicago, Illinois; Department of Radiology (S.A.A., A.S., E.J.R., M.C.H.), Northwestern University Feinberg School of Medicine, Chicago, Illinois; and Department of Radiology (P.M.), University of Miami, Miami, Florida.

Please address correspondence to Michael N. Rozenfeld, DO, Department of Medical Imaging, Ann and Robert H. Lurie Children's Hospital of Chicago, Chicago, IL, 60637; e-mail: michael.rozenfeld@northwestern.edu

<http://dx.doi.org/10.3174/ajnr.A4490>

Services. The NIS is a stratified sample of 20% of all US nonfederal hospitals. Data derived for this study spanned the years 2000–2011.

All patients in this study received a diagnosis of “cerebral aneurysm–nonruptured” (International Classification of Diseases, Ninth Revision, Clinical Modification [ICD9-CM] code 437.3) and a procedural code of either “clipping of aneurysm” (ICD9-CM code 39.51) or any 1 of 3 possible codes for aneurysm coiling: “endovascular total embolization or occlusion of head and neck vessels” (ICD9-CM code 39.72), “endovascular embolization or occlusion of vessels of head and neck by using bare coils” (ICD9-CM code 39.75), or “endovascular embolization or occlusion of vessels of head and neck by using bioactive coils” (ICD9-CM code 39.76). The codes 39.75 and 39.76 were not created until 2009. The ADPCKD group also had a diagnosis of “polycystic kidney disease, autosomal dominant” (ICD9-CM code 753.13), while the control group did not. Patients with a diagnosis of “subarachnoid hemorrhage” (ICD9-CM code 430) were excluded from this study as in prior similar investigations due to the concern of potential coding errors and patients with ruptured intracranial aneurysms being included in our study. Primary end points investigated in this study included in-hospital mortality, length of stay, and total hospital charges. Secondary end points included the diagnoses “iatrogenic cerebrovascular hemorrhage or infarction” (ICD9-CM code 997.02), “intracerebral hemorrhage” (ICD9-CM code 431), “unspecified intracranial hemorrhage” (ICD9-CM code 432.9), “cerebral embolism

with cerebral infarction” (ICD9-CM code 434.11), “dissection of carotid artery” (ICD9-CM code 443.21), and “dissection of vertebral artery” (ICD9-CM code 443.24).

The NIS data were imported into SPSS (IBM, Armonk, New York), and searches were performed by using scripts containing the above codes. Statistical analyses of the data were performed by using χ^2 for categorical variables and *t* test for continuous variables.

RESULTS

During 2000–2011, 189 patients with ADPCKD and unruptured intracranial aneurysms presented for either surgical clipping (*n* = 136) or endovascular coiling (*n* = 53). A control group of 3555 patients without ADPCKD was also analyzed, presenting for either surgical clipping (*n* = 1707) or endovascular coiling (*n* = 1848).

The average age at endovascular coiling in the ADPCKD group was significantly lower than that of the control group (53 versus 58 years) (*P* = .02). The average age at surgical clipping was also significantly lower than that of the control group (50 versus 55 years) (*P* = .00).

There was a mildly increased in-hospital mortality rate in the control group after both coiling and clipping without reaching statistical significance. The mean length of stay was also slightly longer in control subjects compared with patients with ADPCKD after coiling and clipping—only reaching statistical significance in the clipping group. The mean total hospital charges in the control group were significantly greater than those in the ADPCKD group after coiling and clipping (Table 1).

There was a significantly greater incidence of “iatrogenic cerebrovascular hemorrhage or infarction,” “cerebral embolism with cerebral infarction,” and “dissection of carotid artery” in the patients with ADPCKD compared with the control group after endovascular coiling. There was also a significantly greater incidence of “iatrogenic cerebrovascular hemorrhage or infarction” in the ADPCKD group compared with the control group after surgical clipping (Table 2). However, the mean length of hospital stay was not longer in the ADPCKD group, and the total hospital charges were not higher.

Additional analysis within the ADPCKD group revealed a significantly shorter length of stay when the subjects underwent endovascular coiling versus surgical clipping (2.57 versus 5.72 days) (*P* < .01). There was no significant difference in age or total in-hospital charges when comparing clipping and coiling in this population.

DISCUSSION

Our study used the NIS data base to draw from the largest possible sample of patients, and despite the failure of ICD disease codes to fully distinguish primary conditions from adverse events, it suggests that patients with ADPCKD have a significantly increased risk of iatrogenic hemorrhage and infarction, em-

Table 1: Primary end points

	ADPCKD	Controls	P Value
In-hospital mortality			
Coiling	0.0%	0.3%	NS
Clipping	0.0%	0.5%	NS
Mean length of stay (days)			
Coiling	2.57	2.99	NS
Clipping	5.72	6.91	<.01
Mean total hospital charges			
Coiling	\$61,874	\$85,568	<.01
Clipping	\$67,133	\$89,787	<.01

Note:—NS indicates not significant.

Table 2: Secondary end points

	ADPCKD	Controls	P Value
Iatrogenic cerebrovascular hemorrhage or infarction			
Coiling	5 (9.4%)	55 (3.0%)	<.01
Clipping	16 (11.8%)	109 (6.4%)	<.02
Intracerebral hemorrhage			
Coiling	0 (0%)	11 (0.6%)	NS
Clipping	0 (0%)	39 (2.3%)	NS
Unspecified intracranial hemorrhage			
Coiling	0 (0%)	0 (0%)	NS
Clipping	0 (0%)	0 (0%)	NS
Cerebral embolism with cerebral infarction			
Coiling	5 (9.4%)	14 (0.8%)	.00
Clipping	0 (0%)	5 (0.3%)	NS
Dissection of carotid artery			
Coiling	5 (9.4%)	0 (0%)	.00
Clipping	0 (0.0%)	0 (0%)	NS
Dissection of vertebral artery			
Coiling	0 (0%)	0 (0%)	NS
Clipping	0 (0%)	0 (0%)	NS

Note:—NS indicates not significant.

bolic infarction, and carotid artery dissection when undergoing endovascular coiling and a significantly increased risk of iatrogenic hemorrhage or infarction when undergoing surgical clipping. The lack of increased risk of embolic infarction and dissection in the surgical clipping group is presumably due to these adverse outcomes being secondary to catheter manipulation; surgical clipping bypasses the abnormal vessels in these patients.

Patients with ADPCKD undergo aneurysm treatment earlier in life than controls, but it is unclear whether this is because they develop these aneurysms earlier in life or simply because they are detected earlier due to screening.

Most interesting, patients with ADPCKD had a significantly shorter length of hospital stay after clipping compared to patients without ADPCKD and significantly lower in-hospital costs after coiling and clipping. This finding is theorized to be secondary to their lower average age at the time of treatment, which may correlate with fewer comorbidities.

To the authors' knowledge, only 1 similar study to date has been performed.² In that study, which was published in 1992 at a time of presumably higher complication rates, 32 patients with ADPCKD underwent diagnostic cerebral angiography and 25% had transient complications versus 10% in the control group. Two patients with ADPCKD had asymptomatic transient severe occlusive carotid vasospasm, and 1 additional patient had an asymptomatic vertebral artery dissection. The authors of the study concluded that additional caution should be taken in this patient population. Other case reports have also suggested an increased risk of spontaneous dissection of the aorta and internal carotid, vertebral, basilar, and coronary arteries in ADPCKD.^{2,19,20} As with any case report, however, conclusions must be interpreted with caution. Our study builds on this body of knowledge by offering a much larger sample size and additional data analysis and a comparison between endovascular coiling and microsurgical clipping risks.

In our NIS dataset, the in-hospital coiling-related mortality rate in the control group (0.3%) is similar but lower than reported rates in other studies: 2.0%,²¹ 1.8%,²² and 0.6%.²³ Our in-hospital clipping-related mortality rate in the control group (0.5%) is also similar but lower than those reported rates in other studies: 1.8%²¹ and 1.2%.²³ These small differences may be accounted for by a combination of more recent data in our study (2000–2011) and differences in study design ("in-hospital mortality" ICD9 code in our study versus various methods of determining procedure-related mortality in other studies), suggesting accuracy in defining end points with our methodology. Any potential artificial risk reduction compared with other studies would be spread equally across both the ADPCKD and control groups.

While it has been established that there is an increased risk of intracranial aneurysm formation in patients with ADPCKD, screening and treatment algorithms are controversial. Treatment risks have been extensively studied in the general population,^{21–23} but data are sparse regarding the risk in patients with ADPCKD. This study assists in expanding our awareness for this susceptible patient group. Patients with ADPCKD face a significantly increased risk during intracranial aneurysm treatment, whether by clipping or coiling. While this population is exposed to additional risks of embolic infarction and carotid dissection when undergo-

ing endovascular coil embolization, this treatment method was still associated with shorter hospital stays and equivalent in-hospital mortality compared with microsurgical clipping. The final decision of whether to treat, when to treat, and how to treat must be made on an individual patient and aneurysm basis by a multidisciplinary team; the additional overall treatment risks and the additional endovascular catheter-related risks must be considered.

There are limitations in using an administrative data base such as the NIS, given the possibility of coding errors or omissions. Additionally, comorbid patient conditions, patient medications, aneurysm-specific size and anatomy, and/or the complexity of surgical/endovascular treatments cannot be controlled. Unfortunately, there is no way to distinguish a code representing an in-hospital event versus a preadmission event; an issue that may be corrected in ICD-10. ICD-9 codes have, however, been found to have a 66% positive predictive value in correlating with in-hospital adverse events in the surgical population.²⁴ The lack of data on short-term but out-of-hospital mortality is another limitation. It is the authors' opinion that these limitations are at least partially offset by the use of a large dataset, and that any coding errors would be distributed evenly across the patient and control groups.

CONCLUSIONS

Compared with controls, patients with ADPCKD face an increased risk during intracranial aneurysm treatment, whether by endovascular coil embolization or microsurgical clipping. This risk, however, does not translate into longer hospital stays or increased hospital costs. Despite the additional catheterization-related risks of dissection and embolization, coiling results in shorter lengths of stay and no increased risk of mortality compared with clipping.

REFERENCES

1. Schievink WI, Torres VE, Piepgras DG, et al. **Saccular intracranial aneurysms in autosomal dominant polycystic kidney disease.** *J Am Soc Nephrol* 1992;3:88–95 Medline
2. Chapman AB, Rubinstein D, Hughes R, et al. **Intracranial aneurysms in autosomal dominant polycystic kidney disease.** *N Engl J Med* 1992;327:916–20 CrossRef Medline
3. Huston J 3rd, Torres VE, Sulivan PP, et al. **Value of magnetic resonance angiography for the detection of intracranial aneurysms in autosomal dominant polycystic kidney disease.** *J Am Soc Nephrol* 1993;3:1871–77 Medline
4. Rinkel GJ, Djibuti M, Algra A, et al. **Prevalence and risk of rupture of intracranial aneurysms: a systematic review.** *Stroke* 1998;29:251–56 CrossRef Medline
5. Ruggieri PM, Poulos N, Masaryk TJ, et al. **Occult intracranial aneurysms in polycystic kidney disease: screening with MR angiography.** *Radiology* 1994;191:33–39 CrossRef Medline
6. Graf S, Schischma A, Eberhardt KE, et al. **Intracranial aneurysms and dolichoectasia in autosomal dominant polycystic kidney disease.** *Nephrol Dial Transplant* 2002;17:819–23 CrossRef Medline
7. de la Monte SM, Moore GW, Monk MA, et al. **Risk factors for the development and rupture of intracranial berry aneurysms.** *Am J Med* 1985;78:957–64 CrossRef Medline
8. Inagawa T, Hirano A. **Autopsy study of unruptured incidental intracranial aneurysms.** *Surg Neurol* 1990;34:361–65 CrossRef Medline
9. Fox JL. **The incidence of intracranial aneurysm.** In: Fox JL, ed. *Intracranial Aneurysms.* New York: Springer-Verlag; 1983:15–18

10. Stehbens WE. *Pathology of the Cerebral Blood Vessels*. St. Louis: Mosby; 1972:351–470
11. Lozano AM, Leblanc R. **Cerebral aneurysms and polycystic kidney disease: a critical review**. *Can J Neurol Sci* 1992;19:222–27 Medline
12. Chauveau D, Pirson Y, Verellen-Dumoulin C, et al. **Intracranial aneurysms in autosomal dominant polycystic kidney disease**. *Kidney Int* 1994;45:1140–46 CrossRef Medline
13. Chapman AB, Johnson AM, Gabow PA. **Intracranial aneurysms in patients with autosomal dominant polycystic kidney disease: how to diagnose and who to screen**. *Am J Kidney Dis* 1993;22:526–31 CrossRef Medline
14. Hop JW, Rinkel GJ, Algra A, et al. **Case-fatality rates and functional outcome after subarachnoid hemorrhage: a systematic review**. *Stroke* 1997;28:660–64 CrossRef Medline
15. ACROSS Group. **Epidemiology of aneurysmal subarachnoid hemorrhage in Australia and New Zealand: incidence and case fatality from the Australasian Cooperative Research on Subarachnoid Hemorrhage Study (ACROSS)**. *Stroke* 2000;31:1843–50 CrossRef Medline
16. Bichet D, Peters D, Patel AJ, et al. **Cardiovascular polycystins: insights from autosomal dominant polycystic kidney disease and transgenic animal models**. *Trends Cardiovasc Med* 2006;16:292–98 CrossRef Medline
17. Kip SN, Hunter LW, Ren Q, et al. **[Ca²⁺]_i reduction increases cellular proliferation and apoptosis in vascular smooth muscle cells: relevance to the ADPKD phenotype**. *Circ Res* 2005;96:873–80 CrossRef Medline
18. Hassane S, Claij N, Lantinga-van Leeuwen IS, et al. **Pathogenic sequence for dissecting aneurysm formation in a hypomorphic polycystic kidney disease 1 mouse model**. *Arterioscler Thromb Vasc Biol* 2007;27:2177–83 CrossRef Medline
19. Bobrie G, Brunet-Bourgin F, Alamowitch S, et al. **Spontaneous artery dissection: is it part of the spectrum of autosomal dominant polycystic kidney disease?** *Nephrol Dial Transplant* 1998;13:2138–41 CrossRef Medline
20. Itty CT, Farshid A, Talaulikar G. **Spontaneous coronary artery dissection in a woman with polycystic kidney disease**. *Am J Kidney Dis* 2009;53:518–21 CrossRef Medline
21. Wiebers DO, Whisnant JP, Huston J 3rd, et al; International Study of Unruptured Intracranial Aneurysms Investigators. **Unruptured intracranial aneurysms: natural history, clinical outcome, and risks of surgical and endovascular treatment**. *Lancet* 2003;362:103–10 CrossRef Medline
22. Naggara ON, Lecler A, Oppenheim C, et al. **Endovascular treatment of intracranial unruptured aneurysms: a systematic review of the literature on safety with emphasis on subgroup analyses**. *Radiology* 2012;263:828–35 CrossRef Medline
23. Brinjikji W, Rabinstein AA, Nasr DM, et al. **Better outcomes with treatment by coiling relative to clipping of unruptured intracranial aneurysms in the United States, 2001–2008**. *AJNR Am J Neuroradiol* 2011;32:1071–75 CrossRef Medline
24. Houglund P, Nebeker J, Pickard S, et al. **Using ICD-9-CM codes in hospital claims data to detect adverse events in patient safety surveillance**. In: Henriksen K, Battles JB, Keyes MA, et al, eds. *Advances in Patient Safety: New Directions and Alternative Approaches. Vol. 1: Assessment*. Rockville: Agency for Healthcare Research and Quality; 2008. <http://www.ncbi.nlm.nih.gov/books/NBK43647/>. Accessed September 14, 2014

Treatment of Unruptured Intracranial Aneurysms in Autosomal Dominant Polycystic Kidney Disease: Primum Non Nocere

Autosomal dominant polycystic kidney disease (ADPKD) belongs to the most common genetic disorders, with approximately 12.5 million individuals involved worldwide. The disease is a well-known risk factor for intracranial aneurysms (IAs).¹ The rupture of an IA is associated with a high risk of serious complications or death,^{2,3} yet universal screening for IAs in ADPKD remains controversial. It is mainly due to the potential risk connected to pre-emptive treatment of IAs and the cost of screening.⁴

Indeed, according to the study of Rozenfeld et al,⁵ patients with ADPKD have an increased risk for complications during treatment of unruptured IAs compared with the general population. The difference in the complication rate between patients with and without ADPKD is especially striking in cases of endovascular coiling. Most probably, it is attributable to ADPKD-specific, ciliopathy-related, dysfunction of the vascular wall, which is *nota bene* the main pathomechanism of vascular manifestations of ADPKD, including aneurysm formation, hypertension, and others.⁶

However, quitting or reducing screening for IAs is not a solution because screening potentially leads to the protection of life or health of numerous relatively young people; the average age at IA rupture in ADPKD is approximately 40 years, and the risk of death or persistent disability after the rupture is estimated to be almost 50%.^{2,7} On the other hand, most IAs detected by screening are small; thus, the risk for their rupture is low.⁸ Additionally, the risk for progression of IAs in ADPKD is quite low and comparable with that in the general population.^{9,10} Therefore, the key issue is to make decisions on treatment only in patients with substantial risk for IA rupture; in most patients with ADPKD and IA, watchful surveillance is required rather than treatment.

The problem is that the rupture-risk assessment is still challenging. Current treatment guidelines are similar in patients with and without ADPKD.¹¹ However, due to the differences in pathogenesis and clinical characteristics between IAs in ADPKD and the general population, IAs in ADPKD may be considered a distinct clinical entity. Therefore, treatment rules applicable for the general population may not be fully appropriate in ADPKD. There is effort to improve the assessment of risk for IA progression and rupture with clinical and radiographic features¹² and a molecular

biology approach.^{13,14} However, these new risk factors have to be tested in the ADPKD population to verify their utility in this particular group.

Until now, data on risk factors for IA rupture in ADPKD are limited. According to Ring and Spiegelhalter,¹⁵ IA rupture tends to cluster in ADPKD families, which strongly suggests a role of genetic factors, which, however, still need to be identified. Among clinical features, headache was recently proposed as a factor predictive for IA rupture.¹⁶ Most surprising, headache was previously not even considered as an indication for screening for IAs in ADPKD.¹⁷

In summary, considering the relatively low risk for rupture in most IAs in patients with ADPKD and the increased risk of complications connected to their treatment, the treatment decisions must always be cautious and individualized. Additionally, effort should be made to improve the assessment of the IA rupture risk, including searching for ADPKD-specific risk factors.

REFERENCES

1. Chapman AB, Devuyst O, Eckardt KU, et al; Conference Participants. **Autosomal-dominant polycystic kidney disease (ADPKD): executive summary from a Kidney Disease: Improving Global Outcomes (KDIGO) Controversies Conference.** *Kidney Int* 2015;88:17–27 CrossRef Medline
2. Gieteling EW, Rinkel GJ. **Characteristics of intracranial aneurysms and subarachnoid haemorrhage in patients with polycystic kidney disease.** *J Neurol* 2003;250:418–23 CrossRef Medline
3. Zuka M, Onoe T, Kawano M, et al. **Sudden death of a young male with previously undiagnosed autosomal dominant polycystic kidney disease (ADPKD).** *Leg Med (Tokyo)* 2011;13:35–38 CrossRef Medline
4. Klein JP. **On the role of screening for intracranial aneurysms in autosomal dominant polycystic kidney disease.** *AJNR Am J Neuroradiol* 2013;34:1560–61 CrossRef Medline
5. Rozenfeld MN, Ansari SA, Mohan P, et al. **Autosomal dominant polycystic kidney disease and intracranial aneurysms: is there an increased risk of treatment?** *AJNR Am J Neuroradiol* 2015 Sep 3. [Epub ahead of print] CrossRef Medline
6. Rahbari-Oskoui F, Williams O, Chapman A. **Mechanisms and management of hypertension in autosomal dominant polycystic kidney disease.** *Nephrol Dial Transplant* 2014;29:2194–201 CrossRef Medline
7. Chauveau D, Pirson Y, Verellen-Dumoulin C, et al. **Intracranial an-**

- eurysms in autosomal dominant polycystic kidney disease. *Kidney Int* 1994;45:1140–46 CrossRef Medline
8. Xu HW, Yu SQ, Mei CL, et al. **Screening for intracranial aneurysm in 355 patients with autosomal-dominant polycystic kidney disease.** *Stroke* 2011;42:204–06 CrossRef Medline
 9. Irazabal MV, Huston J 3rd, Kubly V, et al. **Extended follow-up of unruptured intracranial aneurysms detected by presymptomatic screening in patients with autosomal dominant polycystic kidney disease.** *Clin J Am Soc Nephrol* 2011;6:1274–85 CrossRef Medline
 10. Jiang T, Wang P, Qian Y, et al. **A follow-up study of autosomal dominant polycystic kidney disease with intracranial aneurysms using 3.0 T three-dimensional time-of-flight magnetic resonance angiography.** *Eur J Radiol* 2013;82:1840–45 CrossRef Medline
 11. Ars E, Bernis C, Fraga G, et al; Spanish Working Group on Inherited Kidney Disease. **Spanish guidelines for the management of autosomal dominant polycystic kidney disease.** *Nephrol Dial Transplant* 2014;29 (suppl 4):iv95–105 CrossRef Medline
 12. Tominari S, Morita A, Ishibashi T, et al; Unruptured Cerebral Aneurysm Study Japan Investigators. **Prediction model for 3-year rupture risk of unruptured cerebral aneurysms in Japanese patients.** *Ann Neurol* 2015;77:1050–59 CrossRef Medline
 13. Zhang LT, Wei FJ, Zhao Y, et al. **Intracranial aneurysm risk factor genes: relationship with intracranial aneurysm risk in a Chinese Han population.** *Genet Mol Res* 2015;14:6865–78 CrossRef Medline
 14. Xu J, Ma F, Yan W, et al. **Identification of the soluble form of tyrosine kinase receptor Axl as a potential biomarker for intracranial aneurysm rupture.** *BMC Neurol* 2015;15:23 CrossRef Medline
 15. Ring T, Spiegelhalter D. **Risk of intracranial aneurysm bleeding in autosomal-dominant polycystic kidney disease.** *Kidney Int* 2007;72:1400–02 CrossRef Medline
 16. Niemczyk M, Niemczyk S, Bujko M, et al. **Headache as a manifestation of intracranial aneurysm in autosomal dominant polycystic kidney disease.** *Neurol Neurochir Pol* 2015;49:126–28 CrossRef Medline
 17. Bajwa ZH, Sial KA, Malik AB, et al. **Pain patterns in patients with polycystic kidney disease.** *Kidney Int* 2004;66:1561–69 CrossRef Medline

M. Niemczyk

Department of Immunology, Transplant Medicine and Internal Diseases
Medical University of Warsaw
Warsaw, Poland

<http://dx.doi.org/10.3174/ajnr.A4538>

REPLY:

We would like to sincerely thank Dr Niemczyk for his commentary on our recent article. We agree that despite the increased risks of aneurysm repair in patients with autosomal dominant polycystic kidney disease (ADPCKD), aneurysm screening programs are beneficial in this population.¹ The issue then arises of how to risk-stratify these patients once aneurysms are discovered. As Dr Niemczyk states, the aneurysms in this patient population must be treated as unique entities and the traditional risk-stratification methods may not be entirely accurate. While it is known that patients with ADPCKD present with subarachnoid hemorrhage earlier in life compared with the general population, once the aneurysm ruptures, they have mortality rates similar to those of the general population.²⁻⁵ Little else is known, however, about the potentially increased risks of rupture in this patient group.

The recently published Unruptured Intracranial Aneurysm Treatment Score lists ADPCKD as an independent risk factor for rupture, with a risk score equivalent to that of hypertension, drug abuse, and Japanese or Finnish ethnicity.⁶ Another recently published PHASES (Population, Hypertension, Age, Size of Aneurysm, Earlier SAH, and Site of Aneurysm) scoring system does not specifically take into account ADPCKD status but does state that Finnish or Japanese ethnicity increases the risk of aneurysm rupture by 2.0–3.6 times.⁷ These findings raise the question of whether patients with ADPCKD should be approached with a treatment paradigm similar to that in these high-risk groups.

We recommend that all treatment-related decisions be made on an aneurysm- and patient-specific basis by multidisciplinary consensus. With this in mind, further research is needed to better risk-stratify aneurysms in patients with ADPCKD.

<http://dx.doi.org/10.3174/ajnr.A4657>

REFERENCES

1. Rozenfeld MN, Ansari SA, Shaibani A, et al. **Should patients with autosomal dominant polycystic kidney disease be screened for cerebral aneurysms?** *AJNR Am J Neuroradiol* 2014;35:3–9 CrossRef Medline
2. de la Monte SM, Moore GW, Monk MA, et al. **Risk factors for the development and rupture of intracranial berry aneurysms.** *Am J Med* 1985;78(6 pt 1):957–64 CrossRef Medline
3. Schievink WI, Torres VE, Piepgras DG, et al. **Saccular intracranial aneurysms in autosomal dominant polycystic kidney disease.** *J Am Soc Nephrol* 1992;3:88–95 Medline
4. Lozano AM, Leblanc R. **Cerebral aneurysms and polycystic kidney disease: a critical review.** *Can J Neurol Sci* 1992;19:222–27 Medline
5. Chapman AB, Johnson AM, Gabow PA. **Intracranial aneurysms in patients with autosomal dominant polycystic kidney disease: how to diagnose and who to screen.** *Am J Kidney Dis* 1993;22:526–31 CrossRef Medline
6. Etmnan N, Brown RD Jr, Beseoglu K, et al. **The unruptured intracranial aneurysm treatment score: a multidisciplinary consensus.** *Neurology* 2015;85:881–89 CrossRef Medline
7. Greving JP, Wermer MJ, Brown RD Jr, et al. **Development of the PHASES score for prediction of risk of rupture of intracranial aneurysms: a pooled analysis of six prospective cohort studies.** *Lancet Neurol* 2014;13:59–66 CrossRef Medline

M.N. Rozenfeld

S.A. Ansari

Department of Radiology

Northwestern University Feinberg School of Medicine

Chicago, Illinois

P. Mohan

Department of Radiology

University of Miami

Miami, Florida

A. Shaibani

E.J. Russell

M.C. Hurley

Department of Radiology

Northwestern University Feinberg School of Medicine

Chicago, Illinois

Cerebral Angiography for Evaluation of Patients with CT Angiogram-Negative Subarachnoid Hemorrhage: An 11-Year Experience

J.J. Heit, G.T. Pastena, R.G. Nogueira, A.J. Yoo, T.M. Leslie-Mazwi, J.A. Hirsch, and J.D. Rabinov

ABSTRACT

BACKGROUND AND PURPOSE: CT angiography is increasingly used to evaluate patients with nontraumatic subarachnoid hemorrhage given its high sensitivity for aneurysms. We investigated the yield of digital subtraction angiography among patients with SAH or intraventricular hemorrhage and a negative CTA.

MATERIALS AND METHODS: An 11-year, single-center retrospective review of all consecutive patients with CTA-negative SAH was performed. Noncontrast head CT, CTA, DSA, and MR imaging studies were reviewed by 2 experienced interventional neuroradiologists and 1 neuroradiologist.

RESULTS: Two hundred thirty patients (mean age, 54 years; 51% male) with CTA-negative SAH were identified. The pattern of SAH was diffuse (40%), perimesencephalic (31%), sulcal (31%), isolated IVH (6%), or identified by xanthochromia (7%). Initial DSA yield was 13%, including vasculitis/vasculopathy (7%), aneurysm (5%), arteriovenous malformation (0.5%), and dural arteriovenous fistula (0.5%). An additional 6 aneurysms/pseudoaneurysms (4%) were identified by follow-up DSA, and a single cavernous malformation (0.4%) was identified by MRI. No cause of hemorrhage was identified in any patient presenting with isolated intraventricular hemorrhage or xanthochromia. Diffuse SAH was due to aneurysm rupture (17%); perimesencephalic SAH was due to aneurysm rupture (3%) or vasculitis/vasculopathy (1.5%); and sulcal SAH was due to vasculitis/vasculopathy (32%), arteriovenous malformation (3%), or dural arteriovenous fistula (3%).

CONCLUSIONS: DSA identifies vascular pathology in 13% of patients with CTA-negative SAH. Aneurysms or pseudoaneurysms are identified in an additional 4% of patients by repeat DSA following an initially negative DSA. All patients with CT-negative SAH should be considered for DSA. The pattern of SAH may suggest the cause of hemorrhage, and aneurysms should specifically be sought with diffuse or perimesencephalic SAH.

ABBREVIATION: IVH = intraventricular hemorrhage

Nontraumatic subarachnoid hemorrhage occurs in 30,000 patients per year in the United States, which accounts for 5% of strokes.¹ Patient mortality approximates 45% within a month after SAH,¹ and the identification of a treatable cause of SAH is imperative.

Cerebral aneurysm rupture accounts for most SAHs,² but a

cause of hemorrhage is not identified in 15%–20% of patients.^{2–4} Prior studies have demonstrated that the pattern of SAH on a noncontrast head CT may predict the probability of identifying a causative vascular lesion, though CT angiography or digital subtraction angiography is needed to identify these lesions.^{5–9}

The evaluation of SAH varies, and no consensus exists as to the best algorithm. Increasingly, CTA is performed in the evaluation of SAH, given its noninvasive nature and wide availability. CTA has a reported a sensitivity of 97%–100% for the detection of intracranial aneurysms.^{10–13} However, it fails to identify a cause for SAH in 5%–30% of patients.^{14,15} DSA remains the criterion standard in the diagnosis of vascular lesions resulting in SAH with a reported sensitivity of 99%.^{16,17} Given the superior sensitivity of DSA and the importance of identifying a treatable cause of SAH, DSA is frequently performed in patients presenting with SAH and negative CTA findings.

Prior studies demonstrated that DSA identifies a cause of SAH

Received May 12, 2015; accepted after revision June 22.

From the Department of Radiology (J.J.H.), Interventional Neuroradiology Division, Stanford University Hospital, Stanford, California; Department of Radiology (G.T.P.), Albany Medical Center, Albany, New York; Departments of Neurology, Neurosurgery, and Radiology (R.G.N.), Emory University School of Medicine, Marcus Stroke and Neuroscience Center, Atlanta, Georgia; Department of Neuroradiology and Interventional Neuroradiology (T.M.L.-M., J.A.H., J.D.R.), Massachusetts General Hospital, Boston, Massachusetts; and Texas Stroke Institute (A.J.Y.), Plano, Texas.

Please address correspondence to James D. Rabinov, MD, Interventional Neuroradiology, Gray 241, Massachusetts General Hospital, 55 Fruit St, Boston, MA 02114; e-mail: jrabinov@partners.org

<http://dx.doi.org/10.3174/ajnr.A4503>

Table 1: Demographic data of patients presenting with subarachnoid or isolated intraventricular hemorrhage without a causative lesion on CTA

	Total	Men	Women
No. of Patients	230	118	112
Mean age (yr)	54	55	54
Age range	19–92	21–92	19–87
SAH found by CT	216	106	110
SAH found by lumbar puncture	14	7	7
Mean time between CTA and DSA (days)	1.5	1.0	2.0
Time range between CTA and DSA (days)	0–110	0–5	0–110
Second follow-up study performed (No. of patients)	169	86	83
Mean time between initial and follow-up study (days)	33	24	42
Time range between initial and follow-up study (days)	0–1836	0–203	0–1836
Second follow-up modality			
CTA	54	28	26
DSA	98	45	53
MRI/MRA	17	10	7

in 4%–14% of patients with negative CTA findings.^{3,4,14,18–20} Moreover, the diagnostic yield of repeat DSA after initially negative DSA findings is reported to be between 4% and 16%.^{14,15,21} We describe our experience with initial and repeat DSA in patients with CTA negative for SAH during an 11-year period at a large neurovascular referral center.

MATERIALS AND METHODS

Patient Selection

We retrospectively reviewed the radiology data base and medical records of all patients who presented to our hospital (Massachusetts General Hospital) during an 11-year period (January 1, 2002, through December 31, 2012) with the following: 1) nontraumatic subarachnoid hemorrhage or isolated intraventricular hemorrhage identified by noncontrast head CT or xanthochromia on lumbar puncture, 2) initial evaluation with a CTA that failed to identify a cause of SAH, and 3) at least 1 cerebral DSA. If an initial cerebral DSA was negative for SAH, patients underwent additional studies.

Follow-up DSA was planned in all patients at an interval of 7–10 days unless there was a contraindication such as arterial dissection or death, and some patients underwent DSA in a shorter time interval due to a clinical deterioration or other evidence of cerebral arterial vasospasm. If a diagnosis was made by a noninvasive imaging study, including CTA or MR imaging/MRA, a follow-up DSA was not performed. Noninvasive imaging studies were performed at the discretion of the physician caring for the patient.

Incidental aneurysms identified by DSA were not considered causative of SAH and comprised additional aneurysms distinct from the ruptured lesions or aneurysms remote from the region of SAH. The study was approved by the institutional review board of our hospital and complied with the Health Insurance Portability and Accountability Act.

Image Acquisition and Analysis

NCCT was performed with standard protocols by using a 16- or 64-section helical CT scanner (LightSpeed; GE Healthcare, Milwaukee, Wisconsin). Axial NCCT images were obtained with 120–140 kV(peak), 170 mA, and 5-mm-section-thickness reconstruction. CTA was performed by axial acquisition from the base of the C1 vertebral body to the vertex by using an 0.5 pitch,

1.25-mm collimation, 350 maximal mA, 120 kVP, and 22-cm FOV. We administered 65–85 mL of iodinated contrast by power injector at 4–5 mL/s into an antecubital vein, and image acquisition was initiated with either a fixed 25-second delay after injection, SmartPrep software (GE Healthcare), or semiautomatic contrast bolus triggering. Axial, coronal, and sagittal maximum-intensity-projection images were available at the time of study review and curvilinear 3D reformations were created by an independent processing laboratory.

MR imaging and MRA were performed on either 1.5T or 3T scanners (Signa 1.5T; GE Healthcare; or Tim Trio 3T; Siemens, Erlangen, Germany) by using standard departmental and vendor protocols.

DSA was performed in a biplane neuroangiography suite (Axioim Artis; Siemens) following transfemoral arterial access under intravenous conscious sedation or general anesthesia. Biplanar DSA images were obtained after selective catheterization of the bilateral common carotid arteries and at least 1 vertebral artery and injection with iodinated contrast. Additional selective injection of the internal, external, or contralateral vertebral artery was performed at the discretion of the neurointerventionalist. 3D rotational angiography was performed at the discretion of the interventional neuroradiologist. Standard views typically included frontal, lateral, and oblique views of each selected vessel.

All NCCT, CTA, and DSA images were independently reviewed by 2 interventional neuroradiologists and 1 neuroradiologist to determine the presence and pattern of SAH, including the following: 1) absence of SAH, or 2) perimesencephalic, 3) sulcal, and 4) diffuse SAH. Perimesencephalic SAH was considered largely within the interpeduncular, prepontine, ambient, quadrigeminal plate or premedullary cistern with minimal extension into the medial Sylvian fissures. This imaging review was performed near the end of the 11-year study period when the manuscript was being prepared. The presence of intraventricular hemorrhage (IVH) was also identified. CTA images were reviewed for a vascular cause of SAH. If vessel irregularity was identified, DSA was performed to determine whether the irregularity represented vasospasm in the region of SAH versus a vasculitis or vasculopathy and for the presence of an aneurysm. If an aneurysm was identified by DSA after a CTA negative for SAH, the CTA was reviewed retrospectively. These studies were included as false-negative ones.

Medical Record Review

Patient demographic information and clinical outcome were reviewed in the electronic Longitudinal Medical Record system available at our hospital.

Statistical Analysis

Statistical analysis was performed by using Excel (Microsoft, Redmond, Washington) and XLSTAT (Addinsoft, New York, New York). A *P* value of .05 was statistically significant.

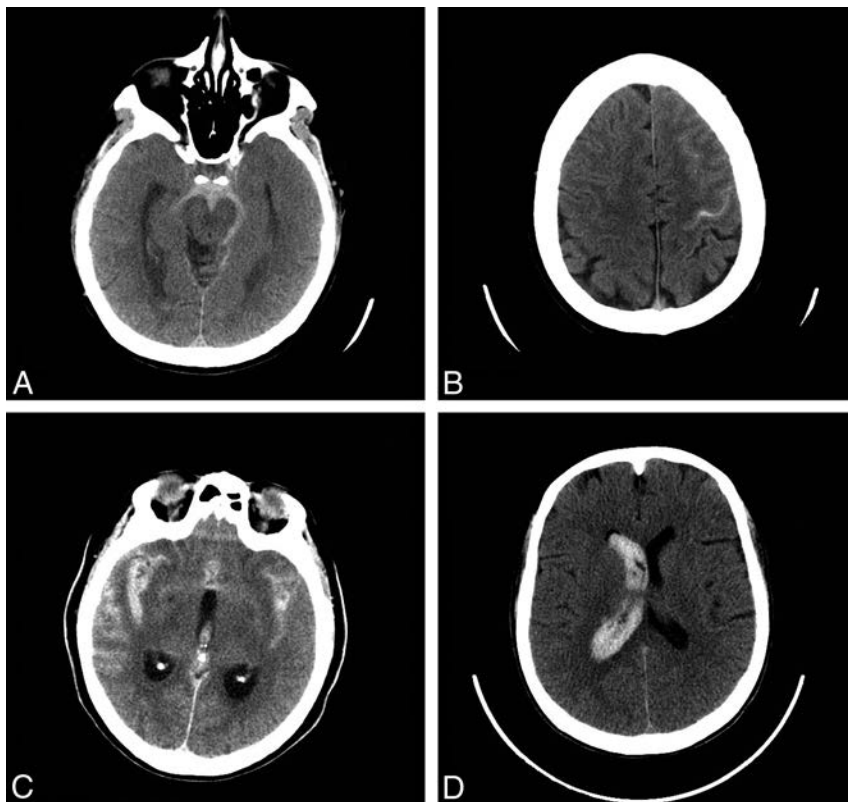


FIG 1. Noncontrast head CT examples of SAH. Perimesencephalic SAH: axial image from a noncontrast head CT demonstrates acute SAH in the prepontine and interpeduncular cistern, consistent with a perimesencephalic pattern of SAH (A). Sulcal SAH: axial image from a noncontrast head CT demonstrates acute SAH in the left precentral sulcus and in the sulci overlying the left middle frontal gyrus, consistent with a sulcal pattern of SAH (B). Diffuse SAH: axial image from a noncontrast head CT demonstrates acute SAH in the bilateral Sylvian fissures, overlying the sulci of the bilateral temporal lobes, consistent with a diffuse pattern of SAH. Note also intraventricular hemorrhage within the third ventricle (C). Isolated IVH: axial image from a noncontrast head CT demonstrates acute intraventricular hemorrhage casting the right lateral ventricle (D).

Table 2: Pattern of subarachnoid hemorrhage and the presence of intraventricular hemorrhage

	All	Men	Women
Pattern of SAH			
None	29 (13%)	15 (14%)	14 (12%)
Perimesencephalic	71 (31%)	38 (34%)	33 (28%)
Sulcal	37 (16%)	15 (14%) ^a	22 (18%)
Diffuse	93 (40%)	43 (39%)	50 (42%)
Xanthochromia on lumbar puncture	16 (7%)	8 (7%)	8 (7%)
Isolated intraventricular hemorrhage	13 (6%)	7 (6%)	6 (5%)

^a $P = .0001$ by Fisher exact test.

RESULTS

From January 1, 2002, to December 31, 2012, 1288 patients presented with nontraumatic SAH. CTA identified an aneurysm as the cause of SAH in 1058 patients (82%), and the CTAs typically provided sufficient data for treatment triage by microsurgical clipping or endovascular coil embolization. The 1058 patients with aneurysms identified by CTA were excluded from the analysis. The remaining 230 patients had SAH or isolated IVH and a CTA that failed to reveal a causative lesion. These 230 patients (17.9% of patients with SAH) included 118 men (51%) and 112 women (49%), and the average patient age was 54 years (Table 1).

SAH was identified by CT in 216 patients (94%) and by CSF xanthochromia on lumbar puncture in 14 patients (6%). In

patients with SAH identified by CT, the SAH distribution was perimesencephalic in 71 patients (31%), sulcal in 37 patients (16%), and diffuse in 93 patients (40%). Representative imaging examples of each type of SAH are shown in Fig 1. Sulcal SAH was identified in 22 women and 15 men (18% and 14%, respectively; $P < .001$), and there was no significant difference in the prevalence of other distributions of SAH between men and women (Table 2). Isolated IVH was identified in 13 patients (6%) by CT (Table 2).

All 230 patients underwent an initial cerebral DSA within a mean of 1.5 days (median, 1 day; range, 0–14 days; and a single outlier performed at 110 days). These studies identified a causative lesion for SAH in 29 patients (13%), including 12 aneurysms (5%), 15 cases of vasculitis or vasculopathy (7%), 1 arteriovenous malformation (0.05%), and 1 dural arteriovenous fistula (0.05%). Vasculitis or vasculopathy (Fig 2) was identified in 11 female patients and 4 men (73% and 27%, respectively; $P = .03$), and there was no significant difference in the prevalence of other causative lesions between men and women (Table 3).

No causative lesion for SAH was identified by initial DSA, CTA, or MR imaging in patients with xanthochromia

on lumbar puncture and no CT evidence of SAH (16 patients, Table 4). Similarly, no causative lesion for SAH was identified by DSA, CTA, or MR imaging in patients with isolated IVH (13 patients, Table 4).

In patients with perimesencephalic SAH (71 patients), 2 aneurysms (3%) and 1 case of vasculitis/vasculopathy (1.5%) were identified (Table 4). However, no source of the hemorrhage was identified in 68 of these patients (96%). By contrast, in patients presenting with sulcal SAH (37 patients), 12 cases of vasculitis/vasculopathy (30%), 1 AVM (3%), and 1 dural AVF (3%) were identified. No aneurysms were identified that resulted in a sulcal pattern of SAH. In patients with diffuse SAH (93 patients), 16 aneurysms (17%) and no other vascular lesions were identified.

Additional studies were performed in 169 patients who had an initial CTA negative for SAH and DSA, including repeat DSA (98 patients), repeat CTA (54 patients), MR imaging/MRA (17 patients), or a combination of these modalities. These follow-up studies were performed within a mean of 33 days (median, 8 days; range, 0–252 days with an outlier at 1836 days; Table 1). A causative lesion for SAH was identified through these follow-up studies in an additional 7 patients (4%). Six de novo aneurysms/pseudoaneurysms were identified by CTA (and subsequently also by DSA, Figs 3 and 4), and all 6



FIG 2. Cerebral arterial vasculitis identified on DSA. A 45-year-old woman who presented with sulcal SAH (arrow) isolated to the left Sylvian fissure (A). A CTA at the time of admission demonstrated multifocal arterial narrowing (arrowheads) within the bilateral anterior and middle cerebral arteries (B). DSA identified more extensive bilateral arterial irregularity with multifocal narrowing and dilation that was consistent with vasculitis.

Table 3: Diagnosis as determined by digital subtraction angiography

	All	Men	Women
Diagnosis after initial DSA			
No causative lesion	201 (87%)	110 (55%) ^a	91 (45%)
Aneurysm	12 (5%)	3 (25%)	9 (75%)
Arteriovenous malformation	2 (1%)	1 (50%)	1 (50%)
Arteriovenous fistula	1 (0.5%)	1 (100%)	0 (0%)
Vasculitis/vasculopathy	15 (7%)	3 (21) ^b	11 (79%)

^a $P = .01$ by Fisher exact test.

^b $P = .03$ by Fisher exact test.

patients initially presented with a diffuse pattern of SAH. One cavernous malformation was identified by MR imaging in a patient who presented with xanthochromia (Table 5).

The neurologic complication rate from diagnostic cerebral angiography was <0.5% in all patients.

DISCUSSION

The use of CTA as a primary imaging and triage technique in patients presenting with SAH results in decreased time to diagnosis and reduced medical costs.²² At our large neurovascular referral center, all patients presenting with SAH undergo a CTA of the head, and this technique identified an aneurysm as the cause of SAH in 82% of patients during an 11-year period. For much of this period, the bulk of patients who underwent subsequent craniotomy for ruptured aneurysms did not undergo preoperative DSA examination.

We investigated the yield of DSA in the remaining 230 patients with SAH and a negative initial evaluation by CTA (17.9% of all patients presenting with nontraumatic SAH). Initial DSA determined the cause of SAH in 13% of these patients, corresponding to a 13% false-negative rate of CTA, which is similar to that in prior studies.^{7,23,24} By contrast, other studies have found a lower yield of 4%–7% of DSA in patients with SAH and a negative initial evaluation by CTA,^{5,6,25} possibly reflecting differences in patient populations. 3D rotational angiography was not routinely performed, and the benefit of this technique in the evaluation of SAH remains controversial.^{26,27} These data further underscore the importance of pursuing DSA in patients with CTA negative for SAH to identify a treatable vascular pathology.

Vascular Lesions Resulting in SAH

The most common identified cause of SAH in our series was vasculitis or vasculopathy, including Call-Flemming or reversible cerebral vasoconstriction syndrome, which accounted for 7% of the abnormalities identified on the initial DSA (Fig 2). Vascular narrowing and irregularity on DSA may also be seen in patients with vasospasm following SAH. However, vasospasm typically occurs 3–5 days after initial intracranial hemorrhage, is most commonly observed after rupture of an intracranial aneurysm, and is most strongly correlated with a diffuse pattern of SAH.²⁸ By contrast, the vascular narrowing and irregularity identified in our series was identified by DSA performed within the first 2 days of presentation with SAH. Moreover, the pattern of SAH in patients with vasculitis or vasculopathy was sulcal (11 patients) or perimesencephalic (1 patient), and these patterns are less commonly associated with vasospasm than diffuse patterns of hemorrhage. These differences strongly suggest that the vascular narrowing and irregularity in these patients are most consistent with a primary vascular pathology rather than vasospasm.

The second most frequent cause of SAH in our series was rupture of an intracranial aneurysm (12 patients; 5%). Repeat DSA identified an additional 6 patients with de novo aneurysms or pseudoaneurysms. Thus, aneurysms were identified in 18 patients, which accounts for an 8% yield of DSA for this pathology. Types of aneurysms that may potentially be missed by initial CTA include small bifurcation aneurysms or those on a curve of a vessel, dissecting aneurysms (Fig 3), perforator aneurysms (Fig 4), and small infectious or myxomatous aneurysms. This yield of initial DSA is slightly higher than that in prior studies, which identified aneurysms in approximately 2% of patients with CTA negative for SAH.^{5,7} This discrepancy in the yield of DSA for the detection of aneurysms may reflect differences in the patient populations, the size of patient cohorts, or even differences in the sensitivity of CTA for aneurysms among different centers.

Vascular lesions resulting in abnormal arteriovenous shunting, including AVMs and dural AVFs, were uncommonly identified by DSA in our series. Only 1 AVM and 1 dural AVF were identified, both of which presented with a sulcal pattern of SAH. The relative rarity of AVMs and AVFs in our series may reflect the

Table 4: Subarachnoid hemorrhage pattern and final diagnosis^a

	Pattern of SAH				
	No SAH ^b	Perimesencephalic	Sulcal	Diffuse	IVH
No source identified	0	68 (96%)	24 (65%)	79 (85%)	13 (100%)
Aneurysm/pseudoaneurysm	0	2 (3%)	0	16 (17%)	0
AVF	0	0	1 (3%)	0	0
AVM	0	0	1 (3%)	0	0
Vasculitis	0	1 (1.5%)	12 (32%)	0	0
Cavernous malformation	1 (3%)	0	0	0	0

^a Percentages reflect patient percentage with a vascular pathology within each SAH pattern.

^b "No SAH" refers to patients with xanthochromia or isolated IVH.

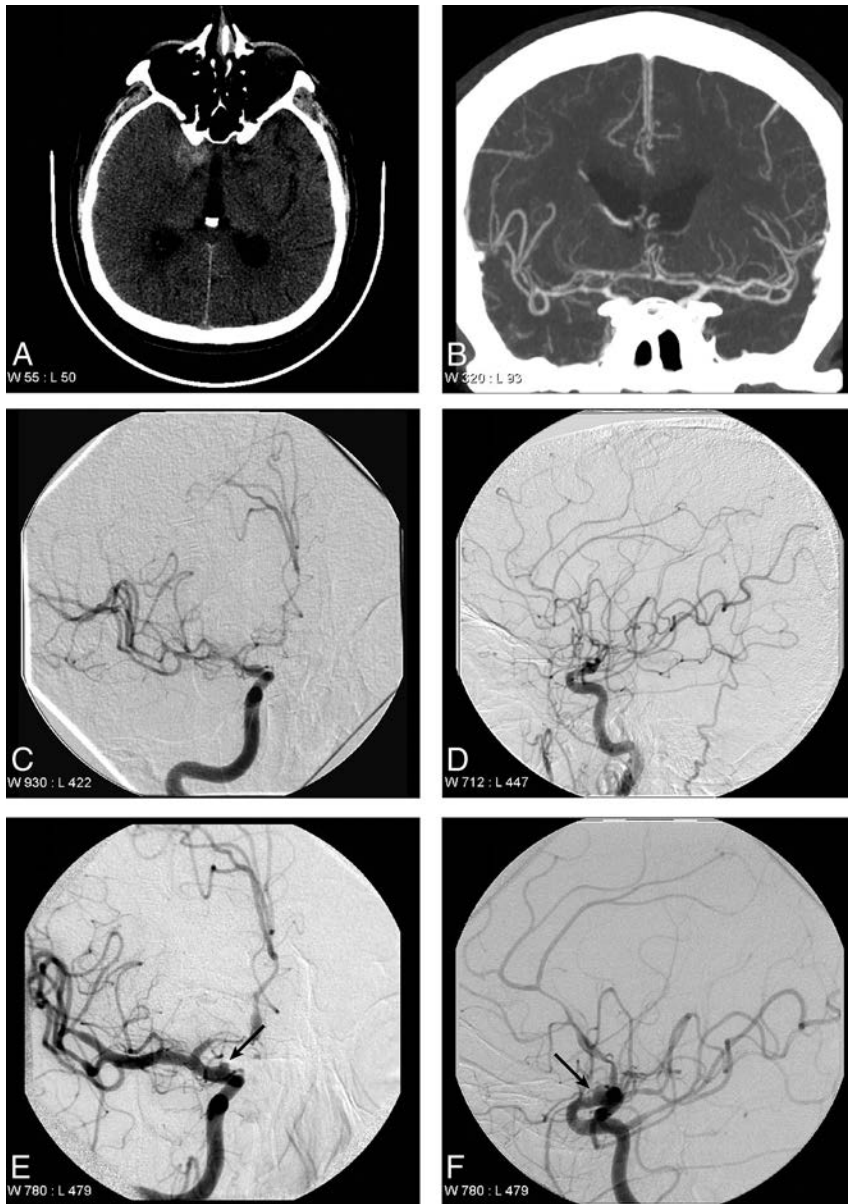


FIG 3. Supraclinoid internal carotid artery aneurysm identified on repeat DSA. A 72-year-old man who presented with perimesencephalic SAH that is localized near the right clinoid process (A). An initial CTA performed on the day of presentation did not identify a lesion responsible for the SAH (B). DSA performed on the day after presentation demonstrates relative narrowing of the right supraclinoid internal carotid artery, the right middle cerebral artery, and the right anterior cerebral artery in the anteroposterior (C) and lateral (D) projections, which was thought to represent early vasospasm. A follow-up DSA was performed 7 days after presentation, which demonstrates an irregular saccular outpouching (arrows) arising from the supraclinoid internal carotid artery in the anteroposterior (E) and lateral (F) projections, consistent with a dissecting aneurysm.

high sensitivity of CTA for the detection of these lesions, which would lead to their exclusion in our study. Moreover, patients with ruptured AVMs frequently present with intraparenchymal hemorrhage and SAH. At our institution, patients with intraparenchymal hemorrhage most often undergo MR imaging to exclude the presence of an underlying mass lesion. Our MR imaging protocols include advanced sequences such as arterial spin-labeling and susceptibility-weighted imaging, which have been shown to be very sensitive for arteriovenous shunting.^{29,30} Based on this diagnostic algorithm, a presumptive diagnosis of an AVM or dural AVF is typically made by CTA and MR imaging at our institution, which likely accounts for the relative paucity of these lesions in this series.

Patterns of SAH and Cause of Hemorrhage

In our series, the distribution of SAH was diffuse (40%), perimesencephalic (31%), sulcal (16%), or identified by lumbar puncture (13%), which is similar to the distribution identified in prior studies.^{5,7,20} Similar to authors in prior studies,^{2,13} we found the distribution of SAH to be highly correlated with specific vascular lesions, as described in detail below.

The yield of DSA in patients with diffuse SAH was 17%, which is similar to the 10%–15% in prior studies.^{5,7} Aneurysms were the only pathology identified that resulted in diffuse SAH, and most of these aneurysms (12 patients; 13%) were identified on initial DSA. However, 6 additional de novo aneurysms/pseudoaneurysms were identified on repeat DSA in patients with diffuse SAH (see below). Therefore, we recommend careful inspection for the presence of aneurysms in patients presenting with diffuse SAH.

By contrast, the yield of DSA in patients presenting with perimesencephalic hemorrhage was 4.5%, which is similar to the 0%–5% yield in prior studies.^{5,7–9} Perimesencephalic SAH typically correlates with a more benign clinical course compared with other patterns of SAH and is the least likely pattern to result in a positive finding on DSA.^{2,31} Several studies have argued that no further investigation is necessary

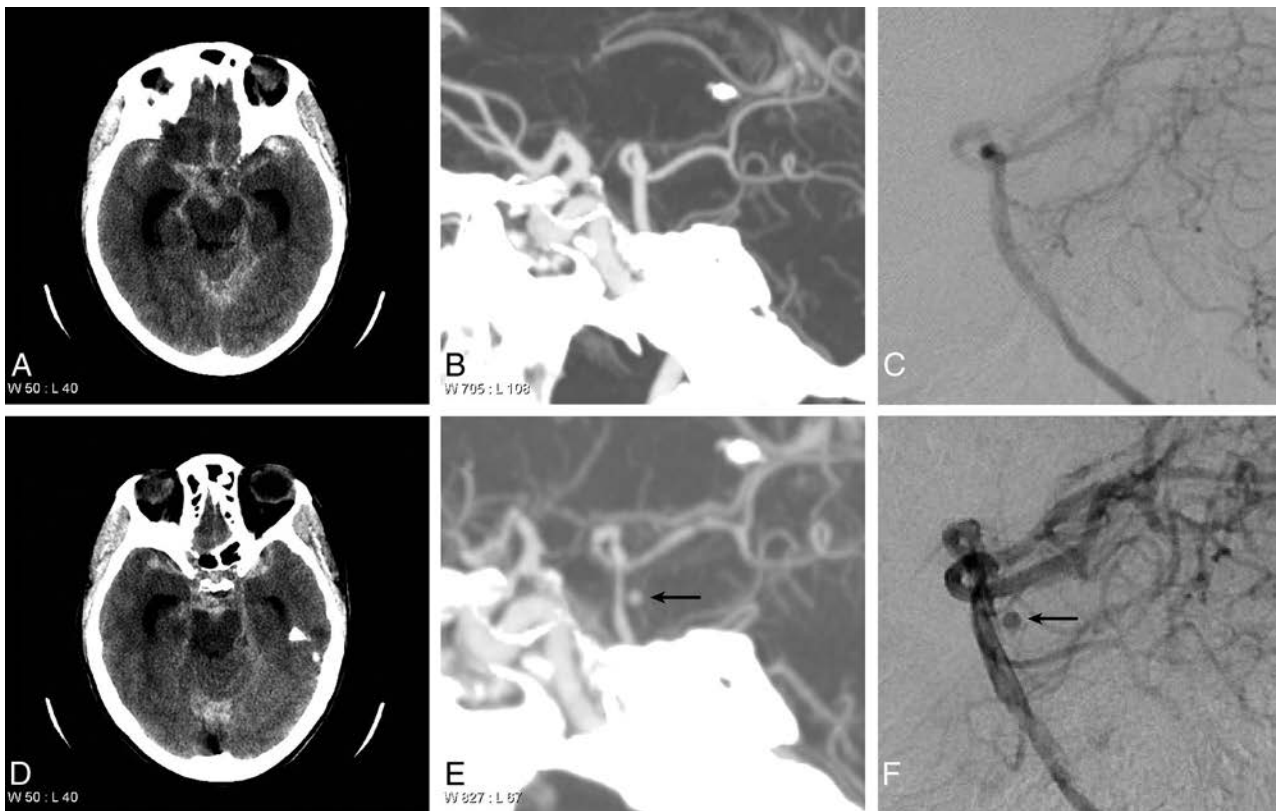


FIG 4. Basilar artery aneurysm identified on repeat CTA and DSA. A 65-year-old woman who presented with diffuse SAH in the basal cisterns and bilateral Sylvian fissures. Note hydrocephalus (A and D). A maximum-intensity-projection image from a CTA (B) and a DSA (C) performed on the day of presentation demonstrate no evidence of an aneurysm arising from the basilar artery. A follow-up CTA (E) and DSA (F) performed 7 days after presentation demonstrate an aneurysm arising from the posterior aspect of the basilar artery, consistent with a perforator artery aneurysm.

Table 5: Additional diagnosis identified on follow-up CTA, DSA, or MRI

	All	Men	Women
Total No. of patients undergoing follow-up studies	169	86	83
Additional diagnosis after follow-up studies:			
Aneurysm/pseudoaneurysm	6 (4%)	3 (3%)	3 (4%)
Cavernous malformation	1 (0.6%)	0 (0%)	1 (1%)

in patients with CTA negative for SAH based on a negative yield of DSA in their series.^{5,9} By contrast, we and others^{2,3} have found that though the yield of DSA was low in these patients, an aneurysm was responsible for perimesencephalic SAH in 3% of patients. We also found a single case of vasculitis accounting for perimesencephalic SAH, which resulted in an active change to the clinical management of this patient. On the basis of these data and the low risk of DSA, we recommend that all patients presenting with CTA negative for perimesencephalic SAH continue to undergo DSA.

A sulcal pattern of SAH resulted in the highest yield of DSA, with a finding rate of 38%. Similar to a prior study,⁶ nearly one-third (32%) of patients with sulcal SAH were found to have vasculitis or vasculopathy. We found a single AVM and a single dural AVF that resulted in a sulcal pattern of SAH. No aneurysms resulted in sulcal SAH. All of these vascular pathologies were identified on the initial DSA, suggesting that follow-up DSA is not

required for diagnostic purposes in patients presenting with sulcal SAH. Most interesting, sulcal SAH was significantly more likely to be found in women. Although the reported incidence of central nervous system vasculitis is equal among men and women,³² other cerebral vasculopathies, including reversible cerebral vasoconstriction syndrome, are more common in women, which may account for this difference in our series.³³

The yield of DSA in patients with either xanthochromia or isolated IVH was zero in our series. However, prior studies have found aneurysms as a cause of xanthochromia in approximately 8% of patients.³⁴ Similarly, prior studies have found a high yield of DSA in patients with isolated IVH, though the sensitivity of CTA in the setting of isolated IVH has been poorly described.³⁵ Therefore, at least 1 DSA is prudent in these patients.

Follow-Up Diagnostic Studies

At our institution, patients with CTA negative for SAH and negative findings on initial DSA undergo further imaging evaluation. We found an additional 6 aneurysms/pseudoaneurysms in 169 patients on repeat DSA performed 1 week after the initial DSA (4% detection rate). Similarly, prior studies have found a repeat DSA yield of 4%–16% in patients presenting with SAH and an initial CTA and DSA negative for SAH.^{7,20,23,24,36} Nondetection of a ruptured aneurysm on initial DSA may be due to vasospasm of the parent vessel, compression of the aneurysm by an adjacent hematoma, development of a de novo aneurysm/pseudoaneu-

rysm, or a small size of the aneurysm in combination with these factors.³⁷ Most interesting, the 6 aneurysms found on repeat DSA were also prospectively identified by repeat CTA that was performed for vasospasm triage purposes before the repeat DSA. It would be of interest to determine the sensitivity of CTA in the delayed detection of a ruptured aneurysm among a greater number of patients.

An MR imaging performed after a negative initial DSA identified a cortical cavernous malformation as a cause of SAH in a single patient. This patient initially presented with an acute headache and NCCT that was negative for intracranial hemorrhage. Xanthochromia was identified by lumbar puncture, which eventually led to the diagnosis. Cavernous malformations have previously been identified as a cause of perimesencephalic SAH,³⁸ though SAH is an uncommon presentation of these lesions.

Limitations

The limitations of this study include a selection bias due to the study occurring at a large tertiary care and neurovascular referral center and the retrospective nature of the study. This selection bias may limit the generalizability of our findings.

CONCLUSIONS

Careful evaluation of patients presenting with CTA negative for SAH should include DSA, even in case of perimesencephalic SAH, given the significant 13% yield of DSA in identifying a vascular pathology that resulted in the hemorrhage. Furthermore, continued investigation is prudent by CTA, DSA, and/or MR imaging in patients with an initial DSA negative for SAH after a CTA negative for SAH, given a 4% yield of these follow-up studies.

Disclosures: Raul G. Nogueira—UNRELATED: Consultancy: Covidien (Study of Tamoxifen and Raloxifene Trial core lab); OTHER RELATIONSHIPS: Stryker/Concentric Medical: Trevo 2 Trial Principal Investigator, DWI/PWI and CTP Assessment in the Triage of Wake-Up and Late Presenting Strokes Undergoing Neurointervention Trial Principal Investigator (unpaid); Covidien/ev3: Solitaire Flow Restoration Device versus the Merci Retriever in Patients with Acute Ischaemic Stroke; and Solitaire With the Intention For Thrombectomy as PRIMARY Endovascular Treatment Trials Steering Committee (unpaid); Covidien: 3D Separator Trial Executive Committee (unpaid). Joshua A. Hirsch—UNRELATED: Consultancy: Medtronic, CareFusion, Comments: Medtronic, ongoing consultancy concerning interventional spine; CareFusion, taught a non-Continuing Medical Education course; Stock/Stock Options: Intratech, Brainstorm.

REFERENCES

1. Bederson JB, Connolly ES Jr, Batjer HH, et al; American Heart Association. **Guidelines for the management of aneurysmal subarachnoid hemorrhage: a statement for healthcare professionals from a special writing group of the Stroke Council, American Heart Association.** *Stroke* 2009;40:994–1025 CrossRef Medline
2. Rinkel GJ, Wijdicks EF, Hasan D, et al. **Outcome in patients with subarachnoid haemorrhage and negative angiography according to pattern of haemorrhage on computed tomography.** *Lancet* 1991; 338:964–68 CrossRef Medline
3. Duong HH, Melançon DD, Tampieri DD, et al. **The negative angiogram in subarachnoid haemorrhage.** *Neuroradiology* 1996;38:15–19 CrossRef Medline
4. Kaim A, Prose M, Kirsch E, et al. **Value of repeat-angiography in cases of unexplained subarachnoid hemorrhage (SAH).** *Acta Neurol Scand* 1996;93:366–73 Medline
5. Agid R, Andersson T, Almqvist H, et al. **Negative CT angiography findings in patients with spontaneous subarachnoid hemorrhage:**

when is digital subtraction angiography still needed? *AJNR Am J Neuroradiol* 2010;31:696–705 CrossRef Medline

6. Agid R, Lee SK, Willinsky RA, et al. **Acute subarachnoid hemorrhage: using 64-slice multidetector CT angiography to “triage” patients’ treatment.** *Neuroradiology* 2006;48:787–94 CrossRef Medline
7. Delgado Almandoz JE, Crandall BM, Fease JL, et al. **Diagnostic yield of catheter angiography in patients with subarachnoid hemorrhage and negative initial noninvasive neurovascular examinations.** *AJNR Am J Neuroradiol* 2013;34:833–39 CrossRef Medline
8. Schievink WI, Wijdicks EF. **Pretruncal subarachnoid hemorrhage: an anatomically correct description of the perimesencephalic subarachnoid hemorrhage.** *Stroke* 1997;28:2572 Medline
9. Cruz JP, Sarma D, Noel de Tilly L. **Perimesencephalic subarachnoid hemorrhage: when to stop imaging?** *Emerg Radiol* 2011;18:197–202 CrossRef Medline
10. Fox AJ, Symons SP, Aviv RI. **CT angiography is state-of-the-art first vascular imaging for subarachnoid hemorrhage.** *AJNR Am J Neuroradiol* 2008;29:e41–42; author reply e46–47 CrossRef Medline
11. Prestigiacomo CJ, Sabit A, He W, et al. **Three dimensional CT angiography versus digital subtraction angiography in the detection of intracranial aneurysms in subarachnoid hemorrhage.** *J Neurointerv Surg* 2010;2:385–89 CrossRef Medline
12. Kershenovich A, Rappaport ZH, Maimon S. **Brain computed tomography angiographic scans as the sole diagnostic examination for excluding aneurysms in patients with perimesencephalic subarachnoid hemorrhage.** *Neurosurgery* 2006;59:798–801; discussion 801–02 CrossRef Medline
13. Kelliny M, Maeder P, Binaghi S, et al. **Cerebral aneurysm exclusion by CT angiography based on subarachnoid hemorrhage pattern: a retrospective study.** *BMC Neurol* 2011;11:8 CrossRef Medline
14. Bradac GB, Bergui M, Ferrio MF, et al. **False-negative angiograms in subarachnoid haemorrhage due to intracranial aneurysms.** *Neuroradiology* 1997;39:772–76 CrossRef Medline
15. Urbach H, Zentner J, Solymosi L. **The need for repeat angiography in subarachnoid haemorrhage.** *Neuroradiology* 1998;40:6–10 CrossRef Medline
16. Luo Z, Wang D, Sun X, et al. **Comparison of the accuracy of subtraction CT angiography performed on 320-detector row volume CT with conventional CT angiography for diagnosis of intracranial aneurysms.** *Eur J Radiol* 2012;81:118–22 CrossRef Medline
17. Yeung R, Ahmad T, Aviv RI, et al. **Comparison of CTA to DSA in determining the etiology of spontaneous ICH.** *Can J Neurol Sci* 2009; 36:176–80 CrossRef Medline
18. Forster DM, Steiner LL, Hakanson SS, et al. **The value of repeat pan-angiography in cases of unexplained subarachnoid hemorrhage.** *J Neurosurg* 1978;48:712–16 CrossRef Medline
19. Huttner HB, Hartmann M, Köhrmann M, et al. **Repeated digital subtraction angiography after perimesencephalic subarachnoid hemorrhage?** *J Neuroradiol* 2006;33:87–89 CrossRef Medline
20. Jung JY, Kim YB, Lee JW, et al. **Spontaneous subarachnoid haemorrhage with negative initial angiography: a review of 143 cases.** *J Clin Neurosci* 2006;13:1011–17 CrossRef Medline
21. Nishioka H, Torner JC, Graf CJ, et al. **Cooperative study of intracranial aneurysms and subarachnoid hemorrhage: a long-term prognostic study, III: subarachnoid hemorrhage of undetermined etiology.** *Arch Neurol* 1984;41:1147–51 CrossRef Medline
22. Hoh BL, Cheung AC, Rabinov JD, et al. **Results of a prospective protocol of computed tomographic angiography in place of catheter angiography as the only diagnostic and pretreatment planning study for cerebral aneurysms by a combined neurovascular team.** *Neurosurgery* 2004;54:1329–40; discussion 1340–42 CrossRef Medline
23. Delgado Almandoz JE, Jagadeesan BD, Refai D, et al. **Diagnostic yield of repeat catheter angiography in patients with catheter and computed tomography angiography negative subarachnoid hemorrhage.** *Neurosurgery* 2012;70:1135–42 CrossRef Medline

24. Topcuoglu MA, Ogilvy CS, Carter BS, et al. **Subarachnoid hemorrhage without evident cause on initial angiography studies: diagnostic yield of subsequent angiography and other neuroimaging tests.** *J Neurosurg* 2003;98:1235–40 CrossRef Medline
25. Dalyai R, Chalouhi N, Theofanis T, et al. **Subarachnoid hemorrhage with negative initial catheter angiography: a review of 254 cases evaluating patient clinical outcome and efficacy of short- and long-term repeat angiography.** *Neurosurgery* 2013;72:646–52; discussion 651–52 CrossRef Medline
26. Ringelstein A, Mueller O, Mönninghoff C, et al. **3D rotational angiography after non-traumatic SAH.** *Rofo* 2014;186:675–79 CrossRef Medline
27. van Rooij WJ, Peluso JP, Sluzewski M, et al. **Additional value of 3D rotational angiography in angiographically negative aneurysmal subarachnoid hemorrhage: how negative is negative?** *AJNR Am J Neuroradiol* 2008;29:962–66 CrossRef Medline
28. Fisher CM, Kistler JP, Davis JM. **Relation of cerebral vasospasm to subarachnoid hemorrhage visualized by computerized tomographic scanning.** *Neurosurgery* 1980;6:1–9 CrossRef Medline
29. Jagadeesan BD, Delgado Almandoz JE, Moran CJ, et al. **Accuracy of susceptibility-weighted imaging for the detection of arteriovenous shunting in vascular malformations of the brain.** *Stroke* 2011;42:87–92 CrossRef Medline
30. Zaharchuk G, Bammer R, Straka M, et al. **Arterial spin-label imaging in patients with normal bolus perfusion-weighted MR imaging findings: pilot identification of the borderzone sign.** *Radiology* 2009;252:797–807 CrossRef Medline
31. van Gijn J, van Dongen KJ, Vermeulen M, et al. **Perimesencephalic hemorrhage: a nonaneurysmal and benign form of subarachnoid hemorrhage.** *Neurology* 1985;35:493–97 CrossRef Medline
32. Salvarani C, Brown RD Jr, Calamia KT, et al. **Primary central nervous system vasculitis: analysis of 101 patients.** *Ann Neurol* 2007;62:442–51 CrossRef Medline
33. Singhal AB, Hajj-Ali RA, Topcuoglu MA, et al. **Reversible cerebral vasoconstriction syndromes: analysis of 139 cases.** *Arch Neurol* 2011;68:1005–12 CrossRef Medline
34. Wallace AN, Dines JN, Zipfel GJ, et al. **Yield of catheter angiography after computed tomography negative, lumbar puncture positive subarachnoid hemorrhage [corrected].** *Stroke* 2013;44:1729–31 CrossRef Medline
35. Flint AC, Roebken A, Singh V. **Primary intraventricular hemorrhage: yield of diagnostic angiography and clinical outcome.** *Neurocrit Care* 2008;8:330–36 CrossRef Medline
36. Maslehaty HH, Barth HH, Petridis AKA, et al. **Special features of subarachnoid hemorrhage of unknown origin: a review of a series of 179 cases.** *Neurol Res* 2012;34:91–97 CrossRef Medline
37. van Gijn J, Rinkel GJ. **Subarachnoid haemorrhage: diagnosis, causes and management.** *Brain* 2001;124:249–78 CrossRef Medline
38. Yaghi S, Oomman S, Keyrouz SG. **Non-aneurysmal perimesencephalic subarachnoid hemorrhage caused by a cavernous angioma.** *Neurocrit Care* 2011;14:84–85 CrossRef Medline

Stent Retriever Thrombectomy in Patients Who Are Ineligible for Intravenous Thrombolysis: A Multicenter Retrospective Observational Study

F. Dorn, S. Prothmann, M. Patzig, H. Lockau, C. Kabbasch, O. Nikoubashman, T. Liebig, C. Zimmer, H. Brückmann, M. Wiesmann, H. Stetefeld, H. Poppert, A. Reich, L. Kellert, and G. Fesl

ABSTRACT

BACKGROUND AND PURPOSE: Intravenous thrombolysis with rtPA is the standard of care for patients with acute ischemic stroke within 4.5 hours after symptom onset. However, a considerable number of patients are ineligible for IV thrombolysis due to various contraindications. Recent studies have proved the superiority of mechanical thrombectomy for patients with large-vessel occlusions in combination with IV rtPA compared with IV rtPA alone. We aimed to demonstrate the efficacy of mechanical thrombectomy for patients who are ineligible for IV rtPA.

MATERIALS AND METHODS: Patients from the stroke registries of 4 dedicated centers who were treated with mechanical thrombectomy from January 2010 to October 2014 were retrospectively evaluated. Inclusion criteria were the following: acute stroke due to proved large-artery occlusion, ineligibility for IV thrombolysis, and a timeframe of ≤ 4.5 hours between stroke and the start of mechanical thrombectomy. Recanalization success, periprocedural complications, clinical outcome, and hemorrhages were evaluated.

RESULTS: One hundred thirty endovascular recanalization procedures were identified. The locations were the following: proximal ICA in 17 (13.1%), terminus ICA in 25 (19.2%), M1 segment in 77 (59.2%), and M2 segment in 11 (8.5%). TICI 2b/3 results were achieved in 101 (77.7%), and an mRS score of 0–2 in 47 patients (37.9%). There was a significant correlation between TICI 2b/3 results and good clinical outcomes (87.2% versus 6.8%; $P = .048$). A good clinical result was most frequent when recanalization was achieved within 4.5 hours (37/74 = 50% versus 10/50 = 20.0%; $P = .001$). Symptomatic hemorrhage occurred in 13.1% of patients; mortality was 24.2%. Periprocedural complications were recorded in 10 patients (7.7%).

CONCLUSIONS: Mechanical thrombectomy can achieve good clinical outcomes in patients with acute large-artery occlusion ineligible for IV thrombolysis, in particular when recanalization is reached early.

ABBREVIATIONS: ESCAPE = Endovascular Treatment for Small Core and Anterior Circulation Proximal Occlusion With Emphasis on Minimizing CT to Recanalization Times; EXTEND IA = Extending the Time for Thrombolysis in Emergency Neurologic Deficits–IntraArterial; MR CLEAN = Multicenter Randomized Clinical Trial of Endovascular Treatment for Acute Ischemic Stroke in the Netherlands; SWIFT PRIME = Solitaire With the Intention for Thrombectomy as Primary Endovascular Treatment Trial; REVASCAT = Randomized Trial of Revascularization with the Solitaire FR Device Versus Best Medical Therapy in the Treatment of Acute Stroke Due to Anterior Circulation Large Vessel Occlusion Presenting within Eight Hours of Symptom Onset

Intravenous treatment with recombinant tissue-plasminogen activator has been proved effective and has been the standard therapy for patients with acute ischemic stroke within 4.5

hours after symptom onset for many years.¹ However, the percentage of patients eligible for treatment with IV thrombolysis is limited, not only because of the restricted time window² but also due to various medical conditions such as recent surgery, anticoagulation, coagulation abnormalities, and history of intracranial hemorrhage.³

Patients with acute stroke symptoms secondary to a large-artery occlusion are at high risk of poor clinical outcome. Furthermore, they are known to respond poorly to IV rtPA alone.^{4–8}

During the past decade, several endovascular techniques have been established to improve the success of recanalization and thus the clinical outcomes of these patients, including intra-arterial thrombolysis, mechanical thrombectomy, and permanent stent angioplasty.^{9–12} Fully retrievable stent-based thrombectomy devices (stent retrievers) were introduced in 2008¹³ and today are

Received April 26, 2015; accepted after revision June 27.

From the Departments of Neuroradiology and Radiology (F.D., H.L., C.K., T.L.) and Neurology (H.S.), University Hospital of Cologne, Cologne, Germany; Departments of Neuroradiology (S.P., C.Z.) and Neurology (H.P.), Klinikum Rechts der Isar, Technical University, Munich, Germany; Departments of Neuroradiology (F.D., M.P., H.B., G.F.) and Neurology (L.K.), University Hospital of Munich, Munich, Germany; and Departments of Neuroradiology (O.N., M.W.) and Neurology (A.R.), University Hospital of Aachen, Aachen, Germany.

F. Dorn and S. Prothmann contributed equally to this work.

Please address correspondence to Franziska Dorn, MD, University Hospital of Munich, Department of Neuroradiology, Marchioninstr 15, 81377 Munich, Germany; e-mail: franziska.dorn@med.uni-muenchen.de

<http://dx.doi.org/10.3174/ajnr.A4520>

the technical standard of care for endovascular recanalization treatment in most stroke centers. While several studies and case series have shown high recanalization success of >80%–90%,^{14–19} the first randomized trials proving a clear clinical benefit compared with sole IV therapy were published only recently.^{20–24}

The aim of this study was to complement the existing data by proving the efficacy of endovascular treatment for the subgroup of patients with large-artery occlusions located in the anterior circulation who are ineligible for primary IV thrombolysis within a time window of 4.5 hours.

MATERIALS AND METHODS

Patient Selection

From the stroke registries of 4 stroke centers, we retrospectively evaluated all patients who underwent endovascular therapy between January 2010 and October 2014 and met the following criteria: acute stroke symptoms secondary to large-artery occlusion and contraindications for IV thrombolysis despite a time from symptom onset to the start of endovascular therapy of ≤ 4.5 hours. One-hundred eight patients (83.1%) underwent the CT stroke protocol, and 22 patients (16.9%), MR imaging.

The decision for treatment for all patients was based on the clinical presentation and the imaging findings. A team of stroke neurologists examined all patients on admission, and the National Institutes of Health Stroke Scale scores were recorded. The patients included in this series had an NIHSS score of at least 10 or fluctuating symptoms. All patients underwent CT or MR imaging before treatment. If possible, multiparametric imaging was performed by using CT/CT angiography and CT perfusion imaging or MR imaging/MR angiography, including the acquisition of FLAIR images, diffusion-weighted images, and a gradient-echo T2* sequence. Imaging criteria for exclusion from endovascular therapy were visible infarction of more than one-third of the vessel territory, no relevant mismatch on CT perfusion imaging, and evidence of hemorrhage. There was no limit to the patient age.

Procedural Data

Final reperfusion success was rated on the basis of the Thrombolysis In Cerebral Infarction scale. Successful reperfusion was defined as TICI scores 2b and 3.²⁵ The start of angiography was defined as the time of the femoral artery puncture, and the first persistent reperfusion result was used for time-to-reperfusion measures.

Endovascular Procedure

All except 8 procedures were performed with the patient under general anesthesia. Endovascular treatment consisted of arterial catheterization of the occluded vessel with a microcatheter and delivery of a stent retriever by withdrawal of the microcatheter. This was followed by a maneuver to withdraw the stent retriever under either continuous aspiration by using a distal access catheter or proximal balloon occlusion. The procedure was repeated until the best possible recanalization result was achieved. Procedures involved the following stent retrievers: Solitaire FR (Covidien, Irvine, California) in 88 (67.7%), Trevo/Trevo ProVue (Stryker, Kalamazoo, Michigan) in 32 (24.6%), pREset thrombus

retriever (Phenox, Bochum, Germany) in 7 (5.4%), and a combination of Solitaire and Trevo in 3 procedures (2.3%).

Follow-Up Imaging and Clinical Outcome

All patients underwent CT and/or MR imaging at 18 ± 6 hours after the intervention. The images were rated for hemorrhagic transformation or cerebral hemorrhage. According to the criteria of the European Cooperative Acute Stroke Study III, symptomatic hemorrhage was defined as any intracranial hemorrhage with clinical deterioration, as indicated by an NIHSS score that was > 4 points or more than the value at baseline.¹

Good clinical outcome after 3 months was defined as an mRS of 0–2.

Statistical Analysis

Statistical analysis was performed by using SPSS 22.0.0.0 (IBM, Armonk, New York). To test categorical variables for differences, the χ^2 test was performed. Mann-Whitney *U* tests and Student *t* tests were used for comparison of continuous variables. A *P* value of $< .05$ was statistically significant.

RESULTS

We identified 130 patients with large-vessel occlusion in the anterior circulation who underwent endovascular recanalization procedures within 4.5 hours after symptom onset and were ineligible for IV thrombolysis. Table 1 gives an overview of the relevant patient data. The mean age was 68.8 years (range, 18–90 years), 64 patients were women (49.2%), and 66 patients (50.8%) were men. The occlusions were located as follows: the proximal ICA in 17 (13.1%), ICA terminus in 25 (19.2%), proximal M1 segment in 71 (54.6%), postbifurcal M1 segment in 6 (4.6%), and M2 segment in 11 (8.5%). A TICI 2b or 3 recanalization result was achieved in 101/130 patients (77.7%). Anticoagulation with phenprocoumon was the most common contraindication for IV thrombolysis (44 patients, 33.8%). Twenty-one patients (16.2%) had a recent history of stroke with corresponding lesions on MR imaging, and 23 patients (17.7%) had a history of recent surgery. Ten patients (7.7%) with evidence for an extracranial occlusion of the ICA were not treated with IV thrombolysis but with antiplatelet medication in preparation for stent placement to reduce the risk of hemorrhage, and 6 patients (4.6%) were under full-dose heparin for numerous disorders. Two patients (1.5%) had not received IV rtPA due to epileptic onset of stroke symptoms; 5 (3.8%), because of known metastasizing cancer; 2 (1.5%), because of gastrointestinal bleeding; 2 (1.5%), because of previous trauma; 3 (2.3%), because of a history of intracranial hemorrhage; 1 (0.8%), because of diagnosed coagulative disorder; and 1 (0.8%), because of an intracranial aneurysm detected by CT angiography. In 10 patients (7.7%), contraindication could not be evaluated. Table 2 gives a detailed overview of the contraindications.

The NIHSS score at admission was available in 120/130 patients (92.3%). The mean NIHSS score was 16.32 ± 6.40 (minimum, 2 with fluctuating symptoms; maximum, 34). Modified Rankin Scale scores after 3 months were available in 124/130 patients (95.4%). A good clinical outcome (mRS 0–2) was achieved

Table 1: Relevant patient data listed for all patients^a

Patient Data	
No. of patients	130
Mean age (yr)	68.8 (min. 18, max. 90)
Sex	
Female	64 (49.2%)
Male	66 (50.8%)
Median NIHSS score on admission (range)	16.32 ± 6.4 (min. 2, max. 34)
Intracranial occlusion site	
Proximal ICA + distal ICA/MCA	17 (13.1%)
Terminus ICA	25 (19.2%)
M1	77 (59.2%)
Main branch	71 (54.6%)
Postbifurcal segment	6 (4.6%)
M2	11 (8.5%)
Reperfusion results	
TICI 0	5 (3.6%)
TICI 1	4 (3.1%)
TICI 2a	22 (15.4%)
TICI 2b	46 (35.4%)
TICI 3	55 (42.3%)
Time from stroke onset to groin puncture (minutes) (mean)	175.7 ± 45.4 (min. 65, max. 270)
Time from stroke onset to final recanalization (minutes) (mean)	246.0 ± 71.7 (min. 94, max. 432)
mRS after 3 months (n = 124)	
0	17 (13.1%)
1	12 (9.2%)
2	18 (13.8%)
3	17 (13.1%)
4	16 (12.3%)
5	14 (10.8%)
6	30 (23.1%)
Symptomatic hemorrhage	17 Patients (13.1%)
Periprocedural complications	10 (7.7%)
SAH	6 (4.6%)
Thrombus lost	1 (0.8%)
Dissection	2 (1.6%)
Loss of device	2 (1.6%)

Note:—Max. indicates maximum; min, minimum.

^a Numbers of patients and percentage are displayed unless otherwise noted.

Table 2: Summary of contraindications against IV thrombolysis

Contraindication	No. of Patients (n = 130)
Phenprocoumon (INR > 1.7)	44 (33.8%)
Recent surgery	23 (17.7%)
Recent stroke	21 (16.2%)
Emergency stentangioplasty	10 (7.7%)
IV heparin	6 (4.6%)
Metastasizing cancer	5 (3.8%)
History of ICH	3 (2.3%)
Previous trauma	2 (1.5%)
Epileptic onset	2 (1.5%)
Gastrointestinal bleeding	2 (1.5%)
Coagulative disorder	1 (0.8%)
Intracranial aneurysm	1 (0.8%)
Not evaluable	10 (7.7%)

Note:—INR indicates international normalized ratio; ICH, intracerebral hemorrhage.

in 47/124 patients (37.9%). The recanalization was successful (TICI 2b/3) in 101/130 patients (77.7%). Forty-one (87.2%) of the 47 patients with a good clinical outcome after 3 months had TICI 2b/3 recanalization, whereas only 6 had a TICI 0–2a result (6.8%; $P = .048$). The mean time from stroke onset to groin puncture was 175.7 ± 45.4 minutes (minimum, 65 minutes; maximum, 270 minutes), and the mean time from stroke onset to final recanalization was 246.0 ± 71.7 minutes (minimum, 94; maximum, 432 minutes). A favorable clinical outcome was more frequent in patients with an occlusion of the M2 (5/11 patients,

45.5%) and M1 segments (30/76 patients, 40.5%) and was least frequent in patients with an occlusion of the terminus ICA (6/24, 25.0%). A good clinical result was more frequent when recanalization was achieved within 4.5 hours compared with patients with longer recanalization times (37/74 = 50% versus 10/50 = 20.0%; $P = .001$). If recanalization was achieved within 6 hours from onset ($n = 107$), 43 patients (40.2%) had a good outcome, whereas in only 4 of 17 patients (23.5%) exceeding the time window of 6 hours was a good outcome noted ($P = .085$).

The mean number of passages was 3.3.^{1–15} A good recanalization result (TICI 2b or 3) was most likely in procedures with only 1 stent retriever passage compared with procedures with ≥ 2 stent retriever passages (25/27 = 92.6% versus 76/103 = 73.8%; $P = .039$). Furthermore, the chance for a good clinical outcome was significantly higher after a recanalization that required only 1 passage (16/26 = 61.5% versus 31/98 = 31.6%; $P = .007$).

Altogether, intracranial hemorrhage was detected in 37 patients (28.5%), of whom 17 had symptomatic hemorrhages (13.1%). Intracranial hemorrhage occurred in 4/44 patients (9.1%) who were under sufficient anticoagulation with phenprocoumon at the time of stroke (international normalized ratio > 1.7) and in 3/6 patients who were under effective IV heparin at the time of stroke (50.0%). The incidence of hemorrhage was 66.7% (2/3) in patients with a history of intracerebral hemorrhage, 13.0% in patients with history of recent surgery (3/23), 14.3% (3/21) in patients with recent ischemic stroke, and 20.0% (1/5) in patients who were not eligible for IV thrombolysis because of metastasizing cancer. The 1 patient with a previously diagnosed coagulative disorder did not develop hemorrhage. None of the patients who received antiplatelet medication for subsequent extra- or intracranial stent placement experienced hemorrhage. The mortality rate after 3 months was 24.2% (30/124 patients). Periprocedural complications occurred in 10 patients (7.7%): subarachnoid hemorrhage in 6 (4.6%), thrombus lost with occlusion of a previously nonaffected territory (A2 segment in 1 patient [0.8%], dissection in 1 [0.8%], and loss of the device in 2 [1.6%]).

DISCUSSION

To the best of our knowledge, we present the largest series of patients with acute occlusions of anterior large intracranial arteries who were ineligible for IV treatment and were primarily referred to sole endovascular therapy by using stent retrievers. So far, retrospective studies and prospective trials providing evidence for the benefit of endovascular treatment in this specific patient group are nonexistent. The Thrombectomy in Patients Ineligible for IV tPA trial (THRILL) was planned with the intention of showing a benefit of stent retriever based thrombectomy in patients who were ineligible for IV fibrinolysis, but enrollment was stopped and the results of this multicentric German/Austrian study are not available.²⁶

Since the introduction of stent retrieval in 2008,¹³ several case series have proved the technical effectiveness of the method, with potentially high rates of successful recanalization in patients with acute stroke symptoms secondary to large-vessel occlusion. Furthermore, the superiority of stent retrievers in terms of revascularization abilities and clinical success in

comparison with the first-generation Merci clot retriever devices (Concentric Medical, Mountain View, California) has been verified in 2 randomized studies.^{27,28} However, before December 2014, the only proved effective treatment for acute ischemic stroke was IV thrombolysis. This has now changed with the publication of 4 randomized studies: Multicenter Randomized Clinical Trial of Endovascular Treatment for Acute Ischemic Stroke in the Netherlands (MR CLEAN),²⁰ Endovascular Treatment for Small Core and Anterior Circulation Proximal Occlusion With Emphasis on Minimizing CT to Recanalization Times (ESCAPE),²¹ Extending the Time for Thrombolysis in Emergency Neurologic Deficits–Intra-Arterial (EXTEND IA),²² Solitaire With the Intention for Thrombectomy as Primary Endovascular Treatment Trial (SWIFT PRIME),²³ and the Randomized Trial of Revascularization with the Solitaire FR Device Versus Best Medical Therapy in the Treatment of Acute Stroke Due to Anterior Circulation Large Vessel Occlusion Presenting within Eight Hours of Symptom Onset (REVASCAT).²⁴ All of these studies compared endovascular treatment with IV thrombolysis alone, and all confirmed a benefit of the endovascular approach for certain patients.

Stent retriever devices were used in 82% and 86% of the interventional arms of MR CLEAN and ESCAPE, respectively, and in 100% of the interventional arms of EXTEND-IA, SWIFT PRIME, and REVASCAT. We used stent retrievers in all cases, resulting in a recanalization success of 77.7% (TICI 2b/3). This rate is within the range of ESCAPE (72.4%), EXTEND-IA (86.2%), and SWIFT PRIME (88.0%) and higher compared with the rather modest successful recanalization rate of MR CLEAN (58.7%).

The rate of good clinical outcomes varied widely in the recently published randomized trials, from 32.6% in MR CLEAN to 71.4% in EXTEND-IA. In our series, the clinical result after 3 months was available in a considerably high number of patients (95.4%), and an mRS of 0–2 was reached by 37.9% of them. Compared with the results of MR CLEAN, the higher percentage of successful recanalization certainly contributes to the better clinical outcome in our series; furthermore, the median time from stroke onset to groin puncture was shorter in our series (176 minutes) compared with MR CLEAN (260 minutes). However, the recanalization times were also shorter compared with ESCAPE (241 minutes) and EXTEND-IA, and both studies resulted in a higher percentage of patients with a favorable clinical outcome. We reason that comorbidities in our patient cohort ineligible for IV therapy contributed to the lower rate of good clinical outcomes compared with these studies.

Another parameter that should be discussed in this context is the lack of IV thrombolysis in our patient group. Intravenous thrombolytic treatment is frequently performed in patients with larger-artery occlusions before endovascular treatment by a “bridging” concept. However, the additional benefit from this regimen is unclear. Whereas the stent retriever series of Dávalos et al¹⁵ showed that patients had significantly better outcomes after IV thrombolysis and stent retriever thrombectomy compared with patients who were treated with stent retriever thrombectomy alone, this result could not be verified in the following Solitaire FR Thrombectomy for Acute Revascularisation trial (STAR)¹⁷ or

other studies. Most patients in the interventional arm of MR CLEAN (87.1%), ESCAPE (72.7%), and REVASCAT (68.0%) and all of the patients in the interventional arm of EXTEND-IA and SWIFT PRIME received IV thrombolysis before endovascular treatment, whereas due to various contraindicating conditions, none of the patients in our study received IV bridging therapy. We cannot know whether additional IV thrombolysis would have changed the number of patients with a favorable clinical outcome in our series significantly, and we cannot exclude this factor contributing to the comparably low number of patients with good clinical results despite successful recanalization in our series (at least when compared with ESCAPE, EXTEND-IA and SWIFT PRIME). Certainly, further evaluation and discussion of this matter will be necessary.

The exciting results of MR CLEAN, ESCAPE, EXTEND-IA, SWIFT PRIME, and REVASCAT will potentially change the guidelines for acute stroke management regimens in the near future. Until then endovascular recanalization is limited to decisions on a case-by-case basis, and IV thrombolysis remains the recommended standard of care for all patients with ischemic stroke within a time window of 4.5 hours. Henceforth, careful selection of patients and an evidence-based definition of subgroups that most likely benefit from endovascular therapy will be necessary to allow the development of responsible decision algorithms.

Contraindications for IV thrombolysis are frequent and most commonly include anticoagulative abnormalities and a history of recent surgery. Furthermore, IV thrombolysis is avoided in patients with conceivable indications for acute stent placement (eg, due to a dissection or stenosis) to avoid bleeding complications. According to most institutional guidelines, therapy for patients with contraindications for IV thrombolysis is limited to (noncausal) medical care, including the control of blood pressure and laboratory and vital parameters in a dedicated stroke care unit. Particularly for these patients, the chance of a (causal) endovascular treatment approach addressing the underlying pathology in the acute stroke phase may be of great benefit.

Certainly, the potential benefit of any medical therapy has to be balanced against a potential risk for adverse events. We found a periprocedural complication rate of 7.7% in our series, which is comparable with the results of the MR CLEAN and other trials and consisted of SAH, thrombus loss with subsequent infarction in previously not affected vessel territories, hemodynamically relevant dissections of extracranial arteries, and loss of devices.

Symptomatic intracranial hemorrhage after mechanical thrombectomy occurs in 4%–12% in larger case series and trials.^{14–19} Symptomatic hemorrhage was not increased in the interventional arm compared with the control group in MR CLEAN (7.7% versus 6.4%), ESCAPE (3.6% versus 2.7%), EXTEND-IA (0% for Solitaire, 6% for controls), SWIFT PRIME (0% versus 3.1%), and REVASCAT (1.9% in both groups). In our series, symptomatic hemorrhage occurred in 13.1% of patients; it occurred in a high percentage of patients who developed stroke under IV heparin (50%) but in <10% of patients who were under phenprocoumon at the time of stroke. However, due to the small

number of patients with IV heparin in our series, these results have to be interpreted carefully.

The present study has several limitations, and the results have to be interpreted with care. Due to its retrospective design, this multicenter study is prone to selection bias. There is no control group and no randomized patient selection. In addition, the patient cohort is not homogeneous for various reasons (eg, the included patients had acute strokes of different etiologies and with different vessel-occlusion patterns).

CONCLUSIONS

Our series indicates a potential benefit of stent retriever–based thrombectomy in patients with large-artery occlusions of the anterior circulation who are ineligible for IV thrombolysis. Successful and early recanalization was the most important factor for a good clinical outcome. Further prospective, controlled randomized studies will be necessary to prove the effectiveness of endovascular therapy for this specific patient group.

Disclosures: Sascha Prothmann—UNRELATED: Consultancy: phenox (proctor); Grants/Grants Pending: DFG grant, Flowmodel Aneurysm (grant pending); Payment for Lectures (including service on Speakers Bureaus): Boston Scientific, Covidien, Travel/Accommodations/Meeting Expenses Unrelated to Activities Listed: Acandis, AB Medica, phenox, Sequent Medical, MicroVention, Covidien. Thomas Liebig—UNRELATED: Consultancy: Sequent Medical, Stryker, Acandis, Comments: consultant and proctor. Martin Wiesmann—UNRELATED: consultancy: Stryker Neurovascular, Philips; Grants/Grants Pending: Covidien,* MicroVention*; Payment for Lectures (including service on Speakers Bureaus): Bracco, Siemens; Royalties: Springer; Payment for Development of Educational Presentations: Abbott,* AB Medica,* Acandis,* Bayer,* Bracco,* B. Braun Medical,* Codman Neurovascular,* Covidien,* Dahlhausen,* MicroVention,* Penumbra,* phenox,* Philips Healthcare,* Siemens,* St. Jude,* Stryker Neurovascular.* Henning Stetefeld—UNRELATED: Travel/Accommodations/Meeting Expenses Unrelated to Activities Listed: Pfizer, Boehringer Ingelheim, Bayer, Comments: subsidized travel, accommodations, and meeting expenses. Holger Poppert—UNRELATED: board membership: Deutsche Stiftung Neurologie*; Consultancy: Bayer Healthcare, Boehringer Ingelheim, Daiichi Sankyo; Payment for Lectures (including service on Speakers Bureaus): Bayer Healthcare, Boehringer Ingelheim, Bristol-Myers Squibb, Roche; Travel/Accommodations/Meeting Expenses Unrelated to Activities Listed: Boehringer Ingelheim.* *Money paid to the institution.

REFERENCES

1. Hacke W, Kaste M, Bluhmki E, et al; ECASS Investigators. **Thrombolysis with alteplase 3 to 4.5 hours after acute ischemic stroke.** *N Engl J Med* 2008;359:1317–29 CrossRef Medline
2. Lees KR, Bluhmki E, von Kummer R, et al; ECASS, ATLANTIS, NINDS and EPITHET rt-PA Study Group. **Time to treatment with intravenous alteplase and outcome in stroke: an updated pooled analysis of ECASS, ATLANTIS, NINDS, and EPITHET trials.** *Lancet* 2010;375:1695–703 CrossRef Medline
3. Jauch EC, Saver JL, Adams HP Jr, et al; American Heart Association Stroke Council; Council on Cardiovascular Nursing; Council on Peripheral Vascular Disease; Council on Clinical Cardiology. **Guidelines for the early management of patients with acute ischemic stroke: a guideline for healthcare professionals from the American Heart Association/American Stroke Association.** *Stroke* 2013;44:870–947 CrossRef Medline
4. Alexandrov AV. **Ultrasound enhanced thrombolysis for stroke.** *Int J Stroke* 2006;1:26–29 CrossRef Medline
5. Bhatia R, Hill MD, Shobha N, et al. **Low rates of acute recanalization with intravenous recombinant tissue plasminogen activator in ischemic stroke: real-world experience and a call for action.** *Stroke* 2010;41:2254–58 CrossRef Medline
6. Riedel CH, Zimmermann P, Jensen-Kondering U, et al. **The importance of size: successful recanalization by intravenous thrombolysis**

7. **sis in acute anterior stroke depends on thrombus length.** *Stroke* 2011; 42:1775–77 CrossRef Medline
7. Lindsberg PJ, Mattle HP. **Therapy of basilar artery occlusion: a systematic analysis comparing intra-arterial and intravenous thrombolysis.** *Stroke* 2006;37:922–28 CrossRef Medline
8. von Kummer R, Hacke W. **Safety and efficacy of intravenous tissue plasminogen activator and heparin in acute middle cerebral artery stroke.** *Stroke* 1992;23:646–52 CrossRef Medline
9. Furlan A. **Intra-arterial prourokinase for acute ischemic stroke: the PROACT II Study—a randomized controlled trial.** *JAMA* 1999;282:2003–11 CrossRef Medline
10. Smith WS, Sung G, Saver J, et al. **Mechanical thrombectomy for acute ischemic stroke: final results of the Multi MERCI trial.** *Stroke* 2008;39:1205–12 CrossRef Medline
11. Smith WS, Sung G, Starkman S, et al; MERCI Trial Investigators. **Safety and efficacy of mechanical embolectomy in acute ischemic stroke: results of the MERCI trial.** *Stroke* 2005;36:1432–8 CrossRef Medline
12. Penumbra Pivotal Stroke Trial Investigators. **The Penumbra Pivotal Stroke trial: safety and effectiveness of a new generation of mechanical devices for clot removal in intracranial large vessel occlusive disease.** *Stroke* 2009;40:2761–68 CrossRef Medline
13. Pérez MA, Miloslavski E, Fischer S, et al. **Intracranial thrombectomy using the Solitaire stent: a historical vignette.** *J Neurointerv Surg* 2012;4:e32 CrossRef Medline
14. Castaño C, Dorado L, Guerrero C, et al. **Mechanical thrombectomy with the Solitaire AB device in large artery occlusions of the anterior circulation: a pilot study.** *Stroke* 2010;41:1836–40 CrossRef Medline
15. Dávalos A, Pereira VM, Chapot R, et al. **Retrospective multicenter study of Solitaire FR for revascularization in the treatment of acute ischemic stroke.** *Stroke* 2012;43:2699–705 CrossRef Medline
16. Dorn F, Stehle S, Lockau H, et al. **Endovascular treatment of acute intracerebral artery occlusions with the Solitaire stent: single-center experience with 108 recanalization procedures.** *Cerebrovasc Dis* 2012;34:70–77 CrossRef Medline
17. Pereira VM, Gralla J, Dávalos A, et al. **Prospective, multicenter, single-arm study of mechanical thrombectomy using Solitaire Flow Restoration in acute ischemic stroke.** *Stroke* 2013;44:2802–07 CrossRef Medline
18. Roth C, Papanagiotou P, Behnke S, et al. **Stent-assisted mechanical recanalization for treatment of acute intracerebral artery occlusions.** *Stroke* 2010;41:2559–67 CrossRef Medline
19. San Román L, Obach V, Blasco J, et al. **Single-center experience of cerebral artery thrombectomy using the TREVO device in 60 patients with acute ischemic stroke.** *Stroke* 2012;43:1657–59 CrossRef Medline
20. Berkhemer OA, Fransen PS, Beumer D, et al. **A randomized trial of intraarterial treatment for acute ischemic stroke.** *N Engl J Med* 2015; 372:11–20 CrossRef Medline
21. Goyal M, Demchuk AM, Menon BK, et al; ESCAPE Trial Investigators. **Randomized assessment of rapid endovascular treatment of ischemic stroke.** *N Engl J Med* 2015;372:1019–30 CrossRef Medline
22. Campbell BC, Mitchell PJ, Kleinig TJ, et al; the EXTEND-IA Investigators. **Endovascular therapy for ischemic stroke with perfusion-imaging selection.** *N Engl J Med* 2015;372:1009–18 CrossRef Medline
23. Saver JL, Goyal M, Bonafe A, et al; SWIFT PRIME Investigators. **Stent-retriever thrombectomy after intravenous t-PA vs. t-PA alone in stroke.** *N Engl J Med* 2015;372:2285–95 CrossRef Medline
24. Jovin TG, Chamorro A, Cobo E, et al; REVASCAT Trial Investigators. **Thrombectomy within 8 hours after symptom onset in ischemic stroke.** *N Engl J Med* 2015;372:2296–306 CrossRef Medline
25. Higashida RT, Furlan AJ, Roberts H, et al; Technology Assessment Committee of the American Society of Interventional and Therapeutic Neuroradiology; Technology Assessment Committee of the

Society of Interventional Radiology. **Trial design and reporting standards for intra-arterial cerebral thrombolysis for acute ischemic stroke.** *Stroke* 2003;34:e109–37 CrossRef Medline

26. Bendszus M, Thomalla G, Knauth M, et al. **Thrombectomy in patients ineligible for iv tPA (THRILL).** *Int J Stroke* 2015;10:950–55 CrossRef Medline
27. Saver JL, Jahan R, Levy EI, et al; SWIFT Trialists. **Solitaire flow re-**

toration device versus the Merci retriever in patients with acute ischaemic stroke (SWIFT): a randomised, parallel-group, non-inferiority trial. *Lancet* 2012;380:1241–49 CrossRef Medline

28. Nogueira RG, Lutsep HL, Gupta R, et al; TREVO 2 Trialists. **Trevo versus Merci retrievers for thrombectomy revascularisation of large vessel occlusions in acute ischaemic stroke (TREVO 2): a randomised trial.** *Lancet* 2012;380:1231–40 CrossRef Medline

Combination of Multicatheter Plus Stent or Balloon for Treatment of Complex Aneurysms

H.J. Jeon, B.M. Kim, D.J. Kim, K.Y. Park, J.W. Kim, and D.I. Kim



ABSTRACT

BACKGROUND AND PURPOSE: Coiling of complex aneurysms is still difficult even with current adjuvant techniques. This study sought to evaluate the safety and effectiveness of a combination of multicatheter plus stent or balloon for the treatment of complex aneurysms.

MATERIALS AND METHODS: All complex aneurysms that underwent coiling with the combination technique were identified from prospectively maintained neurointerventional data bases. “Complex aneurysm” was defined as a wide-neck aneurysm with branch incorporation into or a deep lobulation of the sac. The clinical and angiographic outcomes were retrospectively analyzed.

RESULTS: Sixty-two complex aneurysms (12 ruptured, 50 unruptured) in 62 patients (mean age, 57 years; male/female ratio, 12:50) were treated with a combination technique by using a multicatheter plus stent ($n = 42$, 3 ruptured) or balloon ($n = 20$, 9 ruptured). Treatment-related morbidity (grade 3 hemiparesis) occurred in 1 patient (1.6%). Except for 1 patient who had treatment-related morbidity, none of the other patients with unruptured aneurysms developed new neurologic symptoms at discharge. Nine of the 12 patients with ruptured aneurysms had good outcomes (Glasgow Outcome Score, 4 or 5) at the latest follow-up (mean, 32 months; range, 6–72 months), and 1 patient died from an initial SAH. Posttreatment control angiograms revealed complete occlusion in 27, neck remnant in 34, and incomplete occlusion in 1 aneurysm. At least 1 follow-up catheter or MR angiogram was available in 80.6% ($n = 50$) (mean, 21 months; range, 6–65 months). There were 4 minor and 3 major recurrences (14.0%).

CONCLUSIONS: In this case series, the combination technique by using multicatheter plus stent or balloon seemed safe and effective for the treatment of complex aneurysms.

Technical advances with devices such as catheters, balloons, and stents have widened the indications and improved the outcomes of coiling for the treatment of intracranial aneurysms. A wide-neck, branch incorporation into the sac and a lobulated sac are well-known anatomic features of aneurysms that make the conventional coiling procedure difficult. These complicated anatomic features increase the risk of incomplete coiling, complications such as compromise of the parent vessel or branching artery, and posttreatment recurrence. Some case series have already reported the feasibility of adjunctive techniques for aneurysms with difficult anatomic characteristics and have presented good proce-

dural outcomes.^{1–6} However, the coiling procedure of an aneurysm with a wide neck plus an incorporated branch and/or lobulated sac still remains a technical challenge.^{6,7} In this regard, those aneurysms should be defined as “complex aneurysms.” On the other hand, a simple combination of already well-known techniques can make it easy to coil such complex aneurysms. To our knowledge, however, the feasibility and clinical and angiographic outcomes of combination techniques for these complex aneurysms have not yet been demonstrated. In this study, we evaluated the safety and effectiveness of a combination technique such as multicatheter plus stent or balloon for complex aneurysms.

MATERIALS AND METHODS

All complex aneurysms that underwent coiling with the combination technique were identified from prospectively maintained neurointerventional data bases in 2 academic tertiary referral hospitals between July 2007 and June 2014. A “complex aneurysm” was defined as a wide-neck aneurysm with an incorporated branch into and/or a deep lobulation (more than one-third of the aneurysm height) of the sac; “wide neck” meant that the neck diameter was ≥ 4 mm or the dome-to-neck ratio was ≤ 1.5 .

Received April 22, 2015; accepted after revision July 10.

From the Department of Neurosurgery (H.J.J.), Hallym University College of Medicine, Kangdong Sacred Heart Hospital, Seoul, Korea; and Departments of Radiology (B.M.K., D.J.K., J.W.K., D.I.K.) and Neurosurgery (K.Y.P.), Severance Hospital, Yonsei University College of Medicine, Seoul, Republic of Korea.

Please address correspondence to Byung Moon Kim, MD, PhD, Interventional Neuroradiology, Department of Radiology, Severance Stroke Center, Severance Hospital Yonsei University College of Medicine, 50 Yonsei-ro, 120-752, Seodaemun-gu, Seoul, Republic of Korea; e-mail: bmoon21@hanmail



Indicates article with supplemental on-line photo.

<http://dx.doi.org/10.3174/ajnr.A4526>

During the study period of 7 years, 1307 patients with 1423 aneurysms were treated with coiling in the 2 hospitals. One hundred twenty-one (8.5%) of the 1423 aneurysms met the definition of complex aneurysms in this study. Patient informed consent was obtained before treatment. The institutional review board approved this retrospective study with a waiver of informed consent for study inclusion. All relevant clinical and imaging data were obtained from electronic medical charts, PACSs, and a prospectively registered neurointerventional data base. The clinical and angiographic outcomes were retrospectively analyzed.

Coiling with the Combination Technique

All patients with unruptured aneurysms who were scheduled for stent-assisted coil embolization received premedication with dual antiplatelet medication (aspirin, 100 mg, and clopidogrel, 75 mg) for at least 5 days. Dual antiplatelet medication was maintained for at least 3 months and then was changed to aspirin monotherapy. For patients with ruptured aneurysms who underwent stent placement, a bolus of dual antiplatelet medication (aspirin, 100–500 mg, and clopidogrel, 300 mg) was given just after completion of the procedure. After the introduction of a guiding catheter, a bolus of heparin, 3000 IU, was injected and then heparin, 1000 IU, was given as a booster every hour. For anterior circulation complex aneurysms, a 6F Shuttle guide sheath (Cook, Bloomington, Indiana) was placed in the relevant internal carotid artery. For posterior circulation complex aneurysms, a single 6F Shuttle sheath was placed in the dominant vertebral artery or 2 Envoy guiding catheters of 5F or 6F diameter (Codman & Shurtleff, Raynham, Massachusetts) were placed in the bilateral vertebral arteries.

The combination technique was initially used in 21 complex aneurysms, and in the remaining 41 complex aneurysms, it was performed in the same session after failure of 1 of the following: the multicatheter, balloon-assisted, or stent-assisted technique. Therefore, approximately 51% (62/121) of the complex aneurysms were treated with this combined technique during the study period. For ruptured aneurysms, the balloon was preferentially chosen as an adjunctive device. Preshaped or steam-shaped 0.010-inch Excelsior microcatheters (Stryker, Kalamazoo, Michigan) were used for aneurysm selection and coil delivery with a 0.014-inch microguidewire (Traxcess; MicroVention, Tustin, California; or Synchro; Boston Scientific, Natick, Massachusetts). The adjunctive balloons in this study were HyperForm/HyperGlide (Covidien, Irvine, California) and Scepter C balloons (MicroVention). The stents used in this study included Enterprise (Codman & Shurtleff) and Neuroform (Stryker) stents.

Outcome Measures

“Treatment-related morbidity” was defined as the development of any new neurologic deficit due to treatment-related complications that were still present at discharge. “Treatment-related mortality” was defined when the patient died from treatment-related complications during clinical follow-up. The clinical outcomes of the patients with subarachnoid hemorrhage were evaluated by the Glasgow Outcome Score. A good outcome was defined as a Glasgow Outcome Score of 4 or 5. The clinical outcome at the latest

Summary of complex aneurysms and the results of the combination technique using multicatheter plus stent or balloon

No. of patients	62
Age (yr) (mean)	54.0 ± 12.0
Male/female	12 (19.4%):50 (80.6%)
Presentation (No.)	62
Ruptured	12 (19.4%)
Unruptured	50 (80.6%)
Type of complex aneurysms	
Wide neck plus branch incorporated	41 (66.1%)
Wide neck plus deep lobulation	16 (25.8%)
Wide neck plus both	5 (8.1%)
Sac diameter (mm) (mean) (range)	8.7 ± 3.4 (3.5–19.0)
Neck diameter (mm) (mean) (range)	6.0 ± 2.3 (3.2–14.0)
Location of complex aneurysm	
Internal carotid artery	29 (46.8%)
Middle cerebral artery	5 (8.1%)
Anterior cerebral artery	8 (12.9%)
Basilar artery	20 (32.2%)
Type of combination technique	
Multicatheter plus stent (No.)	42 (67.7%)
Multicatheter plus balloon (No.)	20 (32.3%)
Treatment-related morbidity	1 (1.6%)
Treatment-related mortality	0
Immediate angiographic outcome	
Complete	27 (43.6%)
Neck remnant	34 (54.8%)
Incomplete	1 (1.6%)
Follow-up angiograms (No.)	50 (80.6%)
Duration (mo) (mean) (range)	21 (6–65)
Follow-up results	
Improved or stable	43 (86.0%)
Minor recurrence	4 (8.0%)
Major recurrence	3 (6.0%)

follow-up was defined as the final outcome. If the latest clinical follow-up was >3 months at the point of the analysis of this study, a telephone interview was obtained to determine the patient’s clinical status.

Immediate postcoiling angiographic outcome was analyzed according to the Raymond scale. Follow-up angiographic outcome was classified into 3 categories: improved/stable, minor recurrence when the recurred aneurysm did not require retreatment, and major recurrence when the recurred aneurysm required retreatment. The need for retreatment was determined on the basis of a discussion among 2 neurointerventionists and 3 vascular neurosurgeons in a weekly neurovascular conference.

RESULTS

The Table summarizes the characteristics of complex aneurysms and the results of the combination technique by using the multicatheter plus stent or balloon.

Sixty-two complex aneurysms (12 ruptured and 50 unruptured) in 62 patients (mean age, 57; male/female ratio = 12:50) were treated with a combination technique either multicatheter plus stent ($n = 42$, 3 ruptured) or balloon ($n = 20$, 9 ruptured). Treatment-related morbidity occurred in 1 patient (1.6%) who had a grade 3 right hemiparesis due to an embolic occlusion of the incorporated left anterior choroidal artery, but there was no treatment-related mortality. Except for that patient, no other patient with an unruptured aneurysm developed a new neurologic symptom. Nine of the 12 patients with ruptured aneurysms exhibited

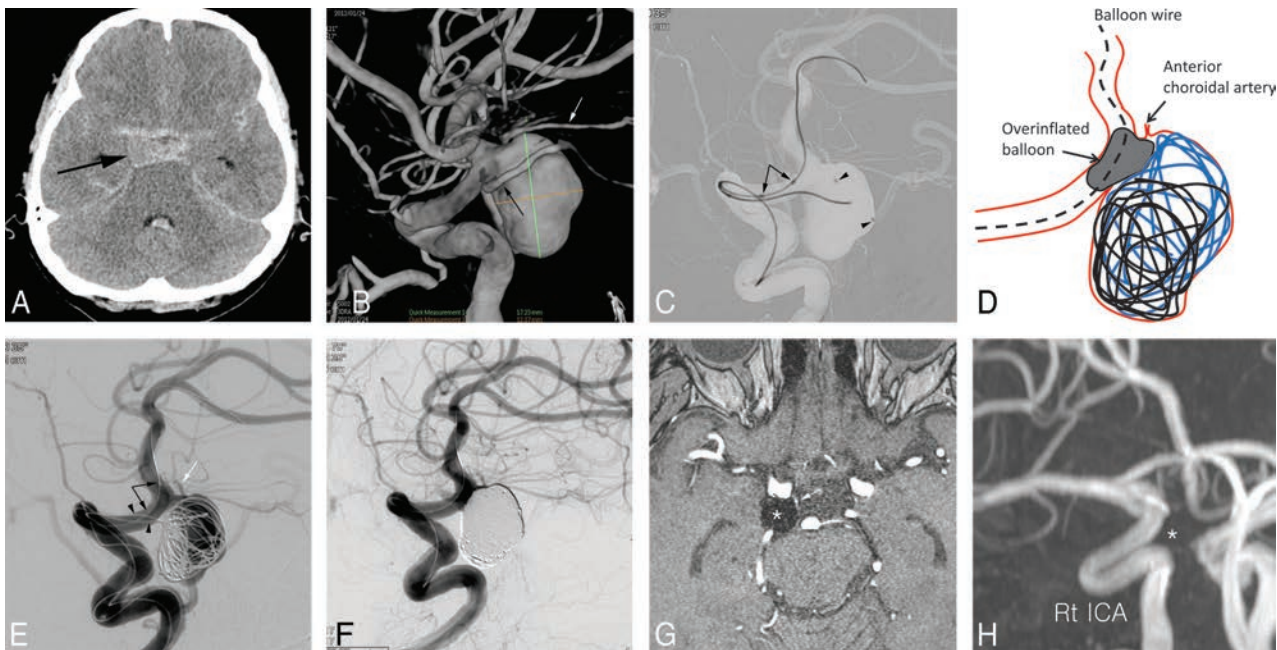


FIG 1. A 58-year-old man presenting with Hunt and Hess grade 3 subarachnoid hemorrhage. *A*, Unenhanced CT shows diffuse subarachnoid hemorrhage in the basal cistern. The *arrow* indicates the ruptured aneurysm. *B*, The 3D reconstruction image shows a 17-mm posterior communicating artery (*black arrow*) aneurysm with incorporation of the anterior choroidal artery (*white arrow*). *C*, A spot image shows HyperForm balloon (*arrow*) navigation after positioning 2 microcatheters (*arrowheads*) in the aneurysm sac. *D*, An illustration explains the technique for treating this aneurysm. During the protection of the anterior choroidal artery by an overinflated balloon, a stable coil frame basket is made by interleaving 2 coils. *E*, Angiogram after balloon deflation confirms a stable coil basket without compromising the origin of the incorporated anterior choroidal artery (*white arrow*). *Arrowheads* indicate 2 microcatheters for coil delivery, and *black arrows* indicate proximal and distal balloon markers. *F*, Completion control angiogram shows complete occlusion of the aneurysm sac with preservation of the incorporated anterior choroidal artery. The 40-month follow-up MR angiogram source (*G*) and MIP reconstruction (*H*) images show no recurrence (*asterisk*) and a patent anterior choroidal artery (*white arrow*).

good outcomes (Glasgow Outcome Score of 4 or 5) at the last follow-up (mean, 32 months; range, 6–72 months), and 1 patient died as a consequence of the initial subarachnoid hemorrhage. Posttreatment control angiograms showed complete occlusion in 27, neck remnants in 34, and incomplete occlusion in 1 aneurysm. At least 1 follow-up angiogram was available in 80.6% ($n = 50$; mean, 21 months; range, 6–65 months). Seven (14%) of the 50 patients were followed by MR angiography alone. Recurrence occurred in 7 aneurysms (14.0%), including 4 minor and 3 major recurrences.

DISCUSSION

Endovascular coiling has been increasingly used for wide-neck aneurysms due to rapid advances in devices and techniques.^{1–12} However, if wide-neck aneurysms have an incorporated branch and/or deeply lobulated sac, coiling is more difficult and there is potentially an increased risk of incomplete coiling, a thromboembolic event, or branching occlusion and posttreatment recurrence. The unique configuration of this aneurysm usually demands a more elaborate coiling technique and can be recognized as a complex and difficult aneurysm in view of the coiling procedure.

To some extent, the multicatheter technique can handle the wide-neck aneurysm via interleaving 2 or 3 coils or locking the first or second coil to make a stabilizing coil basket, and it is useful for accessing the lobulated sac by separating the catheter positions.^{5,6,8,13} In a recent case series, treatment-related morbidity and mortality with a dual-microcatheter technique were 1% and

2%, respectively.⁵ This technique can also intentionally protect the incorporated branch by placing 1 catheter or coil into the branch.^{6,11,12,14} Although balloons and stents were originally designed for preventing coil prolapse and enhancing coil-packing attenuation, slight overinflation of a compliant balloon or “gator backing” of open cell stent struts can additionally protect the branch incorporated with the parent artery of a wide-neck aneurysm.^{6,7,15}

A combination technique is intended to provide the advantages of both the multicatheter technique and a stent or balloon technique. In the combination technique, a balloon or stent is used to protect the aneurysm neck, and multicatheters are used to form and stabilize the coil basket to preserve the incorporated branch (Fig 1) and/or to uniformly pack the lobulated sac with coils (Fig 2).¹⁶ This approach may be a relatively complex procedure, even though it uses already known devices. There may also be complications associated with additional instruments, such as an increase in thromboembolic events and device-related problems. For these reasons, in this study, treatment via the combination technique was initially planned in only one-third of the complex aneurysms, while in two-thirds of the aneurysms, a conventional multicatheter, balloon-, or stent-assisted technique was initially attempted. For the complex aneurysms initially treated with the combination technique, it was anticipated that the multicatheter, balloon, or stent alone could not achieve preservation of an incorporated branch or stability of the coil basket due to a wide neck with incorporated branches and/or deep lobulation (Fig 3).

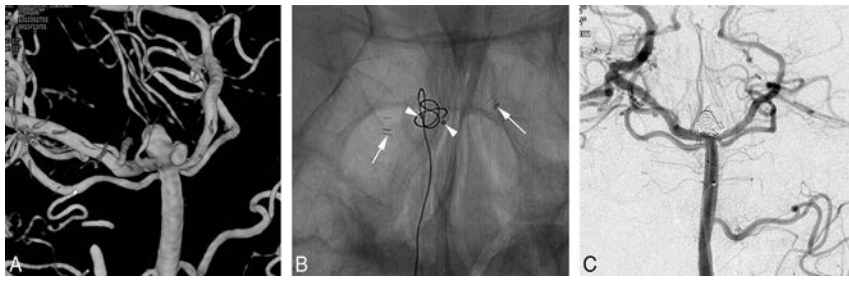


FIG 2. A 27-year-old woman with underlying Moyamoya disease and an unruptured basilar tip aneurysm. *A*, The 3D reconstruction image shows an unruptured basilar tip aneurysm with a deep lobulation. *B*, A spot image shows coil placement after positioning 2 microcatheter tips (*arrowheads*) in the large and small lobes of the sac, respectively, and horizontal stent placement (*arrows*) via the posterior communicating artery. *C*, Completion control angiogram shows uniform coil packing of the lobulated sac, resulting in complete occlusion of the aneurysm.

Given the accumulation of experience since the previously reported cases series,^{6,9,11,12} the complexity of the technique used has not limited the ability to obtain satisfactory results. In the cases focused on preserving an incorporating branch, interleaving 2 coils stabilized the initial coil basket to preserve the incorporated branch, while the overinflated balloon prevented coils from moving toward the incorporated branch (Fig 1). In other cases with a very wide neck and a shallow aneurysm with an acute-angled incorporating branch, a multicatheter-plus-stent system was a more reliable choice than a multicatheter-plus-balloon system (Fig 3). Overall, stents (67.7%) have been used more than balloons (32.3%) for covering the wide neck, but in ruptured cases, balloons (75.0%) were preferred because stents may be associated with hemorrhagic complications.¹⁷ For cases with a very wide neck and deep lobulation, each lobe of the aneurysm was selected by using 2 microcatheters that had different distal tip shapes (preshaped or steam-shaped). Each lobe could be completely embolized with different coils suitable for the respective shape and size during the protection of the parent artery from coil protrusion by the stent (Fig 2).

When using the combined technique for a branch-incorporated aneurysm, the embolizing coil size was matched to the aneurysm depth, rather than the largest or mean diameter of the aneurysm, with an oversized stent or a supercompliant balloon (HyperForm). When the incorporated branch was intended to be protected with a coil, the appropriate preshaped or steam-shaped catheter was used for facing the origin of the incorporated branch (Fig 3 and On-line Fig 1). Usually, for facing the catheter tip to the origin of an ophthalmic artery or an acutely angled middle cerebral artery branch, a preshaped S (Stryker Neurovascular, Fremont, California) or steam-shaped S catheter was useful. As a protection coil for a small incorporated branch, a helical coil with size matched to or slightly greater than the size of the origin of the incorporated branch was chosen (Fig 3 and On-line Fig 1). The complex or 3D coil was occasionally useful for protection of a relatively larger incorporated branch such as a fetal-type posterior cerebral artery. For the deeply lobulated and shallow aneurysm without an incorporated branch, the appropriate preshaped or steam-shaped catheters were chosen for facing each catheter tip to the respective lobe of the aneurysm. Then each coil size was matched to or slightly greater than the largest size of each lobe. If possible, the stent size was matched to the parent artery size. The

balloon was not overinflated, with room for coil placement. Thus, most often 2 coils were packed in each lobe partially intermingling at the confluence of each lobe (Fig 2). After we made a stable coil basket, smaller helical coils were always used for further coil packing without breaking the initial shape of the coil basket.

A major concern about the combination technique for coiling of a complex aneurysm is a possibly increased risk of treatment-related complications resulting from unfavorable aneurysm geometry and the use of additional instruments. The overall incidence of treatment-related complications was reported to be 7.9%–17.1% and 9.4%–12.2% with balloon- and stent-assisted techniques, respectively.^{1,18–21} The multicatheter technique also ranged from 0% to 13.3%.^{5,13,22,23} Notably, in our series, treatment-related morbidity occurred in only 1 patient (1.6%), which is acceptable in comparison with the reported results from the literature focusing only on wide necks and is also remarkable because adding an adjunctive device may lead to an increase in adverse events like thromboembolism and intraprocedural rupture.^{24,25}

Another concern is a possible increase in the recanalization rate after frequent incomplete coiling due to the complicated characteristics of the aneurysm. However, through the combination technique, only 1 incomplete coiling occurred in our study. Although there was a 14% recurrence (3 major and 4 minor recurrences) on follow-up imaging (mean, 21 months), this recurrence rate is favorably comparable with the results reported in the literature.^{4,15,20,21,24–26} An intentional dog-ear remnant in coiling of a branch-incorporated aneurysm cannot be helped, though a dog-ear remnant may be a risk factor for recurrence. There was, however, no significant predictor of recurrence in this study. It may be due to the small number of cases included. Another explanation is that because an incorporated branch was mostly a small or tiny branch except for the posterior communicating artery, hemodynamic stress due to the incorporated branch might also be a little increased and less likely to affect the recurrence rate. In addition, in the case series of coiling of a branch-incorporated aneurysm, the recurrence rate was not greater than those in the literature.⁶ Finally, all 3 major recurrent aneurysms were successfully retreated by additional coiling without any complications.

A flow diverter may be an effective alternative to coiling for these complex aneurysms.²⁷ Unfortunately, no type of flow diverter was launched in our country until November 2014, so it was not available during the study period. Our series demonstrated that the combination technique is not related to a higher complication rate than a single adjunctive device for the treatment of complex aneurysms. Furthermore, the combination strategy for complex aneurysms had a safety and effectiveness favorably comparable with the single adjunctive endovascular techniques in previous studies.^{1–3,8,9,13–15,17–19,22–26}

Our study had several limitations due to its retrospective design and the relatively small number of cases. Therefore, the se-

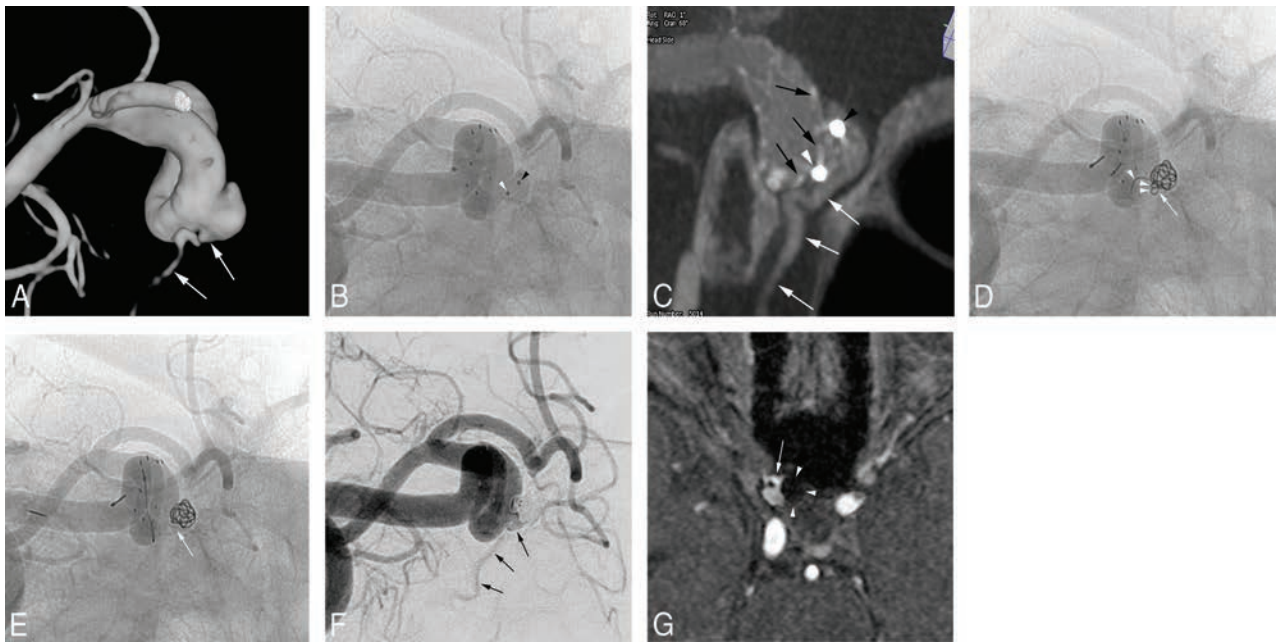


FIG 3. A 59-year-old woman presenting with an unruptured right ophthalmic artery aneurysm. *A*, The 3D reconstruction shows a wide-neck and shallow aneurysm with incorporation of the ophthalmic artery. *Arrows* indicate the ophthalmic artery. Unsubtracted angiogram (*B*) and flat panel CT (*C*) after Neuroform stent placement show 2 microcatheter tips in the aneurysm sac, one of which faces the ophthalmic artery origin. *Black arrows* indicate the struts of the Neuroform stent, and *white arrows* indicate the ophthalmic artery. Note that the 1 catheter tip (*white arrowhead*) faces the ophthalmic artery origin and the other catheter tip (*black arrowhead*) faces the aneurysm dome. *D*, While a helical 1.5 mm × 2 cm coil (*arrowheads*) occupies the region (*arrow*) where the ophthalmic artery branches off and the stent protects the aneurysm neck, an initial coil basket is successfully formed by using the other catheter. *E*, After retrieval of the protection coil, the initial coil basket is stable and the region from which the ophthalmic artery branches off is well-preserved. *F*, Completion angiogram indicates that the aneurysm was nearly completely embolized with intentional preservation of the region from which the ophthalmic artery (*arrows*) branches off. *G*, The 6-month follow-up MR angiogram source image shows no recurrence. The *arrow* indicates the ophthalmic artery origin, and *arrowheads* indicate the coiled aneurysm.

lection bias was inevitable, but it might be somewhat lowered because our data of endovascular treatment were consecutively and prospectively registered. Second, although we preferred balloons to stents in ruptured cases on the basis of the literature,^{17,21} we were not able to demonstrate which device was better for complex aneurysms. Third, angiographic follow-up was not available in all cases; therefore, this lack of follow-up may have somewhat underestimated the recurrence rate. In addition, 7 of the 50 patients who underwent follow-up imaging were followed by MR angiography alone. This type of follow-up might underestimate the recurrence rate a little further.

Finally, this study did not have a control group. Many of the aneurysms might be coilable by using balloon remodeling or stent assistance, and even a single microcatheter. Actually, Kim et al reported a case series about the coiling of a branch-incorporated aneurysm by using multicatheter, balloon, or stent.⁶ Also, a lobulated aneurysm can be coilable by using a multicatheter or single catheter plus a balloon or stent. However, in our experience, this type of coiling took longer and was technically more demanding. In our own experience, the longer it took for coiling, the more frequently procedure-related (especially thromboembolic) complications occurred. Furthermore, in a few cases in which the aneurysm was shallow and had a wide neck and a branch incorporated, it was very difficult to complete coiling by using a single catheter plus balloon/stent or multicatheter. In our own cases in this study, we thought that a combination of multicatheter plus balloon or stent made the coiling time shorter and the procedure easier than multicatheter, balloon-remodeled, or stent-assisted

technique alone. Therefore, despite these limitations, because this study showed satisfactory results in terms of safety and effectiveness, the combination technique described here may provide helpful information in daily practice.

CONCLUSIONS

In this small case series, the combination technique by using a multicatheter plus stent or balloon had very low morbidity and an acceptable recurrence rate for the treatment of a complex aneurysm with a wide neck and an incorporated branch or deep lobulation. The combination technique may be a viable option for coiling of complex aneurysms.

Disclosures: Dong Joon Kim—UNRELATED: Payment for Lectures (including service on Speakers Bureaus); Covidien, Comments: lectures on acute stroke management.

REFERENCES

- Shapiro M, Babb J, Becske T, et al. **Safety and efficacy of adjunctive balloon remodeling during endovascular treatment of intracranial aneurysms: a literature review.** *AJNR Am J Neuroradiol* 2008;29:1777–81 CrossRef Medline
- Generic JC, Biondi A, Piotin M, et al; French SENAT Investigators. **Safety and efficacy of Neuroform for treatment of intracranial aneurysms: a prospective, consecutive, French multicentric study.** *AJNR Am J Neuroradiol* 2013;34:1203–08 CrossRef Medline
- Fargen KM, Hoh BL, Welch BG, et al. **Long-term results of Enterprise stent-assisted coiling of cerebral aneurysms.** *Neurosurgery* 2012;71:239–44; discussion 244 CrossRef Medline
- Starke RM, Durst CR, Evans A, et al. **Endovascular treatment of**

- unruptured wide-necked intracranial aneurysms: comparison of dual microcatheter technique and stent-assisted coil embolization. *J Neurointerv Surg* 2015;7:256–61 CrossRef Medline
5. Durst CR, Starke RM, Gaughen JR Jr, et al. **Single-center experience with a dual microcatheter technique for the endovascular treatment of wide-necked aneurysms.** *J Neurosurg* 2014;121:1093–101 CrossRef Medline
 6. Kim BM, Park SI, Kim DJ, et al. **Endovascular coil embolization of aneurysms with a branch incorporated into the sac.** *AJNR Am J Neuroradiol* 2010;31:145–51 CrossRef Medline
 7. Lubicz B, Lefranc F, Levivier M, et al. **Endovascular treatment of intracranial aneurysms with a branch arising from the sac.** *AJNR Am J Neuroradiol* 2006;27:142–47 Medline
 8. Baxter BW, Rosso D, Lowmie SP. **Double microcatheter technique for detachable coil treatment of large, wide-necked intracranial aneurysms.** *AJNR Am J Neuroradiol* 1998;19:1176–78 Medline
 9. Rho MH, Kim BM, Suh SH, et al. **Initial experience with the new double-lumen sceptor balloon catheter for treatment of wide-necked aneurysms.** *Korean J Radiol* 2013;14:832–40 CrossRef Medline
 10. Kim BM, Kim DJ, Kim DI. **Stent application for the treatment of cerebral aneurysms.** *Neurointervention* 2011;6:53–70 CrossRef Medline
 11. Kim BM, Kim DI, Park SI, et al. **Coil embolization of unruptured middle cerebral artery aneurysms.** *Neurosurgery* 2011;68:346–53; discussion 353–54 CrossRef Medline
 12. Ihn YK, Kim BM, Suh SH, et al. **Coil-protected embolization technique for a branch-incorporated aneurysm.** *Korean J Radiol* 2013;14:329–36 CrossRef Medline
 13. Kim DJ, Kim BM, Park KY, et al. **Coil embolization of overwide and undertall small intracranial aneurysms with double microcatheter technique.** *Acta Neurochir (Wien)* 2014;156:839–46 CrossRef Medline
 14. Cho YD, Kang HS, Kim JE, et al. **Microguidewire protection of wide-necked aneurysms incorporating orifices of tortuous acute-angled vessels: a novel approach.** *Neuroradiology* 2014;56:553–59 CrossRef Medline
 15. McLaughlin N, McArthur DL, Martin NA. **Use of stent-assisted coil embolization for the treatment of wide-necked aneurysms: a systematic review.** *Surg Neurol Int* 2013;4:43 CrossRef Medline
 16. Nakahara T, Kutsuna M, Yamanaka M, et al. **Coil embolization of a large, wide-necked aneurysm using a double coil-delivered microcatheter technique in combination with a balloon-assisted technique.** *Neurol Res* 1999;21:324–26 Medline
 17. Bodily KD, Cloft HJ, Lanzino G, et al. **Stent-assisted coiling in acutely ruptured intracranial aneurysms: a qualitative, systematic review of the literature.** *AJNR Am J Neuroradiol* 2011;32:1232–36 CrossRef Medline
 18. Pierot L, Spelle L, Leclerc X, et al. **Endovascular treatment of unruptured intracranial aneurysms: comparison of safety of remodeling technique and standard treatment with coils.** *Radiology* 2009;251:846–55 CrossRef Medline
 19. Pierot L, Cognard C, Anxionnat R, et al; CLARITY Investigators. **Remodeling technique for endovascular treatment of ruptured intracranial aneurysms had a higher rate of adequate postoperative occlusion than did conventional coil embolization with comparable safety.** *Radiology* 2011;258:546–53 CrossRef Medline
 20. Nishido H, Piotin M, Bartolini B, et al. **Analysis of complications and recurrences of aneurysm coiling with special emphasis on the stent-assisted technique.** *AJNR Am J Neuroradiol* 2014;35:339–44 CrossRef Medline
 21. Shapiro M, Becske T, Sahlein D, et al. **Stent-supported aneurysm coiling: a literature survey of treatment and follow-up.** *AJNR Am J Neuroradiol* 2012;33:159–63 CrossRef Medline
 22. Chung EJ, Shin YS, Lee CH, et al. **Comparison of clinical and radiologic outcomes among stent-assisted, double-catheter, and balloon-assisted coil embolization of wide neck aneurysms.** *Acta Neurochir (Wien)* 2014;156:1289–95 CrossRef Medline
 23. Kwon OK, Kim SH, Oh CW, et al. **Embolization of wide-necked aneurysms with using three or more microcatheters.** *Acta Neurochir (Wien)* 2006;148:1139–45; discussion 1145 CrossRef Medline
 24. Sluzewski M, van Rooij WJ, Beute GN, et al. **Balloon-assisted coil embolization of intracranial aneurysms: incidence, complications, and angiography results.** *J Neurosurg* 2006;105:396–99 CrossRef Medline
 25. Consoli A, Vignoli C, Renieri L, et al. **Assisted coiling of saccular wide-necked unruptured intracranial aneurysms: stent versus balloon.** *J Neurointerv Surg* 2014 Nov 26. [Epub ahead of print] CrossRef Medline
 26. Geyik S, Yavuz K, Yurttutan N, et al. **Stent-assisted coiling in endovascular treatment of 500 consecutive cerebral aneurysms with long-term follow-up.** *AJNR Am J Neuroradiol* 2013;34:2157–62 CrossRef Medline
 27. Becske T, Kallmes DF, Saatci I, et al. **Pipeline for uncoilable or failed aneurysms: results from a multicenter clinical trial.** *Radiology* 2013;267:858–68 CrossRef Medline

High-Resolution C-Arm CT and Metal Artifact Reduction Software: A Novel Imaging Modality for Analyzing Aneurysms Treated with Stent-Assisted Coil Embolization

I. Yuki, Y. Kambayashi, A. Ikemura, Y. Abe, I. Kan, A. Mohamed, C. Dahmani, T. Suzuki, T. Ishibashi, H. Takao, M. Urashima, and Y. Murayama



ABSTRACT

BACKGROUND AND PURPOSE: Combination of high-resolution C-arm CT and novel metal artifact reduction software may contribute to the assessment of aneurysms treated with stent-assisted coil embolization. This study aimed to evaluate the efficacy of a novel Metal Artifact Reduction prototype software combined with the currently available high spatial-resolution C-arm CT prototype implementation by using an experimental aneurysm model treated with stent-assisted coil embolization.

MATERIALS AND METHODS: Eight experimental aneurysms were created in 6 swine. Coil embolization of each aneurysm was performed by using a stent-assisted technique. High-resolution C-arm CT with intra-arterial contrast injection was performed immediately after the treatment. The obtained images were processed with Metal Artifact Reduction. Five neurointerventional specialists reviewed the image quality before and after Metal Artifact Reduction. Observational and quantitative analyses (via image analysis software) were performed.

RESULTS: Every aneurysm was successfully created and treated with stent-assisted coil embolization. Before Metal Artifact Reduction, coil loops protruding through the stent lumen were not visualized due to the prominent metal artifacts produced by the coils. These became visible after Metal Artifact Reduction processing. Contrast filling in the residual aneurysm was also visualized after Metal Artifact Reduction in every aneurysm. Both the observational ($P < .0001$) and quantitative ($P < .001$) analyses showed significant reduction of the metal artifacts after application of the Metal Artifact Reduction prototype software.

CONCLUSIONS: The combination of high-resolution C-arm CT and Metal Artifact Reduction enables differentiation of the coil mass, stent, and contrast material on the same image by significantly reducing the metal artifacts produced by the platinum coils. This novel image technique may improve the assessment of aneurysms treated with stent-assisted coil embolization.

ABBREVIATIONS: MAR = Metal Artifact Reduction; HR = high-resolution

Stent-assisted coil embolization has recently become a common treatment strategy for wide-neck aneurysms.¹⁻⁴ However, poor visibility of the deployed stent during the procedure is considered a limitation because digital subtraction angiography does not allow the visualization of many intracranial stents. Ovalization or kinking of the deployed stent in the parent artery is another limitation.⁵⁻⁸ This phenomenon, also called “inappropri-

ate stent apposition,” can hinder the growth of neointimal coverage on the stent.⁹ Consequently, treated patients are required to undergo a prolonged postprocedural antiplatelet therapy.

Recent reports show that C-arm CT with contrast has superior spatial resolution compared with conventional CT and allows the visualization of both the deployed stent and the contrast material.^{8,10-12} However, once coil embolization is completed, prominent metal artifacts produced by the platinum coils degrade the image quality in the region adjacent to the coil mass, making it extremely difficult to evaluate the minuscule structures around the coil mass.

A new prototype software, Metal Artifact Reduction (MAR; Siemens, Erlangen, Germany), dramatically reduces the metal artifacts in C-arm CT imaging by using a novel image-reconstruction algorithm.^{13,14} Combined with currently available high spatial-resolution C-arm CT prototype implementation, the software enables visualization of meticulous structures around highly attenuated materials like platinum coils.

Received January 27, 2015; accepted after revision June 17.

From the Department of Neurosurgery, The Jikei University School of Medicine, Tokyo, Japan.

This work was supported by a Siemens Research Grant.

Part of this paper was previously presented at: International Stroke Conference, February 12–14, 2014; San Diego, California.

Please address correspondence to Ichiro Yuki, MD, Department of Neurosurgery, The Jikei University School of Medicine, 105-8461 Nishi-Shinbashi 3-25-8, Minato-ku, Tokyo, Japan; e-mail: ichiroyuki@gmail.com; @ichirodyna

Indicates open access to non-subscribers at www.ajnr.org

<http://dx.doi.org/10.3174/ajnr.A4509>

To evaluate the efficacy of MAR, we treated experimental aneurysms with coil embolization by using a stent-assisted technique. Images obtained by using the high-resolution (HR) C-arm CT were processed with MAR. The images before and after MAR processing were compared, and an observational and quantitative analysis was performed.

MATERIALS AND METHODS

Image Acquisition

The images were acquired by using a floor-mounted neuroangiographic unit equipped with 1920×2480 cesium iodide-amorphous silicon flat panel detectors covering an area of approximately 30×40 cm (Artis zee floor; Siemens). The motorized frontal C-arm, typically used for 3D rotational angiography or soft-tissue-optimized C-arm CT, was used to acquire 496 projection images over a 200° arc (rotation time, 20 seconds) at 80 kV(peak) and a total of 260 mAs. The radiation dose for 1 rotational acquisition ranged from 187 to 233 mGy, depending on the position of the scanned animal and the actual conditions of the scan. The focal spot and source-to-detector distances were 0.3 and 1200 mm, respectively. The objects of interest were positioned at the center of rotation, 750 mm from the source.

To maximize spatial resolution, we used a nonbinned mode instead of the 2×2 pixel binning typically used to provide superior contrast resolution for soft-tissue imaging of the C-arm CT. The source projection frames were acquired in a 512×512 matrix covering an FOV of 22 cm diagonally. The rotational datasets were processed with a “normal” (or “sharp”) kernel type, and each acquisition was reconstructed to 2 volume datasets with a 512×512 matrix and an isotropic voxel size ranging from 0.06 to 0.08 mm (corresponding to approximately 30×30 mm and 40×40 mm FOVs, respectively). The first of these 2 volumes was uncorrected and showed significant metal artifacts, whereas the second featured a metal artifacts correction obtained through the application of the MAR prototype software.

In Vitro Evaluation of the Intracranial Stent by High-Resolution C-Arm CT

To compare the image quality produced by conventional C-arm CT with that of the novel HR C-arm CT, 2 Neuroform stents (4.5×20 mm) (Stryker Neurovascular, Kalamazoo, Michigan) were deployed in a silicone vessel model that simulated a bifurcation of a 4-mm vessel. This was scanned by 2 different types of C-arm CT modalities: one with a conventional C-arm CT (Axiom Artis dBA; Siemens), and the other with the high-resolution C-arm CT (Artis zee floor). The 3D volume-rendering images were created by using a Syngo Workplace (Siemens). The obtained 2 images were compared.

Creation of Swine Sidewall Aneurysms followed by Stent-Assisted Coil Embolization

All of the animal experiments were approved by The Jikei University Animal Research Committee. In every treated swine, a sidewall aneurysm was surgically created on each common carotid artery by using a venous graft. Eight experimental aneurysms were created in 6 swine. The aneurysms were designed to be uniformly approximately 6–8 mm in size. To reproduce a wide-neck aneu-

rysm, we adjusted the size of the neck to 4–5 mm in length. The detailed surgical technique was described elsewhere.¹⁵

After the creation of an aneurysm on each side of the common carotid artery, a 6F short sheath was placed on the right femoral artery. Using the sheath, we advanced a 6F guiding catheter to the ipsilateral common carotid artery and DSA was performed to confirm sufficient contrast filling in the aneurysm. Via the guiding catheter, a microcatheter, Excelsior 1018 (Stryker), was placed in the aneurysm. An intracranial stent was then deployed across the neck of the aneurysm via another microcatheter, Excelsior XT-27 (Stryker).

Three aneurysms were treated with Neuroform EZ stents (Stryker Neurovascular). One aneurysm was treated with an Enterprise stent (Codman & Shurtleff, Raynham, Massachusetts), and 4 were treated with a prototype stent with a closed-cell design (4×20 mm). Using a jailing technique, we deployed 3 coils of different sizes into the aneurysms, including Matrix² (Stryker), 10×30 cm; GDC-10 (Stryker), 6×10 cm; and GDC-10, 3×6 cm. Every aneurysm was intentionally left underpacked so that the residual aneurysm could be evaluated postoperatively. In 2 aneurysms, part of the deployed coil was intentionally herniated through the stent lumen, to simulate a situation sometimes encountered in the clinical setting.

HR C-Arm CT with Contrast (Intra-Arterial Injection Protocol) followed by MAR Processing

Using the guiding catheter placed at the proximal common carotid artery, we injected 20% diluted contrast material with an injection speed of 2 mL/s for 22 seconds. The image-acquisition-delay time was set at 2 seconds. The raw data of the HR C-arm CT was sent to a postprocessing workstation syngo XWP (Siemens), and the 3D reconstruction of the obtained images was performed by using syngo InSpace software (Siemens). These were saved as the original preprocessing images.

The raw data of the obtained images were then reconstructed by using the MAR prototype software. The post-MAR images were further processed by using an image-processing application, Aquarius iNtuition, Version 4.4.7.108.0 (TeraRecon, San Mateo, California) to build modified volume-rendering images.

Observer Analysis of the Efficacy of MAR Image Processing

Observational analysis of the efficacy of MAR was performed by using a previously reported analytic method.¹⁴ Five independent neurointerventionalists assessed the quality of pre- and post-MAR processed images in a blinded fashion. During the review, observers were allowed to adjust the window-level settings to optimize viewing. The quality of reconstructed images was rated by using a 3-point scale (1 for “insufficient for evaluation,” 2 for “sufficient for evaluation,” and 3 for “excellent”). Questions included the following: 1) visibility of the stent directly adjacent to the coil mass, and 2) visibility of the parent artery adjacent to the coil mass. Interobserver analyses were performed by using the Wilcoxon signed rank test. Statistical significance was set at a 2-tailed $P = .05$.

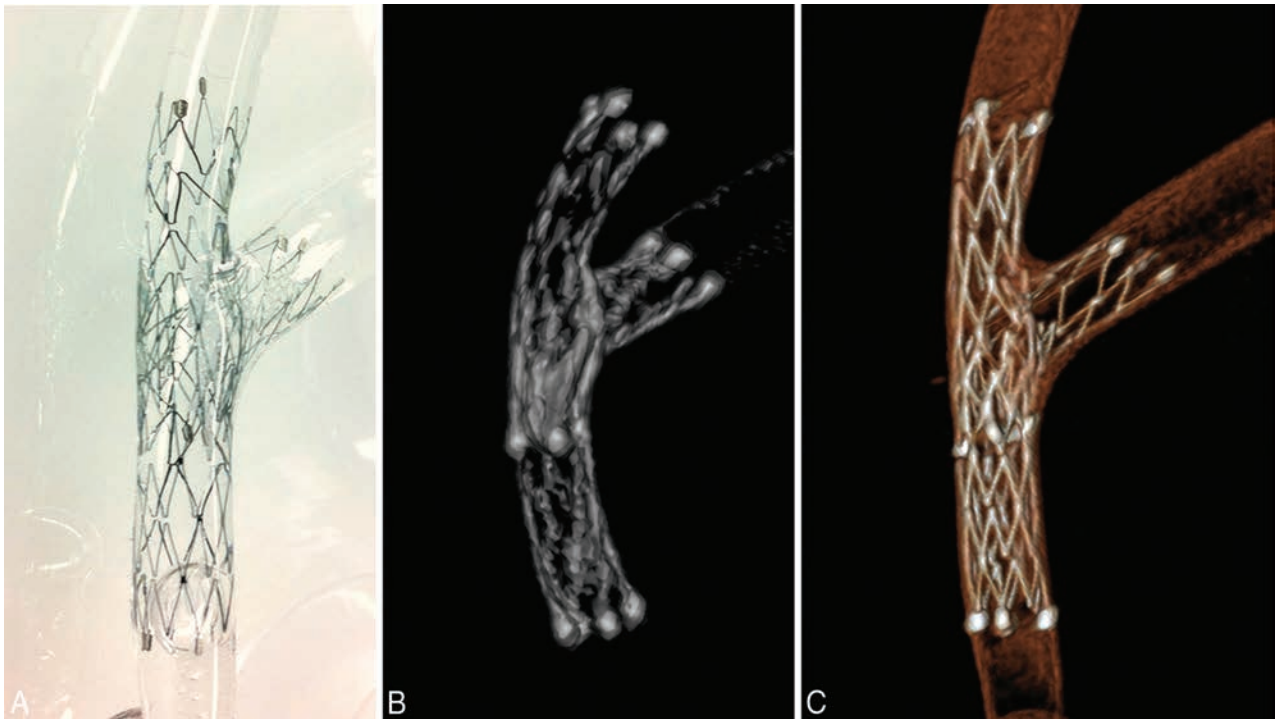


FIG 1. Comparison of the image quality of conventional C-arm CT versus high-resolution C-arm CT. *A*, Two Neuroform stents (4×20 mm) are placed at the bifurcation of a silicone vessel model by using a stent-in-stent technique. *B*, The 3D reconstruction image of the conventional C-arm CT. *C*, The 3D reconstruction image of the high-resolution C-arm CT image. Note the improved visualization of meticulous structures of the stent.

Quantitative Analysis of the Efficacy of MAR and HR C-Arm CT

Quantitative analysis of the efficacy of MAR was also performed by measuring the volume of the streak artifacts produced by the coil material. First, by using 3D reconstruction data of a post-MAR image, we created the baseline coil image by setting the window level that provided the best visualization of the coil mass alone. The volume of the metal obtained from this baseline coil image was defined as “baseline metal volume.” This volume was calculated by using a free open-source software package for image analysis and scientific visualization (3D Slicer, Version 4.3; <http://www.slicer.org>).

Second, the window level of the post-MAR image was adjusted for optimal visualization of the parent artery, stent, and coil mass. The same window level was also applied to the pre-MAR image. This adjusted viewing was defined as “optimized visualization” pre- and post-MAR. The volume of the object observed in each of these optimized visualizations (ie, pre- and post-MAR) was then calculated by using the same software, 3D Slicer.

Last, the baseline metal volume was subtracted from each of the pre- and post-MAR volumes, and the differences between the obtained volumes (pre-MAR in optimized visualization minus baseline metal volume and post-MAR in optimized visualization minus baseline metal volume) were considered as the amount of streak artifacts produced by the coil mass.

The average volume of streak artifacts in the pre-MAR images was compared with the average volume calculated in the post-MAR image. Statistical analysis was performed by the Student *t* test. Significance was set at a 2-tailed $P = .05$.

RESULTS

***In Vitro* Evaluation of the Intracranial Stent by High-Resolution C-Arm CT**

A photograph of the Neuroform stents deployed in a silicone vessel model by using the stent-in-stent technique is shown in Fig 1A. The image obtained by using the conventional C-arm CT (Fig 1B) shows the 2 Neuroform stents (4×20 mm) placed in the silicone vessel model with limited visualization of detailed structures (eg, stent struts). The image obtained by the HR C-arm CT (Fig 1C) demonstrates the meticulous structures of the deployed stents, including the small gaps between the struts, which were the structural features of the open-cell-design stent.

HR C-Arm CT with Contrast Injection followed by MAR

All 8 aneurysms in the 6 swine were successfully created and were treated by coil embolization by using the stent-assisted technique. Embolization was stopped before complete occlusion of the aneurysm so that the residual aneurysm could be evaluated by post-treatment angiography.

In all aneurysms, thin-section MIP images of the HR C-arm CT obtained immediately after the procedure revealed metal artifacts produced by the coil mass. In the pre-MAR image, the image quality near the coil mass was degraded due to the metal artifacts, and differentiating the coils from the stent was difficult. The thin-section MIP images of the post-MAR image showed reduction of the metal artifacts (Fig 2A). The microcatheter placed in the aneurysm via the stent struts became visible after MAR (Fig 2B).

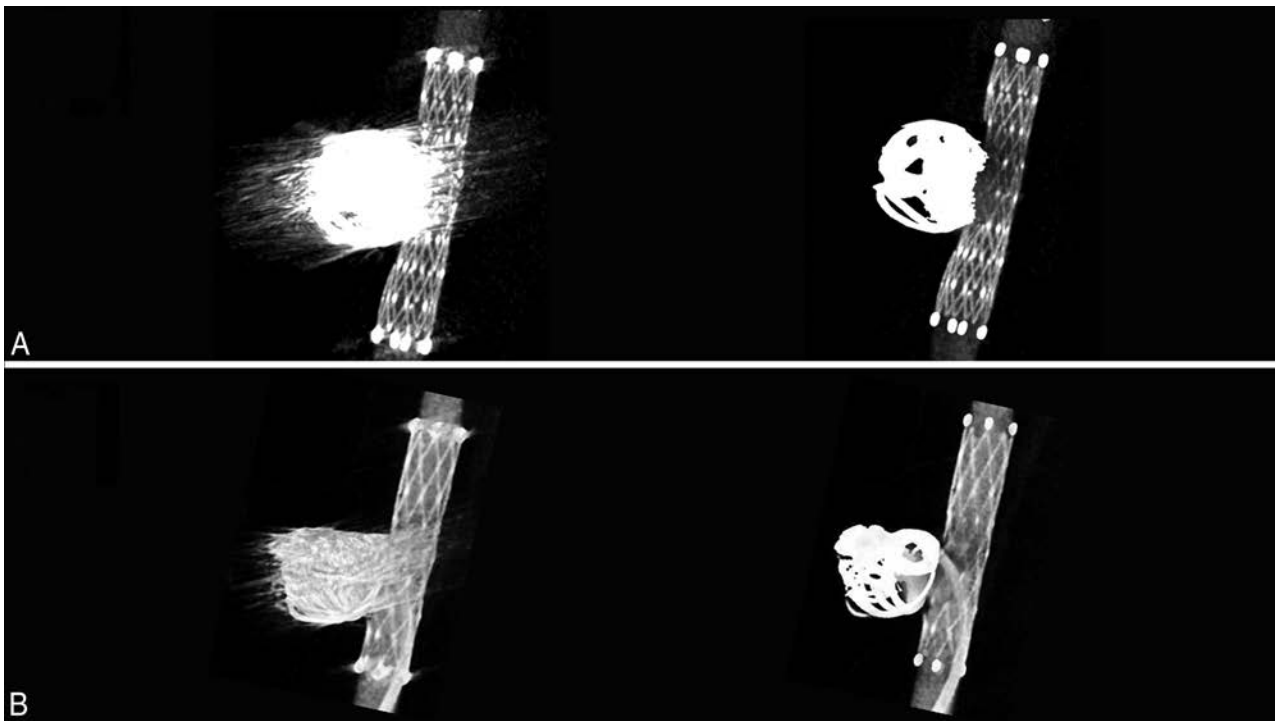


FIG 2. Thin-section MIP images of the aneurysms treated with stent-assisted coil embolization. *A*, Comparison of the pre- (*left*) and post-MAR (*right*) images of an aneurysm treated with a combination of bare platinum coils and a Neuroform stent (4×20 mm) reveals improved visibility of the stent structures near the coil mass after MAR processing. *B*, Another aneurysm that was treated with coil embolization by using a Neuroform stent. Note the improved visibility of the microcatheter inserted in the aneurysm and contrast filling in the aneurysm after the MAR processing (*right*).

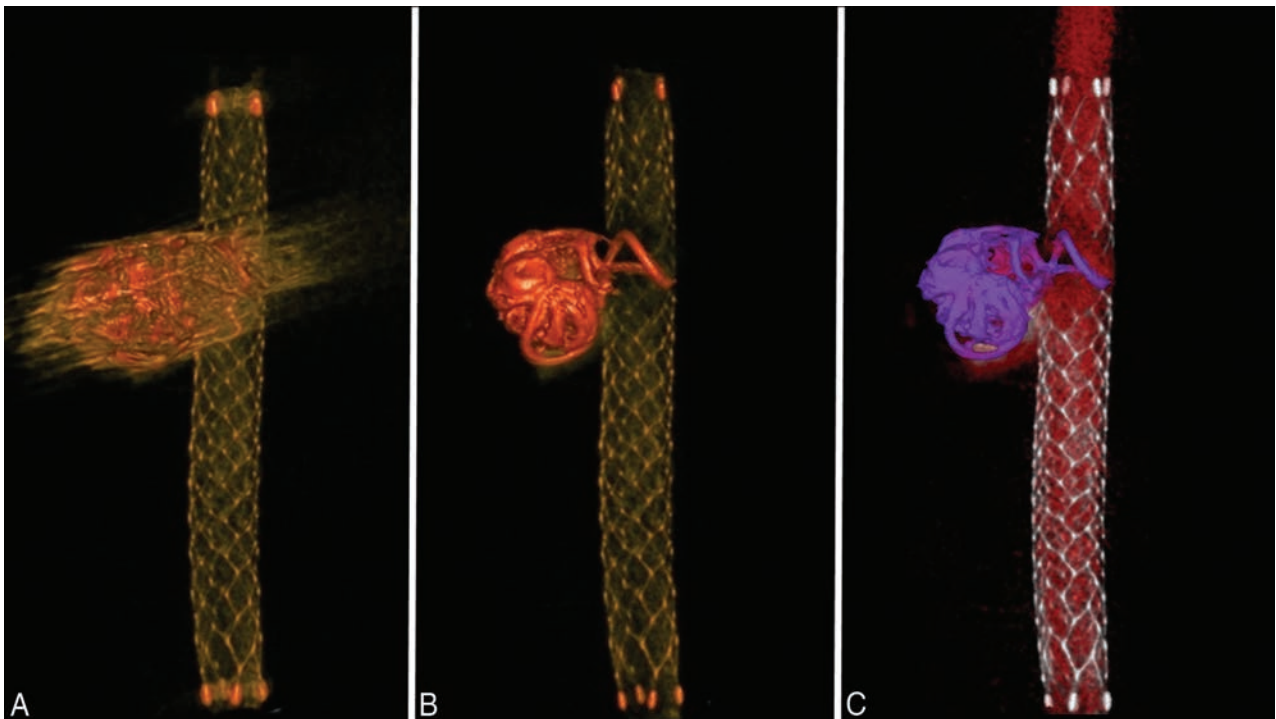


FIG 3. Volume-rendering images of an aneurysm treated by using an Enterprise stent. A volume-rendering image of an aneurysm treated with an Enterprise stent shows that the visibility of the structures around the coil mass in the pre-MAR image (*A*) improves after MAR processing (*B*). *C*, The post-MAR image is further processed by using an image-processing application, Aquarius iNtuition, to create a special volume-rendering image. Different colors are selected on the basis of the range of Hounsfield units. The coil mass (purple) is differentiated from the stent (silver) and contrast (red). The coil loop that protrudes into the stent lumen is also well-visualized.

The volume-rendering images of an aneurysm treated with coil embolization by using an Enterprise stent are shown in Fig 3. Again, the visibility of the structures around the coil mass in the pre-MAR

image (Fig 3A) was improved after MAR processing (Fig 3B). The post-MAR image was further processed by using an image-processing application, Aquarius iNtuition, Version 4.4.7.108.0, to build special

volume-rendering images (Fig 3C). The coil mass (purple) is clearly differentiated from the stent (silver), and the coil loop protruding into the stent lumen is clearly visualized.

Observer Analysis of the Efficacy of MAR and HR C-Arm CT

The results of the observer study are summarized in the Table. First, the stent visibility near the orifice of the coil mass was evaluated by using the pooled data analysis. In the pre-MAR images, 77.5% of the samples rated had a score of 1 (insufficient for the diagnosis), while

Results of the observer study rating the visibility of pre- and post-MAR images

Score ^a	Pre-MAR (%)	Post-MAR (%)	Improvement after MAR Wilcoxon Signed Rank Test
Stent visibility			
1	77.5	0.0	Improved after MAR $P < .0001$
2	22.5	40.0	
3	0.0	60.0	
Parent artery visibility			
1	75.0	12.5	Improved after MAR $P < .0001$
2	22.5	30.0	
3	2.5	60.0	
Overall			
1	76.3	6.3	Improved after MAR $P < .0001$
2	22.5	35	
3	1.3	60.0	

^a Score 1 indicates insufficient for diagnosis; score 2, sufficient for diagnosis; score 3, excellent.

22.5% had a score of 2 (sufficient for the diagnosis). No sample was rated 3 (excellent). In the post-MAR images, 0%, 40%, and 60% of the samples rated had scores of 1, 2, and 3, respectively.

Similarly, the visibility of the parent artery near the coil mass was evaluated. In the pre-MAR images, 75% of the samples rated had a score of 1, 22.5% had 2, and 2.5% had 3. In the post-MAR images, 12.5%, 30%, and 60% of the samples had scores of 1, 2, and 3, respectively.

Overall, in the pre-MAR images, 76.3% of the samples had a score of 1, 22.5% had 2, and 1.3% had 3. In the post-MAR images, 6.3% of the samples had a score of 1, 35% had 2, and 60% had 3.

By the Wilcoxon matched pairs signed rank test, for all categories, the pooled scores given by the observers to the C-arm CT images before MAR were significantly improved after the images were processed with MAR ($P < .0001$).

Quantitative Analysis of the Efficacy of MAR and HR C-Arm CT

The baseline coil image is shown in Fig 4A. Using the workstation syngo Workplace, we adjusted the width and level of the window, the slab thickness, and the position of the images in the post-MAR image (Fig 4B). The same parameters were applied to the pre-MAR image (Fig 4C). The baseline coil volume was subtracted from both the pre- and post-MAR images, and the difference was defined as the “streak artifacts.”

The volume of streak artifacts in the pre-MAR images was compared with that in the post-MAR images (Fig 5). In all 8 aneurysms, the volume of streak artifacts calculated in the pre-MAR images was significantly reduced in the post-MAR images. The

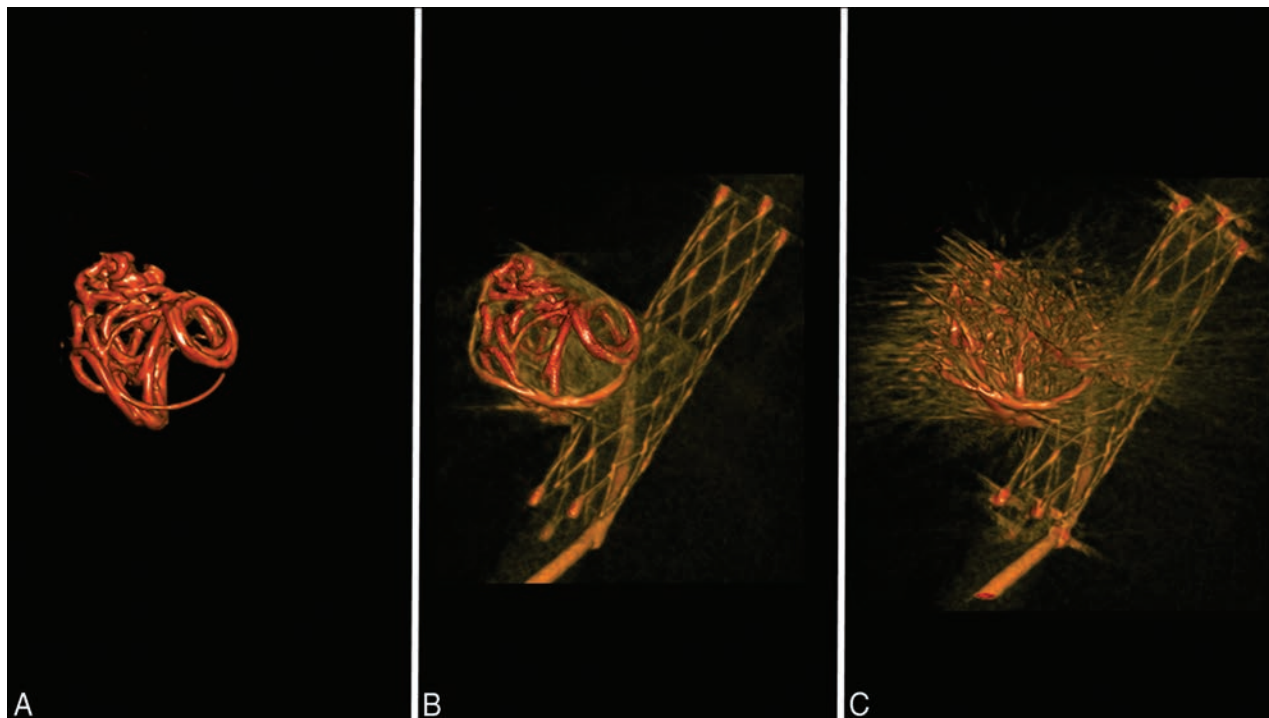


FIG 4. Quantitative measurement of the streak artifacts. *A*, Using the 3D reconstruction data of a post-MAR image, we calculated the baseline metal volume by setting the window level that provides the best visualization of the high-attenuation metal component. *B*, The window level of the post-MAR image is adjusted for the optimal visualization of the parent artery, stent, and coil mass. *C*, The same window level is applied to the pre-MAR image. The volume of the streak artifacts is determined by the difference of the volume of the pre-MAR image and the volume of post-MAR image. The volume of each image is calculated by using the image analysis software 3D Slicer.

Results of Quantitative Analysis: Volume of Streak Artifact

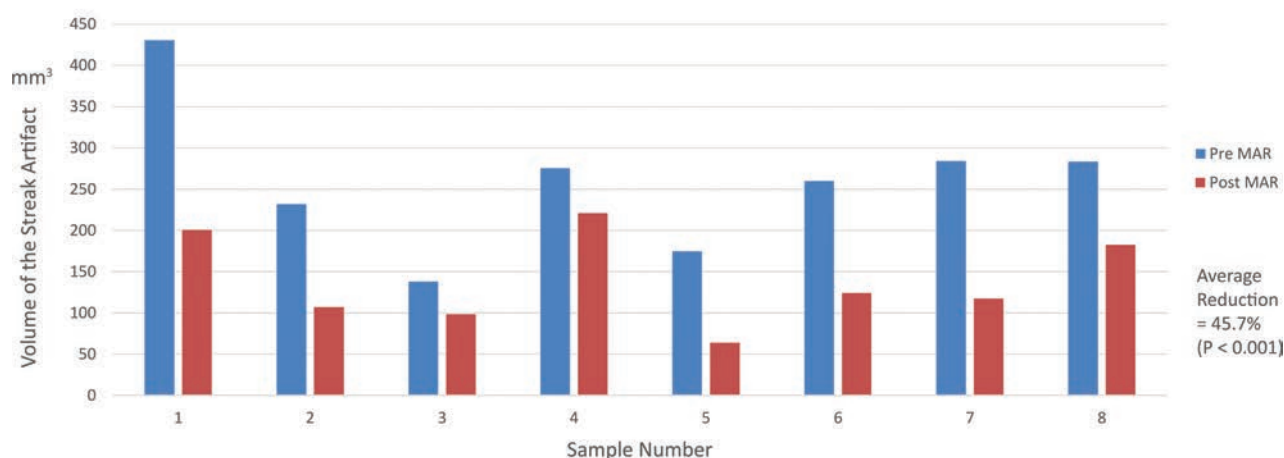


FIG 5. Quantitative analysis of streak artifacts. A graph compares the volume of streak artifacts of the pre- and post-MAR images. In all 8 samples, the volume of streak artifacts in the pre-MAR images is significantly reduced in the post-MAR images. The average artifacts reduction for all samples is 45.7% ($P = .001$).

greatest volume reduction was observed in sample 5, in which the volume of streak artifacts decreased from 174.6 to 63.9 mm³, yielding a 63.4% artifacts reduction. The lowest volume reduction was seen in sample 4, from 275.1 to 220.8 mm³, yielding an artifacts reduction of 19.8%. The average artifacts reduction for all samples was 45.7%. By the Student *t* test, there was a statistically significant difference between the examined datasets ($P = .00034$).

DISCUSSION

Application of Metal Artifact Reduction Software on Currently Available High-Resolution C-Arm CT Images

van der Bom et al¹⁴ reported the efficacy of a metal artifacts correction software on high-resolution C-arm CT images of patients treated with stent-assisted coil embolization. They concluded that the MAR software they used was not capable of fully removing artifacts caused by the implants, even though the image quality of the C-arm CT data was drastically improved after MAR.

The algorithm of the MAR used in the aforementioned study is based on the procedure proposed by Prell et al,¹³ whereas the algorithm used in the present work is a modified and extended implementation of the procedure.¹⁶ The main difference is a higher dimension of the matrix used for the reconstruction of the C-arm CT volume (512³ compared with 256³), resulting in a potentially higher resolution of the obtained images with relatively smaller voxel sizes for the same FOV. Compared with the currently available normal-resolution C-arm CT images, the quality of the postprocessing images was further improved, allowing better differentiation among the stent, coils, and contrast dye.

Results of the observational analysis revealed significant improvement in the visibility of the meticulous structures after MAR, which was probably due to the prominent reduction in streak artifacts, as shown in the results of the quantitative analysis. Moreover, the high spatial resolution may have contributed to the improved visibility of the minuscule structures after MAR.

Limitations of the Study

The swine aneurysm model used in this study simulates the similar size (of the aneurysm and parent artery) and similar biofluid mechanical parameters (ie, cardiac output and blood viscosity) observed in human aneurysms. However, the parent arteries in human aneurysms are normally more tortuous and are surrounded by a skull. Whether the quality of the images presented in this study can be reproduced in the clinical setting is uncertain.

The effectiveness of the metal artifact reduction can be influenced by the volume and attenuation of the high-attenuating material adjacent to the target vessel. If the stent was surrounded by high-attenuating materials, visualization of the stent will become more challenging. The aneurysm model used in this study was a wide-neck aneurysm, though it does not necessarily represent an extremely wide-neck/fusiform aneurysm. Further study investigating the effectiveness of the MAR in such aneurysms treated with stent-assisted coiling should be conducted.

The quantitative analysis of the metal artifacts focuses on the measurement of the streak artifacts, the high-attenuation radiating artifacts from the coil material that are components of several different types of artifacts, including noise, beam-hardening, partial volume effect, and scatter. Because the streak artifacts are only 1 component of such complex phenomena, establishing a measurement method for the true metal artifacts in reconstructed image data is essential. Notably, the calculated streak artifacts in this study not only include the true artifacts arising from the coil but also the following: 1) part of the stent in the considered volume of interest, 2) the contrast medium in the parent artery confined in that same VOI, and 3) artifacts related to other high-attenuation objects (eg, vertebral bones in the VOI).

One acquisition of the HR DynaCT (Siemens) in this study required a radiation dose of 187–233 mGy. If one knows that 1 biplane DSA acquisition with a frame rate of 4 frames/s and high magnification (eg, 11 cm diagonal) requires approximately 150 mGy, this dose is considered justifiable if the information ob-

tained from the sequence is essential for the decision-making in the course of treatment. However, it is still crucial to minimize the radiation dose by collimating the ROI as much as possible.

Future Applications

When an extremely wide-neck aneurysm or a fusiform aneurysm is treated with a stent-assisted technique, separating the coil mass from the parent artery in the DSA images often becomes difficult. Intraoperative use of the C-arm CT with MAR may allow distinguishing the stent, parent artery, and coils. This distinction may contribute to the prevention of technical complications during the procedure.

Second, to date, most patients undergo prolonged antiplatelet therapy after stent-assisted coil embolization due to the concern of a thromboembolic event related to the deployed stent. In fact, in the field of cardiovascular intervention, studies have shown that inappropriate stent apposition causes delay in neointimal coverage, which can lead to the increased risk of a thromboembolic event.⁹

Intra-arterial sonography or intravascular optical coherence tomography is the imaging modality mainly used for the evaluation of post-coronary stent placement. None of these modalities, however, are currently applicable to the intracranial artery, which is extremely tortuous and vulnerable compared with the coronary artery.

A combination of HR C-arm CT and MAR may contribute to the risk assessment of thromboembolic events related to the stent-assisted coil embolization by providing information about the postoperative stent apposition in the treated artery.

CONCLUSIONS

The combination of currently available high spatial-resolution C-arm CT with a prototype implementation of MAR enables the differentiation of the coil mass, stent, and contrast material by significantly reducing the metal artifacts produced by the platinum coils. This novel image technique allows improved visualization of meticulous structures around the coil mass and may contribute to the evaluation of aneurysms treated with stent-assisted coil embolization.

Disclosures: Ichiro Yuki—RELATED: Grant: Siemens*; Support for Travel to Meetings for the Study or Other Purposes: Siemens; Provision of Writing Assistance, Medicines, Equipment, or Administrative Support: Stryker provided stents used in the experiment; UNRELATED: Patents (planned, pending or issued): 1) UC Case No. 2010-085-one (Method and Apparatus for a Surface-Modified Coil Material for Treatment of Brain Aneurysm); 2) UC Case No. 2009-668-one (Dual Rotational Stent Apparatus); 3) UC Case No. 2011-135-1; SSD No. 105837.00023 (Bioactive Spiral Coil Coating); Travel/Accommodations/Meeting Expenses Unrelated to Activities Listed: Siemens (for attending an international meeting). Ashraf Mohamed—UNRELATED: Employment: Siemens (full-time); Stock/Stock Options: Siemens (\$30,000). Toshihiro Ishibashi—RELATED: Stryker Japan,* Siemens*; Consulting Fee or Honorarium: Stryker Japan; UNRELATED: Consultancy: Stryker Japan; Grants/Grants Pending: Stryker Japan,* NTT DOCOMO,* Siemens.* Yuichi Murayama—RELATED: Grant: Siemens*; Support for Travel to Meetings for the Study or Other Purposes: Siemens; UNRELATED: Grants/Grants Pending: Siemens*; Payment for Lectures (including service on Speakers Bureaus): Siemens. *Money paid to the institution.

REFERENCES

1. Chalouhi N, Jabbour P, Singhal S, et al. **Stent-assisted coiling of intracranial aneurysms: predictors of complications, recanalization, and outcome in 508 cases.** *Stroke* 2013;44:1348–53 CrossRef Medline
2. Fiorella D, Albuquerque FC, Deshmukh VR, et al. **Usefulness of the Neuroform stent for the treatment of cerebral aneurysms: results at initial (3–6-mo) follow-up.** *Neurosurgery* 2005;56:1191–201; discussion 1201–02 CrossRef Medline
3. Geyik S, Yavuz K, Yurttutan N, et al. **Stent-assisted coiling in endovascular treatment of 500 consecutive cerebral aneurysms with long-term follow-up.** *AJNR Am J Neuroradiol* 2013;34:2157–62 CrossRef Medline
4. Wakhloo AK, Linfante I, Silva CF, et al. **Closed-cell stent for coil embolization of intracranial aneurysms: clinical and angiographic results.** *AJNR Am J Neuroradiol* 2012;33:1651–56 CrossRef Medline
5. Tsuruta W, Matsumaru Y, Hamada Y, et al. **Analysis of closed-cell intracranial stent characteristics using cone-beam computed tomography with contrast material.** *Neurol Med Chir (Tokyo)* 2013;53:403–08 CrossRef Medline
6. Heller R, Calnan DR, Lanfranchi M, et al. **Incomplete stent apposition in Enterprise stent-mediated coiling of aneurysms: persistence over time and risk of delayed ischemic events.** *J Neurosurg* 2013;118:1014–22 CrossRef Medline
7. Heller RS, Malek AM. **Parent vessel size and curvature strongly influence risk of incomplete stent apposition in Enterprise intracranial aneurysm stent coiling.** *AJNR Am J Neuroradiol* 2011;32:1714–20 CrossRef Medline
8. Patel NV, Gounis MJ, Wakhloo AK, et al. **Contrast-enhanced angiographic cone-beam CT of cerebrovascular stents: experimental optimization and clinical application.** *AJNR Am J Neuroradiol* 2011;32:137–44 CrossRef Medline
9. Foin N, Gutiérrez-Chico JL, Nakatani S, et al. **Incomplete stent apposition causes high shear flow disturbances and delay in neointimal coverage as a function of strut to wall detachment distance: implications for the management of incomplete stent apposition.** *Circ Cardiovasc Interv* 2014;7:180–89 CrossRef Medline
10. King RM, Chueh JY, van der Bom IM, et al. **The effect of intracranial stent implantation on the curvature of the cerebrovasculature.** *AJNR Am J Neuroradiol* 2012;33:1657–62 CrossRef Medline
11. Heller RS, Malek AM. **Successful detection of embologenic ulceration in a symptomatic non-hemodynamic intracranial stenosis using C-arm cone beam CT.** *J Neurointerv Surg* 2013;5:e3 CrossRef Medline
12. Struffert T, Lang S, Adamek E, et al. **Angiographic C-arm CT visualization of the Woven EndoBridge cerebral aneurysm embolization device (WEB): first experience in an animal aneurysm model.** *Clin Neuroradiol* 2014;24:43–49 CrossRef Medline
13. Prell D, Kalender WA, Kyriakou Y. **Development, implementation and evaluation of a dedicated metal artefact reduction method for interventional flat-detector CT.** *Br J Radiol* 2010;83:1052–62 CrossRef Medline
14. van der Bom IM, Hou SY, Puri AS, et al. **Reduction of coil mass artifacts in high-resolution flat detector conebeam CT of cerebral stent-assisted coiling.** *AJNR Am J Neuroradiol* 2013;34:2163–70 CrossRef Medline
15. Murayama Y, Viñuela F, Suzuki Y, et al. **Ion implantation and protein coating of detachable coils for endovascular treatment of cerebral aneurysms: concepts and preliminary results in swine models.** *Neurosurgery* 1997;40:1233–43; discussion 1243–44 CrossRef Medline
16. Stidd DA, Theessen H, Deng Y, et al. **Evaluation of a metal artifacts reduction algorithm applied to postinterventional flat panel detector CT imaging.** *AJNR Am J Neuroradiol* 2014;35:2164–69 CrossRef Medline

Evaluation of the Angiographic Grading Scale in Aneurysms Treated with the WEB Device in 80 Rabbits: Correlation with Histologic Evaluation

A. Rouchaud, W. Brinjikji, Y.-H. Ding, D. Dai, Y.Q. Zhu, H.J. Cloft, D.F. Kallmes, and R. Kadirvel



ABSTRACT

BACKGROUND AND PURPOSE: The WEB Occlusion Score has been proposed to assess angiographic outcomes for intracranial aneurysms treated with the Woven EndoBridge (WEB) device. Using a large series of experimental aneurysms treated with the WEB, we had the following objectives: 1) to compare angiographic outcomes as measured by the WEB Occlusion Scale with histologic results, and 2) to assess interobserver and intraobserver agreement of the WEB Occlusion Scale.

MATERIALS AND METHODS: Intracranial aneurysms were created in 80 rabbits and treated with WEB devices. Animals were sacrificed at last follow-up for histologic evaluation. DSA was performed just after the deployment of the device and at follow-up. Four investigators independently and retrospectively graded the DSA twice according to the WEB Occlusion Scale. One histopathologist blinded to the angiographic results graded the occlusion according to a 4-point scale patterned on the WEB Occlusion Scale. Intra- and interobserver agreement were evaluated for DSA. Follow-up angiographic grading and histologic reference were compared to determine the WEB Occlusion Scale accuracy for complete (with or without recess filling) versus incomplete occlusion and adequate (complete occlusion or neck remnant) versus inadequate occlusion.

RESULTS: Inter- and intraobserver weighted κ for the angiographic WEB Occlusion Scale were, respectively, 0.76 and 0.76, indicating substantial agreement. The sensitivity and specificity of the WEB Occlusion Scale for complete occlusion at follow-up compared with the histologic reference standard were, respectively, 75% and 83.3%, with an overall accuracy of 80%. Similarly, for adequate occlusion at follow-up, sensitivity was 97.7%, specificity was 64.9%, and overall accuracy was 82.5%.

CONCLUSIONS: The WEB Occlusion Scale appears to be consistent, reliable, and accurate compared with a histologic reference standard.

ABBREVIATIONS: WEB = Woven EndoBridge; WOS = WEB Occlusion Scale

The Woven EndoBridge (WEB) device (Sequent Medical, Aliso Viejo, California) is a new and promising tool in the treatment of wide-neck and bifurcation intracranial aneurysms.¹⁻⁴ The endosaccular implant conforms to the aneurysm wall and spans the aneurysm neck to essentially function as a flow diverter at the aneurysm neck–parent artery interface. Initial experimental and clinical studies have demonstrated that the WEB is both safe and effective in the treatment of intracranial aneurysms.¹⁻⁹

Because the mechanism of action of the device differs from that in flow diverters and endosaccular coils, developing tools to assess angiographic occlusion has become a recent priority among many neurointerventionists, and several grading scales have been proposed.^{4,7-10} Perhaps the most commonly used scale is the WEB Occlusion Scale (WOS).⁷ However, none of these scales, including the WOS, has previously been validated with histologic studies, to our knowledge. In a large series of elastase-induced aneurysms in rabbits treated with the WEB device, the objectives of this study were the following: 1) to compare angiographic outcomes as measured by the WOS with histologic results, and 2) to assess interobserver and intraobserver agreement of the WOS.

MATERIALS AND METHODS

In Vivo Experiments

The Institutional Animal Care and Use Committee at our Institution approved the animal procedures. Elastase-induced aneu-

Received May 26, 2015; accepted after revision July 14.

From the Neuroradiology Research Laboratory (A.R., Y.-H.D., D.D., Y.Q.Z., D.F.K., R.K.), Mayo Clinic College of Medicine, Rochester, Minnesota; and the Department of Radiology (A.R., W.B., H.J.C., D.F.K.), Mayo Clinic, Rochester, Minnesota.

Please address correspondence to Aymeric Rouchaud, MD, Neuroradiology Research Laboratory, Mayo Clinic, 200 First St SW, Rochester, MN 55905; e-mail: Rouchaud.Aymeric@mayo.edu; aymeric.rouchaud@gmail.com

Indicates article with supplemental on-line tables.

<http://dx.doi.org/10.3174/ajnr.A4527>

rysms were created in 80 New Zealand white rabbits. Aneurysm creation procedures were performed as previously described by our study group.¹¹ Aneurysms were treated at least 3 weeks after aneurysm creation.¹² No antiplatelet therapy was used before or after treatment. During the device-deployment procedure, animals were anesthetized, the right femoral artery was exposed, and a 5F sheath was inserted, followed by injection of 500 U of heparin through the sheath. A 5F guide catheter (Envoy; Codman & Shurtleff, Raynham, Massachusetts) was advanced into the aortic arch. Digital subtraction angiography was performed with contrast injection through the guide catheter. A microcatheter (Renegade Hi-Flo; Boston Scientific, Natick, Massachusetts) was advanced into the aneurysm lumen over a microguidewire (Transend EX; Stryker, Kalamazoo, Michigan) through the guide catheter. The WEB size was selected according to the aneurysm size. After deployment of the device, the microcatheter was removed and DSA was performed through the guide catheter at the brachiocephalic trunk immediately and 5 minutes following device implantation. Follow-up angiographic evaluation was performed at the sacrifice end point according to the WEB Occlusion Scale as described by Fiorella et al.⁷ Animals were sacrificed with a lethal injection of pentobarbital. Aneurysm and parent artery tissue were immediately fixed in 10% neutral buffered formalin.

Angiographic Evaluations

Four investigators independently and retrospectively examined selected images of the posttreatment and follow-up DSA to grade the occlusion status according to the WEB Occlusion Scale. These readings were performed twice by each of the investigators at 2-month intervals to analyze the intraobserver correlation in the readings. The WEB Occlusion Scale is a 4-point scale using the following grades: complete aneurysm occlusion, complete occlusion with recess filling, aneurysm neck remnants, and aneurysm remnants. The investigators also evaluated the modification of the aneurysm occlusion status between posttreatment and follow-up DSA as follows: improvement, stable, or recurrence. To compare follow-up DSA readings and histologic findings, we dichotomized DSA results as complete occlusion (with or without proximal recess filling) or incomplete occlusion (neck remnant or aneurysm remnant); similarly, we dichotomized DSA results as adequate occlusion (complete occlusion or neck remnant) or inadequate occlusion (aneurysm remnant), according to previous studies.^{8,13} In case of disagreement among readers, a fifth reader adjudicated between adequate or inadequate occlusion.

Histopathologic Processing and Analysis

One histopathologist blinded to the angiographic results did the processing and analysis for healing evaluation. Aneurysm samples were processed at 1000- μm intervals in a coronal orientation, permitting long-axis sectioning of the aneurysm neck, with use of an IsoMet Low Speed Saw (Buehler, Lake Bluff, Illinois). After the device segments were carefully removed under a dissecting microscope, the samples were then re-embedded in paraffin, sectioned at 5–6 μm , and stained with hematoxylin-eosin. The sections

were evaluated by using our previously reported evaluation criteria.¹⁴

The histologic results for each aneurysm were evaluated according to a 4-point histologic scale, patterned on the angiographic WEB Occlusion Scale with the same items: complete aneurysm occlusion, complete occlusion with recess filling, aneurysm neck remnants, and aneurysm remnants.

Statistical Analysis

Statistical analysis was performed by using the statistical software package SAS 9.0 (SAS Institute, Cary, North Carolina). Interobserver and intraobserver agreement was assessed by using the quadratic weighted κ statistic. κ statistics for interobserver agreement were calculated between each observer. Mean κ values were calculated as well. The ANOVA intraclass correlation between readers was calculated. The sensitivity, specificity, and accuracy of DSA evaluations at last angiographic follow-up were calculated by using the histologic findings as a reference standard. These were calculated on a per-reading basis.

RESULTS

Population

Eighty consecutively treated rabbits were included in this study. The length of follow-up varied from 30 to 365 days, with a mean length of follow-up of 101.4 days. Rabbits were sacrificed at day 30 ($n = 27$), day 50 ($n = 5$), day 90 ($n = 30$), day 180 ($n = 12$), or day 365 ($n = 6$). A Single-Layer WEB was used in 55% of cases ($n = 44$), and a Dual-Layer WEB was used in 45% of cases ($n = 36$).

Angiographic Results

Eight readings were performed for each of the 80 posttreatment and 80 follow-up DSAs (4 readers doing the same reading twice at 2-month intervals). Immediate posttreatment DSA showed 8.3% complete occlusion ($n = 53/640$ readings), 3.8% ($n = 24$) complete occlusion with recess filling, 12.7% ($n = 81$) neck remnants, and 75.3% ($n = 482$) aneurysm remnants. At last follow-up DSA, we observed 24.6% complete occlusion ($n = 157/639$ readings), 21.6% ($n = 138$) complete occlusion with recess filling, 30.8% ($n = 197$) neck remnants, and 23.0% ($n = 147$) aneurysm remnants.

The interobserver weighted κ coefficient for agreement of the occlusion grade according to the angiographic WEB occlusion scale was 0.76 (95% CI, 0.76–0.82), indicating substantial agreement among readers (range, 0.68–0.81). The intraobserver κ for the 2 sequential readings of the angiographic results was also substantial at 0.76 (95% CI, 0.72–0.81), ranging from 0.58 to 0.85. The ANOVA intraclass correlation among readers was 0.86 (95% CI, 0.81–0.90) for the first reading and 0.82 (95% CI, 0.76–0.87) for the second reading. The overall intraclass correlation score for both readings was 0.84 (95% CI, 0.79–0.88). Inter- and intraobserver agreement is presented in On-line Tables 1 and 2.

Variation of the aneurysm occlusion status between posttreatment and follow-up DSA showed 73.3% ($n = 469/640$) improvement, 16.6% ($n = 106$) stable occlusion, and 10.1% ($n = 65$) increase of opacification of the aneurysms compared with posttreatment DSA. The intra- and interreader κ was 0.73 (95% CI, 0.70–0.77) and 0.78 (95% CI, 0.71–0.84), respectively. These data are summarized in Table 1.

Table 1: Inter- and intraobserver κ agreement for follow-up DSA readings

	R1	R2	R3	R4
R1	0.748 (0.599–0.897) ^a	0.755 (0.690–0.819)	0.723 (0.656–0.790)	0.658 (0.587–0.730)
R2		0.847 (0.772–0.923) ^a	0.745 (0.680–0.811)	0.700 (0.632–0.767)
R3			0.823 (0.744–0.903) ^a	0.711 (0.644–0.778)
R4				0.582 (0.474–0.691) ^a

Note:—R indicates reader.

^a Intraobserver κ results.

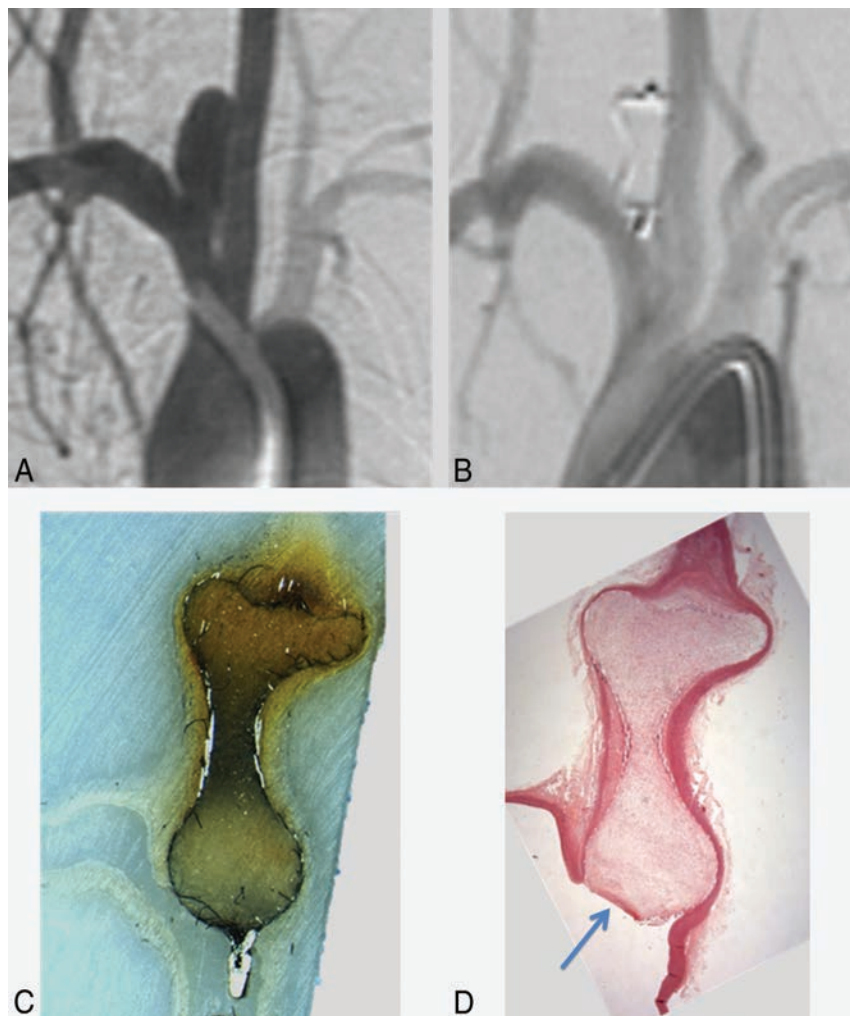


FIG 1. Complete aneurysm occlusion. Angiographic-histologic correlation. Pretreatment DSA shows an aneurysm on the right subclavian artery at the origin of the right common carotid artery (A). Follow-up DSA shows complete occlusion of the aneurysm (B). An all-mount histologic sample shows complete occlusion of the aneurysm, filled with conjunctive tissue and with any lack of organized tissue in to the aneurysm cavity or at the level of the neck (C). Photomicrograph (hematoxylin-eosin, original magnification $\times 100$) shows complete coverage of the neck with endothelial tissue with complete healing (D) and organized connective tissue within the aneurysm lumen.

Complete versus Incomplete Occlusion

We dichotomized follow-up DSA results as complete versus incomplete occlusion. The interobserver κ at follow-up was 0.63 (95% CI, 0.56–0.70), ranging from 0.42 to 0.76; the intraobserver κ was 0.71 (95% CI, 0.55–0.88), ranging from 0.47 to 0.85.

To compare with histologic findings, a fifth reader was needed in 31.2% cases (25/80) to adjudicate between complete or incomplete occlusion. The adjudicated dichotomized DSA evaluation yielded 40% (32/80) complete occlusion and 60% (48/80) incomplete occlusion.

toology agreed for incomplete occlusion. In 8 (10%) cases, DSA suggested a complete occlusion but histology identified incomplete, and similarly, 8 (10%) cases that had been misassessed as incomplete by DSA were found to have complete occlusion on histology (Table 2). Sensitivity and specificity of the DSA for the diagnosis of complete versus incomplete occlusion at follow-up compared with the histologic results as the reference standard were respectively 75% (95% CI, 56%–88%) and 83.3% (95% CI, 69%–92%). The overall accuracy of the DSA evaluation com-

Adequate versus Inadequate Occlusion

We dichotomized DSA results as adequate occlusion (complete healing or proximal recess persistence) versus inadequate occlusion (neck or aneurysm remnants). The interobserver κ at follow-up was 0.69 (95% CI, 0.64–0.73), ranging from 0.50 to 0.79; the intraobserver κ was 0.75 (95% CI, 0.62–0.89), ranging from 0.55 to 0.85.

To compare the DSA results with histologic findings, we determined a consensus value to allocate in the adequate versus inadequate occlusion group, according to the most present value without need for a fifth reader to adjudicate. The consensus dichotomized DSA evaluation yielded 68.8% (55/80) adequate occlusion and 31.2% (25/80) inadequate occlusion.

Histologic Results

Histologic evaluation at the time of follow-up DSA depicted 18.8% complete healing ($n = 15/80$ aneurysms) and 21.2% ($n = 17$) proximal recess persistence; 13.8% of cases ($n = 11$) had aneurysm neck remnants, and 46.2% ($n = 37$) had aneurysm remnants. We observed, respectively, 40% (32/80) complete occlusions, 60% (48/80) incomplete occlusions, 53.8% (43/80) adequate, and 46.2% (37/80) inadequate occlusions.

Correlation between Angiographic and Histologic Results

Illustrative correlations between follow-up DSA and histology are presented in Figs 1 and 2.

Correlation for the Diagnosis of Complete Occlusion

We observed 24 (30%) cases for which DSA and histologic evaluations agreed for complete occlusion (complete occlusion with or without recess filling) and 40 (50%) cases for which DSA and histology agreed for incomplete occlusion.

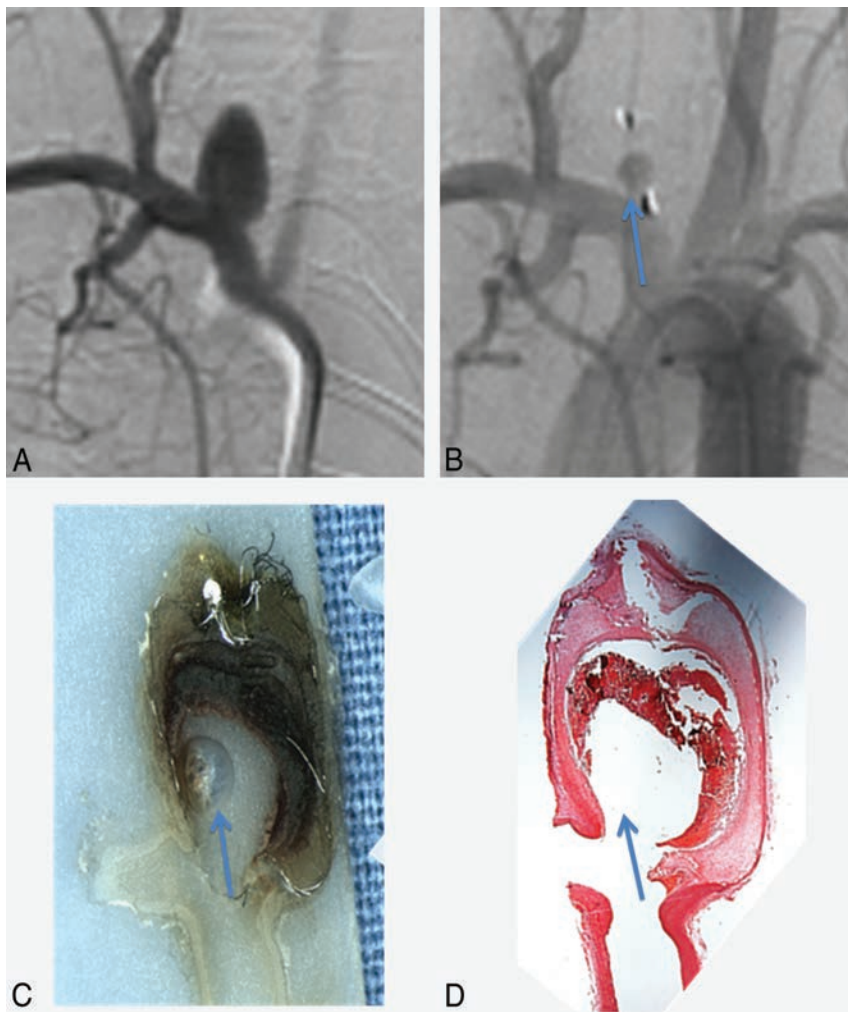


FIG 2. Aneurysm remnant. Angiographic-histologic correlation. Pretreatment DSA shows an aneurysm on the right subclavian artery at the origin of the right common carotid artery (A). Follow-up DSA shows partial filling of the aneurysm sac (blue arrow, B). An all-mount histologic sample shows a lack of filling of the aneurysm by the conjunctive tissue (blue arrow, C). Photomicrograph (hematoxylin-eosin, original magnification $\times 100$) shows a lack of coverage of the neck by endothelial tissue and filling of the aneurysm pouch with a partial thrombosis in the aneurysm sac (D).

Table 2: Correlations between the histologic reference standard and the follow-up DSA WOS evaluation: contingency table for complete versus incomplete occlusion

Histology Grading	Follow-Up DSA Grading		
	Complete Occlusion or Recess Filling	Residual Neck or Residual Aneurysm	Total
Complete occlusion or recess filling	24	8	32
Residual neck or residual aneurysm	8	40	48
Total	32	48	80

pared with the reference standard histology was 80% (95% CI, 65%–90%).

Correlation for the Diagnosis of Adequate Occlusion

We observed 42 (52.5%) cases for which DSA and histologic evaluations agreed for adequate occlusion (complete occlusion or neck remnant) and 24 (30%) cases for which DSA and histology agreed for inadequate occlusion. In 13 (16.2%) cases, DSA suggested an adequate occlusion but histology identified inadequate occlusion, and similarly 1 (1.3%) case was misassessed as inadequate

by DSA but was found to have adequate occlusion on histology (Table 3). Sensitivity and specificity of the DSA for the diagnosis of adequate versus inadequate occlusion at follow-up compared with the histologic results as the reference standard were respectively 97.7% (95% CI, 86.2%–99.9%) and 64.9% (95% CI, 47.4%–79.3%). The overall accuracy of the DSA evaluation compared with the reference standard histology was 82.5% (95% CI, 73.8%–91.9%).

DISCUSSION

Using a histologic reference standard, our study performed on a large series of experimental aneurysms demonstrates that the angiographic WOS is sensitive, specific, and accurate in assessing aneurysm occlusion following treatment of intracranial aneurysms with the WEB device. In addition, we found a substantial level of inter- and intraobserver agreement for the WEB Occlusion Scale. These findings suggest that the WEB Occlusion Scale is an easily reproducible and accurate tool in assessing aneurysm occlusion following treatment with the WEB device.

Our current results are in accordance with the clinical study published by Fiorella et al,⁷ which reported a κ value statistic at 0.779 (95% CI, 0.70–0.86). Our study is the first to compare angiographic assessment of aneurysm occlusion after treatment with the intrasaccular WEB device with histologic controls. Assessment of occlusion is challenging following treatment with the WEB because the angiographic appearance differs from that of coiled or intraluminal flow-diverter-treated aneurysms.⁷ The proximal surface of the WEB is slightly recessed into the body of the device, thus forming a concave “marker recess” at the parent artery–aneurysm interface, to avoid any protrusion of the device in the parent artery. This marker recess opacification can be mistaken for residual filling of the aneurysm neck.

The WEB Occlusion Scale (WOS),¹⁵ based on the modified Raymond Scale, has been developed for the standardized reporting of angiographic occlusion assessment achieved with intrasaccular mesh implants, taking into account the distinction between recess opacification and aneurysm neck remnant. In this scale, complete aneurysm occlusion with or without opacification of the proximal recess is considered complete occlusion⁷; complete occlusion and neck remnant are considered adequate angiographic outcomes according to previous studies.^{13,15,16} This scale has

Table 3: Correlations between the histologic reference standard and the follow-up DSA WOS evaluation: contingency table for adequate versus inadequate occlusion

Histology Grading	Follow-Up DSA Grading		Total
	Adequate Occlusion	Inadequate Occlusion	
Adequate occlusion	42	1	43
Inadequate occlusion	13	24	37
Total	55	25	80

been used in several previous studies and is also used in currently ongoing clinical trials: WEB Clinical Assessment of IntraSaccular Aneurysm Therapy (www.clinicaltrials.gov, NCT 01778322) and Wide Neck Bifurcation Intracranial Aneurysms; Intracranial Aneurysms (NCT 02191618). No other large-scale study has been published comparing histologic findings with DSA in the setting of the evaluation of aneurysm occlusion either for coiled or flow-diverter-treated aneurysms. However, several studies have reported that interobserver and intraobserver agreement rates for the assessment of aneurysm occlusion following both coiling and flow-diverter treatment are moderate to substantial.^{13,16-19} The degree of agreement seen in our study for the WOS is similar to that reported in prior studies of coiling and flow-diverter-treated aneurysms. At a time when consensus definitions for reporting angiographic outcomes following endovascular treatment of intracranial aneurysms are required, scales that are both easily reproducible and histologically validated are of the utmost importance.^{20,21}

Limitations

Our study is limited by its retrospective nature and the use of only selected images for the DSA readers' assessment. Readers did not have access to the complete angiographic run when assessing angiographic occlusion. Furthermore, only 1 experienced reader evaluated the histologic samples. However, this reader was blinded to the DSA outcomes. Another limitation of this study is that rabbits were sacrificed at different time points, which can modify the outcomes after WEB implantation, depending on the length of follow-up.

CONCLUSIONS

This study confirms the consistency and reliability of the WEB Occlusion Scale for DSA evaluation of WEB-treated aneurysms with substantial interobserver and intraobserver agreement. Furthermore, the WEB Occlusion Scale appears to be accurate compared with a histologic reference standard, which is of great importance to justify its use in clinical studies for the evaluation of the WEB device.

ACKNOWLEDGMENTS

We thank Ravi Lingineni, BST, from the Department of Health Sciences Research of Mayo Clinic, for his contribution to statistical analysis.

Disclosures: Waleed Brinjikji—UNRELATED: Grants/Grants Pending: Brain Aneurysm Foundation.* David F. Kallmes—RELATED: Grant: Sequent Medical.* Comments: preclinical research studies; UNRELATED: Board Membership: GE Healthcare (Cost-Effectiveness Board membership); Consultancy: ev3/Covidien/Medtronic.* Comments: planning and implementing clinical trials, Steering Committee membership;

Grants/Grants Pending: MicroVention,* Codman,* Surmodics,* NeuroSigma,* ev3/Covidien/Medtronic.* Comments: preclinical research and clinical trials; Royalties: University of Virginia Patent Foundation, Comments: Spinal Fusion; Travel/Accommodations/Meeting Expenses Unrelated to Activities Listed: ev3/Covidien/Medtronic.* Comments: FDA panel presentation, open comments section. Ramathan Kadirvel—UNRELATED: Grants/Grants Pending: National Institutes of Health.* *Money paid to the Institution.

REFERENCES

- Pierot L, Klisch J, Cognard C, et al. **Endovascular WEB flow disruption in middle cerebral artery aneurysms: preliminary feasibility, clinical, and anatomical results in a multicenter study.** *Neurosurgery* 2013;73:27–34; discussion 34–25 CrossRef Medline
- Lubicz B, Mine B, Collignon L, et al. **WEB device for endovascular treatment of wide-neck bifurcation aneurysms.** *AJNR Am J Neuroradiol* 2013;34:1209–14 CrossRef Medline
- Klisch J, Sychra V, Strasilla C, et al. **The Woven EndoBridge cerebral aneurysm embolization device (WEB II): initial clinical experience.** *Neuroradiology* 2011;53:599–607 CrossRef Medline
- Ding YH, Lewis DA, Kadirvel R, et al. **The Woven EndoBridge: a new aneurysm occlusion device.** *AJNR Am J Neuroradiol* 2011;32:607–11 CrossRef Medline
- Pierot L, Moret J, Turjman F, et al. **WEB treatment of intracranial aneurysms: feasibility, complications, and 1-month safety results with the WEB DL and WEB SL/SLS in the French Observatory.** *AJNR Am J Neuroradiol* 2015;36:922–27 CrossRef Medline
- Papagiannaki C, Spelle L, Januel AC, et al. **WEB intrasaccular flow disruptor—prospective, multicenter experience in 83 patients with 85 aneurysms.** *AJNR Am J Neuroradiol* 2014;35:2106–11 CrossRef Medline
- Fiorella D, Arthur A, Byrne J, et al. **Interobserver variability in the assessment of aneurysm occlusion with the WEB aneurysm embolization system.** *J Neurointerv Surg* 2015;7:591–95 CrossRef Medline
- Caroff J, Mihalea C, Dargento F, et al. **Woven Endobridge (WEB) device for endovascular treatment of ruptured intracranial wide-neck aneurysms: a single-center experience.** *Neuroradiology* 2014; 56:755–61 CrossRef Medline
- Pierot L, Liebig T, Sychra V, et al. **Intrasaccular flow-disruption treatment of intracranial aneurysms: preliminary results of a multicenter clinical study.** *AJNR Am J Neuroradiol* 2012;33:1232–38 CrossRef Medline
- Pierot L, Klisch J, Gaurvit J, et al. **P-009 WEB endovascular treatment of wide-neck bifurcation aneurysms: short- and midterm results in a European study.** *J Neurointerv Surg* 2014;6(suppl 1):A25 CrossRef
- Altes TA, Cloft HJ, Short JG, et al. **1999 ARRS Executive Council Award. Creation of saccular aneurysms in the rabbit: a model suitable for testing endovascular devices—American Roentgen Ray Society.** *AJR Am J Roentgenol* 2000;174:349–54 CrossRef Medline
- Fujiwara NH, Cloft HJ, Marx WF, et al. **Serial angiography in an elastase-induced aneurysm model in rabbits: evidence for progressive aneurysm enlargement after creation.** *AJNR Am J Neuroradiol* 2001;22:698–703 Medline
- Gherasim DN, Gory B, Sivan-Hoffmann R, et al. **Endovascular treatment of wide-neck anterior communicating artery aneurysms using WEB-DL and WEB-SL: short-term results in a multicenter study.** *AJNR Am J Neuroradiol* 2015;36:1150–54 CrossRef Medline
- Dai D, Ding YH, Danielson MA, et al. **Histopathologic and immunohistochemical comparison of human, rabbit, and swine aneurysms embolized with platinum coils.** *AJNR Am J Neuroradiol* 2005; 26:2560–68 Medline
- Lubicz B, Klisch J, Gaurvit JY, et al. **WEB-DL endovascular treatment of wide-neck bifurcation aneurysms: short- and midterm results in a European study.** *AJNR Am J Neuroradiol* 2014;35:432–38 CrossRef Medline
- Cloft HJ, Kaufmann T, Kallmes DF. **Observer agreement in the assessment of endovascular aneurysm therapy and aneurysm recurrence.** *AJNR Am J Neuroradiol* 2007;28:497–500 Medline

17. McDonald JS, Carter RE, Layton KF, et al. **Interobserver variability in retreatment decisions of recurrent and residual aneurysms.** *AJNR Am J Neuroradiol* 2013;34:1035–39 CrossRef Medline
18. Suh SH, Cloft HJ, Lanzino G, et al. **Interobserver agreement after Pipeline embolization device implantation.** *AJNR Am J Neuroradiol* 2013;34:1215–18 CrossRef Medline
19. Tollard É, Darsaut TE, Bing F, et al. **Outcomes of endovascular treatments of aneurysms: observer variability and implications for interpreting case series and planning randomized trials.** *AJNR Am J Neuroradiol* 2012;33:626–31 CrossRef Medline
20. Meyers PM, Schumacher HC, Higashida RT, et al. **Reporting standards for endovascular repair of saccular intracranial cerebral aneurysms.** *AJNR Am J Neuroradiol* 2010;31:E12–24 Medline
21. Raymond J, White PM, Molyneux AJ. **Scales, agreement, outcome measures, and progress in aneurysm therapy.** *AJNR Am J Neuroradiol* 2007;28:501–02 Medline

Evaluation for Blunt Cerebrovascular Injury: Review of the Literature and a Cost-Effectiveness Analysis

A. Malhotra, X. Wu, V.B. Kalra, J. Schindler, C.C. Matouk, and H.P. Forman



ABSTRACT

BACKGROUND AND PURPOSE: Evaluation for blunt cerebrovascular injury has generated immense controversy with wide variations in recommendations regarding the need for evaluation and the optimal imaging technique. We review the literature and determine the most cost-effective strategy for evaluating blunt cerebrovascular injury in trauma patients.

MATERIALS AND METHODS: A comprehensive literature review was performed with data extracted to create a decision-tree analysis for 5 different strategies: anticoagulation for high-risk (based on the Denver screening criteria) patients, selective DSA or CTA (only high-risk patients), and DSA or CTA for all trauma patients. The economic evaluation was based on a health care payer perspective during a 1-year horizon. Statistical analyses were performed. The cost-effectiveness was compared through 2 main indicators: the incremental cost-effectiveness ratio and net monetary benefit.

RESULTS: Selective anticoagulation in high-risk patients was shown to be the most cost-effective strategy, with the lowest cost and greatest effectiveness (an average cost of \$21.08 and average quality-adjusted life year of 0.7231). Selective CTA has comparable utility and only a slightly higher cost (an average cost of \$48.84 and average quality-adjusted life year of 0.7229). DSA, whether performed selectively or for all patients, was not optimal from both the cost and utility perspectives. Sensitivity analyses demonstrated these results to be robust for a wide range of parameter values.

CONCLUSIONS: Selective CTA in high-risk patients is the optimal and cost-effective imaging strategy. It remains the dominant strategy over DSA, even assuming a low CTA sensitivity and irrespective of the proportion of patients at high-risk and the incidence of blunt cerebrovascular injury in high-risk patients.

ABBREVIATIONS: BCVI = blunt cerebrovascular injury; NMB = net monetary benefit; QALY = quality-adjusted life year

Blunt cerebrovascular injury (BCVI), defined as blunt trauma to the carotid and/or vertebral arteries, has a reported incidence ranging from 0.18% to 2.7% in blunt trauma admissions, higher in patients imaged with risk factors as defined by the Denver screening criteria and a high injury severity score.^{1,2} Arterial injury resulting in thrombosis and distal thromboembolism can result in BCVI-related stroke. A latent, asymptomatic period of

10–72 hours has been reported between injury and the onset of neurologic complications, during which antithrombotic therapy may improve neurologic outcome. Screening and early detection of BCVI within the clinically silent period can reduce the risk of stroke, improving the prognosis greatly.^{3–5} Multiple strategies have been suggested, generating debates between aggressive imaging for all blunt trauma admissions and selective screening of patients.^{6–8} In a recent study, 30% of patients had no radiographic or clinical risk factors, and the authors proposed more liberalized screening for BCVI.⁷

Digital subtraction angiography has been considered the reference standard for BCVI detection.^{9,10} Increasingly, CT angiography is used in emergency departments to assess patients.¹¹ There is considerable variation in the reported sensitivity of CTA for BCVI detection in the literature, and its ability to replace DSA has not been validated, to our knowledge. In a multidisciplinary survey in 2011, 60% of practitioners in North America reported using CTA for screening, while 15% continue to use DSA.¹² There

Received May 29, 2015; accepted after revision June 26.

From the Departments of Diagnostic Radiology (A.M., X.W., V.B.K., C.C.M., H.P.F.), Neurology (J.S.), and Neurosurgery (J.S., C.C.M.), Yale School of Medicine, New Haven, Connecticut.

Please address correspondence to Ajay Malhotra, MD, MMM, Department of Diagnostic Radiology, Yale School of Medicine, 333 Cedar St, New Haven, CT 06520-8042; e-mail: ajay.malhotra@yale

Indicates article with supplemental on-line table and bibliography.

Indicates article with supplemental on-line photos.

Evidence-Based Medicine Level 2.

<http://dx.doi.org/10.3174/ajnr.A4515>

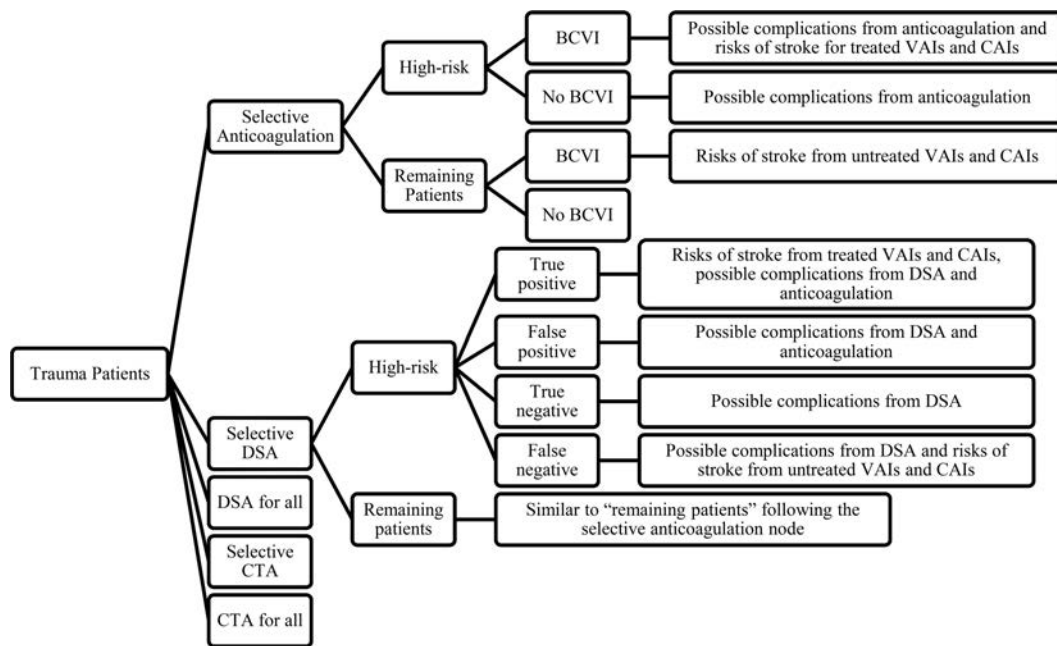


FIG 1. Flow chart of the simplified model. VAI indicates vertebral artery injury; CAI, carotid artery injury.

was wide variability in the choice of imaging and anticoagulation treatment of traumatic cerebrovascular injury, both on an individual basis and among specialties.

The Eastern Association for the Surgery of Trauma Management Guidelines in 2010 found no level 1 evidence for the appropriate technique for the screening and diagnosis of BCVI or for the treatment of BCVI.²

We decided to review the literature for the evaluation and management of BCVI and perform a cost-effectiveness study, incorporating all possible strategies and the direct costs as well as the complication rates of each strategy, in an attempt to determine the optimal strategy from a health care payer perspective.

MATERIALS AND METHODS

Approval from the institutional review board was not required because no actual patients were involved in this study, with all parameters obtained from literature.

Model Description

An economic decision analysis was developed to evaluate 5 possible strategies for adult blunt trauma admissions for BCVI (assuming an average age of 40 years) during a 1-year horizon. The mathematic model was constructed by using TreeAge Pro Suite 2014 (TreeAge Software, Williamstown, Massachusetts).

The 5 possible strategies were the following: no imaging with selective anticoagulation only for high-risk patients, DSA for all trauma admissions, DSA for high-risk patients (as per the Denver screening criteria), CTA for all admissions, and CTA for high-risk patients. For survivors of stroke, complications from anticoagulation and the angiographic procedure were discussed. Patients with false-positive results could also experience complications from anticoagulation and the angiographic procedure. A patient with true-negative findings would only experience complications from DSA or CTA, including a contrast-induced allergic-like reaction and contrast-induced nephropathy. Complications spe-

cific to DSA included those at the arterial puncture site and from the catheter within the intracranial arteries, resulting in transient ischemic attack, stroke, and even death. As per the International Organization for Medical Physics, the risk of radiation-induced cancer and cancer death should not be estimated for doses of ≤ 100 mSv, markedly greater than the 3–6 mSv dose of radiation from CTA and the slightly higher dose from DSA.^{13–15} A patient with false-negative findings would have a higher risk of stroke due to a delayed diagnosis of BCVI. The survivors of stroke experience complications similar to those who have true-positive findings.

In selective screening strategies, the outcomes of patients in the high-risk population were discussed as those in DSA/CTA for all strategies, but with higher risks of stroke. Patients not in a high-risk population would not undergo an angiographic work-up and thus would not experience any procedural complications. Patients with BCVI within that population would have a delayed diagnosis with a higher risk of stroke.

In the selective anticoagulation strategies, high-risk patients would undergo anti-coagulation therapy, with associated costs and bleeding risks. The low-risk patients would not undergo any imaging or treatment with increased risk of stroke or a stroke-related mortality (Fig 1).

Statistical Analysis

The cost-effectiveness model was constructed from a health care payer perspective by using Medicare reimbursement values for costs when possible and literature values otherwise. This practice is recommended by the US Panel on Cost-Effectiveness in Health and Medicine.¹⁶ Outcomes were assessed as utility function, quantified by quality-adjusted life years (QALYs), based on World Health Organization cost-effectiveness guidelines.¹⁷

Two important indicators were used to assess the cost-effectiveness of the 5 strategies. The first was the incremental cost-effectiveness ratio, defined as

Table 1: BCVI screening criteria

Signs and symptoms	Arterial hemorrhage/expanding cervical hematoma Cervical bruit Focal neurologic deficit Neurologic examination incongruous with head CT scan findings Stroke on secondary CT scan
Risk factors	Maxillo facial fractures—Le Fort II or III fracture Cervical spine fracture patterns: extension into the transverse foramen, C1–C3 vertebral fractures Skull base fracture extending to involve the carotid canal Diffuse axonal injury with GCS score <6 Near hanging with anoxic brain injury

Note:—GCS indicates Glasgow Coma Scale. Table adapted from Cothren et al.³⁴

$$\frac{\text{Cost of Strategy 1} - \text{Cost of Reference Strategy}}{\text{Expected Utility of Strategy 1} - \text{Expected Utility of Reference Strategy}}$$

The incremental cost-effectiveness ratio reflects the amount of additional expense for strategy 1 to achieve a full unit of incremental QALY with respect to the reference strategy, and the reference strategy is often chosen as the one of lowest cost. The incremental cost-effectiveness ratio was compared against the standard willingness-to-pay threshold of \$50,000/QALY. A strategy would be acceptable and cost-effective if it has the highest effectiveness among all strategies with an incremental cost-effectiveness ratio below willingness to pay.

The other indicator was net monetary benefit (NMB), defined as

$$\text{Expected Utility} \times \text{Willingness to Pay} - \text{Cost.}$$

The formula quantifies the benefits of a strategy in dollar amounts.

Base case calculation and a Monte Carlo simulation were performed. The base case calculation used the most probable value for each parameter, giving the average cost and effectiveness for a large cohort of patients. The Monte Carlo analysis with probabilistic sampling ran 10,000 iterations, simulating 10,000 hypothetical patients over the distributional range of each parameter. To test the robustness of our conclusion against different variables, we performed several sensitivity analyses. The sensitivity of CTA, the incidence of BCVI in all trauma admissions, the proportion of high-risk patients in all trauma admissions, the proportion of patients with BCVI having risk factors, and the risk of hemorrhage secondary to anticoagulation treatment varied from 0% to 100%.

Clinical Parameters

The probability assigned to each path is the product of all probabilities along its nodes. These parameters were derived from multiple published studies. The incidence of BCVI in blunt trauma admissions was calculated as a weighted average of all studies included in the systematic review by Franz et al¹ according to the number of patients in each study. The total number of blunt trauma admissions was 116,993, and the total number of BCVIs was 1011, giving an incidence of 0.86%. Four studies reported the number of BCVIs with high-risk factors, and the weighted average was obtained to extrapolate the incidence of BCVI in high-risk patients.^{1,6-8,18} The proportion of high-risk populations in all blunt trauma admissions was derived from the weighted average of 2 studies totaling nearly 30,000 patients.^{6,7}

Costs and Outcomes

Costs and utilities were assigned at each terminal node. Costs were quantified with US dollars in 2014 values, and utilities were measured in quality-adjusted life years. No discount rates were used because the study span was 1 year.

Costs were derived from Medicare when a single or several Current Procedural Terminology codes were involved and from published literature values otherwise, as recommended by the US Panel on Cost-Effectiveness Analysis in Health and Medicine. Specifically, the cost of stroke was calculated by dividing the lifetime stroke cost obtained by the difference between the average age at occurrence of BCVI (40 years of age) and the average life span of people in the United States (78.9 years of age).^{6,7,19-21} We acknowledge that our methodology for calculating the cost might be inaccurate, but the value is close to that reported in recent literature.²²

A list of all parameters and their values is presented on the On-line Table.

There are several assumptions made in this model:

- 1) The model was constructed with more than a 1-year horizon because BCVI is not a recurrent event. Minor complications with low costs and little reduction in QALY or those with rare incidence are excluded.
- 2) The major complications secondary to DSA include allergy-like reactions (mild or severe), stroke (transient ischemic attack or permanent stroke), hematoma, and nephropathy.
- 3) CTA complications include allergy-like reactions (mild or severe) and nephropathy, with the same risks as those caused by DSA.
- 4) The major complication of anticoagulation treatment is hemorrhage.
- 5) Complications such as groin hematoma, contrast nephropathy, mild allergy-like reaction, and transient ischemic attack are assumed to incur costs but negligible reduction in effectiveness, with patients having a good outcome on recovery.

RESULTS

Base Case Calculation

In the base case calculation, parameters with distributions were assumed to be at its mean or most probable value. Expected costs and utilities for each strategy were calculated, and incremental cost-effectiveness ratios were compared against a willingness-to-pay threshold of \$50,000/QALY. The result showed that selective anticoagulation had the lowest cost and highest effectiveness (an average cost of \$21.08 and average QALY of 0.7231), and it would thus be the opti-

mal strategy regardless of the willingness-to-pay threshold. Similarly, selective CTA would also be the optimal imaging strategy regardless of the value of the willingness-to-pay threshold (an average cost of \$48.84 and average QALY of 0.7229).

The summary is provided in Table 2 in the order of descending effectiveness.

Monte Carlo Simulation

A Monte Carlo simulation was performed with 10,000 iterations. The acceptability curve showed that selective CTA was the most cost-effective imaging strategy in all iterations, even at a willingness to pay of \$100,000/QALY.

A scatterplot of selective CTA against selective DSA is presented in Fig 2. The incremental effectiveness of selective DSA versus selective CTA in all iterations was negative (selective DSA has worse outcomes), and the incremental costs were positive (selective DSA is more expensive), suggesting that selective DSA is less cost-effective than selective CTA.

Sensitivity Analysis

The sensitivity of CTA, the incidence of BCVI in all trauma admissions, the proportion of high-risk patients in all trauma admissions, and the proportion of patients with BCVI having risk factors varied from 0% to 100%. All 4 results showed selective anticoagulation to be the most cost-effective strategy and selective

CTA to be the optimal imaging strategy (On-line Figs 1–4). As the proportion of high-risk patients increases, selective DSA progressively becomes an unfavorable strategy due to the complications and costs of DSA.

To compensate for the lack of literature reporting risk of hemorrhage secondary to anticoagulation specifically in trauma patients, we performed a sensitivity analysis, varying the incidence of hemorrhage. When the risk of hemorrhage secondary to anticoagulation is higher than 8%, selective CTA is more cost-effective than selective anticoagulation and becomes the optimal strategy overall (On-line Fig 5).

DISCUSSION

Multiple studies have shown the benefits of early diagnosis and treatment of BCVI before onset of neurologic symptoms. Patients with BCVI can have significant morbidity and almost a 20% stroke-related mortality.^{3,4,20,23} Institution of adequate anti-thrombotic therapy was shown by Cothren et al²⁰ in 2005 to reduce the incidence of ischemic neurologic events from 21% in untreated patients to 0.5% in treated patients. They found screening for BCVI with 4-vessel cerebrovascular angiography to be cost-effective when performed in patients at high-risk based on the Denver screening criteria. However, there has been significant controversy in defining both the patient population at risk for BCVI and the optimal screening technique.

In defining the high-risk population for BCVI, different protocols have been recommended, including the Denver screening criteria.^{4,20} However, by using the classically defined risk factors, Emmett et al²⁴ found 16% (19 of 117 patients) and Stein et al⁶ found 21.8% of BCVI patients with no risk factors. Using the Denver modification of screening criteria, Beliaev et al⁸ found the screening to have a sensitivity of 97% and a specificity of 42% and proposed that CTA be used only in high-risk patients.

The choice of technique should be based on comprehensive considerations, including both the sensitivity and specificity of the imaging technique as well as the risk of complications and costs. Increasing use of CTA has been reported to increase BCVI screening, reduce the time to diagnosis, and prevent stroke.^{25,26} A negative CTA result has been shown to be associated with a low risk of subsequent neurologic complications in trauma patients.^{3,27,28} However DSA, the reference standard for BCVI detection, continues to be recommended despite being invasive, labor-intensive, and available only in specialized centers.^{3,4,9,25,29-31} Most injuries missed on CTA are grade I injuries with luminal irregularity, but these have been shown to carry a significant risk of stroke.³

In a meta-analysis comparing the accuracy of CTA against DSA for BCVI, Roberts et al¹⁰ reported a pooled sensitivity of 66% and specificity of 97% for

Table 2: Base case calculation results

Strategy	Cost (\$)	Effectiveness (QALY)
Selective anticoagulation	21.08	0.7231074
Selective CTA	48.84	0.7229382
Selective DSA	284.62	0.7228022
CTA for all	419.11	0.7229337
DSA for all	5594.16	0.7196092

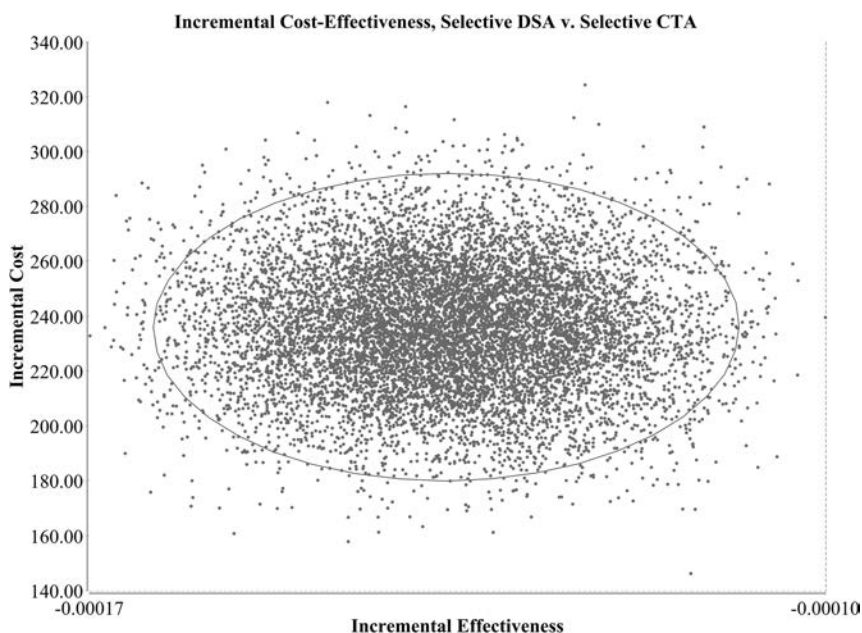


FIG 2. Scatterplot of incremental cost (cost of selective DSA and cost of selective CTA) versus incremental effectiveness (effectiveness of selective DSA and effectiveness of selective CTA). The incremental effectiveness in all iterations was negative (selective DSA has worse outcomes), and the incremental costs were positive (selective DSA is more expensive), suggesting that selective DSA is less cost-effective than selective CTA.

CTA, with slightly better results for carotid-versus-vertebral artery injury. The sensitivity was significantly greater among studies using CT scanners with 16 versus <16 sections per rotation. However even with CT scanners with ≥ 16 sections per rotation and CTA being read by neuroradiologists, the sensitivity remained below 80%.¹⁰ Repeat injections during DSA can be performed if there are artifacts or suboptimal contrast filling, an option not available with CTA. In addition, DSA is performed by neuroangiographers with greater expertise in the assessment of BCVI, compared with CTA, which might be interpreted by general radiologists. A significant CTA learning curve has been described in which the diagnostic accuracy of CTA improved with time, with the specificity and negative predictive value climbing to 100% in the latter half of the study.²⁹

There is great heterogeneity in the reported diagnostic performance of CTA and lack of uniform, unbiased comparison with DSA. Paulus et al¹¹ reported an improved sensitivity of 64-detector row CTA and 32-detector row CTA, with a sensitivity of 68% and a specificity of 92% in 594 patients who met the screening criteria for BCVI and underwent both CTA and DSA. However, there was no blinding or mention of whether the findings could be seen on CTA retrospectively. All 52 false-negative CTA findings of BCVI were in 20 of 594 patients, and whether these CTAs were of optimal quality was not specified. The authors calculated that 0.4% of the study population could have been harmed if CTA had been used as the sole BCVI evaluation, while 0.5% of the patients had significant cerebrovascular complications from DSA. They, therefore, changed their protocol to perform DSA only in patients with positive CTA findings of BCVI or with unexplained neurologic deficits, despite the 68% sensitivity of CTA in their study. The justification given for DSA following positive CTA findings was the low specificity and positive predictive value of CTA (92% and 36%, respectively). However, these results are in stark contrast to the meta-analysis by Roberts et al in which CTA had a specificity of 99% for both carotid and vertebral artery injury, and DSA was proposed instead, with negative CTA results due to the low sensitivity of CTA.

Administration of antithrombotic agents in patients without contraindications has been shown to reduce the rate of neurologic sequelae after BCVI.^{4,23,32} No significant difference in outcome has been shown between heparin and antiplatelet agents.^{3,32,33} Although the reported bleeding complications with pelvic fractures or solid organ injuries are uncommon, there has been a hesitancy to use antithrombotic treatment.³²

Given all these controversies, we constructed the model incorporating the factors discussed above when possible and performed sensitivity analyses otherwise. The results of our study demonstrate that despite assuming a relatively low sensitivity of CTA, selective CTA would still be more cost-effective due to its lower cost and low complication risks. The 66% sensitivity used in our model was from a meta-analysis totaling 5704 carotid and vertebral artery injuries.¹⁰ To compensate for the wide variability reported in the literature on the sensitivity of CTA versus DSA, we performed a sensitivity analysis by varying CTA sensitivities ranging from 0% to 100%. The results showed that selective anticoagulation would be dominant among all 5 strategies. Among all imaging strategies, selective CTA had the highest NMB and would

be the more optimal imaging test for patients with suspected BCVI because the complication rates of DSA were even higher than the incidence of BCVI in screened trauma admissions.

With different definitions of high-risk patients,^{15,17} the proportion of these patients among all trauma admissions and the incidence of BCVI in this group might also vary. Sensitivity analyses varying the proportion of high-risk patients among all trauma admissions and the incidence of BCVI among them were also performed to account for this limitation. When the values varied between 0% and 100%, anticoagulation demonstrated the highest NMB, with selective CTA being the optimal imaging strategy under all possible scenarios.

In the base case calculation, selective anticoagulation of high-risk patients showed the highest cost-effectiveness. Antithrombotic treatment has been shown to reduce the stroke rate significantly in patients with BCVI. However, from an individual perspective, anticoagulating all patients may not be a feasible option, given the possibility of contraindications to anticoagulation and the risk of bleeding. In addition, the differences in both utility and cost between selective anticoagulation and selective CTA were relatively small, suggesting that selective CTA should be considered if an imaging study is to be performed to confirm or rule out the possibility of BCVI. Even when cost is not a major consideration, selective CTA results in higher utility among all imaging strategies.

Due to a lack of literature on the risk of bleeding after antithrombotic treatment in patients with blunt trauma, we performed a sensitivity analysis, which demonstrated that selective CTA replaced selective anticoagulation as the most cost-effective imaging strategy when the risk of hemorrhage secondary to anticoagulation was >8%.

Some of the studies included used the Memphis or other criteria to define patients at high-risk for BCVI. The heterogeneous use of screening criteria may lead to an inconsistent estimate of the BCVI incidence in high-risk patients.

Selective CTA in patients with risk factors according to Denver screening criteria would be the optimal and more cost-effective imaging strategy, even assuming a 100% sensitivity of DSA and a low sensitivity for CTA.

CONCLUSIONS

Our analyses show that selective CTA in high-risk patients is the optimal and cost-effective imaging strategy for evaluation of BCVI in blunt trauma patients. Even if the CTA sensitivity is assumed to be low compared to DSA, or the proportion of patients at high-risk is over a wide range, selective CTA remains the preferred modality.

REFERENCES

1. Franz RW, Willette PA, Wood MJ, et al. **A systematic review and meta-analysis of diagnostic screening criteria for blunt cerebrovascular injuries.** *J Am Coll Surg* 2012;214:313–27 CrossRef Medline
2. Bromberg WJ, Collier BC, Diebel LN, et al. **Blunt cerebrovascular injury practice management guidelines: the Eastern Association for the Surgery of Trauma.** *J Trauma* 2010;68:471–77 Medline
3. Biffi WL, Moore EE, Elliott JP, et al. **The devastating potential of blunt vertebral arterial injuries.** *Ann Surg* 2000;231:672–81 CrossRef Medline

4. Miller PR, Fabian TC, Croce MA, et al. **Prospective screening for blunt cerebrovascular injuries: analysis of diagnostic modalities and outcomes.** *Ann Surg* 2002;236:386–93; discussion 393–95 CrossRef Medline
5. Edwards NM, Fabian TC, Claridge JA, et al. **Antithrombotic therapy and endovascular stents are effective treatment for blunt carotid injuries: results from longterm followup.** *J Am Coll Surg* 2007;204:1007–13; discussion 1014–15 CrossRef Medline
6. Stein DM, Boswell S, Sliker CW, et al. **Blunt cerebrovascular injuries: does treatment always matter?** *J Trauma* 2009;66:132–43; discussion 143–44 CrossRef Medline
7. Bruns BR, Tesoriero R, Kufera J, et al. **Blunt cerebrovascular injury screening guidelines: what are we willing to miss?** *J Trauma Acute Care Surg* 2014;76:691–95 CrossRef Medline
8. Beliaev AM, Barber PA, Marshall RJ, et al. **Denver screening protocol for blunt cerebrovascular injury reduces the use of multi-detector computed tomography angiography.** *ANZ J Surg* 2014;84:429–32 CrossRef Medline
9. Goodwin RB, Beery PR 2nd, Dorbish RJ, et al. **Computed tomographic angiography versus conventional angiography for the diagnosis of blunt cerebrovascular injury in trauma patients.** *J Trauma* 2009;67:1046–50 CrossRef Medline
10. Roberts DJ, Chaubey VP, Zygun DA, et al. **Diagnostic accuracy of computed tomographic angiography for blunt cerebrovascular injury detection in trauma patients: a systematic review and meta-analysis.** *Ann Surg* 2013;257:621–32 CrossRef Medline
11. Paulus EM, Fabian TC, Savage SA, et al. **Blunt cerebrovascular injury screening with 64-channel multidetector computed tomography: more slices finally cut it.** *J Trauma Acute Care Surg* 2014;76:279–83; discussion 284–75 CrossRef Medline
12. Harrigan MR, Weinberg JA, Peaks YS, et al. **Management of blunt extracranial traumatic cerebrovascular injury: a multidisciplinary survey of current practice.** *World J Emerg Surg* 2011;6:11 CrossRef Medline
13. Hendee W. **Risk of medical imaging.** *Med Phys* 2013;40:040401 CrossRef Medline
14. Sabarudin A, Yusof MZ, Mohamad M, et al. **Radiation dose associated with cerebral CT angiography and CT perfusion: an experimental phantom study.** *Radiat Prot Dosimetry* 2014;162:316–21 CrossRef Medline
15. Han A, Yoon DY, Kim ES, et al. **Value of CT angiography for the detection of intracranial vascular lesions in patients with acute severe headache.** *Eur Radiol* 2013;23:1443–49 CrossRef Medline
16. Weinstein MC, Siegel JE, Gold MR, et al. **Recommendations of the Panel on Cost-Effectiveness in Health and Medicine.** *JAMA* 1996;276:1253–58 CrossRef Medline
17. Tan-Torres Edejer T, Baltussen R, Adam T, et al, eds. *Making Choices in Health: WHO Guide to Cost-Effectiveness Analysis.* Geneva: World Health Organization; 2003
18. Kopelman TR, Leeds S, Berardon NE, et al. **Incidence of blunt cerebrovascular injury in low-risk cervical spine fractures.** *Am J Surg* 2011;202:684–88; discussion 688–89 CrossRef Medline
19. US Census Bureau. **Expectation of Life at Birth, and Projections.** 2008. <http://www.census.gov/compendia/statab/2012/tables/12s0104.pdf>. Accessed November 26, 2014
20. Cothren CC, Moore EE, Ray CE Jr, et al. **Screening for blunt cerebrovascular injuries is cost-effective.** *Am J Surg* 2005;190:845–49 Medline
21. Kaye D, Brasel KJ, Neideen T, et al. **Screening for blunt cerebrovascular injuries is cost-effective.** *J Trauma* 2011;70:1051–56; discussion 1056–57 CrossRef Medline
22. Hannon N, Daly L, Murphy S, et al. **Acute hospital, community, and indirect costs of stroke associated with atrial fibrillation: population-based study.** *Stroke* 2014;45:3670–74 CrossRef Medline
23. Fabian TC, Patton JH Jr, Croce MA, et al. **Blunt carotid injury. Importance of early diagnosis and anticoagulant therapy.** *Ann Surg* 1996;223:513–22; discussion 522–25 CrossRef Medline
24. Emmett KP, Fabian TC, DiCocco JM, et al. **Improving the screening criteria for blunt cerebrovascular injury: the appropriate role for computed tomography angiography.** *J Trauma* 2011;70:1058–63; discussion 1063–65 CrossRef Medline
25. Eastman AL, Muraliraj V, Sperry JL, et al. **CTA-based screening reduces time to diagnosis and stroke rate in blunt cervical vascular injury.** *J Trauma* 2009;67:551–56; discussion 555–56 CrossRef Medline
26. Schneider NP, Simons R, Nicolaou S, et al. **Utility of screening for blunt vascular neck injuries with computed tomographic angiography.** *J Trauma* 2006;60:209–15; discussion 215–16 CrossRef Medline
27. Berne JD, Cook A, Rowe SA, et al. **A multivariate logistic regression analysis of risk factors for blunt cerebrovascular injury.** *J Vasc Surg* 2010;51:57–64 CrossRef Medline
28. Utter GH, Hollingworth W, Hallam DK, et al. **Sixteen-slice CT angiography in patients with suspected blunt carotid and vertebral artery injuries.** *J Am Coll Surg* 2006;203:838–48 CrossRef Medline
29. Malhotra AK, Camacho M, Ivatury RR, et al. **Computed tomographic angiography for the diagnosis of blunt carotid/vertebral artery injury: a note of caution.** *Ann Surg* 2007;246:632–42; discussion 642–43 CrossRef Medline
30. DiCocco JM, Emmett KP, Fabian TC, et al. **Blunt cerebrovascular injury screening with 32-channel multidetector computed tomography: more slices still don't cut it.** *Ann Surg* 2011;253:444–50 CrossRef Medline
31. Parks NA, Croce MA. **Use of computed tomography in the emergency room to evaluate blunt cerebrovascular injury.** *Adv Surg* 2012;46:205–17 CrossRef Medline
32. Cothren CC, Moore EE, Biffi WL, et al. **Anticoagulation is the gold standard therapy for blunt carotid injuries to reduce stroke rate.** *Arch Surg* 2004;139:540–45; discussion 545–56 CrossRef Medline
33. Wahl WL, Brandt MM, Thompson BG, et al. **Antiplatelet therapy: an alternative to heparin for blunt carotid injury.** *J Trauma* 2002;52:896–901 CrossRef Medline
34. Cothren CC, Biffi WL, Moore EE, et al. **Treatment for blunt cerebrovascular injuries: equivalence of anticoagulation and antiplatelet agents.** *Arch Surg* 2009;144:685–90 CrossRef Medline

The Moving Carotid Artery: A Retrospective Review of the Retropharyngeal Carotid Artery and the Incidence of Positional Changes on Serial Studies

D.E. Lukins, S. Pilati, and E.J. Escott

ABSTRACT

BACKGROUND AND PURPOSE: Retropharyngeal carotid arteries are a clinically relevant anatomic variant. Prior studies have documented their incidence, but only a single case report has discussed the change in position of the carotid artery to and from a retropharyngeal location. The purpose of this study was to determine the prevalence of retropharyngeal carotid arteries and to evaluate the change in position of retropharyngeal carotid arteries over serial CT examinations of the neck.

MATERIALS AND METHODS: A retrospective review of 306 CT examinations of the neck in 144 patients was performed. Patients with previous neck surgery or neck masses displacing the carotid arteries were excluded. The position of each carotid artery was evaluated on each examination. In patients with prior examinations, change or lack of change in position was recorded. The data were reviewed to assess changes in the position of the carotid arteries.

RESULTS: Of the 144 patients evaluated, 34 were excluded. The final number of examinations included in the study was 249. Sixty-three of 110 patients had at least 1 comparison study. Twenty-three retropharyngeal carotid arteries were present on the baseline examination in 17 (15.5%) of 110 patients. There was documented change to or from a retropharyngeal position in 4 (6.3%) of 63 patients with comparison studies.

CONCLUSIONS: The phenomenon of migration of the carotid arteries to and from a retropharyngeal position with time is confirmed by our study. It is important for physicians to be aware of this phenomenon to avoid potential procedural complications.

Retropharyngeal carotid arteries are a well-known anatomic variant in the neck. Descriptions of this phenomenon date back to at least 1925.¹ Clinical implications of this anatomic variant, including potential procedural complications, are also described in the literature of the early 20th century² and in more recent publications.³⁻⁷ Complications include potentially lethal hemorrhage from injury to the internal carotid artery during surgical procedures involving the pharynx, including tonsillectomy, peritonsillar abscess drainage, and transoral tumor resection. Ligation of the ICA to control hemorrhage may result in hemiplegia.⁸ During a transoral approach for blocking of the glossopharyngeal nerve, there may be inadvertent arterial puncture or

injection of local anesthetic into the retropharyngeal ICA.³ Additionally, there is a risk of injury to and resultant hemorrhage from the retropharyngeal ICA during tracheal intubation.³ The retropharyngeal carotid artery has also been implicated as a potential contributing factor to obstructive sleep apnea, given its alteration of pharyngeal anatomy.³

Various theories have been proposed regarding the cause of retropharyngeal carotid arteries. Congenital alterations of the normal anatomy and increasing tortuosity of the arteries with age have both been suggested as possible causes.⁶ In addition to increasing age, atherosclerosis and hypertension have also been linked with abnormalities of the carotid arteries, including tortuosity, kinking, and coiling.⁹ Prior studies have documented the incidence of retropharyngeal carotid arteries.¹⁰ A recent study evaluated the position of the internal carotid arteries on cervical spine MR imaging. In this study, retropharyngeal carotid arteries (defined by these authors as medial to the uncovertebral joint) were present in 2.6% of patients.¹⁰ To date, only a single case report¹¹ (from the otolaryngology literature) has discussed the change in position of the carotid artery to and from a retropharyngeal location at 2 time points. In our own daily practice, we have noticed this change in position, which, in our experience,

Received March 25, 2015; accepted after revision July 7.

From the Departments of Radiology (D.E.L., E.J.E.) and Otolaryngology Head and Neck Surgery (E.J.E.), University of Kentucky, Lexington, Kentucky; and Department of Radiology (S.P.), John H. Stroger Jr Hospital of Cook County, Chicago, Illinois.

Paper previously presented at: American Society of Neuroradiology Annual Meeting and the Foundation of the ASNR Symposium, May 17–22, 2014; Montreal, Quebec, Canada.

Please address correspondence to Douglas E. Lukins, MD, University of Kentucky, 800 Rose St, HX-302, Lexington, KY 40536; e-mail: douglas.lukins@uky.edu

<http://dx.doi.org/10.3174/ajnr.A4533>

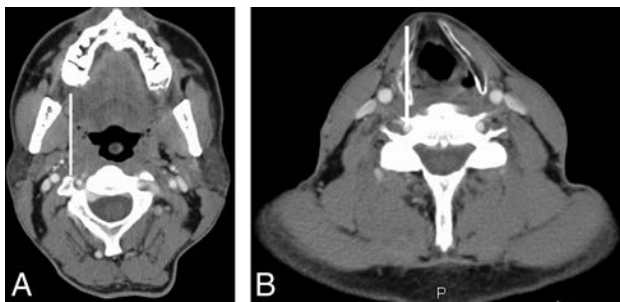


FIG 1. Reference for grading the position of the carotid artery: axial contrast-enhanced CT images of the neck soft tissues at the level of the oropharynx (A) and hypopharynx (B). The vertical reference lines represent the lateral margin of the pharynx. The lines are drawn along the lateral margin of the oropharyngeal wall/palatine tonsil in A and the inner cortex of the thyroid cartilage (which approximates the lateral hypopharyngeal wall) in B. The position of the carotid artery at each level can then be graded with respect to these reference lines.

seems to occur at the level of the oropharynx and hypopharynx. The purpose of this study was to evaluate the incidence of retropharyngeal carotid arteries and their change in position over serial CT examinations of the neck.

For the purposes of this article, any reference to the carotid artery collectively refers to the common carotid artery, external carotid artery (proximal to the occipital artery), and cervical internal carotid artery.

MATERIALS AND METHODS

Patient Demographics

Approval was obtained from the University of Kentucky institutional review board. Contrast-enhanced CT examinations of the neck soft tissues obtained during 2012 were retrospectively evaluated in 144 patients. Patient medical record number, age, sex, and diagnosis were recorded in a spreadsheet (Excel; Microsoft, Redmond, Washington). Patients with a history of more than local neck surgery, such as extensive neck dissection that was considered to cause architectural distortion in the areas of interest, laryngectomy, or thyroidectomy, were excluded from the study. Patients with neck masses displacing the carotid arteries were also excluded, as were patients with scans that were severely degraded by motion artifacts.

Image Analysis

The examinations were all reviewed by a subspecialty board-certified neuroradiologist with or without a research assistant. The date of each initial CT examination was recorded, and the position of the carotid artery was evaluated. The right and left carotid arteries were evaluated separately. The position of the carotid artery was graded by using a scale of 0–3, with 0 indicating a lateral position with respect to the pharynx (lateral to the line in Fig 1); 1, a marginally retropharyngeal position (contacting the line); 2, a completely retropharyngeal position (medial to the line); and 3, a midline position (Fig 1). For carotid arteries that were given grade 1 or higher, the segment of the artery that was graded the highest (ie, positioned most toward a midline retropharyngeal location) was recorded (common carotid artery, ICA, external carotid artery). Additionally, the level of the pharynx at which the carotid artery was retropharyngeal was recorded. Finally, the prevalence

of retropharyngeal carotid arteries was tabulated. The position of the ICAs at the level of the nasopharynx was not included because, in our experience, there has been no observed change in position of the ICA at this level and the fairly high frequency of vascular loops graded 2 at the level of the nasopharynx mask changes in carotid artery position at the level of the oropharynx and hypopharynx due to our method of recording only the segment with the highest grade. The goal of the study was to document changes in the position of the carotid arteries at the level of the oropharynx and hypopharynx on serial studies; therefore, our effort was focused on these levels.

The carotid arteries (of each patient) were graded with regard to the presence and extent of vessel involvement by atherosclerotic disease. Atherosclerotic plaque volume was subjectively graded on a scale of 0–3, with 0 indicating no visible plaque; 1, mild; 2, moderate; and 3, severe plaque volume, and this number was recorded on the spreadsheet. It was not feasible to calculate the degree of stenosis in the carotid arteries because of the venous phase of enhancement on most of the examinations. Additionally, patients were placed into 3 categories based on the position of the carotid arteries on the baseline examination: those with at least 1 retropharyngeal carotid artery, those with at least 1 marginal carotid artery, and those with no marginal or retropharyngeal carotid artery. The average grade of atherosclerosis was calculated for each category. These data were used to evaluate any correlation between the degree of atherosclerosis and carotid artery position.

The electronic medical record was reviewed for each patient for the presence or absence of a diagnosis of hypertension on the patient's problem list. Two separate electronic medical record systems were reviewed, 1 with inpatient data and the other with outpatient data. This information was recorded on the spreadsheet.

The position of the patient's head was recorded for each CT examination. Head position was tracked on each examination by numerically grading the head position in each of 3 planes. These included "nod" or up-and-down motion of the head, "turn" or left-and-right rotation of the head about the axis of the spine, and "tilt" or left-and-right angulation of the head relative to an anteroposterior axis (Fig 2). Rotation (in each of the 3 planes) of 0°–9° was given a score of 0, rotation of 10°–19° was given a score of 1, and rotation of 20°–29° was given a score of 2, and so on. Direction was indicated by "L/R" for left or right or "U/D," up or down.

After the initial CT examination was reviewed, prior examinations (up to 4) were reviewed as well. The carotid artery position was compared and recorded as either the same or different from the initial examination. If different, the exact position was graded and recorded. Additionally, head position was graded and recorded for all comparison examinations.

Statistical Analysis

Data were analyzed for correlation between age and carotid artery position, degree of atherosclerosis and carotid artery position, and diagnosis of hypertension and carotid artery position by using statistical software (JMP Pro 11.1.1; SAS Institute, Cary, North Carolina). The grades for left-and-right carotid artery po-

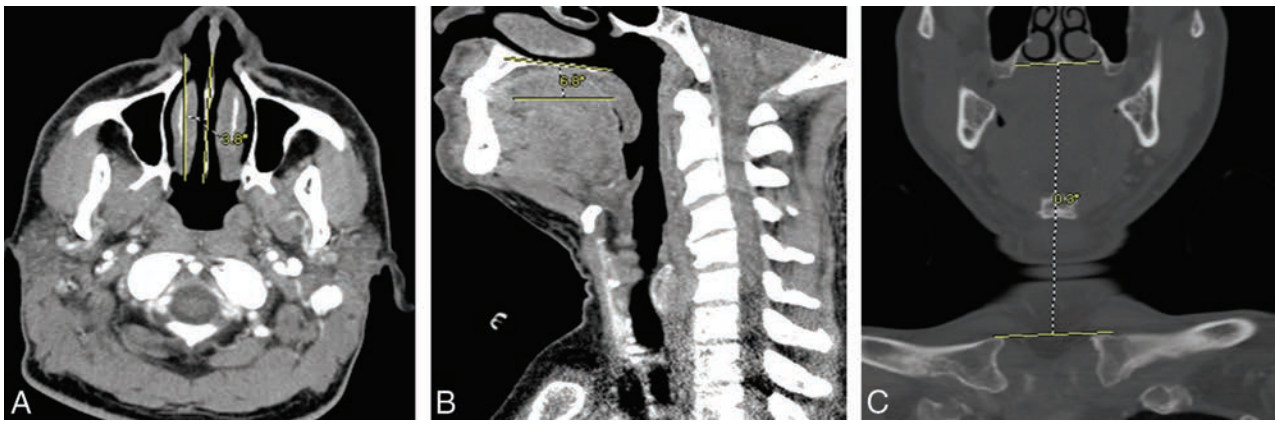


FIG 2. Images representing the “turn” (A), “nod” (B), and “tilt” (C) axes used to calculate head position. A, The amount of rotation in the “turn” axis was measured in degrees of rotation of the nasal septum with respect to the vertical. B, The amount of rotation in the “nod” axis was measured in degrees of rotation of the hard palate from the horizontal. C, The amount of rotation in the “tilt” axis was measured in degrees of rotation of the hard palate with respect to a line drawn along the superior aspects of the clavicular heads.

Table 1: Patient characteristics and carotid position

	Only Lateral	At Least 1 Marginal and No Retropharyngeal	At Least 1 Retropharyngeal
Age (yr) (mean) (min–max)	44.9 (4–74)	55.5 (2–76)	60.5 (37–78)
Atherosclerosis grade (mean) (min–max)	0.55 (0–3)	1.00 (0–3)	1.12 (0–3)

Note:—min indicates minimum; max, maximum.

sitions in each patient were averaged to create a single grade for each patient, and an ordinal logistic regression was performed between age and average carotid artery position. A Fisher exact test was performed to assess the correlation between the degree of atherosclerosis and carotid artery position as well as diagnosis of hypertension and carotid artery position.

RESULTS

Thirty-four of 144 patients were excluded, leaving 110 patients in the study. A prior operation was the most common reason for exclusion from the study. Of the 34 patients excluded, 24 were because of a prior neck operation. Two patients were excluded because of neck masses or lymph nodes that displaced 1 of the carotid arteries. Four patients were excluded for lack of IV contrast that limited assessment of the carotid artery position. Two patients were excluded for extensive soft-tissue emphysema. One patient was excluded for ICA occlusion; and 1 patient, for motion artifacts. Of the 110 patients included in the study, the average patient age was 50.4 years, with a range of 2–82 years. Nine patients (8%) were in the pediatric population (younger than 18 years of age). There were 72 males and 38 females, constituting 65% and 35% of the study population, respectively.

Most patients, 74 composing 75.0% of the population, had a diagnosis of cancer. Among these patients, cancer of the aerodigestive tract was the most common diagnosis (29.9%), followed by hematologic malignancies such as lymphoma and leukemia (16.7%). Less common malignancies in the study population included sinonasal cancer, salivary gland cancer, endocrine gland cancer, and skin cancer. The remaining patients with diagnoses other than malignancy (36, 25.0%) were placed in an “other” category. These patients were imaged for reasons such as neck swelling, airway stenosis, sialoadenitis, abscess, and primary hyperparathyroidism.

Among the patients included in the study, the average grade of atherosclerosis was 0.76 on a scale of 0–3. The average grade of atherosclerosis in patients whose carotid arteries showed a change in position from lateral to retropharyngeal was 1 compared with an average grade of 0.75 in the nonchanging population. Patients in the retropharyngeal category had an average grade of atherosclerosis of 1.12. Patients in the marginal category had an average grade of atherosclerosis of 1.00. Patients without a retropharyngeal or marginal carotid artery had an average grade of atherosclerosis of 0.56 (Table 1). There was no statistically significant correlation ($P = .128$) between the increasing degree of atherosclerosis and increasing average carotid artery grade; however, there was a trend toward a marginal or retropharyngeal position with increasing atherosclerosis grade.

Of the 110 patients included in the study, 63 had at least 1 prior comparison examination. Some comparison studies dated back to 2000. A total of 249 examinations were evaluated, including initial examinations and comparisons. On the anchor examinations (the initial examination that was viewed for each patient), 17 of 110 patients (15.5%) had at least 1 retropharyngeal carotid artery. Three additional patients had retropharyngeal carotid arteries on comparison examinations, but not on the anchor examination. When we took this finding into account, 20 of 110 patients (18.2%) had at least 1 retropharyngeal carotid artery. The average age of patients with at least 1 retropharyngeal carotid artery was 60.5 years compared with patients with at least 1 marginal carotid artery (average age, 55.5 years) and patients without a retropharyngeal or marginal carotid artery (average age, 44.9 years). The youngest patient with a retropharyngeal carotid artery was 37 years of age, and the oldest patient was 78 years. The ICA was the most common retropharyngeal segment seen on the anchor examinations in our study population (61%). The common carotid artery was the next most common retropharyngeal segment (25%). Of note, the external carotid artery (proximal to the occipital artery) was retropharyngeal in 2 patients; this finding

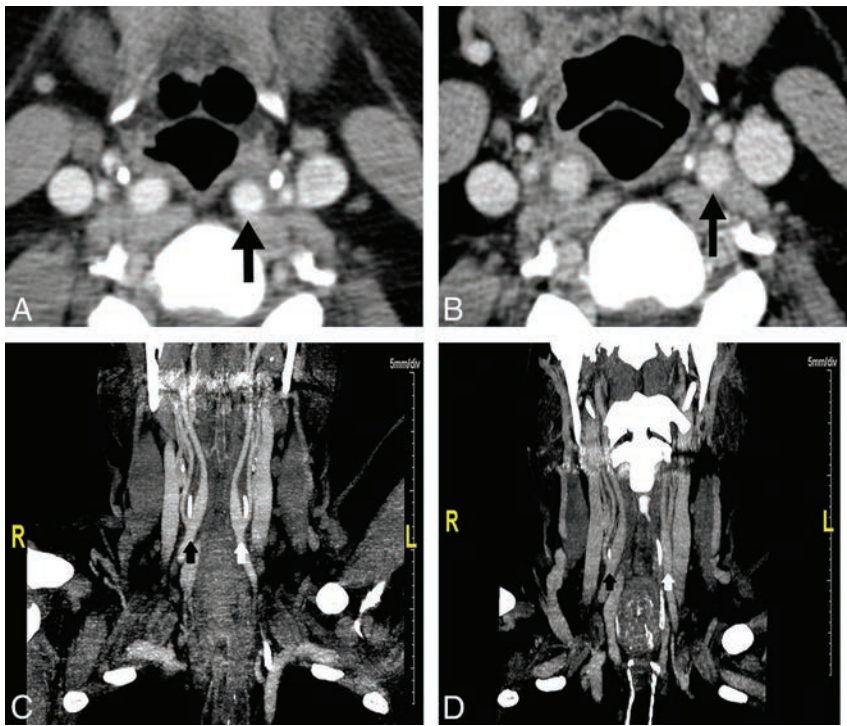


FIG 3. A 58-year-old man with mantle cell lymphoma. *A*, The proximal left internal carotid artery (arrow) position is retropharyngeal (grade 2). The proximal left external carotid artery can be seen lateral to the internal carotid artery. This image was obtained immediately superior to the common carotid bifurcation. The superior cornu of the thyroid cartilage lies between and just anterior to the 2 structures. *B*, On a scan obtained 1 year earlier, the proximal left internal carotid artery (arrow) position is lateral (grade 0). The proximal left external carotid artery can be seen just anterior to the internal carotid artery, and the superior cornu of the thyroid cartilage lies medial to the internal carotid artery. This image was also obtained immediately superior to the common carotid bifurcation. *C*, A coronal reformatted image shows the right common carotid bifurcation (black arrow) and the left common carotid bifurcation (white arrow). The superior cornu of the thyroid cartilage can be seen between the proximal internal and external carotid arteries bilaterally. Both internal carotid arteries are retropharyngeal. *D*, A coronal reformatted image from the examination obtained 1 year earlier (shown in *B*) shows that the proximal left internal carotid artery (white arrow) lies lateral to the superior cornu of the thyroid cartilage, whereas the proximal right internal carotid artery remains retropharyngeal.

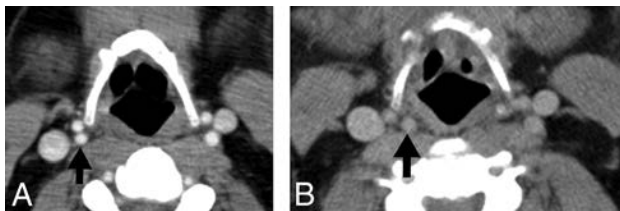


FIG 4. A 46-year-old man with Hodgkin lymphoma. *A*, The right internal carotid artery (arrow) position is lateral (grade 0). Both the proximal internal and external carotid arteries are lateral to the greater cornu of the hyoid bone. This image was obtained immediately above the level of the common carotid bifurcation. *B*, On a scan obtained 6 months earlier, the proximal right internal carotid artery (arrow) position is retropharyngeal (grade 2), located medial to the greater cornu of the hyoid bone. This image was also obtained immediately above the level of the common carotid bifurcation.

was unexpected. In addition, the carotid bifurcation was completely retropharyngeal bilaterally in 1 patient.

Logistic regression showed a statistically significant ($P < .001$) correlation between increasing age and increasing average carotid artery grade. For example, the youngest patient included in our study (2 years of age) would have a 92.7% chance of having no retropharyngeal carotid artery (average grade, 0) and a 0.5%

chance of having bilateral retropharyngeal carotid arteries (average grade, 2), whereas the oldest patient included in our study (82 years) would have a 27.0% chance of having no retropharyngeal carotid artery and a 15.4% chance of having bilateral retropharyngeal carotid arteries.

Twenty-two patients had a diagnosis of hypertension, and 88 patients did not have a diagnosis of hypertension in the electronic medical record systems. The average age of patients with a diagnosis of hypertension was 60.3 years, and the average age of those without a diagnosis of hypertension was 48.6 years. The average carotid position (on the scale of 0–3) in patients with a diagnosis of hypertension was 0.568, and the average carotid position in those without a diagnosis of hypertension was 0.381. Of the 22 patients with a diagnosis of hypertension, 5 (22.7%) had at least 1 retropharyngeal carotid artery. Of the 88 patients without a diagnosis of hypertension, 12 (13.6%) had at least 1 retropharyngeal carotid artery. There was no statistically significant correlation ($P = .334$) between a diagnosis of hypertension and increasing average carotid artery grade.

Within the group of 63 patients with comparison examinations, 4 patients (6.3%) showed interval change in the position of a carotid artery from lateral to retropharyngeal or vice-versa between examinations (Figs 3 and 4). Of

these 4 patients with interval change in position of the carotid arteries, the change in position occurred at the level of the oropharynx in 3 patients and at the level of the hypopharynx in 1 patient. The carotid artery that changed position was on the right in 2 patients and on the left in the other 2 patients. The segment involved was the ICA in 3 patients and the common carotid artery in the single remaining patient. The imaging features and demographic and clinical data of the 4 patients with a change in position of the carotid arteries between examinations are shown in Table 2.

Two patients whose carotid arteries changed position from lateral to retropharyngeal or vice-versa between examinations showed no change in head position between the scans when the change in position of the carotid artery occurred. The other 2 patients whose carotid artery position changed from lateral to retropharyngeal or vice-versa showed a change in the “nod” axis from 0° to 10°–19° down. One of these patients had a retropharyngeal carotid artery when the head was in the 10°–19° down position and a lateral carotid artery when the head was in the neutral position. The other patient showed the opposite pattern, in which the carotid artery was retropharyngeal in the neutral position and lateral with the head in the 10°–19° down position.

Table 2: Demographic data, diagnoses, and imaging features of patients with moving carotid arteries

Patient	Age (yr)	Sex	Diagnosis	Atherosclerosis Grade	Moving Segment	Level of Retropharyngeal Carotid	Time Interval between Scans (mo)	Head Position
1	58	Male	HematoCA	0	Left ICA	Oropharynx	8	Tilted 10° down between scans
2	46	Male	HematoCA	0	Right ICA	Oropharynx	6	Neutral; no change
3	71	Male	Skin cancer	2	Left CCA	Hypopharynx and oropharynx	4	Tilted 10° down between scans
4	56	Female	Lung cancer	2	Right ICA	Oropharynx	2	Neutral; no change

Note:—CCA indicates common carotid artery; HematoCA, hematologic malignancy.

In contrast, another patient changed head position from 30°–39° up to 20°–29° down between 2 scans and showed no change in position of the carotid arteries.

DISCUSSION

We showed an incidence of retropharyngeal carotid arteries on the anchor studies of 15.5%; and 18.2% of patients had at least 1 retropharyngeal carotid artery found over the course of their studies. Prior studies have shown a prevalence of retropharyngeal carotid arteries of 2.6%.¹⁰ The higher prevalence of retropharyngeal carotid arteries between our study and other studies may be related to differences in the method of determining retropharyngeal position and differences in patient demographics. Additionally, some prior studies have only commented on the retropharyngeal position of the internal carotid artery, while our study has shown that the common carotid artery and external carotid artery may also have a retropharyngeal position. Because we have demonstrated that the retropharyngeal carotid artery is not a static phenomenon, prior studies that only documented its presence at a single time point may have underestimated the true prevalence.

The average age of patients with retropharyngeal carotid arteries (60.5 years) was greater compared with those with marginal (55.5 years) or lateral (44.9 years) carotid arteries. Furthermore, statistical analysis of our data revealed a significant correlation between increasing patient age and the likelihood of having a retropharyngeal carotid artery. The association of increasing age with the presence of retropharyngeal or marginal carotid arteries was expected, because older patients tend to have a greater degree of tortuosity of the carotid arteries.¹²

Among our patient population, there was a trend toward association of higher grades of atherosclerosis with retropharyngeal carotid arteries compared with marginal or lateral carotid arteries. This finding was expected because patients with atherosclerotic disease frequently demonstrate tortuosity of the carotid arteries,⁹ and this tortuosity would logically predispose to deviation of the artery from its usual anatomic position. However, statistical analysis of our data failed to confirm that a true correlation was present. Perhaps if a larger sample size were available, a correlation would have been found, and this could potentially be a focus of further investigation.

Our data did not show a statistically significant correlation between a diagnosis of hypertension and an increasing likelihood of having a retropharyngeal carotid artery. This may have been due to incomplete charting or underreporting of hypertension in the electronic medical record, because some of the patients in our study may have been referred to our medical center for subspecialty care. In this

case, the diagnosis of hypertension might have been made by their primary care provider at another institution but not entered into our electronic medical record system.

Our study demonstrated that 6.3% of patients had a change in position of the carotid arteries from retropharyngeal to lateral or vice-versa between any comparison examination and the anchor examination. To our knowledge, this incidence has never previously been evaluated. A recent case report¹¹ documented the phenomenon of variability in the position of the retropharyngeal ICA. Variation in pharyngeal wall diameter and position of the hyoid bone with the respiratory cycle were discussed as potential explanations, but the physiology explaining this change in the position of the ICAs was thought to remain unclear. Additionally, the authors discussed whether the change in position of the retropharyngeal ICA was a fixed alteration of the anatomy of the neck or a transient variation in the position of the ICA. A recent study of the motion of parapharyngeal and retropharyngeal structures during swallowing has shown that there is anterior and medial displacement of the ICA and external carotid artery during pharyngeal contraction.¹³ In our study, the variability in the position of the retropharyngeal carotid arteries was at the level of the hyoid bone in all patients (Figs 2 and 3). The ICA may potentially be temporarily held in a retropharyngeal position by the tip of the greater cornu of the hyoid bone after being drawn anteromedially by pharyngeal contraction during swallowing, though this theory cannot be confirmed by our study, and the duration of the carotid artery being located in any given position cannot be known in our patient population. However, given the lack of change in carotid position in most of our patients, most carotid arteries must be relatively fixed in the retropharyngeal, marginal, or lateral positions. Much more frequent CT examinations would need to be performed on each patient to understand and fully evaluate the dynamic nature of this phenomenon.

The change in position of the head between examinations seemed to have no clear association with the change in the position of the carotid artery from lateral to retropharyngeal or vice-versa. Two of the patients whose carotid arteries changed position between examinations showed no change in head position. The other 2 patients whose carotid arteries changed position showed inconsistent findings, with 1 patient demonstrating a retropharyngeal carotid artery with the head in the neutral position and the other demonstrating a retropharyngeal carotid artery with the head tilted down. Additionally, many of the patients in our study showed large changes in head position between examinations with no change in carotid artery position.

Our patient population comprised mostly adults (92%). This greater proportion of CT examinations performed in adults was likely due to a greater prevalence of head and neck cancer and lymphoproliferative disorders in the adult population as well as awareness of the risks of ionizing radiation to pediatric patients and resultant avoidance of CT by referring providers. While our patient population did include some pediatric patients, the results of the study apply mostly to adults because the patient population was skewed toward adults.

Most of our patient population (65%) was male. This may potentially be explained by a higher incidence of head and neck cancer in males compared with females¹⁴ and by the large proportion of patients with cancer in our study. For this reason, however, our results may not necessarily apply to the population as a whole. Koreckij et al¹⁰ found that an aberrant course to the carotid arteries was more common in female patients and was associated with significantly greater spondylosis and kyphosis than in age-matched controls.

The retropharyngeal carotid artery is a clinically important anatomic variant, and numerous complications associated with this anatomic variant have been reported in the literature. These include hemorrhage from the ICA during surgical procedures involving the pharynx,⁸ inadvertent puncture of and injection of anesthetic into the ICA during transoral blocking of the glossopharyngeal nerve,³ and injury of the ICA during tracheal intubation.³ Ligation of the ICA to control hemorrhage after these complications may result in hemiplegia.⁸ Additionally, the presence of a retropharyngeal ICA may be a contributing factor to obstructive sleep apnea.³ For these reasons, it is important to communicate the presence of a retropharyngeal carotid artery to the clinician. A carotid artery moving into and out of a retropharyngeal position further complicates matters, in that the clinician may assume that it is not present on the basis of a single imaging study and then may encounter it during an operation or in the clinic.

Our study was limited by a number of factors. The relatively small sample size may have led to overestimation or underestimation of the prevalence of retropharyngeal carotid arteries and position-changing carotid arteries. It also may have limited our ability to make a correlation between the degree of atherosclerosis and the likelihood of a retropharyngeal carotid artery. The inhomogeneous patient population in our study may also have skewed our results, though we attempted to exclude patients with conditions that would be expected to have an effect on carotid position. The inconsistent patient positioning between imaging examinations may have had an effect on carotid position, though this was unavoidable in a retrospective study and our results do not suggest that changes in patient positioning have an effect on carotid position.

CONCLUSIONS

Retropharyngeal carotid arteries are a clinically important anatomic variant, shown to occur in 18.2% of the patients in our study. Knowledge of the presence of this variant in a particular patient may allow the clinician to avoid potential complications related to surgical procedures and endotracheal intubation. Our results show that change in the position of the carotid artery from lateral to retropharyngeal or vice-versa is not an uncommon phenomenon, occurring in 6.3% of our patients. Although we did not isolate any definite causes, knowledge of this phenomenon may result in heightened awareness among physicians and therefore aid in the prevention of complications associated with this anatomic variant.

REFERENCES

1. Kelly AB. **Tortuosity of the internal carotid in relation to the pharynx.** *J Laryngol Otol* 1925;40:15–23 CrossRef
2. Skillern PG. **Anomalous internal carotid artery and its clinical significance in operations on tonsils.** *JAMA* 1913;60:172–73 CrossRef
3. Marcucci C, Thomas P, Sewell DA. **Retropharyngeal carotid artery: an important anatomic variation for the anesthesiologist.** *Anesthesiology* 2009;111:454–55 CrossRef Medline
4. Mousa AY, AbuRahma AF. **Retropharyngeal internal carotid artery: a rare presentation with significant clinical implications.** *Ann Vasc Surg* 2013;27:1189.e1–4 CrossRef Medline
5. Ozgur Z, Celik S, Govsa F, et al. **A study of the course of the internal carotid artery in the parapharyngeal space and its clinical importance.** *Eur Arch Otorhinolaryngol* 2007;264:1483–89 CrossRef Medline
6. Paulsen F, Tillman B, Christofides C, et al. **Curving and looping of the internal carotid artery in relation to the pharynx: frequency, embryology and clinical implications.** *J Anat* 2000;197:373–81 CrossRef Medline
7. Srinivasan S, Ali SZ, Chwan LT. **Aberrant retropharyngeal (submucosal) internal carotid artery: an under-recognized, clinically significant variant.** *Surg Radiol Anat* 2013;35:449–50 CrossRef Medline
8. Pfeiffer J, Ridder GJ. **A clinical classification system for aberrant internal carotid arteries.** *Laryngoscope* 2008;118:1931–36 CrossRef Medline
9. Del Corso L, Moruzzo D, Conte B, et al. **Tortuosity, kinking, and coiling of the carotid artery: expression of atherosclerosis or aging?** *Angiology* 1998;49:361–71 CrossRef Medline
10. Koreckij J, Alvi H, Gibly R, et al. **Incidence and risk factors of the retropharyngeal carotid artery on cervical magnetic resonance imaging.** *Spine* 2013;38:E109–12 CrossRef Medline
11. Gupta A, Shah AD, Zhang Z, et al. **Variability in the position of the retropharyngeal internal carotid artery.** *Laryngoscope* 2013;123:401–03 CrossRef Medline
12. Hong JT, Kim TH, Kim IS, et al. **The effect of patient age on the internal carotid artery location around the atlas.** *J Neurosurg Spine* 2010;12:613–18 CrossRef Medline
13. Chitose S, Haraguchi M, Nagata S, et al. **Analysis of passive motion of para- and retropharyngeal structures during swallowing using dynamic magnetic resonance imaging.** *Dysphagia* 2014;29:387–95 CrossRef Medline
14. Jemal A, Bray F, Center MM, et al. **Global cancer statistics.** *CA Cancer J Clin* 2011;61:69–90 CrossRef Medline

Usefulness of Pseudocontinuous Arterial Spin-Labeling for the Assessment of Patients with Head and Neck Squamous Cell Carcinoma by Measuring Tumor Blood Flow in the Pretreatment and Early Treatment Period

 N. Fujima,  D. Yoshida,  T. Sakashita,  A. Homma,  A. Tsukahara,  K.K. Tha,  K. Kudo, and  H. Shirato



ABSTRACT

BACKGROUND AND PURPOSE: For the assessment of the treatment response in non-surgical treatment, tumor blood flow provides the functional information of the tumor which is different from the morphological information such as tumor volume. The purpose of this study was to evaluate the diagnostic value of tumor blood flow values obtained by pseudocontinuous arterial spin-labeling in patients with head and neck squamous cell carcinoma.

MATERIALS AND METHODS: Forty-one patients with head and neck squamous cell carcinoma were evaluated by using pseudocontinuous arterial spin-labeling. Quantitative tumor blood flow was calculated at the pretreatment and the early treatment periods in all the patients, and the percentage change of tumor blood flow between the two was calculated. At the early treatment period, based on their tumor volume reduction rate, we divided the patients into stable disease and partial response groups for a subgroup analysis. The local control or failure was confirmed either by histopathology or by radiologic evaluation within the follow-up.

RESULTS: Pretreatment tumor blood flow in patients in the failure group was significantly lower than that in patients in the local control group. In the subgroup analysis of patients with stable disease, the percentage change of tumor blood flow was significantly larger (due to the tumor blood flow increase from pretreatment value) in the local control group than in the failure group. In addition, in patients with a partial response, the percentage change of tumor blood flow was significantly smaller (due to the tumor blood flow decrease from the pretreatment value) in the local control group than in the failure group. The accuracy for determination of the local control group or the failure group in pretreatment tumor blood flow was 0.83 and that in the combination use of the percentage change of tumor blood flow and tumor volume in the early treatment period was 0.93.

CONCLUSIONS: Tumor blood flow obtained by pseudocontinuous arterial spin-labeling can be useful for the determination of local control. The combined use of the percentage change of tumor blood flow and tumor volume had particularly high diagnostic accuracy.

ABBREVIATIONS: HNSCC = head and neck squamous cell carcinoma; pCASL = pseudocontinuous arterial spin-labeling; PR = partial response; SCC = squamous cell carcinoma; SD = stable disease; TBF = tumor blood flow; TV = tumor volume

Nonsurgical, organ-preserving treatments, including chemotherapy, radiation therapy, and combinations of these approaches, are important therapeutic modalities for patients with

head and neck squamous cell carcinoma (HNSCC).¹⁻³ Detecting early treatment response can impact and improve patient care by allowing tailoring of treatment and optimization of follow-up strategy. Early treatment responses are usually assessed by anatomic imaging with CT or MR imaging to detect morphologic changes of the tumor, as noted in the Response Evaluation Criteria in Solid Tumors rules.⁴ However, studies reported that morphologic changes are limited in their ability to predict treatment response,^{5,6} and, thus, such information alone is not always sufficient for assessing the local control or failure at the primary site. In contrast, the measurement of tumor blood flow (TBF) provides functional information because tumor perfusion reflects neovascularity or angiogenic activity, which is closely related to

Received May 6, 2015; accepted after revision July 6.

From the Department of Diagnostic and Interventional Radiology (N.F., D.Y., A.T., K.K.), Hokkaido University Hospital, Sapporo, Japan; Departments of Otolaryngology—Head and Neck Surgery (T.S., A.H.) and Radiation Medicine (K.K.T., H.S.), Hokkaido University Graduate School of Medicine, Sapporo, Japan; and Global Station for Quantum Medical Science and Engineering (K.K.T., H.S.), Global Institution for Collaborative Research and Education, Sapporo, Japan.

This study received grant support from the Ministry of Education, Culture, Sports, Science, and Technology, Japan (ID 25861047).

Paper previously presented in part at: Joint Annual Meeting of the International Society for Magnetic Resonance in Medicine-European Society for Magnetic Resonance in Medicine and Biology, May 10–16, 2014; Milan, Italy.

Please address correspondence to Noriyuki Fujima, MD, PhD, Department of Diagnostic and Interventional Radiology, Hokkaido University Hospital, N15, W7, Kita-Ku, Sapporo 060-8638, Japan; e-mail: Noriyuki.Fujima@mb9.seikyousei.jp

 Indicates open access to non-subscribers at www.ajnr.org

<http://dx.doi.org/10.3174/ajnr.A4513>

tumor growth.⁷ In patients with HNSCC, the TBF is usually assessed by a dynamic contrast-enhanced method.^{8–11} However, this method is somewhat invasive and requires IV placement and contrast injection, and repetitive scanning is sometimes difficult, especially during chemotherapy when renal dysfunction frequently occurs (approximately 25%–42%) in patients given cisplatin.^{12,13} Because of the difficulties of repetitive scanning, there have been few studies of the changes in TBF with repetitive scanning over the treatment period, and the number of patients in these reports is quite small, at 10 to <20 patients.^{14–16} Thus, the role and potential of TBF measurement during treatment remain unclear. TBF measurement by pseudocontinuous arterial spin-labeling (pCASL), which was introduced for the noninvasive measurement of tissue blood flow without the need for a contrast agent and with no radiation exposure,^{17,18} was recently demonstrated to be feasible and applicable for HNSCCs¹⁹; pCASL thus has potential for the evaluation of treatment effects in patients with HNSCC without the risks with repetitive scanning of contrast-induced nephropathy during chemotherapy and increased radiation exposure. The purpose of the present study was to evaluate the diagnostic value of TBF assessed by pCASL for the determination of local control or failure in patients with HNSCC.

MATERIALS AND METHODS

Patients

The study protocol was approved by our institutional review board, and written informed consent was obtained from all the patients. From September 2010 to August 2013, 45 consecutive patients who were referred to our hospital to receive superselective arterial infusions of cisplatin with concomitant radiation therapy for a diagnosis of nasal, sinonasal, or oropharynx cancer were enrolled in this prospective study with the following inclusion criteria: 1) histopathologic diagnosis of HNSCC, and 2) plan for a full course of curative treatment with a radiation dose of 70 Gy. In all the patients, MR scanning, including pCASL, was performed in both the pretreatment and early treatment period, as described below. Among these 45 patients, 4 discontinued treatment due to severe complications and were excluded. A total of 41 patients, therefore, were considered eligible for this study: 36 men (mean age, 61.2 years; range, 46–77 years) and 5 women (mean age, 57.4 years; range 43–69 years). The histopathologic diagnoses were squamous cell carcinoma (SCC) in all the patients. The primary lesions of the 41 patients, detail of histopathologic information, and T stage were as follows: nasal or sinonasal cavity in 24 patients (well differentiated in 3, moderate in 10, poor in 11; keratinizing type in 9, nonkeratinizing type in 15; T1/2 in 1, T3 in 8, T4a in 11, and T4b in 4) and oropharynx in 17 patients (well differentiated in 3, moderate in 11, poor in 3; keratinizing type in 12, nonkeratinizing type in 5; T1/2 in 4, T3 in 1, T4a in 9, and T4b in 3). The treatment regimen was superselective arterial infusions of cisplatin with concomitant radiation therapy for all the patients. Treatment details were as follows: arterial infusion of cisplatin (100–120 mg/m² per wk for 4 weeks) to the dominant blood supply of the primary tumor by using a microcatheter, with concurrent radiation therapy of a total of 70 Gy in 35 fractions. MR imaging scans, including pCASL, were performed in all the patients before treatment and again in the early treatment period.

The time intervals between the pretreatment pCASL and the beginning of the treatment ranged from 1 to 25 days (mean, 9.2 days). MR scanning in the early treatment period was performed on delivery of 16–20 Gy (mean, 19.1 Gy) of the total 70 Gy, which occurred just after the second arterial infusion of cisplatin.

Clinical End Point

For all the patients, clinical and radiologic follow-ups were performed after the treatment to determine the final diagnosis of failure or local control at the primary site. After treatment or during follow-up, based on the patients' radiologic findings: 1) surgical resection was performed in the patients in whom a residual mass lesion was suspected, and 2) a biopsy was performed in the patients with thickened posttreatment granulation tissue. In addition, careful follow-up was performed in the patients with no mass lesion and/or granulation tissue. Local failure at the primary site was determined by histopathologic confirmation of HNSCC by biopsy specimen or surgical resection, or by enlargement of residual tumor during follow-up. Local control at the primary site was determined by histopathologic confirmation of the absence of HNSCC by surgical resection, the absence of enlargement of the possible residual tumor, or the absence of a new lesion in the posttreatment granulation tissue within the follow-up period, which was at least 1 year.

MR Imaging Protocol

All MR imaging was performed by using a 3T unit (Achieva TX; Philips Healthcare, Best, the Netherlands) with a 16-channel neurovascular coil. First, conventional MR images were obtained to evaluate the primary tumor. These images included 1) axial T1WI with a spin-echo sequence (TR, 450 milliseconds; TE, 10 milliseconds; FOV, 240 × 240 mm; 512 × 512 matrix; section thickness, 5 mm; intersection gap, 30%; scanning time, 2 minutes and 12 seconds), and 2) axial T2WI with a TSE sequence with fat suppression (TR, 4500 milliseconds; TE, 70 milliseconds; TSE factor, 9; FOV, 240 × 240 mm; 512 × 512 matrix; section thickness, 5 mm; intersection gap, 30%; scanning time, 2 minutes and 6 seconds).

In the pCASL scanning, coronal T2WI was performed to obtain anatomic localization of the carotid artery for positioning of the labeling slab. A T1 map was also obtained to measure the longitudinal relaxation in the tumor tissue, and the map was used for the TBF quantification. The acquisition of pCASL was performed by using multishot spin-echo echo-planar imaging to obtain control and labeled images. The labeling slab was placed just under the bifurcation of the internal and external carotid arteries by using coronal T2WI as a reference for the labeling of arterial water. The control images were obtained without the labeling of arterial water by using the same imaging scheme of the labeled images. The MR parameters of the pCASL were as follows: labeling duration, 1650 milliseconds; postlabel delay, 1280 milliseconds; TR, 3619 milliseconds; TE, 18 milliseconds; flip angle, 90°; number of shots, 2; FOV, 230 × 230 mm; matrix, 80 × 80; section thickness, 5 mm; number of sections, 15; acceleration factor for parallel imaging, 2; scanning time, 5 minutes and 11 seconds. All the sections were placed in parallel with the anterior/posterior commissure line. Each section was carefully placed at the same

level in the scans taken at the pretreatment and early treatment period by using the sagittal scout image. The patients were instructed not to swallow, move their tongue, open their mouth, or make any other voluntary motion during the pCASL scan.

The coronal T2WI was obtained by TSE sequence with the following parameters: TR, 4500 milliseconds; TE, 70 milliseconds; TSE factor, 9; FOV, 240 × 240 mm; matrix, 512 × 512; section thickness, 4 mm; intersection gap, 30%; scanning time, 2 minutes and 6 seconds. For the T1 map, we used a gradient-echo sequence with Look-Locker readout by constant flip angle with the following parameters: TR, 7 milliseconds; TE, 1.7 milliseconds; flip angle, 7°; FOV, 230 × 230 mm; matrix, 256 × 256; section thickness, 10 mm (single section acquisition); scanning time, 6 seconds.

Data Analysis

TBF Calculation by pCASL. We calculated the TBF of the pCASL (f) from the signal difference (ΔM), which was calculated by subtracting the labeled image from the control image, by using the previously described equation²⁰:

$$1) \quad f = \frac{\Delta M \lambda R_{1a} \exp(\omega R_{1a})}{2M_0 \alpha} [1 - \exp(-\gamma R_{1a})]^{-1}$$

in which R_{1a} is the longitudinal relaxation rate of blood (0.67 seconds⁻¹), γ is the labeling time (1.65 seconds), ω is the postlabeling delay time (1.28 seconds), α is the labeling efficiency (0.85), and λ is the blood/tumor-tissue water partition coefficient (1.0 g/mL).^{21,22} M_0 is the equilibrium magnetization of the tumor tissue, which was estimated from the signal intensity of the control image and the tumor longitudinal relaxation rate obtained with the T1 map. By using Equation 1, we created the TBF maps on a pixel-by-pixel basis. We used mathematical software (Matlab version 2012a; MathWorks, Natick, Massachusetts) to calculate the TBF values for both pCASLs.

Tumor ROI Delineation. Each patient's primary tumor was outlined by a board-certified neuroradiologist (A.T.) with 18 years of experience. The delineation was performed on the axial T2WI with a polygonal ROI, and the ROI was then copied onto a TBF map (Fig 1). ROI delineation was performed by using ImageJ software (National Institutes of Health, Bethesda, Maryland) to include the soft-tissue mass (and to exclude the normal or inflammatory tissue) in the ROI obtained from the T2WI findings. T1WI was also used as a guide to determine the ROI. To avoid vascular artifacts in the ROI, the area of the vessel signal void was also delineated on the T2WI, and this area was excluded from TBF measurement. Any strong high signal area with T2WI that indicated necrosis was also excluded. The TBF value of pCASL in each patient was determined as the mean of the TBF values in the delineated ROI. If the tumor extended into 2 or more sections on the TBF map, then the mean TBF of all pixels in all ROIs of the tumor was calculated as the TBF value. The percentage change of TBF between the pretreatment and early treatment period was calculated as follows: percentage change of TBF = 100 × (TBF at the early treatment period)/(pretreatment TBF) – 100.

Tumor Volume Measurement. Each tumor ROI used in the TBF analysis was also used for measurement of the tumor volume (TV). The TV was calculated as follows: [TV] = (size of ROI) ×

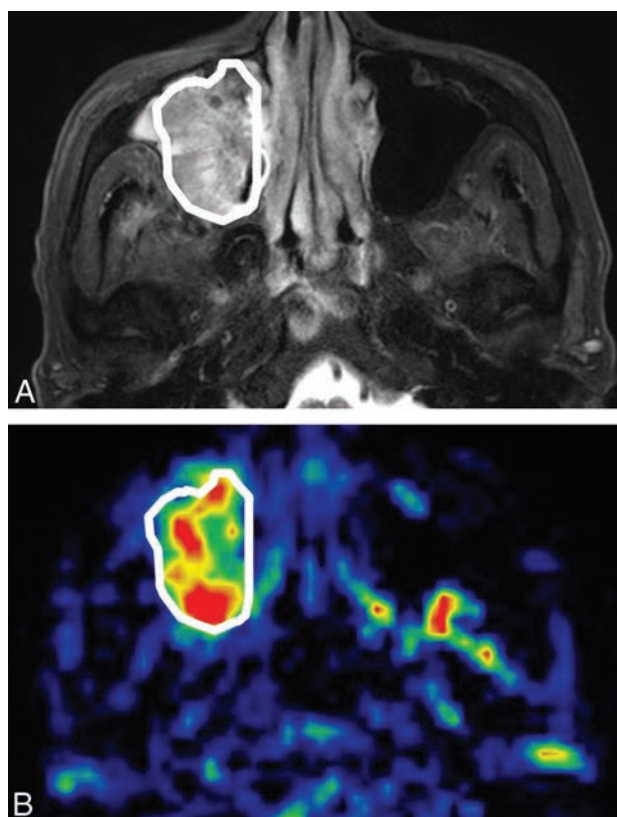


FIG 1. Tumor ROI delineation. An example of the tumor ROI delineation (a 68-year-old man with right maxillary cancer). *A*, The tumor was delineated on the axial T2WI with a polygonal ROI. *B*, After the delineation, the ROI was copied to the corresponding TBF map.

(section thickness). If the tumor extended beyond 2 sections, then the sum of the TVs in all the sections was calculated. The percentage change of TV between the pretreatment and early treatment periods was also calculated as follows: percentage change of TV = 100 × (TV at the early treatment period)/(pretreatment TV) – 100. For the subgroup analysis, we divided the 41 patients into 2 groups based on the Response Evaluation Criteria in Solid Tumors criteria by using their TV values in the pretreatment and early treatment periods as follows: patients whose percentage change of TV reduction between the pretreatment and early treatment period was ≥30% (ie, percentage change of a TV of –30% or less) made up the partial response (PR) group, and those whose percentage change of TV reduction was <30% (percentage change of TV of more than –30%) formed the stable disease (SD) group. Although the diameter of the tumor's long axis at the primary site was used for the size evaluation along with Response Evaluation Criteria in Solid Tumors criteria, this value is sometimes unreliable in head and neck tumors because of their complicated shapes, and, therefore, we used the TV for the size evaluation in the present study.

Statistical Analysis

A Mann-Whitney U test was used to compare pretreatment TBF and TV values between the local control and the failure groups. The same test was used to compare the percentage changes of TBF and TV in the early treatment period between the local control and the failure groups. The subgroup analysis of the percentage

change of TBF was performed by dividing the patients according to TV change in the early treatment period into PR and SD groups. The percentage change of TBF was compared between the patients in the local control group and in the failure group by using a Mann-Whitney *U* test in the PR and SD groups, respectively. If a significant difference was observed, then receiver operating characteristic curves were constructed for the calculation of the area under the curve and for the determination of the best diagnostic accuracy by using the closest point to the upper left corner of the receiver operating characteristic curve in the division of the local control and failure groups.

In addition, to investigate the relationship between TBF based on the location of each primary lesion and the result of the local control group or the failure group, the patients were divided into the group of patients with a lesion in the nasal or sinonasal cavity ($n = 24$) and those with a lesion in the oropharynx ($n = 17$). For each primary lesion, Mann-Whitney *U* tests were then used to compare pretreatment TBF values, the percentage change of TBF at the early treatment period, and for subgroup analysis of the patients with SD and those with PR between the local control and failure groups. *P* values $<.05$ were accepted as significant. Statistical software (SPSS; IBM, Armonk, New York) was used for the analysis.

RESULTS

We successfully obtained pCASL images of the 41 primary tumors in both the pretreatment and early treatment periods. Among the 41 patients, 11 were found to be in the failure group (8 patients with nasal or sinonasal cavity SCC, T stage of T3 in 2, T4a in 4, and T4b in 2; 3 patients with oropharynx SCC, T stage of T4a in 2, and T4b in 1). Nine patients with local failure were confirmed by histopathologic findings. Two patients with local failure and 30 with local control were determined by clinical diagnosis at follow-up (mean, 26 months; range, 12–43 months).

In the analysis of all the patients, the pretreatment TBF in the 11 patients in the failure group (109.6 ± 28.5 mL/100 g/min) was significantly lower than that in the 30 patients in the local control group (142.3 ± 34.5 mL/100 g/min) ($P < .01$) (Fig 2). Although there was a tendency for larger pretreatment TV values in the failure group patients (38.4 ± 27.1 mL) compared with the patients in the local control group (24.8 ± 19.1 mL), the difference was not significant ($P = .15$). In the early treatment period, there was no significant difference in the percentage change of TBF between the failure group ($-3.9\% \pm 11.4\%$) and the local control group ($-15.8\% \pm 34.1\%$) ($P = .19$) or in the TV values between the failure group ($-32.3\% \pm 20.1\%$) and the local control group ($-41.0\% \pm 21.0\%$) ($P = .24$). In the subgroup analysis, 17 patients achieved SD and 24 patients achieved only a PR, based on the percentage change in the TV values. In the subgroup analysis of patients with SD, the percentage change of TBF among the patients in the failure group ($-0.9\% \pm 11.9\%$) was significantly smaller than that in the patients in the local control group ($23.0\% \pm 17.2\%$) ($P < .01$) (Fig 3).

In addition, the subgroup analysis of patients with PR revealed that the percentage change of TBF in the patients in the failure group ($-9.2\% \pm 9.7\%$) was significantly larger than that in the patients in the local control group ($-35.2\% \pm 21.0\%$) ($P < .01$),

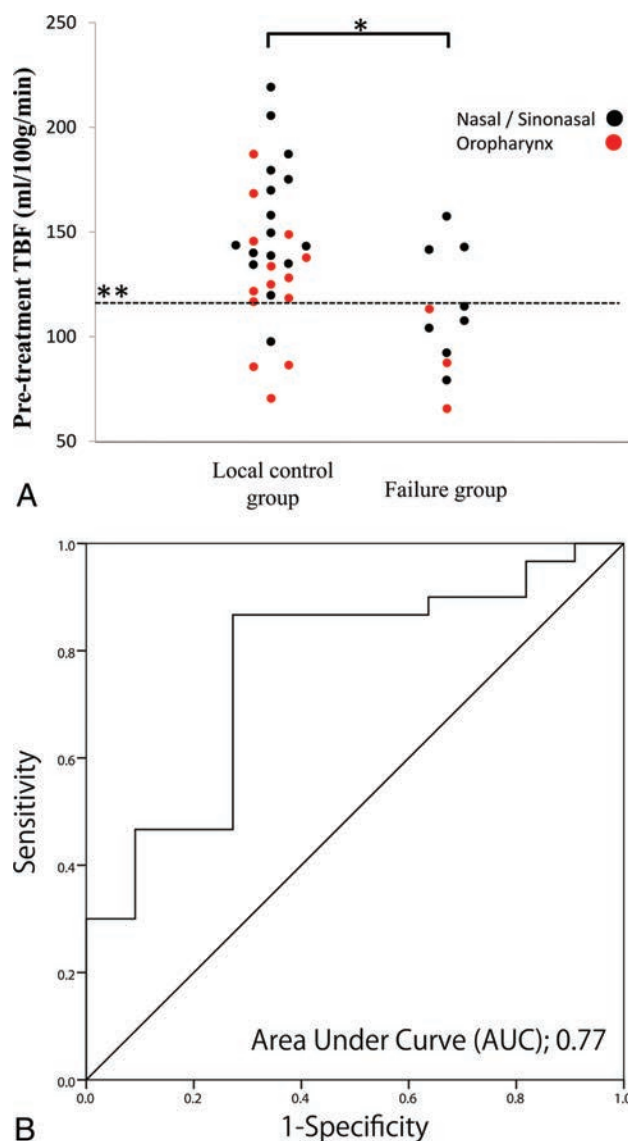


FIG 2. Pretreatment TBF in all the patients. A, The pretreatment TBF in patients in the failure group (109.6 ± 28.5 mL/100 g/min) was significantly lower than that in patients in the local control group (142.3 ± 34.5 mL/100 g/min) ($P < .01$) (A, *). B, The receiver operating characteristic curve analysis revealed the area under the curve of 0.77 ($P < .01$), with the best diagnostic accuracy of 0.83 (34/41), sensitivity of 0.87 (26/30), and specificity of 0.73 (8/11), with a threshold value of 115 mL/100 g/min (A, **).

which was the inverse of the trend in the SD group (Fig 3). In the receiver operating characteristic curve analysis, the best accuracy for the determination of failure or local control group in pretreatment TBF was 0.83 (34/41), with a sensitivity of 0.87 (26/30) and specificity of 0.73 (8/11) when the threshold was set at 115 mL/100 g/min (area under the curve, 0.77; $P < .01$) (Fig 2). In the subgroup analysis of patients with SD, the best accuracy for the percentage change of TBF was 0.94 (16/17), with a sensitivity of 1.0 (10/10) and specificity of 0.86 (6/7) when the threshold was set at 7.0% (area under the curve, 0.94; $P < .01$) (Fig 3). In the subgroup analysis of patients with a PR, the best accuracy for the percentage change of TBF was 0.92 (22/24), with a sensitivity of 0.95 (19/20) and specificity of 0.75 (3/4) when the threshold was set at the range of -8.0% to -14.0% (area under the curve, 0.89; $P < .01$)

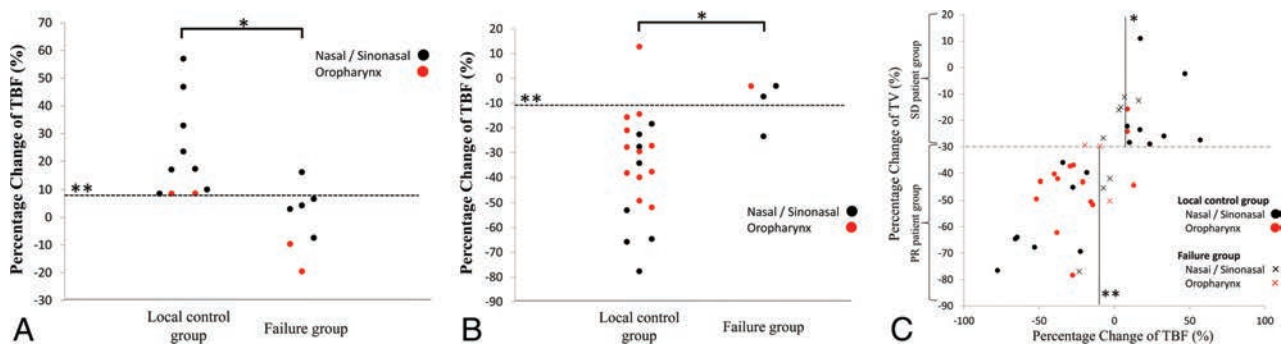


FIG 3. Percentage change of TBF in the early treatment period in the subgroup analyses of patients with SD and patients with PR. **A**, Subgroup analysis of patients in the SD group (the patients with $\leq 30\%$ TV reduction in the early treatment period); the percentage change of TBF in the failure group ($-0.9\% \pm 11.9\%$) was significantly lower than that in the local control group ($23.0\% \pm 17.2\%$) ($P < .01$) (*); the best diagnostic accuracy of 0.94 (16/17) with sensitivity of 1.0 (10/10) and specificity of 0.86 (6/7), with the threshold value 7% (**) was revealed by receiver operating characteristic analysis. **B**, Subgroup analysis of the PR patient group (the patients with $>30\%$ TV reduction in the early treatment period); the percentage change of TBF in the failure group ($-9.2\% \pm 9.7\%$) was significantly higher than that in the local control group ($-35.1\% \pm 21.0\%$) ($P < .01$) (*). The best diagnostic accuracy of 0.92 (22/24) with a sensitivity of 0.95 (19/20) and specificity of 0.75 (3/4), with a threshold value in the range -8.0% to -14.0% (**) was revealed by receiver operating characteristic analysis. **C**, Two-dimensional plot graph with the percentage change of TV on the vertical axis and the percentage change of TBF on the horizontal axis; when the threshold line was set to 7% (*) in the patients in the SD group, and the threshold was in the range -8.0% to -14.0% (**) in the PR patient group, the sensitivity, specificity, and accuracy for the division of failure and local control group were 0.97 (29/30), 0.82 (9/11), and 0.93 (38/41), respectively.

(Fig 3). When the SD and PR groups were combined in the subgroup analysis, the accuracy of the percentage change of TBF was 0.93 (38/41), with 0.97 sensitivity (29/30) and 0.82 specificity (9/11) with the setting of threshold in both SD and PR groups (7.0%; patients of the SD group; -8.0 to -14.0% , patients of the PR group) (Fig 3).

In the analysis based on tumor location, the pretreatment TBF values in the failure group with a nasal or sinonasal cavity lesion (117.5 ± 27.3 mL/100 g/min) were significantly lower than those of the local control group (154.3 ± 33.4 mL/100 g/min) ($P < .05$). In addition, among the patients with an oropharynx SCC, the pretreatment TBF values of the failure group (88.8 ± 23.8 mL/100 g/min) were significantly lower than those of the local control group ($126.7.3 \pm 31.7$ mL/100 g/min) ($P < .05$). At the early treatment period, there was no significant difference in the percentage change of TBF between the failure and local control groups in both the nasal and/or sinonasal cavity SCC ($-1.4\% \pm 11.8\%$ and $-6.4\% \pm 42.4\%$; $P = .59$) and patients with oropharynx SCC ($-10.7\% \pm 8.3\%$ and $-23.0\% \pm 21.0\%$; $P = .42$). Among the patients with nasal and/or sinonasal cavity SCC, in the SD group ($n = 13$: failure in 5, local control in 8), the percentage change of TBF in the failure group ($-4.5\% \pm 8.4\%$) was significantly smaller than that in the local control group ($26.6\% \pm 17.6\%$) ($P < .05$), and in the PR group ($n = 11$: failure in 3, local control in 8), the percentage change of TBF in the failure group ($-11.2\% \pm 10.7\%$) was significantly larger than that in the local control group ($-39.4\% \pm 32.5\%$) ($P < .05$). Among the patients with an oropharynx SCC, in the SD group ($n = 4$: failure in 2, local control in 2), the percentage change of TBF in the failure group ($-14.6\% \pm 7.0\%$) tended to be smaller than that in the local control group ($8.6\% \pm 0.03\%$). In addition, in the PR group ($n = 11$: failure in 1, local control in 10), the percentage change of TBF in the patients in the failure group (-3.1%) tended to be greater compared with that in the local control group ($-28.3\% \pm 17.6\%$), though no significant differences were observed ($P = .28$ and $P = 0.31$, respectively).

DISCUSSION

In this study, all pCASL scanning and TBF calculations were successfully performed in both the pretreatment and early treatment period. Although TBF measurement by pCASL in HNSCCs was recently reported to be feasible,¹⁹ there have been no reports on the use of this parameter in a clinical setting. Thus, the present study is the first to report the clinical usefulness of pCASL as a predictive factor in patients with HNSCC.

In regard to pretreatment TBF, patients in the failure group included in our study exhibited lower values than patients in the local control group. In each primary lesion of the nasal or sinonasal cavity and oropharynx, the same tendency of lower pretreatment TBF was observed in the failure group compared with its respective local control group. A past reported review article introduced several studies that describe the use of pretreatment TBF measured by a dynamic contrast-enhanced perfusion technique for assessments of the prognosis of patients undergoing chemoradiotherapy.²³ Most of these studies concluded that lower pretreatment TBF values indicated a poor prognosis. Our present findings showed the same trend as these previous reports.

With respect to the percentage change of TBF in the early treatment period, we observed that the patients in the failure group showed 1) significantly smaller percentage changes in the SD group, and 2) larger percentage changes in the PR group than the patients in the local control group. Truong et al¹⁴ reported that an initial increase in TBF in the early treatment period (2 weeks after the treatment started) in patients undergoing chemoradiotherapy predicted a good treatment result. The results of their report showed the same trend as that seen in the present study in regard to the patients who achieved SD status. In contrast, Surlan-Popovic et al¹⁵ and Gandhi et al¹⁶ reported that the follow-up TBF values during chemoradiotherapy were significantly lower in the patients with a good treatment response compared with those with a poor response, though more delayed timing was used in the study by Surlan-Popovic et al¹⁵ (the point of 40 Gy in a total of 65 Gy of radiation therapy) and the study by

Gandhi et al¹⁶ (after 1 cycle of induction chemotherapy; 3–4 weeks after the treatment start) for the TBF measurement compared with the present study and the study by Truong et al.¹⁴ These descriptions of TBF decreases in patients with good treatment responses also showed the same trend as that seen in our present patients with PR.

In regard to these findings, we had several hypotheses. The good prognosis in patients with an increase in TBF has been attributed to an increase in tumor oxygenation, which affects the sensitivity of the treatment effect in radiation therapy.^{16,24} We speculated that the initial TBF increase was caused by a decrease in the internal pressure of the tumor, which was derived from the initial treatment effect of cytotoxicity (ie, an increase in the extracellular space due to the destruction of tumor cells) in chemoradiotherapy,^{25–27} which resulted in the decrease in compression of intratumoral arteries. We suspected that such intratumoral changes reflected the initial TBF increase, probably observed as an initial treatment effect before the macroscopic TV reduction occurred. In contrast, the good prognosis in our patients with a TBF decrease reflected a progressed treatment effect, such as a decrease in an intratumoral arteriovenous shunt or a reduced volume of the vascular bed after chemoradiotherapy or damage to the endothelial cells of blood vessels by radiation therapy,^{28–30} and these changes in the tumor are likely to be observed at a more advanced period when the TV reduction has gradually occurred over the course of treatment compared with the initial TBF increase. However, in the present study population, these 2 trends of TBF increase or decrease were observed at the same time point during the treatment. The reason for this was probably related to the heterogeneity in the sensitivity of treatment response with tumors.^{31,32} We suspected that tumors with marked TV reduction even in the early treatment period would show a greater response to treatment compared with others, and we thus observed such a reversed TBF trend along with the change in the TV reduction rate at the same time point during treatment.

Several of our patients had local failure even though marked TV reduction was observed in the early treatment period in their cases. We suspected that this was because there will be intratumoral heterogeneity in treatment responses, such as that shown by a hypoxic lesion around the necrotic tissue or a deep area of the tumor with lower perfusion.^{19,33} Such lesions would continue to show little change of either TBF or TV, whereas other tumor lesions would show a volume reduction with marked TBF change.

Predicting the treatment result of local control or failure can provide useful information for decision-making regarding additional chemotherapy and the planning of earlier salvage surgery after the current chemoradiotherapy. For example, radiation therapy is often replanned due to a reduction in irradiated TV after an interim evaluation. The local distribution of TBF percentage change might be useful for replanning radiation therapy, as with ¹⁸F-FDG-PET.³⁴ In the case of arterial infusion therapy, the dose distribution of drug infusion in each artery can also be adjusted, depending on the regional percentage change of TBF in each arterial territory.

The present study had several limitations. First, the distribution of the primary tumor sites leaned heavily toward the nasal or sinonasal cavity (24 of the 41 cases). To avoid a heterogeneous

treatment plan, one of the study's inclusion criteria was treatment with an arterial infusion of cisplatin with concomitant radiation therapy. Systemic chemoradiotherapy tends to be the most commonly used treatment method for HNSCCs, especially in the oropharynx, but, with this therapy, it can sometimes be difficult to set the early treatment period due to the use of induction chemotherapy or to variation in the courses of chemotherapy drug administration. Second, no comparisons with other noninvasive parameters were conducted. The ADC measured from DWI has been widely investigated, and recent studies investigated the prediction of treatment response as well as the early detection of treatment response.^{23,25} Because TBF is a different biologic parameter than ADC, the combined use of both parameters could yield a more accurate prognosis. Further studies are needed to examine these points. Third, the patient number in the subgroup analysis based on SD and PR groups was quite small, and thus, the value of diagnostic accuracy from receiver operating characteristic analysis may not have much sufficient reliability. To address these problems, further analysis with greater numbers of patients will be considered necessary than in the current study. Fourth, other tumor environment factors, such as histologic differentiation, human papillomavirus status, and T stage, were not fully investigated as additional subgroup analysis. Because these factors may have a complex relationship with each other, the correlations among these factors and the identification of the factors that are related to the prognosis should be clarified in further studies.

CONCLUSIONS

The TBF values obtained by pCASL can provide useful information for the prediction of the local control: 1) higher pretreatment TBF values were suggested to indicate a local control, and 2) an increase in TBF in patients with a small TV reduction (–30% or less) in their primary tumor at the early treatment period and a decrease in TBF in patients with a large TV reduction (more than –30%) were each suggested to indicate a local control. In particular, the use of the percentage change of TBF combined with the percentage change of TV had high diagnostic accuracy for predicting the local control.

Disclosures: Noriyuki Fujima—RELATED: Grant: The Ministry of Education, Culture, Sports, Science, and Technology, Japan (ID 25861047). Kohsuke Kudo—UNRELATED: Grants/Grants Pending: NEXT Program,* JSPS KAKENHI Grant*; Payment for Lectures (including service on speakers bureaus): GE Healthcare, Toshiba Medical Systems, Hitachi Medical Systems, Philips Medical Systems, Siemens Medical Systems, Bayer Healthcare. Hiroki Shirato—UNRELATED: Grants/Grants Pending: Hitachi,* Mitsubishi Heavy Industry,* Shimadzu,* Comments: For radiotherapy research; Patients (planned, pending or issued): Hitachi*; Royalties: Olympus.* *Money paid to the institution.

REFERENCES

1. Homma A, Oridate N, Suzuki F, et al. **Superselective high-dose cisplatin infusion with concomitant radiotherapy in patients with advanced cancer of the nasal cavity and paranasal sinuses: a single institution experience.** *Cancer* 2009;115:4705–14 CrossRef Medline
2. Wong SJ, Harari PM, Garden AS, et al. **Longitudinal Oncology Registry of Head and Neck Carcinoma (LORHAN): analysis of chemoradiation treatment approaches in the United States.** *Cancer* 2011; 117:1679–86 CrossRef Medline
3. Kimata Y, Uchiyama K, Ebihara S, et al. **Postoperative complications and functional results after total glossectomy with microvascular**

- reconstruction.** *Plast Reconstr Surg* 2000;106:1028–35 CrossRef Medline
4. Eisenhauer EA, Therasse P, Bogaerts J, et al. **New response evaluation criteria in solid tumours: revised RECIST guideline (version 1.1).** *Eur J Cancer* 2009;45:228–47 CrossRef Medline
 5. Cao Y, Popovtzer A, Li D, et al. **Early prediction of outcome in advanced head-and-neck cancer based on tumor blood volume alterations during therapy: a prospective study.** *Int J Radiat Oncol Biol Phys* 2008;72:1287–90 CrossRef Medline
 6. Fujima N, Kudo K, Yoshida D, et al. **Arterial spin labeling to determine tumor viability in head and neck cancer before and after treatment.** *J Magn Reson Imaging* 2014;40:920–28 CrossRef Medline
 7. Folkman J, Klagsbrun M. **Angiogenic factors.** *Science* 1987;235:442–47 CrossRef Medline
 8. Faggioni L, Neri E, Bartolozzi C. **CT perfusion of head and neck tumors: how we do it.** *AJR Am J Roentgenol* 2010;194:62–69 CrossRef Medline
 9. Li XS, Fan HX, Zhu HX, et al. **The value of perfusion CT in predicting the short-term response to synchronous radiochemotherapy for cervical squamous cancer.** *Eur Radiol* 2012;22:617–24 CrossRef Medline
 10. Agrawal S, Awasthi R, Singh A, et al. **An exploratory study into the role of dynamic contrast-enhanced (DCE) MRI metrics as predictors of response in head and neck cancers.** *Clin Radiol* 2012;67:e1–5 CrossRef Medline
 11. Bisdas S, Medov L, Baghi M, et al. **A comparison of tumour perfusion assessed by deconvolution-based analysis of dynamic contrast-enhanced CT and MR imaging in patients with squamous cell carcinoma of the upper aerodigestive tract.** *Eur Radiol* 2008;18:843–50 CrossRef Medline
 12. de Jongh FE, van Veen RN, Veltman SJ, et al. **Weekly high-dose cisplatin is a feasible treatment option: analysis on prognostic factors for toxicity in 400 patients.** *Br J Cancer* 2003;88:1199–206 CrossRef Medline
 13. Daugaard G, Abildgaard U, Holstein-Rathlou NH, et al. **Renal tubular function in patients treated with high-dose cisplatin.** *Clin Pharmacol Ther* 1988;44:164–72 CrossRef Medline
 14. Truong MT, Saito N, Ozonoff A, et al. **Prediction of locoregional control in head and neck squamous cell carcinoma with serial CT perfusion during radiotherapy.** *AJNR Am J Neuroradiol* 2011;32:1195–201 CrossRef Medline
 15. Surlan-Popovic K, Bisdas S, Rumboldt Z, et al. **Changes in perfusion CT of advanced squamous cell carcinoma of the head and neck treated during the course of concomitant chemoradiotherapy.** *AJNR Am J Neuroradiol* 2010;31:570–75 CrossRef Medline
 16. Gandhi D, Chepeha DB, Miller T, et al. **Correlation between initial and early follow-up CT perfusion parameters with endoscopic tumor response in patients with advanced squamous cell carcinomas of the oropharynx treated with organ-preservation therapy.** *AJNR Am J Neuroradiol* 2006;27:101–06 Medline
 17. Lanzman RS, Robson PM, Sun MR, et al. **Arterial spin-labeling MR imaging of renal masses: correlation with histopathologic findings.** *Radiology* 2012;265:799–808 CrossRef Medline
 18. Binnewijzend MA, Kuijter JP, Benedictus MR, et al. **Cerebral blood flow measured with 3D pseudocontinuous arterial spin-labeling MR imaging in Alzheimer disease and mild cognitive impairment: a marker for disease severity.** *Radiology* 2013;267:221–30 CrossRef Medline
 19. Fujima N, Kudo K, Tsukahara A, et al. **Measurement of tumor blood flow in head and neck squamous cell carcinoma by pseudo-continuous arterial spin labeling: comparison with dynamic contrast-enhanced MRI.** *J Magn Reson Imaging* 2015;41:983–91 CrossRef Medline
 20. Wang Z, Aguirre GK, Rao H, et al. **Empirical optimization of ASL data analysis using an ASL data processing toolbox: ASLtbx.** *Magn Reson Imaging* 2008;26:261–69 CrossRef Medline
 21. van Osch MJ, Teeuwisse WM, van Walderveen MA, et al. **Can arterial spin labeling detect white matter perfusion signal?** *Magn Reson Med* 2009;62:165–73 CrossRef Medline
 22. Wheeler RH, Ziessman HA, Medvec BR, et al. **Tumor blood flow and systemic shunting in patients receiving intraarterial chemotherapy for head and neck cancer.** *Cancer Res* 1986;46:4200–04 Medline
 23. Srinivasan A, Mohan S, Mukherji SK. **Biologic imaging of head and neck cancer: the present and the future.** *AJNR Am J Neuroradiol* 2012;33:586–94 CrossRef Medline
 24. Bhatnagar P, Subesinghe M, Patel C, et al. **Functional imaging for radiation treatment planning, response assessment, and adaptive therapy in head and neck cancer.** *Radiographics* 2013;33:1909–29 CrossRef Medline
 25. King AD, Chow KK, Yu KH, et al. **Head and neck squamous cell carcinoma: diagnostic performance of diffusion-weighted MR imaging for the prediction of treatment response.** *Radiology* 2013;266:531–38 CrossRef Medline
 26. Kauppinen RA. **Monitoring cytotoxic tumour treatment response by diffusion magnetic resonance imaging and proton spectroscopy.** *NMR Biomed* 2002;15:6–17 CrossRef Medline
 27. Berrak S, Chawla S, Kim S, et al. **Diffusion weighted imaging in predicting progression free survival in patients with squamous cell carcinomas of the head and neck treated with induction chemotherapy.** *Acad Radiol* 2011;18:1225–32 CrossRef Medline
 28. Zwelling LA, Kohn KW. **Mechanism of action of cis-dichlorodiammineplatinum(II).** *Cancer Treat Rep* 1979;63:1439–44 Medline
 29. Leek RD, Landers RJ, Harris AL, et al. **Necrosis correlates with high vascular density and focal macrophage infiltration in invasive carcinoma of the breast.** *Br J Cancer* 1999;79:991–95 CrossRef Medline
 30. Martin DF, Fischer JJ. **Radiation sensitivity of cultured rabbit aortic endothelial cells.** *Int J Radiat Oncol Biol Phys* 1984;10:1903–06 CrossRef Medline
 31. Kojima H, Endo K, Moriyama H, et al. **Abrogation of mitochondrial cytochrome C release and caspase-3 activation in acquired multi-drug resistance.** *J Biol Chem* 1998;273:16647–50 CrossRef Medline
 32. Godwin AK, Meister A, O'Dwyer PJ, et al. **High resistance to cisplatin in human ovarian cancer cell lines is associated with marked increase of glutathione synthesis.** *Proc Natl Acad Sci U S A* 1992;89:3070–74 CrossRef Medline
 33. Evans SM, Du KL, Chalian AA, et al. **Patterns and levels of hypoxia in head and neck squamous cell carcinomas and their relationship to patient outcome.** *Int J Radiat Oncol Biol Phys* 2007;69:1024–31 CrossRef Medline
 34. Delouya G, Igidbashian L, Houle A, et al. **¹⁸F-FDG-PET imaging in radiotherapy tumor volume delineation in treatment of head and neck cancer.** *Radiother Oncol* 2011;101:362–68 CrossRef Medline

Protrusion of the Infraorbital Nerve into the Maxillary Sinus on CT: Prevalence, Proposed Grading Method, and Suggested Clinical Implications

J.E. Lantos, A.N. Pearlman, A. Gupta, J.L. Chazen, R.D. Zimmerman, D.R. Shatzkes, and C.D. Phillips

ABSTRACT

BACKGROUND AND PURPOSE: The infraorbital nerve arises from the maxillary branch of the trigeminal nerve and normally traverses the orbital floor in the infraorbital canal. Sometimes, however, the infraorbital canal protrudes into the maxillary sinus separate from the orbital floor. We systematically studied the prevalence of this variant.

MATERIALS AND METHODS: We performed a retrospective review of 500 consecutive sinus CTs performed at our outpatient centers. The infraorbital nerve protruded into the maxillary sinus if the entire wall of the infraorbital canal was separate from the walls of the sinus. We recorded the length of the bony septum that attached the infraorbital canal to the wall of the maxillary sinus and noted whether the protrusion was bilateral. We also measured the distance from the inferior orbital rim where the infraorbital canal begins to protrude into the sinus.

RESULTS: There was a prevalence of 10.8% for infraorbital canal protrusion into the maxillary sinus and 5.6% for bilateral protrusion. The median length of the bony septum attaching the infraorbital canal to a maxillary sinus wall, which was invariably present, was 4 mm. The median distance at which the infraorbital nerve began to protrude into the sinus was 11 mm posterior to the inferior orbital rim.

CONCLUSIONS: Although this condition has been reported in only 3 patients previously, infraorbital canal protrusion into the maxillary sinus was present in >10% of our cohort. Identification of this variant on CT could help a surgeon avoid patient injury.

ABBREVIATIONS: IOC = infraorbital canal; ION = infraorbital nerve

CT of the paranasal sinuses is an important diagnostic technique in the work-up of patients with known or suspected disease of the nasal cavity and paranasal sinuses. CT gives the surgeon a roadmap for surgery and alerts the surgeon to the presence of potentially clinically relevant anatomic variants. Many sinonasal variants are important to identify since their presence may increase the risk of surgical error.¹ With the advent of endoscopic techniques, surgery of the paranasal sinuses has expanded to involve complex procedures that were once reserved for open approaches. Thus, it is extremely important to identify such variations from the normal sinus anatomy, especially in patients who are likely to require extended

endoscopic sinus surgery for etiologies such as inverted papilloma, mucocele, trauma, or malignant tumor.

The infraorbital nerve is the distal portion of the maxillary nerve (V2), which originates as the second division of the trigeminal nerve (fifth cranial nerve). After the maxillary nerve traverses the foramen rotundum, it enters the pterygopalatine fossa and gives off nasal and palatine branches before exiting through the inferior orbital fissure and terminating as the infraorbital nerve (ION). The ION then enters the infraorbital canal (IOC) through the infraorbital groove. The IOC is a bony canal typically within the orbital process of the maxilla, synonymous with the floor of the orbit. The ION exits the IOC through the infraorbital foramen of the anterior maxilla. Variably, the IOC can protrude into the maxillary sinus separate from the floor of the orbit. This may leave the ION susceptible to injury during endoscopic or open sinus surgery. To date, just 3 case reports exist in the literature describing this variant,^{2,3} with no large studies describing the frequency with which it occurs. The aim of this study was to establish the prevalence of infraorbital nerve protrusion into the maxillary sinus and define its common characteristics. This variation is of clinical importance in sinus surgery, and we suggest an accompa-

Received March 31, 2015; accepted after revision June 17.

From the Departments of Radiology (J.E.L., A.G., J.L.C., R.D.Z., C.D.P.) and Otolaryngology (A.N.P.), Weill Cornell Medical College, New York, New York; and Department of Radiology (D.R.S.), Lenox Hill Hospital, New York, New York.

Please address correspondence to Joshua E. Lantos, MD, Weill Cornell Medical College, Department of Radiology, 535 E 68th St, New York, NY 10065; e-mail: jol9057@med.cornell.edu

<http://dx.doi.org/10.3174/ajnr.A4588>

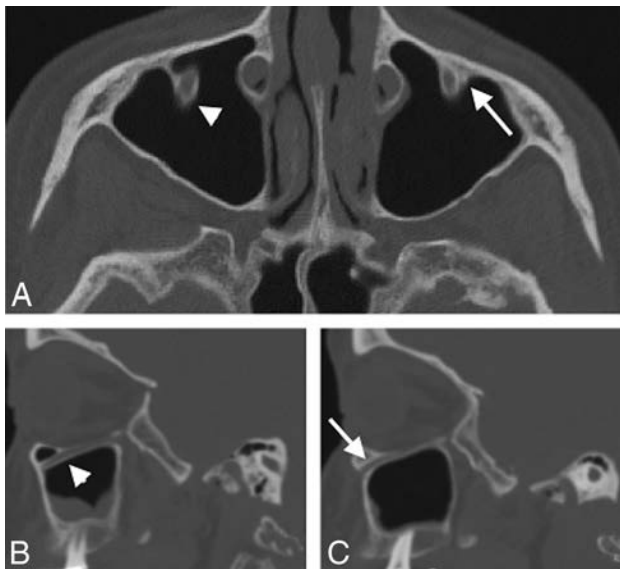


FIG 1. Axial (A), right parasagittal (B), and left parasagittal (C) sinus CT images in a 55-year-old woman show unilateral right-sided protrusion of the ION into the maxillary sinus (arrowheads in A and B). While part of the wall of the left IOC protrudes into the sinus, the entire circumference of the IOC is not distinct from the anterior maxillary sinus wall; this feature is confirmed on the sagittal image through the left maxillary sinus (arrows in A and C). Additionally, no measurable bony septum connects the IOC to the wall of the maxillary sinus. This distinction was chosen to define protrusion of the ION into the maxillary sinus.

nying grading scale to relay the degree of protrusion to the surgeon.

MATERIALS AND METHODS

A retrospective image review of sinus CTs performed at our institution was conducted after obtaining institutional review board approval, including a waiver for informed consent. Five hundred consecutive sinus CTs performed on 500 distinct patients at our outpatient centers from February 2, 2014 to July 31, 2014 were included in the study. Most patients had known or suspected sinus inflammatory disease and were referred by an otorhinolaryngologist. All CTs reviewed were acquired in the axial plane at 0.625 mm and reconstructed in a bone algorithm at 1.25 mm in the axial plane. Sagittal and coronal reconstructions in either bone or soft-tissue algorithms at 1.5-mm thickness were also performed on all studies. Coverage on all CT scans was from the vertex of the skull through the level of the hard palate; expanded coverage was performed to fuse data with endoscopic instrumentation in these potential surgical candidates. No CT scans were excluded due to technical inadequacy or an inability to identify the IOC.

CTs were performed on one of our several scanners including a LightSpeed Pro-16 or HD-750 scanner (GE Healthcare, Milwaukee, Wisconsin) and were reviewed on a PACS on bone window settings (width/level, 4095/600) by a neuroradiology fellow (J.E.L.). The IOC was considered to protrude into the maxillary sinus if the entire wall of the IOC was not in contact with any of the walls of the maxillary sinus on a single image (Fig 1). When this variant was present and a bony septum connected the IOC with a wall of the maxillary sinus, the maximal depicted length of the septum on axial images was measured (Fig 2A). In patients

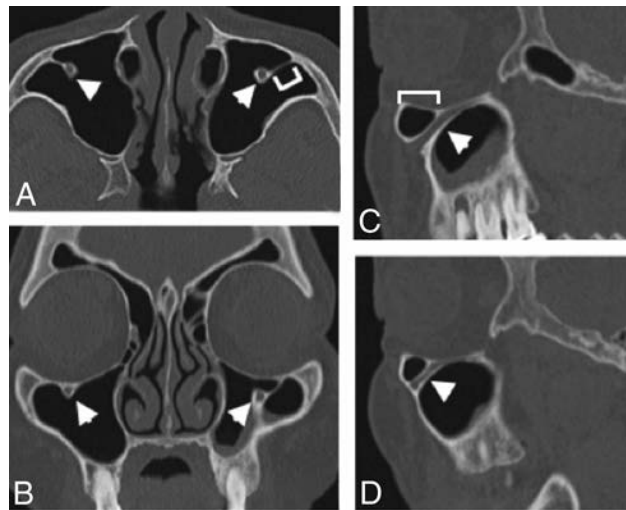


FIG 2. Axial (A), coronal (B), left parasagittal (C), and right parasagittal (D) CT images in a 72-year-old woman show bilateral protrusion of the ION (arrowheads) into the maxillary sinus. The septum attaching the IOC to the anterior wall of the sinus was measured (bracket in A) on the axial image. The distance at which protrusion begins posterior to the inferior orbital rim (bracket in C) was measured on the sagittal image.

The 54 patients composing our group of patients with IOC protrusion broken down into 3 groups^a

Class	Septum Length	No. of Patients	Median Age (yr)	Female/Male	Bilateral (%)
1	1–3 mm	26	62.5	15:11	12 (46%)
2	4–6 mm	18	48.5	9:9	8 (44%)
3	7–11 mm	10	43.5	5:5	8 (80%)

^a The most medial septum was chosen in patients with multiple septa.

with >1 septum, the most medial septum attaching to the anterior wall was measured. The presence of multiple maxillary sinus bony septa attached to the IOC was recorded. We noted from which wall of the maxillary sinus (anterior, posterior, or medial) the septum arose. On sagittal images, we also measured the distance at which the ION began to protrude into the sinus, measuring posteriorly from the fixed anatomic landmark of the inferior orbital rim (Fig 2C). Note was made of whether the protruding IOC was unilateral or bilateral. Patients with IOC protrusion were divided into 3 classes based on maximal septum length: 1–3; 3–6; and ≥ 7 mm.

RESULTS

The study population consisted of 272 females (54.4%) and 228 males (46.6%) with a median age of 47 years (range, 6–95 years). Protrusion of the IOC into the maxillary sinus was identified in 54 patients (10.8%); it was bilateral in 28 (5.6%) and unilateral in 26 (5.2%). All protruding IOCs were anchored to a wall of the maxillary sinus by at least 1 bony septum. The median length of the septum attaching the IOC to the wall of the maxillary sinus was 4 mm (range, 1–11 mm). The median distance posterior to the inferior orbital rim at which the ION began to protrude into the sinus was 11 mm (range, 5–24 mm). Of the 54 patients with a protruding IOC, 26 (48%) had a bony septum measuring 1–3 mm, 18 (33%) had a bony septum measuring 4–6 mm, and 10 (19%) had a bony septum measuring ≥ 7 mm (Table). One patient had a single bony septum attached to the posterior wall of the

sinus; otherwise, all patients with posterior septa had additional bony attachments to the anterior wall. No patient had a bony attachment to the medial wall of the sinus. A second septum attached to a protruding IOC was present in 9 patients, and a second septum was bilateral in 4 patients. A third septum was present in 1 patient unilaterally.

DISCUSSION

In our study of 500 consecutive sinus CTs performed at our outpatient centers, we found that IOC protrusion into the maxillary sinus had a prevalence of 10.8%. At present, only 3 case reports exist describing this anatomic variant.^{2,3} Maillieux et al² described 2 patients: One demonstrated IOC protrusion bilaterally, and 1 had unilateral protrusion. Elnil et al³ described a third patient in whom the finding was bilateral. No formal definition exists for IOC protrusion into the maxillary sinus. Because we aimed to define a clinically relevant variant that may place a patient at greater surgical risk, we considered IOC protrusion into the sinus present if the entire 360° of the wall of the IOC was not in contact with a wall of the maxillary sinus on at least 1 axial CT image. With this definition, 1 of the 2 patients reported by Maillieux et al may not have had IOC protrusion based on the images provided in that publication.

A bony septum attaching the protruding IOC to a wall of the maxillary sinus was invariably present in our study, and we found a wide range in the length of this septum. The length of this septum is important because the further into the sinus the IOC protrudes, the more susceptible it may be to injury during sinus surgery. When multiple septa were present, we measured the most medial septum attaching to the anterior wall because we thought it gave a more representative measurement of how far into the sinus the IOC protruded. Sometimes lateral attachments were very long and did not reflect the degree of protrusion relative to protruding IOCs with single attachment. Additionally, the medial septum was thought to be more clinically relevant because endoscopic sinus surgery more frequently takes place in the medial maxillary sinus.

At the lower end of our septum length range (1–3 mm), IOC protrusion may not be of clinical significance, and reporting the small distance of protrusion can convey that to the clinician. Of our 500 patients, however, 28 (5.6%) had septa measuring >3 mm and 10 (2%) had septa measuring >6 mm. It has not yet been established at what length the septum becomes clinically relevant. We chose to group our patients into 3 classes based on the length of the septum attached to the protruding IOC (Table). Possibly only 1 group (class 3, those with the longest septa), will prove to be clinically relevant, similar to the Keros classification of the length of the lateral lamella of the cribriform plate, in which only type 3 is considered clinically relevant, placing the patient at the highest surgical risk for iatrogenic injury.⁴

We also measured the distance at which the IOC begins to protrude into the maxillary sinus posterior to the inferior orbital rim because the inferior orbital rim is a fixed anatomic landmark and it may be a useful way for a surgeon to conceptualize the degree of protrusion before an intervention. The IOC began to protrude into the sinus more proximally with a longer measurement. As with the length of the bony septum, it is not clear at this

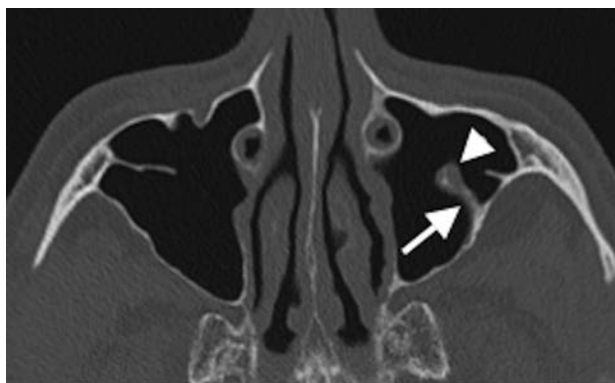


FIG 3. Axial CT image in a 56-year-old man shows left-sided protrusion of the ION into the maxillary sinus (*arrowhead*) attached to a single posterior septum (*arrow*). This was the only patient with a septum attaching a protruding IOC to the posterior wall of the maxillary sinus without an additional septum attaching to the anterior wall.

time at what point this measurement becomes clinically relevant. Nevertheless, stating this measurement may give a surgeon an idea of the severity of the protrusion and in what location to expect the nerve when entering the sinus.

The wall to which a septum attaches is important to note as well; while we did not find a patient with an attachment to the medial wall, such a septum could theoretically be at greater risk during maxillary antrostomy. Only 1 patient had a single septum attaching a protruding IOC to the posterior wall (Fig 3), with the remaining patients all having at least 1 such septum attached to the anterior wall.

The significance of a protruding IOC into the maxillary sinus has not been fully addressed in the literature. For a sinonasal variant to be considered relevant, 1 of the following 4 must be true: The variant impairs normal drainage pathways, hinders endoscopic access to distal areas, serves as a focus for occult disease, or increases the risk of surgical error.¹ Examples of anatomic variants detectable on CT that may increase the risk of iatrogenic injury include sphenothmoid (Onodi) cells, optic nerve or internal carotid artery protrusion into the sphenoid sinus, insertion of the intersphenoid sinus septum onto the carotid canal, and aeration of the anterior clinoid process. A sphenothmoid cell is a posterior ethmoid cell that pneumatizes superiorly above the sphenoid sinus and posteriorly beyond the anterior sphenoid face, with the optic nerve being intimately related to its lateral wall. It places the optic nerve at increased risk of injury during posterior ethmoidectomy; the reported incidence of this variant ranges from 8% to 14%.⁵ Optic nerve or internal carotid artery canal dehiscence and protrusion into the sphenoid sinus increase the risk of injury to those structures as well. Most of the literature supports a prevalence of optic nerve dehiscence of 0.7%–8%.⁶ Reported prevalence for optic nerve protrusion ranges from 8% to 35%, but no consensus definition exists for what constitutes protrusion, despite effort at developing a classification scheme.⁷ The prevalence of internal carotid artery dehiscence and protrusion varies widely from 1.5% to 30% and 5.2% to 67%, respectively, with variation potentially depending on the study population.⁶ Aeration of the anterior clinoid process has a reported prevalence of 12%–19%,^{8,9} and when optic nerve protrusion is

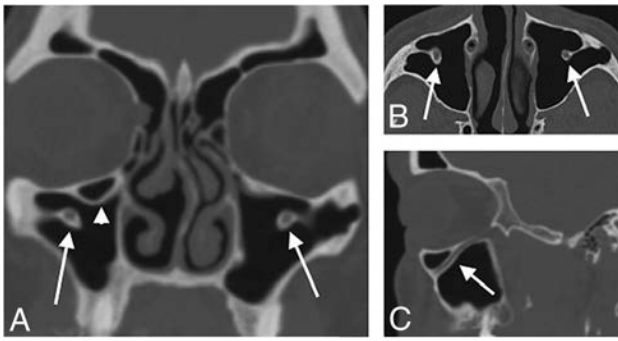


FIG 4. Coronal (A), axial (B), and right parasagittal (C) CT images in a 58-year-old man show bilateral protrusion of the IOC into the maxillary sinus. On the coronal image, an infraorbital ethmoid (Haller) cell is seen on the right (arrowhead) just medial and superior to the protruding IOC (arrow). Bilateral protrusion is seen on the axial image (arrows), and confirmation of protrusion is seen on the sagittal image through the right maxillary sinus. The presence of a protruding IOC near an infraorbital cell is important for the endoscopic surgeon to know preoperatively, in the event that the infraorbital cell is targeted during sinus surgery.

present, there is a 56% chance of ipsilateral anterior clinoid aeration.⁹ Insertion of an intersphenoid sinus septum onto the carotid canal has been reported in 4.7%.¹⁰ The 10.6% prevalence for the presence of IOC protrusion into the maxillary sinus observed in this study is comparable with these other variants that are commonly accepted as reportable on sinus CT.

Authors of prior case reports of ION protrusion believed that this variant leads to an increased risk during endoscopic sinus surgery; thus, those authors advocated mentioning this variant in preoperative sinus CT reports.^{2,3} The long-term consequence of injury to the ION is best described in the setting of trauma, specifically in zygomaticomaxillary complex fractures, in which injury to the ION occurred in 64.4% of cases in 1 series of 478 patients with unilateral fractures.¹¹ Traumatic ION injury results in ipsilateral paresthesias and numbness of the nose and lip, and we would expect similar outcomes in the setting of iatrogenic injury to a protruding ION during sinus surgery. Iatrogenic ION injury with subsequent paresthesia has been described in rhinoplasty, presumably after the ION exited the maxilla through the infraorbital foramen.¹² Iatrogenic injury to the ION has also been reported in the setting of endoscopic sinus surgery, requiring canine fossa puncture for insertion of an endoscope or microdebrider for extensive maxillary sinus disease, as seen in polyposis and extensive fungal debris. One review of 37 such canine punctures found evidence of long-term injury to 6 of 37 (16%) IONs,¹³ including facial pain and paresthesias. While the ION is usually visualized after buccal mucosa incision and lifting of the periosteum, noting ION protrusion on preoperative CT will alert the surgeon to the possibility that the ION could be in an unexpected location.

We suggest that the presence of a protruding IOC should be characterized when there are nearby anatomic variants such as an infraorbital ethmoid (Haller) cell, which are likely to be part of the surgical dissection (Fig 4). As can be seen in Fig 4, this patient has a class 3 protrusion of the IOC and the ION is in close approximation to the infraorbital ethmoid cell. In attempting to adequately resect this cell with curved instrumentation, whether

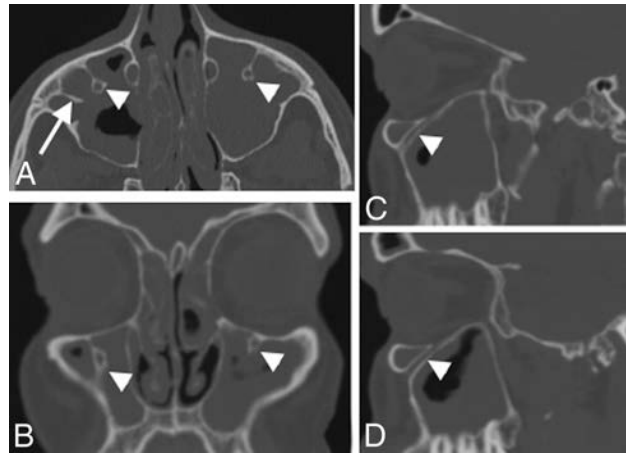


FIG 5. Axial (A), coronal (B), right (C), and left (D) parasagittal CT images of a 42-year-old man show extensive paranasal sinus inflammatory disease and also demonstrate bilateral protrusion of the IOC (arrowheads) into the maxillary sinus. Incidental note is made of an additional bony septum in the right maxillary sinus (arrow in A). For this surgical candidate, the IOC position should be mentioned in the report.

powered or blunt, one could easily inadvertently disrupt the ION in this position. Simply unroofing the bone from the nerve and creating a dehiscence may cause the patient to have neuropathy of the ION. Chandra and Kennedy¹⁴ described a similar variant to the protruding IOC, in which the IOC coursed within the inferior lamella of an infraorbital ethmoid (Haller) cell rather than within the inferior orbital wall. This location would put the ION at a risk similar to that of a protruding IOC because the IOC is not in the expected location of the orbital floor; thus, the ION is not as well-protected. We did not, however, find this variant in our imaging review of 500 patients.

Other disease processes of the maxillary sinus, such as chronic inflammation or neoplasm, may put the protruding ION at risk. Extensive inflammatory disease within the maxillary sinus may cause the bony canal to be weakened or dehiscent (Fig 5). Antrochoanal polyps can originate from the anterior wall of the maxillary sinus, in the location of many of our protruding IONs and their bony septa, and endoscopic dissection along the anterior aspect of the maxillary sinus requires curved powered tissue debriders and angled telescopes for visualization. Resection of an inverted papilloma requires a wide local excision around its lateral maxillary sinus wall origin due to the 6%–10% rate of malignant transformation.¹⁵ An endoscopic approach requires the use of angled burrs to remove the bone intimately associated with the origin of the inverted papilloma. In each of these instances, a protruding ION would be at an increased risk of injury.

Open surgical approaches to the maxillary sinus also place the ION at risk of injury. The Caldwell-Luc procedure is an open approach through the gingivobuccal sulcus into the maxillary sinus, most commonly used to address difficult pathology not amenable to endoscopic techniques, such as resection of neoplasm, recurrent antrochoanal polyp, dentigerous cyst, and fungal disease. Access to the orbit and pterygoid space can also be achieved through this approach.^{16,17} Furthermore, an antral punch to introduce a balloon dilation catheter to approach the maxillary infundibulum is being used with increasing frequency.¹⁸ These

open, anterior approaches to the maxillary sinus place a protruding ION at increased risk of iatrogenic injury because most are connected to a bony septum attached to the anterior maxillary sinus wall. Thus, we believe that in the presurgical setting, identification of the location of the ION should be part of the routine search pattern for interpreting physicians to reduce the risk of ION injury.

The prevalence of 10.8% of IOC protrusion in this cohort suggests that it is a common anatomic variation, though its prevalence in the general population not referred for imaging is unknown. Although we have no reason to suspect it, IOC protrusion into the maxillary sinus may be more common in individuals with known or suspected sinus inflammatory disease. In this instance, our prevalence would not be applicable to the general population, and future studies may help confirm that our number is generalizable to the greater population. Furthermore, we suggest a classification that can be used to easily convey the degree of protrusion to the surgeon. At this time, because the rate of iatrogenic injury to the protruding ION is unknown, the clinical utility of this classification scale is not clear. Still, because there are an estimated 250,000 endoscopic sinus surgical procedures per year performed in the United States and the maxillary sinus is the most commonly instrumented sinus, a rate of 10.8% ION protrusion is of particular clinical relevance.¹⁹

CONCLUSIONS

To date, only 3 case reports in the literature have described protrusion of the IOC into the maxillary sinus rather than within the orbital process of the maxilla (orbital floor). Using the definition that the entire wall of the IOC had to be separate from all walls of the maxillary sinus on a single image, we found a prevalence of 10.8% for this variant during review of 500 CT scans. The distance of protrusion into the sinus should be noted because this information may help avoid iatrogenic injury during surgical intervention.

REFERENCES

1. Earwalker J. **Anatomic variants in sinonasal CT.** *Radiographics* 1993; 13:381–415 CrossRef Medline
2. Mailleux P, Desgain O, Ingabire MI. **Ectopic infraorbital nerve in a maxillary sinus septum: another potentially dangerous variant for sinus surgery.** *JBR-BTR* 2010;93:308–09 Medline
3. Elnil H, Al-Tubaikh JA, El Beltagi AH. **Into the septum I go, a case of**

4. **bilateral ectopic infraorbital nerves: a not-to-miss preoperative sinonasal CT variant.** *Neuroradiol J* 2014;27:146–49 CrossRef Medline
4. Stammberger HR, Kennedy DW; Anatomic Terminology Group. **Paranasal sinuses: anatomic terminology and nomenclature.** *Ann Otol Rhinol Laryngol Suppl* 1995;167:7–16
5. Kantarci M, Karasen RM, Alper F, et al. **Remarkable anatomic variations in paranasal sinus region and their clinical importance.** *Eur J Radiol* 2004;50:296–302 CrossRef Medline
6. Anusha B, Baharudin A, Phillip R, et al. **Anatomical variations of the sphenoid sinus and its adjacent structures: a review of existing literature.** *Surg Radiol Anat* 2014;36:419–27 CrossRef Medline
7. DeLano MC, Fun FY, Zinreich SI. **Relationship of the optic nerve to the posterior paranasal sinuses: a CT anatomic study.** *AJNR Am J Neuroradiol* 1996;17:669–75 Medline
8. Avci E, Bandemci G, Ozturk A. **Microsurgical landmarks for safe removal of the anterior clinoid process.** *Minim Invasive Neurosurg* 2005;48:268–72 CrossRef Medline
9. Chen YL, Lee LA, Lim KE. **Surgical consideration to optic nerve protrusion according to sinus computed tomography.** *Otolaryngol Head Neck Surg* 2006;134:499–505 CrossRef Medline
10. Hamid O, El Fiky L, Hassan O, et al. **Anatomic variations of the sphenoid sinus and their impact on trans-sphenoid pituitary surgery.** *Skull Base* 2008;18:9–15 CrossRef Medline
11. Sakavicious D, Juodzybalys G, Kubilius R, et al. **Investigation of infraorbital nerve injury following zygomaticomaxillary complex fractures.** *J Oral Rehabil* 2008;35:903–16 CrossRef Medline
12. Meyer M, Moss AL, Cullen KW. **Infraorbital nerve palsy after rhinoplasty.** *J Craniomaxillofac Surg* 1990;18:173–74 CrossRef Medline
13. Robinson SR, Baird R, Le T, et al. **The incidence of complications after canine fossa puncture performed during endoscopic sinus surgery.** *Am J Rhinol* 2005;19:203–06 Medline
14. Chandra RK, Kennedy DW. **Surgical implications of an unusual anomaly of the infraorbital nerve.** *Ear Nose Throat J* 2004;83:766–67 Medline
15. von Buchwald C, Bradley PJ. **Risks of malignancy in inverted papilloma of the nose and paranasal sinuses.** *Curr Opin Otolaryngol Head Neck Surg* 2007;15:95–98 CrossRef Medline
16. Barzilai G, Greenberg E, Uri N. **Indications for Caldwell-Luc approach in the endoscopic era.** *Otolaryngol Head Neck Surg* 2005;132: 219–20 CrossRef Medline
17. Matheny KE, Duncavage JA. **Contemporary indications for the Caldwell-Luc procedure.** *Curr Opin Otolaryngol Head Neck Surg* 2003;11:23–26 CrossRef Medline
18. Stankiewicz J, Tami T, Truitt T, et al. **Transantral, endoscopically guided balloon dilatation of the ostiomeatal complex for chronic rhinosinusitis under local anesthesia.** *Am J Rhinol Allergy* 2009;23: 321–27 CrossRef Medline
19. Bhattacharyya N. **Ambulatory sinus and nasal surgery in the United States: demographics and perioperative outcomes.** *Laryngoscope* 2010;120:635–38 CrossRef Medline

Ultrasound of the Hypoglossal Nerve in the Neck: Visualization and Initial Clinical Experience with Patients

 S. Meng,  L.F. Reissig,  C.-H. Tzou,  K. Meng,  W. Grisold, and  W. Weninger

ABSTRACT

BACKGROUND AND PURPOSE: The hypoglossal nerve, providing motor innervation for the tongue, can be affected in many diseases of the neck and skull base, leading to dysarthria, dysphagia, and ultimately atrophy of the tongue. We determined the feasibility of direct visualization of the hypoglossal nerve in the neck with ultrasound, testing this technique on healthy volunteers and evaluating it in clinical practice.

MATERIALS AND METHODS: The study consisted of 4 parts: first, ultrasound-guided perineural ink injections along the course of the hypoglossal nerve at 24 sides of 12 fresh, nonembalmed cadaver necks. Subsequently, the specimens were dissected to confirm the correct identification of the nerve. The second part was examination of healthy volunteers with ultrasound and measurement of cross-sectional areas for generating reference data. The third part was scanning of healthy volunteers by 2 resident physicians with little and intermediate experience in ultrasound. Fourth was examination with ultrasound of patients with motor symptoms of the tongue.

RESULTS: The hypoglossal nerve was correctly identified bilaterally in all cadaveric specimens (24/24) and all volunteers (33/33). The cross-sectional area ranged from 1.9 to 2.1 mm². The resident physicians were able to locate the nerve in 19 of 22 cases, demonstrating that locating the nerve is reproducible and feasible even with intermediate experience in ultrasound. Finally, alterations of the hypoglossal nerve in disease states could be depicted.

CONCLUSIONS: Direct, reliable, and reproducible visualization of the extracranial hypoglossal nerve with ultrasound is feasible.

ABBREVIATION: US = ultrasound

The hypoglossal nerve provides motor innervation for the entire tongue with the exception of the palatoglossal muscle. The nerve leaves the medulla oblongata between the olive and the pyramid in the preolivary groove, passes through the premedullary cistern, and exits the skull through the hypoglossal canal. Inferior to the skull base, the nerve descends lateral to the carotid artery, traveling with the glossopharyngeal, vagal, and accessory nerves; the carotid artery; and the internal jugular vein within the carotid space. At the level of the mandibular angle, the nerve courses anteriorly, caudal to the posterior belly of the digastric muscle, toward the hyoid bone. Here, the nerve enters the submandibular space, passes between the mylohyoid and the hyo-

glossal muscles into the sublingual space, and finally enters the body of the tongue.¹

A lesion of the hypoglossal nerve can cause dysarthria, dysphagia, and tongue paralysis, and unilateral atrophy of the tongue muscles may result. Denervation of the tongue can be secondary to radiation therapy due to formation of fibrotic tissue around the nerve, infection, lymphadenopathy, tumor entrapping or infiltrating the nerve, neurogenic tumors arising within the nerve, or trauma, with iatrogenic trauma resulting from carotid endarterectomy, neck dissection, or tonsillectomy being among the more common causes of hypoglossal nerve dysfunction. There are also reports of carotid and vertebral artery dissections leading to hypoglossal nerve injury.²⁻¹⁸ In a large case series of hypoglossal nerve palsies, the site of the lesion could not be localized in 6%.⁹

In the radiologic diagnostic work-up, a segmental imaging approach is advised.¹⁹⁻²¹ The medullary, cisternal, and skull base segments can be well examined with the existing protocols of MR imaging and CT. In the carotid and submandibular spaces, these imaging modalities are also recommended, but the nerve itself is usually not depicted.^{19,20,22} We are not aware of any study of the

Received April 27, 2015; accepted after revision May 22.

From the Departments of Radiology (S.M.), Ear, Nose, and Throat Diseases (K.M.), and Neurology (W.G.), KFJ Hospital, Vienna, Austria; and Center for Anatomy and Cell Biology (S.M., L.F.R., W.W.) and Division of Plastic and Reconstructive Surgery (C.-H.T.), Department of Surgery, Medical University of Vienna, Vienna, Austria.

Please address correspondence to Stefan Meng, MD, Center for Anatomy and Cell Biology, Währinger Str 13, 1090 Vienna, Austria; e-mail: stefan.meng@meduniwien.ac.at

<http://dx.doi.org/10.3174/ajnr.A4494>

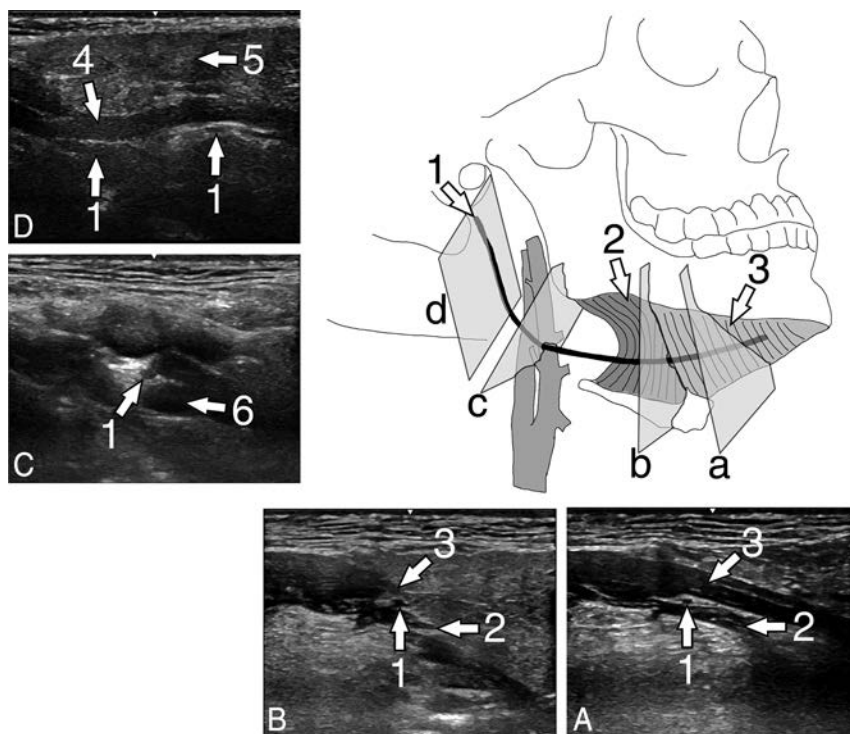


FIG 1. Illustration of the hypoglossal nerve with exemplary US scans of the hypoglossal nerve of a healthy volunteer. *A*, Transversal scan at the floor of the mouth in a coronal body plane. *B*, Transversal scan at the posterior rim of the hyoglossal muscle in a coronal body plane. *C*, Transversal scan in a paracoronal body plane at the crossing of the nerve with the external carotid artery. *D*, Longitudinal scan at the carotid space in a paracoronal body plane. 1 = hypoglossal nerve, 2 = hyoglossal muscle, 3 = mylohyoid muscle, 4 = stylohyoid and styloglossal muscles, 5 = parotid gland, 6 = external carotid artery.

feasibility of the direct visualization of the extracranial hypoglossal nerve, though ultrasound (US) has been increasingly used to visualize peripheral nerves to diagnose and localize pathologies affecting them.^{23,24}

The aim of our study was to test the feasibility of direct visualization of the extracranial hypoglossal nerve with US in fresh cadavers, healthy volunteers, and patients with a suspected lesion of the hypoglossal nerve. A secondary objective was to provide data on the cross-sectional area of the hypoglossal nerve in our volunteer sample as a reference.

MATERIALS AND METHODS

Our study consisted of 4 parts: In the first part, the cadaveric study, we examined the technical feasibility of visualization of the extracranial hypoglossal nerve with US in fresh human specimens. In the second part, the volunteer study, we examined individuals and performed measurement of the nerve cross-sectional areas. In the third part, the reproducibility study, we evaluated whether 2 resident physicians with little and intermediate experience in US were capable of locating the hypoglossal nerve in a second group of healthy volunteers. The last part was a clinical evaluation, in which we performed US scans of patients with a known pathology of the neck and tongue palsy or, in one case, screened for neurofibromatosis. We visualized the pathology and the affected hypoglossal nerve. All 4 parts of this study were performed according to the regulations of the local ethics committees.

Cadaveric Study

For this study, we examined 24 neck sides from fresh, nonembalmed cadavers of 5 women and 7 men, with a mean age of 78.25 ± 11.23 years (median, 79 years; maximum, 97 years; minimum, 58 years). They donated their bodies to the Department of Anatomy. According to the medical records, they had no neuromuscular or neck and throat disease.

All cadaver specimens were scanned with a portable US system (LOGIQ e; GE Healthcare, Milwaukee, Wisconsin) by using a linear wide-band array transducer with an imaging frequency of 4.2–13 MHz (L4–12t-RS, LOGIQ e; GE Healthcare). A radiologist with 8 years of experience in clinical and interventional ultrasound performed US scans and US-guided injections.

The cadaver was placed in a supine position, with the neck in maximum extension. Then the US transducer was positioned at the sublingual space aligned parallel to the coronal body plane (Fig 1*D*). The hypoglossal nerve was localized as an oval hypoechoic structure in the space between the mylohyoid and the hyoglossal muscles. From this starting position, the nerve was tracked medially into the tongue and laterally to the

carotid space with slight adjustments of the scan plane (Fig 1*C*, *-B*). Within the carotid space, the hypoglossal nerve was tracked further as it turns cranially and courses parallel to the carotid vessels to the skull base (Fig 1*B*, *-A*). Along the course from the sublingual space to the end of the carotid space at the skull base, in steps of 1–2 cm, a 23-ga syringe needle aligned parallel to the US scan plane was advanced from the skin to the nerve. The needle tip was positioned at the perineural sheath of the hypoglossal nerve. There, a small amount (approximately 0.01 mL) of India ink diluted 1:10 with saline solution and thickened with Nutrilis (Nutricia, Erlangen, Germany) was injected. The ink was thickened to minimize the spread of the color. During the US scan, the injected ink was digitally documented as small pockets of hypoechoic fluid around the nerve.

Immediately after the injection procedure, the cadaver was dissected by 2 experienced anatomists. Using surgical scalpels and forceps, they exposed the hypoglossal nerve from the entry of the nerve into the tongue to the region inferior to the skull base. The distribution of the ink was photo-documented.

Volunteer Study

Thirty-three healthy volunteers (17 men, 16 women) without any known neuromuscular or neck and throat disease, with an average age of 44.9 ± 11.85 years (median, 43 years; maximum, 70 years; minimum, 27 years) were recruited from the authors' families and the hospital staff. Written informed consent was obtained from all volunteers. Using the same examination protocol and US hard-

ware as in the cadaveric study, the same radiologist scanned the test individuals.

Cross-sectional areas of the hypoglossal nerve were measured at 2 distinct locations at both sides of the volunteers' necks. The first position was at the posterolateral border of the mylohyoid muscle (Fig 1C). Here, the US transducer was rotated to a position transverse to the long axis of the hypoglossal nerve. A still image of the cross-section of the nerve was stored. The second position was at the crossing of the nerve with the external carotid artery (Fig 1B). Here again, the US scanning plane was aligned transverse to the long axis of the nerve, and an US still image was stored. The actual measurement of the cross-sectional area at these 2 positions was performed after the scanning procedure on a personal computer by using the software ImageJ (National Institutes of Health, Bethesda, Maryland) for greater ease of use.

Reproducibility Study

A second group of 11 healthy volunteers (7 women and 4 men) without any known neuromuscular or neck and throat disease, with an average age of 48 ± 10.13 years (median, 4 years; maximum, 61 years; minimum, 27 years) was recruited from the hospital staff. Written informed consent was obtained from all volunteers.

After a short introduction of a few minutes on the scanning technique, in particular by using Fig 1, an ear, nose, and throat diseases resident physician with little experience in US (<1 year) and a radiology resident physician with intermediate experience in US (4 years) scanned the test individuals by using the same examination protocol and US hardware as in the cadaveric study.

The assigned task was to locate the hypoglossal nerve at the 2 locations defined in the volunteer study described above. These were at the posterolateral border of the mylohyoid muscle (Fig 1C) and at the crossing of the nerve with the external carotid artery (Fig 1B).

A total scanning time limit of 5 minutes for each volunteer neck side was set. The primary investigator checked the results presented by the resident physicians.

Clinical Evaluation

Between 2014 and 2015, we examined 6 patients with hypoglossal nerve palsy and a prior operation of the hypoglossal nerve and a patient with neurofibromatosis, who were referred to our department. These patients (4 men and 2 women) with a mean age of 54.3 years were examined with the same US hardware as described in the cadaveric study. US still images were recorded. The US findings were correlated with the known clinical history and course.

RESULTS

Cadaveric Study

In all specimens (24/24), we could identify the hypoglossal nerve within the slit between the mylohyoid and hyoglossal muscles in the sublingual space by using US. From this scanning position, it was also possible to track the nerve medially until it entered the tongue, laterally into the carotid space, and further cranially along the carotid arteries accompanied by the vagal, glossopharyngeal, and accessory nerves (Fig 1). The most cranial part of the course

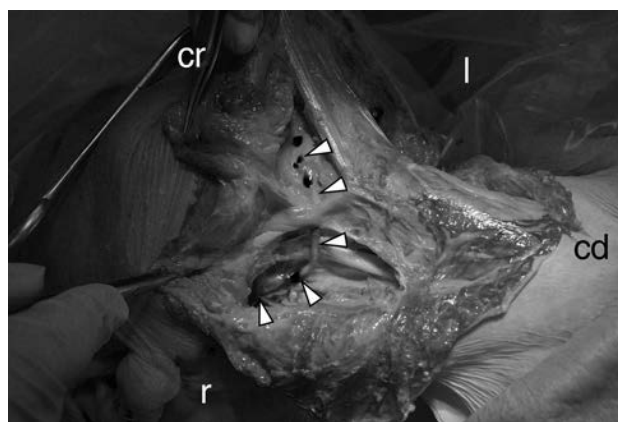


FIG 2. Dissection situs of the right side of a neck. View from ventrolateral. Note the exposed hypoglossal nerve (arrowheads) with dark ink markings along its course. Cr indicates cranial; cd, caudal; r, right; l, left.

within the carotid space, just beneath the skull base, could not be visualized completely because it was deep within the neck covered by the styloid and mastoid processes. In the dissection, the injected ink was found exclusively at the perineural sheath of the hypoglossal nerve (Fig 2). No ink was found inside the nerve or within any other structure of the neck but the perineural sheath of the hypoglossal nerve.

Volunteer Study

Following the protocol developed in the prior cadaveric study, we were able to visualize the hypoglossal nerve in all volunteers (33/33). It was possible to take reference measurements of the cross-sectional areas of the hypoglossal nerve at the posterolateral rim of the mylohyoid muscle and at the crossing with the external carotid artery in all specimens. Our measurement results are presented in Table 1.

We encountered minor difficulties tracking the hypoglossal nerve with US throughout its course due to the lower image quality in persons with beards and due to the limited space for US transducer movements in volunteers with large collar sizes and short necks. However, we were able to locate the nerve and perform the required measurements.

Reproducibility Study

Both resident physicians were able to locate the hypoglossal nerve in 19 of 22 neck sides. The radiology examiner with intermediate experience in US failed to locate the hypoglossal nerve in only 1 neck side. The otorhinolaryngologist with little experience in US failed to find the nerve in 3 neck sides within the set time limit of 5 minutes per neck side. Both examiners extensively used the color Doppler mode. For both examiners, this facilitated distinguishing the nerve from small blood vessels because both structures may have a similar morphology in gray-scale ultrasound.

Clinical Evaluation

Our US examination revealed a variety of pathologies. Our sample included 6 patients with conditions such as iatrogenic scar tissue around a nerve (Fig 3), nerve infiltration by oropharyngeal carcinoma (Fig 4), surgical end-to-side nerve coaptation (Fig 5), partial nerve transfer, and a neurofibroma (Fig 6). Medical his-

Table 1: Summary of US scan measurements of volunteer hypoglossal nerve cross-sectional areas

	Right Side (Mean) (Median, SD, Maximum, Minimum)	Left Side (Mean) (Median, SD, Maximum, Minimum)
Location 1 At the posterolateral rim of the mylohyoid muscle (mm ²)	1.9 (2, 0.6, 3, 0.8)	1.9 (2, 0.6, 4, 1)
Location 2 At the crossing of the hypoglossal nerve with the external carotid artery (mm ²)	2.1 (1.7, 0.6, 3, 0.8)	2.1 (2.1, 0.5, 3.4, 1.1)

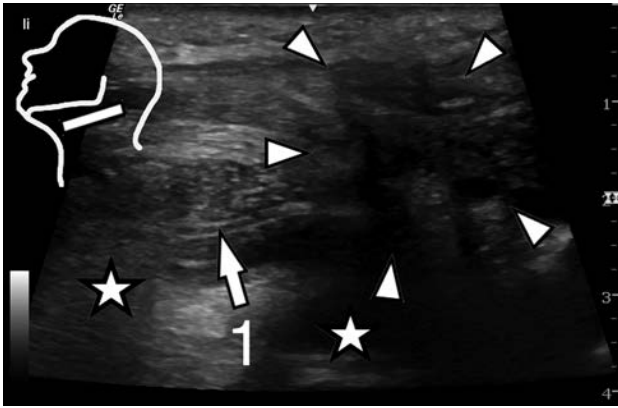


FIG 3. Parasagittal US scan at the floor of the mouth of patient 1 (Table 2). Note the hypoglossal nerve entering the region with extensive scar tissue after a neck dissection operation. Inset: position of the US transducer; 1 = hypoglossal nerve, asterisks = body of the tongue, arrowheads = scar tissue.

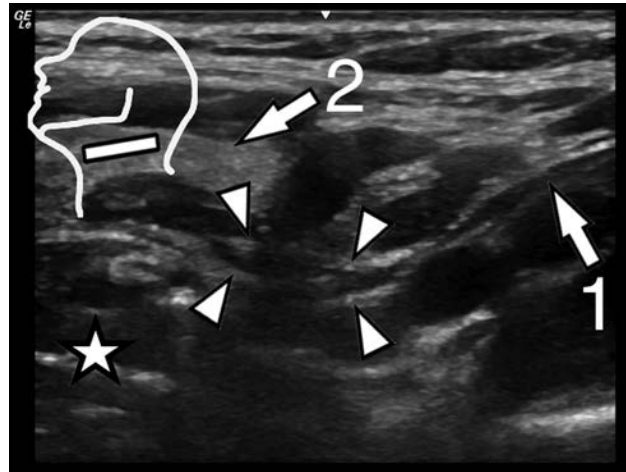


FIG 5. Parasagittal US scan at the carotid space of patient 3 (Table 2). Anterior to the carotid space the hypoglossal nerve is thickened focally after a facial nerve end-to-side coaptation. Inset: position of the US transducer; 1 = hypoglossal nerve, 2 = submandibular gland, asterisk = body of the tongue, arrowheads = coaptation site.

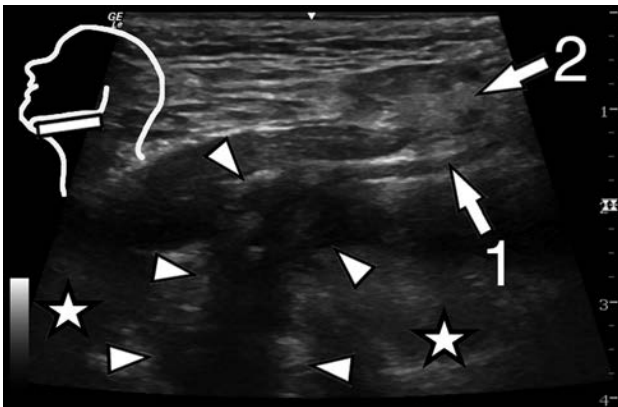


FIG 4. Parasagittal US scan at the floor of the mouth of patient 2 (Table 2). The hypoglossal nerve is directly infiltrated by a squamous cell carcinoma of the tongue base. Inset: position of the US transducer; 1 = hypoglossal nerve, 2 = submandibular gland, asterisks = body of the tongue, arrowheads = squamous cell carcinoma of the tongue base.

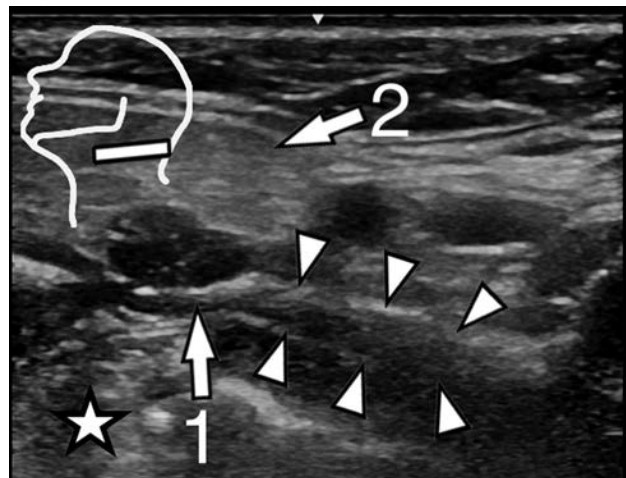


FIG 6. Parasagittal US scan at the carotid space of patient 6 (Table 2). The hypoglossal nerve is thickened markedly in the carotid space due to formation of a fibroma. Inset: position of the US transducer; 1 = hypoglossal nerve, 2 = submandibular gland, asterisk = body of the tongue, arrowheads = fibroma.

tory, US findings, and the assumed diagnosis of our patients are listed in Table 2.

In all patients, the extracranial course of the nerve and the pathologies affecting the nerve could be visualized. Image quality was lower in patients with prior operations and subsequent extensive scar tissue in the scanned region.

DISCUSSION

Paralysis of the tongue can be a symptom of a heterogeneous spectrum of pathologies, and imaging of the potentially affected regions in the central and peripheral nervous system is an essential element of the diagnostic work-up. In case of a suspected lesion of

the hypoglossal nerve, radiologic standards have been established. The medullary, cisternal, and skull base segments of the hypoglossal nerve course are examined with CT and MR imaging according to the strengths of these imaging modalities in imaging soft-tissue or bony structures. For the neck segment of the hypoglossal nerve, CT and MR imaging have also been advocated as the primary imaging modalities.¹⁹⁻²¹ Here, the hypoglossal nerve is assessed indirectly by delineating the muscles innervated by the

Table 2: Summary of patient histories and US findings

No.	Age (yr)	Sex	History	Clinical Details on Referral	US findings
1	50	M	Squamous cell carcinoma of the tonsil, neck dissection	Hypoglossal nerve palsy	Scar tissue around the nerve (Fig 3)
2	72	M	Squamous cell carcinoma of the tongue base	Hypoglossal nerve palsy	Tumor infiltration of the nerve (Fig 4)
3	33	F	Facial nerve end-to-side coaptation to the hypoglossal nerve after tongue palsy after cerebellopontine angle tumor resection	Tongue paresis	Nerve coaptation site with focal hypoglossal nerve thickening (Fig 5)
4	68	F	Partial hypoglossal nerve transfer for facial nerve reconstruction after malignant parotid gland tumor resection	Tongue weakness	Nerve transfer site with focal thickening and fibrosis
5	48	M	Squamous cell carcinoma of the tonsil, neck dissection, radiotherapy, chemotherapy	Hypoglossal palsy	Scar tissue entrapment of the hypoglossal nerve
6	55	M	Neurofibromatosis	Screening	Neurofibroma (Fig 6)

nerve and by detecting potential pathologies that are in the vicinity of the expected course of the nerve. Muscle atrophy or muscle denervation changes can indirectly indicate pathology of the hypoglossal nerve, but they are not direct proof. Furthermore, small lesions and pathologic processes originating from the hypoglossal nerve itself may remain undetected.

So far, US has been described as insufficient to give useful information concerning the hypoglossal nerve.¹⁹ Hence, a reliable imaging protocol for the direct visualization of the nerve has not yet been established, to our knowledge. In the cadaveric study, we developed and verified an US imaging protocol for the reliable visualization of the extracranial hypoglossal nerve, with the exception of the segment directly beneath the hypoglossal canal. We applied this protocol in healthy volunteers and patients.

Although there are many nerves and nerve-like structures in the neck, our ink injections and subsequent dissections show that the nerve can be correctly identified and traced with US. The minor US scanning difficulties we encountered during the examination of healthy volunteers and patients are generally known problems in head and neck US. A large patient collar size and a short neck impede transducer movements and could require the use of lower US transducer frequencies and thus lead to a lower image resolution. Typically, a generally lower US image quality results from beards, prior operations, and prior radiation therapy.

It was possible to visualize the extracranial portion of the hypoglossal nerve in all cadaveric specimens, volunteers, and patients. The only exception was an approximately 1-cm-long segment of the hypoglossal nerve just beneath the external opening of the hypoglossal canal. Here, the US scan was blocked by the styloid and mastoid processes, and we could not develop an alternative sonographic window. From our point of view, this limitation can only be overcome with other image modalities such as CT and/or MR imaging.

The US examinations in the first, second, and fourth part of this study were performed by the highly experienced primary investigator. Physicians with little and intermediate experience in US could locate the hypoglossal nerve in >86% and >95% of cases, respectively, however, after a brief training of a few minutes. Thus, we are confident that a focused examination of the hypoglossal nerve with US is feasible in clinical routine. As noted in the observation of the resident physicians' scanning, we strongly rec-

ommend the use of color Doppler because it seems to facilitate the perception of the hypoglossal nerve position.

A notable shortcoming of our study design is the retrospective character of the clinical part in combination with the low number of cases with hypoglossal nerve pathologies. Nevertheless, primary hypoglossal nerve pathologies are rare, and the focus of our study was to demonstrate the feasibility of visualizing the hypoglossal nerve in different settings. A prospective clinical trial evaluating US versus CT and MR imaging is the next logical step, and we are planning such a study.

In the examination of our patients, all alterations of the nerve itself were focal thickenings and easy to perceive; thus, no comparisons with reference nerve diameters were necessary. Given that some pathologies, for example polyneuropathies, might lead to nerve thickening or thinning over a long segment,²⁵⁻²⁷ in such cases, reference data might be helpful in detecting the pathology. The marginally smaller cross-sectional area of the hypoglossal nerve at the distal measurement point (1.9 versus 2.1 mm²) can be explained by the branching of the ansa cervicalis.

A radiologic imaging protocol can only be successfully introduced in daily hospital routine if the necessary device is part of the standard equipment. In our study, we used US hardware that is relatively inexpensive and widely available. Furthermore, identifying the hypoglossal nerve between the mylohyoid and hyoglossal muscles is simple. Following our protocol, US can be easily used to assess the extracranial hypoglossal nerve and can complement existing imaging algorithms.

CONCLUSIONS

We demonstrated that with US, it is possible for even relatively inexperienced examiners to reliably and directly visualize most of the extracranial course of the hypoglossal nerve. We also present reference measurements of the cross-sectional area of the hypoglossal nerve. In a small group of patients, we depicted structural alterations of the nerve and of its immediate surroundings resulting from pathologies and prior operations.

ACKNOWLEDGMENTS

We thank Muna Nourafza, MD, for her valuable comments during the preparation of the article.

Disclosures: Wolfgang Weninger—UNRELATED: Grants/Grants Pending: Wellcome Trust, UK (Deciphering the Mechanisms of Developmental Disorders); Payment for Lectures (including service on Speakers Bureaus): IMC-Krems, FH-St Pölten, FH-CampusWien.

REFERENCES

1. Standing S. *Gray's Anatomy: The Anatomical Basis of Clinical Practice*. Edinburgh: Churchill Livingstone; 2008
2. Andrioli G, Rigobello L, Mingrino S, et al. **Tapia's syndrome caused by a neurofibroma of the hypoglossal and vagus nerves: case report.** *J Neurosurg* 1980;52:730–32 CrossRef Medline
3. Cheng VS, Schultz MD. **Unilateral hypoglossal nerve atrophy as a late complication of radiation therapy of head and neck carcinoma: a report of four cases and a review of the literature on peripheral and cranial nerve damages after radiation therapy.** *Cancer* 1975;35:1537–44 CrossRef Medline
4. Cunningham EJ, Bond R, Mayberg MR, et al. **Risk of persistent cranial nerve injury after carotid endarterectomy.** *J Neurosurg* 2004;101:445–48 CrossRef Medline
5. Ferguson GG, Eliasziw M, Barr HW, et al. **The North American Symptomatic Carotid Endarterectomy Trial: surgical results in 1415 patients.** *Stroke* 1999;30:1751–58 CrossRef Medline
6. Friedman L, Eisenberg AA. **Neurofibroma of the hypoglossal nerve.** *Ann Surg* 1935;101:834–38 CrossRef Medline
7. Junquera L, Gallego L. **Images in clinical medicine: denervation atrophy of the tongue after hypoglossal-nerve injury.** *N Engl J Med* 2012;367:156 CrossRef Medline
8. Karvounaris DC, Symeonidis N, Triantafyllou A, et al. **Ectopic parathyroid adenoma located inside the hypoglossal nerve.** *Head Neck* 2010;32:1273–76 CrossRef Medline
9. Keane JR. **Twelfth-nerve palsy: analysis of 100 cases.** *Arch Neurol* 1996;53:561–66 CrossRef Medline
10. Kum YS, Kim JK, Cho CH, et al. **Intraneural reticular perineurioma of the hypoglossal nerve.** *Head Neck* 2009;31:833–37 CrossRef Medline
11. Lin YS, Jen YM, Lin JC. **Radiation-related cranial nerve palsy in patients with nasopharyngeal carcinoma.** *Cancer* 2002;95:404–09 CrossRef Medline
12. Mahadevappa K, Chacko T, Nair AK. **Isolated unilateral hypoglossal nerve palsy due to vertebral artery dissection.** *Clin Med Res* 2012;10:127–30 CrossRef Medline
13. Mohanty SK, Barrios M, Fishbone H, et al. **Irreversible injury of cranial nerves 9 through 12 (Collet-Sicard syndrome): case report.** *J Neurosurg* 1973;38:86–88 CrossRef Medline
14. Mokri B, Silbert PL, Schievink WI, et al. **Cranial nerve palsy in spontaneous dissection of the extracranial internal carotid artery.** *Neurology* 1996;46:356–59 CrossRef Medline
15. Stricker T, Steinlin M, Willi UV, et al. **Hypoglossal nerve palsy associated with deep cervical lymphadenopathy.** *Neurology* 1998;50:1926–27 CrossRef Medline
16. Tong Y. **Role of duplex ultrasound in the diagnosis and assessment of carotid body tumour: a literature review.** *Intractable Rare Dis Res* 2012;1:129–33 CrossRef Medline
17. Williamson J, Leopold G, Prabhu V, et al. **Successful treatment of a rare metastatic malignant carotid body tumour in a young adult, with conservative surgery and local radiotherapy.** *J Laryngol Otol* 2012;126:428–31 CrossRef Medline
18. Sharp CM, Borg HK, Kishore A, et al. **Hypoglossal nerve paralysis following tonsillectomy.** *J Laryngol Otol* 2002;116:389–91 CrossRef Medline
19. Alves P. **Imaging the hypoglossal nerve.** *Eur J Radiol* 2010;74:368–77 CrossRef Medline
20. La'porte SJ, Juttla JK, Lingam RK. **Imaging the floor of the mouth and the sublingual space.** *Radiographics* 2011;31:1215–30 CrossRef Medline
21. Thompson EO, Smoker WR. **Hypoglossal nerve palsy: a segmental approach.** *Radiographics* 1994;14:939–58 CrossRef Medline
22. Sharma B, Dubey P, Kumar S, et al. **Isolated unilateral hypoglossal nerve palsy: a study of 12 cases.** *J Neurol Neurosci* 2010;2:5
23. Lieba-Samal D, Pivec C, Platzgummer H, et al. **High-resolution ultrasound for diagnostic assessment of the great auricular nerve: normal and first pathologic findings.** *Ultraschall Med* 2014 May 13. [Epub ahead of print] CrossRef
24. Park JK, Jeong SY, Lee JH, et al. **Variations in the course of the cervical vagus nerve on thyroid ultrasonography.** *AJNR Am J Neuroradiol* 2011;32:1178–81 CrossRef Medline
25. Weiss MD, Oakley JC, Meekins GD. **Hypoglossal neuropathy in Lewis-Sumner syndrome masquerading as motor neuron disease.** *Neurology* 2006;67:175–76 CrossRef Medline
26. Winter WC, Juel VC. **Hypoglossal neuropathy in hereditary neuropathy with liability to pressure palsy.** *Neurology* 2003;61:1154–55 CrossRef Medline
27. Zaidman CM, Al-Lozi M, Pestronk A. **Peripheral nerve size in normals and patients with polyneuropathy: an ultrasound study.** *Muscle Nerve* 2009;40:960–66 CrossRef Medline

Elucidating Metabolic Maturation in the Healthy Fetal Brain Using ^1H -MR Spectroscopy

I.E. Evangelou, A.J. du Plessis, G. Vezina, R. Noeske, and C. Limperopoulos



ABSTRACT

BACKGROUND AND PURPOSE: ^1H -MRS provides a noninvasive way to study fetal brain maturation at the biochemical level. The purpose of this study was to characterize in vivo metabolic maturation in the healthy fetal brain during the second and third trimester using ^1H -MRS.

MATERIALS AND METHODS: Healthy pregnant volunteers between 18 and 40 weeks gestational age underwent single voxel ^1H -MRS. MR spectra were retrospectively corrected for motion-induced artifacts and quantified using LCModel. Linear regression was used to examine the relationship between absolute metabolite concentrations and ratios of total NAA, Cr, and Cho to total Cho and total Cr and gestational age.

RESULTS: Two hundred four spectra were acquired from 129 pregnant women at mean gestational age of 30.63 ± 6 weeks. Total Cho remained relatively stable across the gestational age ($r^2 = 0.04, P = .01$). Both total Cr ($r^2 = 0.60, P < .0001$) as well as total NAA and total NAA to total Cho ($r^2 = 0.58, P < .0001$) increased significantly between 18 and 40 weeks, whereas total NAA to total Cr exhibited a slower increase ($r^2 = 0.12, P < .0001$). Total Cr to total Cho also increased ($r^2 = 0.53, P < .0001$), whereas total Cho to total Cr decreased ($r^2 = 0.52, P < .0001$) with gestational age. The cohort was also stratified into those that underwent MRS in the second and third trimesters and analyzed separately.

CONCLUSIONS: We characterized metabolic changes in the normal fetal brain during the second and third trimesters of pregnancy and derived normative metabolic indices. These reference values can be used to study metabolic maturation of the fetal brain in vivo.

ABBREVIATIONS: GA = gestational age; tCho = total Cho (glycerol 3-phosphocholine + phosphocholine); tCr = total Cr (phosphocreatine + Cr); tNAA = total NAA (NAA + *N*-acetyl aspartylglutamate)

^1H -MR spectroscopy provides a noninvasive method to study brain maturation at the biochemical level. Early metabolic changes observed by ^1H -MRS may precede morphologic brain changes¹ and overt clinical signs of disease,² which makes it an invaluable tool for providing insights into the mechanisms of

brain insult and antecedents of injury. The spectra obtained by ^1H -MRS depict several metabolites dominated by a large water resonance. When this water signal is suppressed, the metabolites emerge at different resonant frequencies and are expressed as parts per million. Each metabolite reflects specific cellular and biochemical processes. *N*-acetylaspartate is considered a neuronal-axonal marker with a neuronal bioenergetic role³⁻⁵ found in the brain and spinal cord, creatine is involved in energy metabolism through the Cr kinase reaction generating phosphocreatine, and, in turn, adenosine triphosphate,⁶ and choline containing compounds of glycerol 3-phosphocholine and phosphocholine which is present at high levels in glial cells⁷ as intermediaries in the synthesis of acetylcholine.⁸ Lactate, a by-product of anaerobic metabolism, is not normally present but may be detectable by ^1H -MRS in certain pathologies.⁹⁻¹¹

The application of ^1H -MRS in studying the fetal brain in vivo has been explored since the 1990s,¹² and a number of reviews have been published.¹³⁻¹⁵ However, there is a paucity of standardized ^1H -MRS measurements and reference values for fetal brain metabolites from normal healthy pregnancies. Small sample sizes

Received April 27, 2015; accepted after revision June 21.

From the Divisions of Diagnostic Imaging and Radiology (I.E.E., G.V., C.L.) and Fetal and Transitional Medicine (A.J.D.P., C.L.), Children's National Medical Center, Washington, DC; Departments of Pediatrics (I.E.E., A.J.D.P., G.V., C.L.) and Radiology (I.E.E., G.V.), The George Washington University School of Medicine and Health Sciences, Washington, DC; and Applied Science Laboratory, GE Healthcare, Berlin, Germany (R.N.).

This study was funded by the Canadian Institutes of Health Research: MOP-81116 (C. Limperopoulos).

Paper previously presented in part at: Annual Meeting of the Pediatric Academic Societies, May 4-7, 2013; Washington, DC.

Please address correspondence to Catherine Limperopoulos, PhD, Diagnostic Imaging and Radiology/Fetal and Transitional Medicine, Children's National Medical Center, 111 Michigan Ave NW, Washington, DC 20010; e-mail: climpero@childrensnational.org

Indicates open access to non-subscribers at www.ajnr.org

<http://dx.doi.org/10.3174/ajnr.A4512>

have also limited the wide application and diagnostic value of this approach in the fetus. The purpose of this article was to characterize prospectively the trajectory of in vivo metabolic brain maturation of the healthy fetus in the second and third trimesters, and to provide reliable reference values for the interpretation of single voxel ¹H-MRS of the fetal brain.

MATERIALS AND METHODS

Subjects

This Health Insurance Portability and Accountability Act compliant prospective study was approved by the institutional review board of Children's National Medical Center, and written informed consent was obtained by all the study participants. Healthy volunteers between 18 and 40 weeks of pregnancy were consecutively recruited from 2011 through 2014 in low-risk obstetric clinics. In 2012, the protocol was amended to include serial studies of the same subject. Inclusion criteria were normal fetal sonography studies and the absence of any maternal medical conditions that might interfere with normal fetal growth and development (eg, chronic hypertension, preeclampsia, intrauterine growth restriction, placental abnormalities, gestational diabetes, and a known history of congenital heart disease).^{16,17} Those with multiple gestations, evidence of congenital infection, documented prenatal chromosomal abnormalities, fetal sonography findings of dysmorphic features, dysgenetic brain lesions, or anomalies of other organ systems, and any maternal contraindication to MR (eg, mechanical heart valve, pacemaker, or any other ferromagnetic implants) were also excluded. No maternal or fetal sedation was used during the MR studies. Retrospectively, those with incidental findings or abnormalities documented in the MR imaging report by the pediatric neuroradiologist (G.V.) were also excluded from the study cohort.

MR Imaging and Spectroscopy Acquisition

MR imaging and single voxel ¹H-MRS data for all the subjects were acquired on a 1.5T MR scanner (Discovery MR450; GE Healthcare, Milwaukee, Wisconsin) using an 8-channel surface coil (GE Healthcare) as part of a comprehensive MR imaging protocol. Anatomic single-shot FSE T2WI with TR = 1100 milliseconds and TE = 160 milliseconds, field of view 320 × 320 mm², 2-mm section thickness, and 40–60 sections for total brain coverage was acquired in all 3 orthogonal planes. The MR images were reviewed by a neuroradiologist to exclude structural brain abnormality. A single-voxel point-resolved spectroscopy sequence with chemical shift selective suppression was used with TR = 1500 milliseconds; TE = 144 milliseconds; 128–192 excitations that contained 2048 complex points that covered a spectral bandwidth of 2500 Hz, with the phase of all 3 radiofrequency excitation pulses alternating from 0° to 180°; 16 nonwater-suppressed excitations as reference data; and 6 outer volume suppression pulses around an isotropic voxel, either 25 × 25 × 25 or 30 × 30 × 30 mm³, depending on gestational age (GA) and brain size, with an acquisition time of 3:48 or 5:24 minutes, respectively. The voxel was placed in the middle of the brain posterior to the basal ganglia, encompassing the thalamus and hypothalamus, while avoiding the scalp and extracranial tissues and preventing contamination of the spectra by unwanted lipid signals (Fig 1), using

the anatomic T2WI for guidance. Automatic prescanning and shimming procedures were performed, followed by fine adjustment of the center frequency, transmitter and receiver gains, and linear shims. Before the spectra acquisition, the water suppression level was verified to be >95%, and the line width at full width at half maximum to be ≤4 Hz, which indicated good quality shimming and high spectral resolution for water suppression to accurately resolve the adjacent Cho and Cr peaks at 3.19 ppm and 3.02 ppm, respectively. Mean transmit and receive gains (R1, R2) were 166 ± 6, 13 ± 1 and 29 ± 2, respectively, for all acquired spectra. During the course of the study, the stability and drift of the MR scanner center frequency, transmit gains, and receive gains (R1, R2) were monitored weekly with quality assurance scans of the "Braino" MR spectroscopy sphere phantom (GE Healthcare) using the single-voxel point-resolved spectroscopy sequence.

MR Spectroscopy Processing

Raw spectra as P-files were transferred to an off-line Linux workstation (The Linux Foundation, San Francisco, California) for correction of motion-induced artifacts due to fetal movement and maternal breathing during acquisition using a retrospective methodology described previously.¹⁸ Resulting spectra were then fitted to basis spectra using the LCMoDel software (<http://www.lcmoDel.com/>)¹⁹ (to calculate metabolite concentrations in the chemical shift range of 4.0–1.0 ppm using the unsuppressed water signal as the internal reference).²⁰ The MR visible water concentration²¹ in the voxel was calculated to be 50,013 mmol/L using the mean water content in the ex vivo cerebrum as 901 ± 11.48 g/M, in the range of 18–40 weeks of gestation,²² and the molar mass of water, which is approximately 18.02 g/M.²³ This was set in the LCMoDel parameter "WCONC" rather than 35,880 mmol/L used as the default value for white matter, which underestimates the absolute metabolite concentrations.^{24,25} Based on the LCMoDel output, MR spectra with line width at full width at half maximum of >0.1 ppm (approximately 6 Hz) and/or SNR of <3 were excluded. Metabolite concentrations with a confidence level of the Cramer-Rao lower bounds²⁶ of >20% were also excluded from the subsequent analysis. LCMoDel analysis was restricted to fit to the simulated basis spectra of glycerol 3-phosphocholine, phosphocholine, Cr, phosphocreatine, NAA, *N*-acetyl aspartylglutamate, and lactate. Due to the low signal and spectral resolution of TE = 144 milliseconds at 1.5T, the sums of the absolute concentrations total NAA (tNAA) = NAA + *N*-acetyl aspartylglutamate, total Cho (tCho) = glycerol 3-phosphocholine + phosphocholine, total Cr (tCr) = phosphocreatine + Cr, and lactate were used in the analysis because they represent more accurate estimates, as shown from the lower confidence level %SD of the Cramer-Rao lower bounds obtained. The -CrCH₂ correction term simulated as a negative CrCH₂ singlet approximately 3.94 ppm was used to correct for attenuation of the CrCH₂ singlet due to water suppression and differential relaxation effects at the long TE.²⁷ T1 and T2 relaxation corrections were not applied due to unavailable literature data for the fetal brain between 18 and 40 weeks of pregnancy and because T2 errors in each metabolite have little effect on the metabolite concentrations (approximately 2%).²¹ A summary of the quality statistics of the MR spectra acquired is shown in Table 1.

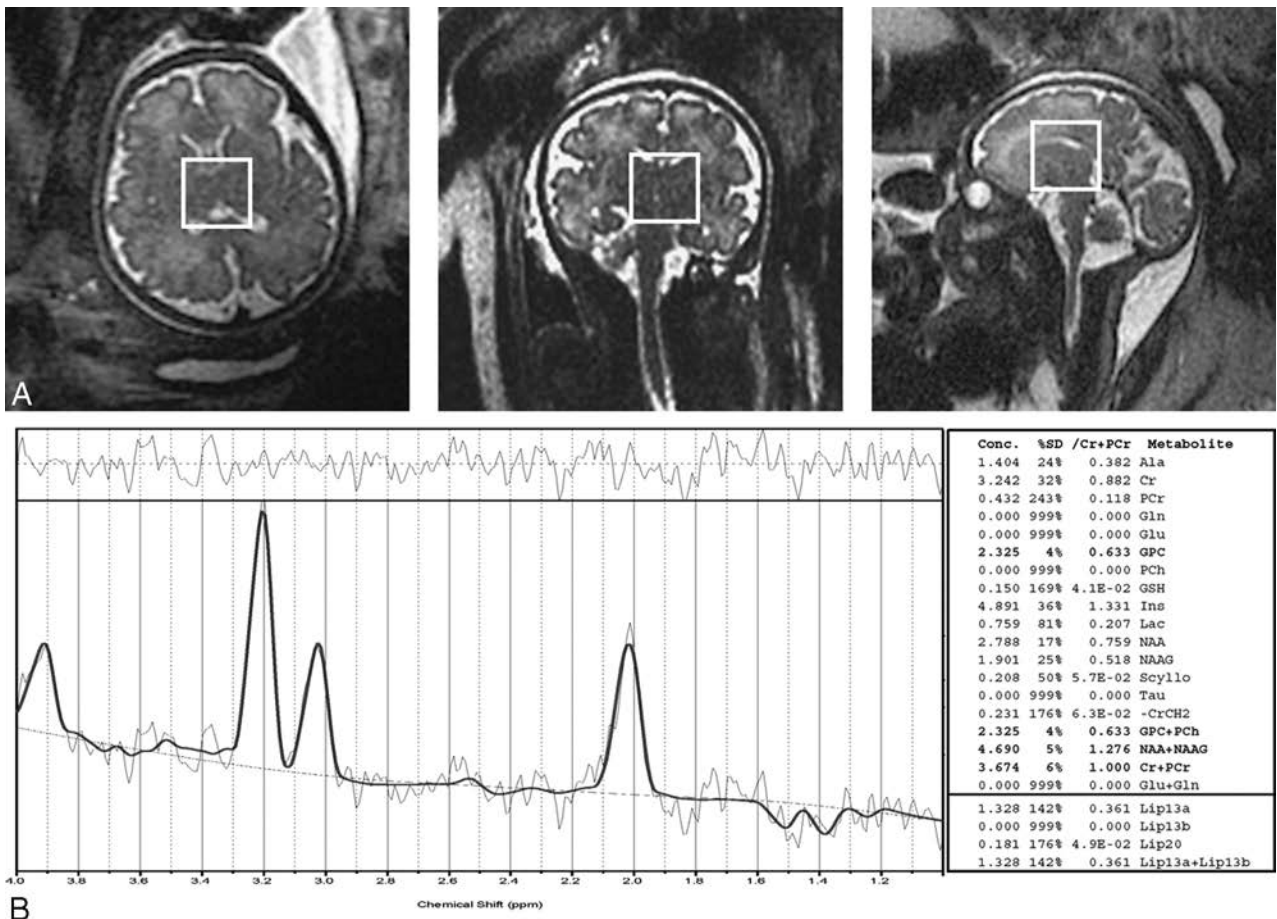


FIG 1. A, T2-weighted single-shot fast spin-echo MR imaging (TR/TE = 1100/160 milliseconds, 2-mm thickness) in all 3 orthogonal planes (axial, coronal, and sagittal), showing voxel placement (white rectangle) in a fetus of 35.87 weeks gestation. B, ¹H-MRS acquired using a point-resolved spectroscopy sequence (TR/TE = 1500/144 milliseconds, voxel 30 × 30 × 30 mm) quantified using LCModel.

Table 1: Quality statistics of MR spectra acquired: FWHM, SNR, and %SD Cramer-Rao lower bounds in the whole study cohort^a

Spectra	FWHM, ppm	SNR	%SD tNAA	%SD tCho	%SD tCr
n = 153	0.07 ± 0.02	7.25 ± 2.59	9.98 ± 5.51	4.80 ± 1.56	10.28 ± 4.70

Note:—FWHM indicates line width at full width at half maximum.

^a Values are rounded to 2 decimal places.

Statistical Analysis

Descriptive statistics, including means, standard deviations, and frequencies were used to characterize the study cohort. Linear regression analysis (least squares method) was used to fit a straight line with 95% confidence intervals (CIs) to the absolute metabolite concentrations and ratios as a function of GA.²⁸⁻³⁰ The goodness of fit was assessed using the coefficient of determination (r^2) and the standard deviation of the residuals. The slope of the linear regression was tested at $P < .05$ as indicative of significance. The intraclass correlation coefficient was used to assess scan-rescan measurement reliability within an ANOVA framework. The intraclass correlation coefficient represents concordance and evaluates the level of agreement between raters in measurements, in which 1 is perfect agreement and 0 is no agreement at all.³¹ The coefficient of variation, defined as the standard deviation of the mean difference between 2 measurements divided by the mean of all measurements was also used as a measure of dispersion.³² The coefficient of variation and intraclass correlation coefficient are most commonly used in ¹H-MRS studies.³³⁻³⁵ The analysis was

performed using GraphPad Prism 6.05 software (GraphPad Software, San Diego, California). Results are presented as mean (SD) unless otherwise noted.

RESULTS

A total of 204 MR spectra were acquired from 129 healthy pregnant women during their second and third trimester of pregnancy (mean GA, 30.63 ± 6 weeks). Seventy-one spectra (34.8%) were acquired during the second trimester and 133 (65.2%) during the third trimester. Five subjects' MR spectra (2.45%) were excluded from the analysis due to excessive maternal and fetal movement, lipid contamination, and/or low SNR that precluded any quantification of the metabolite concentrations and metabolite ratios. Three were in the second trimester (mean GA, 25.43 ± 1 week), and 2 were in the third trimester (mean GA, 34.21 ± 1 week). An additional 14 MR spectra of the 204 (6.86%) were also excluded from the analysis at the quantification stage because their metabolite concentrations had a >20% confidence level of the Cramer-Rao lower bounds.²⁶ Twenty-five MR spectra (12.25%) were acquired twice during the examination when time permitted. Of those patients who had 2 MR spectra, the one MR spectrum with higher quality (ie, higher SNR, narrower line width at full width half maximum, and lower %SD of the Cramer-Rao lower bounds) was used in the analysis. An additional 7 randomly se-

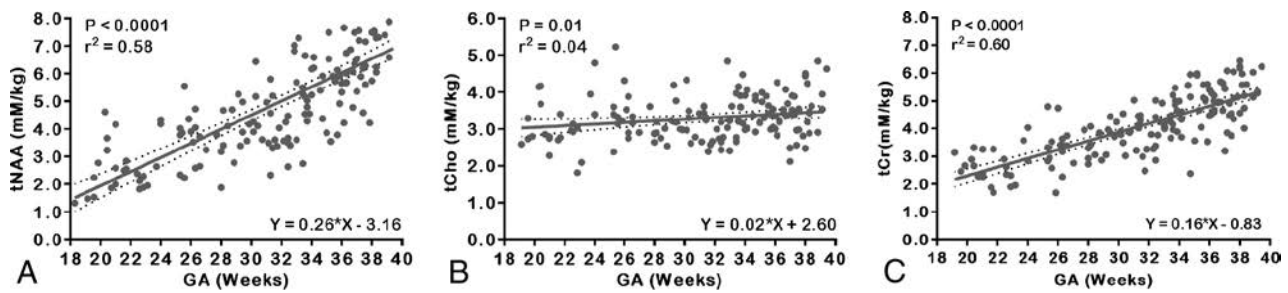


FIG 2. Scatterplots of absolute metabolite concentrations relative to the water signal and linear regression straight line fits with mean (solid line) and 95% CIs (dotted lines). A, tNAA. B, tCho. C, tCr.

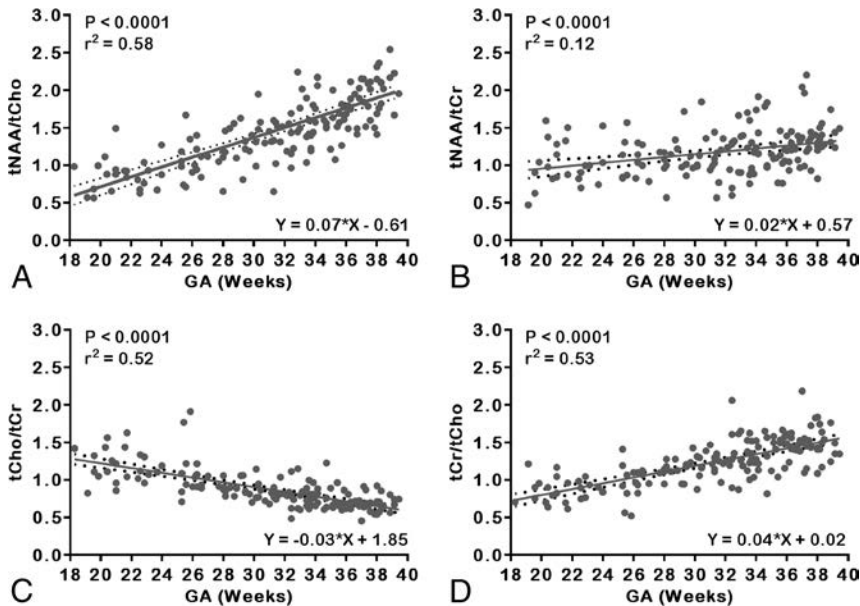


FIG 3. Scatterplots of metabolite concentration ratios and linear regression straight line fits with mean (solid line) and 95% CIs (dotted lines). A, tNAA:tCho. B, tNAA:tCr. C, tCho:tCr. D, tCr:tCho.

lected pregnant women had 7 MR spectra (3.43%) acquired (2 in the second trimester and 5 in the third trimester; mean GA, 31.27 ± 4 weeks) that were used for intrasession reproducibility. The remaining 153 MR spectra (75%) (mean GA, 31.3 ± 6 weeks) were included in the final analysis. These included 34 subjects who underwent 2 serial scans, one in the second trimester (mean GA, 25.6 ± 5 weeks) and one in the third trimester (mean GA, 35.0 ± 3 weeks). All the participants' MR images were reviewed by an experienced pediatric neuroradiologist (G.V.) and were found to have structurally normal brains. Postnatal MR studies were performed on 71% of neonates who returned for follow-up MR studies. All the neonates had a structurally normal brain after birth.

Metabolic Maturation during Second and Third Trimesters

Metabolic profiles in the fetal brain changed significantly with advancing GA. Figure 2 depicts the main absolute metabolite concentrations detected in the fetal brain of the entire cohort across GA, with the best-fit straight line and corresponding 95% CIs. Absolute concentrations of each metabolite using the unsuppressed tissue water as an internal reference and corrected for cerebral water content were also calculated in mM/kg. The tNAA exhibited a significant increase ($r^2 = 0.58$, $P < .0001$) with ad-

vancing GA from 18 to 40 weeks. The tCho increased linearly with GA and was relatively stable across gestation, ($r^2 = 0.04$, $P = .01$) compared with tCr, which increased with GA ($r^2 = 0.60$, $P < .0001$), which made tCho ideal as a denominator for the metabolite ratios.

The tNAA to tCho [tNAA:tCho] also exhibited a significant increase with increasing GA ($r^2 = 0.58$, $P < .0001$), whereas tNAA to tCr [tNAA:tCr] exhibited a slower yet significant increase ($r^2 = 0.12$, $P < .0001$) from 18 to 40 weeks. Similarly, tCho:tCr and tCr:tCho showed a significant exponential increase with GA ($r^2 = 0.52$, $P < .0001$; $r^2 = 0.53$, $P < .0001$, respectively). Figure 3 depicts the main metabolite concentration ratios detected in the fetal brain of the entire cohort across GAs, with the best-fit line and corresponding 95% CIs.

Analysis was also performed by stratifying the cohort into 2 groups, that is, those patients who underwent MR studies in the second trimester (43/153 [28%]; mean GA, 23.62 ± 2.82 weeks) versus the third trimester of pregnancy (110/153 [72%]; mean GA, 34.31 ± 3 weeks) to compare metabolic profiles in each trimester alone. In the second trimester group, tCho and tNAA:tCr did not exhibit a significant increase with GA. Conversely tNAA, tNAA:tCho, tCr:tCho, and tCr exhibited a small but significant increase with GA ($r^2 = 0.17$, $P = .007$; $r^2 = 0.12$, $P = .02$; $r^2 = 0.10$, $P = .034$; $r^2 = 0.20$, $P = .003$, respectively), whereas tCho:tCr significantly decreased with increasing GA ($r^2 = 0.23$, $P = .0015$). In the third trimester alone, tNAA exhibited the highest increase with GA ($r^2 = 0.41$, $P < .0001$), whereas tNAA:tCr and tCho exhibited a small yet significant increase with GA ($r^2 = 0.06$, $P = .009$). Both tNAA:tCho and tCr exhibited a significant increase with GA ($r^2 = 0.37$, $P < .0001$; $r^2 = 0.39$, $P < .0001$, respectively). Similarly, tCr:tCho increased significantly with GA ($r^2 = 0.20$, $P < .0001$), whereas tCho:tCr decreased with GA ($r^2 = 0.20$, $P < .0001$). The normative values for the absolute metabolite concentrations and their corresponding ratios per week of gestation for the study cohort are summarized in Table 2.

In a subset of 21 subjects, 4 in the second trimester (mean GA, 23.29 ± 3.5 weeks) and 17 in the third trimester (mean GA,

Table 2: Normative mean absolute metabolite concentrations and ratios per GA in weeks for the whole cohort^a

	GA, wk										
	18–20	20–22	22–24	24–26	26–28	28–30	30–32	32–34	34–36	36–38	38–40
tNAA, mM/kg	1.87 ± 0.62	3.01 ± 0.91	2.63 ± 0.96	3.76 ± 1.07	3.32 ± 0.78	4.09 ± 0.77	4.27 ± 1.05	4.96 ± 1.44	5.69 ± 1.24	6.52 ± 1.50	7.58 ± 1.27
tCho, mM/kg	2.55 ± 0.72	3.15 ± 0.65	3.12 ± 0.89	3.58 ± 0.85	3.13 ± 0.40	3.16 ± 0.46	3.15 ± 0.52	3.29 ± 0.64	3.43 ± 0.37	3.44 ± 0.75	3.70 ± 0.65
tCr, mM/kg	2.34 ± 0.83	2.59 ± 0.58	2.72 ± 0.71	3.30 ± 1.06	3.21 ± 0.50	3.68 ± 0.52	3.81 ± 0.69	4.28 ± 0.64	4.78 ± 0.96	5.01 ± 0.79	5.37 ± 0.63
tNAA:tCho	0.76 ± 0.21	0.95 ± 0.22	0.85 ± 0.21	1.07 ± 0.32	1.06 ± 0.20	1.31 ± 0.24	1.37 ± 0.30	1.50 ± 0.31	1.66 ± 0.29	1.93 ± 0.43	2.07 ± 0.26
tNAA:tCr	0.89 ± 0.36	1.17 ± 0.28	0.97 ± 0.24	1.25 ± 0.61	1.04 ± 0.22	1.12 ± 0.24	1.14 ± 0.29	1.17 ± 0.32	1.23 ± 0.32	1.32 ± 0.32	1.41 ± 0.15
tCho:tCr	1.14 ± 0.24	1.25 ± 0.26	1.14 ± 0.13	1.17 ± 0.44	0.99 ± 0.11	0.86 ± 0.11	0.84 ± 0.12	0.78 ± 0.16	0.74 ± 0.16	0.69 ± 0.10	0.69 ± 0.09
tCr:tCho	0.91 ± 0.20	0.83 ± 0.18	0.88 ± 0.10	0.95 ± 0.31	1.02 ± 0.10	1.17 ± 0.14	1.21 ± 0.16	1.33 ± 0.27	1.39 ± 0.17	1.49 ± 0.23	1.47 ± 0.19

^a Values are rounded to 2 decimal places.

Table 3: Summary of the reproducibility statistics^a

Metabolite Concentration	CV, %	ICC (95% CI)
tNAA	6.15	0.90 (0.35–0.97)
tCho	9.30	0.72 (0.62–0.95)
tCr	5.43	0.96 (0.77–0.99)

Note:—CV indicates coefficient of variation; ICC, intraclass correlation.

^a Values are rounded to 2 decimal places.

34.75 ± 2.6 weeks), there was quantifiable lactate in the LCModel fitted spectra with %SD confidence level of Cramer-Rao lower bounds of 16.14 ± 3.1, which was higher than the uncertainty of other metabolite concentrations. Absolute metabolite concentration of lactate was 4.36 ± 2.13 mmol/L/kg, which showed greater variability than the other metabolite concentrations. In all these subjects, none of their postnatal MR studies showed evidence of lactate or any structural brain abnormalities.

Reproducibility and Repeatability

Seven MR spectra (3.43%) acquired at random from 7 study participants (2 in the second trimester and 5 in the third trimester; mean GA, 31.27 ± 4 weeks) were used in intrasession reproducibility of the results. These were acquired an average of 20 minutes apart to test reproducibility and repeatability of voxel placement and subsequent absolute metabolite concentration quantification. Scan-rescan coefficient of variation was 6.15% for tNAA, 9.30% for tCho, and 5.43% for tCr. Intraclass correlation coefficient was highest for tCr, which showed high concordance with repeated measurements. The reproducibility statistics are shown in Table 3.

DISCUSSION

In this study, we demonstrated that absolute metabolite concentrations and metabolite ratios using ¹H-MRS can be successfully obtained from the in vivo fetal brain in >75% of cases. In so doing, we provided normative data at TE = 144 milliseconds for metabolic development of the fetal brain over the latter half of gestation in the largest cohort of healthy fetuses to date. We demonstrated that metabolite ratios in the normal fetal brain change with GA as energy demands and cellular maturation increases and cerebral structure evolves. We quantified the detection of the tNAA peak from 18 weeks onward; to our knowledge, this is the earliest detection of tNAA in vivo reported to date. Also to our knowledge, this is the first study to provide absolute metabolite concentrations corrected for water concentration of the fetal brain (cerebrum) and provided clinically relevant values in units of mM/kg. This represents a more accurate estimation of the absolute metabolite concentrations otherwise underestimated if this correction is not used.²⁵ Inherent limitations with metabolite ra-

tios and misconceptions that they self-correct for type of scanner, localization method differences, gain instabilities, regional susceptibility variations, and partial volume effects are addressed using absolute metabolite concentrations in addition to ratios.³⁶

This is also the first study to report intrasession reproducibility and repeatability in fetal ¹H-MRS. Although it is difficult to achieve high reproducibility due to the inherent fetal motion and voxel placement, our results compared favorably with similar studies in the liver³⁴ and adult brain^{33,37} that used similar voxel sizes to acquire MR spectra.

Very few studies have explored fetal brain ¹H-MRS in vivo. Most of these studies reported metabolite peak ratios or metabolite areas that are very different and might not be clinically significant from the absolute metabolite concentrations or ratios that LCModel quantifies. Heerchap and van den Berg¹² first performed a feasibility study of 6 healthy third-trimester fetuses using long acquisition times (>10 minutes). Fenton et al³⁸ reported metabolites in a small sample using a short breath-hold technique, but spectral quality remained poor. Subsequently, Kok et al³⁹ studied 36 normal third trimester fetuses and described a significant increase in both NAA:Cr and NAA:Cho, whereas Cho:Cr decreased with increasing GA. Using maternal sedation, Girard et al²⁸ performed clinically indicated studies in 58 fetuses in which fetal MR imaging studies were found to be structurally normal. However, they reported ratios of each metabolite to the total metabolite sum, which makes these data difficult to compare with other studies. Also, their long acquisition times (twice as long as our study) and their voxel placement in the centrum semiovale was different enough from ours to be able to make any meaningful comparisons. Most recently, Berger-Kulemann et al⁴⁰ retrospectively evaluated, with a 55% success rate, ¹H-MRS of 75 fetuses referred for MR imaging for suspected brain abnormalities.⁴¹ It is important to note that, unlike other studies, our inception cohort only included low-risk healthy pregnant volunteers, which constituted a truly representative normative sample. We also demonstrated a higher success in interpretable ¹H-MRS in the absence of maternal sedation.

The increase in both tNAA:tCho and tNAA:tCr with advancing GA described in our study may be attributed to dendritic and synaptic development.⁵ The tCho peak observed in our MR spectra was composed of both phosphocholine and glycerol 3-phosphocholine. These compounds are involved in membrane synthesis and degradation.⁷ This tCho peak, however, only reflects a small part of the tissue level of Cho-containing compounds. More than 90% of the latter is phosphatidylcholine, a major constituent of the phospholipids that form myelin,^{42,43} which cannot be detected by ¹H-MRS.⁴⁴ The tCho exhibits a higher concentration

during early life than in adulthood, which indicates that Cho-containing compounds are turned over more rapidly during early human development^{24,45} and decrease over the first 5 years of life.^{46,47} We also showed that tCho:tCr decreases with increasing GA, whereas tCho remains relatively stable until the beginning of myelination toward the end of the third trimester of pregnancy and early postnatal period.^{45,48} One study reported that absolute Cr levels remain stable during gestation, which may serve as a reliable

reference (denominator) for quantifying changes in other metabolites.²⁹ Analysis of our data indicated that tCho may be a more-appropriate reference metabolite for the developing fetal brain because it remains at relatively constant levels from 18 to 40 weeks of gestation, as shown by the tCho linear regression straight line plot and shown from the absolute metabolite concentrations quantified using the unsuppressed tissue water as an internal reference²⁰ in Table 2. However, there is a small increase in tCho when considering the cohort in the third trimester alone, which likely indicated the start of myelination.

Lactate was observed in a small subset of our cohort. Berger-Kulemann et al⁴⁰ found lactate in 2 of their 6 normal fetuses (33.3%), whereas Story et al³⁰ described lactate in 3 healthy fetuses (7%) with normal deliveries and postnatal outcomes. The investigators postulate that lactate may be an important source of energy for the normally developing brain. Lactate is also normally present in CSF.⁴⁹ The voxel used in this study contained heterogeneous brain tissue, including contamination by CSF, which led to the detection of lactate signal. Because our choice of TE (144 milliseconds) is specific to lactate, it is likely more frequently detected when present. Furthermore, the absolute metabolite concentration of lactate exhibited a greater variability than any of the other metabolites, which indicated that the fluctuating baseline might also be responsible for its detection. No lactate peak was identified in the postnatal ¹H-MRS. Further studies are needed to investigate the presence and predictive value of lactate in the healthy fetus.

The choice of TE often depends on the metabolite of interest. In this study, we chose TE = 144 milliseconds because this has a better-defined baseline and less baseline distortion over TE = 35 milliseconds, which allowed for a more accurate quantification as indicated by lower %SD of the Cramer-Rao lower bounds. In addition, our normative fetal ¹H-MRS studies were performed to be able to compare brain metabolites in a cohort of fetuses with complex congenital heart disease, in which we selected TE = 144 milliseconds to detect and differentiate lactate from lipids at 1.3 to 1.4 ppm by J-modulation/inversion of the lactate doublet peaks.

Strengths of our study included the largest known sample size of healthy normal fetal studies, the prospective design, and the successful acquisition and correction of motion-induced artifacts, which yielded high-quality spectra in >75% of the studies. Limitations included the fact that single voxel fetal brain ¹H-MRS requires an additional anatomic scan for voxel placement and is usually relatively large to increase SNR. This is needed given the magnitude and frequency of fetal-maternal motion to ensure that it remains within the brain. However, the voxel usually contains white-gray matter and CSF.¹⁵ To overcome this limitation would require tissue segmentation to resolve tissue constituents from

which the MR spectrum is acquired, which is currently not possible in utero.³⁹

This study demonstrated the feasibility of obtaining noninvasive metabolic information from the fetal brain with a high success rate and good reproducibility using ¹H-MRS. Normative reference values of absolute metabolite concentrations and ratios in the fetal brain in the second and third trimesters of pregnancy are provided for the largest sample to date. This is also the first study to retrospectively correct the acquired MR spectra for motion-induced artifacts before quantification, which yielded high-quality spectra. These data will aid clinicians in interpreting ¹H-MRS of the fetal brain, complementing structural MR imaging, and allowing detection of early deviation from these norms in the compromised fetus. In the future, detection of such deviation from normal metabolic development may allow interventions that minimize irreversible brain injury.

ACKNOWLEDGMENTS

The authors thank the clinical research coordinators, the MR technologists, and the volunteers and their families for participating in this study.

Disclosures: Iordanis Evangelou—RELATED: Grant: Canadian Institutes of Health Research (MOP-81116)*; UNRELATED: Board Membership: ImPossible MR, LLC; Consultancy: GE Healthcare Coils, MR Instruments; Employment: ImPossible MR, LLC; Grants/Grants Pending: Veterans Affairs, Department of Defense,* Chronic Effects of Neurotrauma Consortium (CENC0039P); Stock/Stock Options: ImPossible MR, LLC, Ralph Noeske—UNRELATED: Employment: GE Healthcare. *Money paid to the institution.

REFERENCES

1. Fayed N, Morales H, Modrego PJ, et al. **White matter proton MR spectroscopy in children with isolated developmental delay: does it mean delayed myelination?** *Acad Radiol* 2006;13:229–35 CrossRef Medline
2. Broom KA, Anthony DC, Lowe JP, et al. **MRI and MRS alterations in the preclinical phase of murine prion disease: association with neuropathological and behavioural changes.** *Neurobiol Dis* 2007;26:707–17 CrossRef Medline
3. Barker PB. **N-acetyl aspartate—a neuronal marker?** *Ann Neurol* 2001;49:423–24 CrossRef Medline
4. Moffett JR, Ross B, Arun P, et al. **N-Acetylaspartate in the CNS: from neurodiagnostics to neurobiology.** *Prog Neurobiol* 2007;81:89–131 CrossRef Medline
5. Urenjak J, Williams SR, Gadian DG, et al. **Specific expression of N-acetylaspartate in neurons, oligodendrocyte-type-2 astrocyte progenitors, and immature oligodendrocytes in vitro.** *J Neurochem* 1992;59:55–61 CrossRef Medline
6. Sartorius A, Lugenbiel P, Mahlstedt MM, et al. **Proton magnetic resonance spectroscopic creatine correlates with creatine transporter protein density in rat brain.** *J Neurosci Methods* 2008;172:215–19 CrossRef Medline
7. Gill SS, Small RK, Thomas DG, et al. **Brain metabolites as 1H NMR markers of neuronal and glial disorders.** *NMR Biomed* 1989;2:196–200 CrossRef Medline
8. Katz-Brull R, Koudinov AR, Degani H. **Choline in the aging brain.** *Brain Res* 2002;951:158–65 CrossRef Medline
9. José da Rocha A, Túlio Braga F, Carlos Martins Maia A Jr, et al. **Lactate detection by MRS in mitochondrial encephalopathy: optimization of technical parameters.** *J Neuroimaging* 2008;18:1–8 CrossRef Medline
10. Wolfberg AJ, Robinson JN, Mulkern R, et al. **Identification of fetal cerebral lactate using magnetic resonance spectroscopy.** *Am J Obstet Gynecol* 2007;196:e9–e11 CrossRef Medline

11. Charles-Edwards GD, Jan W, To M, et al. **Non-invasive detection and quantification of human foetal brain lactate in utero by magnetic resonance spectroscopy.** *Prenat Diagn* 2010;30:260–66 CrossRef Medline
12. Heerschap A, van den Berg PP. **Proton magnetic resonance spectroscopy of human fetal brain.** *Am J Obstet Gynecol* 1994;170:1150–51 CrossRef Medline
13. Brighina E, Bresolin N, Pardi G, et al. **Human fetal brain chemistry as detected by proton magnetic resonance spectroscopy.** *Pediatr Neurol* 2009;40:327–42 CrossRef Medline
14. Pugash D, Krssak M, Kulemann V, et al. **Magnetic resonance spectroscopy of the fetal brain.** *Prenat Diagn* 2009;29:434–41 CrossRef Medline
15. Story L, Damodaram MS, Allsop JM, et al. **Proton magnetic resonance spectroscopy in the fetus.** *Eur J Obstet Gynecol Reprod Biol* 2011;158:3–8 CrossRef Medline
16. Limperopoulos C, Tworetzky W, McElhinney DB, et al. **Brain volume and metabolism in fetuses with congenital heart disease: evaluation with quantitative magnetic resonance imaging and spectroscopy.** *Circulation* 2010;121:26–33 CrossRef Medline
17. Clouchoux C, Guizard N, Evans AC, et al. **Normative fetal brain growth by quantitative in vivo magnetic resonance imaging.** *Am J Obstet Gynecol* 2012;206:173.e1–8 CrossRef Medline
18. Evangelou IE, Noeske R, Limperopoulos C. **Retrospective correction of motion induced artifacts in 1H magnetic resonance spectroscopy of the fetal brain.** In: *Proceedings of the IEEE 12th International Symposium on Biomedical Imaging*, Brooklyn, New York. April 16–19, 2015:853–57
19. Provencher SW. **Estimation of metabolite concentrations from localized in vivo proton NMR spectra.** *Magn Reson Med* 1993;30:672–79 CrossRef Medline
20. Longo R, Bampo A, Vidimari R, et al. **Absolute quantitation of brain 1H nuclear magnetic resonance spectra. Comparison of different approaches.** *Invest Radiol* 1995;30:119–203 CrossRef Medline
21. Kreis R, Ernst T, Ross BD. **Development of the human brain: in vivo quantification of metabolite and water content with proton magnetic resonance spectroscopy.** *Magn Reson Med* 1993;30:424–37 CrossRef Medline
22. Diem K, Lentner C. *Scientific Tables*. Basle: J.R. Geigy; 1970
23. Ganguly A. *Fundamentals of Physical Chemistry*. New Delhi: Pearson Education India; 2012
24. Kreis R, Hofmann L, Kuhlmann B, et al. **Brain metabolite composition during early human brain development as measured by quantitative in vivo 1H magnetic resonance spectroscopy.** *Magn Reson Med* 2002;48:949–58 CrossRef Medline
25. Tomiyasu M, Aida N, Endo M, et al. **Neonatal brain metabolite concentrations: an in vivo magnetic resonance spectroscopy study with a clinical MR system at 3 Tesla.** *PLoS One* 2013;8:e82746 CrossRef Medline
26. Cavassila S, Deval S, Huegen C, et al. **Cramér-Rao bounds: an evaluation tool for quantitation.** *NMR Biomed* 2001;14:278–83 CrossRef Medline
27. Provencher SW. **Automatic quantitation of localized in vivo 1H spectra with LCModel.** *NMR Biomed* 2001;14:260–64 CrossRef Medline
28. Girard N, Gouny SC, Viola A, et al. **Assessment of normal fetal brain maturation in utero by proton magnetic resonance spectroscopy.** *Magn Reson Med* 2006;56:768–75 CrossRef Medline
29. Kok RD, van den Berg PP, van den Bergh AJ, et al. **Maturation of the human fetal brain as observed by 1H MR spectroscopy.** *Magn Reson Med* 2002;48:611–16 CrossRef Medline
30. Story L, Damodaram MS, Allsop JM, et al. **Brain metabolism in fetal intrauterine growth restriction: a proton magnetic resonance spectroscopy study.** *Am J Obstet Gynecol* 2011;205:483.e1–8 CrossRef Medline
31. Stanish WM, Taylor N. **Estimation of the intraclass correlation coefficient for the analysis of covariance model.** *Am Stat* 1983;37:221–24 CrossRef
32. Kirkwood TB. **Geometric means and measures of dispersion.** *Biometrics* 1979;35:908–09
33. Marshall I, Wardlaw J, Cannon J, et al. **Reproducibility of metabolite peak areas in 1H MRS of brain.** *Magn Reson Imaging* 1996;14:281–92 CrossRef Medline
34. van Werven JR, Hoogduin JM, Nederveen AJ, et al. **Reproducibility of 3.0 Tesla magnetic resonance spectroscopy for measuring hepatic fat content.** *J Magn Reson Imaging* 2009;30:444–48 CrossRef Medline
35. Gasparovic C, Bedrick EJ, Mayer AR, et al. **Test-retest reliability and reproducibility of short-echo-time spectroscopic imaging of human brain at 3T.** *Magn Reson Med* 2011;66:324–32 CrossRef Medline
36. Li BS, Wang H, Gonen O. **Metabolite ratios to assumed stable creatine level may confound the quantification of proton brain MR spectroscopy.** *Magn Reson Imaging* 2003;21:923–28 CrossRef Medline
37. Wijtenburg SA, Rowland LM, Edden RA, et al. **Reproducibility of brain spectroscopy at 7T using conventional localization and spectral editing techniques.** *J Magn Reson Imaging* 2013;38:460–67 CrossRef Medline
38. Fenton BW, Lin CS, Macedonia C, et al. **The fetus at term: in utero volume-selected proton MR spectroscopy with a breath-hold technique—a feasibility study.** *Radiology* 2001;219:563–66 CrossRef Medline
39. Kok RD, van den Bergh AJ, Heerschap A, et al. **Metabolic information from the human fetal brain obtained with proton magnetic resonance spectroscopy.** *Am J Obstet Gynecol* 2001;185:1011–15 CrossRef Medline
40. Berger-Kulemann V, Brugger PC, Pugash D, et al. **MR spectroscopy of the fetal brain: is it possible without sedation?** *AJNR Am J Neuroradiol* 2013;34:424–31 CrossRef Medline
41. Brunel H, Girard N, Confort-Gouny S, et al. **Fetal brain injury.** *J Neuroradiol* 2004;31:123–37 CrossRef Medline
42. Smith ME. **A regional survey of myelin development: some compositional and metabolic aspects.** *J Lipid Res* 1973;14:541–51 Medline
43. Podbielska M, Banik NL, Kurowska E, et al. **Myelin recovery in multiple sclerosis: the challenge of remyelination.** *Brain Sci* 2013;3:1282–324 CrossRef Medline
44. Miller BL, Chang L, Booth R, et al. **In vivo 1H MRS choline: correlation with in vitro chemistry/histology.** *Life Sci* 1996;58:1929–35 CrossRef Medline
45. Hüppi PS, Posse S, Lazeyras F, et al. **Magnetic resonance in preterm and term newborns: 1H-spectroscopy in developing human brain.** *Pediatr Res* 1991;30:574–78 CrossRef Medline
46. Danielsen ER, Ross B. *Magnetic Resonance Spectroscopy Diagnosis of Neurological Diseases*. New York: M. Dekker; 1999
47. Pouwels PJ, Brockmann K, Kruse B, et al. **Regional age dependence of human brain metabolites from infancy to adulthood as detected by quantitative localized proton MRS.** *Pediatr Res* 1999;46:474–85 CrossRef Medline
48. Holland BA, Haas DK, Norman D, et al. **MRI of normal brain maturation.** *AJNR Am J Neuroradiol* 1986;7:201–08 Medline
49. Nagae-Poetscher LM, McMahon M, Braverman N, et al. **Metabolites in ventricular cerebrospinal fluid detected by proton magnetic resonance spectroscopic imaging.** *J Magn Reson Imaging* 2004;20:496–500 CrossRef Medline

Intensity of MRI Gadolinium Enhancement in Cerebral Adrenoleukodystrophy: A Biomarker for Inflammation and Predictor of Outcome following Transplantation in Higher Risk Patients

W.P. Miller, L.F. Mantovani, J. Muzic, J.B. Rykken, R.S. Gawande, T.C. Lund, R.M. Shanley, G.V. Raymond, P.J. Orchard, and D.R. Nascene

ABSTRACT

BACKGROUND AND PURPOSE: Outcomes following hematopoietic stem cell transplantation for higher risk childhood-onset cerebral adrenoleukodystrophy are variable. We explored whether a brain MR imaging gadolinium intensity scoring system improves prediction of neurologic outcome.

MATERIALS AND METHODS: We developed a 4-point scale of gadolinium intensity relative to the choroid plexus: 0 = no enhancement; 1 = hypointense; 2 = isointense; 3 = hyperintense. The interobserver concordance of the scale was assessed on 30 randomly chosen studies. Scores were generated for 64 evaluable patients and compared with CSF chitotriosidase levels, a known inflammatory marker correlating with outcomes following transplantation. For 25 evaluable higher risk patients (Loes ≥ 10), the gadolinium intensity score was compared with longer term posttransplantation clinical change.

RESULTS: The gadolinium intensity scoring system showed good interobserver reproducibility ($\kappa = 0.72$). Of 64 evaluable boys, the score positively correlated with average concomitant CSF chitotriosidase activity in nanograms/milliliter/hour: 0: 2717, $n = 5$; 1: 3218, $n = 13$; 2: 6497, $n = 23$; and 3: 12,030, $n = 23$ ($P < .01$). For 25 evaluable higher risk patients, more intense pretransplantation brain MR imaging gadolinium enhancement predicted greater average loss on the adrenoleukodystrophy neurologic function scale following transplantation: 0/1: adrenoleukodystrophy neurologic function scale score difference = 4.3, $n = 7$; 2/3: adrenoleukodystrophy neurologic function scale score difference = 10.4, $n = 18$ ($P = .05$).

CONCLUSIONS: Gadolinium enhancement intensity on brain MR imaging can be scored simply and reproducibly for cerebral adrenoleukodystrophy. The enhancement score significantly correlates with chitotriosidase. In boys with higher risk cerebral disease (Loes ≥ 10), the enhancement score itself predicts neurologic outcome following treatment. Such data may help guide treatment decisions for clinicians and families.

ABBREVIATIONS: ALD = adrenoleukodystrophy; cALD = cerebral adrenoleukodystrophy; CHIT = chitotriosidase; Δ NFS = change in NFS score; GIS = brain MRI gadolinium intensity scale score; HSCT = hematopoietic stem cell transplantation; NFS = adrenoleukodystrophy neurologic function scale score

Adrenoleukodystrophy (ALD) is an X-linked peroxisomal disorder affecting approximately 1 in 21,000 males. Mediated by elevated concentrations of very long chain fatty acids, the disease may manifest as central nervous system demyelination, primary

hypoadrenalism, and/or primary hypogonadism. The disease results from pathogenic mutations in the peroxisomal transporter *ABCD1* gene, but genotype does not predict the presentation, and different presentations may occur within the same family.^{1,2}

In 35% of affected males, cerebral involvement (cerebral adrenoleukodystrophy [cALD]) begins in childhood. This devastating phenotype is characterized by rapidly progressive central nervous demyelination and, if untreated, usually death within years of onset of clinical signs and symptoms.³ Postmortem analyses of affected brains have implicated mononuclear inflammatory mechanisms.⁴⁻⁶ Radiographic changes generally precede clinical neurologic disease by several years in childhood cALD and are characterized by symmetric, expanding white matter lesions.⁷ Consistent with known neuroinflammatory histopathology, gadolinium enhancement is typically observed near the leading edge of active demyelination and, when present, strongly predicts dis-

Received April 20, 2015; accepted after revision June 15.

From the Division of Pediatric Blood and Marrow Transplant (W.P.M., T.C.L., P.J.O.), Department of Pediatrics; and Departments of Diagnostic Radiology (J.B.R., R.S.G., D.R.N.) and Neurology (G.V.R.), University of Minnesota Medical Center, Minneapolis, Minnesota; Division of Hematology and Oncology (L.F.M.), Department of Pediatrics, University of Sao Paulo, Sao Paulo, Brazil; University of Minnesota Medical School (J.M.), Minneapolis, Minnesota; and Biostatistics Core (R.M.S.), Masonic Cancer Center, University of Minnesota, Minneapolis, Minnesota.

Weston P. Miller and Luiz F. Mantovani contributed equally to this work.

Please address correspondence to Weston Peter Miller, MD, University of Minnesota, Pediatric Blood and Marrow Transplantation, 420 Delaware St, SE, MMC 484, Minneapolis, MN 55455; e-mail: mill4991@umn.edu

<http://dx.doi.org/10.3174/ajnr.A4500>

Hearing/auditory processing problems	1
Aphasia/apraxia	1
Loss of communication	3
Vision impairment/fields cut	1
Cortical blindness	2
Swallowing difficulty or other central nervous system dysfunction	2
Tube feeding	2
Running difficulties/hyperreflexia	1
Walking difficulties/spasticity/spastic gait (no assistance)	1
Spastic gait (needs assistance)	2
Wheelchair required	2
No voluntary movement	3
Episodes of urinary or fecal incontinency	1
Total urinary or fecal incontinency	2
Nonfebrile seizures	1
Possible Total	25

FIG 1. The cerebral adrenoleukodystrophy neurologic function scale used to evaluate gross clinical neurologic status for the higher risk cALD cohort pretransplantation and at most recent posttransplantation follow-up. Note that a score of zero denotes absence of clinical signs of cerebral disease. Maximal signs within a domain score the total of all grades within that domain (for example, a patient with “total urinary or fecal incontinency” scores 3, for the sum of episodes of incontinency [$n = 1$] and total incontinency [$n = 2$]).

ease progression.^{8,9} The cALD brain MR imaging severity scale of Loes et al¹⁰ is commonly used to quantify radiographic disease burden in adrenoleukodystrophy. Increasing Loes scores denote accumulating white matter disease and atrophy in defined neuro-anatomic or functional regions: periventricular/subcortical areas (parieto-occipital, anterior-temporal, and frontal), corpus callosum, visual and auditory pathways, frontopontine-corticospinal projection fibers (internal capsule and brain stem), basal ganglia, cerebellum, and anterior thalamus. For patients with ALD with no cerebral involvement, the Loes score is by definition zero, while maximal cerebral involvement on the scale (Loes = 34) correlates with profound neurologic impairment.¹⁰

Although experimental gene therapy trials are currently underway, allogeneic hematopoietic stem cell transplantation (HSCT) remains the standard therapy to arrest cerebral disease progression in cALD.³ Most important, long-term functional outcome analyses have demonstrated critical dependence on cerebral white matter disease burden as measured by the Loes score at the time of transplantation.¹¹ Most patients with Loes of <10 are lacking signs of cerebral disease as measured on the ALD neurologic function scale (NFS, Fig 1)¹² and are seriously considered for HSCT. For these standard-risk patients with cALD (Loes <10 at HSCT), gross neurologic function following transplantation nearly uniformly remains the same on the NFS. However, outcomes after transplantation for higher risk disease (Loes ≥ 10 at HSCT) are considerably more difficult to prognosticate and range from mild clinical progression to profound devastation.¹³ For such higher risk patients, the absolute pretransplantation Loes score alone does not predict neurologic outcome.

Despite effort aimed at early detection, many boys still arrive at ALD diagnosis because of neurologic impairment from higher risk cALD (Loes ≥ 10). In these cases, clinicians and families face difficult decisions regarding the use of HSCT, a procedure that carries significant risk of injury and mortality.¹⁴ Therefore, addi-

tional prognostic indicators are sought of likely benefit from HSCT in these higher risk patients with cALD, who already demonstrate extensive cerebral white matter disease burden at diagnosis.

In previous reports, a strong correlation between pretransplantation chitotriosidase enzyme activity (CHIT, elaborated by activated monocytes) in plasma and CSF and clinical neurologic change at 1 year following HSCT for cALD have been observed.¹⁵ In that analysis, higher CSF CHIT in the pretransplantation setting strongly correlated with clinical neurologic worsening for a nonstratified cALD cohort (standard and higher risk patients combined).

We have anecdotally observed a possible correlation between the intensity of gadolinium enhancement on pre-HSCT brain MR imaging and clinical neurologic outcomes following HSCT in higher risk cALD (Loes ≥ 10). In this single-institution study, we established a simple gadolinium intensity scoring (GIS) system for cALD brain MR imaging and applied it to a large patient cohort. We explored the reproducibility of the GIS and its correlation with concomitant CSF CHIT. Finally, we analyzed the pretransplantation GIS predictive value for posttransplantation neurologic outcomes in higher risk cALD.

MATERIALS AND METHODS

Cohort Identification and CSF Chitotriosidase Activity Determination

All patients confirmed to have ALD by diagnostic plasma very long chain fatty acid profile and who underwent evaluation at the University of Minnesota after January 1, 2000, were considered for this retrospective study. CSF CHIT activity and CHIT genotypes were determined by methods previously described.¹⁵

Because 1 aim of our analysis was to assess a correlation between GIS and CSF CHIT in cALD regardless of how limited or extensive white matter disease may be, all patients with cALD, regardless of Loes score, were included for analysis of GIS and CSF CHIT correlation if they had the following: 1) an untreated MR imaging evaluable for GIS (pretransplantation, if the patient proceeded to HSCT), and 2) concomitant CSF CHIT data. For patients genotypically determined to be heterozygous CHIT null ($CHIT^{WT}/CHIT^0$, seen in approximately 35% of the general population), CSF CHIT activity reported for this study was set to twice that measured in the assay. Patients were excluded for analysis of GIS and CSF CHIT correlation for the following reasons: 1) They were genotypically homozygous CHIT null ($CHIT^0/CHIT^0$, seen in approximately 5% of the general population), because these patients are not capable of producing the enzyme; or 2) they did not demonstrate MR imaging evidence of cerebral disease (Loes = 0).

Because previous reports have shown standard-risk patients with cALD (Loes <10 at the time of HSCT) to demonstrate no-to-minimal worsening in posttransplantation general clinical neurologic function,¹³ only higher risk patients with cALD (Loes ≥ 10 at the time of transplantation) were considered for retrospective analysis of the correlation between pretransplantation GIS and neurologic function outcomes posttransplantation. These higher risk patients were included in this study if the following conditions were met: 1) a pretransplantation brain MR imaging was evaluable for GIS; 2) the pretransplantation Loes score was ≥ 10 ; and 3) robust donor hematopoietic engraftment

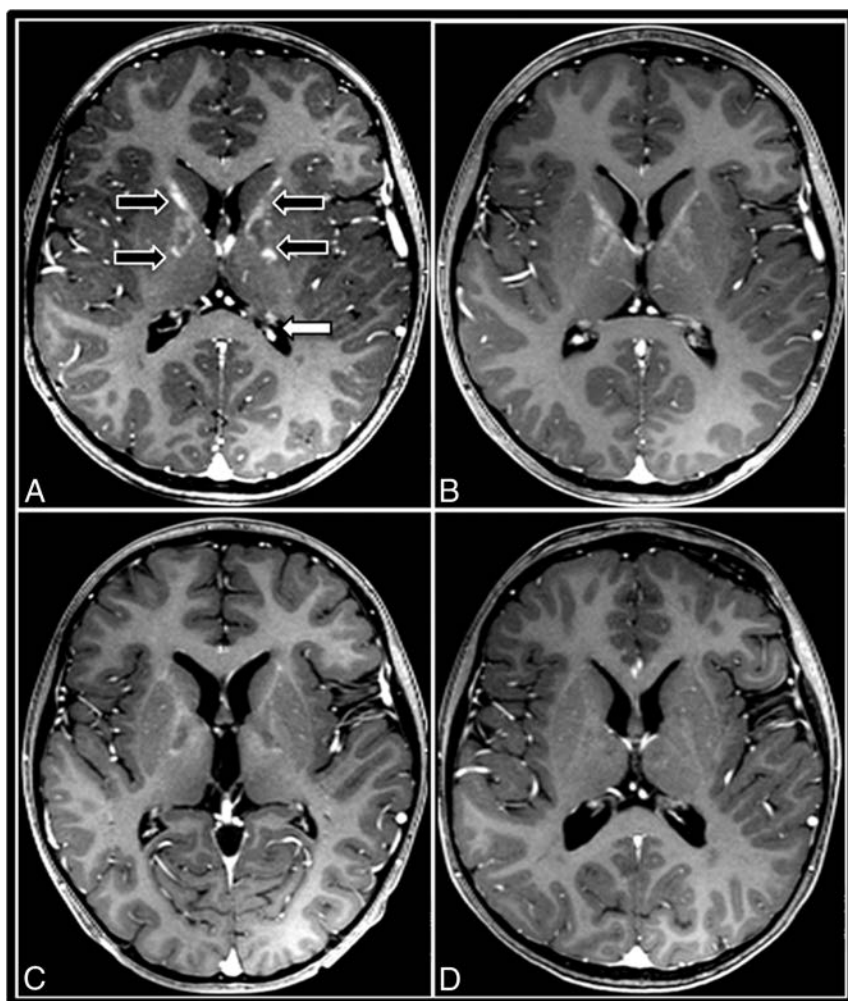


FIG 2. A gadolinium intensity scoring system for cerebral adrenoleukodystrophy demonstrated by successive postcontrast T1WI of a 7-year-old boy with ALD primarily involving the internal capsule. This patient exhibits all 4 grades of GIS, from initial intense contrast enhancement progressing to nonenhancement. A, Pre-HSCT MR imaging demonstrates GIS = 3 in the internal capsules (black arrows) with maximal lesion enhancement hyperintense to the choroid plexus (white arrow). B, Thirty days post-HSCT, the GIS is 2, because maximal lesion enhancement equal to the choroid plexus is observed. C, Later, MR imaging exhibits GIS = 1 with maximal lesion enhancement hypointense to the choroid plexus. D, Ninety days after successful HSCT, resolution of contrast enhancement is seen (GIS = 0).

(≥80%) was achieved following transplantation. Patients were excluded if death resulted from transplant-related complications.

All patients receiving transplants were treated on protocols approved by the institutional review board and following the provision of informed consent. For each patient, the best available allograft according to standard institutional guidelines was chosen. The transplant conditioning regimen was dependent on the appropriate protocol available to the patient at the time of transplantation. Antimicrobial prophylaxis and therapy, graft-versus-host disease prophylaxis, and blood product supportive care followed standard institutional guidelines.

ALD MR Imaging Severity (Loes) Score and Gadolinium Intensity Score Assignment

Brain MR imaging studies included in this analysis were prospectively assigned a severity score according to the Loes system by a single neuroradiologist (D.R.N.) who was blinded to CHIT data and neurologic outcomes.¹⁰

Gadolinium intensity scores were determined from 3D-T1-weighted MPRAGE (TR, 1900 ms; TE, 2.19 ms; TI, 900 ms; 1 average; flip angle, 9°; section thickness, 0.9 mm; voxel size, 0.9 × 0.9 × 0.9 mm; matrix, 256 × 256) images obtained approximately 5 minutes following intravenous dosing of either Magnevist (gadopentetate dimeglumine; Bayer HealthCare Pharmaceuticals, Wayne, New Jersey), 0.1 mmol/kg, or Gadavist (gadobutrol; Bayer Schering Pharma, Berlin, Germany), 0.05 mmol/kg.

Because gadolinium enhancement intensity may vary due to interscan differences in timing of the IV contrast bolus, we developed the GIS so that the enhancement intensity would be internally controlled. Each brain MR imaging was assigned a GIS as follows: 0 = no contrast enhancement; 1 = maximal lesion enhancement less than that of the choroid plexus; 2 = maximal lesion enhancement of equal intensity to that of the choroid plexus; 3 = maximal lesion enhancement more intense than that of the choroid plexus (Fig 2). All GISs used for analysis were assigned by a single neuroradiologist (D.R.N.) who was blinded to CHIT data and neurologic outcomes.

The Fleiss κ was used to assess interrater agreement among 3 neuroradiologists (D.R.N., J.B.R., R.S.G.) on 30 randomly selected scans. Good interobserver reliability was observed ($\kappa = 0.72$).¹⁶

Neurologic Function Scale Score Assignment

For higher risk patients with cALD (Loes ≥10 at HSCT) who had undergone trans-

plantation, clinical cerebral disease severity was scored immediately before HSCT and at the latest posttransplantation follow-up by using the ALD NFS (Fig 1).¹² NFS assignment was performed from retrospective review of clinical notes by a single investigator (W.P.M.) who was blinded to radiographic GIS, Loes, and CHIT data. Change in NFS (Δ NFS) was defined as the difference between the NFS at the most recent follow-up and the baseline NFS obtained immediately before HSCT. For patients who died of cALD disease progression following HSCT, the most recent NFS was set to the maximum (25) at the time of death.

Study Objectives and Statistical Analyses

The main objective of this retrospective cohort study was to determine, in all evaluable patients with cALD, whether brain MR imaging gadolinium intensity correlates with CSF CHIT, an inflammatory biomarker shown to be associated with neurologic

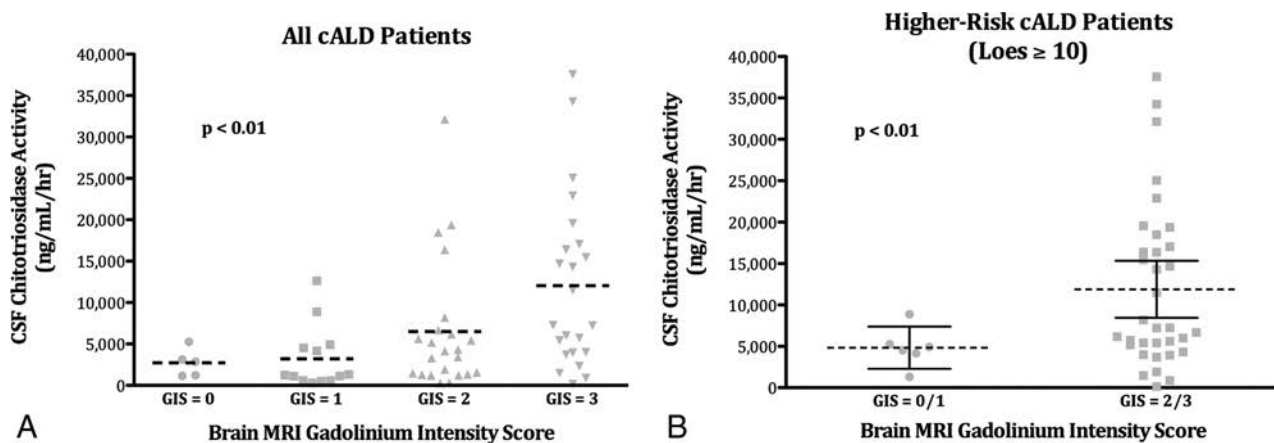


FIG 3. CSF chitotriosidase activity correlates with the brain MR imaging gadolinium intensity score in cALD. A, The mean value of CSF CHIT activity (dashed line) by GIS for the entire evaluable cALD cohort ($n = 64$). B, The mean value of CSF CHIT activity (dashed line) and 95% confidence intervals (solid bars) by GIS for patients with higher risk cALD ($Loes \geq 10$; $n = 40$).

function at 1 year following transplantation for cALD. A secondary objective was to determine whether pretransplantation GIS correlates with long-term change in neurologic function (ΔNFS) in higher risk patients with cALD ($Loes \geq 10$) undergoing HSCT.

Comparisons of mean CSF CHIT activity levels across each cALD GIS were made by the Kruskal-Wallis test. Comparison of mean CSF CHIT activity by the GIS group in higher risk patients with cALD ($Loes \geq 10$) was performed with the t test by using the Welch correction for disparate variance. Comparison of change in the NFS by the GIS group in higher risk patients with cALD ($Loes \geq 10$) was performed with the t test.

RESULTS

Brain MR Imaging Gadolinium Intensity Score Correlates Strongly with CSF Chitotriosidase Activity in cALD

Sixty-four boys with cALD were evaluable for simultaneous CSF CHIT and brain MR imaging GIS. Very few patients ($n = 5$) demonstrated no gadolinium enhancement ($GIS = 0$). The remaining cohort ($n = 59$) was distributed relatively equally among nonzero GIS. For the entire group, mean CSF CHIT varied significantly between GIS cohorts (Fig 3). GIS, mean CSF CHIT activity (nanogram/milliliter/hour), and number of patients observed were as follows: $GIS = 0$, 2717, $n = 5$; $GIS = 1$, 3218, $n = 13$; $GIS = 2$, 6497, $n = 23$; and $GIS = 3$, 12,030, $n = 23$ ($P < .01$, difference in mean CHIT across GIS groups).

When one considers higher risk patients with cALD only ($Loes \geq 10$), CSF CHIT varied significantly by GIS (Fig 3). Because of low patient numbers in this cohort subset, a binary GIS status was assigned. Patients with low GIS (1/2, $n = 6$) demonstrated a mean CHIT of 4844 ng/mL/h (95% CI, 2429–7393 ng/mL/h), while those with high GIS (2/3, $n = 34$) showed a mean CHIT of 11,892 ng/mL/h (95% CI, 8461–15,322 ng/mL/h; $P < .01$, difference in mean CHIT).

Pretransplant Brain MR Imaging Gadolinium Intensity Score Correlates with Longer Term Clinical Neurologic Outcome following HSCT in Higher Risk Patients with cALD

Twenty-five patients with higher risk cALD ($Loes \geq 10$ at HSCT) and near-complete donor hematopoietic engraftment following HSCT (>80% at most recent follow-up) were evaluable for long-

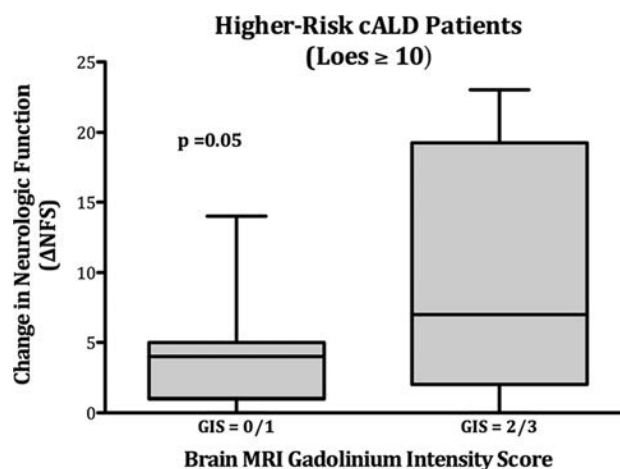


FIG 4. Change in the neurologic function score after HSCT correlates with the pretransplantation MR imaging gadolinium intensity score in higher risk cALD. ΔNFS by pretransplant brain MR imaging GIS status is shown for patients with higher risk cALD ($Loes \geq 10$ at transplantation). Seven patients had low GIS status (0/1), while 18 had high GIS status (2/3) on pretransplantation MR imaging. Solid rectangles show the first quartile (bottom), median (midline), and third quartile (top) results; whiskers define range.

term change in neurologic function (ΔNFS) based on pretransplantation brain MR imaging GIS (Fig 4). Seven patients with low GISs (0/1) demonstrated a mean ΔNFS of 4.3 at an average post-transplantation follow-up of 3 years. Eighteen patients with high GISs (2/3) experienced a mean ΔNFS of 10.4 at an average post-transplantation follow-up of 1 year 10 months ($P = .05$, difference in mean ΔNFS).

The distribution of transplantation, demographic, and Loes characteristics between the 2 groups is shown in the Table.

DISCUSSION

Currently, allogeneic hematopoietic stem cell transplantation is considered the best treatment for “standard-risk” childhood cerebral adrenoleukodystrophy ($Loes$ brain MR imaging severity score < 10).^{3,11,13} In these children with relatively low-level cerebral white matter involvement at the time of HSCT, gross neurologic function on the ALD NFS is generally normal before trans-

Demographic, transplant, and Loes characteristics in higher risk patients with cALD (Loes ≥ 10) analyzed for neurologic function change by pretransplantation gadolinium intensity score

	GIS 0/1 (n = 7)	GIS 2/3 (n = 18)	Difference (95% CI)
Age at HSCT (yr)			
Mean	10.1	9.0	1.2 (–1.9–4.2)
IQR	8.1–13.3	6.8–10.0	
Pre-HSCT Loes			
Mean	12.6	14.0	–1.5 (–3.3–0.4)
IQR	11–14	11–16	
Donor chimerism (%) ^a			
Mean	98.7	97.1	1.6 (–2.1–5.3)
IQR	100–100	92–100	

Note:—IQR indicates interquartile range.

^a Donor chimerism reflects the percentage of donor hematopoietic engraftment at the most recent follow-up.

plantation and remains largely unchanged afterward. However, a significant proportion of patients with cALD present at diagnosis with advanced, often-symptomatic cerebral disease. Owing to greater white matter involvement (Loes ≥ 10), these patients with cALD are considered at higher risk for poor neurologic outcomes after transplantation.

In a recent analysis, 30 consecutive higher risk patients (Loes ≥ 10) were reported to have a median Δ NFS of 7.5 (interquartile range, 4–19; range, 0–23) when analyzed at a median of 2.1 years after HSCT. Such highly variable and unpredictable neurologic outcomes (ranging from mild, if any, changes to significant neurologic impairment) make for difficult decisions by both clinicians and families, especially because no other effective therapies for higher risk cALD currently exist. Moreover, while large analyses have shown consistently favorable neurologic outcomes for patients with a pretransplantation Loes < 10 , the absolute pre-HSCT Loes score within the higher risk cALD group (pretransplant Loes ≥ 10) has not been proved solely prognostic.¹³ Therefore, additional predictive biomarkers for this challenging patient subset are sought.

Recently, a tight correlation between pretransplantation CHIT activity in CSF and neurologic outcomes at 1 year following HSCT for all cALD has been reported.¹⁵ Because CHIT is elaborated by activated monocytes and macrophages, this marker may quantify active neuroinflammation in patients with cALD. However, CHIT assay is not readily available to most clinicians when assessing boys with cALD. Furthermore, baseline CHIT has not yet been shown within the higher risk cALD subset to be a clear predictor of neurologic function after HSCT.

Radiographic strategies for the quantification of neuroinflammation are limited. While the Loes score is an objective measurement of brain regions affected by demyelination, it does not reflect the volume of brain involved, and it does not quantify contrast enhancement. Practical volumetric analysis of the affected white matter or of areas involved by inflammation is not easily performed with standard clinical PACSs from most vendors. Therefore, we developed a simple scoring system based on the maximal intensity of enhancement observed on each cALD brain MR imaging, positing a correlation between the degree of enhancement and active neuroinflammation. Because observer judgment of MR imaging gadolinium enhancement intensity is fundamentally relative, our system incorporates intrascan intensity in the highly vas-

cular choroid plexus as a normalizing reference. Indeed, we found the scoring system to have high interobserver reproducibility among neuroradiologists.

Using this scale, we showed that higher gadolinium enhancement intensity scores on the untreated cALD brain MR imaging positively correlated with concomitant CSF CHIT. Furthermore, for patients with higher risk cALD at the time of HSCT (Loes ≥ 10), we observed an association between higher pretransplantation GISs and worse longer term neurologic functional outcomes. There were relatively fewer higher risk patients with cALD (Loes ≥ 10) in our evaluable cohort who had lower GIS status at baseline (4% with GIS = 0%; and 24% with GIS = 1). However, our findings suggest significantly better neurologic outcomes for this group deemed at higher risk by the Loes score (Δ NFS of only 4.3 versus Δ NFS of 10.4 for higher risk patients with GIS = 2/3) at a long-term posttransplantation follow-up. Although the mechanism of action of HSCT for cALD is not well-understood, it may, in part, exert its desired effect (arresting further myelin loss) by quelling neuroinflammation. In the higher risk patients with cALD (Loes ≥ 10), the baseline absolute Loes score—which tallies discrete regions within the cerebrum, brain stem, and cerebellum with radiographically evident demyelination—has not been observed to independently correlate with posttransplantation neurologic outcome. However, the Loes system neither accounts for nor attempts to quantify radiographic evidence of neuroinflammation. In fact, among evaluable higher risk patients with cALD in this current analysis (Loes ≥ 10), gadolinium enhancement intensity as measured by GIS did not correlate with absolute Loes scores (data not shown). Therefore, biomarkers that do address this component of active cALD may add prognostic value.

A hindrance to better understanding of HSCT for cALD is the relative rarity of the disorder. Although this cohort is considered large in the field, our study is limited due to few evaluable patients. In particular, confidence in the utility of the pretransplantation GIS to predict neurologic outcomes following HSCT for higher risk cALD (Loes ≥ 10) would be greater if more such patients were evaluable. Ultimately, a matrix of various “measures” of cerebral disease burden before HSCT (clinical, neuropsychologic, tissue biomarkers, Loes severity, and gadolinium intensity status) may better predict likely longer term outcomes for this challenging cALD population.

CONCLUSIONS

Brain MR imaging gadolinium enhancement in cALD can be quantified with a simple, reproducible scoring system. When applied to MR imaging studies of untreated boys, the gadolinium intensity score shows a strong positive correlation with the activity of cerebrospinal chitotriosidase, an enzyme elaborated by activated monocytes and previously shown to correlate with neurologic function at 1 year posttransplantation in all patients with cALD undergoing HSCT. In higher risk patients with cALD (Loes ≥ 10), a subset for whom prediction of neurologic outcomes following HSCT has been difficult, the baseline brain MR imaging gadolinium intensity status appears to significantly predict long-term neurologic functional change. Although this study was performed by using a dedicated 3T MR imaging protocol with fixed T1WI parameters, we believe this method will likely yield useful

information regardless of scanner manufacturer, field strength, or sequence parameters. These findings may help to inform clinician and parental decision-making for higher risk patients with cALD who seek transplantation intervention.

Disclosures: Ryan M. Shanley—UNRELATED: Grants/Grants Pending: National Institutes of Health.* Gerald V. Raymond—UNRELATED: Consultancy: Department of Health and Human Services; Expert Testimony: various medicolegal cases; Grants/Grants Pending: Patient-Centered Outcomes Research Institute.* Paul J. Orchard—UNRELATED: Other: Phase 2/3 Study of the Efficacy and Safety of Hematopoietic Stem Cells Transduced With Lenti-D Lentiviral Vector for the Treatment of Childhood Cerebral Adrenoleukodystrophy.* Comments: Our institution is participating in a clinical trial of gene therapy for this disease. The company sponsoring the trial is Bluebird Bio. As Principal Investigator of the study, I have some salary support for the study. However, the gene therapy study does not support the investigations reported in this article. *Money paid to the institution.

REFERENCES

- Engelen M, Kemp S, de Visser M, et al. **X-linked adrenoleukodystrophy (X-ALD): clinical presentation and guidelines for diagnosis, follow-up and management.** *Orphanet J Rare Dis* 2012;7:51 CrossRef Medline
- Moser H, Raymond G, Dubey P. **Adrenoleukodystrophy: new approaches to a neurodegenerative disease.** *JAMA* 2005;294:3131–34 CrossRef Medline
- Mahmood A, Raymond G, Dubey P, et al. **Survival analysis of haematopoietic cell transplantation for childhood cerebral X-linked adrenoleukodystrophy: a comparison study.** *Lancet Neurol* 2007;6:687–92 CrossRef Medline
- Powers JM, Pei Z, Heinzer AK, et al. **Adreno-leukodystrophy: oxidative stress of mice and men.** *J Neuropathol Exp Neurol* 2005;64:1067–79 CrossRef Medline
- Powers JM, Liu Y, Moser AB, et al. **The inflammatory myelinopathy of adreno-leukodystrophy: cells, effector molecules, and pathogenetic implications.** *J Neuropathol Exp Neurol* 1992;51:630–43 CrossRef Medline
- Berger J, Forss-Petter S, Eichler FS. **Pathophysiology of X-linked adrenoleukodystrophy.** *Biochimie* 2014;98:135–42 CrossRef Medline
- Moser HW, Raymond GV, Lu SE, et al. **Follow-up of 89 asymptomatic patients with adrenoleukodystrophy treated with Lorenzo's oil.** *Arch Neurol* 2005;62:1073–80 CrossRef Medline
- Melhem ER, Loes DJ, Georgiades CS, et al. **X-linked adrenoleukodystrophy: the role of contrast-enhanced MR imaging in predicting disease progression.** *AJNR Am J Neuroradiol* 2000;21:839–44 Medline
- Loes DJ, Fatemi A, Melhem ER, et al. **Analysis of MRI patterns aids prediction of progression in X-linked adrenoleukodystrophy.** *Neurology* 2003;61:369–74 CrossRef Medline
- Loes DJ, Hite S, Moser H, et al. **Adrenoleukodystrophy: a scoring method for brain MR observations.** *AJNR Am J Neuroradiol* 1994;15:1761–66 Medline
- Peters C, Charnas LR, Tan Y, et al. **Cerebral X-linked adrenoleukodystrophy: the international hematopoietic cell transplantation experience from 1982 to 1999.** *Blood* 2004;104:881–88 CrossRef Medline
- Moser HW, Raymond GV, Koehler W, et al. **Evaluation of the preventive effect of glyceryl trioleate-trierucate (“Lorenzo’s oil”) therapy in X-linked adrenoleukodystrophy: results of two concurrent trials.** *Adv Exp Med Biol* 2003;544:369–87 CrossRef Medline
- Miller WP, Rothman SM, Nascene D, et al. **Outcomes after allogeneic hematopoietic cell transplantation for childhood cerebral adrenoleukodystrophy: the largest single-institution cohort report.** *Blood* 2011;118:1971–78 CrossRef Medline
- Appelbaum FR, Thomas E. *Thomas’ Hematopoietic Cell Transplantation: Stem Cell Transplantation.* Oxford: Wiley-Blackwell; 2009
- Orchard PJ, Lund T, Miller W, et al. **Chitotriosidase as a biomarker of cerebral adrenoleukodystrophy.** *J Neuroinflammation* 2011;8:144 CrossRef Medline
- Fleiss JL, Levin B, Paik MC. *Statistical Methods for Rates and Proportions.* New York: John Wiley & Sons; 2003

Treatment of 213 Patients with Symptomatic Tarlov Cysts by CT-Guided Percutaneous Injection of Fibrin Sealant

K. Murphy, A.L. Oaklander, G. Elias, S. Kathuria, and D.M. Long



ABSTRACT

BACKGROUND AND PURPOSE: There has been a steady progression of case reports and a small surgical series that report successful surgical treatment of Tarlov cysts with concomitant relief of patients' symptoms and improvement in their neurological dysfunction, yet patients are still told that these lesions are asymptomatic by physicians. The purpose of this study was to analyze the efficacy and safety of intervention in 213 consecutive patients with symptomatic Tarlov cysts treated by CT-guided 2-needle cyst aspiration and fibrin sealing.

MATERIALS AND METHODS: This study was designed to assess outcomes in patients who underwent CT-guided aspiration and injection of ≥ 1 sacral Tarlov cyst at Johns Hopkins Hospital between 2003 and 2013. In all, 289 cysts were treated in 213 consecutive patients. All these patients were followed for at least 6 months, 90% were followed for 1 year, and 83% were followed for 3–6 years. The aspiration-injection procedure used 2 needles and was performed with the patients under local anesthesia and intravenous anesthesia. In the fibrin-injection stage of the procedure, a commercially available fibrin sealant was injected into the cyst through the deep needle (Tisseel VH).

RESULTS: One year postprocedure, excellent results were obtained in 104 patients (54.2% of patients followed), and good or satisfactory results were obtained in 53 patients (27.6%). Thus, 157 patients (81.8%) in all were initially satisfied with the outcome of treatment. At 3–6 years postprocedure, 74.0% of patients followed were satisfied with treatment. There were no clinically significant complications.

CONCLUSIONS: The aspiration-injection technique described herein constitutes a safe and efficacious treatment option that holds promise for relieving cyst-related symptoms in many patients with very little risk.

ABBREVIATION: TC = Tarlov cyst

Perineurial Tarlov cysts (TC) are extrathecal CSF-filled cavities in the perineurial recesses around dorsal spinal nerve roots. Composed of vascularized connective tissue lined with flattened arachnoid tissue, TCs characteristically contain nerve root fibers and ganglion cells in their walls or cavities and tend to be sacral.^{1,2} They are also notable for their restricted connection to the subarachnoid space and thus exhibit delayed filling during spinal myelography.¹ The initial characterization

of these structures was cadaveric anatomic variants of unknown clinical significance^{3,4}; the neurosurgeon I.M. Tarlov recognized TCs in patients and established that some cause neurologic symptoms that can be cured neurosurgically.^{5–10} His 1953 monograph detailed their pathology, including compression and distortion of local nerves and hemorrhage.¹⁰ Ensuing work has established that TCs can cause axial sacrococcygeal pain; intrathecal hypotension; perineal pain; sensory loss; and bladder, bowel, and sexual dysfunction.^{11–13} Radicular symptoms have also been recognized,¹⁴ as have electrophysiologic correlates¹² and links to collagen dysfunction (eg, Ehlers-Danlos and Marfan syndromes).^{15,16}

Diagnosis preferentially begins with dedicated sacral MR imaging, which is more sensitive than CT or standard lumbosacral MR imaging.¹⁷ TCs are visualized (but not always reported) on 1%–2% of sacral MRIs, with approximately 25% of these believed to cause symptoms.¹⁸ It is often necessary to evaluate subarachnoid connectivity with myelography to distinguish TCs from intradural ectasias, subarachnoid cysts, and meningeal diverticula—cystic abnormalities that are frequently confused with TCs and for

Received February 22, 2015; accepted after revision June 13.

From the Department of Radiology (K.M., G.E.), University of Toronto, Toronto, Ontario, Canada; Departments of Neurology (A.L.O.) and Pathology (Neuropathology) (A.L.O.), Massachusetts General Hospital, Harvard Medical School, Boston, Massachusetts; Russell H Morgan Department of Radiology and Radiological Science (S.K.), Johns Hopkins Hospital, Baltimore Maryland; and Neuroscience Consults (D.M.L.), Lutherville, Maryland.

This work was supported in part by research grants from the US Public Health Service (NIH K24NS9892).

Please address correspondence to Kieran Murphy, MB, FRCPC, FSIR, Department of Radiology, Room 3 mc 424, Toronto Western Hospital, 399 Bathurst St, Toronto, ON, Canada M5T 2S8; e-mail: Kieran.murphy@uhn.ca

Indicates open access to non-subscribers at www.ajnr.org

<http://dx.doi.org/10.3174/ajnr.A4517>

which intracystic injection is contraindicated to avoid intrathecal spread and arachnoiditis.

Despite misimpressions in many clinical circles that TCs are always asymptomatic, there has been steady progress in developing the interventional treatments required for definitive management of symptoms. Conservative approaches including analgesic/anti-inflammatory medication and physical therapy have achieved varying degrees of success in reducing cyst-associated symptoms.¹⁹ Surgical methods, meanwhile, include lumbar-peritoneal and cystosubarachnoidal drainage and shunting^{20,21}; bipolar cautery to shrink cysts¹⁷; decompressive laminectomy²²⁻²⁴; and laminectomy with either total cyst resection,^{1,10,25,26} partial cyst wall resection,²⁷ or duroplasty/plication of cyst walls.²⁸ Despite standard limitations such as malfunction and infection after shunting, persistence of pain after laminectomy, and radicular deficits after ablative procedures, a prior review found that 88.6% of patients in the studies evaluated were satisfactorily relieved by surgery according to the outcome criteria of each report.¹⁴ Microsurgical techniques, such as laminectomies with electrophysiology-guided cyst wall fenestration/imbrication and myofascial flap repair and closure, are also used, and while these are potentially less effective, they appear to cause fewer adverse events and preserve neural tissue better.²⁹⁻³²

Minimally invasive percutaneous techniques have also emerged. In 1994, Paulsen et al¹³ reported immediate symptom relief lasting up to 3 months after single-needle aspiration of symptomatic TCs in 5 patients. Lee et al³³ then described using a patient's temporary response to cyst aspiration as a diagnostic maneuver to select candidates for surgery. In 1997, Patel et al³⁴ first described injecting autologous fibrin glue into aspirated cysts. Four of 4 patients exhibited marked improvement without recurrence during 23 months, with 1 achieving lasting relief. They postulated that fibrin deposition on cyst walls would impede CSF ingress, trigger fibrosis, and, ideally, promote cyst contracture. Zhang et al³⁵ subsequently reported that 100% of 31 patients treated with intracystic fibrin glue injection achieved satisfactory relief without recurrence during 28 months of follow-up. This methodology was further refined by the development by Murphy et al³⁶ of the 2-needle technique evaluated in this report. Maintaining an equilibrium of intracystic pressure during aspiration-injection, this procedure reduced pressure-related procedural radicular pain sometimes noted with the single-needle technique and perhaps improved fibrin sealant filling.

MATERIALS AND METHODS

Study Design

This study, initiated in 2003 after receiving institutional approval, assessed outcomes in all patients who underwent CT-guided 2-needle aspiration-injection of ≥ 1 symptomatic sacral TC at Johns Hopkins Hospital between 2003 and 2012. Assessments were repeated at 3 months postprocedure, 1 year postprocedure, and yearly thereafter.

Patient Selection

The study cohort was drawn from patients referred with apparently symptomatic sacral TCs. Although 6 patients were treated for cervical, thoracic, or lumbar TCs, these are not discussed here because they were too few to satisfactorily analyze. Referred pa-

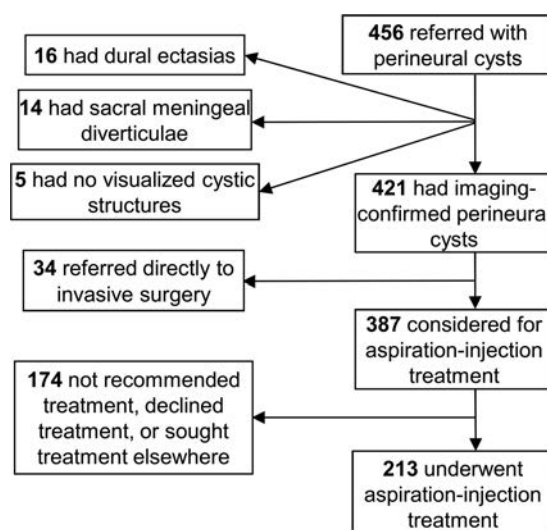


FIG 1. Patient recruitment flowchart for aspiration-injection therapy.

tients were vetted for inclusion as illustrated in Fig 1. First, a diagnosis of TC was confirmed by scanning all patients with lumbar and sacral MR imaging to identify, characterize, and localize any cystic structures present. All studies were read independently by both an interventional neuroradiologist and a participating neurosurgeon. TCs were identified according to the classification criteria of Goyal et al² and Wilkins.³⁷ Patients in whom MR imaging inadequately defined subarachnoid connectivity underwent myelography to assess the rapidity of contrast spread into the cyst, and only those without significant connectivity (ie, those with slowly filling cysts) were considered for inclusion.

Depending on the seriousness of their condition and their willingness to enter the study, patients with imaging-confirmed sacral TCs were either referred to invasive surgery or considered for aspiration-injection treatment. Those who remained in consideration underwent further examination and testing to determine whether their symptoms could be attributed to visualized cysts (ie, whether their TCs were symptomatic). Confirmation of symptomatic cysts required that axial pain be in the immediate anatomic vicinity of the cyst, that radicular symptoms and signs occur only in the appropriate distribution of cyst-bearing segments, and that other potential pain generators be excluded by imaging or other diagnostic testing. Additionally, 104 patients in whom the symptoms of cysts were particularly uncertain underwent diagnostic sacral blockade of cyst-bearing roots; this was performed in the standard fashion through the most convenient posterior sensory foramen and used fluoroscopic or CT guidance to place a needle on the cyst-bearing root, superior to the cyst, and near the next root above. Pain relief commensurate with the agent used and lack of pain relief with control blocks were required for attribution of symptoms to the blocked cyst.

Exclusion Criteria. All patients with cystic abnormalities other than perineural cysts and patients with cysts possessing considerable (wide-neck) direct communication with the subarachnoid space were rejected. Patients who lacked the ability to communicate in English; had the probability of inadequate follow-up (eg, those who lived outside North America); had any *Diagnostic and Statistical Manual of Mental Disorders* diagnosis; had unexplained

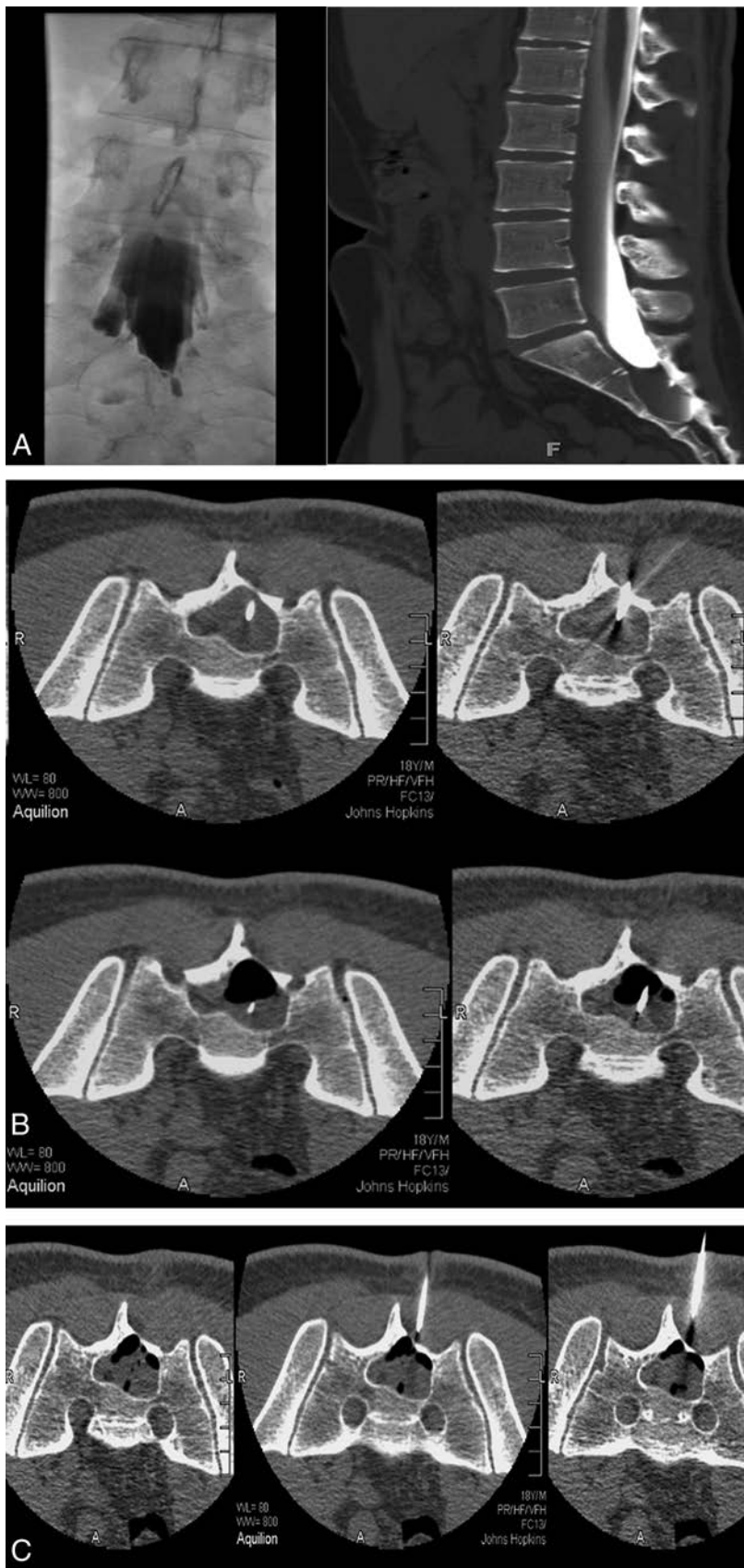


FIG 2. A, CT myelogram and myelogram showing minimal filling of a large right S2 Tarlov cyst with a narrow neck. There is significant remodelling of S2 and S3. B, With 18-ga spinal needles in place, one deeper than the other, partial aspiration has developed an air-fluid level. C, Injection of fibrin fills the cyst 80%. The volume of fibrin injected is close to the volume of CSF aspirated.

symptoms that were not clearly related to cyst-bearing roots or (as assessed by a neurosurgery nurse practitioner) the presence of ≥ 2 Waddell signs (to exclude patients whose pain may have considerable nonorganic components); and patients with any other probable identified pain generator besides TCs were also all rejected for treatment.

Physical Examination

All patients were seen by an experienced nurse practitioner who obtained a typical neurosurgical history with review of systems and medical history. All patients were also seen by a neurosurgeon and underwent history, physical evaluation of the spine, and neurologic evaluation, focusing on the symptomatic area of the spine. In addition, all patients underwent a detailed history and physical evaluation of the territories supplied by cyst-bearing nerve roots. All patients with pelvic, abdominal, or genital symptoms were also seen by a gynecologist and/or urologist. Urodynamics were obtained if recommended by the urologist.

Pain and function were evaluated by the Lumbar Spine Outcomes Questionnaire scale, a validated outcome measure in spinal disease that permits quantification of pain and neurologic loss (including bowel, bladder, or sexual dysfunction) and can be administered satisfactorily by telephone.³⁸ In addition to the severity measures, pain was also described in terms of its spatial and temporal characteristics, with aggravating and alleviating factors taken into account.

Treatment

All patients had a detailed discussion of treatment options including no treatment, pharmacologic pain management, invasive surgery, and aspiration-injection. That aspiration-injection was a new and novel technique was emphasized. All patients were given written material explaining these points in accordance with institutional review board guidelines. Patients who elected the aspiration-injection procedure were seen by the interventional neuroradiologist and were engaged in a second discussion of the procedure and its risks and benefits.

Method of Aspiration-Injection

All patients included in our cohort were treated by using the aspiration-injection technique previously described by Murphy et al.³⁶ Briefly, aspiration was preceded by performance of diagnostic CT (Aquilion 16-detector row multidetector CT unit; Toshiba Medical Systems, Tokyo, Japan) to select the level providing access to the cyst through the thinnest overlying bone. Sedation was induced intravenously. The back was prepared in the usual sterile fashion, with local anesthesia infiltrated into the skin, fat, muscles, and periosteum overlying the sacrum. Two 18-ga needles were advanced into the cyst with CT fluoroscopy (13 frames per second, 3 adjacent 2-, 4-, and 2-mm sections) (Fig 2). The tip of the first needle was typically placed deep in the cyst, while the second was placed more superficially. The stylets were removed from both needles, and fluid was aspirated via the deeper needle. The more superficial needle served as a venting tube during the aspiration process, allowing air to enter the cyst. Following aspiration, an air-fluid level developed; this was monitored intermittently with CT fluoroscopy for evidence of rapid cyst refilling, which would indicate a connection to the thecal sac. (We avoided using iodinated contrast agents to monitor cyst fluid levels because these fill up the cyst, complicate fibrin injection, and impair fibrin binding while providing no appreciable additional information compared with air-fluid levels). A commercially available fibrin sealant composed of human/bovine fibrin, fibrinolysis inhibitor, thrombin, and calcium chloride was next injected into the cyst through the deep needle (Tisseel VH; Baxter Healthcare, Deerfield, Illinois).

Following our observation that completely filling cysts with sealant often temporarily exacerbated postprocedural radicular pain (likely due to swelling sealant compressing the affected nerve root or nearby nociceptors), we adjusted the technique so that sealant injection was halted when CT fluoroscopy indicated that the cavity was approximately 75% full rather than 100% full. This step was found to address the postoperative pain issue without compromising efficacy. Both needles were then withdrawn, and the puncture sites were covered with an antibiotic ointment and a sterile dressing. Patients were observed for 2 hours after the completion of the procedure before being discharged. They were asked to stay locally for 1 night and were permitted to return to their normal physical activity immediately but were advised not to undertake strenuous physical exercise for 2–3 weeks. If multiple cysts were present, typically only 2 were treated per session, so some patients returned for repeat sessions.

Outcome Assessments

Outcomes were evaluated in the clinic or by telephone at 1 day and at 6 and 12 weeks postprocedure by an experienced nurse practitioner or a neurosurgeon. Lumbar sacral MR imaging was repeated at 12 weeks and 1 year postprocedure. Subsequent yearly MRIs were recommended but not required. The primary outcomes, pain and function, were assessed by using the Lumbar Spine Outcomes Questionnaire. An “excellent” outcome required complete pain relief according to the Lumbar Spine Outcomes Questionnaire scale, discontinuation of all pain medications and treatments, and improvement or stabilization of other cyst-linked neurologic signs and symptoms so that no further treatments were required. Patients also had to report satisfaction with the

Table 1: Imaging findings

Findings	No. of Patients
Position/No. of root nerves involved	
Unilateral, single root	113
Bilateral, single root	78
Bilateral, ≥ 2 roots	22
Nerve root localization	
L4	1
L5	1
S1	16
S2	142
S3	120
S4–S5	9
Aspirated cyst size, cm	
1–2	1
2–3	111
3–4	32
>4	8

outcome of their procedure and willingness to undergo it again for the same result. A “good/satisfactory” outcome required pain to have “improved quite a bit” on the Lumbar Spine Outcomes Questionnaire scale plus discontinuation of narcotic analgesics. Neurologic deficits had to be commensurate with adequate function or no further progression. Patients also had to be satisfied with the results and not seeking further treatment. All outcomes other than “excellent” or “good/satisfactory” were reported as treatment failures even if some improvement was noted.

RESULTS

The 213 patients described in this article had all been followed for at least 6 months by the time of submission, with 192 (90.1%) of these patients having been followed for 1 year and 177 (83.1%) having been followed for between 3 and 6 years.

Characterization of Cysts

Overall, the 213 patients treated had 289 cysts among them. One hundred forty-four patients had unilateral cysts and symptoms, and 69 patients had bilateral cysts. Multiple cysts ranged from 2 to 9, and the average was 3 for each patient in whom multiple cysts were treated bilaterally. Nine patients had S4 or S5 cysts, but none were symptomatic in isolation. These imaging findings are summarized in Table 1.

Neurologic Symptoms and Signs

Local pain in the region of the cyst that was aggravated by sitting down was the most common symptom in our cohort, though S1, S2 sciatica and neuropathy were also prevalent. Patients with isolated S2 root cysts and no evidence of S1 nerve root compression characteristically had sciatica proceeding no further than the medial heel and immediately adjacent sole. Additionally, many patients had generalized sacral and/or lumbar pain; pelvic and/or perineal pain; and sexual, bladder, or bowel dysfunctions. Common bladder symptoms included incontinence, urinary frequency or urgency, and an inability to fully empty the bladder, while bowel dysfunction tended to involve urgency or mild incontinence. The most common physical neurologic abnormality observed in our patients was an absent ankle reflex. Weakness of plantar flexion was also prevalent, as were cyst-related sensory

Table 2: Neurologic symptoms and signs

Symptom/Sign	No. of Presenting Patients
Local pain	210
L4, L5 neuropathy	2
S1, S2 sciatica	151
S1, S2 neuropathy	137
Generalized sacral/lumbar pain	189
Pelvic/perineal pain	209
Bladder dysfunction	92
Sexual dysfunction	92
Bowel dysfunction	62
Absent Achilles reflex	130
Weakness of plantar flexion	87
Paralysis of plantar flexion	2
Paralysis of dorsiflexion	2
Rectal sphincter tone reduction	61
Bladder sphincter impairment	92
Cyst-related sensory loss	
L4	1
L5	1
S1	16
S2	137
S3, S4, S5	97

loss, reduced rectal sphincter tone, and bladder sphincter impairment. Sensory loss most frequently occurred in the perineal region and usually comanifested with perineal pain. Two patients with cysts that compressed the L5 nerve root exhibited weakness of dorsiflexion and complete footdrop. Table 2 summarizes the presenting signs and symptoms in treated patients.

Aspiration-Injection Outcome

At 1 year postprocedure, “excellent” results had been obtained in 104 patients (54.2%), and “good/satisfactory” results had been obtained in 53 patients (27.6%). Thus, 157 patients (81.8%) in all were initially satisfied with the outcome of treatment. In 7 of the patients who were not satisfactorily treated, the aspiration-injection procedure was not technically feasible. In the remainder, the intervention was performed but failed to yield satisfactory results at 1 year postprocedure.

During the 3- to 6-year follow-up, “excellent” results were obtained in 106 patients (59.9%). This outcome represented an increase from the equivalent statistic at 1 year; all those patients who were classified as having excellent results at 1 year maintained this status into the latter follow-up period, and an additional 2 patients in the “good/satisfactory” category at 1 year now qualified as having excellent results. Twenty-five patients (14.1%) now rated their outcome as “good/satisfactory,” a decline from the number that did so at 1 year. Overall, 131 patients (74.0%) were satisfied with treatment at 3- to 6-year follow-up. Only 2 patients have reported recurrence of symptoms after >6 years.

Table 3 presents a breakdown of the aspiration-injection therapy outcomes with respect to individual signs and symptoms.

Re-Aspiration

Twenty-three patients (10.8% of the treated cohort) underwent re-aspiration within the first 6 months due to recurrent symptoms after immediate short-term relief. Thirteen patients (6.1% of the treated cohort) underwent re-aspiration after 6 months. Two of

Table 3: Outcome of aspiration-injection therapy

Symptom/Sign	Outcome		
	Excellent	Good	Unchanged
Local pain	87 (41.4%)	72 (34.3%)	51 (24.3%)
Sciatica/neuropathy	81 (53.6%)	32 (21.2%)	38 (25.2%)
Perineal pain/sensory loss	86 (41.4%)	70 (33.5%)	53 (25.4%)
Bladder/sexual dysfunction	30 (32.6%)	38 (41.3%)	24 (26.1%)
Bowel dysfunction	22 (35.5%)	23 (37.1%)	17 (27.4%)
Plantar flexion weakness	44 (50.6%)	20 (23.0%)	23 (26.4%)
Plantar flexion paralysis	0 (0%)	0 (0%)	2 (100%)
Dorsiflexion paralysis	0 (0%)	0 (0%)	2 (100%)
Rectal sphincter reduction	22 (36.1%)	23 (37.7%)	16 (26.2%)

these had the procedure between 6 and 12 months after the initial aspiration. In 7, re-aspiration was undertaken after the first year, and in 3, after 2 years. One re-aspiration failed, but all the others conferred satisfactory relief again. One patient underwent 3 re-aspirations for recurrent symptoms at 2-year intervals. Repeat MR imaging demonstrated fluid-filled cysts in all patients who underwent re-aspiration, indicating cyst reaccumulation following the initial procedure.

Complications

There were no documented infections or nerve injuries in the treated cohort. One patient had a mild nonspecific allergic reaction with systemic hives, which led to overnight hospitalization as a precaution, but they resolved without incident. Three patients appeared to experience elevated inflammation; all inflammation resolved without treatment during 2–4 weeks, however.

Seven patients had symptoms of spinal fluid leak and required a postprocedure blood patch for control. Twenty patients had increased sciatica following the procedure, which resolved within <3 months. One patient had increased sciatica that persisted for >3 months but eventually resolved. Seven patients had severely increased local pain; this resolved in 6 of these patients within 3 months. Three patients described an increase in all symptoms, including bowel and bladder dysfunction, immediately following injection, though all were transient and resolved within 3 months. There was no incidence of aseptic meningitis.

Surgical Outcome

Patients who had been referred for surgery initially and 11 patients who failed aspiration and were subsequently referred for surgery were followed on the same schedule used for patients undergoing aspiration. Of the initial 34 patients referred for surgery, 31 (91.2%) achieved excellent or satisfactory relief and were satisfied with their surgical outcome. The remaining 3 patients underwent surgery that proved to be partially successful, but they continued to have symptoms afterward. Nonetheless, no worsening of patients’ conditions or significant increases in neurologic deficits resulted from surgery in these cases. Of the 11 patients who failed aspiration and were referred to surgery, all had successful relief of symptoms.

DISCUSSION

Contrary to popular sentiments in the medical community, current data indicate that at least some TCs are symptomatic. Beyond the simple correlational finding that a consistent set of symptoms

is associated with certain cysts, perhaps the strongest evidence for this position is the well-documented effectiveness of surgical treatment of apparently symptomatic cysts. Since Tarlov described the successful resection of symptomatic perineurial cysts in 1953,¹⁰ there has been a steady progression of case reports and small surgical series that reported successful surgical treatment of such cysts with concomitant relief of patient symptoms and improvement in their neurologic dysfunction.¹⁹⁻³² If one accepts the authors' criteria for success, collation of the outcomes of these studies indicates that 88.6% of patients were satisfactorily relieved of symptoms with relatively low morbidity and mortality (no deaths or serious neurologic worsening were reported). Similarly, this study found that 91.2% of the 34 patients referred directly for surgical obliteration (as opposed to aspiration-injection treatment) of their cysts achieved excellent or satisfactory outcomes, while the remainder reported at least some improvement and had no worsening of symptoms or neurologic signs. Relief of symptoms and signs following treatment has long been used in neurosurgery to justify attribution of both to specific pathology; the success of herniated disc excision and decompression of spinal stenosis, for instance, has (supported by excellent clinical research data) helped cement symptomatic attribution to their respective pathologies. As such, this body of evidence strongly supports the contentions that some TCs are symptomatic and that these symptoms can be relieved by surgical intervention.

Such a position is also bolstered by the favorable results obtained by several studies^{13,33-37} that treated symptomatic TCs with variants of the aspiration-injection technique, including the current article. Moreover, we believe that our data help justify the image-guided aspiration of probable symptomatic cysts and their injection with fibrin sealant as a less-invasive alternative treatment to surgical measures. The initial and long-term success rates for this technique are high enough to hold promise for its adoption as an adequate and efficacious therapy option, with 81.8% of treated patients satisfied with the intervention in terms of its effects on their symptoms at 1 year postprocedure and 74.0% satisfied at 3- to 6-year follow-up. Additionally, our data indicate that aspiration-injection treatment is associated with low morbidity and adverse events: No instances of neurologic injury occurred among those treated in our cohort, and only 8 patients had minor complications (all of which resolved without need for further operations). Only 4 patients reported worsened pain following the procedure but 2 of these recovered shortly afterward and a third was lost to follow-up.

Of special note is the utter lack of instances of postprocedural aseptic meningitis (reported by Patel et al³⁴ to have occurred in 75% of patients) in our series; we surmise this may be because we treated only narrow-neck cysts, thus avoiding fibrin reflux into the thecal sac and subarachnoid space. That all of the 11 patients who failed aspiration treatment were subsequently successfully treated with surgery also indicates that the former procedure does not reduce the chance or extent of success for the latter; this indication reinforces the potential of aspiration-injection as a useful first-option treatment for TC.

The simple discovery of a cyst does not justify attribution of the symptoms to that cyst, but cysts of <10 mm have, in our experience, occasionally been symptomatic. Attribution should

be based on the location of the cyst and the ability of these factors to explain (via likely effects on cyst-bearing or neighboring nerve roots) local pain and associated signs and symptoms, as well as temporary relief of symptoms with controlled diagnostic blockade of cyst-bearing nerve roots and the absence of another plausible generator to explain pain and other signs or symptoms. One should not overstate the prevalence of symptomatic Tarlov cysts, especially the prevalence of symptomatic Tarlov cysts that require surgical or percutaneous intervention. In this study, a considerable proportion of patients of the larger group of referred patients were found to be adequately managed by pharmacologic means alone without significant evidence of progression.

Why are these cysts symptomatic in the first place? Certainly, the pathologic changes associated with perineurial cysts are rather striking: Nerves within the cyst-bearing dorsal nerve roots, structures notoriously sensitive to compression, may be distorted, compressed, and injured by the bulging cyst, and adjacent nerves are often also compressed.^{1,10} Given that afferent nerves populate this area, one may make a direct link between such pathologic changes and the (not infrequently) accompanying radicular symptoms, such as neuropathic pain, paresthesias, and sensory loss/neurophysiologic abnormalities. Additionally, cyst pressure is known to be great enough to erode sacral bone and has been hypothesized to sensitize dural and/or periosteal nociceptors.^{10,39} It is possible that this second mechanism is primarily responsible for the local, nociceptive pain that often characterizes symptomatic cysts. Meanwhile, the worsening of both radicular and local symptoms with time could be attributed to the gradual enlargement that some cysts may undergo.^{1,17}

Finally, one should wonder why the fibrin sealant used in the aspiration-injection procedure would be effective in treating symptomatic TCs for the long-term, because the compound is slowly absorbed in the body so that permanent cyst obliteration would not occur. Our underlying hypothesis (shared by Patel et al³⁴) was that the injection of sealant into the cyst would thicken the wall of the cyst via fibrosis and block the 1-way valve at the neck of the cyst, reducing the entry of spinal fluid (and thereby preventing the cyst from distending and compressing local nerves or stimulating nearby nociceptors). This hypothesis remains unproven from these data. Still, some support exists for such a position. In the case of subsequent neurosurgical procedure after the injection of fibrin sealant, the formation of a thin impermeable membrane is reported to be evident in the operative site.

CONCLUSIONS

Despite widespread belief to the contrary, it has been known for some 70 years that perineurial cysts are sometimes symptomatic and that associated symptoms and signs may be relieved by successful treatment of the troublesome cyst. Surgical methods are effective but are often complicated by infection, postoperative CSF leak, or damage to neural tissue; these make them an imperfect first-option treatment and suggest the need for a percutaneous image-guided approach. The aspiration-injection technique described herein constitutes a safe and efficacious treatment option, and one that holds promise for relieving cyst-related symptoms in many patients with very small risk.

Disclosures: Donlin M. Long—UNRELATED: Consultancy: SKK Corp, Comments: consulting related to lumbar disc herniation treatment; Expert Testimony: medico-legal consultant for medical malpractice and personal injury.

REFERENCES

1. Tarlov IM. **Spinal perineurial and meningeal cysts.** *J Neurol Neurosurg Psychiatry* 1970;33:833–43 CrossRef Medline
2. Goyal RN, Russell NA, Benoit BG, et al. **Intraspinal cysts: a classification and literature review.** *Spine (Phila Pa 1976)* 1987;12:209–13 CrossRef Medline
3. Rexed B. **Arachnoidal proliferations with cyst formation in human spinal nerve roots at their entry into the intervertebral foramina: preliminary report.** *J Neurosurg* 1947;4:414–21 CrossRef Medline
4. Tarlov IM. **Perineurial cysts of the spinal nerve roots.** *Arch Neurol Psychiatry* 1938;40:1067–74 CrossRef
5. Tarlov IM. **Cysts (perineurial) of the sacral roots: another cause (removable) of sciatic pain.** *J Am Med Assoc* 1948;138:740–44 CrossRef Medline
6. Tarlov IM. **Cysts of the sacral nerve roots: clinical significance and pathogenesis.** *AMA Arch Neurol Psychiatry* 1952;68:94–108 CrossRef Medline
7. Tarlov IM. **Cysts (perineurial) of the sacral nerve roots: another cause of the sciatic or sacral cauda equina syndrome.** *J Neuropathol Exp Neurol* 1952;11:88–89 Medline
8. Tarlov IM. **Cysts of sacral nerve roots: pathogenesis and clinical significance.** *AMA Arch Neurol Psychiatry* 1953;69:391–92 Medline
9. Tarlov IM. **Sacral nerve-root cysts: pathogenesis and clinical significance.** *J Nerv Ment Dis* 1953;117:156–57 CrossRef Medline
10. Tarlov IM. *Sacral Nerve-Root Cysts: Another Cause of the Sciatic or Cauda Equina Syndrome.* Springfield: Charles C. Thomas; 1953
11. Abbott KH, Leimbach WH, Retter RH. **The role of perineurial sacral cysts in the sciatic and sacrococcygeal syndromes: a review of the literature and report of 9 cases.** *J Neurosurg* 1957;14:5–21 CrossRef Medline
12. Cattaneo L, Pavesi G, Mancina D. **Sural nerve abnormalities in sacral perineurial (Tarlov) cysts.** *J Neurol* 2001;248:623–24 CrossRef Medline
13. Paulsen RD, Call GA, Murtagh FR. **Prevalence and percutaneous drainage of cysts of the sacral nerve root sheath (Tarlov cysts).** *AJNR Am J Neuroradiol* 1994;15:293–97; discussion 298–99 Medline
14. Oaklander AL, Long DM, Larvie M, et al. **Case records of the Massachusetts General Hospital: Case 7–2013—a 77-year-old woman with long-standing unilateral thoracic pain and incontinence.** *N Engl J Med* 2013;368:853–61 CrossRef Medline
15. Isono M, Hori S, Konishi Y, et al. **Ehlers-Danlos syndrome associated with multiple spinal meningeal cysts: case report.** *Neurol Med Chir (Tokyo)* 1999;39:380–83 CrossRef
16. Doi H, Sakurai S, Ida M, et al. **A case of sacral meningeal cyst with Marfan syndrome [in Japanese].** *No Shinkei Geka* 1999;27:847–50 Medline
17. Rodziewicz GS, Kaufman B, Spetzler RF. **Diagnosis of sacral perineurial cysts by nuclear magnetic resonance.** *Surg Neurol* 1984; 22:50–52 CrossRef Medline
18. Langdown AJ, Grundy JR, Birch NC. **The clinical relevance of Tarlov cysts.** *J Spinal Disord Tech* 2005;18:29–33 CrossRef Medline
19. Hiers RH, Long D, North RB, et al. **Hiding in plain sight: a case of Tarlov perineurial cysts.** *J Pain* 2010;11:833–37 CrossRef Medline
20. Bartels RH, van Overbeeke JJ. **Lumbar cerebrospinal fluid drainage for symptomatic sacral nerve root cysts: an adjuvant diagnostic procedure and/or alternative treatment? Technical case report.** *Neurosurgery* 1997;40:861–64; discussion 864–65 CrossRef Medline
21. Morio Y, Nanjo Y, Nagashima H, et al. **Sacral cyst managed with cyst-subarachnoid shunt: a technical case report.** *Spine* 2001;26: 451–53 CrossRef Medline
22. Siqueira EB, Schaffer L, Kranzler LI, et al. **CT characteristics of sacral perineurial cysts: report of two cases.** *J Neurosurg* 1984;61:596–98 CrossRef Medline
23. Sá MC, Sá RC. **Tarlov cysts: report of four cases [in Portuguese].** *Arq Neuropsiquiatr* 2004;62:689–94 CrossRef Medline
24. Tanaka M, Nakahara S, Ito Y, et al. **Surgical results of sacral perineurial (Tarlov) cysts.** *Acta Med Okayama* 2006;60:65–70 Medline
25. Nishiura I, Koyama T, Handa J. **Intrasacral perineurial cyst.** *Surg Neurol* 1985;23:265–69 CrossRef Medline
26. Voyadzis JM, Bhargava P, Henderson FC. **Tarlov cysts: a study of 10 cases with review of the literature.** *J Neurosurg* 2001;95:25–32 Medline
27. Strully KJ, Heiser S. **Lumbar and sacral cysts of meningeal origin.** *Radiology* 1954;62:544–49 CrossRef Medline
28. Yücesoy KK, Naderi S, Ozer H, et al. **Surgical treatment of sacral perineurial cysts: a case report.** *Kobe J Med Sci* 1999;45:245–50 Medline
29. Mummaneni PV, Pitts LH, McCormack BM, et al. **Microsurgical treatment of symptomatic sacral Tarlov cysts.** *Neurosurgery* 2000; 47:74–78; discussion 78–79 CrossRef Medline
30. Guo D, Shu K, Chen R, et al. **Microsurgical treatment of symptomatic sacral perineurial cysts.** *Neurosurgery* 2007;60:1059–65; discussion 1065–66 CrossRef Medline
31. Rasmussen MM, Clemmensen D, Karabegovic S, et al. **A novel microsurgical method for the treatment of spinal nerve root cysts.** *Dan Med J* 2012;59:A4539 Medline
32. Caspar W, Papavero L, Nabhan A, et al. **Microsurgical excision of symptomatic sacral perineurial cysts: a study of 15 cases.** *Surg Neurol* 2003;59:101–05; discussion 105–06 CrossRef Medline
33. Lee JY, Impekoven P, Stenzel W, et al. **CT-guided percutaneous aspiration of Tarlov cyst as a useful diagnostic procedure prior to operative intervention.** *Acta Neurochir (Wien)* 2004;146:667–70 CrossRef Medline
34. Patel MR, Louie W, Rachlin J. **Percutaneous fibrin glue therapy of meningeal cysts of the sacral spine.** *AJR Am J Roentgenol* 1997;168: 367–70 CrossRef Medline
35. Zhang T, Li Z, Gong W, et al. **Percutaneous fibrin glue therapy for meningeal cysts of the sacral spine with or without aspiration of the cerebrospinal fluid.** *J Neurosurg Spine* 2007;7:145–50 CrossRef Medline
36. Murphy K, Wyse G, Schnupp S, et al. **Two-needle technique for the treatment of symptomatic Tarlov cysts.** *J Vasc Interv Radiol* 2008;19: 771–73 CrossRef Medline
37. Wilkins RH. **Intraspinal cysts.** In: Wilkins RH, Rengachary SS, eds. *Neurosurgery.* New York: McGraw-Hill; 1985:2061–70
38. Bendebba M, Dizerega GS, Long DM. **The Lumbar Spine Outcomes Questionnaire: its development and psychometric properties.** *Spine J* 2007;7:118–32 CrossRef Medline
39. Dastur HM. **The radiological appearances of spinal extradural arachnoid cysts.** *J Neurol Neurosurg Psychiatry* 1963;26:231–35 CrossRef Medline

Clinical Outcomes of Patients with Delayed Diagnosis of Spinal Dural Arteriovenous Fistulas

W. Brinjikji, D.M. Nasr, J.M. Morris, A.A. Rabinstein, and G. Lanzino

ABSTRACT

BACKGROUND AND PURPOSE: Spinal dural arteriovenous fistulas are commonly missed on imaging or misdiagnosed as inflammatory or neoplastic processes. We reviewed a consecutive series of spinal dural arteriovenous fistulas referred to our institution that were missed or misdiagnosed on initial imaging and studied the clinical consequences of missing or misdiagnosing the lesion.

MATERIALS AND METHODS: We reviewed spinal dural arteriovenous fistulas diagnosed at our institution between January 1, 2000, and November 1, 2014. A lesion was defined as “misdiagnosed” if initial MR imaging or CT myelography demonstrated characteristic imaging features of spinal dural arteriovenous fistula but the patient was clinically or radiologically misdiagnosed. Outcomes included length of delay of diagnosis, increased disability (increase in mRS or Aminoff motor disability of ≥ 1 point) between initial imaging evaluation and diagnosis date, and posttreatment disability.

RESULTS: Fifty-three consecutive spinal dural arteriovenous fistulas that were initially misdiagnosed despite having characteristic imaging findings on MR imaging or CT myelography were included in our study. Eight patients (18.9%) underwent spinal angiography before referral, which was interpreted as having negative findings but was either incomplete (6 cases) or retrospectively demonstrated the spinal dural arteriovenous fistulas (2 cases). The median time of delayed diagnosis was 6 months (interquartile range, 2–14 months). Fifty-one patients (96.2%) had increased disability between the initial study, which demonstrated features of a spinal dural arteriovenous fistula, and diagnosis. Thirty-two patients (60.4%) developed a new requirement for a walker or wheelchair. Following treatment, 21 patients (41.2%) had an improvement of 1 point on the mRS or Aminoff motor disability scale.

CONCLUSIONS: Delayed diagnosis of spinal dural arteriovenous fistula with characteristic imaging features results in high rates of additional disability that are often irreversible despite surgical or endovascular treatment of the fistula.

ABBREVIATION: SDAVF = spinal dural arteriovenous fistula

Spinal dural arteriovenous fistulas (SDAVFs) are spinal vascular lesions that classically present with vague symptoms such as leg dysesthesias and exertional leg weakness but slowly progress to severe myelopathy with paraplegia and sphincter dysfunction.¹ Because of the nonspecific nature of their presenting symptomatology and insidious onset, SDAVFs often go clinically undiagnosed or are misdiagnosed as peripheral neuropathy, spinal stenosis, multiple sclerosis, transverse myelitis, or radiculopathies.²

Despite the vague clinical symptoms associated with the initial

presentation of SDAVFs, they typically demonstrate a characteristic imaging appearance. On MR imaging, SDAVFs are characterized by spinal cord enlargement in the lower thoracic region and conus, with T2 hyperintensity across multiple segments and serpiginous, enlarged intradural vessels along the dorsal and ventral aspect of the cord. Gadolinium-enhanced spine MR imaging is often helpful in highlighting the dilated intradural veins and can even demonstrate cord enhancement but is not indispensable for radiologic diagnosis.³ Given the characteristic imaging features of these lesions, they represent a prime opportunity for the radiologist to make an important and often clinically unsuspected diagnosis.

Despite their classic imaging appearance, SDAVFs can remain undiagnosed on imaging or can be misdiagnosed. In a number of cases in the literature, high T2 signal in the conus or prominent vascular flow voids in the intradural space are missed on initial imaging, only to be picked up at follow-up imaging after progres-

Received May 24, 2015; accepted after revision June 30.

From Departments of Radiology (W.B., J.M.M.), Neurology (D.M.N., A.A.R.), Neurosurgery (G.L.), and Center for Science of Healthcare Delivery (G.L.), Mayo Clinic, Rochester, Minnesota.

Please address correspondence to Waleed Brinjikji, MD, Mayo Clinic, 200 First St SW, OL1-112 SMH, Rochester, MN 55905; e-mail: Brinjikji.waleed@mayo.edu; @WBrinjikji

<http://dx.doi.org/10.3174/ajnr.A4504>

sion of the patient's symptoms. In addition, cases exist in which the cord signal was hyperintense on T2-weighted images and the patient was diagnosed with and treated for transverse myelitis or neuromyelitis optica, despite the presence of flow voids.^{2,4,5}

In this study, we examined a consecutive series of patients presenting with imaging findings of SDAVFs that were missed or misdiagnosed. We studied the clinical consequences of delayed diagnosis, such as progression of disability, use of additional imaging, number of months until diagnosis, and improvement of clinical symptoms following treatment.

MATERIALS AND METHODS

Patient Population

Following institutional review board approval, we reviewed a consecutive series of angiographically confirmed SDAVFs diagnosed and/or treated at our institution from January 1, 2000, to November 1, 2014. Patients with clinically or radiologically misdiagnosed SDAVFs had to meet at least 1 of the following criteria as determined by 2 reviewers: 1) Initial MR imaging or CT myelogram of the spine demonstrated characteristic imaging features of an SDAVF, but these findings were not noted in the radiology report; 2) initial MR imaging or CT myelogram of the spine demonstrated characteristic imaging features of an SDAVF, no radiology report was available, and the patient was treated initially for a disease other than an SDAVF without conventional angiography, spinal MRA, or CTA being performed; or 3) an SDAVF was suspected on the basis of imaging, and the patient had a spinal angiography that was incomplete (ie, not all vessels were injected) or showed an SDAVF that was not appreciated, leading to the incorrect interpretation of negative findings.

Our institution is a large tertiary referral center, so most patients received extensive evaluations at other centers before arriving at our institution. Because radiology reports did not always accompany images from outside centers (only 5 cases with outside radiology reports were available), the clinical management of the patient was most often used to indicate whether the SDAVF was missed or misdiagnosed. The definition of characteristic imaging features of SDAVF was high T2 cord signal and/or serpiginous vascular intradural flow voids with or without intramedullary enhancement on MR imaging or a serpiginous blood vessel coursing in the spinal canal on CT myelography. Vascular intradural flow voids were distinguished from CSF pulsations because these were serpiginous flow voids taking the expected shape/morphology of a blood vessel.

Imaging Evaluation

Imaging examinations were simultaneously reviewed by a staff neuroradiologist with 10 years' experience and a senior diagnostic radiology resident. The readers were not blinded to the patient's diagnosis of an SDAVF. MR imaging examinations were reviewed for the following imaging findings: increased T2 signal in the conus, number of levels of high T2 signal, presence of flow voids, and presence of cord enhancement on postgadolinium images. "Serpiginous flow voids" were defined as serpiginous areas of signal loss on T2-weighted imaging. This definition was chosen because such flow voids are not usually seen on T2-weighted images around the lower spinal cord/conus medullaris. "Intramedullary"

enhancement was defined as enhancement of the conus or spinal cord itself rather than surface enhancement of pial vessels, which can be seen in some as normal findings. We compiled imaging findings and scored them by using the recently validated 4-point arteriovenous fistula score, which assigns 1 point to the following clinical/imaging characteristics: 1) 50 years of age or older, 2) T2 hyperintensity extending to at least 5 levels, 3) flow voids, and 4) a subcervical lesion.⁶ A score of ≥ 3 has been found to have a sensitivity of 85% and specificity of 97% in determining the presence of an SDAVF.⁶ CT myelograms were evaluated for the presence of a serpiginous vessel coursing in the intradural space. Conventional spinal angiograms were evaluated for the presence of an SDAVF and angiogram completeness. An angiogram was defined as "incomplete" if the feeding artery seen on a later angiogram was not selectively injected. We also evaluated posttreatment angiograms and spinal MR angiograms for resolution of the SDAVF.

Clinical Evaluation

The clinical evaluation was performed by a vascular neurology fellow (D.M.N.) through a retrospective chart review of clinical notes and neurologic examinations. We collected the following clinical data: time of delay in diagnosis; modified Rankin Scale score on presentation, diagnosis, and 90 days posttreatment; Aminoff score of motor disability at presentation, diagnosis, and 90 days posttreatment; worsening of symptoms (defined as an increase of at least 1 point on the mRS or Aminoff score); interval use of a walker following initial imaging; interval use of a wheelchair following initial imaging; and interval development of sensory symptoms (including dysesthesias and paresthesias) or bowel and bladder symptoms (including neurogenic bladder and incontinence).

Additional Procedures and Imaging

In addition to documenting the type of treatment for the SDAVF, we also collected data on additional imaging and interventions performed before the diagnosis of SDAVF. Data collected on interventions included the use of systemic steroids, IV immunoglobulin, and plasmapheresis between the initial imaging study that demonstrated evidence of the SDAVF and the time the fistula was actually recognized. We also tabulated the number of additional imaging studies that were performed before arriving at the diagnosis of SDAVF.

Statistical Analysis

Because this was a descriptive study, no formal statistical comparisons were performed. We report descriptive statistics including mean, median, and proportions. All analyses were performed with the JMP statistical software package, Version 10.0 (SAS Institute, Cary, North Carolina).

RESULTS

Patient Population

One hundred patients were diagnosed with SDAVFs at our institution during this time. Of these, 53 (40.8%) met our inclusion criteria. The mean age of these patients was 65.0 ± 10.8 years, and 48 patients (90.6%) were older than 50 years of age. Forty-three patients were men (81.1%), and 10 patients were women (18.9%).

Table 1: Patient characteristics and additional procedures

	No. (%)
No.	53
Mean (SD) age	65.0 (10.8)
No. (%) male	43 (81.1)
Mean delay in diagnosis (mo)	9.2 ± 11.1
Symptoms at presentation	
Bilateral motor symptoms	48 (90.6)
Sensory symptoms	20 (37.7)
Bowel or bladder symptoms	13 (24.5)
Focal unilateral motor deficit	3 (5.7)
Initial working diagnosis	
Spinal stenosis	13 (24.5)
Myelopathy NOS	10 (18.9)
Transverse myelitis	9 (17.0)
Ischemic myelopathy	4 (7.6)
Peripheral neuropathy	3 (5.7)
Myopathy	2 (3.8)
NMO	2 (3.8)
CIDP	2 (3.8)
Other	8 (15.1)
Additional interventions	
Systemic steroids	18 (34.0)
IVIg	5 (9.4)
Surgery	6 (11.3)
Biopsy	2 (3.8)
Plasma exchange	4 (7.6)
Rituximab	2 (3.8)
No. of additional spine MRIs or CTs until diagnosis	
1	10 (18.9)
2	8 (15.1)
3	12 (22.6)
4	12 (22.6)
≥5	11 (20.8)

Note:—NOS indicates not otherwise specified; NMO, neuromyelitis optica; CIDP, chronic inflammatory demyelinating polyneuropathy.

The mean number of months between the time when the first imaging study demonstrating findings of SDAVF was performed and the time of diagnosis was 9.2 ± 11.1 months (median, 6 months). The 3 most common working diagnoses for patients who had imaging evidence of SDAVF were spinal stenosis (13 patients, 24.5%), myelopathy not otherwise specified (10 patients, 18.9%), and transverse myelitis (9 patients, 17.0%).

Systemic steroid administration (oral or IV) was the most common medical intervention between the initial imaging study demonstrating the SDAVF and the time of diagnosis (18 patients, 34.0%). Six patients (11.3%) had laminectomies during this interval, 1 patient had a spinal cord biopsy, and 4 patients (7.6%) had plasma exchange. The median number of additional imaging studies performed before diagnosis was 3. Eleven patients (20.8%) had ≥5 additional imaging studies. These data are summarized in Table 1.

Imaging Findings on Arteriovenous Fistula Score

Forty-eight patients (90.6%) had evidence of SDAVFs on MR imaging on initial imaging evaluation, and 5 patients (9.4%) had imaging evidence of SDAVF on CT myelography. Forty-four patients (91.7%) had high T2 signal in the conus on MR imaging, and 46 patients (95.8%) had increased T2 signal in the cord. Thirty-seven patients (77.1%) had at least 5 levels of high T2 cord signal intensity. In 43 patients (89.6%), the high T2 cord signal extended ≥3 levels. Fifty-one patients (96.2%) had flow voids in

Table 2: Imaging characteristics

Imaging Findings	No. (%)
High T2 cord signal (including conus)	46 (95.8)
Increased conus signal	44 (91.7)
Prominent intradural vessel on CT myelography or MRI	51 (96.2)
Cord enhancement	38 (79.2)
High T2 signal and flow void	44 (91.7)

the intradural space on MR imaging or a dilated serpiginous vessel in the intradural space on CT myelography. Thirty-eight patients (79.2%) had spinal cord enhancement. Forty-four patients (91.7%) had both high cord T2 signal and flow voids. In total, 51 patients (96.1%) had an arteriovenous fistula score of ≥3, indicating a high probability of a spinal dural arteriovenous fistula.

Two patients had high T2 signal but no flow voids. In 1 case, the spinal MR imaging had high T2 cord signal extending 6 levels and intramedullary enhancement. The patient was 80 years of age. This patient had an arteriovenous fistula score of 3. The patient was misdiagnosed as having an ischemic myelopathy. The second patient was a 49-year-old man with high T2 conus signal that was interpreted as myelomalacia and cord atrophy due to spinal stenosis. The patient underwent a laminectomy, but his symptoms progressed. Six months following the initial MR imaging, the patient underwent a spinal MRA due to suspicions that his symptoms were due to an SDAVF on the basis of the gradual progression of his symptoms. This patient had an arteriovenous fistula score of 1.

Eight patients (18.9%) underwent spinal angiographies that were interpreted as having negative findings. In all 8 cases, patients were treated for diagnoses other than SDAVF following angiography. In 6 cases (11.3%), the feeding artery was not selectively injected and no SDAVF was visualized. Among these 6 cases, in 2 cases the feeding artery was a hypogastric/internal iliac artery, and in 4 cases, the feeding artery was a radiculomeningeal artery from the lumbar or thoracic levels. In 2 cases, the fistula was present because the angiogram of the culprit artery was selectively injected; however, the angiogram was interpreted as negative. One additional patient had a 5-year delay in the diagnosis of an SDAVF despite imaging findings of high T2 cord signal and flow voids. Imaging findings are summarized in Table 2. Case examples are shown in Figs 1 and 2.

Clinical Progression and Posttreatment Outcomes

At the time of initial imaging evaluation, 51 patients (96.3%) had some motor deficit, 20 patients (37.7%) had sensory symptoms including pain, and 13 patients (24.5%) had bowel or bladder symptoms. At the time of diagnosis, 51 patients (96.2%) had worsening of disability as measured by the mRS and 51 patients (96.2%) had worsening of motor disability as measured by the Aminoff score of motor disability. Forty of 42 patients (95.2%) with an mRS of 0–1 at baseline had worsening of symptoms at the time of diagnosis, and 25 of 35 patients with an Aminoff score of motor disability of 0–1 at baseline had worsening of symptoms at the time of diagnosis (71.4%). Seventeen patients (32.1%) required a wheelchair, 15 patients (28.3%) required a walker, and 15 patients (28.3%) required a cane.

Forty-one patients (77.4%) underwent surgical ligation for initial treatment, and 11 patients (20.8%) underwent endovascu-



FIG 1. A 57-year-old woman with a 3-month history of bilateral lower extremity tingling and progressive lower extremity weakness. *A* and *B*, T2-weighted lumbar spine MR images demonstrate high T2 signal in the conus with multiple flow voids in the intradural space. *C*, T2-weighted MR image of the thoracic spine demonstrates high T2 signal in the lower thoracic cord to the conus. The patient was diagnosed with neuromyelitis optica and received no spinal-vasculature imaging before referral to our institution. Two rounds of IV methylprednisolone (Solu-Medrol) therapy resulted in worsening of symptoms, and rituximab therapy was of no benefit. *D*, Spinal angiography demonstrates the spinal dural AVF with an arterial feeder from the L3 radiculomeningeal artery.

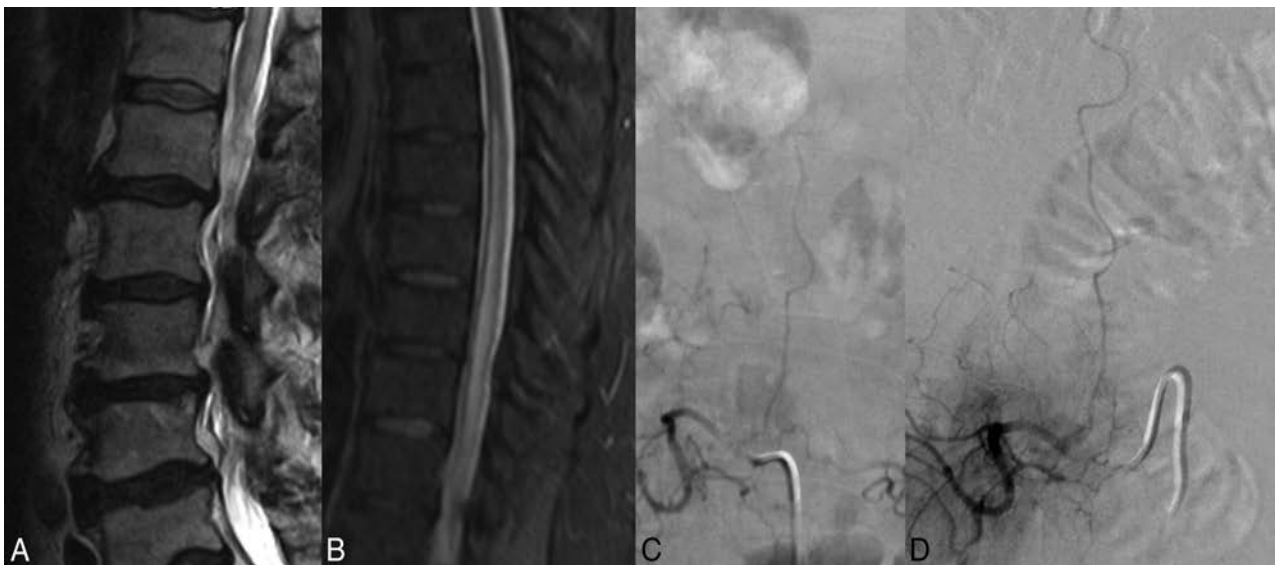


FIG 2. A 68-year-old man with a 3-month history of saddle anesthesia, constipation, difficulty voiding, and numbness in the lower extremities. T2-weighted images of the lumbar and thoracic spine demonstrate high T2 signal in the lower thoracic cord and conus (*A* and *B*). Due to clinical suspicion of SDAVF, an angiogram was obtained before referral to our center. *C*, The angiogram clearly demonstrates the fistula arising from the L2 radiculomeningeal artery; however, it was interpreted as a negative finding. Before the diagnosis was made, the patient underwent an extensive imaging and clinical evaluation, including a panel negative for paraneoplastic syndrome, PET/CT, and lumbar puncture. Two rounds of IV Solu-Medrol therapy resulted in worsening of symptoms. The patient also underwent a T10–T11 laminectomy and 2 spinal cord biopsies. *D*, Repeat spinal angiography re-demonstrates the fistula.

lar embolization. Forty-eight patients had postoperative MRA or spinal angiography, and resolution of the SDAVF on imaging was seen in 46 patients (95.8%). Ninety days following treatment, 29

patients (56.8%) demonstrated no improvement in disability as measured by the mRS and 21 patients (41.2%) had an improvement of at least 1 point on the mRS scale. One patient died due to

Table 3: Clinical outcomes

	Presenting (No.) (%)	At Diagnosis (No.) (%)	90 Days after Treatment (No.) (%)
mRS			
0	0 (0.0)	0 (0.0)	2 (3.9)
1	42 (79.2)	2 (3.8)	8 (15.7)
2	8 (15.1)	12 (22.6)	12 (23.5)
3	3 (5.7)	16 (30.2)	16 (31.4)
4	0 (0.0)	21 (39.6)	10 (19.6)
5	0 (0.0)	2 (3.8)	2 (3.9)
6	0 (0.0)	0 (0.0)	1 (2.0)
Aminoff motor score			
0 (No deficit)	1 (1.9)	1 (1.9)	2 (4.0)
1 (Hyposthenia)	34 (64.2)	9 (17.0)	6 (12.0)
2 (Reduced tolerance)	6 (11.3)	11 (20.8)	5 (10.0)
3 (Need for cane)	12 (22.6)	15 (28.3)	14 (28.0)
4 (Need for crutches or walker)	0 (0)	15 (28.3)	11 (22.0)
5 (Patient in wheelchair)	0 (0)	17 (32.1)	12 (24.0)
Bowel or bladder symptoms			
Yes	13 (24.5)	27 (50.9)	23 (45.1)
No	40 (75.5)	26 (49.1)	28 (54.9)
Sensory symptoms			
Yes	20 (37.8)	28 (52.8)	20 (39.2)
No	33 (62.2)	25 (47.2)	31 (60.8)

complications from metastatic gastric adenocarcinoma (2.0%). On the Aminoff score of motor disability, 47 (94%) patients were either stable (31 patients, 62%) or improved (16 patients, 32%) after treatment, while 3 patients (6.0%) demonstrated worsening of their motor disabilities. At 90 days posttreatment, 12 patients (24.0%) required a wheelchair, 11 patients (22.0%) required a walker, and 14 patients (28.0%) required a cane. These data are summarized in Table 3.

DISCUSSION

Our study of 53 patients with a delayed diagnosis of SDAVF demonstrated a high rate of additional morbidity and disability from the time of imaging evidence of SDAVF to the time of diagnosis. Notably, all patients in our cohort could ambulate independently at the time of the initial imaging study demonstrating the SDAVF, but more than half (32 patients) had become wheelchair-bound or required a walker by the time the SDAVF was recognized. Furthermore, this progression of disability was usually not reversible with treatment of the SDAVF: Only one-third of patients becoming wheelchair-bound by the time of SDAVF diagnosis were able to ambulate with a walker 90 days after treatment. The morbidity associated with delayed diagnosis of SDAVF was likely preventable in most patients. Approximately 90% of patients with a delayed diagnosis had both serpiginous flow voids and high T2 cord signal on the initial imaging evaluation, which are the classic imaging characteristics of SDAVFs, and 96% of patients had abnormal intradural spinal vessels. These findings highlight the importance of a timely diagnosis of SDAVFs and the role of the radiologist in raising clinical suspicion for these lesions.

In general, SDAVFs are associated with a poor natural history. It has been proposed that SDAVFs result from loss of normal physiologic control of the glomerulus of Manelfe, a structure located between 2 layers of the dura mater, composed of ≥ 2 arterioles converging with a vascular ball (glomerulus) and being drained by a single intradural vein. However, the means by which

the glomeruli of Manelfe lose their ability to be physiologically controlled is still unknown. Following formation of the fistula between the radiculomeningeal artery and radicular vein, venous congestion along the longitudinal venous network draining the spinal cord can occur. Congestion is generally most marked in the conus due to its dependent location, resulting in the classic sensorimotor deficits and bowel and bladder symptoms.⁷ Progression of the lesion results in increased venous congestion and, in turn, chronic hypoxia and progressive myelopathy with worsening of symptoms.⁸ The onset of symptoms is often insidious and can take place years after the fistula develops.⁹ In general, when left untreated, symptomatic SDAVFs progress to severe irreversible myelopathy with paraparesis and sphincter dysfunction. However, the natural history of asymptomatic,

incidentally discovered SDAVFs is unknown.¹⁰

So many of these lesions are diagnosed late or misdiagnosed because of the slow and insidious onset of symptoms. SDAVFs have been reported misdiagnosed and even treated as peripheral neuropathy, radiculopathies, multiple sclerosis, intramedullary tumors, neuromyelitis optica, and transverse myelitis.^{11,12} Furthermore, because of the demographic characteristics of patients affected by these lesions (typically older men), they are often misdiagnosed as central spinal canal stenosis secondary to degenerative changes (ie, spinal stenosis), as occurred in approximately 20% of patients in our study. With or without initial misdiagnosis, diagnostic delays are common and can be quite long. In fact, the estimated time from clinical symptom onset to diagnosis ranges from 11 to 27 months, depending on the series.^{13,14}

Because of the protean clinical symptoms of SDAVFs in early stages, imaging plays a central role in the diagnosis of these lesions. As mentioned previously, SDAVFs have a very characteristic imaging appearance, including high T2 conus signal, high contiguous T2 signal in the spinal cord, enhancement, and intradural vascular flow voids.^{3,15} In our series for example, approximately 80% of patients had evidence of high T2 cord signal and flow voids in their initial imaging study. High conus signal was present in 83% of patients, which is important because many patients undergo lumbar spine imaging as the initial evaluation for their symptoms. High conus or cord signal is not a specific finding for SDAVF; however, when detected, the radiologist should consider the possibility of an SDAVF in the correct clinical setting.

In a retrospective study of 78 patients with unexplained myelopathy, Strom et al¹⁶ found that nearly 30% of patients had an SDAVF on angiography. This finding led to the conclusion that spinal angiography should be considered in patients with unexplained myelopathy to allow prompt diagnosis of an SDAVF. Cao et al⁶ proposed a 4-point score to identify SDAVFs, suggesting that patients who meet at least 3 of the following 4 criteria should be referred for spinal angiography: 50 years of age or older, length

of intramedullary lesion ≥ 5 segments, perimedullary dilated vessels, and a subcervical lesion. This scoring system had a sensitivity of 85% and a specificity of 97% for the diagnosis of SDAVF on spinal angiography. Most interesting, all patients in our study met at least 3 of these criteria.

Delayed diagnosis and treatment of SDAVFs are associated with a very poor prognosis. Iovtchev et al² reported a series of 7 patients with delayed (60–730 days) diagnosis of SDAVFs. All 7 patients had become wheelchair-bound by the time of treatment, and 4 remained nonambulatory after treatment of the fistula and rehabilitation. Cenzato et al¹⁷ reviewed 65 patients with SDAVFs undergoing surgical and endovascular treatment and found that patients with the best clinical outcomes were those who had been diagnosed early and had an Aminoff scale score of < 3 before the intervention. While delayed diagnosis was not an independent predictor of poor postoperative outcome in the Cenzato series, it was associated with a higher degree of disability at the time of treatment and thus a poorer clinical outcome following treatment.¹⁷ A previous analysis of 153 patients with SDAVF treated surgically at our institution did not find an independent association between the time from symptom onset to fistula treatment and postoperative prognosis; however, preoperative disability was the strongest determinant of postoperative outcome.¹⁸ In the current study focused on patients with delayed diagnosis, treatment very often took place only once substantial disability had already developed, and all too frequently this disability proved irreversible despite successful obliteration of the fistula.

Recommendations

Our study and others highlight the importance of timely diagnosis of spinal dural arteriovenous fistulas. Because most of these patients will only receive imaging of the lumbar spine without contrast during the initial evaluation of their symptoms, often the only sign of an SDAVF will be a slightly increased signal in the conus with some flow voids. These “edge of the film” findings are commonly missed, highlighting the necessity for the radiologist to specifically examine the conus in every lumbar spine MR imaging. In cases of patients with unexplained myelopathy, a spine MRA should be considered. Spine MRA has a high sensitivity for detection of SDAVFs as does 64–detector row multidetector CTA.^{19,20} In cases in which there is a high clinical suspicion, careful conventional spinal angiography should be performed because it is both safe and the criterion standard for detection of SDAVFs.²¹ In cases in which an artery cannot be accessed or assessed on the first attempt, there should be a low threshold for repeat angiography at a later date to ensure that all vessels are fully evaluated.

Limitations

Our study has limitations. First, most patients included in this study had extensive imaging evaluations performed before referral to our institution. Only a small proportion came with outside imaging reports; thus, we were unable to determine whether the signs of an SDAVF were mentioned in the radiology report and just not followed up clinically or if they were missed or misinterpreted, resulting in a delay in diagnosis. However, we can be certain that these patients were at least clinically misdiagnosed because only a small proportion ever underwent spinal angiography, and of those who did, all were interpreted as

having negative findings. It is possible that the physician taking care of the patient disregarded the imaging diagnosis and treated the patient incorrectly or that patients may have initially refused spinal angiography.

Another limitation is the risk of bias in retrospectively interpreting the initial diagnostic imaging because both reviewers were aware that an SDAVF was present. However, the purpose of this study was not to evaluate the sensitivity of radiologists in detecting SDAVFs; rather, the purpose was to determine the clinical outcomes of those who had characteristic imaging findings but had a delay in diagnosis. We acknowledge that in many cases, the imaging findings could be subtle (ie, subtle flow voids or subtle T2 signal hyperintensity); however, in $> 80\%$ of cases, patients had high T2 cord signal intensity and characteristic T2 flow voids, both characteristics that are highly suggestive of the SDAVF diagnosis. Another limitation is that we retrospectively determined the Aminoff motor disability and mRS scores through chart review. We may have underestimated or overestimated mRS scores, especially those in the 1–3 range. The Aminoff motor disability score, however, is easier to assess in a retrospective chart review because most of the necessary data can be easily abstracted from the documented physical examination (ie, use of a cane, walker or wheelchair, gait instability, and so forth). Last, because ours is a large referral center, there is definitely a risk of referral bias.

CONCLUSIONS

Delayed diagnosis of SDAVFs frequently leads to unnecessary pharmacologic and surgical treatments. Delayed diagnosis of SDAVFs in patients with imaging features of the disease results in high rates of additional morbidity, which is often irreversible despite successful treatment of the fistula. Thus, timely diagnosis of these lesions is essential to avoid additional morbidity from worsening of the myelopathy. Clinicians should have a low threshold for performing noninvasive angiography in patients with unexplained myelopathy.

Disclosures: Alejandro A. Rabinstein—UNRELATED: DJO Global.* Comments: for an investigator-initiated project on upper limb deep venous thrombosis prevention; Royalties: Elsevier,* Oxford.* Comments: for authored books. Giuseppe Lanzino—UNRELATED: Consultancy: Covidien.* *Money paid to the institution.

REFERENCES

1. Marcus J, Schwarz J, Singh IP, et al. **Spinal dural arteriovenous fistulas: a review.** *Curr Atheroscler Rep* 2013;15:335 CrossRef Medline
2. Iovtchev I, Hiller N, Ofra Y, et al. **Late diagnosis of spinal dural arteriovenous fistulas resulting in severe lower-extremity weakness: a case series.** *Spine J* 2015;15:e39–44 CrossRef Medline
3. Morris JM. **Imaging of dural arteriovenous fistula.** *Radiol Clin North Am* 2012;50:823–39 CrossRef Medline
4. Abe T, Tokuda Y, Ishimatsu S, et al. **Spinal dural arteriovenous fistula incidentally discovered.** *J Emerg Trauma Shock* 2011;4:299 CrossRef Medline
5. Aghakhani N, Parker F, David P, et al. **Curable cause of paraplegia: spinal dural arteriovenous fistulae.** *Stroke* 2008;39:2756–59 CrossRef Medline
6. Cao W, Huang L, Ge L, et al. **A simple score (AVFS) to identify spinal dural arteriovenous fistula before spinal digital subtraction angiography.** *J Stroke Cerebrovasc Dis* 2014;23:1995–2000 CrossRef Medline
7. Amanieu C, Hermier M, Peyron N, et al. **Spinal dural arteriovenous fistula.** *Diagn Interv Imaging* 2014;95:897–902 CrossRef Medline

8. Krings T, Mull M, Gilsbach JM, et al. **Spinal vascular malformations.** *Eur Radiol* 2005;15:267–78 CrossRef Medline
9. Houdart E, Redondo A, Saint-Maurice JP, et al. **Natural history of an incidentally discovered spinal dural arteriovenous fistula.** *Neurology* 2001;57:742–43 CrossRef Medline
10. van Rooij WJ, Nijenhuis RJ, Peluso JP, et al. **Spinal dural fistulas without swelling and edema of the cord as incidental findings.** *AJNR Am J Neuroradiol* 2012;33:1888–92 CrossRef Medline
11. McKeon A, Lindell EP, Atkinson JL, et al. **Pearls & oysters: clues for spinal dural arteriovenous fistulae.** *Neurology* 2011;76:e10–12 CrossRef Medline
12. Thiex R, Mayfrank L, Krings T, et al. **Delayed diagnosis of spinal dural arteriovenous fistula in the absence of pathological vessels on MRI.** *Zentralbl Neurochir* 2006;67:94–98 CrossRef Medline
13. Van Dijk JM, TerBrugge KG, Willinsky RA, et al. **Multidisciplinary management of spinal dural arteriovenous fistulas: clinical presentation and long-term follow-up in 49 patients.** *Stroke* 2002;33:1578–83 CrossRef Medline
14. Gilbertson JR, Miller GM, Goldman MS, et al. **Spinal dural arteriovenous fistulas: MR and myelographic findings.** *AJNR Am J Neuroradiol* 1995;16:2049–57 Medline
15. Krings T, Geibprasert S. **Spinal dural arteriovenous fistulas.** *AJNR Am J Neuroradiol* 2009;30:639–48 CrossRef Medline
16. Strom RG, Derdeyn CP, Moran CJ, et al. **Frequency of spinal arteriovenous malformations in patients with unexplained myelopathy.** *Neurology* 2006;66:928–31 Medline
17. Cenzato M, Debernardi A, Stefani R, et al. **Spinal dural arteriovenous fistulas: outcome and prognostic factors.** *Neurosurg Focus* 2012;32:E11 CrossRef Medline
18. Muralidharan R, Mandrekar J, Lanzino G, et al. **Prognostic value of clinical and radiological signs in the postoperative outcome of spinal dural arteriovenous fistula.** *Spine (Phila Pa 1976)* 2013;38:1188–93 CrossRef Medline
19. Condette-Auliac S, Boulin A, Roccatagliata L, et al. **MRI and MRA of spinal cord arteriovenous shunts.** *J Magn Reson Imaging* 2014;40:1253–66 CrossRef Medline
20. Oda S, Utsunomiya D, Hirai T, et al. **Comparison of dynamic contrast-enhanced 3T MR and 64-row multidetector CT angiography for the localization of spinal dural arteriovenous fistulas.** *AJNR Am J Neuroradiol* 2014;35:407–12 CrossRef Medline
21. Forbes G, Nichols DA, Jack CR Jr, et al. **Complications of spinal cord arteriography: prospective assessment of risk for diagnostic procedures.** *Radiology* 1988;169:479–84 CrossRef Medline

Osseous Pseudoprogession in Vertebral Bodies Treated with Stereotactic Radiosurgery: A Secondary Analysis of Prospective Phase I/II Clinical Trials

B. Amini, C.B. Beaman, J.E. Madewell, P.K. Allen, L.D. Rhines, C.E. Tatsui, N.M. Tannir, J. Li, P.D. Brown, and A.J. Ghia



ABSTRACT

BACKGROUND AND PURPOSE: Osseous pseudoprogession on MR imaging can mimic true progression in lesions treated with spine stereotactic radiosurgery. Our aim was to describe the prevalence and time course of osseous pseudoprogession to assist radiologists in the assessment of patients after spine stereotactic radiosurgery.

MATERIALS AND METHODS: A secondary analysis of 2 prospective trials was performed. MRIs before and after spine stereotactic radiosurgery were assessed for response. “Osseous pseudoprogession” was defined as transient growth in signal abnormality centered at the lesion with a sustained decline on follow-up MR imaging that was not attributable to chemotherapy.

RESULTS: From the initial set of 223 patients, 37 lesions in 36 patients met the inclusion criteria and were selected for secondary analysis. Five of the 37 lesions (14%) demonstrated osseous pseudoprogession, and 9 demonstrated progressive disease. There was a significant association between single-fraction therapy and the development of osseous pseudoprogession ($P = .01$), and there was a significant difference in osseous pseudoprogession-free survival between single- and multifraction regimens ($P = .005$). In lesions demonstrating osseous pseudoprogession, time-to-peak size occurred between 9.7 and 24.4 weeks after spine stereotactic radiosurgery (mean, 13.9 weeks; 95% CI, 8.6–19.1 weeks). The peak lesion size was between 4 and 10 mm larger than baseline. Most lesions returned to baseline size between 23 and 52.4 weeks following spine stereotactic radiosurgery.

CONCLUSIONS: Progression on MR imaging performed between 3 and 6 months following spine stereotactic radiosurgery should be treated with caution because osseous pseudoprogession may be seen in more than one-third of these lesions. Single-fraction spine stereotactic radiosurgery may be associated with osseous pseudoprogession. The possibility of osseous pseudoprogession should be incorporated into the prospective criteria for assessment of local control following spine stereotactic radiosurgery.

ABBREVIATIONS: OPP = osseous pseudoprogession; PD = progressive disease; PR = partial response; SSRS = spine stereotactic radiosurgery

Spine stereotactic radiosurgery (SSRS) is a form of stereotactic body radiation therapy that combines advanced treatment delivery techniques (eg, intensity-modulated radiation therapy) with image guidance and rigid immobilization to deliver high doses of conformal radiation to the target while minimizing

exposure to nearby critical structures such as the spinal cord (Fig 1A–C). Imaging plays a critical role not only in diagnosis and therapy planning but also in the post-SSRS evaluation of patients in determining the response to therapy. In evaluating patients following SSRS, we have noticed a phenomenon whereby the intraosseous extent of the lesion transiently enlarges on early post-therapy MRI and simulates progression (Fig 1D–F).

This osseous pseudoprogession (OPP) complicates the early post-SSRS imaging assessment of patients and can lead to uncertainty about the true response. We undertook a secondary analysis of 2 prospective trials performed at our institution to define the prevalence and time course of OPP to provide guidance to interpreting radiologists in assessing the patient after SSRS.

MATERIALS AND METHODS

Patient Population

We performed a secondary analysis of 2 consecutive prospective SSRS trials at our institution. Between 2002 and 2011, 223 patients

Received June 14, 2015; accepted after revision July 14.

From the Departments of Diagnostic Radiology (B.A., J.E.M.), Biostatistics (P.K.A.), Neurosurgery (L.D.R., C.E.T.), Genitourinary Medical Oncology (N.M.T.), and Radiation Oncology (J.L., P.D.B., A.J.G.), The University of Texas MD Anderson Cancer Center, Houston, Texas; and The University of Texas Health Science Center at Houston (C.B.B.), Houston, Texas.

This work was supported in part by the Cancer Center Support Grant (National Cancer Institute Grant P30 CA016672).

Please address correspondence to Behrang Amini, MD, PhD, Department of Diagnostic Radiology, University of Texas MD Anderson Cancer Center, 1400 Pressler St, Unit 1475, Houston, TX 77030; e-mail: bamini@mdanderson.org; @DrBehrangAmini

Indicates open access to non-subscribers at www.ajnr.org

<http://dx.doi.org/10.3174/ajnr.A4528>

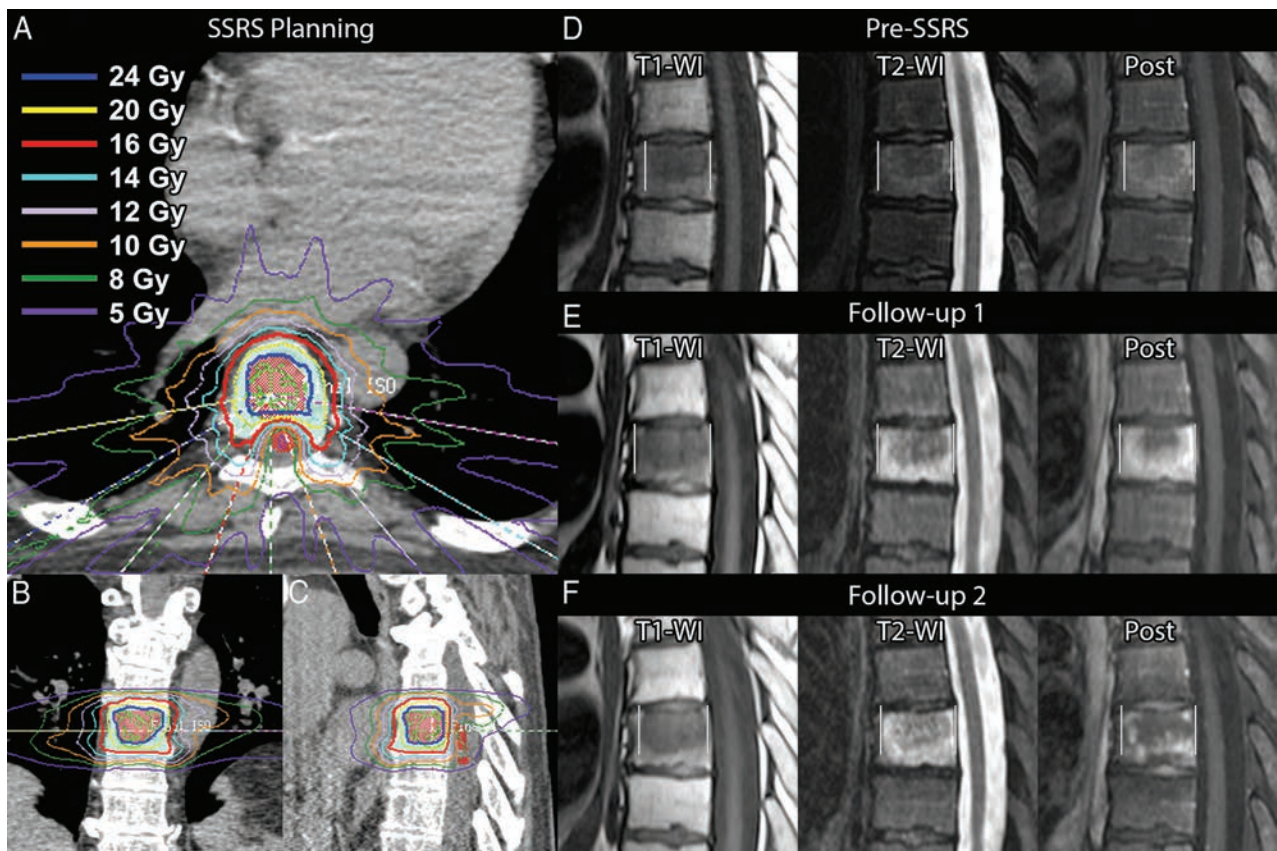


FIG 1. Index case of osseous pseudoprogession (not part of the analysis). A 55-year-old man with metastatic renal cell carcinoma. A–C, Axial, coronal, and sagittal images from the SSRS treatment plan. Twenty-four Gy (blue open area) will be delivered to the gross tumor volume corresponding to the metastasis seen on MR imaging (D), and 16 Gy (red open area), to the remainder of the at-risk vertebral body (clinical tumor volume) in a single fraction. The spinal cord (red shaded area) is spared from high-dose radiation. Other colors correspond to isodose lines as indicated. D, MR image obtained 6 weeks before therapy shows the lesion in the central vertebral body. E, The lesion enlarges on follow-up 1, 6 weeks after SSRS. There is extensive signal abnormality surrounding the lesion. The entire extent of the signal abnormality, including the lesion, is measured in this study (indicated by vertical white lines). F, Surrounding signal abnormality decreases on follow-up 2, 16 weeks following SSRS.

were enrolled in 2 phase I/II trials at our institution, evaluating the use of single-fraction and multiple-fraction SSRS, respectively, in patients with spinal metastases. All patients treated in the initial study received multifraction SSRS. As the safety of multifraction SSRS was established, a second study was initiated in which patients were treated with single-fraction SSRS. The trials were approved by the institutional review board, and written informed consent was obtained from trial participants before enrollment. Eligibility requirements included diagnosis of cancer, Karnofsky Performance Status score of >40 , and MR imaging identifying spinal or paraspinal metastasis within 4 weeks of enrollment. Indications for treatment included oligometastatic disease from a known primary tumor, failure of prior surgery or conventionally fractionated radiation, residual tumor after surgery, medical inoperability, and refusal of surgery. Exclusion criteria included spinal cord compression, unstable spine as determined by a multidisciplinary tumor board, cytotoxic chemotherapy within 1 month of enrollment, and external beam radiation therapy to the current site of disease 3 months before planned SSRS.

Exclusion criteria for the secondary analysis included the following: 1) imaging follow-up of <6 months, 2) the presence of surgical hardware or cement augmentation during the observation period, 3) the presence of significant fracture during the ob-

servation period (“significant fracture” defined as one that results in signal abnormality that could not be differentiated from the lesion), 4) lesions not located in the vertebral body (to allow reproducible measurements), and 5) lesions occupying $>75\%$ of the vertebral body cross-sectional area (to allow determination of lesion growth).

Radiation Therapy Procedure

All patients underwent intensity-modulated, near-simultaneous, CT-guided SSRS by using the EXACT Targeting system CT-on-rails (GE Healthcare, Milwaukee, Wisconsin) or the Trilogy treatment delivery system with On-Board Imager Conebeam CT (Varian Medical Systems, Palo Alto, California), as previously described.^{1,2} Patients were immobilized in a BodyFix 14 stereotactic body frame system (Elekta, Stockholm, Sweden) and aligned by using a BodyFix 14 Target Positioner (Elekta). Treatment planning was performed by using intensity-modulated radiation therapy inverse-treatment planning software (Pinnacle; Philips Medical Systems, Andover, Massachusetts). Verification of target positioning and quality assurance procedures for each case was performed by the radiation oncologist and a dedicated radiation physicist, respectively.

Spinal tumors were prescribed to receive 30 Gy in 5 fractions,

27 Gy in 3 fractions, or 16, 18, or 24 Gy in 1 fraction to the gross tumor volume. "Gross tumor volume" was defined by the visible disease on MR imaging fused with the pretreatment planning CT. "Clinical treatment volume" was defined as gross tumor volume with at-risk contiguous bone marrow. "Planning treatment volume" was defined with no margin to the clinical treatment volume. In most patients, 80%–90% of the target volume received the prescription dose. For the single-fraction protocol, the maximal point dose to 0.01 cm³ of the spinal cord was 10 Gy based on dose-volume histogram analysis. For the multifraction protocol, the spinal cord constraint was maximum dose to 10 Gy for 5-fraction treatments and 9 Gy for the 3-fraction treatments. Radiation treatments were administered on alternating days.

Image Review and Analysis

Patients were seen for follow-up visits and MR imaging every 3 months for 2 years, then every 6 months thereafter. MR imaging was performed in most cases without and with intravenous gadolinium-based contrast material, with exceptions made for compromised renal function (glomerular filtration rate of <30 mL/min/1.73 m²) and patient refusal. The screening review of clinical records and MR images for application of the exclusion criteria (see "Patient Population") was performed by a single reader (C.B.B.). Lesions were measured in consensus by 2 readers (C.B.B. and B.A.) on sagittal T1WI, T2WI fat suppressed, and postcontrast sequences as the greatest anteroposterior extent of signal abnormality (Fig 1E, -F). Because the aim of the study was to define the phenomenon of osseous pseudoprogression, emphasis was placed on the reproducibility of measurements. Axial images were not used for measurement due to scan-to-scan variation related to obliquity.

Lesion response was determined retrospectively by comparing the post-SSRS MRIs with the pre-SSRS baseline study as a partial response (PR, decrease in size of the lesion of >2 mm), stable disease (no growth or growth of <2 mm), progressive disease (PD, continued growth of >2 mm over multiple studies), and osseous pseudoprogression. "OPP" was defined as transient growth of >2 mm in signal abnormality centered at the lesion that was followed by sustained decline (± 2 mm in >3 months) in the size of the area of signal abnormality. The medication history and the response of other bone metastases (if present) were reviewed to ensure that this decline was not due to systemic therapy by checking that no change in systemic therapy occurred following peak lesion size. If systemic therapy was changed following peak lesion size, a determination of OPP was made if other bone lesions enlarged while the SSRS-treated lesion decreased in size (ie, the decrease in size of the SSRS-treated lesion could not be attributed to the change in systemic therapy). If an enlarging lesion failed to meet at least 1 of the above criteria, it was classified as PD. Two millimeters was chosen as the measurement error based on the spatial resolution of MR imaging.

Statistical Analysis

Statistical analysis was performed by using R statistical computing software for Windows (<http://www.r-project.org>) and STATA/MP 14.0 (StataCorp, College Station, Texas). Univariate analysis was performed by using Cox proportional hazards regres-

sion modeling with OPP-free survival as the evaluable end point. The Fisher exact test was used to assess the association between the OPP and non-OPP groups with respect to fractionation regimens (single or multiple). Tumor histology was dichotomized as radiosensitive and radioresistant (ie, sensitive or resistant to conventional radiation therapy), with the latter group consisting of patients with renal cell carcinoma, sarcoma, adenoid cystic carcinoma, and melanoma. Kaplan-Meier analysis and the log-rank test were used for assessment of OPP-free survival. Statistical significance was set for *P* values < .05.

RESULTS

From the initial prospective dataset of 223 patients, 37 lesions in 36 patients met the inclusion criteria and were selected for secondary analysis. Demographic and clinical data are presented in Table 1. The mean age at SSRS was 53 years (range, 32–74 years; 95% CI, 49–56 years). Metastases from renal cell carcinoma, sarcoma, and thyroid carcinoma constituted 67% of cases. Most treated lesions were in the thoracic and lumbar spine (49% and 43%, respectively).

Sixteen lesions (43%) received single-fraction therapy, 15 (41%) received 3 fractions, and 6 (16%) received 5 fractions. The most common dose/fraction combination was 27 Gy at 3 fractions (41%), followed by 24 Gy at 1 fraction (19%), 18 Gy at 1 fraction, 30 Gy at 5 fractions (16% each), and 16 Gy at 1 fraction (8%).

Most lesions (62%) either stabilized or partially responded to therapy during the observation period. The remaining 14 lesions (38%) enlarged on the early post-SSRS scans. Five of these (36%) demonstrated OPP, while 9 (64%) demonstrated progressive disease.

The overall prevalence of OPP among all 37 lesions was 14%. The 5 cases of OPP all received single-fraction SSRS, resulting in a prevalence of 31% when limited to a population of lesions treated with single-fraction radiation therapy. Three of these 5 received 24 Gy, with the remaining 2 treated with 16 and 18 Gy each.

Univariate analysis (Table 2) revealed an association between patient age and the development of OPP (hazard ratio, 1.16; 95% CI, 1.03–1.30). Linear regression failed for the fractionation regimen (single- versus multifraction) due to collinearity (all cases of OPP occurred in lesions treated with single-fraction therapy). The Fisher exact test found a significant association between single-fraction therapy and the development of OPP (*P* = .01), and there was a significant difference in OPP-free survival between single- and multifraction regimens (*P* = .005, Fig 2).

No significant association was found on univariate analysis for the development of OPP with respect to tumor histology (radioresistant versus radiosensitive), dose, or location in the spine (thoracic versus cervical/lumbar).

The apparent change in size of the lesions after SSRS is shown in Fig 3. The time-to-peak lesion size occurred between 9.7 and 24.4 weeks after SSRS (mean, 13.9 weeks; 95% CI, 8.6–19.1 weeks). The mean change in size from the baseline preradiation MR imaging to peak size was 5 mm on T1WI (range, 4–8 mm), 5 mm on T2WI fat suppressed (range, 2–10 mm), and 6 mm on postcontrast images (range, 4–9 mm), with no significant difference among the 3.

The lesions returned to baseline size (within an MR imaging

Table 1: Demographic and clinical data

No.	Age (yr)	Sex	Histology	Level	Dose (Gy)	Fractions	Response
1	57	F	Renal cell carcinoma	L1	24	1	OPP
3	55	M	Renal cell carcinoma	L4	24	1	SD
4	54	F	Renal cell carcinoma	T12	24	1	PD
5	52	M	Renal cell carcinoma	L1	27	3	PR
8	52	M	Renal cell carcinoma	L4	30	5	PD
9	42	M	Renal cell carcinoma	T11	30	5	SD
11	53	F	Renal cell carcinoma	T12	30	5	PR
12	60	F	Breast carcinoma	T8	30	5	SD
13	63	F	Melanoma	L1	27	3	SD
15	58	M	Basal cell carcinoma	T4	30	5	PD
16	32	F	Thyroid carcinoma	L3	30	5	SD
17	46	F	Thyroid carcinoma	L1	27	3	PR
				L2	27	3	SD
18	50	F	Thyroid carcinoma	T11	27	3	SD
19	49	M	Thyroid carcinoma	T6	27	3	PD
20	44	F	Sarcoma	C3	27	3	PR
22	50	F	Sarcoma	T8	27	3	SD
23	70	F	Sarcoma	L2	27	3	PR
24	49	M	Thyroid carcinoma	T1	27	3	SD
25	48	F	Breast carcinoma	T2	18	1	PR
26	51	F	Breast carcinoma	T5	18	1	SD
27	38	F	Lung carcinoma	L1	18	1	SD
29	74	M	Lung carcinoma	L1	18	1	OPP
30	35	M	Sarcoma	T8	16	1	PR
31	50	F	Sarcoma	T5	18	1	PD
32	59	M	Sarcoma	T5	18	1	SD
35	44	M	Renal cell carcinoma	L4	24	1	PD
36	63	M	Renal cell carcinoma	L6	24	1	OPP
37	70	M	Renal cell carcinoma	T12	24	1	OPP
38	65	M	Renal cell carcinoma	C3	24	1	PR
39	61	M	Renal cell carcinoma	T6	27	3	PD
40	33	F	Breast carcinoma	L4	27	3	PD
41	67	M	Colon carcinoma	L3	27	3	PR
42	48	F	Adenoid cystic carcinoma	C2	27	3	PD
43	58	F	Thyroid carcinoma	L2	27	3	PR
44	34	F	Breast carcinoma	T9	16	1	PR
45	65	M	Prostate carcinoma	T6	16	1	OPP

Note:—SD indicates stable disease.

Table 2: Univariate Cox regression analysis for OPP-free survival

Variable	HR	P Value	95% CI	Comment
Age	1.16	.01	1.03–1.30	Continuous
Radiation dose	0.86	.1	0.72–1.03	Continuous
Tumor radiosensitivity	0.70	.7	0.12–4.17	Radiosensitive vs -resistant
Location	0.75	.8	0.13–4.48	T-spine vs C/L-spine
Fraction	–	–	–	Collinearity (all OPP occurred in single-fraction regimens)

Note:—HR indicates hazard ratio; C/L, cervical/lumbar; –, not applicable.

measurement error of ± 2 mm) on T1WI after 23.1–52.4 weeks (mean, 32 weeks). One lesion each on T2WI and postcontrast images did not return to baseline size within the observation period. The mean time to return to baseline size, excluding these lesions, was 30.6 weeks for T2WI (range, 23–37.4 weeks) and 35 weeks for postcontrast images (range, 25.3–52.4 weeks).

DISCUSSION

The phenomenon of pseudoprogression has been classically described in brain lesions following gamma knife therapy.³ With expanded use of stereotactic body radiation therapy, pseudoprogression has been described and analyzed in lung lesions^{4,5} and more recently reported in the soft-tissue components of 2 bone lesions following SSRS.⁶ However, no systematic analysis or even

anecdotal reports of pseudoprogression of lesions confined to bone have been published, to our knowledge.

The absence of these data complicates the follow-up assessment of patients treated with SSRS and can lead to uncertainty regarding the true response to radiation in the setting of clinical trials. Our study provides preliminary information on the prevalence, time course, and risk factors for the development of OPP and can provide guidance on the management of enlarging lesions on early post-SSRS scans.

We found that OPP is common, with a prevalence of 14% overall and 31% when considering its occurrence in the population of patients treated with single-fraction SSRS. All 5 cases of OPP in our study occurred after single-fraction SSRS (24 Gy, 18 Gy, and 16 Gy). A significant association was present between single-fraction therapy and OPP, and there was a significant difference in OPP-free survival between single- and multifraction regimens ($P = .005$, Fig 2). Most interesting, the 2 recently reported cases of pseudoprogression of soft-tissue components of bone lesions have also been in single-fraction regimens.⁶ This finding suggests that the higher biologic dose delivered by single-fraction regimens plays a role in the development of OPP.

The etiology of OPP is likely related to a combination of the effect of radiation on the tumor itself and the adjacent marrow. Tumor growth due to necrosis in response to therapy (chemotherapy and radiation) is a well-known phenomenon,⁷ which likely plays a role in the development of OPP. Indeed, a recent case report in a patient with pseudoprogression in the soft-tissue (epidural)

component of a spine lesion following SSRS showed necrosis in the early (<8 weeks) post-SSRS period.⁶ The effect of radiation on the surrounding bone can be extrapolated from experimental data in animals on the effect of conventional radiation therapy with time and compared with the time course of OPP (Fig 3). In the range of radiation doses used in our study (16–24 Gy), manifestations of radiation on the bone marrow during the first 4 weeks included progressive decrease in marrow cellularity, decrease in the number of sinusoids, and increase in endosteal fibrosis.⁸ This sequence of events was followed by a marked decrease in hematopoietic activity and a marked disruption of sinusoids, with free flow of erythrocytes into parenchymal areas of the marrow.⁸ Hematopoietic cellularity, which normally accounts for the T2 signal

of marrow, was relatively suppressed at this time; however, the extravasation of blood elements through disrupted sinusoids can account for the increase in marrow T2 signal, and the increased permeability of the sinusoids can account for the increased enhancement during the peak of OPP. Later, there is further suppression of marrow hematopoiesis, disappearance of sinusoidal elements, and maximal endosteal fibrosis.⁸ This relatively acellular phase can account for the decrease in marrow T2 signal and enhancement seen on the down-slope of the OPP curve. Following this period, there is patchy early regeneration of marrow and sinusoid-like structures, which progress to an irregular formation of sinusoids within areas of hematopoiesis⁸

and may account for the progressive normalization of marrow signal following the early downslope.

The time-to-peak size in OPP occurred between 9.7 and 24.4 weeks following SSRS and returned to baseline between 23 and 52.4 weeks after SSRS, with slight variation depending on the pulse sequence (Fig 3). This range is earlier than that of the reported time-to-peak lesion size (24–48 weeks) and resolution (60–96 weeks) for early pseudoprogession of brain lesions following gamma knife therapy.^{9,10} This difference is not unexpected, given the differences between the local environments encountered in bone and brain. Temporal evolution information was not obtained in the aforementioned case series on soft-tissue pseudoprogession⁶ because both reported lesions were treated following the development of pseudoprogession due to symptoms (steroids in one case and laminectomy in the other).

The aspect of this study that is most relevant to clinical practice is the guidance it can provide to radiologists on the interpretation of an enlarging lesion on early post-SSRS scans. As noted above, of the 14 lesions in our study that enlarged on early post-SSRS MRI, 5 (36%) represented OPP. The impact of this finding on clinical practice is that enlarging lesions on early post-SSRS scans will require follow-up imaging to elucidate the true response because more than one-third would be expected to have OPP and not true PD.

Our study has several limitations. While our cases were derived from 2 prospective datasets, the data were not randomized and biases may exist between the 2 primary cohorts of patients. A related limitation of this secondary retrospective analysis is the necessity of excluding 187 of the original 223 patients due to a combination of factors that would have complicated detection of OPP (eg, hardware placement, cement augmentation, and moderate to severe pathologic fracture). A larger validation study will be needed before the results of this preliminary study can be confidently generalized.

Another limitation of our study is that many patients were receiving systemic therapy during the observation period. Our retrospective response criteria attempted to account for the effect of systemic therapy by considering OPP when no change in sys-

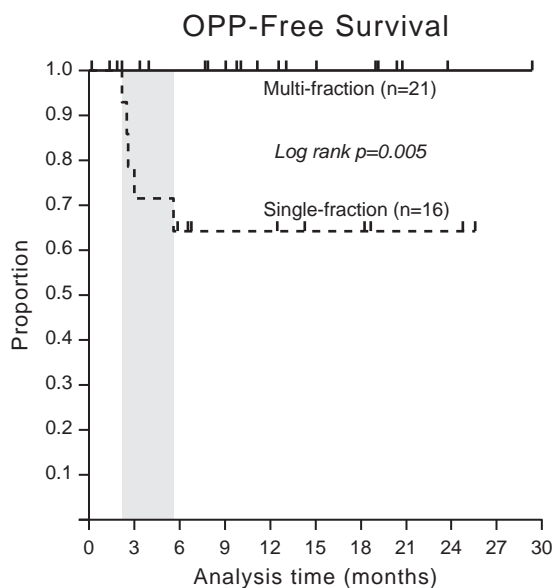


FIG 2. Osseous pseudoprogession-free survival by SSRS fraction status. OPP-free survival is defined as the length of time following SSRS that a patient lives with the disease without development of OPP. Kaplan-Meier analysis shows that there was a significant difference in OPP-free survival between single- and multifraction regimens. The 5 cases of OPP were all treated with single-fraction SSRS and occurred between approximately 3 and 6 months following SSRS (shaded area).

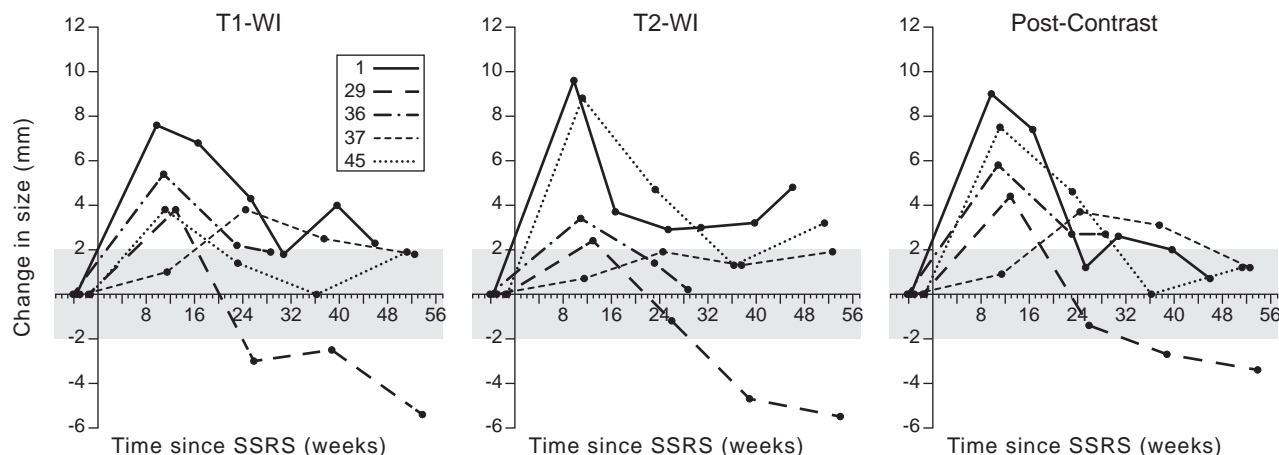


FIG 3. Time course of lesions demonstrating osseous pseudoprogession. Lesions 1, 29, 36, 37, and 45 (see Table 1) demonstrate an initial increase in size followed by a decrease (OPP). The shaded areas correspond to a ± 2 -mm change from baseline, representing measurement error on MR imaging. Similarly, the apparent late increase in lesion size on T2WI in patients 1, 37, and 45 falls within a ± 2 -mm range of the preceding time points and may represent measurement error.

temic therapy had occurred following peak lesion size or, if systemic therapy was changed following peak lesion size, by considering OPP when the response of the treated lesion could be shown to be different from that of other bone lesions (ie, the SSRS-treated lesion decreased in size, while other bone lesions enlarged). However, the effect of synergy between radiation and systemic therapy cannot be entirely eliminated by applying these criteria to a retrospective dataset.

A limitation inherent in our study design, which aimed to describe the time course and prevalence of a new phenomenon, is that it limits comment on imaging features that would allow a prospective differentiation of OPP from PD. A separate, multi-reader study with test and validation arms would be needed to establish criteria for differentiating the 2. However, in the case of pseudoprogession in the brain, findings on conventional MR imaging have been insufficient in making this distinction,¹¹ and advanced imaging techniques such as diffusion and perfusion MR imaging have been investigated for this purpose.¹²

A final limitation relates to the retrospective determination of response based on the change in lesion size with time. While we believe that it is reasonable to assume that persistently enlarging lesions represented PD and transiently enlarging lesions represented OPP, no pathologic proof was available in our patients.

Despite these limitations, our study is the first to describe and systematically analyze the prevalence and time course of OPP following SSRS and can provide guidance in the assessment of the patient after SSRS.

CONCLUSIONS

Progression on MR imaging performed between 3 and 6 months following SSRS should be treated with caution because an osseous pseudoprogession may be seen in more than one-third of these lesions. Serial MR imaging is needed to determine the true response. The possibility of OPP should be incorporated into prospective criteria for the assessment of local control following SSRS.

Disclosures: Charles B. Beaman—UNRELATED: Grants/Grants Pending: Vision Training Grant, Comments: pays my tuition and salary of approximately \$21,000 per year. Laurence D. Rhines—UNRELATED: Consultancy: Stryker, Globus medical, Comments: Educational.

REFERENCES

1. Chang EL, Shiu AS, Lii MF, et al. **Phase I clinical evaluation of near-simultaneous computed tomographic image-guided stereotactic body radiotherapy for spinal metastases.** *Int J Radiat Oncol Biol Phys* 2004;59:1288–94 CrossRef Medline
2. Shiu AS, Chang EL, Ye JS, et al. **Near simultaneous computed tomography image-guided stereotactic spinal radiotherapy: an emerging paradigm for achieving true stereotaxy.** *Int J Radiat Oncol Biol Phys* 2003;57:605–13 CrossRef Medline
3. de Wit MC, de Bruin HG, Eijkenboom W, et al. **Immediate post-radiotherapy changes in malignant glioma can mimic tumor progression.** *Neurology* 2004;63:535–37 CrossRef Medline
4. Huang K, Dahele M, Senan S, et al. **Radiographic changes after lung stereotactic ablative radiotherapy (SABR): can we distinguish recurrence from fibrosis? A systematic review of the literature.** *Radiation Oncol* 2012;102:335–42 CrossRef Medline
5. Dahele M, Palma D, Lagerwaard F, et al. **Radiological changes after stereotactic radiotherapy for stage I lung cancer.** *J Thorac Oncol* 2011;6:1221–28 CrossRef Medline
6. Taylor DR, Weaver JA. **Tumor pseudoprogession of spinal metastasis after radiosurgery: a novel concept and case reports.** *J Neurosurg Spine* 2015;22:534–39 CrossRef Medline
7. Choi H, Charnsangavej C, Faria SC, et al. **Correlation of computed tomography and positron emission tomography in patients with metastatic gastrointestinal stromal tumor treated at a single institution with imatinib mesylate: proposal of new computed tomography response criteria.** *J Clin Oncol* 2007;25:1753–59 CrossRef Medline
8. Knospe WH, Blom J, Crosby WH. **Regeneration of locally irradiated bone marrow, I: dose dependent, long-term changes in the rat, with particular emphasis upon vascular and stromal reaction.** *Blood* 1966;28:398–415 Medline
9. Hayhurst C, Zadeh G. **Tumor pseudoprogession following radiosurgery for vestibular schwannoma.** *Neuro Oncol* 2012;14:87–92 CrossRef Medline
10. Bakardjiev AI, Barnes PD, Goumnerova LC, et al. **Magnetic resonance imaging changes after stereotactic radiation therapy for childhood low grade astrocytoma.** *Cancer* 1996;78:864–73 CrossRef Medline
11. Young RJ, Gupta A, Shah AD, et al. **Potential utility of conventional MRI signs in diagnosing pseudoprogession in glioblastoma.** *Neurology* 2011;76:1918–24 CrossRef Medline
12. Prager AJ, Martinez N, Beal K, et al. **Diffusion and perfusion MRI to differentiate treatment-related changes including pseudoprogession from recurrent tumors in high-grade gliomas with histopathologic evidence.** *AJNR Am J Neuroradiol* 2015;36:877–85 CrossRef Medline

Low Signals on T2* and SWI Sequences in Patients with MS with Progressive Multifocal Leukoencephalopathy

We read with interest the study by Hodel et al¹ concerning the occurrence of cortex, U-fiber, and basal ganglia low signals found on T2* and SWI sequences in 12 patients with MS with progressive multifocal leukoencephalopathy (PML). These low signals were frequent in this series and may occur in presymptomatic patients with PML treated with natalizumab (75% of their 8 asymptomatic patients with PML). We previously published such low intensities in a patient with a PML diagnosis.² We further confirmed the importance of T2* and SWI sequences to detect low signals in a series of 4 patients with PML.³ Pathologic analysis by Hodel et al¹ of a patient with low T2* signal intensities identified astrocytic gliosis associated with abundant microglial and macrophage infiltrates, containing myelin-filled vacuoles. The authors hypothesized that low signal on T2* could be related to accumulation of iron in the macrophages. Although T2* and SWI low signal intensities are not constant in PML, their occurrence may differentiate confluent MS lesions from PML. Consequently, an MR imaging survey of patients at risk for PML (notably patients

with MS treated with natalizumab or those who are immunosuppressed) should include T2* and SWI sequences.

REFERENCES

1. Hodel J, Outteryck O, Verclytte S, et al. **Brain magnetic susceptibility changes in patients with natalizumab-associated progressive multifocal leukoencephalopathy.** *AJNR Am J Neuroradiol* 2015 Aug 27. [Epub ahead of print] CrossRef Medline
2. Carra-Dalliere C, Menjot de Champfleur N, Ayrygnac X, et al. **Quantitative susceptibility mapping suggests a paramagnetic effect in PML.** *Neurology* 2015;84:1501–02 CrossRef Medline
3. Carra-Dalliere C, Menjot de Champfleur N, Deverdun J, et al. **Use of quantitative susceptibility mapping (QSM) in progressive multifocal leukoencephalopathy.** *J Neuroradiol* 2015 Oct 13. [Epub ahead of print] CrossRef Medline

● P. Labauge

● C. Carra-Dalliere

● X. Ayrygnac

Department of Neurology

● N. Menjot de Champfleur

Department Neuroradiology

Montpellier University Hospital

Centre Hospitalo-Universitaire Gui de Chauliac

Montpellier, France

<http://dx.doi.org/10.3174/ajnr.A4632>

REPLY:

We would like to thank Dr Labauge and colleagues for their thoughtful reading of our recent article “Brain Magnetic Susceptibility Changes in Patients with Natalizumab-Associated Progressive Multifocal Leukoencephalopathy” (NTZ-PML).¹

For the survival and functional outcome of patients treated by NTZ, it is crucial to detect PML on the basis of brain MR imaging before symptom onset, when brain involvement is more localized. This is the first clinical report showing the magnetic susceptibility changes in brain NTZ-PML lesions from the asymptomatic to the chronic stages with different MR imaging scanners (1.5T and 3T) and different MR images (T2* and SWI). In this preliminary study, we did not assess the diagnostic accuracy of the hypointense rim sign on susceptibility-weighted MR images for the diagnosis of asymptomatic NTZ-PML, but our data suggest the major role of this technique in clinical routine. Thus, as suggested by Dr Labauge and colleagues, we believe that susceptibility-weighted MR images should be systematically included in the MR imaging protocol performed in patients with suspected PML.

SWI is now available on most MR imaging scanners and should be preferred to T2* due to the higher spatial resolution and the improved lesion conspicuity inherent to this technique. In our experience, SWI was much more sensitive than T2* in detecting a subtle hypointense rim involving the U-fibers, particularly at the asymptomatic stage. Assessing iron accumulation by quantitative susceptibility mapping must be useful as well to better understand the pathophysiology of this new imaging feature, as previously suggested.² However, this approach still needs postprocessing time and cannot be performed in daily clinical practice.

SWI should be interpreted according to other signal anomalies previously reported in the literature for the early diagnosis of PML, including perivascular punctate lesions (enhanced or not on postcontrast T1WI) and hyperintensities on diffusion-weighted images.^{3,4} Awareness of these specific lesion patterns and the use of an adequate MR imaging protocol facilitate an earlier diagnosis of asymptomatic NTZ-PML, associated with a more favorable prognosis.

REFERENCES

1. Hodel J, Outteryck O, Verclytte S, et al. **Brain magnetic susceptibility changes in patients with natalizumab-associated progressive mul-**

- tifocal leukoencephalopathy. *AJNR Am J Neuroradiol* 2015 Aug 27. [Epub ahead of print] CrossRef Medline
2. Carra-Dalliere C, Menjot de Champfleury N, Ayrignac X, et al. **Quantitative susceptibility mapping suggests a paramagnetic effect in PML.** *Neurology* 2015;84:1501–02 CrossRef Medline
3. Yousry TA, Pelletier D, Cadavid D, et al. **Magnetic resonance imaging pattern in natalizumab-associated progressive multifocal leukoencephalopathy.** *Ann Neurol* 2012;72:779–87 CrossRef Medline
4. Hodel J, Outteryck O, Dubron C, et al. **Asymptomatic progressive multifocal leukoencephalopathy associated with natalizumab: diagnostic precision with MR imaging.** *Radiology* 2015 Oct 5. [Epub ahead of print] CrossRef Medline

J. Hodel

University of Lille
Lille, France

Department of Neuroradiology
Roger Salengro Hospital
Lille, France

O. Outteryck

University of Lille
Lille, France

Department of Neurology
Roger Salengro Hospital
Lille, France

S. Verclytte

Department of Radiology
Saint Philibert Hospital
Lille, France

V. Deramecourt

University of Lille
Lille, France

Department of Pathology
Lille University Hospital
Lille, France

A. Lacour

University of Lille
Lille, France

Department of Neurology
Roger Salengro Hospital
Lille, France

J.-P. Pruvo

University of Lille
Lille, France

Department of Neuroradiology
Roger Salengro Hospital
Lille, France

P. Vermersch

University of Lille
Lille, France

Department of Neurology
Roger Salengro Hospital
Lille, France

X. Leclerc

University of Lille
Lille, France

Department of Neuroradiology
Roger Salengro Hospital
Lille, France

<http://dx.doi.org/10.3174/ajnr.A4634>

Flow-Diverter Stents for the Treatment of Saccular Middle Cerebral Artery Bifurcation Aneurysms: Is “Unsuitable” the Right Conclusion?

We read with interest the recent publication by Caroff et al¹ on saccular MCA aneurysm treatment by flow diverters (FDs), in regard to the increasing tendency to use FDs in distal, off-label localizations. We appreciate their important contribution to the subject but remain reserved regarding their strong conclusion. The subject is still under research, but some promising clinical and angiographic outcomes have been published.² We were slightly perplexed by the interpretation of the reported complication rate, taking into account the methodologic limitations of the study due to the small number of subjects.

Various mechanisms of ischemic complications are implicated in flow diversion with covered arteries, which are not always sufficiently represented in a small case series. Thrombosis related to an ineffective anti-aggregation regimen, suboptimal stent apposition on the arterial wall, or distal emboli provoked by the mechanical manipulations inside the arteries are types of complications that should not be confounded with the pure hemodynamic effect of flow diversion on a covered branch. Good discrimination of the various potential ischemic mechanisms is mandatory to obtain a more profound understanding of FD-related complications.

To clear a misunderstanding, we must comment on the complication rates of the case series by Saleme et al³ cited in the discussion. The overall complication rate for the MCA cases in the study was 5% ($n = 1/19$), with a sole side branch–related complication in the MCA aneurysm sub-series. Apart from reporting complication rates, they performed a classification of jailed branches, dividing them into anastomotic or terminal. In this section, a symptomatic angiographic change was defined as any angiographic remodelling at 6 months in patients who reported transient symptoms at any point during the follow-up of 6 months.

These findings, reported in the postprocedural period analysis, usually occurred around 3–4 weeks after stent placement and consisted of either transient symptoms or silent DWI spots. They were reported to delineate the progressive remodelling of jailed branches, as part of the collateral network development of the brain⁴ in the postprocedural period. They were described in patients under effective antiaggregation and should not be confounded with early ischemic findings in patients with inefficient antiaggregation or with immediate flow restriction in the jailed

branches, related to local high metal coverage or stent-deployment defects.

The complications reported in the study of Caroff et al¹ were encountered in the immediate postprocedural period; as they mentioned, the complications seemed to be related mainly to antiaggregation and technical issues. These results are useful to plan further, larger scale studies; they should also be kept in mind in everyday practice. Controlled hypertension in the postprocedural period, avoidance of under- or overinhibition of P2Y12 receptors,² and slight device oversizing are key technical points to consider when covering MCA branches.

The use of FDs in MCA bifurcations is still under research; various parameters need to be clarified and standardized before establishing a consensus for this treatment. Jailing distal terminal intracranial branches such as MCA bifurcations remains a challenging issue, but with a careful hemodynamic case-by-case study and proper patient preparation, FD treatment in such cases may prove to be a useful technique in otherwise challenging complex cases. Further research is underway regarding this subject by several teams; until concrete data see the light, every conclusion should be taken with a grain of salt.

REFERENCES

1. Caroff J, Neki H, Mihalea C, et al. **Flow-diverter stents for the treatment of saccular middle cerebral artery bifurcation aneurysms.** *AJNR Am J Neuroradiol* 2015 Sep 24. [Epub ahead of print] CrossRef Medline
2. Kallmes DF, Hanel R, Lopes D, et al. **International retrospective study of the Pipeline embolization device: a multicenter aneurysm treatment study.** *AJNR Am J Neuroradiol* 2015;36:108–15 CrossRef Medline
3. Saleme S, Iosif C, Ponomarjova S, et al. **Flow-diverting stents for intracranial bifurcation aneurysm treatment.** *Neurosurgery* 2014; 75:623–31; quiz 631 CrossRef Medline
4. Rouchaud A, Leclerc O, Benayoun Y, et al. **Visual outcomes with flow-diverter stents covering the ophthalmic artery for treatment of internal carotid artery aneurysms.** *AJNR Am J Neuroradiol* 2015; 36:330–36 CrossRef Medline

© C. Iosif
© C. Mounayer

Department of Interventional Neuroradiology
Dupuytren University Hospital
Limoges, France

REPLY:

We would like to comment on the letter to the Editor regarding our article “Flow-Diverter Stents for the Treatment of Saccular Middle Cerebral Artery Bifurcation Aneurysms.”¹ We thank Dr Iosif and colleagues for their interest in our work, and we welcome the opportunity to comment on some of their remarks. First, we agree that there are multiple mechanisms involved in thromboembolic complications when using flow-diverter stents (FDSs) and that in some cases, the mechanisms can be unclear. However, we would strongly assert that in our study, complications were almost exclusively related to hemodynamic effects and not due to any technical issues, as suggested in the letter of Dr Iosif and colleagues.

No cases of thrombosis related to ineffective antiaggregation therapy were encountered because all patients were tested for any potential aspirin or clopidogrel resistance with the VerifyNow P2Y12 assay (Accumetrics, San Diego, California) and hematologic lab tests, as performed by Saleme et al.² We admit the possibility that even without biologic resistance to clopidogrel, this medication may be insufficient in those cases in which the covered branch is at very high risk of occlusion due to sudden flow restriction in the first hours after FDS delivery. Therefore, we as a department are considering a switch from clopidogrel to ticagrelor.³

Stent apposition is much easier to obtain at sites of middle cerebral artery bifurcation aneurysms than at sites of carotid siphon aneurysms due to less tortuosity. In addition, in our study, stent apposition was always confirmed with postoperative VasoCT (Philips Healthcare, Best, the Netherlands). If required, FDSs were ballooned to achieve a perfect opening.

Using diffusion-weighted MR imaging, we did not detect any distal emboli in the FDS branch provoked by mechanical manipulations during FDS delivery. In fact, in most cases branch catheterization and FDS positioning were quite simple at these locations.

In addition to these points, blood pressure was strictly controlled during treatment and in an intensive care unit for 12 hours after treatment.

We apologize for any eventual inaccuracies in the analysis of the complication ratio in the study by Saleme et al.² Because we tried to focus only on MCA saccular aneurysms, we excluded all blister aneurysms; this exclusion may have resulted in an overestimation of the morbidity rate from the available data in this study. However, we remain convinced that the use of FDS for the

treatment of saccular MCA bifurcation aneurysms carries a risk of complications. As reported and discussed by Saleme et al, in some cases, ischemic complications will occur in the covered branch territory because the corticopial anastomosis is unable to fully meet the needs of the brain area. However, how to predict this phenomenon from digital subtraction angiography data (even with balloon test occlusion) is not yet clearly understood. Moreover, in our studies, DWI ischemic findings are seen in 43% of cases.

We wish to encourage Iosif and colleagues in their research to clarify the mechanisms of branch modifications with flow diversion; there may be a place for FDSs in the management of lesions that are challenging for surgical clipping and endovascular treatment such as blood blister-like, fusiform MCA aneurysms or difficult, dysplastic, extremely broad-based aneurysms. However, in the case of saccular MCA bifurcation aneurysms, because a meta-analysis from published studies with FDSs showed permanent deficit rates in 10.3% of cases (7/68),^{1,2,4,5} we consider that under the conditions described in the different studies, FDSs are indeed not a “suitable solution” and other endovascular or surgical strategies should be preferred. Therefore, we encourage the rigorous evaluation of last-generation braided stents and new innovative devices that are increasingly becoming available on the market.

REFERENCES

1. Caroff J, Neki H, Mihalea C, et al. **Flow-diverter stents for the treatment of saccular middle cerebral artery bifurcation aneurysms.** *AJNR Am J Neuroradiol* 2015 Sep 24. [Epub ahead of print] CrossRef Medline
2. Saleme S, Iosif C, Ponomarjova S, et al. **Flow-diverting stents for intracranial bifurcation aneurysm treatment.** *Neurosurgery* 2014;75: 623–31; quiz 631 CrossRef Medline
3. Storey RF, Angiolillo DJ, Patil SB, et al. **Inhibitory effects of ticagrelor compared with clopidogrel on platelet function in patients with acute coronary syndromes: the PLATO (PLATElet inhibition and patient Outcomes) PLATELET substudy.** *J Am Coll Cardiol* 2010;56: 1456–62 CrossRef Medline
4. Yavuz K, Geyik S, Saatci I, et al. **Endovascular treatment of middle cerebral artery aneurysms with flow modification with the use of the Pipeline embolization device.** *AJNR Am J Neuroradiol* 2014;35: 529–35 CrossRef Medline
5. Briganti F, Delehay L, Leone G, et al. **Flow diverter device for the treatment of small middle cerebral artery aneurysms.** *J Neurointerv Surg* 2015 Jan 20. [Epub ahead of print] CrossRef Medline

J. Caroff
L. Spelle
J. Moret

Department of Interventional Neuroradiology
Hôpital Bicêtre, Assistance Publique des Hôpitaux de Paris, Paris Sud Université
Paris, France

<http://dx.doi.org/10.3174/ajnr.A4654>

Stents for Idiopathic Intracranial Hypertension: Meta-Analyzed, Hypo-Analyzed, and In Need of a Trial

How did the recent article by Satti et al¹ pass muster? A review of the status of venous sinus stent placement in 2013² included more patients with stents than the so-called meta-analysis review in your October 2015 issue. Seven of the studies cited in the 2013 analysis had only 1 patient each and were not included in the 2015 analysis; stripped of those 7 single patient studies, the 2015 meta-analysis looks much like the 2013 review. Nevertheless, why choose to include in the meta-analysis a study with only 4 patients—or the studies with only 10, 12, 15, or 18 patients? The power in both the 2013 review and the current meta-analysis lies in the 52-patient study by Ahmed et al,³ in which CSF opening pressure, an essential criterion for the diagnosis of idiopathic intracranial hypertension (IIH), was not documented in either 11 or 9 patients depending on which meta-analysis one chooses to read. Likewise, the 2 studies with 15 patients each (Fields et al⁴ and Albuquerque et al⁵) did not record the CSF opening pressure for any of their included patients; and both the 4-patient study (Owler et al⁶) and the 18-patient study (Kumpe et al⁷) did not record CSF opening pressure in 1 and 4 patients, respectively. A study of 10 patients noted to be without recorded CSF opening pressures in the 2013 analysis (Bussi ere et al⁸) is noted in Table 4 of the 2015 meta-analysis as having an opening pressure range of 25–50 cm H₂O. What was the source of that post hoc information?

Given that an elevated CSF pressure is an essential diagnostic criterion of IIH, for which all of these patients were treated, it is therefore possible that as many as 56 of the patients included in the meta-analysis did not meet the criteria for diagnosis of the disease and should not be included in any study of IIH. Given that so little regard was shown for adherence to strict diagnostic criteria to establish the presence of IIH, it is no wonder that there is absolutely no mention of poststenting CSF opening pressure in any of the included studies, which is remarkable because failing to do so missed an opportunity to establish causality. The authors are correct in noting that future studies of operative techniques for this disease should include pre- and postintervention CSF studies, of which I

would suggest that at a minimum these require documented CSF pressures in all patients.

Whether or no IIH actually existed, all patients in the meta-analysis studies underwent the stent-placement procedure and were subject to subsequent complications. Subdural hematoma, noted in passing as a major complication in the meta-analysis, is treated more rigorously in the 2013 review, which noted that all cases of recorded subdural hematomas were treated with open surgical decompression. Therefore, the possibility exists that at least some patients who did not meet the criteria for a diagnosis of IIH underwent an unnecessary procedure that caused a life-threatening complication requiring an emergent operation. Also treated in passing are the 8 patients in the meta-analyzed studies who underwent re-stenting for in-stent/peri-stent restenosis—events that are normally noted as complications in most studies of vascular stents but not so in the Satti article where they are neither listed as complications nor listed as “revisions” in Table 4. There is also the possibility that the 2.2% conversion rate to another treatment technique noted in the meta-analysis may not be accurate. A study from a dedicated multidisciplinary IIH treatment center that is not referenced in the meta-analysis (Goodwin et al⁹) reported that 3 of 18 (16.6%) patients failed venous sinus stent placement and ultimately required a shunt procedure. A conversion to a more invasive procedure as a result of treatment failure should be counted as a complication of the initial procedure.

The only conclusion that can be drawn is that there is a hint of a promise for this procedure in some patients in whom medically refractory IIH is correctly established. Without a controlled trial comparing venous sinus stent placement with either an accepted surgical technique or the best available medical therapy, conclusions cannot be drawn regarding which patients, if any, may benefit from venous sinus stent placement.

REFERENCES

1. Satti SR, Leishangthem L, Chaudry MI. **Meta-analysis of CSF diversion procedures and dural venous sinus stenting in the setting of medically refractory idiopathic intracranial hypertension.** *AJNR Am J Neuroradiol* 2015;36:1899–904 CrossRef Medline
2. Puffer RC, Mustafa W, Lanzino G. **Venous sinus stenting for idio-**

- pathic intracranial hypertension: a review of the literature. *J Neurointerv Surg* 2013;5:483–86 CrossRef Medline
3. Ahmed RM, Wilkinson M, Parker GD, et al. **Transverse sinus stenting for idiopathic intracranial hypertension: a review of 52 patients and of model predictions.** *AJNR Am J Neuroradiol* 2011;32:1408–14 CrossRef Medline
 4. Fields JD, Javedani PP, Falardeau J, et al. **Dural venous sinus angioplasty and stenting for the treatment of idiopathic intracranial hypertension.** *J Neurointerv Surg* 2013;5:62–68 CrossRef Medline
 5. Albuquerque FC, Dashti SR, Hu YC, et al. **Intracranial venous sinus stenting for benign intracranial hypertension: clinical indications, technique, and preliminary results.** *World Neurosurg* 2011;75:648–55 CrossRef Medline
 6. Owler BK, Parker G, Halmagyi GM, et al. **Pseudotumor cerebri syndrome: venous sinus obstruction and its treatment with stent placement.** *J Neurosurg* 2003;98:1045–55 CrossRef Medline
 7. Kumpe DA, Bennett JL, Seinfeld J, et al. **Dural sinus stent placement for idiopathic intracranial hypertension.** *J Neurosurg* 2012;116:538–48 CrossRef Medline
 8. Bussière M, Falero R, Nicolle D, et al. **Unilateral transverse sinus stenting of patients with idiopathic intracranial hypertension.** *AJNR Am J Neuroradiol* 2010;31:645–50 CrossRef Medline
 9. Goodwin CR, Elder BD, Ward A, et al. **Risk factors for failed transverse sinus stenting in pseudotumor cerebri patients.** *Clin Neurol Neurosurg* 2014;127:75–78 CrossRef Medline

● P. Noonan

Department of Radiology
Scott and White Memorial Hospital
Temple, Texas

REPLY:

I appreciate the thorough review and comments on our recent article, “Meta-Analysis of CSF Diversion Procedures and Dural Venous Sinus Stenting in the Setting of Medically Refractory Idiopathic Intracranial Hypertension,”¹ by Dr Noonan. I humbly concede that our meta-analysis of the dural venous sinus stent (DVSS) is not significantly different from the previously published meta-analysis on the topic of DVSS for idiopathic intracranial hypertension (IIH),² though another meta-analysis on DVSS was not the goal of the article. The DVSS portion of the article represented only one-third of the focus of the article. The goal of the article was to compare outcomes and complications of DVSS with traditional surgical approaches (CSF flow diversion and optic nerve sheath fenestration) on the basis of the best available published literature and to highlight that the “standard of care” for medically refractory IIH may not be superior to DVSS. To date, no large meta-analysis has been performed comparing surgical intervention with the DVSS in the setting of IIH. The purpose of this article was to challenge the assertion that surgery, rather than endovascular treatment, should be considered as the first-line standard of care for all patients with medically refractory IIH. Therefore, this article represents a significant and unique contribution to the literature.

The major limitation of the article was the retrospective nature and inconsistent data collection, which are inherent with meta-analysis study designs and are further complicated by comparison of different procedures by different operators focusing on different clinical parameters. This limitation was a considerable challenge, and direct comparison of baseline characteristics and follow-up was impossible.

One criticism raised by Dr Noonan was our approach to exclusion/inclusion of particular articles. This was largely driven by the numbers and was arbitrary. DVSS is a relatively new procedure compared with optic nerve sheath fenestration and CSF flow diversion; therefore, significantly less patient data were available. Data regarding DVSS were incomplete and inhomogeneous, given the current lack of standards (selection and follow-up). We chose to exclude any article deemed to have poor or incomplete data. Articles with a single patient were also excluded because they did not significantly add to the power of the study (7 articles with single patients are already well-described in the literature). Larger patient numbers were, in our opinion, worth the effort required to evaluate and standardize the data to help power the study. The 15-patient cohort from Albuquerque et al³ was included to help power the DVSS subset, despite not providing detailed pretreatment CSF opening pressures, given that the remainder of the data points were documented. Albuquerque et al did report, however, that elevated venous pressures were confirmed in all except 1 patient (18/19 patients).³ In reference to the comments regarding Table 4, venous sinus stenting, Bussière et al² did report CSF opening pressures as a range between 25 and 50 cm H₂O, which was provided in the body of the article under “Materials and Methods.” Strict inclusion criteria were not commonly adhered to in the surgical modalities.

Emergent evacuation of a subdural hematoma is not to be taken lightly and may be less common now, given improved catheter technology with use of flexible large-bore guiding catheters such as the Neuron Max catheter (Penumbra, Alameda, California). Subdural hematomas were reported in only 4/136 patients and resulted in no deaths in the DVSS group. Additionally, the major complication rate in this group was significantly lower than that in the surgical alternatives. I humbly contend that most neurointerventionalists would not consider re-stent placement as a complication, but rather a limitation. If we defined “repeat procedure” as a complication, the CSF flow-diversion group would appear even less appealing to physicians and patients because 154/435 patients required an astonishing additional 428 procedures. This was just during the average follow-up period of 41 months in largely young female patients, with an average age of 31.9 years (potentially, additional procedures might be needed for many more years).

Finally, I would agree with Dr Noonan that there is great promise for the DVSS in the setting of appropriately chosen patients with medically refractory IIH. I would propose incorporation of the following before any stent procedure:

- 1) A multidisciplinary approach (documenting truly medically refractory IIH)
- 2) CSF studies with elevated opening pressures
- 3) Careful imaging selection before venography (MR imaging and MRV with and without contrast)
- 4) Venography confirming stenosis and direct pressure measurements (gradient, ≥ 8 mm Hg) without sedation
- 5) Intervention by using a careful technique (a triaxial approach by using modern ultra-flexible guiding catheters) and the “conduit technique” to minimize the risk of dural sinus injury⁴ and dual antiplatelet therapy minimizes risk of in-stent thrombosis
- 6) Thorough long-term follow-up including clinical examination (symptoms, papilledema, funduscopic examination) and follow-up CSF pressures.

I sincerely hope this article proves to be a valuable contribution to the literature, ideally serving as a stepping stone to better understand the disease and potentially suggesting a new paradigm in the treatment of patients with medically refractory IIH.

REFERENCES

1. Satti SR, Leishangthem L, Chaudry MI. **Meta-analysis of CSF diversion procedures and dural venous sinus stenting in the setting of medically refractory idiopathic intracranial hypertension.** *AJNR Am J Neuroradiol* 2015;36:1899–904 CrossRef Medline
2. Bussière M, Falero R, Nicolle D, et al. **Unilateral transverse sinus stenting of patients with idiopathic intracranial hypertension.** *AJNR Am J Neuroradiol* 2010;31:645–50 CrossRef Medline
3. Albuquerque FC, Dashti SR, Hu YC, et al. **Intracranial venous sinus stenting for benign intracranial hypertension: clinical indications, technique, and preliminary results.** *World Neurosurg* 2011;75:648–52; discussion 592–95 CrossRef Medline
4. Turk A, Manzoor MU, Nyberg EM, et al. **Initial experience with distal guide catheter placement in the treatment of cerebrovascular**

disease: clinical safety and efficacy. *J Neurointerv Surg* 2013;5:247–52
CrossRef Medline

S.R. Satti

Department of Neurointerventional Surgery
Christiana Care Health System
Newark, Delaware

L. Leishangthem

Department of Neurology
Albert Einstein Medical Center
Philadelphia, Pennsylvania

T. Sivapatham

Department of Neurointerventional Surgery
Christiana Care Health System
Newark, Delaware

The authors apologize and state that in the original article “WEB-DL Endovascular Treatment of Wide-Neck Bifurcation Aneurysms: Long-Term Results in a European Study” by L. Pierot, J. Klisch, T. Liebig, J.-Y. Gauvrit, M. Leonardi, N.P. Nuzzi, F. Di Paola, V. Sychra, B. Mine, and B. Lubicz [*AJNR Am J Neuroradiol* 2015;36:2314–19, 10.3174/ajnr.A4445], there is an error in the author affiliations of Prof. M. Leonardi (M.L.). The correct version is given below.

Department of Neuroradiology (M.L.), Ospedale Bellaria, IRCCS Istituto delle Scienze Neurologiche di Bologna and DIMES, Bologna University, Bologna, Italy.

<http://dx.doi.org/10.3174/ajnr.A4643>